Bern University
of Applied Sciences

Empa
Materials Science and Technology



Timber Bridges

International Conference on Timber Bridges ICTB2021 PLUS

09-12 May 2022

Conference Proceedings

Bern University of Applied Sciences and Empa

International Conference on Timber Bridges ICTB 2021PLUS
Conference Proceedings
9 - 12 May 2022

Edited by
Bettina Franke
Steffen Franke

Published by
Bern University of Applied Sciences
Architecture, Wood and Civil Engineering
Solothurnstrasse 102
CH-2504 Biel

www.bfh.ch/ictb
ictb21@bfh.ch

ISBN 9 783906 878126

Berner Fachhochschule
Haute école spécialisée bernoise
Bern University of Applied Sciences

Empa
Materials Science and Technology

Preface

We are pleased to host the International Conference on Timber Bridges- ICTB 2021^{PLUS}.

At this conference, young researchers, and practician/practitioners as well as old hands in the field of timber bridges get the opportunity to share their knowledge while –at the same time- learning from others. The presentations cover topics from the enhancement of wooden materials and components for new timber bridges to the assessment, strengthening and monitoring of existing bridges, both modern and historic ones. Following the conference, in which the theoretical foundations are highlighted, a field trip and excursion to existing old and new timber bridges will provide the opportunity to learn from real cases and continue the knowledge exchange on-site.

The organizers see the conference also as a contribution to the decarbonization of infrastructure for the necessary climate change. The share of wooden bridges in the total number of bridges is small although wood is a high-performance and sustainable material. Modern wood materials and technologies are being increasingly used in the construction of multi-storey buildings. This current development clearly shows that wood is also suitable and competitive as a building material for large structures. Therefore, it is desirable that also the transport infrastructure is increasingly realized with wood. To achieve this, it is necessary to give an impulse in education, research, and exchange of knowledge, so that planners and decision-makers are motivated to work with sustainable materials and technologies in bridge construction. In this context, the authors and speakers of the 4th ICTB will show innovative solutions, present realized projects as well as current research results in order to foster timber bridge construction worldwide and to inspire and convince sceptics and authorities.

The organizers of the conference feel connected to climate neutrality and wood as a material and have organized the conference with commitment.

We hope you benefit from it.

Andreas Müller | Bettina Franke | Robert Widmann | Steffen Franke

Bern University of Applied Sciences, Biel, Switzerland
Empa, Structural Engineering Research Laboratory, Dübendorf, Switzerland

Content

Day 1, 10th May 2022

Infrastructure made of wood - opportunities for decarbonization of the public sector 9
Stefan Zöllig

Våla bridge - Timber network arch footbridge in Ringebu, Norway 17
Anna Weronika Ostrycharczyk, Arne Værnes

Two new pedestrian and cycle bridges between Rupperswil and Auenstein, Switzerland 27
Kurt von Felten, Milo Zimmerli

Innovative large timber foodbridges and dynamic testing in Spain 33
Julio Vivas, Álvaro Magdaleno, Soledad Rodríguez, Antolín Lorenzana

Fruttli-and Rigiaa-Bridge, Timber-UHPC composite structure 41
Edgar Kälin, Peter Rogenmoser

A new pedestrian bridge made of regional beech wood in Adliswil 47
Andreas Burgherr, Ciril Stadler

Pedestrian and cyclist bridges made with durable hardwoods 57
Marcus Schiere, Jos Peters

The road to durable bridge design: An experience from Québec 65
Caroline Frenette

Design, construction and maintenance of structurally protected timber bridges 73
Antje Simon, Markus G. Jahreis, Johannes Koch

Robust Timber bridges without cladding 79
Frank Miebach

Structural Rehabilitation of a Historic Covered Bridge: Bridgeport Covered Bridge 85
Lawrence Jones, Brian Wiens

A reliable method for moisture content measurement at inspections and the results from nine Swedish Timber Bridges, *Niclas Björngrim, Per-Anders Fjellström, Göran Berggren* 99

Effectiveness of structural protection measures for timber bridges – results of a long-term moisture monitoring, *Johannes Koch, Antje Simon, Markus G. Jahreis* 105

Monitoring systems for timber bridges – Moisture content and swinging behaviour 115
Steffen Franke, Bettina Franke, Sébastien Bonifacio, Andreas Müller

Day 2, 11th May 2022

Wooden bridges enrich the world 125
Frank Miebach

Modern timber bridges 129
Rune Abrahamsen

Advanced data logging system for moisture monitoring of timber bridges - background and large scale application, *Kai Simon, Jürgen Hezel, Simon Aicher* 133

Characterization and assessment of the mechanical properties of spruce foundation piles retrieved from bridges in Amsterdam, *Giorgio Pagella, Geert Ravenshorst, Wolfgang Gard, Jan Willem van de Kuilen* 141

Climate respectively moisture induced stresses in block-glued glulam members of timber bridges, *Bettina Franke, Marcus Schiere, Steffen Franke* 151

Vibration serviceability of timber pedestrian bridge based on field test and analysis 159
Shingo Kato, Hideyuki Honda and Atsushi Toyoda

Study of the dynamic response of a timber pedestrian bridge during different construction stages, *Jens Bergenudd, Jean-Marc Battini, Roberto Crocetti, Costin Pacoste* 167

New concepts for timber bridge decks without cross beams: Stress laminated decks and interlocked laminated decks, *Tormod Dyken, Hauke Burkart* 179

Details for timber bridges with asphalt wearing surfaces 185
Andreas Müller, Marcus Schiere

Direct trafficable waterproofing and wearing courses for timber decks, 195
Dirk Uebelhoer, Mareike Vogel, Thomas Volkmer, Adrian Willi Wick

Creating a connecting between asphalt wearing surface and timber bridge decks 201
Marcus Schiere, Andreas Müller, Nicolas Bueche, Christian Angst

Setting the Standard – Advancements in wood bridge design in the Canadian highway bridge design code *Andrew Lehan, David Moses* 213

Fatigue strength of axially loaded steel rods bonded in European ash glulam 223
Bruno Maurer, Ernst Gehri, Thomas Strahm, René Steiger, Christian Affolter

Exploring fatigue rules for timber structures in Eurocode 5 231
Kjell Arne Malo, Francesco Mirko Massaro, Haris Stamatopoulos

Assessment of glulam structures: moisture monitoring and investigation on the effect of climatic conditions on durability, *Placide Uwizeyimana, Marianne Perrin, Florent Eyma* 243

Defect Identification Coupled with Grayscale Image Enhancement Technology 251
Junwon Seo, Euiseok Jeong, James Wacker

Evaluating the Efficacy of Ground-Penetrating Radar as an Inspection Tool for Timber Bridges 257
C. Adam Senalik, James P. Wacker, Xiping Wang

Day 3, 12th May 2022

History and development stages in timber bridge construction in Switzerland 266
Robert Widmann, Andreas Müller

First Swiss wildlife bridge made with timber 279
Lukas Rüegsegger

Climate and moisture monitoring system in the timber wildlife crossing 'Rynetel' 285
Sébastien Bonifacio, Marcus Schiere, Andreas Müller

Preliminary moisture-relevant monitoring results of a timber wildlife bridge 290
Karim Ghazi Wakili, Jan Maurer, Andreas Müller

Structural yield of a pedestrian bridge made of CLT-concrete, con-nected by screws and by notches, *Gonzalo Moltini, Gonzalo Cabrera, Vanesa Baño* 296

Notched Connections for Timber-Concrete Composite Bridges – Investigations on the Fatigue Behaviour, *Simon Mönch, Ulrike Kuhlmann* 305

Sharp metal for timber connections 313
Paolo Grossi, Stephan Schindlauer

Overview EN 1995-2:2022xx and Annex D Examples for Detailing 319
Matthias Gerold

Vibration, Deflections 357
Patricia Hamm

TCC and Integral Bridges 369
Jörg Schänzlin, Alfredo Dias

Sponsoren advertisement

Bern University of Applied Sciences

Empa

Timbatec Timber Construction Engineers Switzerland

Eurotec GmbH

Heco AG

Hüsser Holzleimbau AG

Immer AG

neue Holzbau AG

ProGeo Monitoring Systeme & Services GmbH & Co. KG

Rotho Blaas Srl

Sika Services AG

Timber Structures 3.0 AG

ICTB 2021 PLUS
4th International Conference on Timber Bridges
Biel/Bienne, Switzerland, 9 -12 May 2022



Infrastructure made of wood – opportunities for decarbonization of the public sector

Stefan Zöllig[1]

Abstract

The infrastructural construction sector is one of the largest CO_2 emitters in Switzerland. The main cause is the use of reinforced concrete. By replacing reinforced concrete with wood, infrastructure construction could significantly reduce its emissions and thus substantially contribute to decarbonization. A corresponding political proposal "Research and innovation of wood as a material for use in infrastructure construction as a decarbonization contribution" was adopted in the Swiss federal parliament in November 2021 and will be implemented in the next few years. For this purpose, Bern University of Applied Sciences (BFH AHB) has developed a strategy together with Timbatec Holzbauingenieure Schweiz AG and TS3 AG. Also, a research project for box-girder heavy duty bridges has been started recently.

Climate change

We are living in a time of major climate changes. We all know: It's the carbon emission which destroys the world we live in. Because of fossile fuel burning: Gas, oil, coal. Even if we reduce our carbon emissions to a net zero by 2050, temperatures will climb at least 2°C above pre-industrial times, cp. Figures 1 and 2. But this means a complete stop to the burning of fossil fuels.

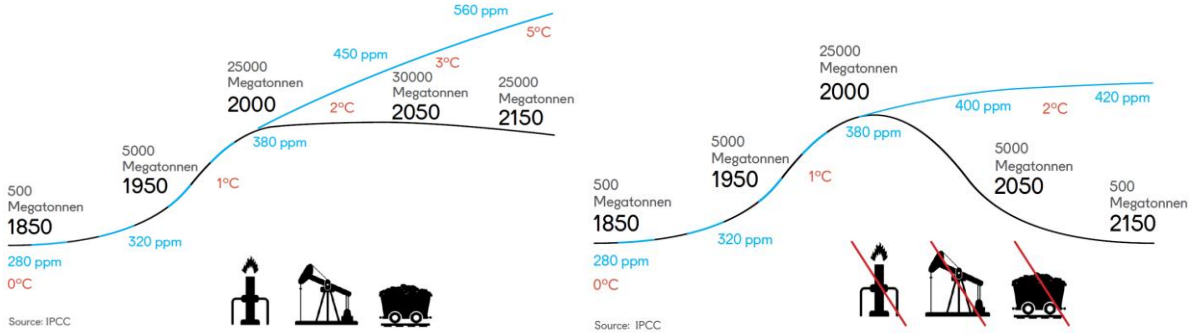


Figure 1 and 2: CO_2 and temperature development over time. Pictures: Timbatec

People think that air traffic is the main problem. It isn't. Global air traffic only accounts for around 3% of CO_2 emissions. Of course, we should not fly excessively. But avoiding flights hardly gains anything measurable. Buildings, on the other hand, contribute around 40% of global CO_2 emissions. 20% of the CO_2 emissions are caused by the construction of buildings, 20% during operation. Did you know that one of the worst drivers of the climate change is the cement production? 9% of the worldwide carbon emissions is caused by the cement production, the basis of all concrete buildings and infrastructure.

All of us probably have concrete in our portfolios. Industrial investments, real estate, infrastructure. Why? Because concrete is good. It's a fascinating material! It's strong, flexible, cheap, available worldwide. But it has a system error, which cannot be solved. Concrete is destroying our habitat! If cement was a country, it would be the third biggest emitor of carbon: China, USA, Cement. And cement is only one ingredient in reinforced concrete. Other ingredients are: Steel, gravel, sand, aggregates, but also the creation of the formwork, transport, assembly, disassembly and replacement after a few cycles. As mentioned, CO_2 emissions during construction add up to about 20% of global CO_2 emissions. IPCC Intergovernmental Panel on Climate Change recommends a maximum of only 2% to stay below the 2°C target, see Figures 3 and 4.

The only way to avert this threat is to completely avoid CO_2-emitting materials in construction: Concrete, bricks, steel, as shown in Figures 5 to 7.

[1] Stefan Zöllig, Co-owner, member of the management board, Timbatec Holzbauingenieure AG, land, sz@timbatec.ch

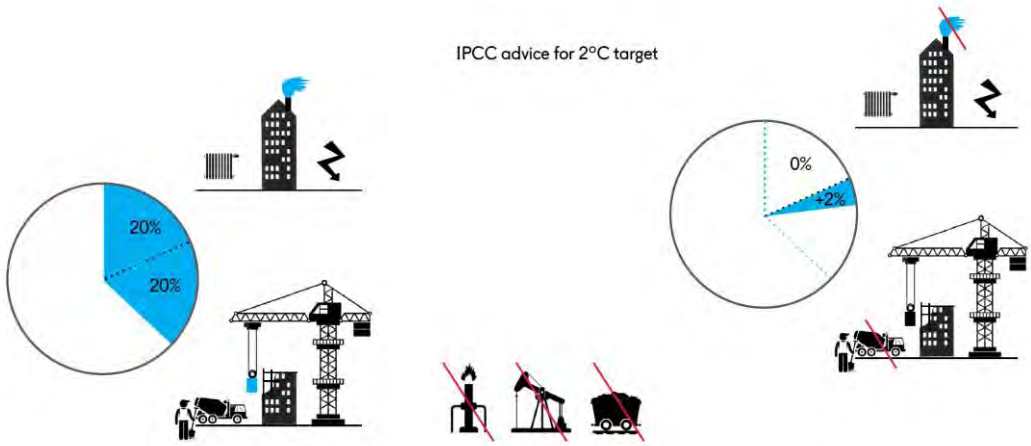


Figure 3 and 4: CO_2 emissions by air traffic and buildings. Pictures: Timbatec



Figure 5, 6, 7: CO_2 - emitting materials to be avoided

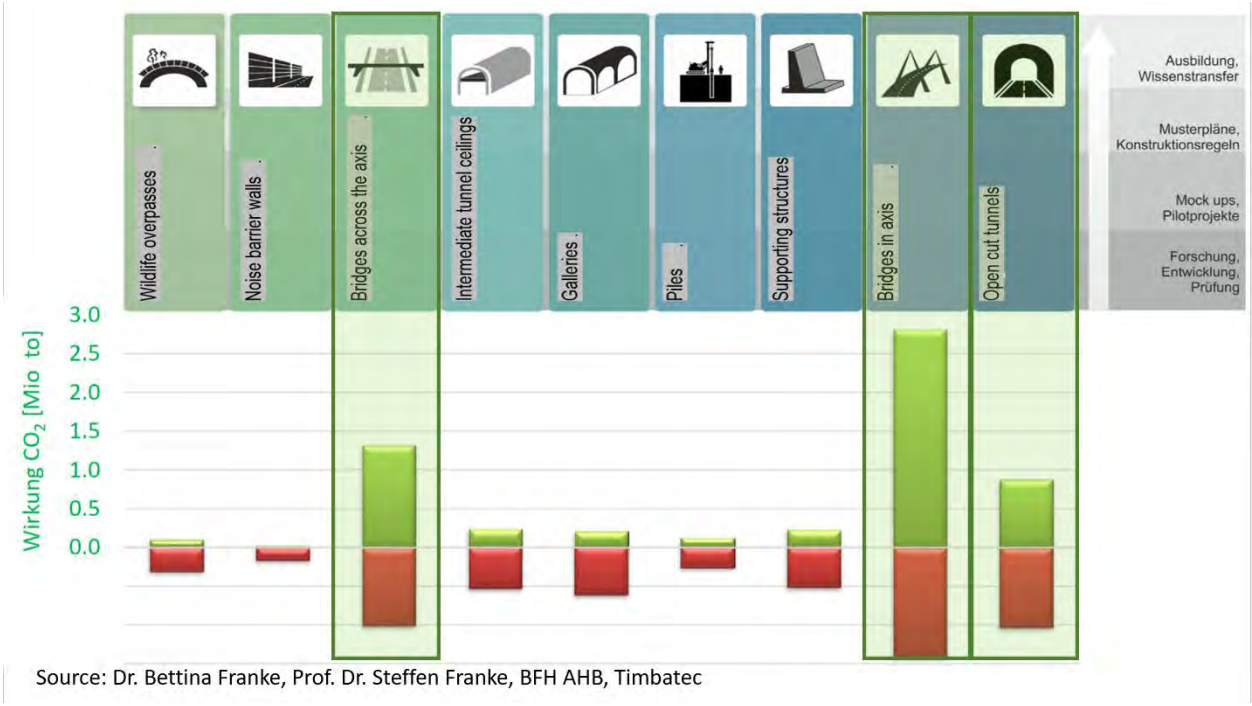


Figure 8 and 9 wood applications in infrastructure.

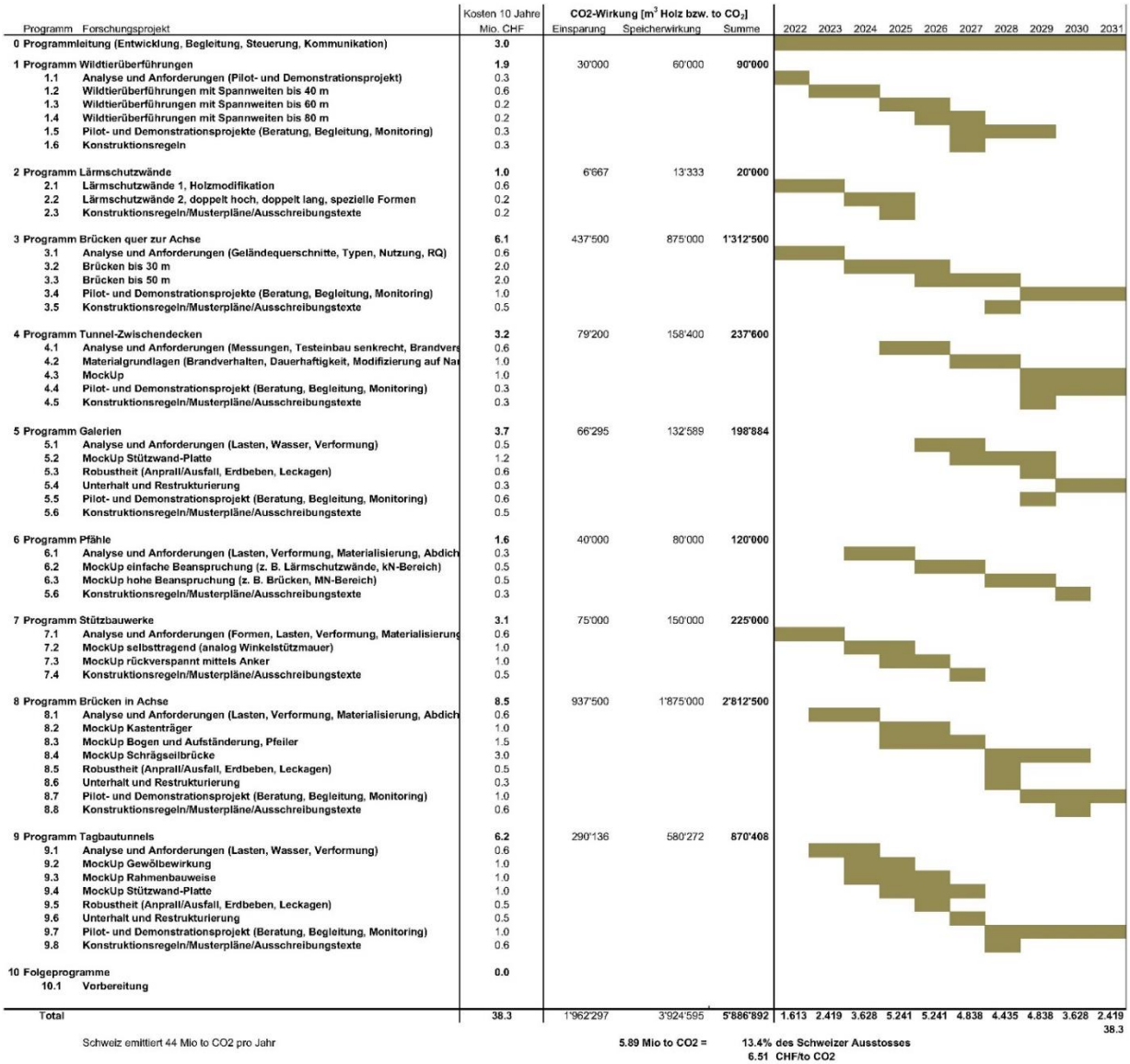


Strategy for infrastructure in wood

The timber industry is already experiencing an increasing demand for timber buildings. Also, the demand for wood infrastructure is increasing. The task now is to replace reinforced concrete in infrastructure (Figures 9 to 11) with CO_2-storing materials such as wood. For this purpose, the Bern University of Applied Sciences AHB has worked out a research and implementation strategy together with Timbatec, Figure 12. Wood could be used in a wide variety of applications in the infrastructure sector.



Figure 9, 10, 11: Rising demand for wood in infrastructure: Bridges across the axis, bridges in axis, open-cut tunnels



Programm	Forschungsprojekt	Kosten 10 Jahre Mio. CHF	CO2-Wirkung [m³ Holz bzw. to CO2] Einsparung	Speicherwirkung	Summe
0	Programmleitung (Entwicklung, Begleitung, Steuerung, Kommunikation)	3.0			
1	Programm Wildtierüberführungen	1.9	30'000	60'000	90'000
1.1	Analyse und Anforderungen (Pilot- und Demonstrationsprojekt)	0.3			
1.2	Wildtierüberführungen mit Spannweiten bis 40 m	0.6			
1.3	Wildtierüberführungen mit Spannweiten bis 60 m	0.2			
1.4	Wildtierüberführungen mit Spannweiten bis 80 m	0.2			
1.5	Pilot- und Demonstrationsprojekte (Beratung, Begleitung, Monitoring)	0.3			
1.6	Konstruktionsregeln	0.3			
2	Programm Lärmschutzwände	1.0	6'667	13'333	20'000
2.1	Lärmschutzwände 1, Holzmodifikation	0.6			
2.2	Lärmschutzwände 2, doppelt hoch, doppelt lang, spezielle Formen	0.2			
2.3	Konstruktionsregeln/Musterpläne/Ausschreibungstexte	0.2			
3	Programm Brücken quer zur Achse	6.1	437'500	875'000	1'312'500
3.1	Analyse und Anforderungen (Geländequerschnitte, Typen, Nutzung, RQ)	0.6			
3.2	Brücken bis 30 m	2.0			
3.3	Brücken bis 50 m	2.0			
3.4	Pilot- und Demonstrationsprojekte (Beratung, Begleitung, Monitoring)	1.0			
3.5	Konstruktionsregeln/Musterpläne/Ausschreibungstexte	0.5			
4	Programm Tunnel-Zwischendecken	3.2	79'200	158'400	237'600
4.1	Analyse und Anforderungen (Messungen, Testeinbau senkrecht, Brandvers	0.6			
4.2	Materialgrundlagen (Brandverhalten, Dauerhaftigkeit, Modifizierung auf Na	1.0			
4.3	MockUp	1.0			
4.4	Pilot- und Demonstrationsprojekt (Beratung, Begleitung, Monitoring)	0.3			
4.5	Konstruktionsregeln/Musterpläne/Ausschreibungstexte	0.3			
5	Programm Galerien	3.7	66'295	132'589	198'884
5.1	Analyse und Anforderungen (Lasten, Wasser, Verformung)	0.5			
5.2	MockUp Stützwand-Platte	1.2			
5.3	Robustheit (Anprall/Ausfall, Erdbeben, Leckagen)	0.6			
5.4	Unterhalt und Restrukturierung	0.3			
5.5	Pilot- und Demonstrationsprojekt (Beratung, Begleitung, Monitoring)	0.6			
5.6	Konstruktionsregeln/Musterpläne/Ausschreibungstexte	0.5			
6	Programm Pfähle	1.6	40'000	80'000	120'000
6.1	Analyse und Anforderungen (Lasten, Verformung, Materialisierung, Abdich	0.3			
6.2	MockUp einfache Beanspruchung (z. B. Lärmschutzwände, kN-Bereich)	0.5			
6.3	MockUp hohe Beanspruchung (z. B. Brücken, MN-Bereich)	0.5			
5.6	Konstruktionsregeln/Musterpläne/Ausschreibungstexte	0.3			
7	Programm Stützbauwerke	3.1	75'000	150'000	225'000
7.1	Analyse und Anforderungen (Formen, Lasten, Verformung, Materialisierung	0.6			
7.2	MockUp selbsttragend (analog Winkelstützmauer)	1.0			
7.3	MockUp rückverspannt mittels Anker	1.0			
7.4	Konstruktionsregeln/Musterpläne/Ausschreibungstexte	0.5			
8	Programm Brücken in Achse	8.5	937'500	1'875'000	2'812'500
8.1	Analyse und Anforderungen (Lasten, Verformung, Materialisierung, Abdich	0.6			
8.2	MockUp Kastenträger	1.0			
8.3	MockUp Bogen und Aufständerung, Pfeiler	1.5			
8.4	MockUp Schrägseilbrücke	3.0			
8.5	Robustheit (Anprall/Ausfall, Erdbeben, Leckagen)	0.5			
8.6	Unterhalt und Restrukturierung	0.3			
8.7	Pilot- und Demonstrationsprojekt (Beratung, Begleitung, Monitoring)	1.0			
8.8	Konstruktionsregeln/Musterpläne/Ausschreibungstexte	0.6			
9	Programm Tagbautunnels	6.2	290'136	580'272	870'408
9.1	Analyse und Anforderungen (Lasten, Wasser, Verformung)	0.6			
9.2	MockUp Gewölbewirkung	1.0			
9.3	MockUp Rahmenbauweise	1.0			
9.4	MockUp Stützwand-Platte	1.0			
9.5	Robustheit (Anprall/Ausfall, Erdbeben, Leckagen)	0.5			
9.6	Unterhalt und Restrukturierung	0.5			
9.7	Pilot- und Demonstrationsprojekt (Beratung, Begleitung, Monitoring)	1.0			
9.8	Konstruktionsregeln/Musterpläne/Ausschreibungstexte	0.6			
10	Folgeprogramme	0.0			
10.1	Vorbereitung				
Total		38.3	1'962'297	3'924'595	5'886'892

2022 2023 2024 2025 2026 2027 2028 2029 2030 2031
1.613 2.419 3.628 5.241 5.241 4.838 4.435 4.838 3.628 2.419
38.3

Schweiz emittiert 44 Mio to CO2 pro Jahr
5.89 Mio to CO2 = 13.4% des Schweizer Ausstosses
6.51 CHF/to CO2

Figure 12: Strategy, Research programs and projects for decarbonization of infrastructure. Graphic BFH AHB, Timbatec.

9 main application areas were evaluated, assessed, and quantified. In estimating the volumes of wood to be used, it was found that there are three predominant areas of high impact: Bridges across the axis, bridges in axis, and open-cut tunnels. In comparison, the other areas are almost negligible.

This strategy does not need to fear the cost-benefit comparison either. In Switzerland alone, 1.96 million tons of CO_2 can be saved and 3.92 million tons of CO_2 can be substituted by replacing concrete. In total, an effect of 5.89 million tons of CO_2 is achievable. This corresponds to 13.4% of Switzerland's annual CO_2 emissions. The costs of the entire strategy amount to CHF 38.3 million, or CHF 6.51/to CO_2.

Taking into account that it takes roughly 5 years from order to execution, there are 25 years left for achieving to net-zero, cp. Figure 13. Therefore 4% of CO_2 emissions will have to be reduced annually over the next 25 years - while construction activity remains unchanged. This will not be possible even with emission-reduced concrete. But if every possible application is ordered in wood, the storage of CO_2 in the wood gives a certain head start, so that the goal remains achievable.



Figure 13: Time lag from order to execution 5 years. Graphic: BFH, Timbatec.

Political homework

It is understandable that the authorities were not waiting for this task. The main task of the road authorities is to create and operate the traffic routes, and to do so as safely and cost-effectively as possible. Sustainable infrastructure in wood is not. If we want the sustainability of the constructions to become the task of the authorities as well, we also have to do the political homework. Jakob Stark, member of the Council of States, and Erich von Siebenthal, member of the National Council, have submitted a motion that has been adopted in both federal chambers by the end of 2021, Figure 14. Not only the road authorities, but all authorities concerned with the construction and operation of infrastructure buildings must now fulfill this task. This also includes, for example, the railroads or the army's buildings.

To enable the widespread use of wood in infrastructure buildings, the legal basis must be established first. So if you want to play a decisive role in your country or state, find a parliamentarian to submit this proposal. Politicians are grateful for well-researched and ready-made proposals. This saves them a lot of work, strengthens their political effectiveness, and raises their sustainability profile in the society.



21.3293 Motion

Submitted by Stark Jakob, Ständerat, Fraktion der Schweizerischen Volkspartei

Research and innovation of wood as a material for use in infrastructure construction as a decarbonization contribution

Text submitted:

The Federal Council is instructed to research the possibilities for decarbonizing infrastructure construction in cooperation with universities and the relevant standards commissions. In particular, it should be examined, and efforts made to supplement or replace reinforced concrete with CO_2-absorbing materials. The focus should be on researching and innovating wood as a material for widespread use in infrastructure construction. A corresponding research and implementation strategy is to be developed.

Explanation:

Infrastructure construction is one of the largest CO_2 emitters in Switzerland. The main cause is the use of reinforced concrete. Cement production (2020: 4 214 785 tons, source cemsuisse.ch), with annual CO_2 emissions of about 2.5 million tons, contributes more than 5 percent to national CO_2 emissions (46.4 million tons).

For the construction of infrastructures, in the building sector, but also in other sectors such as the road sector, various solutions are already available today with materials that do not produce CO_2 during production but store it, such as wood. One cubic meter of wood stores about 1 ton of CO_2 in the long term. When used properly, wood is a very long-term and also cost-effective CO_2 store for infrastructure buildings in all sectors. The advantages over the currently discussed CCS (Carbon Capture and Storage) are obvious: with CCS, one pays a high amount per ton of CO_2 for the pure storage function, whereas this is included in the price when using wood for infrastructure construction, i.e. it is free of charge, so to speak.

In addition, there is the reduction in CO_2 emissions due to the substitution of reinforced concrete with wood; one cubic meter of wood replaces approximately one cubic meter of reinforced concrete. In addition, the energy input per cubic meter of material is significantly lower for wood components than for reinforced concrete.

Although the first promising applications of wood in infrastructure construction are available, increased support for research and innovation is needed so that a significant contribution can be made in time to the storage of CO_2 and the reduction of CO_2 production. Together with universities and standardization associations, a research and implementation strategy should be developed that provides a general basis but also focuses specifically on the various areas and types of structures. The offices involved in the construction of infrastructure buildings, such as ARMASUISSE, ASTRA, BAFU, BAV (SBB), BBL, BFE, BWO OR PUBLICA are to be involved accordingly.

https://www.parlament.ch/de/ratsbetrieb/suche-curia-vista/geschaeft?AffairId=20213293

Figure 14: Full text of the submitted proposal 21.3293 of Ständerat Jakob Stark and Nationalrat Erich Von Siebenthal

Wooden wildlife overpasses in Switzerland

Stefan Zöllig wrote the first study on wildlife bridges made of wood in 1998. Afterwards, it took 22 years until the first wooden wildlife overpasses could be built. So, the first wooden wildlife overpasses of Switzerland were built in 2020 in Rynetel AG (Figure 15) and 2021 in Neuenkirch LU (Figure 16). The wildlife overpass in Rynetel AG is a double arch with 17.5 m span each. The wildlife overpass in Neuenkirch LU is designed as a double single span girder with 17.5 m span each and a center support.

Further wildlife bridges are planned in Ziegelbrücke GL (Figure 17) and in Tenniken BL. The wildlife bridge in Ziegelbrücke GL will be designed as an arch with a span of 57 m.



Figure 15: Built wildlife overpass Rynetel AG, Switzerland. Picture: Nils Sandmeier, Timbatec



Figure 16: Built wildlife overpass Neuenkirch LU, Switzerland. Picture: Nils Sandmeier, Timbatec



Figure 17: Planned wildlife overpass Biberlikopf Ziegelbrücke GL, Switzerland. Picture: Nightnurse Images, Zürich

Research: Heavy duty box girder bridges

To be successful in infrastructure made of wood, it is not enough to criticize reinforced concrete. Nor is the experience gained so far sufficient to be successful in the three determined areas. On the contrary, we must very quickly develop the necessary methods to be able to realize long-span heavy-duty bridges in wood. Previous reinforced concrete bridges were designed as box girders. Can this construction method be transferred to timber construction? To answer this question, Dr.-Ing. Bettina Franke and Prof. Dr. Steffen Franke from the Bern University of Applied Sciences AHB have started a research project together with Stefan Zöllig from Timbatec and TS3 as well as with other business partners. Here, the feasibility of prestressed hollow box girders in wood is evaluated and developed. The TS3 technology, in which CLT cross laminated timber panels are joined together by butt joint bonding, is making an important contribution to this. The joint edges of the CLT panels are CNC-machined and pre-treated in the factory. On site, the CLT panels are arranged in the correct geometry, sealed and grouted with a high-performance casting-resin without applying pressure. This is done in panel plane, but also with miter joints.

This feasibility study is, so to speak, the "entry debate" until the implementation of the Stark motion starts.

Two box-girder modules in the courtyard of the Bern University of Applied Sciences in Biel, as shown in Figures 18 to 20, will be used as working models where the envisaged static models, but also practical exercises can be carried out. It is to be expected that, in the course of the research project, new findings will

emerge that will require adjustments to the model. This is desired and planned in order to be ready for the realization of the first prestressed box girder bridges as soon as possible.

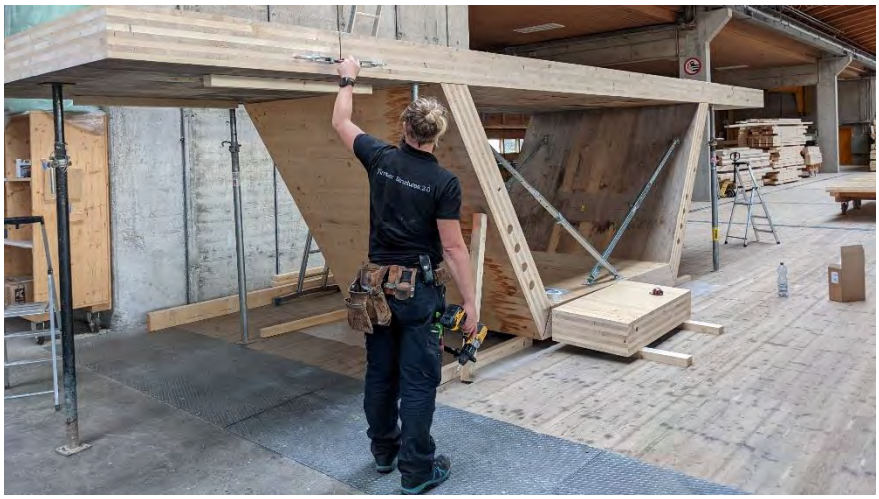


Figure 18: Manufacturing box-girder modules at the factory. Picture: Flück AG, Wangen b. Dübendorf



Figure 19: Installation of the box-girder modules. Picture: Steffen Franke



Figure 20: Box-girder modules in the courtyard of the Bern University of Applied Sciences Biel. Picture: Steffen Franke

Conference Proceedings 4th ICTB (2022)
https://doi.org/10.24451/zqqs-ba50

ICTB 2021 PLUS
4th International Conference on Timber Bridges
Biel/Bienne, Switzerland, 9 -12 May 2022



Våla bridge - Timber network arch footbridge in Ringebu, Norway

Anna Weronika Ostrycharczyk[1], Arne Værnes

Abstract

This paper is about the Våla network arch timber footbridge, located in Ringebu, Norway. The bridge has one span of 52.5 m, and a 3.0 m wide footpath. The arches are made of glulaminated timber, the deck is made of prestressed concrete and hangers and wind truss are made of steel. In the first part of the article a simplified procedure for finding 'semi-optimal' network pattern is presented. It includes defining geometrical features such as: the arch rise, the number of hangers and the type of network pattern. There were 30 network outlines studied in the pre-design phase before the final pattern was chosen. In further part of the article, selected aspects of bridge design, such as material type for main elements and connectors as well as assumptions for numerical model are provided. Finally, description of the main tasks from the execution stage are presented. The article aims to show how to choose a network pattern in a simplified way, and that a network arch bridge can be a successful alternative to more traditional types for medium span timber footbridges.

1 Introduction

The concept of network arch bridge has been introduced in 1966 by Norwegian engineer Per Tveit [1]. Since then, network bridges were built all around the world, especially in Japan, USA and Europe, with emphasis on Germany and Norway. Traditionally, those bridges were made of steel or steel and concrete. In 2016 the first timber network arch bridge (Steien bridge) was built in Alvdal, Norway [2-3]. Since then, in Norway, timber become more often considered a serious candidate for building material for arches. As a result, network bridges with timber arches, like Hellefossbrua (opened in 2019), Prestmyra (opened in 2018) and presented in this paper – Våla footbridge (opened in 2020) has been build.

2 Choice of network pattern

The first part of the paper focuses on the hangers and network pattern, i.e., elements which influence structural performance of the bridge in a critical way. The main idea behind a network pattern is that forces which are acting directly on the deck, are transferred to the arch, just like in a classical arch-bridge with vertical hangers. However, in the network bridges, the 'mobilized' part of the arch is bigger than in the classical ones. Therefore, by using inclined hangers (network outline), the forces in the structure, mainly in hangers and the arch, are more uniformly distributed. This leads to smaller values of extreme forces and, as a result, to the smaller cross-sections of the structural elements.

There were three steps in the procedure of choosing a network pattern for Våla bridge. First, a set of 2D outlines of patterns was created, based on recommendations from the literature. In second step, visual grading was used to limit studied patterns. Finally, forces in hangers, from self-weight of simplified 3D numerical model, were used for pattern comparison.

In the engineering practice there are three most used network pattern types: pattern with constant inclination of hangers (CIH), pattern with constant change of hangers' inclination (CCI) and radial patter (RAD). Information about the patterns can be found, among others, in [4 -5]. In the pre-design phase of Våla-project only the two network pattern types, CCI and RAD, were considered since those patterns are more effective than CIH [6]. The principle of the CCI and RAD patterns outlines is shown in Figure 1.

[1] Anna Weronika Ostrycharczyk, PhD, Structural Engineer, Norconsult AS, Norway, anna.weronika.ostrycharczyk@norconsult.com

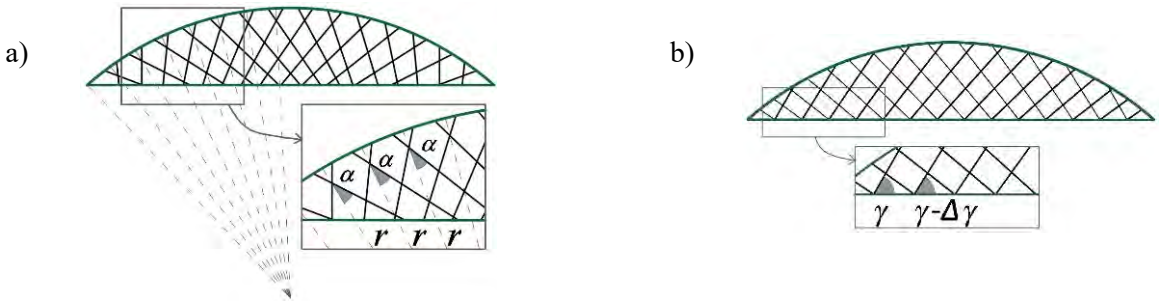


Figure 1 Principle for the outline of the network pattern; a) radial b) constant change of hangers' inclination

A total number of 30 different 2D network patterns was chosen for evaluation, before the final pattern was defined. Among those patterns, two arch rises were considered (8.0 m and 8.4 m), as well as three numbers of hangers (20, 22 and 24, which refers to all hangers in one arch). For the radial pattern, the angle α varied between 28 and 45 degrees. For pattern with constant change of hangers' inclination, starting angle γ varied between 70 and 80 degrees, while angle change $\Delta\gamma$ varied between 2,5 and 3,5 degrees. The parameters like arch rise and number of hangers were chosen based on the author's study [7, 8]. It was assumed that, in all considered patterns, hangers were evenly distributed along the arch. The outlines of the considered patterns are presented in Figure 2, while collection of patterns data and prescribed number of studied pattern is presented in Table 1.

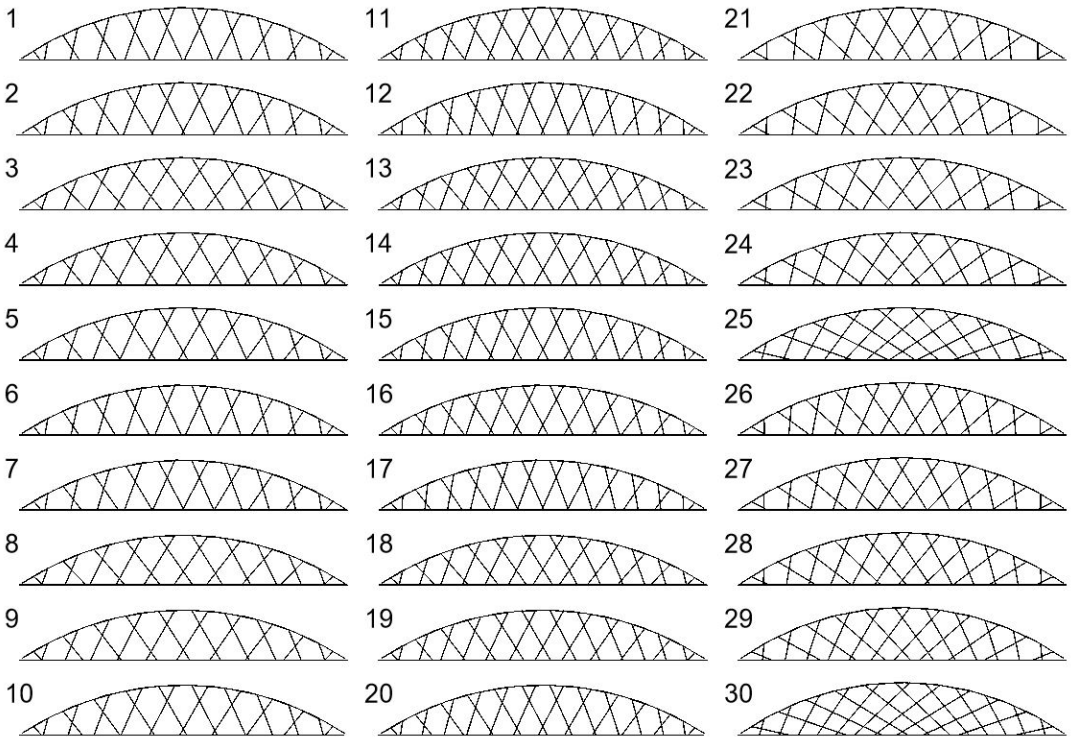


Figure 2 Patterns considered in the pre-design phase of Våla bridge

Table 1 Numbers and parameters of studied patterns

	Pattern type	**CCI**	**RAD**
		Pattern nr (1 to 20)	**Pattern nr (21 to 30)**
Arch rise	8.0 [m]	6 to 10; 16 to 20	-
	8.4 [m]	1 to 5; 11 to 15	21 to 30
Number of hangers	20 [-]	1 to 10	21 to 25
	22 [-]	-	26 to 30
	24 [-]	11 to 20	-



In the pre-designing phase, all 2D patterns were graded visually. The focus was on features listed below.

- The number of hanger's crossings.
  - It is desired, that most of the hangers cross at least twice.
- The location of hanger's crossings (especially on the deck level).
  - It was chosen to avoid two hangers 'landing' on the deck in the same point, or very close to each other, since it leads to the concentration of the stresses in the deck as well as the connectors cannot be unified. It should be pointed out, that patterns' outlines presented in Figure 2 refers to the centreline of the arch, deck and hangers, therefore the real hanger-deck connection point is located above the presented deck-line.
- The angle between the deck and the hanger.
  - Too steep inclination between the deck and the hanger leads to the high bending moment in the arch. It also leads to the big differences between minimum and maximum force in the hanger or making the hanger to slack.
- Aesthetics.
  - Although judgment after aesthetics is not fully objective, it was chosen to avoid patterns which creates two rows of 'rhombic' shapes with similar size along the bridge length.

Table 2 Results from visual grading of hangers

CIH				RAD	
Nr	**Feature**	**Nr**	**Feature**	**Nr**	**Feature**
1	X	11	●●	21	
2	X ●●	12	●●	22	●●
3		13	ae	23	<
4	X	14		24	●● <
5	●●	15	●● ae	25	<
6	X	16	ae	26	
7	X ●●	17	X	27	●●
8		18	ae	28	<
9	●● ae	19		29	<
10	●●	20	ae	30	<

X	low number of hanger's crossings
●●	location of hanger's crossings
<	inclination between hanger and deck
ae	aesthetics

Table 2 shows results from visual grading of all thirty patterns. Numbers 3, 8, 14, 19, 21 and 26 remained unmarked, thus were taken into further consideration. Those patters were used to create a simplified 3D numerical model, to study hangers' axial forces induced by self-weight. Both 2D patterns, and 3D models were created in semi-automatic way, by use of Python script in Dynamo in Revit, and Robot Structural Analysis Professional software [9-11].

In the numerical model the arch was built as a simple beam made of GL30h, with a cross-section of 500x600 mm. The arch was modelled as fixed to the deck at the ends. The deck was modelled as a shell element, made of concrete, with predefined thickens of 350 mm. Hangers, made of steel with diameter of 50 mm, were modelled as beam elements. All rotational degrees of freedom were released at both ends of hangers; thus, they could transfer only tension and compression. In final design, hangers were not exposed to compression. However, in the study-phase, presence of compression in hangers was a factor for determination which pattern's outline is most promising. The whole bridge was modelled like a simply supported beam.

Results from the influence of self-weight on force distribution in hangers, for six selected patterns, are presented in Table 3. The table shows maximum and minimum axial forces in hangers. Note, that a positive value refers to the tension and a negative value refers to the compression; it corresponds to the most common sign convention, and not to the sign convention form Robot Structural Analysis. It is clearly visible, that patterns 21 and 26 are more effective than the others, since all hangers in those two patterns are in tension. In addition, maximum force is smallest in those patterns.

Table 3: Axial forces in hangers induced by self-weight of the structure, for six selected full network patterns; results from pre-design phase

Pattern nr	3	8	14	19	21	26
Min [kN]	-39 *	-43	-53	-57	17	7
Max [kN]	173 **	184	169	177	154	155

* negative value = compression
** positive value = tension

Since the arches in Våla bridge were designed in glulam, and the deck was designed in concrete, it was natural to make the end part of the arch also in concrete. Such solution gives better force distribution in the arch-deck connection, due to uniform material and by avoiding mechanical steel connectors in this area. It is the architect and the designer who decide how long should this concrete part of the arch be. Technical limitations are mainly related to the necessary space for placing rebars and steel connector for glulam arch, casted at the end of the concrete arch. In Våla bridge, it was chosen to run the concrete arch from the deck up to the point of crossing with the first hanger in pattern. Simultaneously this first (and last) hanger was removed from the outline. In Figure 3, the removed hanger is presented as a dashed line. Removal of the first (and last) hanger, combined with the moment-resistant concrete end of the arch, influence positive on bending moments in the arch made of glulam. It leads to smaller values of bending moments.

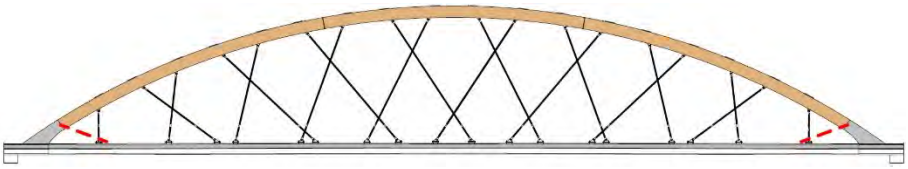


Figure 3 Outline of the network pattern with removed first and last hanger

Having the assumption of first (and last) hanger removed determined, numerical analyses for six considered patters were performed again. Results in form of the minimum and the maximum forces in the hangers, induced from the self-weight are presented in Table 4. Positive value refers to tension. Values in the table show, that with reduced number of hangers, there is only tensile force in all hangers of all studied patterns. However, it is also visible, that the difference between maximum and minimum force is the smallest in pattern 21 and 26. This suggest that those patterns are better than others.

Table 4: Axial forces in hangers induced by self-weight of the structure, for six selected network patterns with reduces number of hangers; results from pre-design phase.

Pattern nr	3	8	14	19	21	26
Min [kN]	28*	26	5	1	52	45
Max [kN]	119	120	114	117	93	85

* positive value = tension

Pattern 21 was chosen for further evaluation in the design phase. Pattern 21 is a radial pattern with angle α of 28 degrees between the arch radius and the hanger. The arch rise is 8.4 m. It was chosen over pattern 26 based on number of hangers: pattern 21 have 18 hangers in one arch (after removing fist and last hanger), and pattern 26 has 20 hangers (after the same reduction procedure).

In case of Våla bridge, difference of two hangers, between pattern 21 and 26, refers to cost of circa 80 thousand NOK (≈ 8 thousand EUR). Note that the cost of the whole bridge was circa 12 million NOK (≈ 1.2 million EUR).



3 Other designing aspects

In this part of the article, description of the structure and some selected aspects of the design of the bridge are presented.

The bridge is design for 100 years lifetime, based on requirements form Eurocodes and Norwegian handbook N400 'Design of bridges'[12] provided by The Norwegian Public Roads Administration. The bridge is 52.5 m long, and 5.9 m wide, while footpath is 3.0 m wide. The traffic load is defined as 5 kN/m^2 for pedestrian load, and 120 kN (40 kN + 80 kN) for a single, service vehicle. The deck is made of prestressed concrete with two tendons on each side. The thickness of the deck varies, between 350 mm in the middle and 650 mm on site, where the tendons are located. The arches are made of GL30h, with cross-section of 550x700 mm. The glulam is preserved by double vacuum-pressure impregnation with Cu-based salt and with creosote, which is still authorized for use in Norway. Creosote increases a self-weight of the wood. According to N400 addition for creosote is equal to 0,5 kN/m^3 or 0,8 kN/m^3 depends on which value is more unfavourable. In the calculations of Våla bru only one addition to weight, 0.8 kN/m^3, was used. The reason for that is small influence of the difference between the heigh and the low value of creosote addition (0.3 kN/m^3), which is less than 1% of weight of the whole bridge, thus negligible. The arches are protected mechanically in addition to chemical impregnation. They are covered with the zinc plates on the top, and with the wooden cladding on the outside, mounted in a way providing necessary ventilation. Due to chosen solution for timber protection, the serviceability class 2 was used in calculations. The arches are inclined towards each other with 6 degrees, which, in combination with wind-truss, provides stability in transverse direction. Although it is natural to make a wind bracing out of wood in wooden bridges, in Våla bridge it was chosen to use steel. Partially due to aesthetic, to balance out the steel hangers, and partially to avoid possible challenge of creosote dripping on the pedestrians.

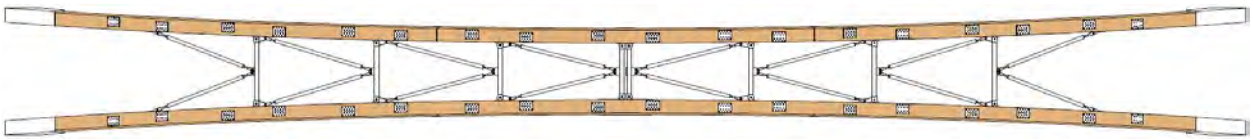


Figure 4 Outline of the wind truss in Våla footbridge.

Wind bracing, presented in Figure 4, is in K-shape and is designed of pipes made of standard carbon steel S355. There are two sizes of the pipes: the transversal ones are bigger, with diameter of 193,7x5mm, and the diagonal ones are smaller, 139,7x6 mm. Size difference is based on the aesthetics. To avoid axial forces in the wind bracing due to the difference in the E-module and temperature expansion in the wood and the steel, the top transversals of the K-shape are split in two independent pipes. Hangers, with diameter of 42 mm are made of carbon steel with minimum yield stress of 520 N/mm^2. Each hanger is divided into two parts, and those parts are connected with the turnbuckle which allows for prestressing the cables. In design process it was chosen to divide hangers on one level: ca. 1.2 m above the deck; see Figure 5. Such placing of division is favourite due to procedure for prestressing since all heavy equipment can be placed directly on the deck and additional lift is not needed. However, in case of some hangers, chosen division placing was located close to the crossing between two of them. It required additional check for space necessary to mount the turnbuckle. When deciding for hangers' division, additional aspect to consider was a minimum length of the lower part of the hanger, which was assumed 500 mm in the project. Finally, the shortest member of the cable was 892 mm long, spreading between the pin and the middle of the turnbuckle. Hangers are connected on the deck level to the steel connectors casted in concrete, and on the arch level to the 'T-plate'. Those 'T-plates' consists of two welded plates: one located on the top of the arch, and the other located in the hole in the arch; see Figure 6. Although usually a stainless steel is used for elements embedded in timber, material used for the discussed connector is a hot dip galvanized and powder coated carbon steel. Such choice was made to avoid contact between carbon steel and stainless steel: hanger vs connector. The connection is also considered replaceable, since it is screwed to the arch from the top and load combination for procedure of hanger replacement was taken into account in the calculations and design. Arch itself is divided in the three parts, see Figure 5. Here, all parts of timber-timber and timber-concrete connectors are made of stainless steel, with use of slotted-in plates and dowels.

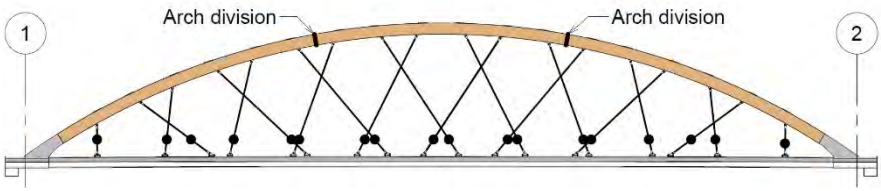


Figure 5 Division of hangers and arch

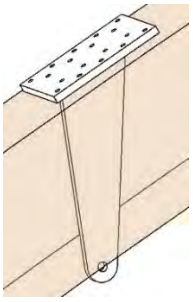


Figure 6 'T-plate' connector

Final numerical model of the bridge was created in Robot Structural Analysis Professional 2019. It was created in similar way to the model in pre-design phase. The deck was modelled as a shell, and the arch, hangers and wind-truss as beams. Considering boundary conditions, pinned support was modelled in one axis, and rolled support in the other axis. Releases of rotational degrees of freedom were placed at the end of hangers and each of element of wind bracing. Rigid links were used to connect the wind truss to the arch, to represent the real structure most accurate, since the beams representing the arch in the numerical model refers to the centreline of the arch. Arches were modelled with inclination toward each other. Connection between the concrete part of the arch and the deck was modelled as fully stiff. The stiffness of the connection at the end of the timber arch was reduced by 30 % in Rx, any by 10% in Ry and Rz directions, where Rx, Ry and Rz are rotational stiffness along the beam and transversally to the beam respectively. Connection between two parts of timber arch was modelled as fully stiff. The assumption for timber-timber connection was based on constant compression in the arch, and positive influence from wind bracing on bending moments, especially on the moment Mz (out of the arch plane).

The main numerical analyses related to the ultimate limit state and serviceability limit state were performed as linear analyses, regardless that hangers can carry only tension force; modelling hangers as 'only tension' automatically change the analysis to nonlinear. Since in all of the considered load cases, all hangers were always in tension, running a linear analysis was a choice of savings of computational time. Additional analyses, like buckling, dynamic or nonlinear with initial imperfection of the arch, etc., were also executed, to cover all requirements for correct (to the best knowledge) design.

4 Bridge erection

The overall order of executed procedures during erection of Våla bridge is presented below.

- Erection of scaffolding for the deck.
- Casting concrete on the deck.
- Casting concrete part of the arch; see number 1 in Figure 7.
- Prestressing the deck with the tendons.
- Mounting the arch on the arch-scaffolding tower; see Figure 8.
- Mounting wind-truss.
- Casting end part of the concrete arch, see number 2 in Figure 7.
- Mounting of hangers.
- Prestressing of hangers.
- Disassembly of scaffolding.

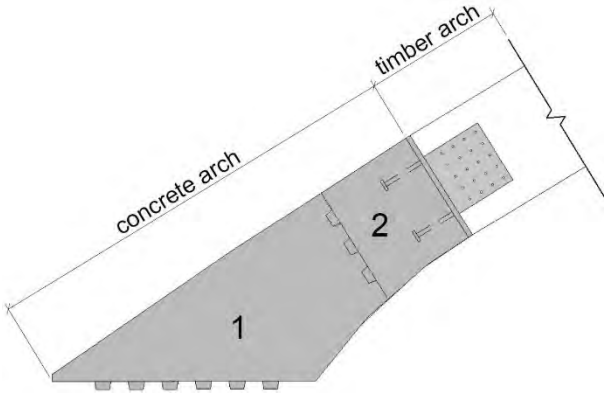


Figure 7 Concrete arch divided into parts according to the technological breaks.

Choice of the scaffolding for the deck was quite important. Since the deck in made of concrete, the scaffolding was necessary. Våla bridge is located above the river and a floodplain. It was assumed that no foundation should be places in the water. Due to limitation of free space between water level and underside of scaffolding, it was chosen to use two different systems of scaffolding. One system had temporary foundation on the edge of the river and spread above the water, while the second system was places directly on the ground, see Figure 8.

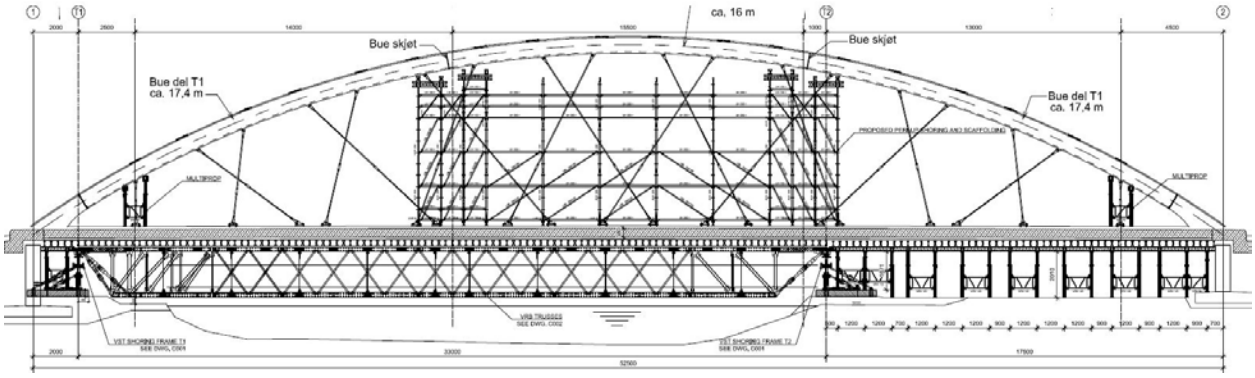


Figure 8 Outline of scaffolding system on Våla bridge

Such solution limits a span for the first type of scaffolding, which resulted in a smaller height of the scaffolding construction. However, it also leaded to the concentration forces in the point where two of systems were joining. Therefore, some ground settling was expected in this area, and responding local camber was formed on the deck. This camber was on the top to the already designed curvature of the deck which should compensate deformation of the construction form the self-weight. Unfortunately, real ground settling was smaller than calculated, and a part of the formed local camber become permanent. This situation, combined with building tolerances led to the challenging procedure of mounting and prestressing of hangers. In case of one hanger, the theoretical length between pin and pin was 7299 mm, while the distance measured on site was 67 mm shorter. Note, that each cable has tolerance of ± 50 mm, and while prestressing it should additionally shorten. Thus, prestressing of cables was an important and precise procedure in Våla bridge. It was executed in the iterative way, in three steps, which can be repeated in a loop. In the first step hangers were prestressed from the centre of the arch towards the ends. It was done simultaneously on both arches, see Figure 9. In the next step, hangers from one set, with inclination toward axis 2, were prestressed following direction from axis 1 to axis 2. Then, the other set, with inclination toward axis 1, was prestressed following direction from axis 1 to axis 2. Note, that one set of hangers consists of those hangers which incline in the same way. In the third step, procedure form step two was repeated, while assuming starting point in axis 2. In Våla bru the required level of prestress was achieved already in the step two, while the step tree was used just for small adjustments. Prestressing took circa one day. Additional verification of hangers' prestress was done around one week later. Prestressing of hangers was the last major work made before scaffolding was removed. Figure 10 and Figure 11 present the bridge under construction.

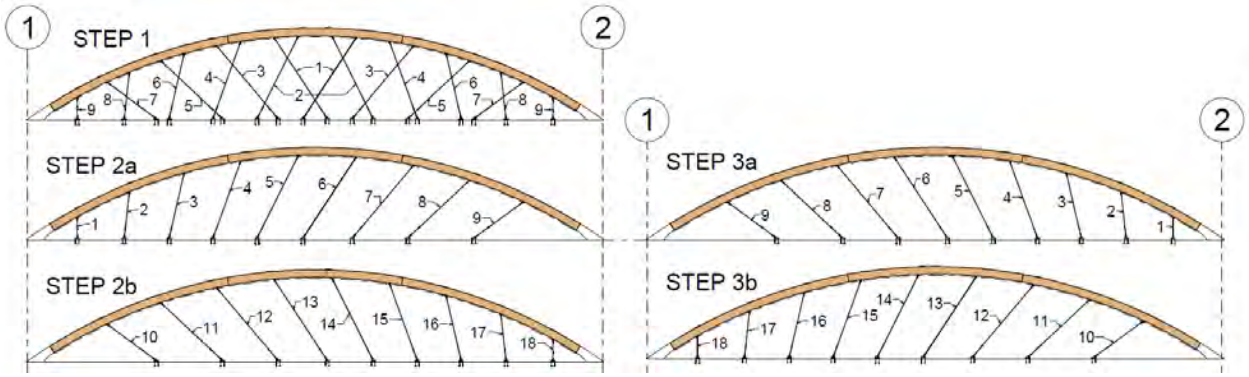


Figure 9 Prestressing procedure of hangers



Figure 10 Våla bru under construction (photo: H. E. Wedum)



Figure 11 Våla bru – scaffolding on flood-plain (photo: H. E. Wedum)

5 Conclusions

This paper summarizes procedure of designing Våla footbridge. In the first part, the simplified procedure of choosing an 'semi-optimal' network pattern was presented. The procedure is based on visual grading of 2D-outline of patterns and studying force distribution in hangers from self-weight. In second part of the paper, some designing aspect of the bridge were described. Selected challenges from the building site and used techniques were presented in the final part of this paper.

The paper shows the importance of right choice of the network patten, and that the network arch timber bridges have a potential for medium span footbridges. Figure 12 and Figure 13 present the completed bridge.



Figure 12 Våla bridge (photo: H. E. Wedum)

6 Acknowledgement

The authors would like to acknowledge people, institutions and companies listed below, for the support given during designing process, execution of the bridge and writing this paper. Thanks go to our colleague Per Kristian Ekeberg from Norconsult AS, Henrik Eineteig Wedum, Anders Brenne, Linda Elisabeth Brateng, Thorstein Kjøs and Johannes Veie from Norwegian Road Administration (SVV), Yngve Olav Aartun from Plan Arkitekter AS, Stig Solbjør from KB Spennteknikk AS and to the contractor Anlegg Øst Entreprenør AS.



Figure 13 Våla bridge (photo: P. K. Ekeberg)

7 References

[1] Tveit P. (1966) The design of network arches. The structural engineer, 7(44):249-259.
[2] Veie J., Abrahamsen R.B. (2013) Steien Network Arch Bridge. In: 2nd International Conference on Timber Bridges. Las Vegas, Nevada USA.
[3] Veie J. (2017) Network arch bridge with glulam arches. Lessons learned and further development. In: 3rd International Conference on Timber Bridges. Skeleftå, Sweden
[4] Schanack F., Brunn B. (2009). Netzgenerierung von Netzwerkbogenbrücken (Generation of network arch hanger arrangements; in German). Stahlbau, 78(7):477-483.
[5] De Zotti A., Pellegrino C., Modena C. (2007) A parametric study of the hanger arrangement in arch bridges. In 5th international conference on arch bridges ARCH '07. Funchal, Madeira, Portugal.
[6] Ostrycharczyk A.W., Malo K.A. (2017) Comparison of network patterns suitable for timber bridges with crossbeams. In: 3rd International Conference on Timber Bridges. Skellefteå, Sweden.
[7] Ostrycharczyk A.W. (2017). Network arch timber bridges with light timber deck on transverse crossbeams; Doctoral thesis at NTNU, 2017:318. Trondheim: Skipnes Komunikasjon as.
[8] Ostrycharczyk A.W., Malo K.A. (2022) Network arch timber bridges with light timber decks and spoked configuration of hangers – Parametric study. Engineering structures, 253:113782.
[9] Python Software Foundation. https://www.python.org/.
[10] Revit 2019, Autodesk.
[11] Robot Structural Professional 2019, Autodesk.
[12] N400 Bruprosjektering (Designing of bridges; in Norwegian) (2015). Norwegian Public Roads Administration.

Conference Proceedings 4th ICTB (2022)
https://doi.org/10.24451/bb0f-9c31

ICTB 2021 PLUS
4th International Conference on Timber Bridges
Biel/Bienne, Switzerland, 9 -12 May 2022

Two new pedestrian and cycle bridges between Rupperswil and Auenstein, Switzerland

Kurt von Felten[1], *Milo Zimmerli*[2]

1 Introduction

The existing road bridges over the Aare and the underwater canal have unfavorably narrow space conditions for cyclists and pedestrians. New pedestrian and bicycle bridges shall create an attractive and safe connection for non-motorized traffic.



Figure 1: Bridge B, three-span girder next to the existing road bridge [Roger Frei, Zurich]

[1] Kurt von Felten (project leader), Dipl. Bauing. HTL, Makiol Wiederkehr AG, Switzerland, vonfelten@holzbauing.ch
[2] Milo Zimmerli (speaker), Holzbauing. BSc FH, Makiol Wiederkehr AG, Switzerland, zimmerli@holzbauing.ch

ICTB 2021 PLUS
4th International Conference on Timber Bridges
Biel/Bienne, Switzerland, 9 -12 May 2022



The two wooden bridges have lengths of 90.50 and 98.50 meters and a usable width of 3.50 m. They are arranged parallel at the downstream end to the existing bridges. The substructure is designed as a timber structure composed of longitudinal main girders made of glulam. The roadway consists of transversely arranged wooden beams, a three-layer slab and a mastic asphalt road surface. A 1.30 m high steel railing with a wooden handrail serves as fall protection. The abutments and the bridge piers are made of reinforced concrete and founded on bored piles.



Figure 2: Bridge A, five-span girder [Roger Frei, Zurich]

2 Design description

The pedestrian and cycle bridges consist of continuous 3- or 5-span wooden girders. The spans are in accordance with the existing road bridges.

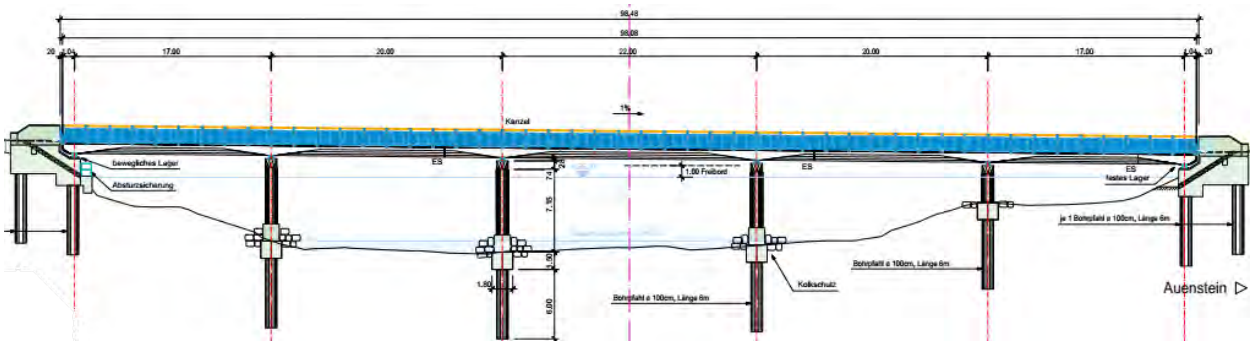


Figure 3: Longitudinal view of Bridge A, five-span girder



The main girders consist of a collection of individual glulam beams (figure 1, 4). The maximum length of glulam is around 40 meters in terms of production and transport. Therefore, the girders had to be transported to the construction site as devided individual parts by truck.

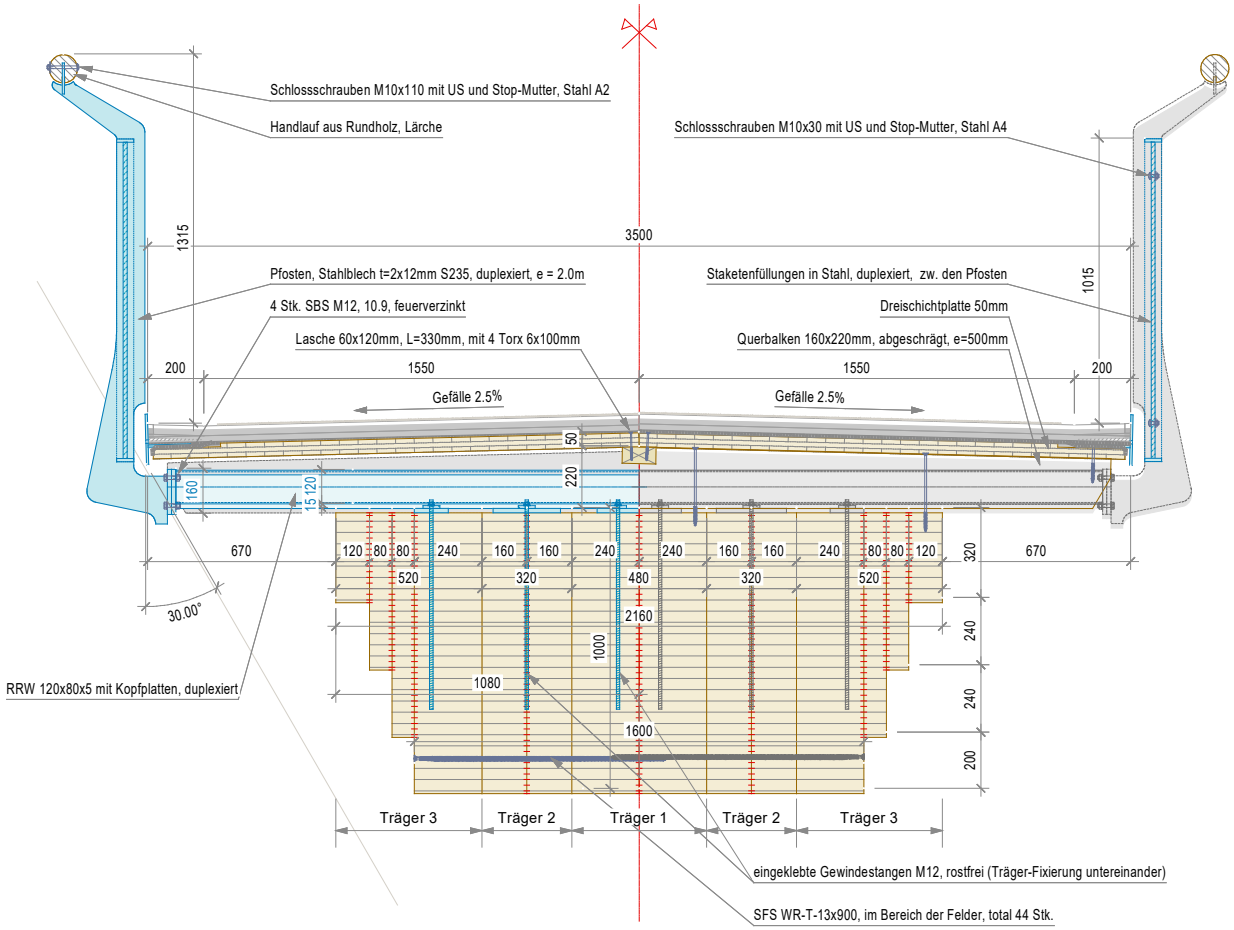


Figure 5: Cross section in the bridge field area

From the existing bridge, they were lifted onto the piers just in time via pendulum lift using two large truck-mounted cranes (figure 6). Thanks to an ingenious arrangement of the joints of the individual girders and multifunctional connecting components in the superstructure, the system is configured to function statically as a continuous girder.

The outermost beams are cove shaped. They have full cross-section at the piers and abutments, tapering off toward the field sections (figure 5). From a structural point of view, this is feasible and brings advantages in terms of structural wood preservation. On the main girder, transversely arranged secondary beams and sloped three-layer slabs form the basis for waterproofing and two-layer mastic asphalt. A monitoring system controls the condition of the waterproofing. The lateral cantilevers of the carriageway serve to protect the main girders. The railing structure is decoupled from the carriageway by connecting the posts to the steel beams running parallel to the secondary beams. The steel beams also serve as static cross connectors between the individual beams to form the main girder as continuous system as described.



Figure 4: Abutment [Roger Frei, Zürich]



3 Photos of the assembly



Figure 6: left: pendulum lift; above: connection of the main girders; below: installation of crossbeams and railing frames



Figure 7: aerial view during construction



Figure 8: Bridge A, five-span girder [Roger Frei, Zurich]

4 Acknowledgement

The project authors of the impressive wooden bridges are the timber construction engineering office Makiol Wiederkehr AG and the civil engineering office Wilhelm+Wahlen Bauingenieure AG. In order to achieve the best design for the client (Canton of Aargau), the architectural office of Edelmann Krell was consulted. The design support of experienced architects has proven successful, as two remarkably attractive bridges have been created. We would like to thank all these involved for their excellent cooperation.

Photographs by Roger Frei, architectural photographer, Zurich

Conference Proceedings 4th ICTB (2022)
https://doi.org/10.24451/02es-hd44

ICTB 2021 PLUS
4th International Conference on Timber Bridges
Biel/Bienne, Switzerland, 9 -12 May 2022



Innovative large timber foodbridges and dynamic testing in Spain

Julio Vivas[1], Álvaro Magdaleno[2], Juan Carlos Santos[1], Soledad Rodríguez[3], Antolín Lorenzana[2]

1 Summary

This work shows the practical methodology used for the dynamic testing and identification of a timber pedestrian walkway located in the *Anillo Verde* trail, upon the N-102 road in Vitoria, Spain. The footbridge is 61 meters long and 3 meters wide and consists of arched glulam structural beams, wood deck and steel cross bracings, designed by Media Madera Ingenieros Consultores. The experimental campaign was carried out in December 2019, just after its erection process. Useful data was collected to estimate its modal properties and to calibrate the corresponding computational model. Also, some serviceability tests were carried out to quantify the vibrations induced when a lone pedestrian transits at different paces. Although there may be some other works with similar objectives and methodology, the peculiarity of this structure is the building material, its large size and the challenging one-step erection process, resulting in a fully functional structural typology with attractive advantages from construction and environmental points of view.

2 Introduction



Fig. 1. Walkers on the Guadalhorce footbridge

With a total length of 270 meters spread and a central span of 70 meters, the Guadalhorce footbridge is one of the largest timber footbridges in Europe and has become a new attraction of the city of Malaga, since its inauguration in October 2020, with thousands of walkers, cyclists and pictures shared on social networks.

This bridge is an excellent example of the latest works carried out by the company Media Madera, a company specialized in the design, calculation an construction of timber bridges for more than 20 years. Taking

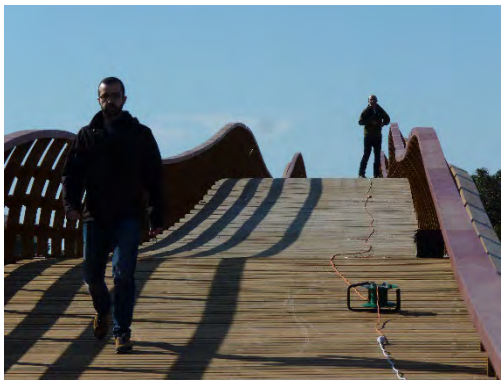
[1] Media Madera Ingenieros Consultores, Asturias, Spain
[2] ITAP, Universidad de Valladolid, Valladolid, Spain
[3] CETEMAS, Centro Tecnológico de la Madera de Asturias, Asturias, Spain

into account the existing background of the brightest timber footbridges built, the structural arch typology constitutes the most immediate and adequate solution for the resistant characteristics of the glue-laminated timber, allowing a high range of economically effective lights between 30 and 80 meters, with which the minimun number of necessary supports is defined.



Fig. 2. The Guadalhorce footbridge during its construction

3 Dynamic testing



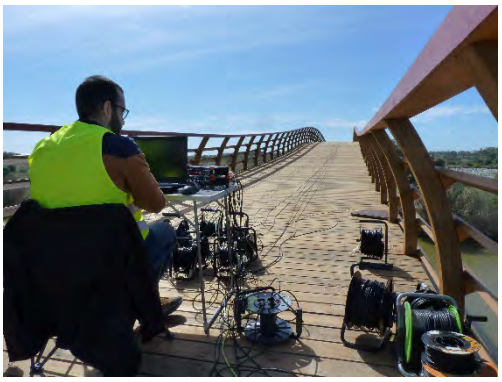


Fig. 3. Dynamic testing of Guadalhorce footbridge

Pedestrian footbridges, like many other building and civil engineering structures, must meet a number of criteria prescribed in standards. Most of the criteria refer to safety conditions. It is also desirable to comply with serviceability conditions, sometimes included as recommendations in the standards and design guidelines [1, 2, 3]. When both the actions and the behaviour of the material are well known, the criteria fulfilment can be check by simulation. This is usually the case with the ultimate strength criteria undergoing overloads, often considered to be quasi-static loading. However, if the behaviour is not so well defined (as in the case of structural timber [4]) or the actions are dynamic ones (as in the case of pedestrian transits) the evaluation by simulation may present serious deficiencies, mainly due to the lack of knowledge of the damping coefficient. Furthermore, with this type of material, the parameters that define the behaviour (both static and dynamic) significantly depend on environmental factors such as humidity and temperature. It is therefore necessary to evaluate on the basis of estimates and to check, once the footbridge has been built, that the estimates are correct or at least conservative. Otherwise, corrective action may be required. Dynamic tests such as those described in this paper are necessary for these checks. Another application of these tests, which is not covered in this work, would be the calibration of the computational model in order to simulate the behaviour in situations that are difficult to experiment with, such as the case of a crowded footbridge.



4 Case study: Dynamic Testing of a 61 meters span timber footbridge

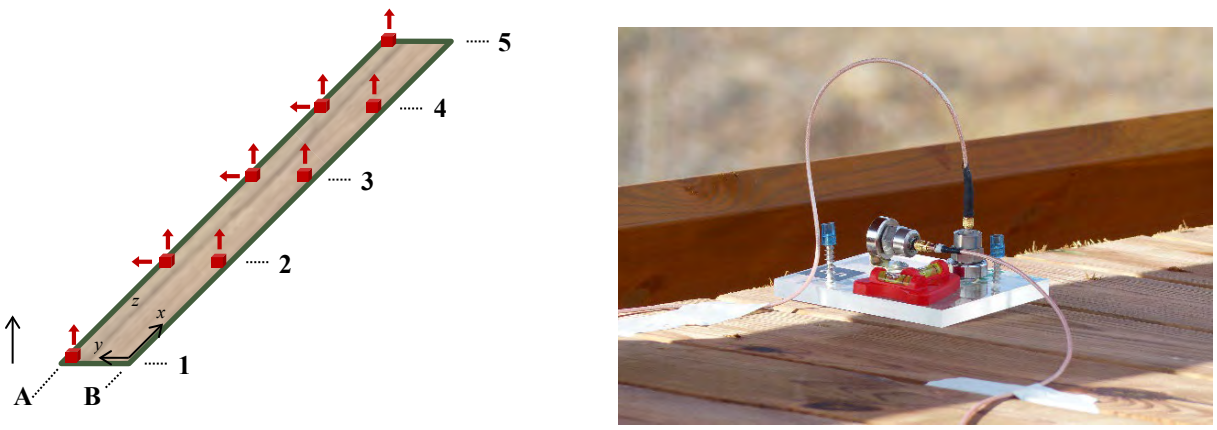


Fig. 4. Green Ring footbridge in Vitoria

In December 2019, the Green Ring (*Anillo Verde*) of Vitoria was completed by placing a footbridge over the N-102 at km 347. The footbridge is designed as a three-hinged arch of 61 m. The width is 3 m and a maximum height above the road is 6 m. Figure 1(a) shows an overview of the whole structure. At the time of its construction, it was the longest single-span footbridge on the iberian peninsula, although in February 2020 it was surpassed by the central span of the footbridge over the Guadalhorce River in Málaga, which is 70 m long. The assembly (Figure 1(b)) was carried out in only 6 hours, the abutments had already been built previously.

The properties of structural class GL28h wood according to EN 14080:2013, density 425 kg/m^3 and bending modulus of elasticity 12600 MPa were taken into account in its project. The total weight is 39.3 tons. To the structural wood are added functional parts (deck and railings) and steel bracing and fittings that can mean about 3 additional tons.

5 Modal testing and identification



(a) (b)

Fig. 5. (a) Layout; (b) detail of the biaxial configuration of the accelerometers



Modal analysis techniques are well established in the literature [5, 6, 7, 8]. Obviously, some instrumental equipment is needed to perform any full-scale tests. This work shows how these means can be reduced to a lightweight and autonomous equipment easily handled by two people. Figure 5(a) shows the layout of the footbridge projected on a horizontal plane where the simplest 5 equidistant measurement sections have been selected along the length of the footbridge. Accelerometers (Figure 5(b)) are placed at these points and oriented in the indicated directions to measure vertical and transversal accelerations. The excitation force required to conduct the experimental modal analysis is induced by a person bouncing on a homemade force plate. This bouncing is applied in two different locations, with the force plate located on point 2A (case I) and with the force plate located on point 3A (case II).

Once the input (bouncing, Figure 6) and the outputs (accelerations) are synchronously registered by means of a proficient and battery-powered datalogger, the frequency response functions (FRFs) relating them, also known as accelerances, can be calculated by means of an estimator such as H_v [5, 6].



Fig. 6. Bouncing on a forceplate.

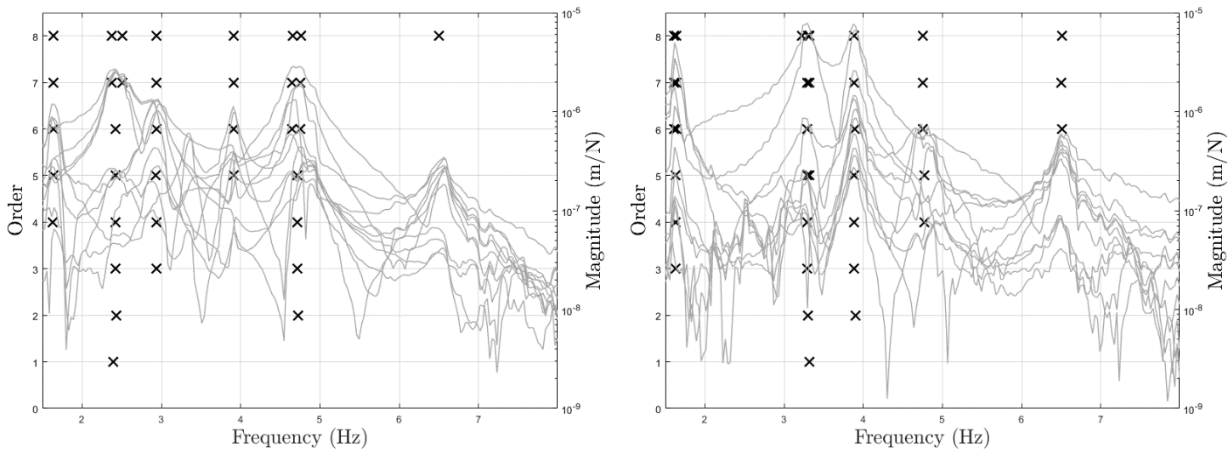
The modal properties of the structure that constitute the expression shown in Eq. (1), which permits to calculate the frequency response function relating an input (i) and an output (k), can be found by means of a curve fitting procedure. Note that this is performed simultaneously for all the FRFs of each case. In that expression, s_r accounts for the eigenvalues of the structure, closely related to the natural frequencies (ω_r) and damping ratios (ζ_r) through Eq. (2). The i-th coordinate of the r-th mode shape is denoted as ϕ_{ri} and n accounts for the order of the modal model, which is the number of modes it is composed of. Finally, j stands for the imaginary unit ($j^2 = -1$) and the symbol $*$ represents the complex conjugate.



$$h_{ik}(\omega) = \sum_{r=1}^{n} \left(\frac{\phi_{ri}\phi_{rk}}{\mathrm{j}\omega - s_r} + \frac{\phi_{ri}^{*}\phi_{rk}^{*}}{\mathrm{j}\omega - s_r^{*}} \right) \quad (1)$$

$$s_r = -\omega_r \zeta_r + \mathrm{j}\,\omega_r \sqrt{1-\zeta_r^2} \quad (2)$$

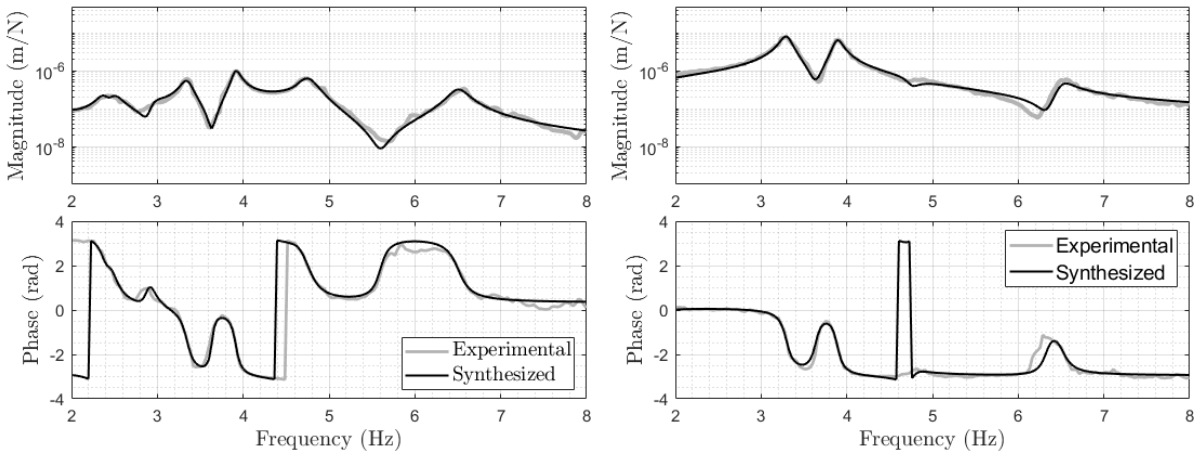
Note that the total amount of modes in the measured frequency range is unknown *a priori*. For this reason, the curve fitting process is repeated several times for each case assuming different orders n. The found modes for each order are plotted together in the known as the stability diagrams shown in Figure 4, which are carefully studied to choose the best model order, i.e., the one which best represents the dynamic behaviour of the structure in the frequency range of interest with the least number of modes. In this case, in the range of interest (between 1 and 8 Hz), an order 8 was considered appropriate in both cases.



(a) (b)

Fig. 7. Stability charts of (a) case I and (b) case II

Figure 5 shows two examples of FRF fitting: Figure 7(a) corresponds to the case I and Figure 8(b), to the case II. In both cases, the FRF corresponding to the point 3A (Z axis) has been plotted. As can be seen, the fitted curve (in solid black), computed from Eq. (1), accurately represents the same dynamic behaviour than the experimental FRF (in solid gray).



(a) (b)

Fig. 8. Examples of A3Z receptance fit of (a) case I and (b) case II



After the visual interpretation of the resulting modes, it is possible to sum up the main results in Table 1, where the last column shows a rough description of the corresponding mode shapes by comparing them to the classical mode shapes of a simple supported beam. Note that the actual mode shapes of the timber structure do not correspond exactly to the ones found in a simple supported beam, but they share similar topological features, like the general shape (bending or torsion) and the number of vibration nodes (points with a null mode shape coordinate). In this sense, the mode shapes described as "1" do not contain any internal vibration node (only the ones associated to the supports), those marked as "2" contain one vibration node located approximately at the middle section, etc.

Table 1. Identified natural frequencies and description of the corresponding mode shapes

Freq. (case I) [Hz]	Freq. (case II) [Hz]	Damping ratio (%)	Mode shape
1.64	1.64	2.91	Lateral Bending 1
2.38	–	2.85	Vertical Bending 2
3.35	3.29	1.90	Vertical Bending 1
3.91	3.89	1.14	Torsion 1
4.65	–	1.95	Torsion 2
4.74	4.75	1.68	Vertical Bending 3
6.51	6.51	2.38	Torsion 3

6 Serviceability assessment

Once the modes have been identified (mode shapes, natural frequencies and damping ratio), determining if any of them is prone to be excited by human locomotion is relatively easy. Usual walking and running are in the range from 95 bpm to 256 bpm (1.58 to 4.26 Hz), which covers the 1st to 4th identified modes. Experimental results are presented by crossing (figure 9) the footbridge at paces matching modes 2 and 3, that are the ones likely to resonate with normal walking and running activities. After the corresponding round-trip transits (90 kg pedestrian with the help of a metronome) the vertical accelerations shown in figures 10 are obtained.

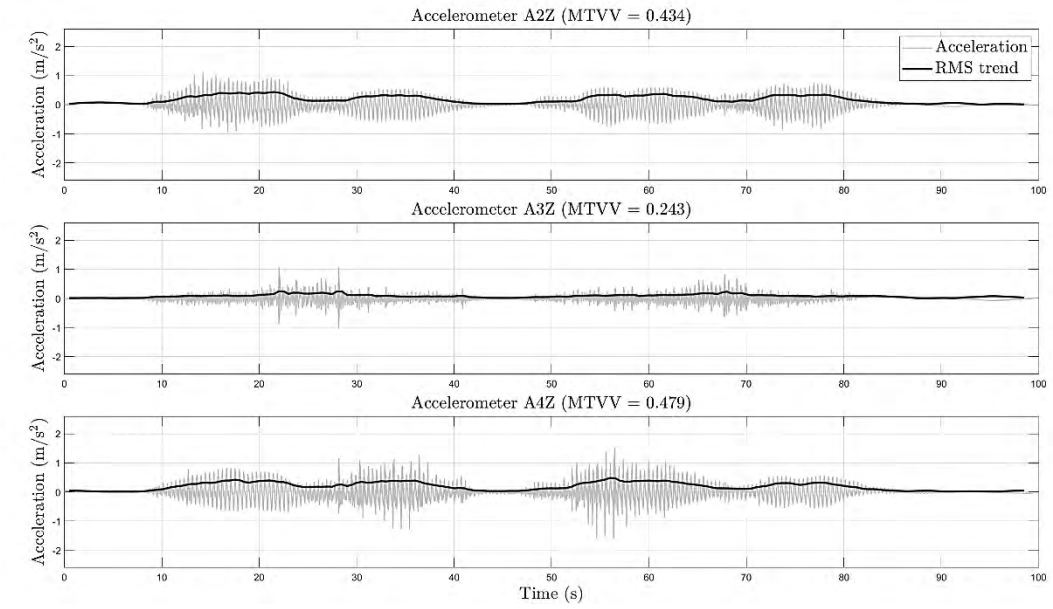


Fig. 9. Transits on the footbridge. A single pedestrian walking test.

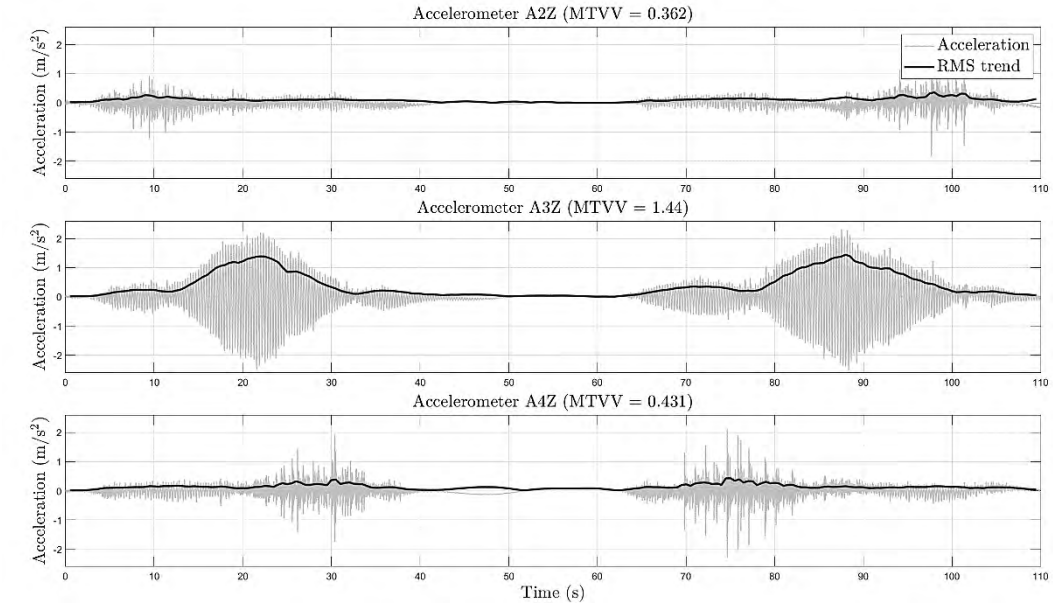


In the first case, peak effective values about 1 m/s^2 and maximum transient vibration values (MTVV) less than 0.5 m/s^2 are obtained.

For the transits at 200 bpm, the processed values are 2.4 m/s^2 peak and 1.44 m/s^2 MTVV. Overall, these values exceed the range of "comfortable footbridge" [9, 10] but given the use of the bridge (immersed in a green trail) the installation of dissipation systems were not prescribed.



(a)



(b)

Fig. 10. Time responses of certain locations. (a) Walking at 143 bpm (VB2). (b) Running at 200 bpm (VB1)



7 Conclusions

When the interest is focused on identifying structures prone to vibrate under pedestrian actions, it has been demonstrated that with portable instrumental equipment and without an external energy supply, modal identification tests can be satisfactorily performed.

Seven modes below 7 Hz have been easily identified in the footbridge under study. Beyond that frequency the task is more difficult without the instrumental support of a mechanical shaker. However, from the serviceability point of view, it is pointless to identify modes at higher frequencies.

Although the design guidelines and the limits they set with regard to comfortability are varied, after the obtained values of MTVV for isolated transits, the footbridge can be classified within the normal comfort range for the intended use.

The MTVV values could be increased in case of synchronized groups of pedestrians [12, 13] or synchronized pedestrian flow. However, the high mass of the structure and the damping of more than 1.5% will make interaction effect difficult to appear. In addition, under high occupancy conditions the damping will increase significantly, making synchronisation even difficult. These ends could be estimated by simulation once the computer model has been calibrated with the results obtained from the modal analysis.

8 Acknowledgement

The authors wish to acknowledge IDEPA and the Ministerio de Economía y Competitividad, Spanish Government, for the partial support through the RTI 2018-098425 Research Project

9 References

[1] Skyshine.com.my
[2] Photogrammetric Techniques in Civil Engineering Material Testing and Structure Monitoring.
[3] SETRA. Technical guide - footbridges - Assessment of vibrational behavior of footbridges under pedestrian loading, Service d'Etudes Techniques des Routes et Autoroutes, 2006.
[4] UNE-EN 1995-2:2010. Eurocódigo 5: Proyecto de estructuras de madera. Parte 2: Puentes. AENOR, 2010.
[5] D. J. Ewins, Modal testing : theory, practice, and application. Research Studies Press, 2000.
[6] N. M. M. Maia and J. M. M. Silva, Theoretical and Experimental Modal Analysis. Research Studies Press, 1997.
[7] N.J. Bertola and I.F.C. Smith, A methodology for measurement-system design combining information from static and dynamic excitations for bridge load testing. Journal of Sound and Vibration, 463, 2019.
[8] J. A. Fabunmi, Spectral basis theory for the identification of structural dynamic systems, AIAA J., vol. 26, no. 6, pp. 726–732, 1988.
[9] M. Setareh and S. Gan, Vibration Testing, Analysis, and Human-Structure Interaction Studies of a Slender Footbridge. Journal of Performance of Constructed Facilities, 32(5), 2018.
[10] A. Srikantha Phani and J. Woodhouse, Viscous damping identification in linear vibration, J. Sound Vib., vol. 303, no. 3–5, pp. 475–500, Jun. 2007.
[11] K. S. Kim, Y. J. Kang, and J. Yoo, Structural parameters identification using improved normal frequency response function method, Mech. Syst. Signal Process., vol. 22, no. 8, pp. 1858–1868, 2008.
[12] E. Shahabpoor, A. Pavic, V. Racic, and S. Zivanovic. Effect of group walking traffic on dynamic properties of pedestrian structures. Journal of Sound and Vibration, 387:207–225, 2017.
[13] J. Sebastian, I. M. Diaz, C. M. Casado, A. V. Poncela, and A. Lorenzana. Evaluacion de la prediccion de aceleraciones debidas al transito peatonal en una pasarela en servicio. Informes de la Construcción, 65(531):335–348, 2013.

Conference Proceedings 4th ICTB (2022)
https://doi.org/10.24451/9cwh-1635

ICTB 2021 PLUS
4th International Conference on Timber Bridges
Biel/Bienne, Switzerland, 9 -12 May 2022



Fruttli-and Rigiaa-Bridge, Timber-UHPC composite structure

Edgar Kälin[1], Peter Rogenmoser[2]

1 Introduction

In 2020 and 2021, two obsolete concrete bridges in central Switzerland at the foot of the Rigi should be replaced.

Innovative timber-UHPC composite bridges were built for 40-tonne loads.

The Fruttli and Rigiaa bridges are located on the access road to the Rigi region. All log and freight transports are handled over this major freight road.

At a bridge inspection, it was determined that repair of the old bridges was no longer technically feasible. Two engineering offices submitted variants for the replacement of the 10 and 16 m long bridges: A conventional proposal for concrete bridges and another proposal for a timber-UHPC composite structure. Due to the lower costs, shorter construction time and ecological aspects, the decision was made in favour of the timber-UHPC composite construction.

After preparatory work on the existing support, the entire bridge superstructure was built within one week. After another 4 days, the bridge was open to traffic.



Figure 1:Fruttli Bridge, Goldau, Switzerland

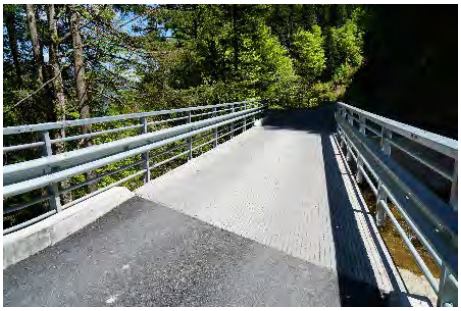


Figure 2:Fruttli Bridge, Goldau, Switzerland



Figure 3: Rigiaa Bridge, Goldau, Switzerland



Figure 4: Rigiaa Bridge, Goldau, Switzerland

2 Construction

The bridges consist of glulam girders, which are shear-resistant connected with a UHPC slab cast on site.

The girders were placed on the abutments, whereby formwork for pouring the bridge slab made of UHPC was already pre-assembled on the outermost girders. The formwork between the timber girders was formed by superimposed 3-layer slabs, which remain in the bridge. The cross-section structure is inspired by that of the Gletschersand Bridge in Grindelwald, which was built by Emch+Berger in 2018 [1].

[1] Edgar Kälin, dipl. Ing. ETH/SIA, Ingenieurbüro Edgar Kälin AG, Switzerland, e.kaelin@ingenieurkaelin.ch
[2] Peter Rogenmoser, Holzbauingenieur, neue Holzbau AG, Switzerland, peter.rogenmoser@neueholzbau.ch

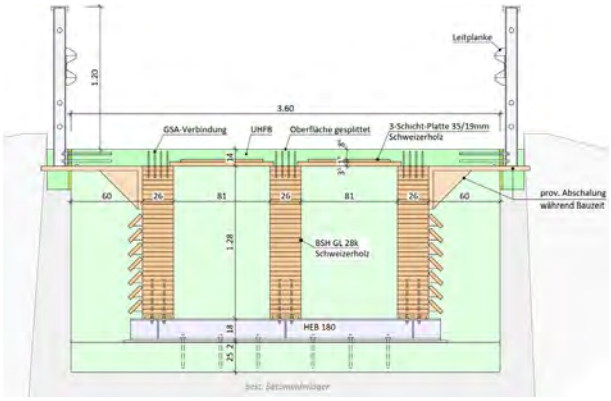


Figure 5: Rigiaa Bridge, Cross section

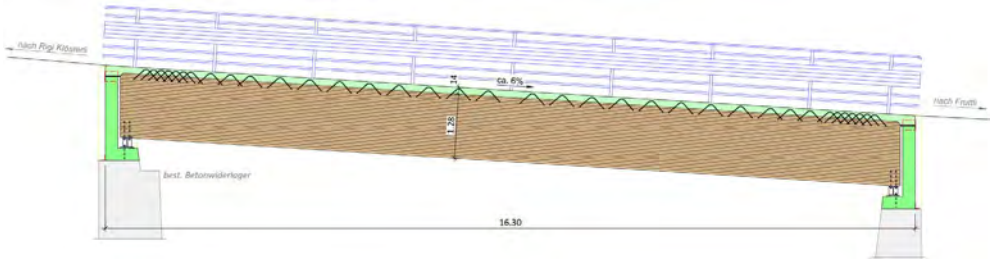


Figure 6: Rigiaa Bridge, Longitudinal section

The main girders at the abutments rest on HEB steel profiles. Threaded rods (GSA® technology) glued transversely to the girders transfer the bearing forces into the abutments via direct steel contact.

To protect the timber from weathering, the deck is cantilevered over the outermost beams. On the Fruttli Bridge, the cantilever is enough to prevent direct weathering of the timber at an assumed driving rain angle of 30°. On the Rigiaa bridge, the timber girders are additionally protected by boarding made of saw-rough boards. The damp-proof coating applied at the factory ensured protection during the construction phase. These measures optimally shield the timber and ensure a long service life.

The UHPC slab cast on site with a thickness of 8.5 cm to 14 cm can be driven over directly. It serves as a seal throughout the entire period of use and, due to the cantilevers, also as weather protection for the timber beams.

To increase sliding resistance of the deck, grooves were finally milled into the surface of the Fruttli bridge. The steel fibres contained in the UHPC that stood up more due to the milling were then flamed with a gas flame. This was a premiere that led to the desired, flawless result.

In contrast, for the Rigiaa bridge, a two-layer UHPC slab with the same overall thickness as for the Fruttli bridge was chosen. On top of the first layer of conventional UHPC with steel fibres, a second layer of UHPC was poured. This second layer contains chippings instead of steel fibers



Figure 7: Rigiaa bridge, Transport of the girders with pre-assembled formwork



Figure 8: Fruttli bridge, Assembly of the girders with the pre-assembled formwork



Figure 9: Rigiaa bridge, the glulam girders placed on the abutments



Figure 10: Fruttli bridge, the reinforced bridge slab



Figure 11: Rigiaa bridge, Mixing UHPC



Figure 12: Fruttli bridge, Mixing UHPC



Figure 13: Rigiaa bridge, casting of the UHPC



Figure 14: Rigiaa bridge, casting of the UHPC



Figure 15: Rigiaa bridge, smoothing of the first layer of the UHPC deck



Figure 16: Fruttli bridge, smoothing of the UHPC deck



Figure 17: Fruttli bridge, Milling the grooves to increase skid resistance

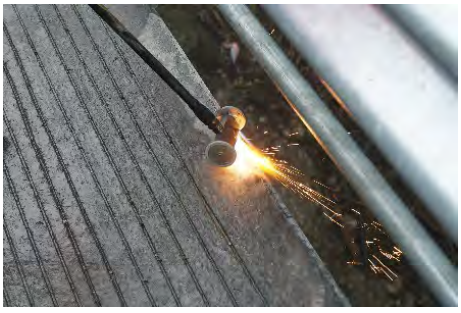


Figure 18: Fruttli bridge, Flaming the surface



Figure 19: Rigiaa bridge, casting the second layer

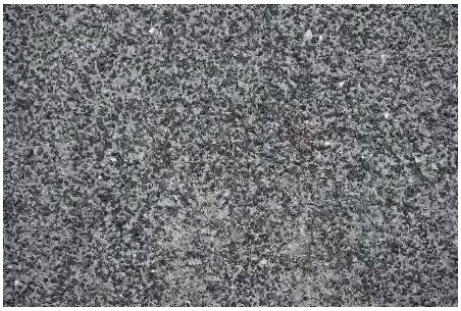


Figure 20: Rigiaa bridge, surface



Figure 21: Rigiaa bridge, lateral view of the girders and the bridge slab



Figure 22: Fruttli bridge, soffit with beams and 3-layer panels

3 UHPC

UHPC stands for **U**ltra-**H**igh **P**erformance, cement-bonded fibre **C**omposite building material. Building with UHPC is regulated in Switzerland in the 2052 standard of the SIA (Swiss Society of Engineers and Architects). Another Name for the material is UHPFRC (**U**ltra-**H**igh **P**erformance, cement-bonded **F**ibre **R**einforced **C**omposite).

The building material UHPC is neither steel nor concrete, but a new type of building material with an independent mode of action.

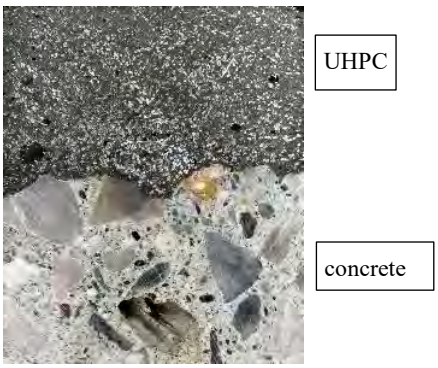


Figure 23: Comparison UHPC and concrete (EPFL, Switzerland)

Figure 23 shows the obvious, pictorial difference between the two building materials. UHPC consists of cement, other fines and hard particles (quartz) with a maximum size of 1 mm. The packing density of these particles is optimised so that the resulting building material no longer has any voids (pores). This cement-bound building material is reinforced by slender short fibres in high dosage. These fibres are made of steel, 15 mm long and 0.2 mm thick, and make up at least 3% of the building material volume. The amount of water needed to set the cement (binder) is so small that during the hardening process of UHPC, the added water is completely consumed for cement setting. Since there is no more free water, no drying process can take place, as is usual with mortar and concrete and leads to the formation of capillary pores. The capillary pores common in conventional concrete are interconnected and thus allow water to enter the concrete from the outside. Water is the necessary precondition for corrosion of the steel reinforcing bars or chemical reactions in the concrete (alkali aggregate reaction), which are the two most common damage mechanisms of reinforced concrete. In contrast, UHPC - as previously explained - has no capillary pores, which means

that no water ingress can take place and thus no damage to the building material can occur. The building material UHPC is waterproof. This watertightness has been proven by many tests. In addition, tests have shown that UHPC is waterproof even under tensile stress. These properties guarantee the building material UHPC a very high durability against climatic influences with water and de-icing salts. UHPC has been used on bridges in Switzerland for 18 years. The experience gained from these applications confirms this very high durability. Accordingly, significantly lower maintenance costs are expected for the Fruttli and Rigiaa bridges than for a conventional concrete bridge.

Due to the impermeability and the very high abrasion resistance of the UHPC, the sealing and waterproofing work required for a concrete or timber bridge can be omitted and no wear layer is required for the roadway.

4 Composite effect

The bond between the glulam girders and the bridge slab is ensured by means of GSA®-HBV shear bond.

Together with the UHPC deck slab, the timber girders form the desired composite girder. Due to its high performance and ductility, the GSA-HBV composite system is ideally suited for bonding with the high-strength UHPC. The GSA® technology is based on threaded rods glued into the timber or, in the case of the HBV system, on glued-in reinforcing steel. The connection is designed in such a way that the reinforcing rods fail ductilely in the fracture state. This excludes the brittle failure modes of the timber or the adhesive. Due to the high stiffness, a practically rigid connection with high fracture resistance is created. GSA-HBV also behaves in an extremely ductile manner (see graphic) and thus reliably distributes the shear flow to all connectors used. The efficient fastener corresponds to the high-quality individual materials, which ultimately results in a beneficial overall system.

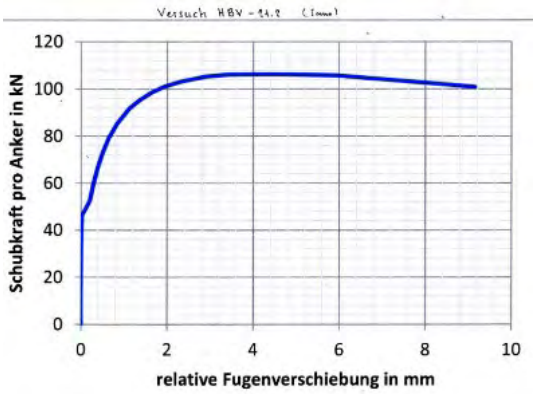


Figure 24: Load-deformation diagram of GSA connections, neue Holzbau AG, Switzerland

5 Sustainability

In terms of global warming potential and resource consumption, the timber-UHPC composite construction has major advantages compared to a conventional concrete construction. There are also small advantages in comparison with a pure UHPC construction, as the following graph shows.

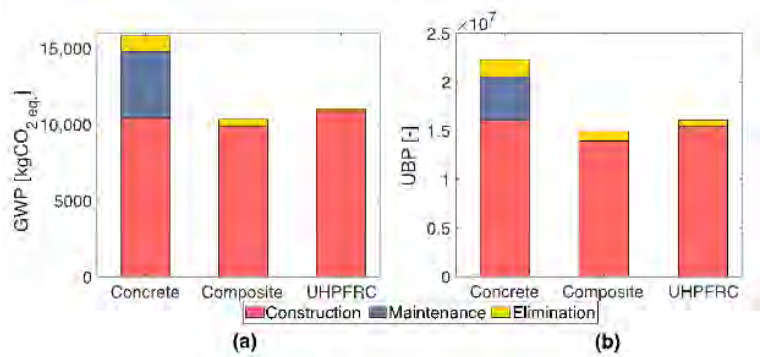


*Figure 25: Environmental impacts of bridge designs over the use span, including construction, maintenance, and elimination processes: **(a)** Global warming potential; **(b)** Ecological scarcity (UBP points) [2]*

The eco-balance can be improved significantly in the future by using an environmentally friendly UHPC mix. An environmentally friendly mix of UHPC has been developed recently where two improvements are made to the standard mix [3]. First, steel fibres are replaced by ultra-high molecular weight polyethylene (UHMW-PE) fibres. Second, 50% of clinker is replaced with limestone fillers.

As this ECO-UHPC provides similar mechanical properties to the standard mix, similar bridge designs are obtained. Additionally, the maintenance and elimination processes of UHPC are not affected as the durability properties of ECO-UHPC are equivalent to the conventional mix. The influence of ECO-UHPC in terms of global warming potential is presented in Figure 24.

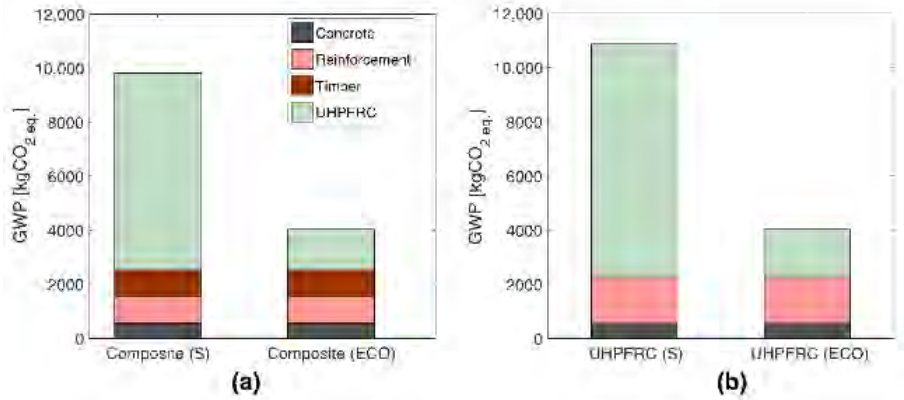


*Figure 26: Influence of using an environmentally friendly UHPC on the bridge's ecological footprint in terms of global warming potential: (**a**) Timber–UHPC composite bridge; (**b**) UHPC bridge.*

For smaller spans and lower loads, the use of sawn timber instead of glulam also improves the life cycle assessment significantly.

6 Conclusions

Today, timber bridges are mainly used as pedestrian bridges, whereas concrete or steel construction dominates in road traffic.

The two bridges on the Rigi are the first timber-UHPC composite bridges in Switzerland that can be driven over by 40 t trucks. They show that this construction method can compete with a conventional concrete construction in terms of price, while at the same time offering great advantages in terms of construction time, durability and ecology. Due to the multifunctionality of the UHPC, very simple constructions with extremely favourable maintenance costs result.

These bridges can therefore be exemplary for other road bridges, also with larger spans.

7 References

[1] Emch +Berger (2018), https://www.emchberger.ch/de/gletschersand-bruecke)

[2] Bertola N., Küpfer C., Kälin E., Brühwiler E. (2021) Assessment of the Environmental Impacts of Bridge Designs Involving UHPFRC, Sustainability, Special Issue "Prefabricated Bridge Elements and Connections: Towards Sustainability in Bridge Construction"

[3] Hajiesmaeili, A.; Denarié, E. Next Generation UHPFRC for Sustainable Structural Applications. In Proceedings of the DSCS 2018: 2nd International Workshop on Durability and Sustainability of Concrete Structures, Moscow, Russia, 6–7 June 2018.

Conference Proceedings 4th ICTB (2022)
https://doi.org/10.24451/p33k-vn37

ICTB 2021 PLUS
4th International Conference on Timber Bridges
Biel/Bienne, Switzerland, 9 -12 May 2022



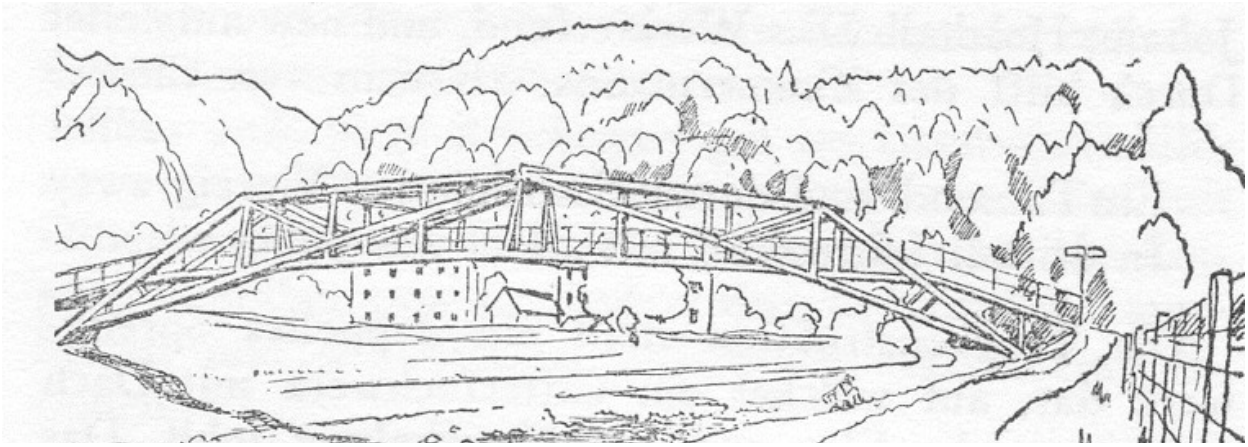
A new pedestrian bridge made of regional beech wood in Adliswil

Andreas Burgherr[1], Ciril Stadler

1 Introduction

The Tüfisteg is a pedestrian bridge over the Sihl in Adliswil. This 45 m long overpass was first built in 1932 as a trussbridge. truss bridges were originally built by the military They are characterised by the fact that they are built of easily accessible, often local material, i.e. wood. This classification for such bridges has been used up to the present day, even though they have long since been built by others than just the military.

The first version of the Tüfisteg was an unroofed truss construction with a suspended roadway. The building material used at the time was tar oil impregnated larch wood.



In 1985, the initial bridge had to be replaced. Following the military tradition, the new bridge was rebuilt as an unroofed truss construction made of solid wood. The side truss constructions formed a flat truss structure with the roadway resting on the lower chords. This bridge was built from CFRP pressure-impregnated spruce and fir wood.



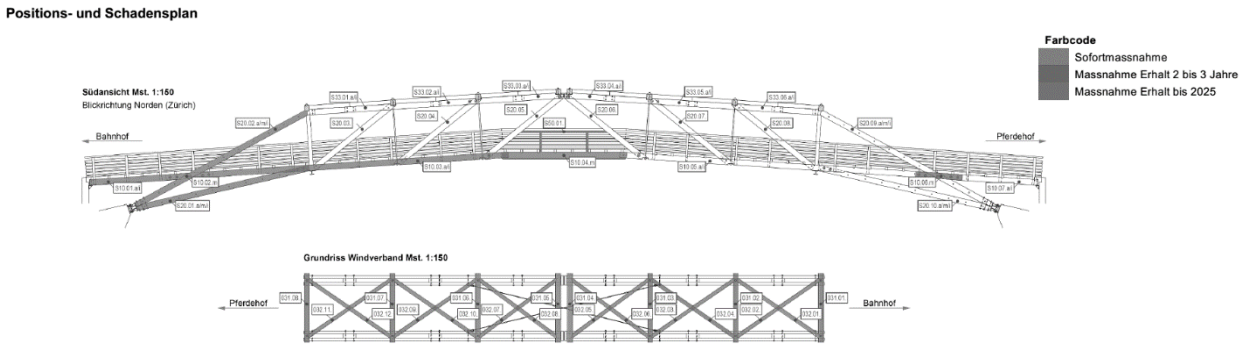
[1] Andreas Burgherr, Managing Director, Timbatec Holzbauingenieure Schweiz AG, Switzerland, ab@timbatec.ch



In 2006, the damage to the structure had progressed so much that the bridge had to be thoroughly renovated. Unfortunately, in the course of this renovation, it was decided to seal the cracks in the solid wood beams with epoxy resin.



A condition analysis from 2017 shows that the bridge is in such a bad state again that it is in need of major rehabilitation. The components rehabilitated with epoxy would all have had to be replaced. However, due to the construction, the primary components could hardly be replaced without dismantling the entire bridge.



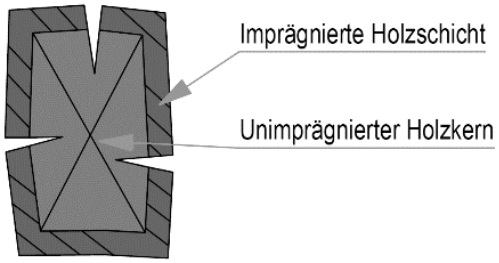
Accordingly, it was decided to replace the bridge altogether. The new bridge should be an unroofed truss bridge that reuses the existing abutments. As with the first bridge from 1932, a technical durability of at least 40 years should be reached.

1.1 Insights from damage analysis

As a basis for the new bridge design, a thorough damage analysis was first carried out.

The following factors turned out to be critical for durability:

- Large cross-sections lead to severe cracking
- Large, cracked cross-sections absorb more moisture and dry out more slowly.
- With large cross-sections, the cross-section core can hardly be impregnated, which remains susceptible to rot in the event of moisture penetration.



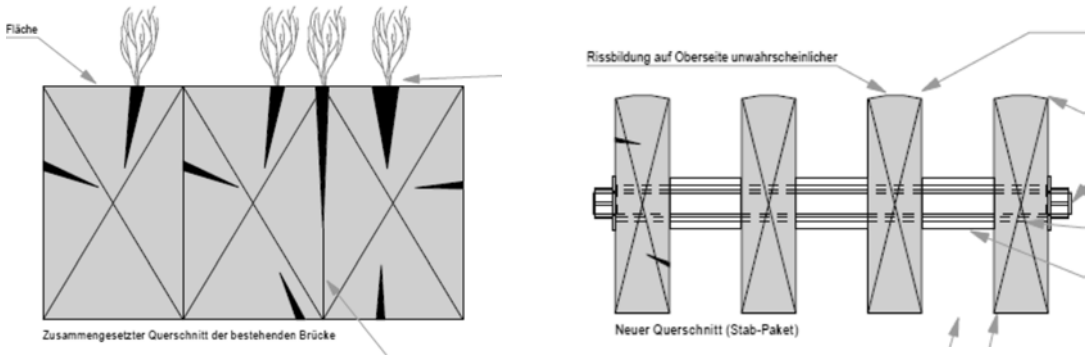
1.2 Solution approach

The new bridge should have similar appearance (truss bridge) and reuse the existing abutments.

Built of solid wood, this again means large and compound cross-sections for coniferous wood. In the case of an unroofed truss bridge, the only structural wood protection that is contemplable are cover and sacrificial boards on the top of the structural components. These can protect the individual beams between the connections. Yet these board covers are of little use in the truss nodes. Here, water can still get into the connection points and lead to moisture penetration.



One solution to this problem is the use of hardwood. Thanks to the higher density compared to coniferous wood, the individual timber cross-sections can be smaller. Formerly large composite cross-sections can be dissolved into air-flushed bar groups with similar load-bearing capacity.



Board-type bar assemblies have a much higher surface-to-volume ratio, which means they dry more quickly and are much less susceptible to cracking.

Now the challenge arises to choose the "appropriate" type of wood. One possibility is to use wood species such as oak, robinia or chestnut. These types of wood have good natural durability, but are relatively very pricey and/or not constantly available in the desired profile dimensions.

Even with the best structural wood protection, localised moisture penetration at contact points can occur in an open, uncovered truss bridge. Even with a construction in oak, damage can occur after only 10 years.

Pressure impregnation can prevent this. Since the critical contact points are usually well protected from direct weathering, chemical wood preservation remains effective in these areas for a very long time. However, this requires wood species that can be impregnated easily and are available as construction timber.

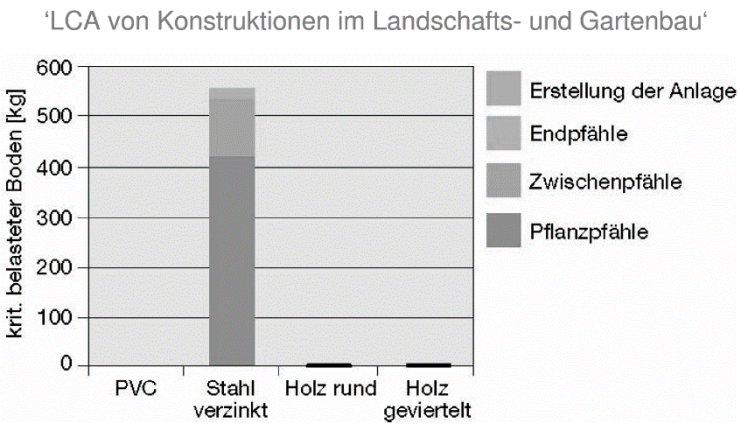
A wood species with high mechanical properties that is available in large quantities is beech. It can easily be impregnated, provided there is no red heart. However, unimpregnated beech has very low natural durability. Accordingly, with beech it is essential that the individual cross-sections can be completely impregnated with wood preservative.

1.3 Pressure impregnation - is this still "state of the art"?

Chemical wood preservation is frowned upon. "If you construct properly, you don't need to poison the wood" or "Pressure-impregnated wood poisons the environment and can only be disposed of later as hazardous waste" are the most frequent reactions when pressure impregnation is mentioned.

But are these statements still true? What used to be true for tar-oil impregnated wood is no longer true for today's salt-based impregnation options.

A study conducted by Empa in 2001 entitled "Life cycle assessment of constructions in gardening and landscaping" compared, among other things, the life cycle assessment of vineyard stakes used in vineyards. The impact of the stakes on the soil was also investigated. Stakes made of plastic, galvanised steel and pressure-impregnated wood were compared. The result was that compared to galvanised steel, the soil load of wooden stakes is negligible.





Applied to a bridge, this means that the leaching of preservatives from the wood is not relevant compared to the zinc from the steel parts.

regarding subsequent recycling, salt-based pressure-impregnated wood is equivalent to painted window frames, door leaves, parquet flooring or resin-covered chipboard for furniture.

If the alternative is only steel and concrete, pressure-treated wood is still considerably better in terms of environmental impact.

1.4 Beech wood in outdoor use - is that possible?

Everyone who deals with wood seems to know: Beech wood is a difficult material and certainly not suitable to be placed where it is exposed to the weather.

Is this statement generally valid, or is there a way of handling beech that makes its use possible? Everyone is looking for utilisations for beech wood. But beech wood sales will hardly be increased only with the now established high-performance components for interior use. There is also a need for low-threshold applications for beech wood on a larger scale.

1.4.1 Balconies Saumacker

In 2014, as part of a pilot project, we planned the use of beech wood outdoors on a balcony on Saumackerstrasse in Zurich. We were looking for planning approaches that would do justice to the specific properties of beech wood.

High residual stresses, deformations: Lamella construction in which each board can deform without great constraints

Low weather resistance: Complete impregnation with wood preservative (CKB).

High mechanical strength: design that takes advantage of this.

In the first few years, the ageing behaviour of the balconies was observed with annual monitoring. It was detected that the construction behaves much better and more benignly than assumed.

Around 40 m3 of local Zurich beech wood was used for the balconies at Saumacker. The balconies were also awarded the Swiss Wood label.







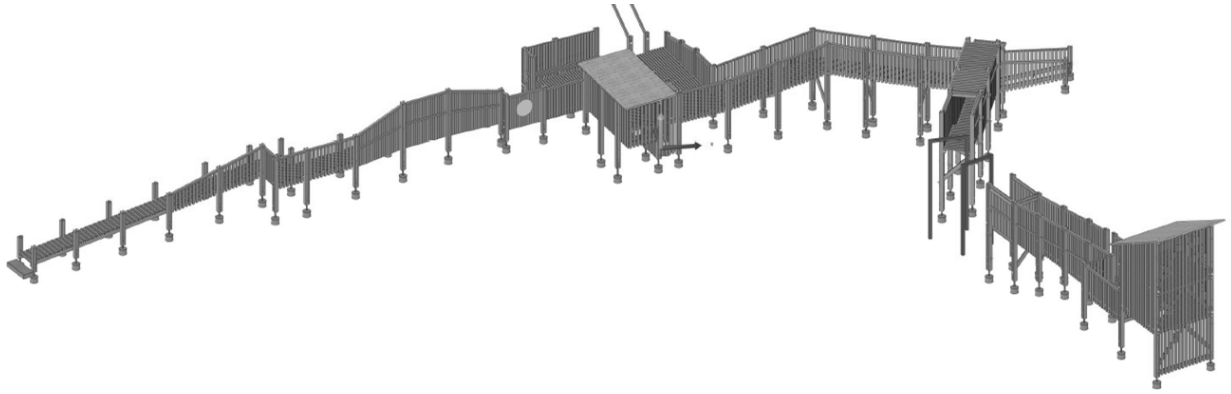
1.4.2 Playground Buchholz

A second opportunity to use beech wood outdoors arose with the renovation of the "Buchholz" playground in Zurich Witikon.





The original playground dates to the 1970s and was built as a "telephone pole construction" at the edge of the forest in an old quarry pit that has since become completely vegetated again. Due to safety deficiencies, the structure was replaced in 2003 by a similar structure made of natural oak and larch wood. After only 10 years, this showed considerable damage (fungal infestation with the oak spore, among others), which by 2015 had become so severe that the facility had to be replaced again.



In an evaluation phase, we concluded that a durability of considerably more than 10 years cannot be guaranteed for a structure constructed with domestic timber under the prevailing climatic conditions without chemical wood protection.

But if chemical wood preservation is necessary, then we will at least live up to the name and build the playground called Buchholz in local beech wood.. Based on Our previously gained knowledge from the beech balconies, we have planned the playground with colourless BKD-5 impregnated beech planks. All existing foundations were reused. The playground was completed in 2017 and has since been monitored annually for its condition and ageing behaviour in this climatically difficult environment.

Here, too, the beech wood playground has so far behaved pleasantly and as expected.



1.5 Previous insights for an open bridge made of beech wood.

When building with beech wood constantly exposed to weather, the type of construction and the treatment of the material must be adapted in favor of the properties of beech wood. In the case of a bridge, the static strains are many times higher than in previous applications. Based on the experience with the two previous projects, we decided on the following framework parameters:

Timber harvest: If possible, only beech wood felled in late autumn. The sap and glucose content must be as low as possible.

Wood quality: No red-core wood, as it is inconvenient to be impregnated.

Cross-sections: Maximum cross-section width 60 mm. Such a plank can build up less residual pressure so that minimal restraint cracks occur.

Construction: All cross-sections are air-flushed on all sides with minimal contact surfaces. All components must be individually replaceable without having to dismantle the bridge.

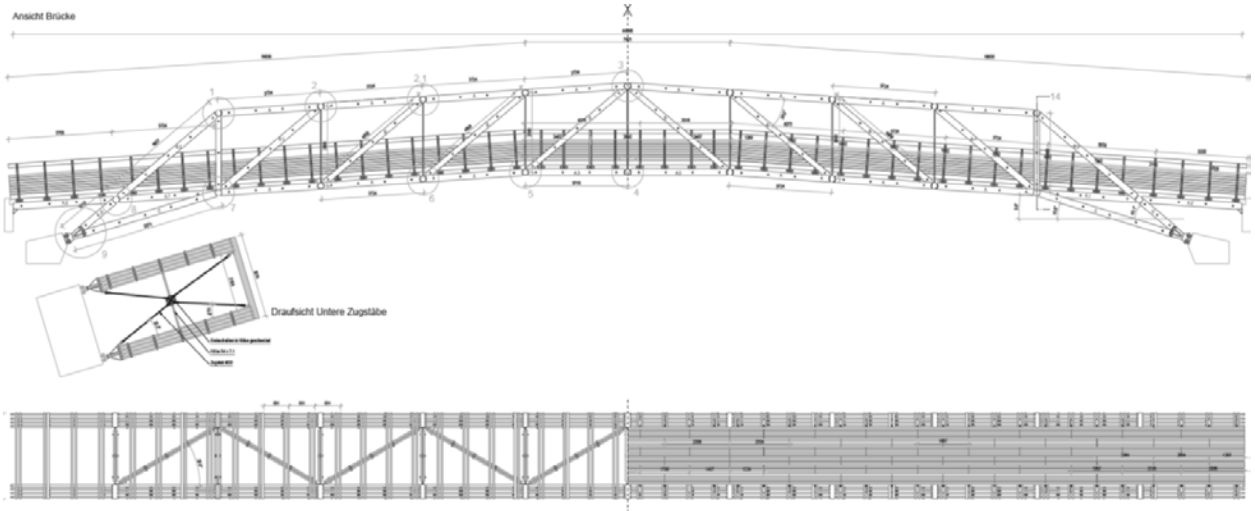
Pressure impregnation: Only executed by an impregnation plant that has experience with beech wood. All components are impregnated twice: Once before and once after joinery. This procedure guarantees thorough impregnation. In addition, strongly throwing or twisting components show up and can be sorted out.

Load-bearing behaviour: The load-bearing behaviour (buckling) of beam groups must be examined/researched in more detail. For this purpose, corresponding tests were carried out as part of a thesis at the BFH.

2 Construction principles of new Tüfisteg made of solid beech wood

2.1 Truss conception

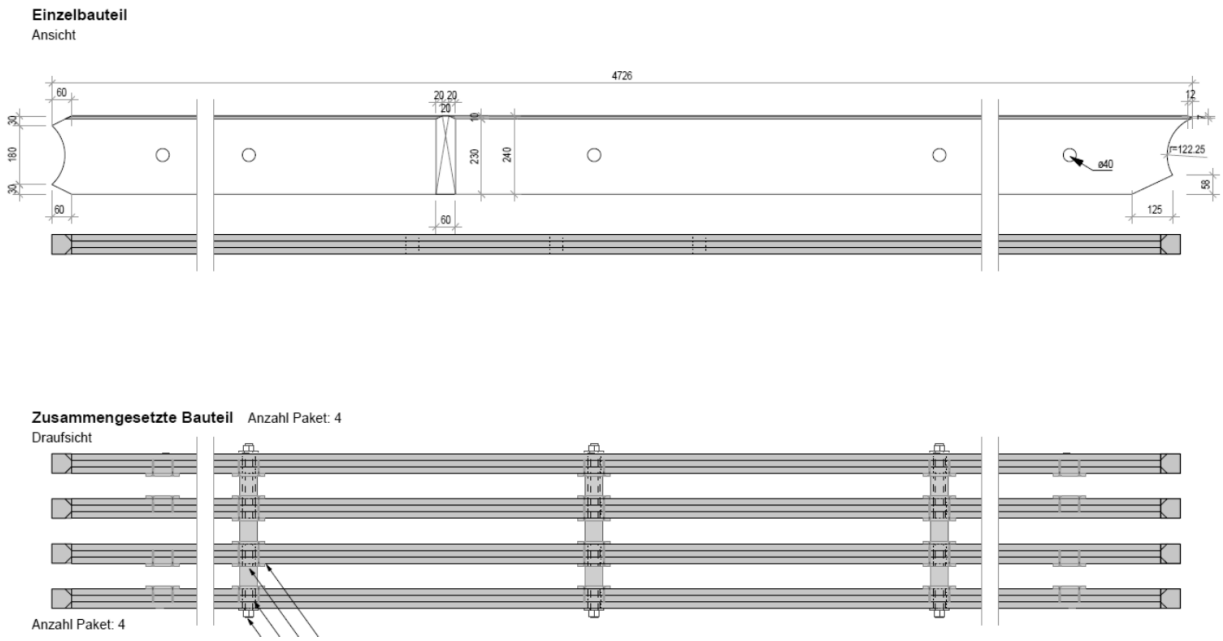
The new bridge conforms with the previous bridge, so that the previous abutments could be reused 1:1. Since the length of the structure in hardwood is limited, the truss struts in the abutments were designed steeper in order to shorten the component lengths. In the same profile, the new bridge now has 8 instead of 6 truss struts.



2.2 Rod groups

In the beech version, the truss chords are arranged in open rod groups by geometrically breaking up the previous assembled beams. These are threaded at regular intervals onto steel tubes with spacer rings and braced with a continuous screw to form a fixed package.

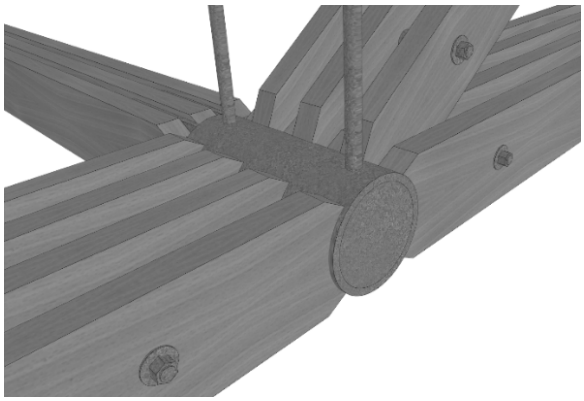
Between the gaps, water can flow off unhindered at any time. Due to the much larger surface, these cross-sections also dry out much quicker after a rainy period. This arrangement also allows for later replacement of individual bars with relatively little effort.

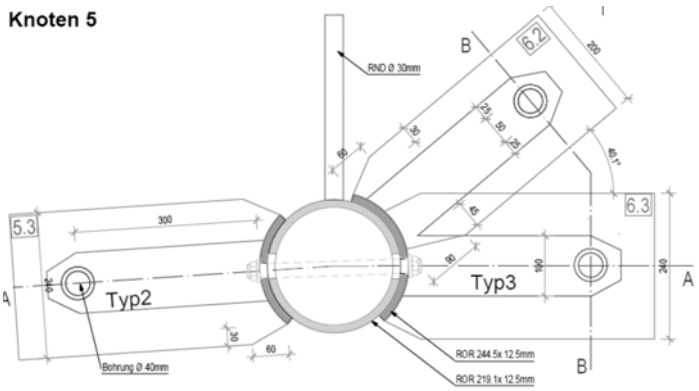


2.3 Node

The connection of the beech rods in the nodes is carried out as a pure compression connection onto a round steel profile. All components subject to tensile stress are again realised with steel tension rods, as in the existing bridge.

The design principle in the nodes is to minimise capillary joints so that water always drains away.

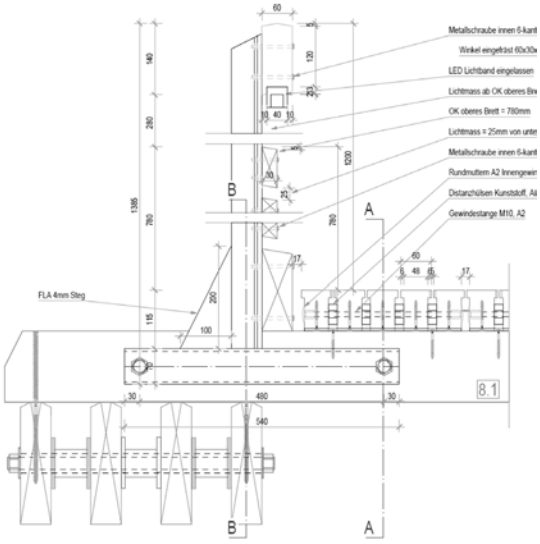


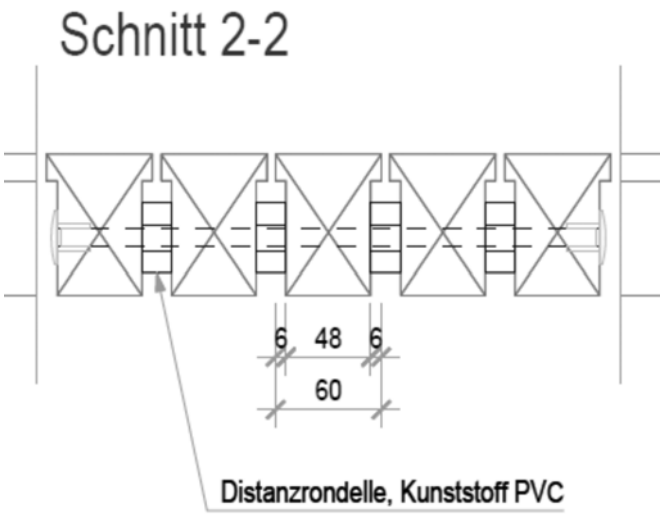




2.4 Roadway

The roadway was also made of beech. T-shaped profiles were assembled into groups of bars. Beech cross-sections were used, which do not meet the strength requirements of the main structure, but can be processed as roadway slats without any problems. As with the existing bridge, the roadway slats were provided with an anti-slip coating made of sanded epoxy.



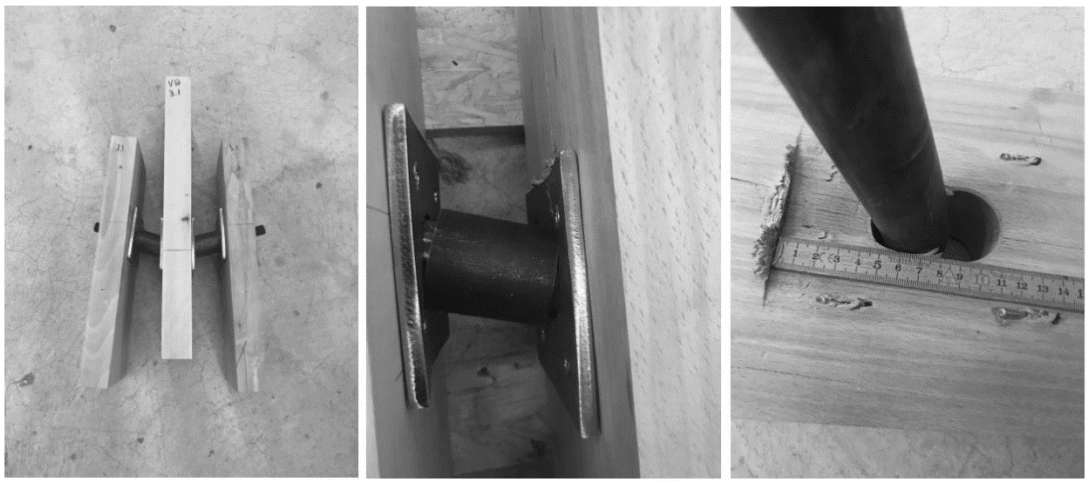


3 Buckling research at Berne University of Applied Science

Since the fasteners are very specific and the composite compression members are generally described very sparsely in the national and international standards, a complex structural analysis model was developed by the Timbatec company for evaluating the stability of the components in the direction of the connection axis. With the help of the model, the effective moment of inertia of the components is calculated via the bending deformation and, in a second step, the stability verifications are carried out on a replacement profile.

Two different test series were carried out as part of a bachelor thesis. With the first test series, the structural analysis model is checked globally. For this purpose, the effective moment of inertia of the components is determined via the bending deformation in the same way as in the model. The second series of tests is used to assess the stiffness of the fasteners and thus to check the model locally regarding the parameters introduced for representing the fasteners as displacement and torsion springs.

These tests served as the basis for the design of the rod packages used for the Tüfisteg.





4 Assembly and first insights

The bridge was mostly pre-assembled in two parts at the factory (Burch Sarnen) and pre-assembled on site. The bridge, which weighed around 30 tonnes, was then lifted into place on the supports using a large pneumatic crane.





During the one-year inspection, it was noted that the beechwood bridge has been behaving very well so far, as expected.

Conference Proceedings 4th ICTB (2022)
https://doi.org/10.24451/c2tk-mp63

ICTB 2021 PLUS
4th International Conference on Timber Bridges
Biel/Bienne, Switzerland, 9 -12 May 2022



Pedestrian and cyclist bridges made with durable hardwoods

Marcus Schiere[1], *Jos Peters*[2]

Abstract

The dense network of waterways and roads is plausibly the reason for a large amount of small timber bridges in the Netherlands. Many of these bridges are made of hardwoods like oak and ekki. These timber species have a higher natural durability than regular softwoods, hence, open structures and simple building methodology are possible. This paper aims at providing an overview of several examples of large timber bridges built in ekki.

1 Introduction

According to a recent study from 2021, there should be about 31000 timber bridges in the Netherlands [1]. Their large number is plausibly related high density of waterways and canals in combination with the large network of bicycle roads. In many of these bridges, ekki and oak are a primary raw building material. These small bridges can also be made of concrete, steel and plastic composites. Ekki has also found its way into many other types of timber structures like lock gates, guide rails, fenders, balconies, sheet piling, terraces, etc (Figure 1). It shows the diversity of applications of hardwood timber in structures exposed directly to water, wind, rain and sun.



Figure 1: several examples of the use of ekki in timber structures other than bridges (from left to right, high to low): Lock gates (Bernhardsluis, Deventer), guide rail (during tests, Lelystad), fenders (location unknown), and stairways and balconies (Kop van Lombok, Utrecht)

[1] Marcus Schiere, Product Manager, Hupkes Wijma B.V., The Netherlands, mjs@hupkeswijma.com
[2] Jos Peters, Timber Engineer, Hupkes Wijma B.V., The Netherlands



Concrete, steel and plastic composites have not always been able to compete with the advantages timber sometimes offers: its workability on the construction site, its durability, and recyclability. In specific scope of LCA, wooden bridges easily outperform plastic composites, concrete and steel counterparts [2].

Before the introduction of ekki from the tropics on the European timber market, oak was used for the construction of these bridges [3]. Ekki has exceptional qualities that are rarely found in softwood [4] or hardwoods from temperate climates: The strength class of Ekki is marked as D70 by the EN 1912 [5] and corresponding properties are found in the EN 338 [6]. The resistance to fungi is marked I/II and the resistance to marine borers M-D in EN 350 [7]. The density at 12% moisture content is 1060 kg/m^3 [8]. Freshly cut, it weighs about 1200 kg/m^3, which means that it is heavier than water. In the floods of 2021 of the Ahr river in Germany for instance, a timber bridge in ekki near Sinzig was still found on its abutments after being submerged. It did not float during the floods, partially due to its weight. Unfortunately, after closer analysis, the abutments had suffered severe damage, along with several structural elements of the bridge, and it was demolished anyway [9].

Forest Stewardship Council (FSC) guarantees a sustainable raw material through forestry practices based on social, economic, and ecological principles further explained in ten rules [10]. The forestry practices are carefully monitored by independent parties. Using certified wood is incredibly important to guarantee future supply of timber. Using sustainable harvested timber helps to protect forests, too.

2 Hardwood timber as a building material

2.1 Timber engineering, joints, connections

Ekki has proven nearly impossible to glue into engineered wood products for structural applications like Glued Laminated Timber (GLT) or Cross Laminated Timber (CLT). However, connections can easily be made using either (1) carpentry joints, (2) connections with mechanical fasteners such as screws, bolts, dowels, in combination with slotted in plates, too (Figure 2). In the design of connections, general rules set by the EN 1995 [11] are used, along with requirements set by national annexes. (3) Separate beams can be dowelled together to form a dowel laminated timber beam [11], like done in the largest span of 15 meters of the ‘Fietsen door de Heide’ bridge in Belgium (Figure 3). In practice, beams with a height of a little over 1 meter and lengths up to 25 meters are built using this technique, making it a easy way to build cyclist in and pedestrian bridges with medium spans, even for light traffic loads such as service vehicles even up to 16 tons.



Figure 2 dowelled connection



Figure 3: 15 meter span of the 'Fietsen door de Heide' with dowel laminated beams

2.2 Dimensions of timbers elements

Ekki can also be obtained from the trees in large dimensions. The timber is known to grow straight, containing only little number of irregularities like knots. A special case are the pillars of the 'Botterbrug' in Harderwijk which are 22 meters long and have a tapered diameter of 60 cm/80 cm (top/bottom) and are made out of one single trunk (Figure 4). These trunks were specially selected in the forest and transported in on single piece by road and sea, to the woodturner and then to the building site.



Figure 4: Illustration of the sizes of pillars used in the 'Botterbrug' in Harderwijk

2.3 Typical bridge typologies

Five construction types are typically identified in the timber bridge construction using ekki: the small bridge using straight beams up to about 8 meters. This is a bridge type that can be constructed in a modular way. Medium spans can be made using dowel laminated beams, up to lengths of about 20 meters, sometimes more. If even longer spans are required, the truss bridge can be used, until now used for lengths up to about 40 meters in bridges like the 'Pieter Smitbrug' and the 'Stönner Meijwaardbrug'. Large spans like these can also be covered using arch type structure or cable stay bridges. Amongst these is the earlier mentioned 'Botterbrug' in Harderwijk spanning a total of 76 meters, crossing the highway A28.

The main structure of each of the bridges of Ekki are unprotected from impact of rain and sun and are built into Service Class 3 in the EN 1995 [11]. Ekki bridges generally achieve service lives of 50 years if at least a minimal maintenance is performed. This has also been observed in sluice doors. Once the service life is reached, most of the structural elements can often be re-used in other structures. Due to the absence of chemicals that extend the longevity of the material, it is also naturally degradable and causes no harm to the environment.

3 Case studies

3.1 The 'Pieter Smitbrug'

The 'Pieter Smitbrug' with a length of 800 meters was the largest cyclist bridge in Europe at the time of its construction. It crosses a canal (Winschoterdiep), a highway (A7), a nature reserve, and a part of a lake 'Oldamstermeer' (Figure 5). It being a bridge of these dimensions makes it an exceptional example of how timber can be used to create infrastructure for pedestrians and cyclists using a renewable material, modular design, with outstanding end of life capabilities. Apart from connecting two smaller towns and thus creating an easy access of each other's education, commercial, and recreational facilities too, the construction of the bridge was also used to strengthen the local ecology. Trees were planted along the new bridge to encourage bats to cross the highway. Nesting boxes for birds were placed below the deck and lighting was especially selected that would not disturb wildlife at night. The bridge was designed for a service life of 80 years. This was achieved by protecting the main structural elements with ekki boards.



Figure 5: Aireal photo of the 'Pieter Smitbrug' along with a detail of the main span (above) and the main span and transport for the production site in Kampen to the building location by boat.

As the main span of the bridge crosses a highway, it was necessary to account for possible collision forces from traffic underneath the bridge [13]. According to the Eurocodes, this needs to be done once the bridge is less than 6 meters above the underlying road. In the Netherlands, this height is increased to 7 meters. These loads are in the order of 200 tons too. This led to the reinforcement of the lower chord of the truss structure with steel. The upper chord and the bracing were made of timber. The bridge was officially opened for use in winter of 2021.

3.2 The 'Stönner Meijwaardbridge'

The 'Stönner Meijwaardbridge' in Oirschot and has a total length of 240 meters. The truss bridge crossing the 'Wilhelminacanal' under an angle has a span of 41 meters and a width between parapets of 4 meters. It connects the town's neighbourhoods located south of the canal with the city center.

Although this bridge was not located over a highway or other road, collision loads had to be accounted for that originated from inland shipping traffic. This also meant that the lower chord of the truss structure had to be reinforced with steel. The upper chord and bracing could be carried out in timber. It still resulted in a slender and elegant bridge, which was officially opened for use in summer of 2020.

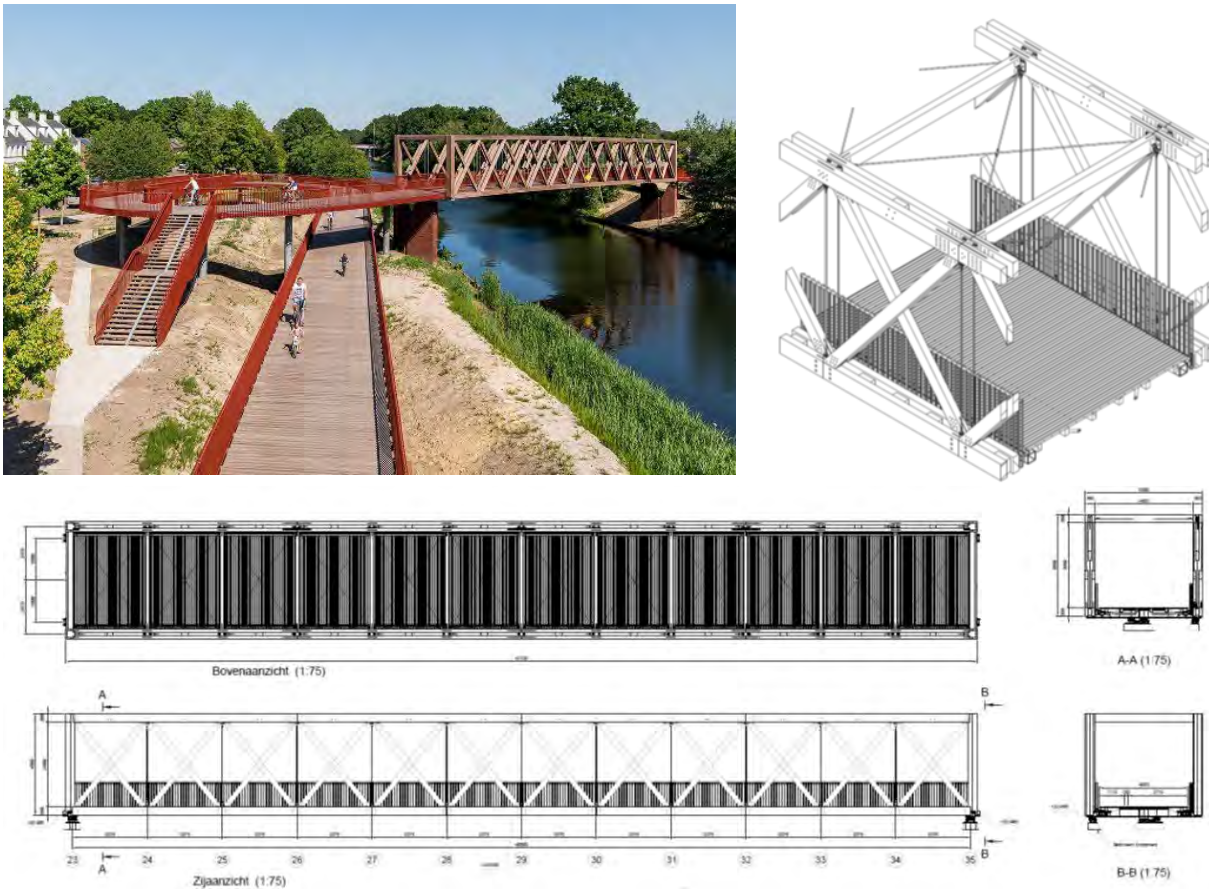


Figure 6: the 'Stonner Meijwaardbridge' (@JDFV, 2020) along with a cross section of the main span (above) and the top and side view of the main span (below)

3.3 Fietsen door de Heide

'Fietsen door de Heide' is part of a touristic cycling route through the national park 'de Hoge Kempen' near Maasmechelen in Belgium. The length of the bridge in this cycling route is almost 300 meters long and has a width between parapets of 3.5 meters. The bridge provides cyclists a look-out point over the moors in a region that is candidate for UNESCO world heritage site. The fine and regular structure of posts and supports refers to the region's long history of coal mines. The architects recently won a prize for its design on the International Design Awards in Los Angeles.

The parapets were made with softwood that was partially obtained from the local forest. The softwood was treated to increase its natural durability. The deck was made of prefabricated concrete elements, which span the distance between the timber supports of 3 meters. In the main span of 15 meters length crossing a road, dowel laminated beams were used to carry not only vertical loads, but collision loads from traffic too. Figure 7 shows a picture of the final bridge and an illustration of the bridges main load bearing system.

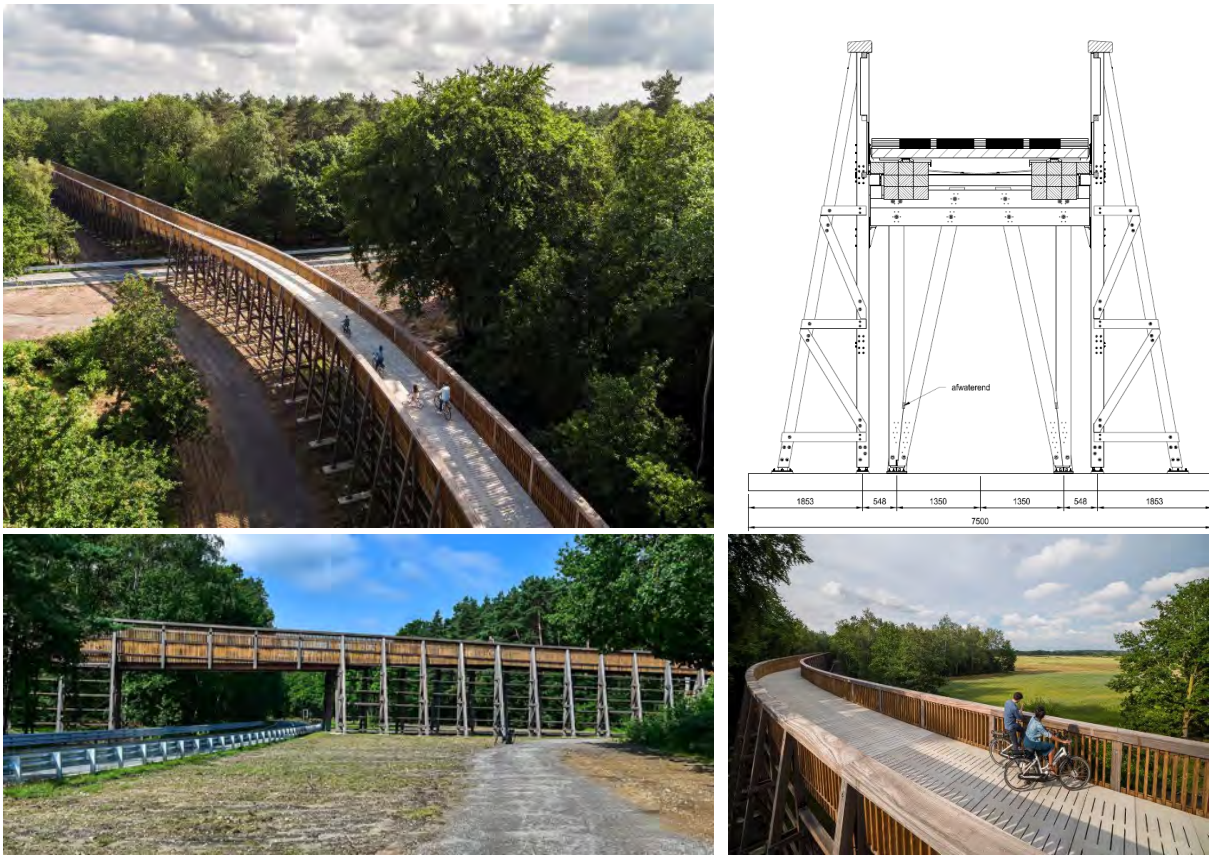


Figure 7: Aerial picture of the highest section of the 'Fietsen door de Heide' (@VisitLimburg) along with a detail of the supporting frames oft he main span (above) and a side view of the main span and the view from the highest point of the bridge (@VisitLimburg)

4 Conclusion

Building with a timber like ekki has offered -and will continue to offer- outstanding possibilities to easily build bridges in timber. Despite difficulties using adhesives so commonly used in engineered wood products, many different types of structures have been made. Design rules and building methods as described in the EN 1995 can be used to make truss structures, arch structures and cable stayed bridges. There are sustainable sources of the timber trough certified chains of supply. The presented case studies have shown that it is a flexible material that fits into a circular approach for modern timber bridge construction to sequester carbon in future infrastructure too.

5 Acknowledgements

The authors would like to acknowlegde the work of our former colleague at Wijma Kampen B.V. Peter Zanen, who was one of the main drivers to set up these highlighted projects within our company.

The authors would also like to thank the customers and project partners involved in these projects being Pieter Smitbrug: Povincie Groningen, gemeente Oldambt, Structon Civiel, Konijnklijke Oosterhof-Holman, NOL architekten, Machinefabriek Rusthoven, en Ohpehn advies en ingenieursbureau, for the Stonner Meijwaardbrug: Gemeente Oirschot, Ballast Nedam, West8, Bureau Waardenburg, wUrck, Wagemaker, Nauta Heeg, and HIG, and ‘Fietsen door de Heide’: Provincie Limburg, Besix, Maat Ontwerpers, Witteveen + Bos.



6 References

[1] Bleijenberg A, Instandhouding civiele infrastructuur, TNO 2021 R10440A, 2021
[2] Hegger S. en de Graaf D., Vergelijkende LCA studie bruggen, Beco, 2013
[3] Oosterhoff, J., Bruggen in Nederland 1800-1940, bruggen van beton, steen en hout, Nederlandse Bruggenstichting, ISBN 978-90-5345-103-8, 1998
[4] Kuilen, J.W. van de, Blass, H.J., Mechanical properties of azobe (Lophira alata), Holz als Roh-und Werkstoff 63, p. 1-10, 2005
[5] EN 1912 Structural Timber - Strength classes - Assignment of visual grades and species, Nederlands Normalisatie-instituut, Postbus 5059, Delft, the Netherlands, 2012
[6] NEN EN 338, Structural timber - Strength classes, Nederlands Normalisatie-instituut, Postbus 5059, Delft, the Netherlands, 2009
[7] NEN EN 350, Durability of wood and wood-based products – testing and classification oft he durability to biological agents of wood and wood based materials, Konijnklijk Normalisatie-instituut, Postbus 5059, Delft, the Netherlands, 2016
[8] Wiselius, S.I. (editor), Houtvademecum 10e druk: Eigenschappen en toepassingen van houtsoorten, 10th edition, Bim Media, ISBN-10 9012582164, 2011
[9] Holz-zentralblatt, Holzbruecke trotz Flut an der Ahr, 30 July 2021
[10] FSC, Principles and Criteria, fsc.org, accessed 4/4/2022.
[11] NEN EN 1995-1-1, Eurocode 5 - Ontwerp en berekening van houtconstructies - Deel 1-1: Algemeen - Gemeenschappelijke regels en regels voor gebouwen, Nederlands Normalisatie-instituut, Postbus 5059, Delft, the Netherlands, 2005
[12] Schelling W., Zur Berechnung nachgiebig zusammengesetzter Biegeträger aus beliebig vielen Querschnitten, in Ehlbeck,J.; Steck,G.: Ingenieurholzbau in Forschung und Praxis. Karlsruhe: Bruderverlag 1982. S.163-196
[13] NEN EN 1991-1-7+C1+A1/NA: Eurocode 1: Belastingen op constructies deel 1-7: Algemene belastingen - Buitengewone belastingen, Nederlands Normalisatie-instituut, Postbus 5059, Delft, the Netherlands, 2019

Conference Proceedings 4th ICTB (2022)
https://doi.org/10.24451/5hzv-kz55



The road to durable bridge design: An experience from Québec

Caroline Frenette [1]

1 Introduction

In Quebec, forests cover more than half of the province territory, representing over 900 000 km². 92% of these forests are on public land and, therefore, under the responsibility of the Quebec government for managing all activities, including forestry. Access to this forest territory represents 475 000 km of forest roads, and nearly 3 000 bridges. The majority of these forest road bridges, also called bridges on multi-use roads, span between 5 and 30 m [1].

Since these forest road bridges are not located on the public traffic road network, they are not governed by the standards of the Ministry of Transportation (MTQ) [2]. If they are built on public land, these bridges are under the responsibility of the Ministry of Forests, Wildlife and Parks (MFFP), and their design and evaluation must follow its specific regulations, adapted from Canadian Highway Bridge Design Code [3][4][5]. Most of these bridges are built by forestry companies to access the resource. Nonetheless, they may be utilized by various users during their lifetime.

For many years, a steel-wood bridge concept has been often used for this type of structure, due to its simplicity erection and economical aspect. This concept includes steel girders seating on a treated wood box foundation, and supporting treated wood crossbeams and a wood running surface, which can be treated or untreated depending on the context [6].

In the last 20 years, a new solution has been developed to replace the steel girders with locally produced glulam girders, taking advantage of a regional material with a low carbon footprint. These timber bridges are mostly made of straight glulam girders supporting treated wood crossbeams and a treated or untreated wood running surface. Since the beginning of 2000, more than 100 of these timber bridges have been built on the forest roads throughout Quebec [7].

Inspections of existing timber bridges have highlighted some durability issues, often related to discontinuous protection of the main glulam structure. In order to pursue the objective of promoting the use of wood in the realization of these infrastructures, work has been undertaken by the government, the industry and Cecobois to improve the initial concept and develop constructive solutions adapted to the Quebec context [7]. The challenge is to provide high quality glulam bridges that offer the desired structural resistance for a minimum life span of 40 to 50 years, while remaining economically competitive with the current steel-wood concept.

Last year, a technical working committee on the evaluation of the load-bearing capacity of timber bridges, bringing together specialists from the MFFP, the MTQ and the industry, has been set up to promote the development of adequate tools and the acquisition of knowledge regarding timber bridges in order to better understand their long-term behaviour.

2 Glulam forest road bridges

As discussed, more than 100 glulam forest road bridges have been built throughout Quebec since 2000. These timber bridges are mostly made of straight local glulam girders supporting treated wood crossbeams and a treated or untreated wood running surface (Figure 1).

To help the expansion of this innovative solution using local glulam, some issues needed to be addressed. Efficient prefabrication techniques have been developed to ensure the competitiveness of this solution, specific detailing has been proposed to avoid degradation of the glulam girders and limit maintenance, and a new evaluation methodology was established to simplify its design.

[1] Caroline Frenette, Professor, Université du Québec à Rimouski, Canada, Caroline_Frenette@uqar.ca



Figure 1: Dalime Bridge - Manufacturing: Nordic Structures – Photo credit: Adrien Williams

1.1 Local glulam

The majority of glulam produced in northern Quebec is made from Black Spruce. This specie is known for its high density and fibre strength, as well as its limited diameter, thin annual rings and small knots. In order to optimize this raw material, a proprietary product, NordicLam, is manufactured by laminating small sections in both directions (Figure 2).

Despite its high strength, black spruce is difficult to treat with chemicals due to the closing of the pit chambers during drying. Therefore, the durability of the infrastructures made with black spruce glulam relies mainly on good design and manufacturing details to avoid the presence of moisture, as well as on effective finishing products to protect the wood against rain and UV rays.



Figure 2: Glulam made of local black spruce (picea mariana) (credit: Nordic Structures)



1.2 Efficient prefabrication techniques

The fabrication and assembly of glulam forest bridges were optimized in order to be economically competitive. Concepts favouring the pre-assembly of girders in groups of 2 or 3 allow efficient connections between the girders and the diaphragms, a fast and easy construction process, as well as an easier installation of a waterproofing protection on top of the girders (Figure 3).

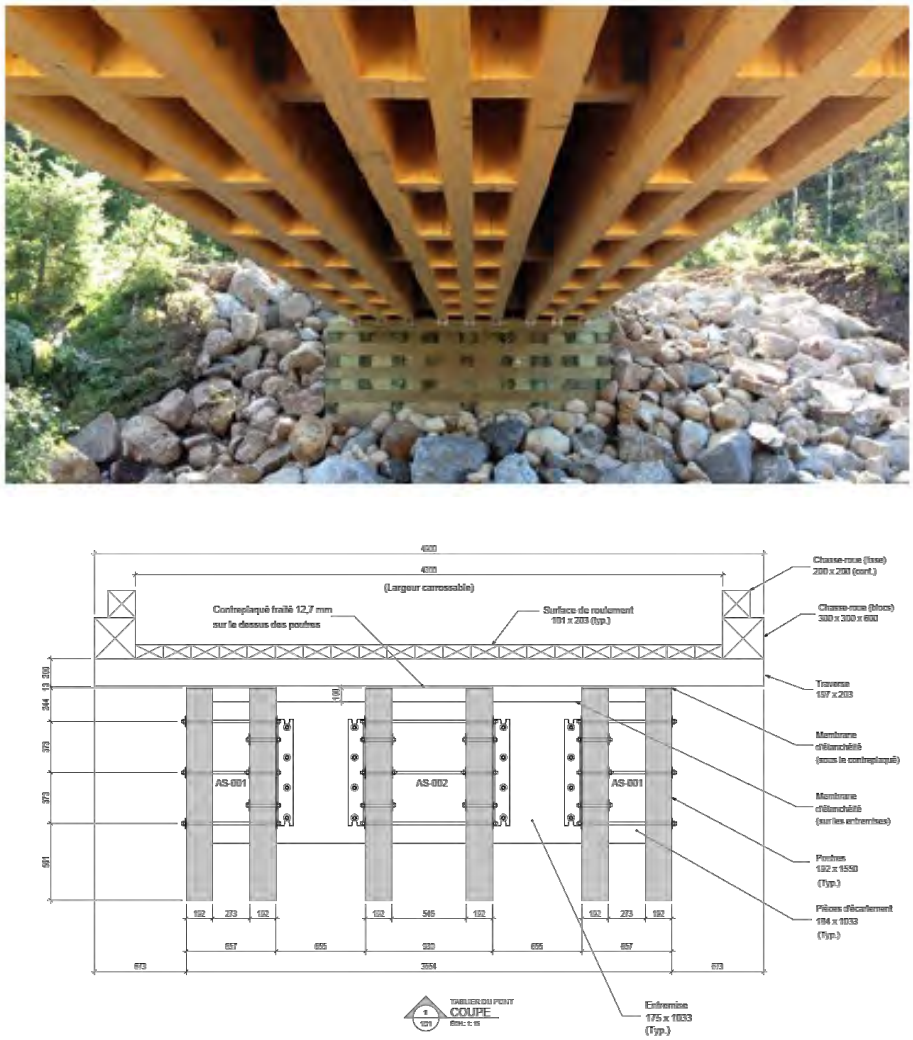


Figure 3: Concept with pre-assembled glulam girders (credit: Nordic Structures)

1.3 Detailing for durability

Several old covered bridges, still in service, demonstrate the durability of timber bridges [8]. Although loads and uses have changed over time, the basic principles of durability have allowed these infrastructures to be in service for years, some for more than a century. Today, without necessarily using a full-bridge cladding, these principles can be used to ensure the durability of modern timber bridges.

In the case of the forest road bridges built in Quebec, the impossibility of chemically treating the local spruce glulam girders requires the development of effective protection solutions. Moreover, maintenance of the bridges built on public land represents a challenge. Firstly, these bridges are often very remote, they can be few hundred kilometres from the nearest town. Secondly, the maintenance of these bridges is under the responsibility of the users, who may change during the lifetime of the bridge. For example, a new bridge may be built to provide access to a new logging area. A few years later, it is no longer required by the forestry company, and remains in place for other users, such as cottagers or hunting and fishing associations.



This particular context explains the importance of providing efficient durability detailing anticipating the possibility of irregular maintenance service. In 2020, Cecobois wrote a guide on the durability of timber bridges in order to present design details that would promote the durability of these glulam forest bridges [7]. In collaboration with several specialists from the government and the industry, design and fabrication details were developed to provide adequate protection of the glulam structure against frequently observed sources of moisture, such as frequent exposure of the edge girders to rain and accumulation of wet sand at the footings.

These recommendations had to consider the use of a semi-waterproof wood deck over the main structure and the impossibility to add a waterproof bituminous surface on these remote bridges. Nonetheless, the continuity of the deck, a sufficient overhang over the side girders and a watertight and durable protection above each girder showed to be efficient to ensure the protection of the girders. In addition, a flashing to protect the end-grain of the crossbeams was recommended. Various solutions were also presented to protect the support of the glulam girders, including the use of a nylon pad to raise the support and prevent rising moisture as well as the extension of the running surface on top of the abutments to prevent the passage of debris.

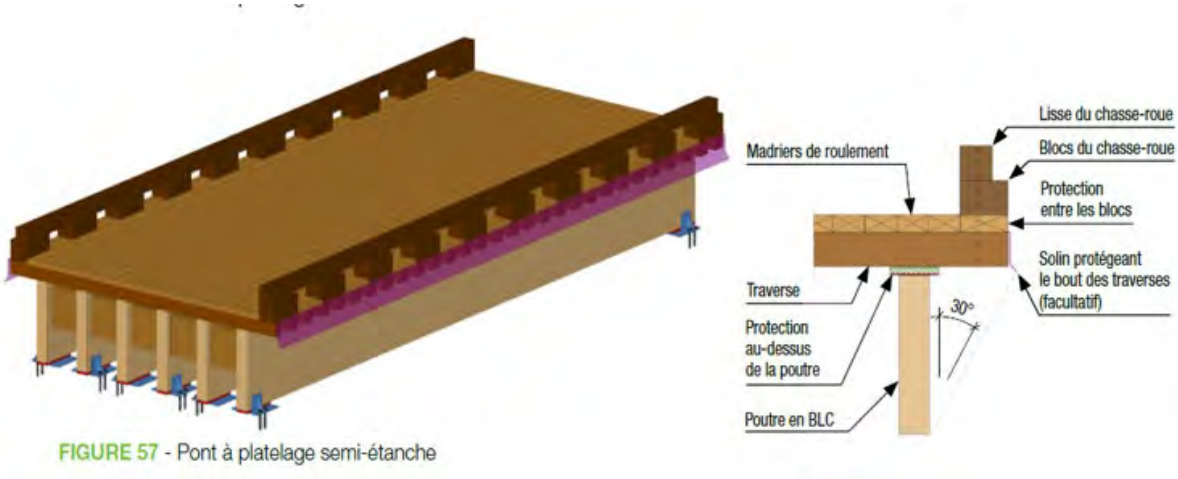


FIGURE 57 - Pont à platelage semi-étanche

Figure 4: Examples of detailing for protection [7]

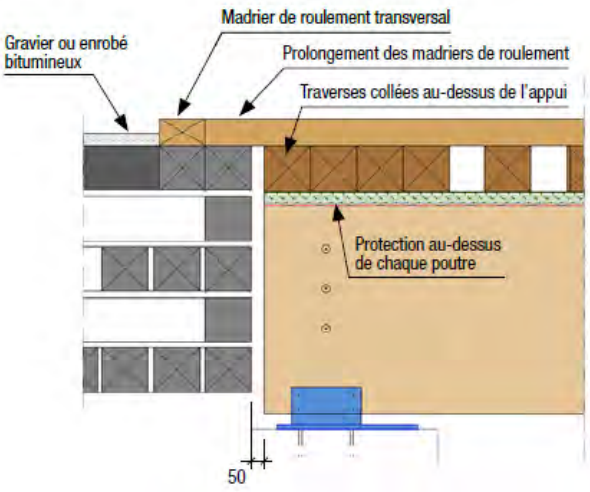


Figure 5: Continuity of the decking to prevent debris accumulation [7]

A new bridge was built recently respecting the recommendations of the Cecobois guide, including the use of a dark opaque finishing product to protect the wood against rain and UV and flashing to provide a 30° angle protection to the main glulam side girders (Figure 6).



Figure 6: Rivière Tachereau Bridge - Manufacturing: Nordic Structures – Photo credit: Stéphane Routhier

1.4 Realistic evaluation methods

As discussed previously, a technical working committee on the evaluation of the load-bearing capacity of timber bridges was created to bring together specialists from the MFFP, the MTQ and the industry. During the work of this technical committee (which is still ongoing), a new evaluation analysis method is being developed to allow a simplified but more representative analysis of forest bridges with glulam girders [9]. This evaluation method would be more adapted to these bridges than the simplified analysis method provided by the Canadian Highway Bridge Code [5], while being less complex than a 3D FEM model.

The proposed evaluation method is performed in two steps: first, a longitudinal analysis and then a transverse analysis. The longitudinal analysis consists in determining the effects produced by a truck load on a lane by treating the bridge as a group of parallel beams. Once the highest load configuration is obtained, the transverse analysis associates the effects of the longitudinal analysis to each girder by considering the transverse distribution of the forces. This distribution considers the flexibility of the glulam girders supporting the deck as spring supports (Figure 7).

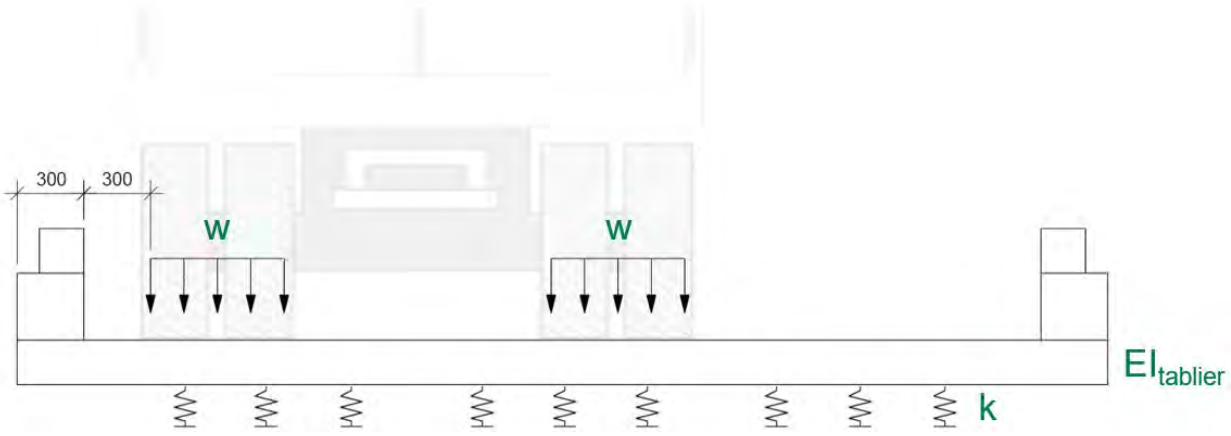


Figure 7: Modelling of the deck as a beam supported on spring supports [9]

3 Glulam traffic road bridges

In addition to the forest road bridges discussed in this paper, few traffic road bridges have been built in Quebec, and are monitored by the Ministry of Transportation (MTQ) [10]. For these bridges, the glulam structure is protected by a waterproof layer and a bituminous rolling surface. Exceptional timber bridges, such as the 160-meter four span Mistissini bridge built on the Cree nation land in Northern Quebec, also show in opportunities of timber bridges in Canada (Figure 8) [11].

In 2017, the Ontario Wood Bridge Reference Guide provided guidance for the design of timber bridge in the Ontario Province and highlighted the need to update the Canadian Highway Bridge Code regarding new technologies in timber bridges [12]. Since then, an active committee has been working on the section 9 of the Canadian Highway Bridge Code to update this section [13].



Figure 8: Mistissini Bridge - Design: Stantec - Manufacturing: Nordic Structures - Photo credit: Stéphane Groleau

4 Conclusion

The construction of glulam bridges appeared in Quebec's forests in the early 2000s and since then, more than 100 bridges using this material have been built on public forest roads throughout Quebec.

A collaborative effort between government and industry specialists has resulted in the development of constructive solutions to ensure future use and longevity of this bridge concept using local black spruce glulam girders.

5 Acknowledgement

The author would like to acknowledge the financial and technical contribution of the government of Quebec, Ministry of Forests, Wildlife and Parks (MFFP) and Ministry of Transportation (MTQ), as well as Nordic Structures, Hexaki, FPInnovations and Cecobois.



6 References

[1] MFFP (2021) Ressources et industries forestières - Portrait statistique 2020, Ministère des Forêts, de la Faune et des Parcs, Québec. Canada. ISBN (PDF) : 978-2-550-90470-0

[2] MTQ (2020). Manuel de conception des structures, Gouvernement du Québec, ministère des Transports, 452 p.

[3] MFFP (2021) Guide d'application du Règlement sur l'aménagement durable des forêts du domaine de l'État, Gouvernement du Québec, ministère des Forêts, de la Faune et des Parcs. https://mffp.gouv.qc.ca/RADF/guide (Consulté 1er décembre 2021)

[4] MFFP (2020) Norme relative aux ponts et aux ouvrages amovibles dans les forêts du domaine de l'État. Gouvernement du Québec, Ministère des Forêts, de la Faune et des Parcs. 11p.

[5] CSA (2019) S6-19 - Canadian Highway Bridge Design Code, Mississauga, Groupe CSA, 950 p.

[6] MTQ (2017). Manuel d'évaluation de la capacité portante des ponts acier-bois, Gouvernement du Québec, ministère des Transports, de la Mobilité durable et de l'Électrification des transports (MTMDET), 154 p.

[7] Cecobois (2020) Guide sur la durabilité des ponts en bois, Centre d'expertise sur la construction commerciale en bois (cecobois), 44 p.

[8] Arbour G. Caron F. et Lefrançois J. (2005). Les ponts couverts au Québec, ministères des transports, Publications du Québec, ISBN : 978-2-551-19636-4. 244 p.

[9] Tahri H, Dumont LP and Frenette C (2022) Rapport technique sur les méthodes d'évaluation de la capacité portante des ponts forestiers en bois. Comité de travail technique sur l'évaluation de la capacité portante des ponts en bois pour Ministère des Forêts, de la Faune et des Parcs. 35 p.

[10] MTQ (2011). Pont Albanel (p-11826) - Structure en bois lamellé-collé de type « NORDIC LAM » performance in situ rapport final, 186 p.

[11] Lefebvre D (2017) Conception d'un pont en bois de 160 mètres de longueur à Mistissini, Québec

[12] CWC (2017) Ontario Wood Bridge Reference Guide. Prepared by Moses Structural Engineers and Brown & Co. Engineering Ltd. for the Canadian Wood Council and the Ontario Ministry of Natural Resources and Forestry. 242 p.

[13] Lehan A and D Moses (2022) Setting the Standard – Advancements in Wood Bridge Design in the Canadian Highway Bridge Design Code. 4th international conference on Timber Bridges. Switzerland.

Conference Proceedings 4th ICTB (2022)
https://doi.org/10.24451/ctzc-yb11

ICTB 2021 PLUS
4th International Conference on Timber Bridges
Biel/Bienne, Switzerland, 9 -12 May 2022



Design, construction and maintenance of structurally protected timber bridges

Antje Simon[1], Markus G. Jahreis, Johannes Koch

1 Introduction

Timber construction is experiencing a renaissance due to the current debate on sustainability and decarbonisation. However, developments in timber bridge construction have been declining for years. Since 2008, when a timber footbridge collapsed in North Rhine-Westphalia, timber bridges have seldom been built in Germany. This damage and numerous other unprotected timber bridges that were improperly planned and built have caused considerable image loss for timber bridge construction.

Using timber as a structural material is a matter of conviction as well as responsibility. An increased application of this ecological and sustainable material should be supported and promoted in bridge construction. For the planning and construction of new timber bridges, it is a basic requirement to provide technical standards that are state of the art. In Germany, comprehensive guidelines are available for the construction of bridges made of reinforced concrete, prestressed concrete, steel and steel-concrete composite. These rules were developed and will be continuously updated by the Federal Highway Research Institute (BASt). A comparable rulebook does not exist for timber bridges. Thus, bridges made of this sustainable material have a considerable competitive disadvantage. The research project ProTimB was initiated in 2016 to rectify that shortfall. Initial results of the project were presented at the ICTB 2017 [1], [2]. The project was concluded in 2019 [3]. This paper presents the results of the research project.

2 The research project ProTimB

2.1 Overview

Technical guidelines guarantee professional state of the art design and construction standards. On the one hand, waiving the rules opens a comprehensive field for creativeness. On the other hand, the risk of serious mistakes in design and construction may rise enormously as a consequence. Especially for timber bridges, insufficient weather protection for the wood can often be identified as a problem. Also, the planning effort increases when details that could actually be standardised have to be newly developed for every new project. Therefore, the research project ProTimB aimed to define standards for structurally protected timber bridges following the generally accepted sets of rules for other materials. The project focused on protected bridges, because the long-term durability of timber bridges can only be achieved by using structural protection measures consistently in all stages of planning, construction and service life.

The outcome of the project is a set of technical guidelines for the design, construction and maintenance of protected timber bridges (Figure 1). Formally, it is inspired by the existing sets of rules for other materials to facilitate their application in practice. The design rules consist of references for planning, samples for structural analysis and 36 new sample drawings (MuZ-HolzBr) [4]. “Recommendations for technical contractual terms for timber bridges (ETV-HolzBr)” have been developed for construction [5]. Regarding maintenance, sample handbooks for the maintenance and inspection of timber bridges and recommendations for object-related damage analysis (OSA-HolzBr) have been compiled. Furthermore, an advanced training course has been conceptualised for timber bridge inspectors. Additionally, nine protected timber bridges crossing rivers were comprehensively monitored [6]. The most important guidelines will be presented in the following. For further details see [3].

[1] Antje Simon, Professor for Timber Construction, University of Applied Sciences Erfurt, Germany, antje.simon@fh-erfurt.de

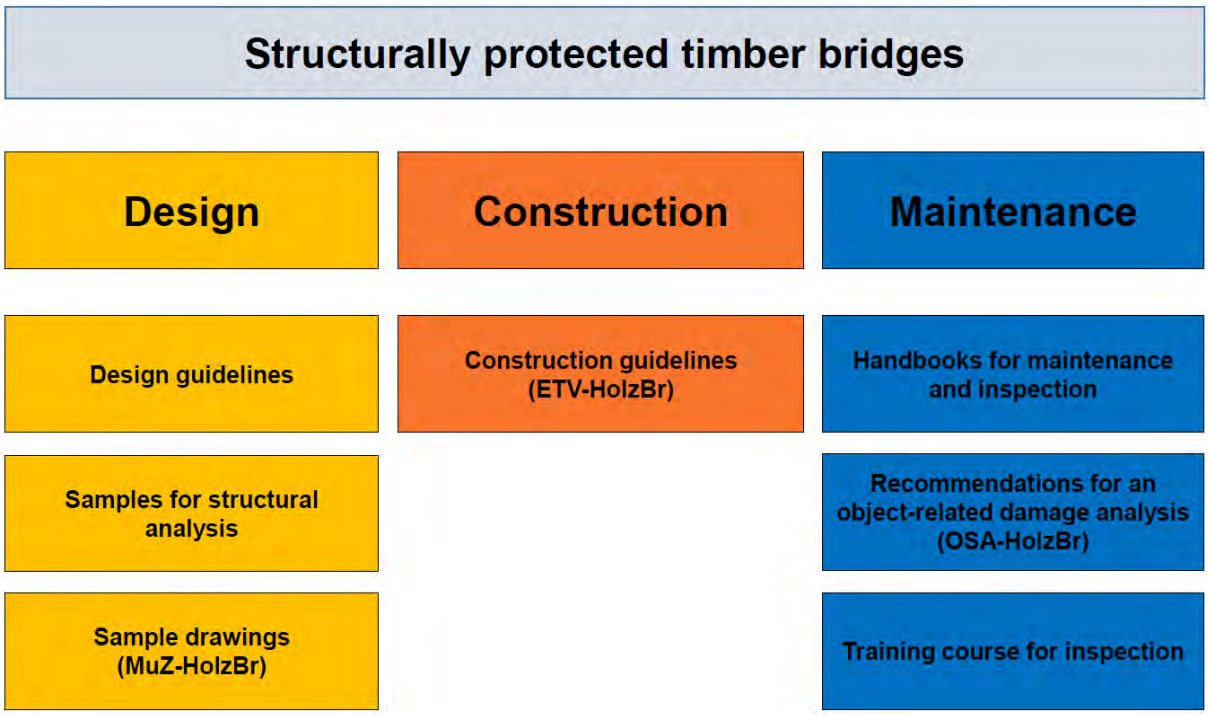


Figure 1: Overview of the new guidelines und project results

2.2 Guidelines for design

The most important document for the design of timber bridges is a set of new sample drawings [7]. Based on formerly developed drawings [8] and [9], it updates and extends them. The 36 drawings show durable and proven solutions for special structural details (Table 1). They are closely related to the familiar drawings (RIZ-Ing) of the Federal Highway Research Institute (BASt).

Table 1: Content of the new sample drawings for protected timber bridges

Drawing	Content
H-Belag 1-4	Variants of pavement and their mounting (closed surfaces as asphalt sealings, concrete- and natural stone slabs and open surfaces using wooden planks)
H-Dicht 1-3	Design of sealings for the timber-superstructure
H-Gel 1-5	Variants of parapets and their fastening
H-Kap 1-2	Mounting of concrete caps on timber structures
H-Lag 1-3	Details for bearings
H-Schutz 1-8	Structural protection measures (covering, cladding, ventilation distances, protrusion)
H-Trog 1-2	Design of cross frames and bracing structures for trough bridges
H-Übe 1-4	Transition structures and expansion joints
H-Was 1-3	Details for drainage and dewatering
H-Zug 1	Accessibility of substructure

Figure 2 shows examples of the drawings explaining the structural protection measures.

ICTB 2021 PLUS
4th International Conference on Timber Bridges
Biel/Bienne, Switzerland, 9 -12 May 2022

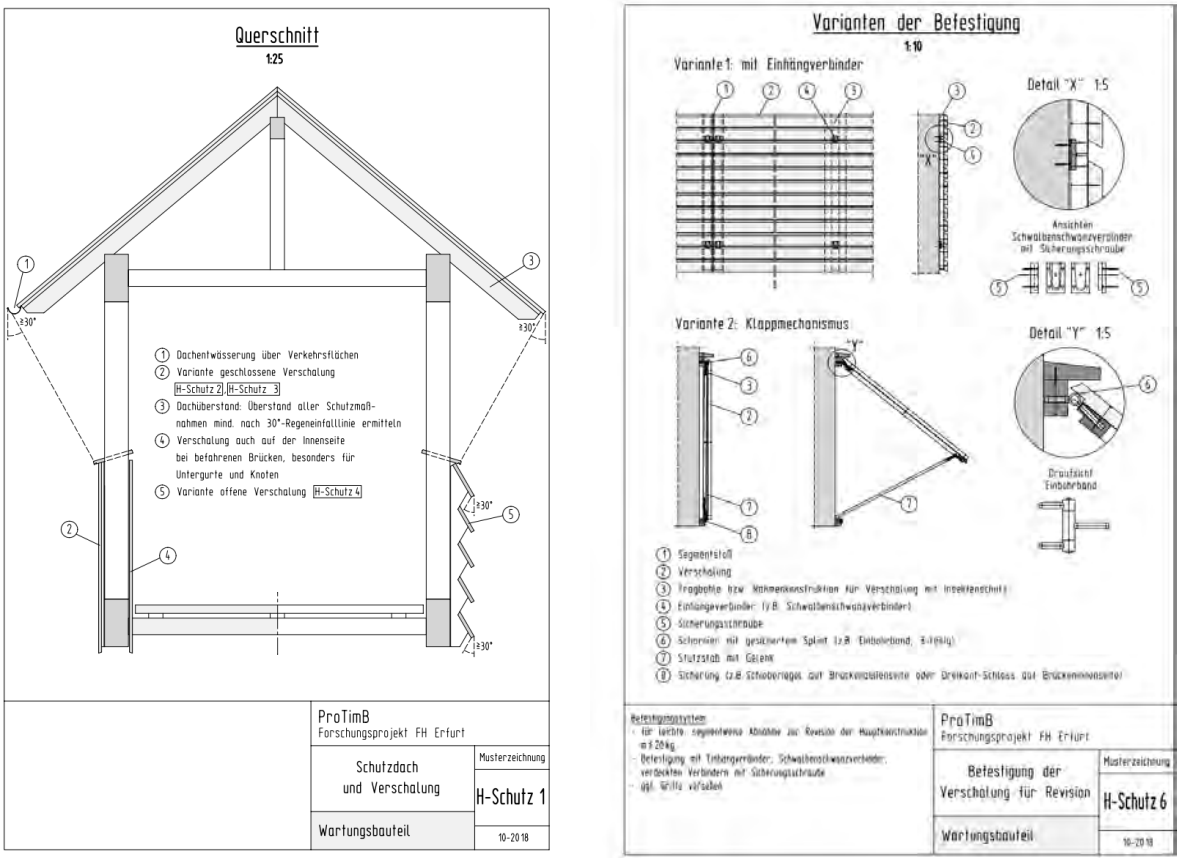


Figure 2: Examples of the new sample drawings regarding structural protection

In addition to the drawings, supplements for the technical design documents are recommended. The appropriate wood species and necessary structural protection measures have to be planned and documented for every single timber member based on their use class according to EN 335 [10] and DIN 68800-1 [11] as shown in Figure 3. Furthermore, it is advisable to plan a monitoring system for every new bridge to recognise structural defects in time. This recommendation has already been implemented in the new European code for timber bridges [12]. Also, the new annex D of EC5-2 showing sample drawings is inspired by the results of the ProTimB project. Samples of structural analyses for simple deck and trough bridges complete the design guidelines.

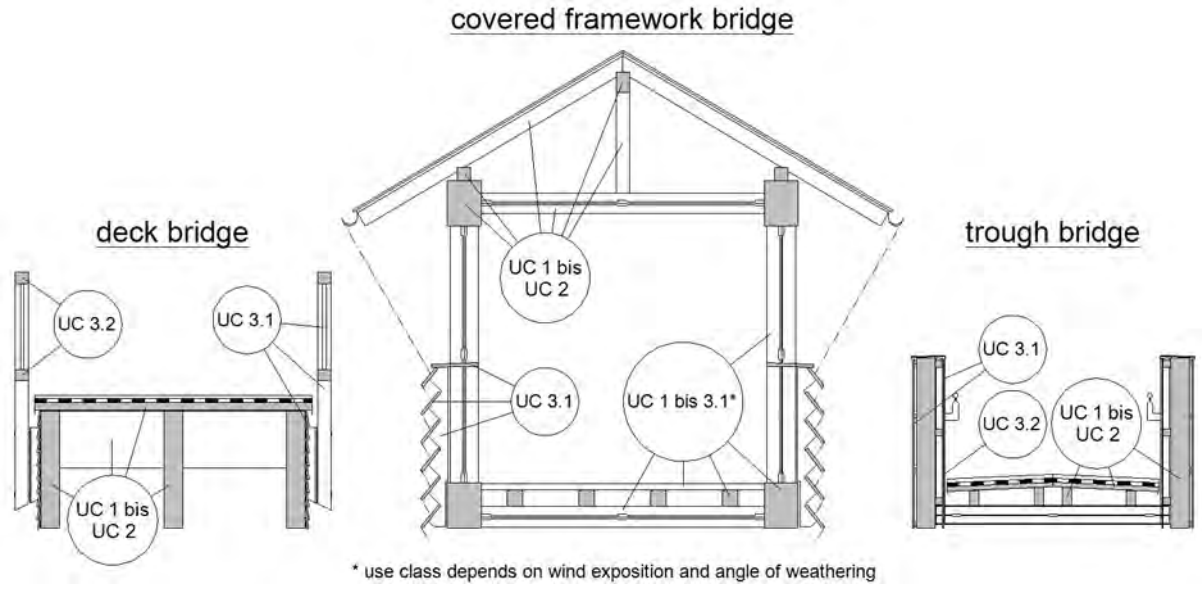


Figure 3: Assignment of timber members to use classes (UC) in different exposure situations



2.3 Guidelines for construction

"Recommendations for technical contractual terms for timber bridges (ETV-HolzBr)" have been developed for construction [5]. This document defines basic material requirements for the timber, engineered wood products, thermally and chemically modified wood, adhesives and steel members. Requirements are provided for minimum dimensions, surface qualities and limits for deformation due to shrinkage and swelling. The production, storage, delivery, quality control and assembly of structural timber members are regulated. Due to quality control, the recommendations define limits for dimensional and moisture tolerances, cracks and surface qualities at the factory and at the construction site. Furthermore, they contain necessary measures to be taken for structural timber protection and the corrosion protection of steel members in timber bridges. It is the first time that recommendations for the design and construction of timber-concrete composite bridges have been listed in a German guideline. Minimum concrete strength and variants of effective connections are defined. Information is given on the service classes and limits for temperature and moisture variation for the correct calculation of hygroexpansion. Suggestions for the design of wildlife bridges with a special focus on sealing and covering layers complete these guidelines.

The guidelines and drawings are available via the website of the University of Applied Sciences Erfurt and the quality association for timber bridges (Qualitätsgemeinschaft Holzbrückenbau).

2.4 Guidelines for maintenance

In Germany, bridge inspection is strictly regulated. Supervision consists of checks and inspections in regular cycles. Every bridge has to be visited twice a year and checked once a year. Additionally, the basic inspection and main inspection have to be performed alternately every three years. The main inspection requires a hands-on check of every structural member and is therefore the most complex and expensive one. Checklists have been developed for annual bridge inspection so that the corresponding road maintenance authority can work effectively (Figure 4). Additionally, a sample handbook for inspection has been written for special types of timber bridges such as framework bridges, cable-stayed bridges or bridges for wildlife. It recommends useful measurement methods and contains special hints for organisation, accessibility, documentation and traffic security during the inspection. Regarding individual structural characteristics, the regular inspection of every timber bridge can be optimized and performed economically using this handbook. If a regular inspection reveals complex damage of unclear cause or unclear dimension of defects, further recommendations are given for the implementation of an object-related damage analysis. This elaboration has been integrated into the guidelines of the BASt and the software for the documentation of bridge inspections.

Bridge Check

Bridge number: …… Road number: ……
Bridge title: ....……..

Occasion: □ yearly check □ after flood
□ after accident □ storm damage
□ others: ……..……..

Date …… Checked by ……..……..

The following aspects have been checked:
□ All structural protection members are intact and functional (covering, sealings, claddings…).
□ All accessible members have been checked for moisture (marks of running water, timber with earth contact, growth of moss and algae…).
□ The timber moisture content has been measured in damp and vulnerable areas.
□ All accessible members have been checked for wood-destroying fungi, mycelium and starting rot.
□ All accessible members have been checked for wood-destroying insects.
□ Protruding connectors have been observed (screws in planks, dowels in knot areas…).

The following changes / damages / moisture content values have been detected:
…….....
The following maintenance measures are necessary:
…….....
…….....

Signature: ……..

Figure 4: Checklist for annual bridge checks



Respecting the principles of structural protection for durable timber bridges is mandatory but not sufficient. Their intended service life of 100 years can only be achieved in combination with regular maintenance. In ProTimB a sample handbook for maintenance has been developed. It explains all useful service measures, their necessary intervals and required technical equipment as well as means of access to facilitate economical maintenance. Service measures include:

- the cleaning of the superstructure, benchings, road surface, bridge drains and drainage channels,
- the removal of vegetation all around the bridge in a radius of at least 2 m,
- the renewal of coatings, sealants, joints,
- the repair of planks, asphalt layer, claddings, cover plates and parapet members.

For every measure, an interval is recommended, taking the structural element's service life and seasonal weathering and pollution into account.

Responsible inspection of timber bridges requires specialist knowledge about the special anisotropic, organic material timber und substantial experience in inspection practice. Bridge inspectors are seldom experts on checking timber bridges because most of the bridges they regularly inspect consist of concrete, brickwork or steel. To familiarise those engineers with the special challenges of timber bridge inspection, a certified advanced training course has been developed.

Besides writing the guidelines, a monitoring system has been installed within the ProTimB project to supervise the development of timber moisture content. It was planned, executed and evaluated at nine protected timber bridges crossing waters in Germany [6]. The bridges demonstrated a timber moisture content lower than the critical 20 mass% for fungal growth. These results prove that the structural protection of timber bridges enables long durability. Critical moisture content values were measured temporarily at two bridges, caused by a defective expansion joint and a special weathering exposition. In both cases, the bridge owners were informed immediately. As a result, they were able to repair the defect and to improve structural protection to prevent serious consequential damages. Providing such a benefit, the monitoring of moisture content at every new timber bridge is highly recommended for at least five years after their construction.

3 Conclusion and View

The new design and construction guidelines are basic regulations for the state of the art planning and construction of durable, aesthetic timber bridges. They formally follow the existing set of rules for concrete and steel and have been provided in a user-friendly format to facilitate their use in practice. Existing competitive disadvantages for timber as a structural material should be repealed by using the research results.

The research has also influenced the updating process for timber bridge code EN 1995-2. In the new code, regulations for structural protection and durability will be significantly extended. Drawing examples for detailing will be contained for the first time in a structural code.

Due to their ecological and sustainable advantages, a significant increase in the market for timber bridges is to be expected in Germany. Aesthetic, well-protected and durable timber bridges of a high-quality standard should characterise our landscape in the future.

4 Acknowledgement

The new guidelines for protected timber bridges were developed within the research project "Protected Timber Bridges (ProTimB)". The research has been supported and funded by the Federal Ministry of Education and Research of Germany, the companies of the Qualitätsgemeinschaft Holzbrückenbau e. V. (Schaffitzel Holzindustrie GmbH + Co. KG, Schmees & Lühn Holz- und Stahlingenieurbau GmbH, Grossmann Bau GmbH) and Setzpfandt Beratende Ingenieure GmbH & Co. KG. The authors thank all partners and supporters for their technical and financial support.



5 References

[1] Simon, A.; Jahreis, M.; Koch, J.; Arndt, R. (2017) New design guidelines for structural protected timber bridges. ICTB 2017, Skelleftea, Sweden

[2] Koch, J.; Arndt, R.; Simon, A. (2017) Moisture monitoring of nine protected timber bridges in Germany. ICTB 2017, Skelleftea, Sweden

[3] Simon, A.; Arndt, R.; Jahreis, M.; Koch, J. (2019) Entwicklung einheitlicher Richtlinien für den Entwurf, den Bau, die Überwachung und Prüfung geschützter Holzbrücken – Protected Timber Bridges (ProTimB). Final research report. University of Applied Sciences Erfurt, Germany

[4] Simon, A.; Jahreis, M.; Koch, J.; Arndt, R. W. (2020) Moderne Holzbrücken planen, bauen, erhalten - Teil 1: Bauwerksentwurf. Bautechnik 97 (2020), Heft 02, Ernst & Sohn, Berlin.

[5] Simon, A.; Koch, J.; Jahreis, M.; Arndt, R. W. (2020) Moderne Holzbrücken planen, bauen, erhalten - Teil 2: Bauausführung und Erhaltung. Bautechnik 97 (2020), Heft 02, Ernst & Sohn, Berlin.

[6] Koch, J.; Simon, A.; Jahreis, M. (2022) Effectiveness of structural protection measures for timber bridges – results of long-term moisture monitoring. ICTB 2021 plus, Biel, Switzerland

[7] Informationsdienst Holz [Hrsg.] (2019) Musterzeichnungen für Holzbrücken, holzbau handbuch Reihe 1, Teil 9, Folge 3.

[8] HARRER Ingenieure (2006) Musterzeichnungen Holzbrücken.

[9] Qualitätsgemeinschaft Holzbrückenbau (2012) Detailzeichnungen Holzbrücken, März 2012.

[10] EN 335 (2013) Durability of wood and wood-based products – Use classes: definitions, application to solid wood and wood-based products

[11] DIN 68800-1 (2019) Wood preservation – Part 1: General

[12] prEN 1995-2 (2022) Eurocode 5 - Design of timber structures – Part 2: Bridges. Final document 19/01/2022

Conference Proceedings 4th ICTB (2022)
https://doi.org/10.24451/dwve-0996

ICTB 2021 PLUS
4th International Conference on Timber Bridges
Biel/Bienne, Switzerland, 9 -12 May 2022

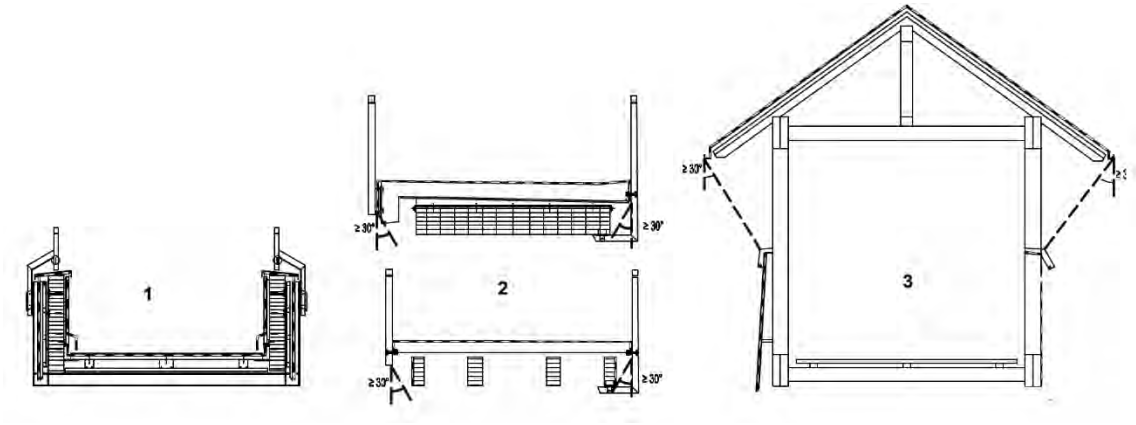


Robust Timber bridges without cladding

Frank Miebach[1], Germany

1 Introduction

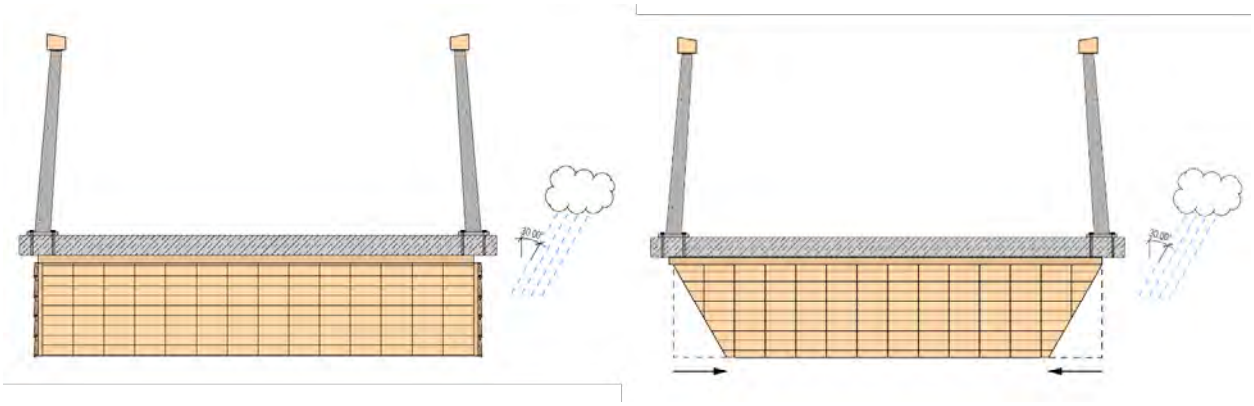
Concerning the Eurocode 1995-2 for timber bridges the preferred design should be dimensioned for a lifespan of 100 years. That means, that only timber bridges with protection are possible and allowed. Hereby the focus is put on constructive elements to ensure a protected bridge:



2 Examples for modern bridge designs without cladding

An easy and well known method of protection are claddings on top and the side areas of a construction. If you put a roof on top you get the so called “covered bridge”.So an additional element guarantees a water drainage against weathering. In the regulation of the EC 1995-2 is now introduced a fix angle for weathering with 30° out of the vertical line, so all elements behind this line can be seen as protected.

This leads to the simple idea to create new bridge designs without cladding – but with waterproof pavement on top. So a pavement function like a roof, and gives enough overhang for the structure.



So different designs could be realized in the last years:

[1] Frank Miebach, Dipl.-Ing. (FH), Founder Ingenieurbüro Miebach, Germany, info@ib-miebach.de



Figure 1: Bridge – Schwäbisch Gmünd (GER) - 2012

2012: First time while stepped geometry follows a 30° angle for protection. Also innovative: waterproof pavement with huge granite plates and transversal gutters



Figure 2: Bridge – Neckartenzlingen (GER)

2017: Dominance of 30° rule follows function: first time with 2m high horizontal beams for bloc glued timber. Covering by overhanging prefab concrete slabs on top.



Figure 3: Bridge – Wangen/Allgäu (GER)



2020: efficient bridge Solution with parallel beams spans over 30m – covered with asphalt on top.



Figure 4: Bridge – Schäftersheim (GER)

2022: Solution for a timber concrete composite (TCC) bridge – also with stepped concrete plate



Figure 5: Bridge – Engelskirchen (GER)

2020: continuous stepped bloc glued beam with horizontal curvature

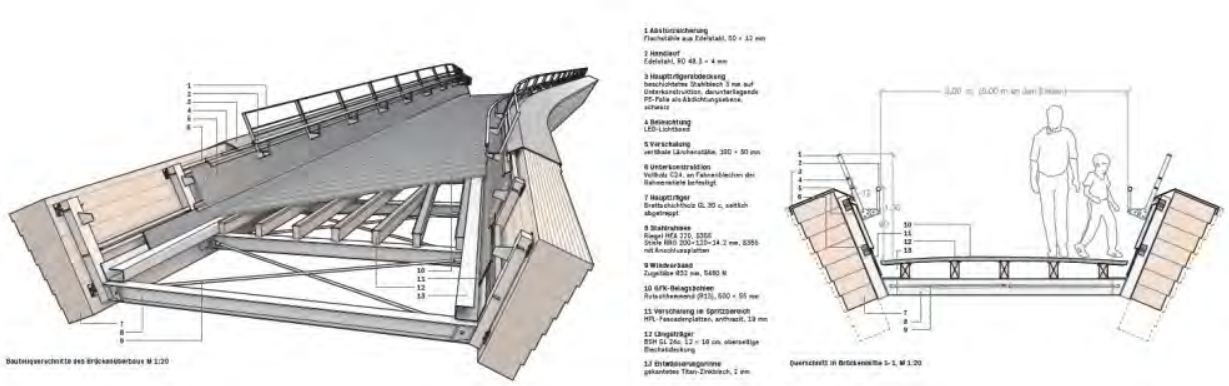


Figure 6: Bridge – Balingen (GER) © *moxon architects*

2022: asymmetric, double twisted beam tilted in 30° line – promising design for through bridges



Figure 7: Bridge – London (UK)

Competition design: arch bridge with cladding on top and interior – without cladding from the outside view



Figure 8: Bridge – Frankenberg (GER)

2022: Form follows static impact: timber design without cladding with correlating overhang of the concrete slabs.



Figure 9: Bridge over motorway A1 Paris (FR) *© exploration architecture, Paris*

In process: solid glulam structure well protected – and with fire resistance for over 120 minutes



Figure 10: competition Bridge – Kinding (GER)

Competition design: under tensioned beam in neighborhood of a historical roman stone bridge

3 Conclusion

The designing of timber bridges without a side cladding bings enormous benefit even for presenting the carrying structure. In the dialog with architects and clients the absence of claddings are perceived very positively, and it gains the possibility for better controlling of the construction. So we see the added value that timber can be demonstratively shown and is given better conditions, especially in competition with other materials.

Important note: the angle of 30° is not valid for all situations! Sometimes a higher value is strongly recommended – in relation to the climate conditions (especially wind driven rain) on site.

Conference Proceedings 4th ICTB (2022)
https://doi.org/10.24451/ra4b-hy72

ICTB 2021 PLUS
4th International Conference on Timber Bridges
Biel/Bienne, Switzerland, 9 -12 May 2022



Structural Rehabilitation of a Historic Covered Bridge: Bridgeport Covered Bridge

Lawrence E. Jones[1], S.E., Brian S. Wiens, S.E.

Abstract

The Bridgeport Covered Bridge was constructed in 1862 by David Inglefield Wood of the Virginia Turnpike Company as a major toll road to support the development of the Comstock Silver Lode across the Sierra Nevada Mountains in western California. The bridge has a substantial span of 63.4 meters (208 feet) over the South Fork of the Yuba River in Nevada County, California. It utilizes a Howe Truss fitted with a supplementary timber arch chord on either side of each main truss. The span has the distinction of being the longest remaining single-span covered bridge in the United States.

After providing a temporary structural stabilization design in 2013, Buehler began the full structural rehabilitation design of the bridge which both maintained the historical nature and detailing of the bridge while also making discrete structural improvements to allow the bridge to continue to be a historical resource for the State of California for many years to come.

1 Introduction

The resiliency of architecture and structure are exemplified by the historic style and nature of a wood covered bridge. Throughout the United States, the expansion of settlers moving west in the 1800s necessitated the development of roads and rail links to connect people and supply chains to the areas of commerce and development. No stranger to these endeavors were the bridge builders of that time who coupled the experience and ingenuity of predecessor projects, civil engineers, and patents, domestic and abroad, to create these vital links built to stand the test of time.

This paper is intended to highlight the history of the Bridgeport Bridge construction and document the techniques utilized to rehabilitate, tune and test a historic covered bridge. Through, and because of, the rehabilitation, much of the historical fabric has remained intact and will be on display for generations to come.

The bridge has a vibrant history of service which has endured many twists and turns in recent years. Design was completed in 2018, construction commenced in 2019, and in the fall of 2021, the bridge was re-opened to the public.

History of the Bridgeport Bridge

Following the discovery of silver in Western Nevada in 1859, the Bridgeport Bridge was constructed along a new toll road in order to provide a safe and direct passage through a portion of the Sierra Nevada mountains towards Sacramento and San Francisco. The bridge was built by David Inglefield Wood in 1862.

Following the peak of the silver mining in 1876, the bridge remained in private ownership until 1901, when it was declared a route along a public highway. The bridge was then utilized for automobile traffic until 1973, when a new concrete span was constructed upstream. In 1986, California State Parks acquired the bridge and adjacent property to develop the South Yuba State Park.

In January 1997, a flood damaged a significant portion of the bridge and was restored later that year. In 2013, the bridge was closed to pedestrian use until it was temporarily stabilized in 2015 and design efforts for the rehabilitation began shortly thereafter.

[1] Lawrence E. Jones, Senior Principal, Buehler Engineering, Inc., United States, ljones@buehlerengineering.com



Components of the Bridgeport Covered Bridge

The Bridgeport Bridge is comprised of timber and iron with stone masonry abutments. The primary bridge structure utilizes a truss on either side of the floor deck which are flanked with a supplemental, segmented arch on the inside and outside face of each truss. The truss has an upper and lower chord with double braces and single counter-braces within the web. The vertical web members consist of two iron tension rods. The chords, braces, counter-braces and tension rods are coincident at cast iron nodes.

Material Investigation

In order to determine the strength of existing materials, material testing and investigation was required during design. The existing structure was assessed for conditions of decay and damage. Most of the primary members observed appeared to be from the original construction.

The original timbers used to construct the bridge were old-growth timber likely sourced very near to the bridge site (Miller & Knapp, 2013). Wood members were visually graded to obtain member allowable stresses. Specific areas of core decay were identified in the top chord along with local crushing at tension rod connections. One tension rod had failed near the top threaded portion of the rod just below the nut. The existing tension rods were tested for strength and microstructure and the wrought iron rod strength was found to be consistent with historic material strengths.

Rehabilitation Design Criteria

The Bridgeport Bridge is located in the foothills of western Nevada County and spans across the southern fork of the Yuba River. Numerous faults have been identified within sixty miles of the site and seismicity is considered “high”. The bridge, being a California Historical Landmark, was designed to the 2013 California Historic Building Code and ASCE 7-10.

No original construction documents or calculations have been found. Early photographs of the bridge show signage limiting the maximum bridge loading to three tons. Early engineering manuals (Engineering Field Manual, 1917) make note that “the maximum uniformly distributed live load will not exceed the maximum uniformly distributed dead load.” A design live load of sixty-five pounds per square foot was used which correlates with historic engineering manuals while also minimizing the degree of member augment or replacement due to gravity load overstress. In preliminary strength assessment studies, the wrought iron tension rods were found to be the weak link (Gasparini, et al., 2016). Early judgments were made during design that many of the tension rods required replacement in order to first improve the structural resiliency of the bridge, and also to maximize the strength and load carrying capacity of the remaining bridge members.

Lateral loads were applied to the bridge per the California Historic Building Code which allows for a twenty-five percent reduction in lateral forces from the current Building Code. Wind and seismic loads were obtained from ASCE 7 and compared to AASHTO loading.

Analytical Modeling

Various tools were used to study and analyze the bridge. The primary structural analysis modeling program used was SAP Ultimate. The bridge members and their connections were modeled to appropriately assign tension-only (iron tension rods) or compression-only members (arch, braces, and counter-braces) to properly simulate the anisotropic members and connections. The analytical model also provided a way to study various loading and construction sequences. Variations were studied which engaged the arch chords at different sequences relative to the release of the shoring for dead loading and introduction of live loading. In the different sequences studied, the arch attracts more load the earlier that it is engaged. Conversely, the truss action (as demonstrated by the upper chord and tension rod demand) diminishes with early arch engagement.

Truss System Description

The Bridgeport Covered Bridge trusses consist of two Howe trusses which are approximately 16’-6” (5.03m) between laminated chord centroids. The components of the truss include horizontally laminated top and bottom chords consisting of eight laminations of approximately 2” (51mm) nominal x 20’-0” (6.10m) DF-L sawn lumber stitched together with bolts and spiked nails. Laminated planks were likely



used in lieu of hewn timbers for economy's sake (Bennett, 2002). The web members consist of two 4-3/4"x 10-1/4" (121mm x 260mm) braces with a single 4-3/4" x 7-3/4" (121mm x 197mm) counter-brace opposing. Two steel tension rods occur at each bay. The work point of the tension rods, strut, counter-strut, and top or bottom chord coincide with a nodal casting. At the abutments, a 12"x16" (305mm x 406mm) bolster beam is located which extends from the abutment out past the location where the arch chord passes the bottom truss chord.

Arch System Description

The arch consists of two 4-3/4" x 13" (121mm x 330mm) chords which abut both the inside face and exterior face of the truss. The arch chords are bolted to each double truss brace with two ¾" (19mm) diameter bolts with blocking between the brace and counter-brace at each bolt attachment.

Which System is Dominant?

From the outset, the most critical aspect of the bridge analysis was understanding the load path and then appropriately modeling and analyzing the structure. With two capable gravity support structural systems (Howe truss and arch), the rehabilitation must honor the original load paths and load sharing so as to minimize new strengthening elements and new stresses in the historic structure. In order to understand the load path, Buehler aimed to consider the original designer's intentions through studying the bridge member's proportions, material strengths, and available historic references.

While there are many bridges around the world built with a combination truss arch system, historical practice and modern interpretations seem to show that there is not uniformity of thought or practice on how these structures are to perform. Across many of the truss-arch combination structures, the arch system is typically proportionally much stiffer than the truss system. German engineer Karl Culmann noted the relative arch stiffness to truss stiffness during his American tour in the mid-nineteenth century (Rinke, 2016). While the stiffness difference between the two systems may suggest a more dominant arch participation, other references suggest the arch has been considered supplementary to the truss. JJ Daniels, a bridge builder who built Long truss bridges (a predecessor patent to the Howe truss), would attach the arch to the truss after falsework removal. (Barker, 2015). Initially, the truss would support the bridge self-weight, with the arch taking the subsequent live loads after engagement.

The Bridgeport Bridge arch is attached to the truss at each strut and as it passes across the bottom chord. Different than a Long truss in that the vertical tension members are slender iron; the truss web members cannot directly apply load to the arch through a vertical member congruent with the load direction. Therefore, a majority of the load transfer into the arch occurs at the connection of the arch to the bottom chord and bolster beam. A study of the bridge structure was performed to review the proportions of the structural members relative to loading. Various historic engineering documents (including Modern American Bridge Building (Tower, 1874)) provide design criteria and member capacity for trussed bridges. While published following the Bridgeport Bridge's erection, it is fair to assume limited changes to design methodology in that time span. Backwards engineering of the upper chord, end brace, and end vertical rod shows very close alignment of member proportion to allowable wood stresses allowed in the 1874 design manual. The 1874 reference provided a 15 ksi (103 MPa) working stress for iron rods; which the study showed was exceeded with a 21 ksi (145 MPa) working stress under dead loads without arch contribution.

The high stress within the end tension rods begs the question of what early value engineering decisions may have been made. It is noted that a 1-1/2" (38mm) square rod would produce a 15 ksi (103 MPa) dead load stress which would correspond to the working stress limit noted in the 1874 publication. Another hypothesis is that the apparent undersized end rods may be attributed to a reduction in end rod stress due to the strength and stiffness increase in this portion of the span from the bolster beam. The 12x16 (305mm x 406mm) bolster beam provides an increased flexural capacity of the bottom chord and detracts from the truss action of the truss assembly. A cursory study model showed that the presence of this bolster beam reduces the forces in the web members by approximately fifteen percent. With this assumption, tension rod stresses would be approximately 18 ksi (124 MPa) which offers better alignment with historic rod capacity. It is unclear how or if the original designers would have estimated the degree to which the bolster beam would decrease truss action.

In addition, construction sequencing studies showed that engaging the arch earlier in the erection sequence would increase arch stress due to the difference in arch stiffness relative to the truss. When the arch is



initially engaged for both dead and live loads, it was found that the arch stress was almost two times higher than when the arch engagement was postponed until live load introduction. This showed that if the Arch chord was assumed to be the primary system, it would be overstressed for historic and modern capacity values without significant strengthening.

Bridge Improvements

Various improvements to the bridge were made in the rehabilitation design. In general, most repairs consisted of the replacement of damaged timber in kind. Truss repairs consisted of complete replacement of the top chord and selective replacement of damaged bottom chord laminations. Improvements were made to the stitching of the laminations with nail spikes, timber screws and stitch bolts. Hidden timber screws were used locally at the midspan where additional lamination displacement was noted and tension stresses were high. Damaged portions of the arch were replaced in kind. The arch bearing hardware appeared to have been incorrectly installed in the 1971 repairs which resulted in a shortened arch span at the south arch. The rehabilitation corrected this condition and provided adjustable arch bearing seats to allow for future arch tuning to increase or decrease force within the arch. Repairs and replacements to the floor decking and exterior siding and roofing were also made. Improvements to the Tension Rods and Abutments are discussed further below.

Tension Rods

The Secretary of the Interior Standards for Rehabilitation (National Park Services) specify that "deteriorated historical features will be repaired rather than replaced. Replacement of missing features will be substantiated by documentary and physical evidence." Results from the structural analysis indicated that the rods were significantly overstressed. Due to the age and condition of the wrought iron rods and the high number of loading fatigue cycles over time, replacement of the existing highly stressed wrought iron rods was recommended.

Iron rods manufactured in the 1850s time period had variable strength characteristics due to archaic manufacturing and quality control issues. (In addition, during the rehabilitation, stamps observed on the rods showed seventeen different foundry identification stamps from foundries all over the world.) Iron is considered a brittle material due to the relatively small elongation of the material prior to tension failure compared to steel. This characteristic is not desirable from a performance or safety standpoint. ASTM A588 grade 50 (345 MPa) weathering steel was considered for replacement of the existing rod material. In addition to strength, the weathering steel was evaluated for texture and finish similarity and found to be the best option due to strength, source availability, and natural corrosion resistance characteristics.

Abutments

The original abutments from 1862 were dry stacked granite blocks resting on a rock outcropping on the north and river cobbles and boulders on the south end. In 1971, the original bridge abutment was raised thirty inches (762 mm) based on documents by Gillett Harris Duranceau Associates Sheets 1-9 (stamped preliminary) dated July 29, 1971. Extensive soil and abutment studies to evaluate the support conditions determined that the existing gravity rock walls were vulnerable to failure due to gravity, soil, lateral, or seismic loads.

New grouted piles and pile caps with abutment walls were placed within the footprint of the existing rock walls. The rock walls were drilled and epoxy doweled to the abutment walls to act as a veneer. Rock joints were cleaned and fully mortared to correct voids.

Tuning

The performance of the Howe truss over time is reliant upon regular monitoring and occasional tightening of the tension rods. Over time, various environmental factors will contribute to the reduction of tensile forces within the tension rods after the initial prestress state. The tension rods pass through the top chord, the horizontal strut perpendicular to the span of the bridge, cast iron nodes (top and bottom) and the bottom chord. Steel plate washers are located above and below the top and bottom chords, respectively, which bear against the chords. After the initial prestress, member seating, the timber volumetric shrinkage losses, and expansion and contraction of the wood and steel members due to temperature changes will all affect the prestress. Most of the prestress loss is expected to occur within the first few months after the initial stressing.



(Gasparini, et al., 2020). After these months, the truss tension rods will be examined and additional tensioning will be performed.

The initial tuning sequence for the Bridgeport Bridge was developed by Tim Andrews of Barns and Bridges of New England and Buehler. In this sequence, the truss was rebuilt in place while suspended from the shoring truss. While suspended, the vertical tension rods are initially tightened finger tight plus half turn. The struts and counter struts are then shimmed or shortened to ensure firm bearing. An epoxy grout was used to fill voids at the cast iron bearing shoe to provide a tight fit. After firm bearing was established, the vertical rods were tightened to a "full effort of a man" using an eighteen inch (457mm) long wrench. Vertical rod pairs were checked for equal tension and diagonals for equal bearing by hammer sounding the members.

Following the initial tuning, the arch chords were replaced and the jacks supporting the bridge structure were lowered to engage the truss and arch. At this point, the structure supported the full dead load of the bridge. During this sequence, camber and deflections were carefully monitored and recorded. During the construction process, continued conversations were had regarding the arch loading sequence. It was determined that allowing the arch to partially engage at the dead loading conditions would help restrict deflection losses while having minimal effect long-term member stresses and connection forces. Load cell monitoring at the arch bearing seats was used to maintain and monitor the arch reaction loads. The bearing seats were adjusted to maintain symmetric loading and keep loading within acceptable tolerance as the full dead load and proof live load on the bridge was introduced. Due to the shoring truss location, elements of the bridge were not able to be re-built until the shoring truss was removed. In order to properly simulate dead loads of the bridge, simulated loads utilizing hung water totes were used. After simulated truck passage proof load, the shoring truss was removed and the remaining bridge stringers, siding, and roofing were installed.

During tuning, a selection of the vertical tension rods and the arch chord members at the buttress bearing seat were instrumented to measure forces in members. Strains in the tension rods, harmonics in the tension rods, force on the arch bearing seat, and strain in the truss bottom chord were recorded at various stages of construction and loading. This data will be helpful in future retuning efforts to evaluate loss of prestress and determine the level of adjustment each rod may require. In future retuning efforts, the arch chords may be utilized to relieve the self-weight loading on the trusses. With this relief, the tension rods may be tightened and creep and camber losses may be able to be re-established.

It must be noted that prestress losses due to the tension rod bearing on the wood top and bottom chords has been a point of refinement within the history of wooden covered bridge construction. The original bearing seat design provided a flat or dimpled surface where it met the truss chords. The rod forces were transferred through the timber chords in compression perpendicular to grain. This action affects the tension rod prestress as the wood shrinks, crushes, or expands due to moisture content changes. Amasa Stone, William Howe's brother-in-law and colleague, is recognized for improving the node casting by integrating a sleeve through the timber truss chords allowing for minimal prestress losses due to wood behavior (Barker, et al., 2015). This sleeve also allowed for improved shear transfer between the web members and the chords. The Bridgeport Bridge node castings did not have this integrated sleeve.

Shoring

A conventional external shoring system was envisioned in the construction documents which was modeled after shoring used in the 1971 repairs utilizing steel shoring towers supported in the river gravels. Due to more intensive CEQA (California Environmental Quality Act) permit issues to protect the habitat in the river channel, the contractor elected to pursue a modular steel truss system that was internal to the bridge structure.

This box steel truss, named the Mabey Truss, was assembled at one end and launched (pushed) through the bridge and across shoring towers located on the amended footings of the temporary stabilization system coincident with the arch to bottom chord intersection point of the bridge.

The shoring truss was intended to carry gravity and lateral wind loads during construction. One complication of this shoring system was the inability to support a fully loaded dead weight of the bridge while allowing for completion the bridge floor decking until the shoring rods that supported the work platform which was suspended below the bottom chord were removed. This limitation in the shoring design



was accommodated by field load testing of the bridge prior to shoring removal and completion of construction.

Repair and Re-Assembly

After disassembly, re-assembly began with repair work on the bottom chord damage. Lamina were replaced and stitched together with GRK timber fasteners. The entire bottom chord assembly was then retro-stitch bolted to strengthen for shear transfer in the staggered laminations. Original cast iron stitch bolts were retained for the historic fabric and augmented with supplemental staggered stitch bolts. For minor wood imperfections, the contractor utilized repair epoxy to fill holes and checks and provide uniform support for the cast iron seats on the truss chords.

New bolster beams were added at both abutments and damaged solid sawn chord sections at ends were replaced with step-lapped connections to laminated chord material. Truss re-assembly and exchange of damaged members continued for the truss bracing to provide base geometry for a completely new laminated top chord. The new top chord consisted of twenty-foot-long (6.10m) 2”x16” (51mm x 406mm) boards which were laminated with GRK timber fasteners and stitch bolted to complete the assembly. Original truss top chord bracing and struts were replaced as needed and re- installed. Steel bracing above the top chord was added in preparation for field drilling of tension rod holes and re-assembly of the rod system. End steel portal frames were attached to the steel top chord bracing assembly. Cast iron seat connections at braces were wedged and filled with epoxy for uniform compression support.

Completion of the initial tuning allowed the assembly of the side walls and roof framing at the center portion of the bridge in preparation for final load testing.

Load Testing

A full-scale dead and moving live load testing program was incorporated into the final approval of the bridge. The dead loads from the skin and decking that were in conflict with the shoring system had to be artificially applied using suspended water totes. The live load testing was accomplished by using calibrated jacks at discrete points against the shoring truss system that was now no longer needed as a gravity support.

Load testing was monitored by a survey of points on the structure to note deflections, strain gages to monitor tension in the bottom chord, and load cells at arch chord seats to monitor compression reactions at abutments. Sounding frequencies of tension rods and arch chord were documented in the testing process.

Future Maintenance and Tuning

The new protective skin on the structure significantly increases the resilience of the wood structure from environmental decay and applied fire retardant will also help protect against California wildfires. The truss is expected to experience long-term creep and shrinkage due to drying and settling of connections. The maintenance plan is to check the tightness of the tension rods and to adjust arch support connection at abutments. The testing process has allowed documentation of tension rod and arch chord sounding frequencies to aid in follow-up adjustments.

Conclusions

The rehabilitation of the Bridgeport Bridge provided an opportunity to preserve a piece of history for many future generations to enjoy and reflect on our past. In the analysis of the Bridgeport Bridge 150 years after its original construction, we were able to apply modern analytical tools and engineering understanding to a statically indeterminate and complex structure. This analysis both validated much of the original design as well as allow improvements to be made where the original design did not meet modern code or design requirements.



References

[1] AASHTO. 2014, *AASHTO LRFD Bridge Design Specifications*, Seventh Edition, 2014, American Association of State Highway and Transportation Officials, Washington D.C.
[2] AASHTO. 2009, *LRFD Guide Specifications for the Design of Pedestrian Bridges*, American Association of State Highway and Transportation Officials, Washington D.C.
[3] ASCE, 2014, *Seismic Evaluation and Retrofit of Existing Buildings*, ASCE/SEI 41-13, American Society of Civil Engineers, Reston, Virginia.
[4] ASCE, 2010, *Minimum Design Loads on Buildings and Other Structures*, ASCE/SEI 7-10, American Society of Civil Engineers, Reston, Virginia.
[5] Barker, James, et al., *Covered Bridges and the Birth of American Engineering*, pp 63, 139, 169, Historic American
[6] Engineering Record, 2015
[7] Bennett, Lola, *Addendum to Bridgeport Covered Bridge*, HAER No. CA-41, Historic American Engineering Record, 2002
[8] Bridgeport Chronological History, www.southyubastatepark.org , Accessed 30 June 2020
[9] CBC, 2013, *California Building Code*, 2013 edition, California Building Standards Commission, Sacramento, California.
[10] David Wood Arrives, www.southyubastatepark.org , Accessed 30 June 2020
[11] FHWA, *Bridge Inspector's Reference Manual*, Publication No. FHWA NHI 12-049, 2012 edition, Federal Highway Administration, Arlington, Virginia
[12] Forest Products Inspection, Inc. 2012, *Bridgeport Bridge Timber Assessment*, FPI Job No. 11182, February 9, 2012, Kelseyville, California.
[13] Gasparini, Dario, et al., *"Long-Term Behavior of Posttensioned Wood Howe Trusses"*, J. Struct. Eng., 2020, 146(7): 04020112. https://doi.org/10.1061/(ASCE)ST.1943-541X.0002655
[14] Gasparini, Dario, et al., *"Strength of Burr-Arch Trusses HAER No. OH-138"*, p 39, Historic American Engineering Record, 2016
[15] Miller, Terry E., and Knapp, Ronald G., America's Covered Bridges: Practical Crossings – Nostalgic Icons, Tuttle Publishing, Singapore, 2013
[16] National Park Service, "The Secretary of the Interior's Standards for Rehabilitation", *Technical Preservation Standards*, nps.gov/tps/standards/rehabilitation/rehab/stand.htm, Accessed 29 June 2020.
[17] Rinke, Mario, "Formal and Structural Multiplicity in Early Truss Design", 2016
[18] Tower, G.B.N., *Instructions on Modern American Bridge Building, Boston*, A. Williams & Company, 1874
[19] Trautwine Jr., John C., and Trautwine 3rd, John C., The Civil Engineer's Pocketbook Eighteenth Edition, John Wiley & Sons, 1907
[20] U.S. Army, Chief of Engineers, *Engineer Field Manual*, Parts I-VII, pp 251-253, Government Printing Office, 1917
[21] Yearby, Jean P., *Bridgeport Covered Bridge*, HAER No. CA- 41, 1985, Historic American Engineering Record, 1985

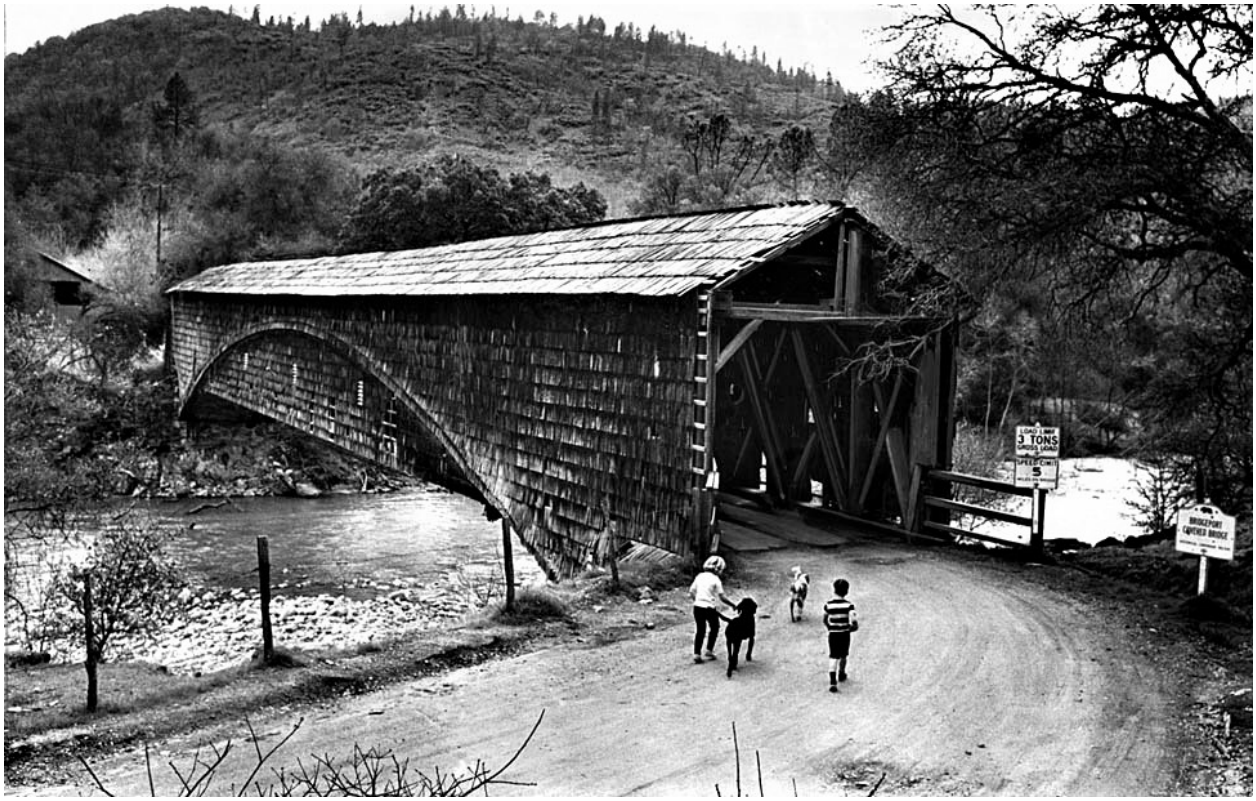


Figure 1 – Bridgeport Bridge circa 1970 (Image courtesy of South Yuba River State Park)

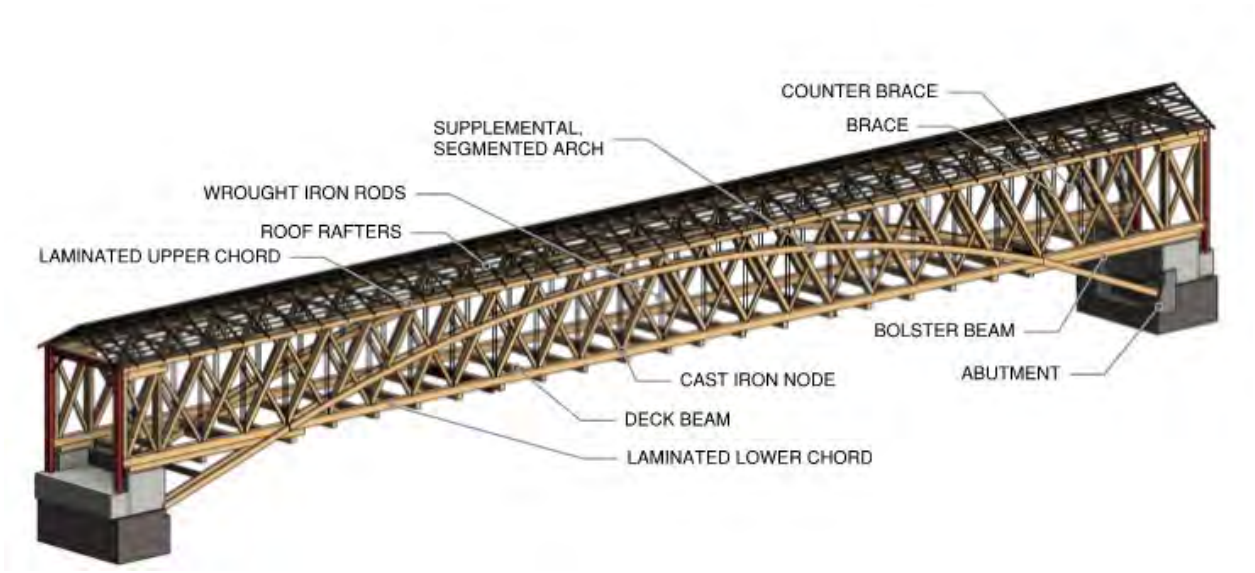


Figure 2 – Graphic of Bridge Components



Figure 3 – Photograph of Bottom Chord Decay prior to repair (Lawrence Jones)



Figure 4 – Launch of shoring (Lawrence Jones)



Figure 5 – Bare bridge with shoring installed (John Rebenstorff)



Figure 6 – Load testing bridge prior to shoring removal (Lawrence Jones)



Figure 7 – Completed Bridge – exterior (Brian Wiens)



Figure 8 – Completed Bridge – Interior (Brian Wiens)

Conference Proceedings 4th ICTB (2022)
https://doi.org/10.24451/40fy-m069

ICTB 2021 PLUS
4th International Conference on Timber Bridges
Biel/Bienne, Switzerland, 9 -12 May 2022



A Reliable Method For Moisture Content Measurement At Inspections And The Results From Nine Swedish Timber Bridges

Niclas Björngrim[1], Per-Anders Fjellström, Göran Berggren

1 Introduction

Timber bridges with stress laminated decks are commonly made of untreated spruce in Sweden and have a required technical life time of 80 years. To meet the lifetime requirement one important part is good water proofing, especially the detailing along the edges. The second part is reliable results from inspections and moisture content measurements. One problem at inspections is to measure moisture content of parts covered by cladding or beneath the water proof membrane. Out of experiences from inspections and commonly used methods a new sensor has been developed by the authors [1]. The sensor is cheap, robust and will last the lifetime of a bridge. Another feature of the sensor is the ability to measure moisture beneath the waterproofing membrane of thick decks. The sensor is a part of scalable system designed for manual measurements and continuous monitoring. As of today, 22 bridges are equipped with a monitoring system using the sensor.

2 Material and method

This paper presents focus on nine modern timber bridges built in Sweden between 1994 and 2020, the bridges are presented listed in Table 1. The Bridges in this study have been monitored and/or inspected by the second author several times over the years.

Moisture measurements

The moisture sensor measures at two depths at each sensor location. Surface moisture content (MC) at (0-45 mm) and internal MC (100 mm – directly under waterproofing membrane). For each bridge installation there is one to two temperature sensors to calibrate the measurements for the temperature. For continuous logging of MC wireless OmniSense S-160-0 sensors has been used.

Inspections

Bridge Main inspections are performed every six years, primary by visual assessment but also aided with tools as impact hammer, MC meter and knife. If damages are found a special inspection is performed to investigate the issue.

Table 1: Bridges in this study.

Bridge	Intended use	Bridge type	Monitoring	Condition
Klockarleden long	Road	Stress lam	Manual	Elevated MC
Klockarleden short	Road	Stress lam	Manual	Elevated MC
Älvsbacka	Pedestrian	Cable stayed	Manual/Continuous	Good
Tvärån	Pedestrian	Stress lam	Manual/Continuous	Elevated MC, condensation
Mobacken	Pedestrian	Stress lam	Manual	Good
Gislaved	Road	Arch/stress lam	Manual/Continuous	High MC at edges
Sundbron	Road	Stress lam	Manual/Continuous	Good
Hörle	Road	Stress lam	Manual	Good
Färgelanda	Pedestrian	Stress lam	Manual	Good

3 Results

The result section presents results from monitoring, inspection and examples of good and bad detailing from the bridges presented.

[1] Niclas Björngrim, Associate Senior Lecturer, Luleå University of Technology, Sweden, niclas.bjorngrim@ltu.se



3.1 Klockarleden short and long,1994

The two consecutive bridges that are similar in construction and appearance. An unusual detail is the outer beams made of oak. The sensors show high surface MC, this originates from a problem with detailing of the edges. On the long bridge this has been exchanged to a better solution and the surface moisture is now normal. The bridge deck underneath the waterproofing membrane show good MC values.



Figure 1. Wet outer beam from Klockarleden short.

3.2 Älvsbacka

Älvsbacka is one of the longest timber bridges in Sweden spaning 130 meters. Monitoring from an earlier system which is no longer operative is reported in [2] and [3]. Today the girders are monitored with twelve retrofitted sensors The bridge is in good condition with MC values around 17-18%.

3.3 Tvärån

A pedestrian bridge equipped with four sensors. The bridge has increased level of surface moisture due to water condesating (Figure 2), which has led to cupping of the bridge deck.



Figure 2. Condensation on bottom of the bridge deck.



3.4 Mobacken

The bridge is a pedestrian bridge with timber decking of treated pine (Figure 3). The bridge has ten sensors factory installed. The manual measurements is showing a MC between 12-16% under the membrane.



Figure 3. Stress laminated deck with a thin rubber membrane and plank decking.

3.5 Sundbron

The bridge is a single lane traffic bridge. During the assembly of the bridge one glulam beam, the outermost with sensors M1-M4 in Figure 4, partly fell in to the water. The wet beam was attached and stressed together with the deck in its wet state. The interface between the wet beam and its neighboring dry beam was monitored and it could be concluded that the high local MC dried down to normal levels after a few months. The placing of the sensors can be seen in Figure 4. The MC for 0-45mm in to the deck is shown in Table 2 and the MC 50-520 mm in to the deck is shown in Table 3. Logging of sensor M1, NV 0-45mm is shown in Figure 5. It can be seen that the MC dries down to around 15% from the initial high MC.

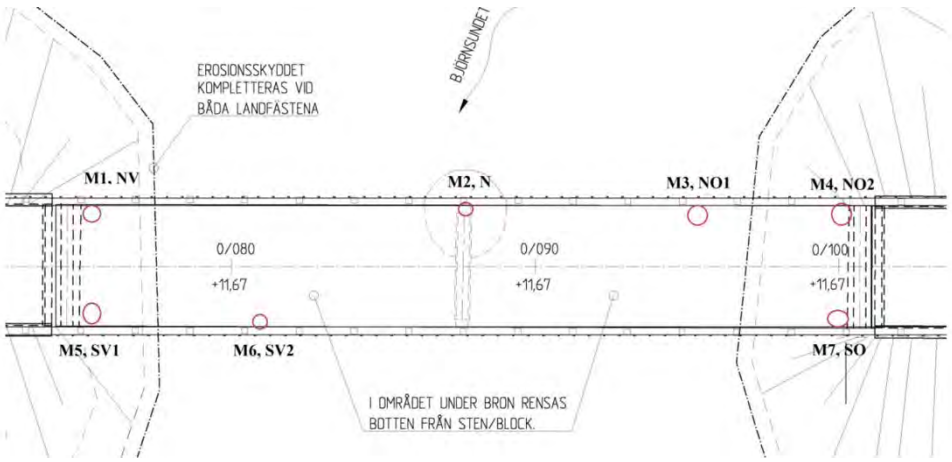


Figure 4. Sensor placing Sundbron.



*Table 2: MC measurements at 0-45mm depth for Sundbron. The * indicates a logger is attached at that measurement point.*

Sensor	6-12-15	26-12-15	11-2-16	28-6-16
M1, NV	23	17	39	*
M2, N	25	24	26	19
M3, NO1	36	30	25	19
M4, NO2	20	20	24	19
M5, SV1	21	22	25	17
M6, SV2	36	33	27	19
M7, SO	17	17	25	18
Temp	3	-3	1	16

Table 3: MC measurements at 50-520mm depth for Sundbron.

Sensor	6-12-15	26-12-15	11-2-16	28-6-16
M1, NV	15	15	22	18
M2, N	21	21	21	19
M3, NO1	27	24	21	18
M4, NO2	15	16	20	23
M5, SV1	15	16	17	17
M6, SV2	28	26	21	19
M7, SO	14	15	19	17

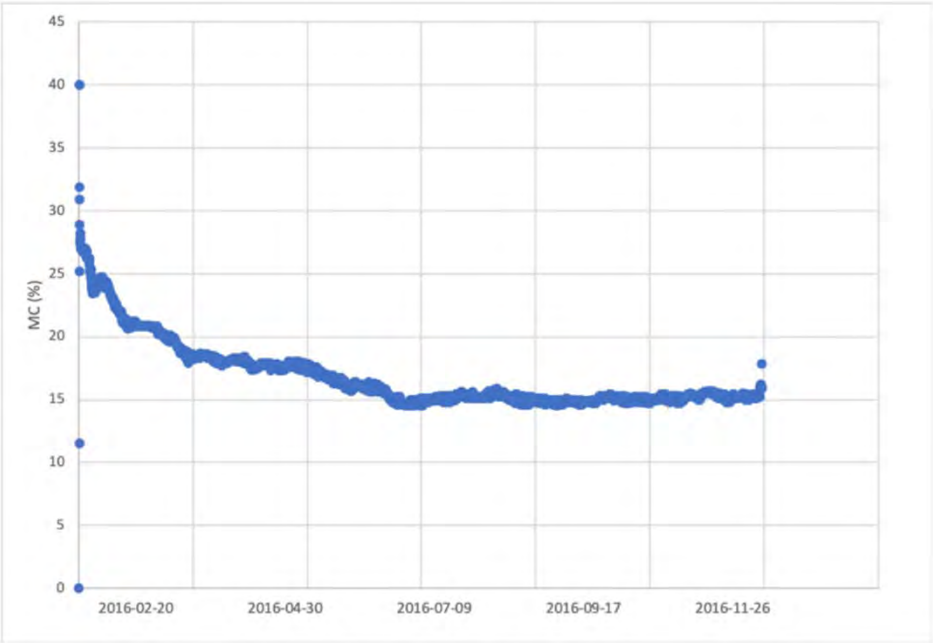


Figure 5. Logging of sensor M1, NV 0-45mm from 11-2-2016 to 15-10-2016.



3.6 Gislaved bridge

The Gislaved bridge is Swedens largest road bridge in timber [4]. The bridge is equipped with 16 retrofitted sensors. This bridge shows the importance of acting fast when monitoring data show high moisture content. Elevated moisture content was determined in 2015 and with no actions taken by the owner, areas with severe decay was found during inspections in 2020. After removing the asphalt several problems were found. The membrane strip on the edge of the deck still had the protective backing on (Figure 6) resulting in no adhesion to the deck. The membrane strip joints were not welded which leads to water penetrating in under the drip edge and into the wood deck.



Figure 6. Detail of Gislaved bridge. Membrane strip not properly attached. Decayed wood is also visible.

3.7 Hörle

A road bridge spanning a railroad with ten retrofitted sensors. The timber deck from three inspections show expected MC where good detailing such as examples in Figure 7 is a contributing reason.



Figure 7. Good detailing of expansion joint drainage and down pipe.



3.8 Färgelanda

A pedestrian bridge with six factory installed sensors. The first inspection was in April 2019 four months after erection. The second inspection was performed in October 2020. In one of the corners of the bridge elevated MC was detected. The 24% measured is possibly condensated water and is expected to be lower during spring and summer.

4 Conclusions

The moisture measuring sensor is a reliable way for managing timber bridges together with inspections. Klockarleden short showed high MC values from the sensor system, but the inspection found that the wood was in good condition although the MC was over fiber saturation point. By improving some of the edge details the surface moisture will decrease as it has for the longer of the two bridges. The monitoring of Sundbron show that even tough water was introduced to the structure during the assembly, the bridge deck dried down to normal MC levels in five months. The Gislaved monitoring system found high MC from the beginning, and when the special inspection was performed flaws from the construction had resulted in decay at the edges of the bridge.

Bridges with good design and detailing, reliable moisture content measurements together with inspections is crucial for timber bridges to last or outlast the technical life time.

5 References

[1] Björngrim, N., Fjellström, P. A., and Hagman, O. (2017). "Factory-mounted and retrofit passive resistance sensors adapted to monitor moisture content in timber bridges," *BioRes.* 12(4), 7218-7227.

[2] Saracoglu, E., & Bergstrand, S. (2015). Continuous monitoring of a long-span cable-stayed timber bridge. *Journal of Civil Structural Health Monitoring*, *5*(2), 183-194.

[3] Kliger, R., Svensson, T., Jansson, H., & Svensson, I. (2013). Vibration response of long cable-stayed timber footbridge–case study. In *Proceedings of International Conference on Timber Bridges 2013-Las Vegas, Nevada USA*.

[4] EKHOLM, K., Nilsson, P., & Johansson, E. (2013). Case Study of the Longest Single Span Timber Bridge for Highway Loads in Sweden. In *Proceedings, 2nd International Conference on Timber Bridges. Washington, DC: WoodWorks–Wood Products Council*.

Conference Proceedings 4th ICTB (2022)
https://doi.org/10.24451/mx3b-we02

ICTB 2021 PLUS
4th International Conference on Timber Bridges
Biel/Bienne, Switzerland, 9 -12 May 2022



Effectiveness of structural protection measures for timber bridges – results of long-term moisture monitoring

Johannes Koch[1], Antje Simon, Markus G. Jahreis

1 Introduction and motivation

Timber has many advantages. These include the high degree of prefabrication and the related, short-closure times during the construction phase, the almost matchless climate-friendly nature of the building material and, of course, its high level of efficiency in its ratio of load-bearing capacity and mass. As a logical consequence, then, it is suggested that Germany should aim for a significant increase in the use of timber in its bridge constructions.

However, an increase in the use of wood can only be achieved by overcoming the poor reputation of timber bridge construction in Germany. As result of poorly planned and inadequately maintained timber bridges in the past, these are generally seen as not being durable [1]. In order to minimise planning and execution errors in the future and to ensure the maintenance of the structures, new guidelines for the design, construction, maintenance and inspection of protected timber bridges have been developed within the research project, "Protected Timber Bridges" ("ProTimB"), at the University of Applied Sciences Erfurt (FHE). The structure of the developed guidelines is based on the existing regulations of the German federal highways. The guidelines can be downloaded from the FHE website [2] and are presented in summarised form on ICTB 2021 PLUS [3].

A second approach, "ProTimB", had the aim of creating a database on timber moisture content in timber bridges built over water. Here, the idea was to reduce the number of restrictive requirements on timber bridge inspections. A guideline for federal road bridges suggests that the durability of timber bridges crossing bodies of water is critical [4]. Therefore, annual major inspections are required for such timber bridges regardless of whether or not the bridge is protected against the ingress of precipitation and moisture. Bridges made of other construction materials need only be inspected every six years.

Short intervals of inspections of non-protected timber bridges are useful, as this type of bridge is subject to the risk of fungal decay due to the timber moisture content being higher than 20 mass%. However, structural protection enables a timber moisture content that is lower than 20 mass%, hence, fungal decay should not occur [5][6] – which would also make the necessity of annual inspections of these protected timber bridges unlikely. Furthermore, it is also very inconvenient for the building owners, as the annual inspections result in high maintenance costs. As a consequence, there is a certain reluctance to building timber bridges. "ProTimB" aimed at demonstrating that timber bridges over bodies of water are not exposed to a higher risk of fungal decay, providing they are structurally protected against precipitation and moisture ingress.

This paper describes the results of a monitoring programme of nine structural protected timber bridges in Germany.

2 Outline of the monitoring programme

2.1 Background

Fresh infestation can only occur if the timber moisture content exceeds the fibre saturation point. The fibre saturation point lies in the range of about 26–34 mass% for local softwood species [7]. Such a high level of moisture content will be reached where the structure is exposed to precipitation and other moisture ingress. A moisture content up to the fibre saturation point can also occur in timber depending on the ambient climate, as it is a hygroscopic material whose moisture content constantly adjusts to the humidity and temperature of the ambient air.

However, the German wood protection standard DIN 68800 requires a long-term timber moisture content at a maximum of 20 mass% for load bearing components [8]. Additionally, it is explained that decay is not

[1] Corresponding Author, Ph.D. student and research assistant, Fachhochschule Erfurt - University of Applied Sciences, Germany, johannes.koch@fh-erfurt.de



expected if the wood is not exposed to a moisture content higher than 20 mass% for more than four months [9].

In order to show that structurally-protected timber bridges are not at a higher risk of decay, a moisture monitoring programme was initiated as a part of the "ProTimB" research project. The intention was to demonstrate that the timber moisture content remains permanently below 20 mass%.

2.2 Overview

The monitoring programme of structurally-protected timber bridges under "ProTimB" was unique with regard to both its systematic and scope in Germany. The timber moisture content and the ambient climate were recorded at nine protected timber bridges of different construction types throughout Germany, as shown in Figure 1 below. All bridges span a river and a part of the foreland, while one bridge in Lörrach additionally spans a highly-frequented, federal road. The first measurement system was implemented in August 2015 on a road bridge in Lohmar-Höngesberg. The other eight systems were implemented in the autumn of 2016. At the bridge in Lörrach, a second measuring system with additional measuring points was set up in 2018. The monitoring systems on five of the nine bridges were removed in summer 2019, at the end of "ProTimB". Yet, the monitoring on the other four bridges that are located in Lohmar-Höngesberg, Lörrach, Wippra and Breitungen continues to the present time.

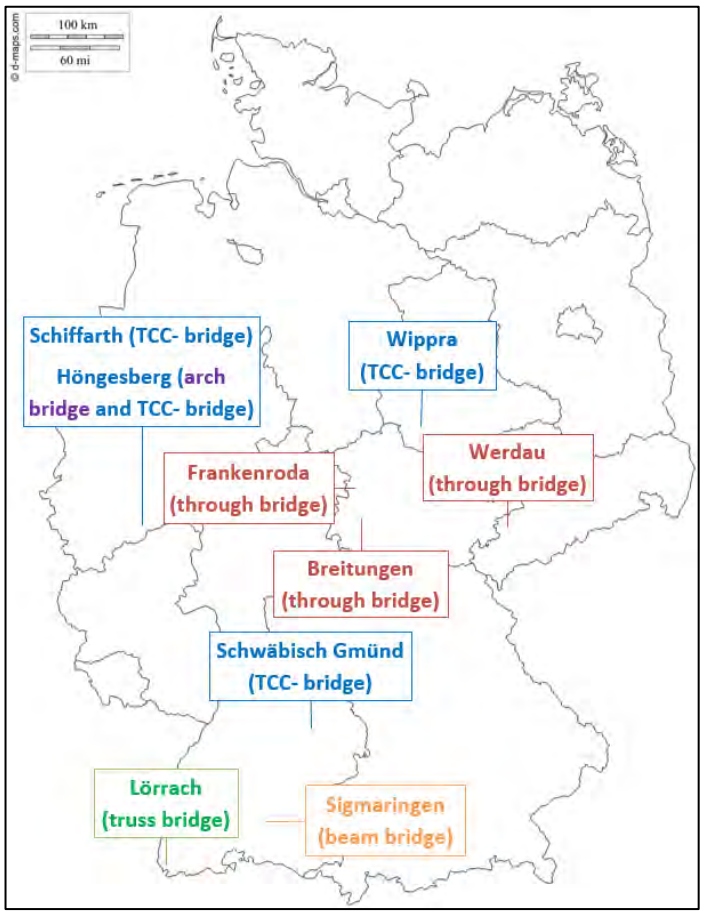


Figure 1: Location and construction type of the bridges within the "ProTimB" monitoring programme

A system with eight pairs of electrodes was implemented at each structure to measure the electrical resistance of the wood, distributed over two or three measuring areas. In each case, there were measuring points with several measuring depths above the waters and in the foreland. Furthermore, the timber temperature, air temperature and relative humidity were also logged at each of the measuring areas. Figure 2 below shows the road bridge in Lohmar-Schiffarth with the implemented equipment and four pairs of electrodes at the two measuring areas.

More details of the implementation of the monitoring systems and the bridges of the programme are given in [10][11][12].



Figure 2: View of the TCC road bridge in Lohmar-Schiffarth (top of the image); measuring area over the foreland (bottom left); measuring equipment in an installation box (bottom centre); measuring area over the River Agger (bottom right of the image)

2.3 Method

The timber moisture content is estimated by using the electrical resistance method, which is standardised for sawn timber [13]. Using experimentally-determined wood species-specific calibration curves, the moisture content of the timber can be derived from the measured resistance. However, the electrical resistance is also influenced by the temperature. Therefore, the timber moisture content has to be calculated from the measured electrical resistance using the calibration curves, and corrected using the measured timber temperature.

The equilibrium moisture content was computed according to the mathematical Hailwood-Horrobin sorption model using the ambient climate conditions, relative humidity and air temperature [14]. Theoretically, this moisture content occurs directly on the wood surface. Given that the timber moisture content is not determined at the surface, but at several depths of the cross section, it should be noted that this calculated value may not exactly match the timber moisture content directly calculated from the measured electrical resistance. Changes in climatic conditions affect the timber moisture content deeper in the cross section with a time delay. Furthermore, no material specific parameters were available for the Hailwood-Horrobin sorption model to calculate the timber moisture content for larch (*Larix decidua*) and European spruce (*Picea abies*) – the species of wood used for the bridges of the monitoring programme. Thus, the equilibrium moisture content for all structures was determined on the base of data for Sitka spruce (*Picea sitchensis*) [15].

However, a comparison between the equilibrium moisture content and the timber moisture content can be used to understand how the ambient climate influences the timber moisture content. Excessive discrepancies could be an indication for free water in the area of the sensors.

3 Results and discussion

3.1 Effectiveness of structural protection measures

Table 1 shows the mean values of the timber moisture content (TMC) and the equilibrium moisture content (EMC) of all nine bridges of the "ProTimB" monitoring programme. It can be observed that at none of the nine bridges do the mean values exceed 20 mass%. Generally, this is a positive trend as concerns the risk of decay.



Table 1: Mean values of the timber moisture content (TMC) and the equilibrium moisture content (EMC) in mass% of the bridges of the "ProTimB" monitoring programme

Location of the bridges	Evaluation period	TMC above foreland [mass%]	TMC above river [mass%]	EMC above foreland [mass%]	EMC above river [mass%]
Lohmar Höngesberg	19.08.2015 - 13.11.2019 04.05.2021 - 31.01.2022	18.6 18.5	17.1 18.2	15.9 15.6	16.3 16.2
Lohmar Schiffarth	21.10.2016 - 18.06.2019	16.0	15.9	16.5	15.7
Wippra	13.10.2016 - 21.01.2022 13.10.2016 - 28.02.2021	18.1	17.8	 no sensor	 17.8
Schwäbisch Gmünd	28.10.2016 - 30.04.2019	15.7	16.1	14.7	15.3
Breitungen	26.10.2016 - 31.01.2022	15.9	15.9	16.6	16.0
Sigmaringen	04.11.2016 - 14.05.2019	16.6	15.9	16.5	16.4
Lörrach System I	03.11.2016 - 31.01.2022	19.1	19.5	15.6	16.2
Lörrach System II	01.02.2018 - 28.04.2021 15.03.2019 - 28.04.2021	 16.3	16.8	no sensor	no sensor
Werdau	24.11.2016 - 06.06.2019	16.0	15.7	16.3	16.0
Frankenroda	23.11.2016 - 27.05.2019	16.5	16.7	16.7	15.9

However, it is also important to take the development of moisture content into account in shorter periods. As described above, 20 mass% should not be exceeded for longer than four months. Examples of the development of the timber moisture content and equilibrium moisture content on two bridges are given in Figures 3 and 4.

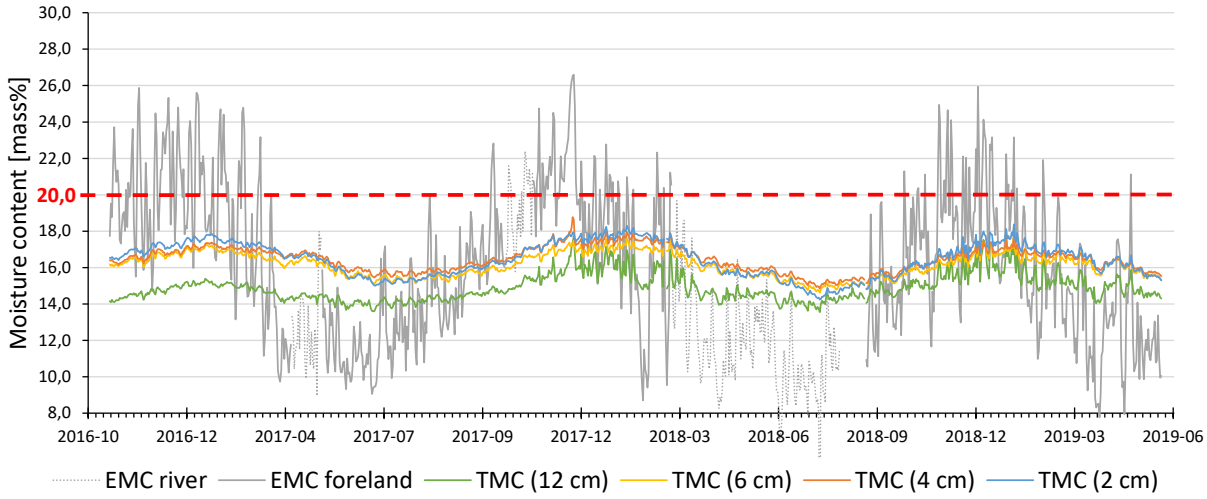


Figure 3: Daily mean values of equilibrium moisture content (EMC) and timber moisture content (TMC) at different measuring depths at the bridge in Lohmar-Schiffarth (measuring area: foreland)

Figure 3 shows the development of moisture content at the bridge in Lohmar-Schiffarth near Cologne at the measuring area above the foreland. The timber moisture content follows the equilibrium moisture content that represents the climate conditions with a time delay. The seasonal climate changes are clearly visible. It can also be seen that the timber moisture content does not exceed the limit of 20 mass% during the whole evaluation period from October 2016 to Jun 2019. Figure 3 is representative of the measuring results of the bridges in Schwäbisch Gmünd, Breitungen, Werdau and Frankenroda. At all of these, the timber moisture content remains below 20 mass%. Therefore, decay is not expected in the measuring areas. It should be taken into consideration that the measurements are only punctual and not distributed over the whole superstructures. However, the results show that the structural wood protection measures are effective.

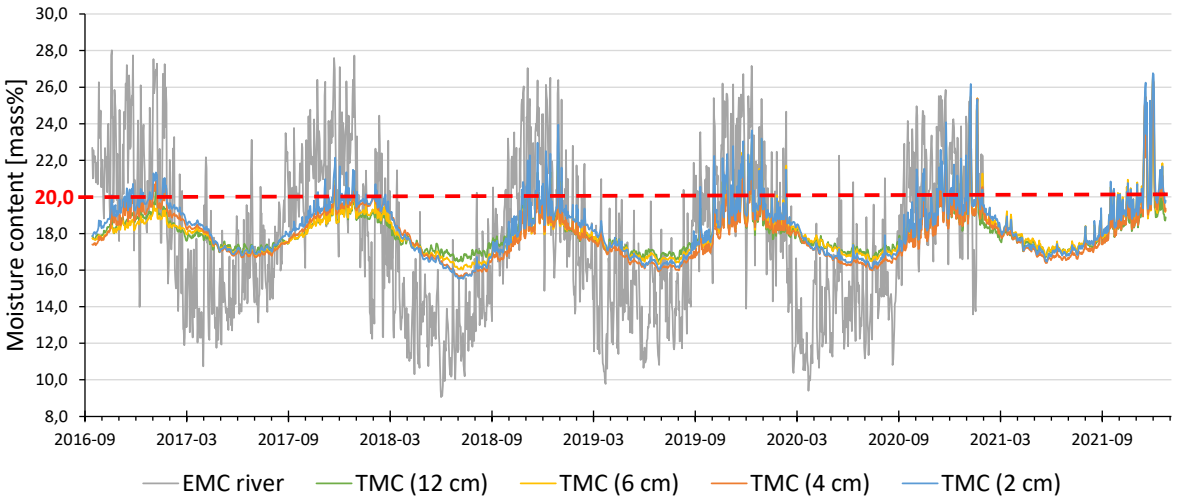


Figure 4: Daily mean values of equilibrium moisture content (EMC) and timber moisture content (TMC) at different measuring depths at the Birkberg bridge in Wippra (measuring area: foreland)

On the other hand, there are areas with exceeded moisture content in the winter periods, which is shown in Figure 4. This occurs at the bridges in Wippra, Lohmar-Höngesberg and Lörrach, as well as Sigmaringen in certain periods. In the graph it can be seen that the period of higher moisture level over 20 mass% is limited to three or four months per year. The wood usually dries back to an acceptable level after February. These short periods of higher moisture level are also acceptable in preventing the risk of decay.

However, when looking at the mean values of the moisture content in Table 1, a number of other questions arise. Most bridges have a mean value of 16 mass%. The bridges of Lohmar-Höngesberg and Wippra are at 18 mass%, and at Lörrach a little higher at 19 mass%. The question here is why this is the case.

Figure 4 shows that the moisture content is directly related to the climate conditions represented by the equilibrium moisture content. There are no unusual offsets on the graph. Thus, the continuously 2 mass% higher moisture level at the Birkberg bridge in a valley near to Wippra appears to be a consequence of the more humid and colder climate in the Harz mountains. The higher equilibrium moisture content for this location confirms this.

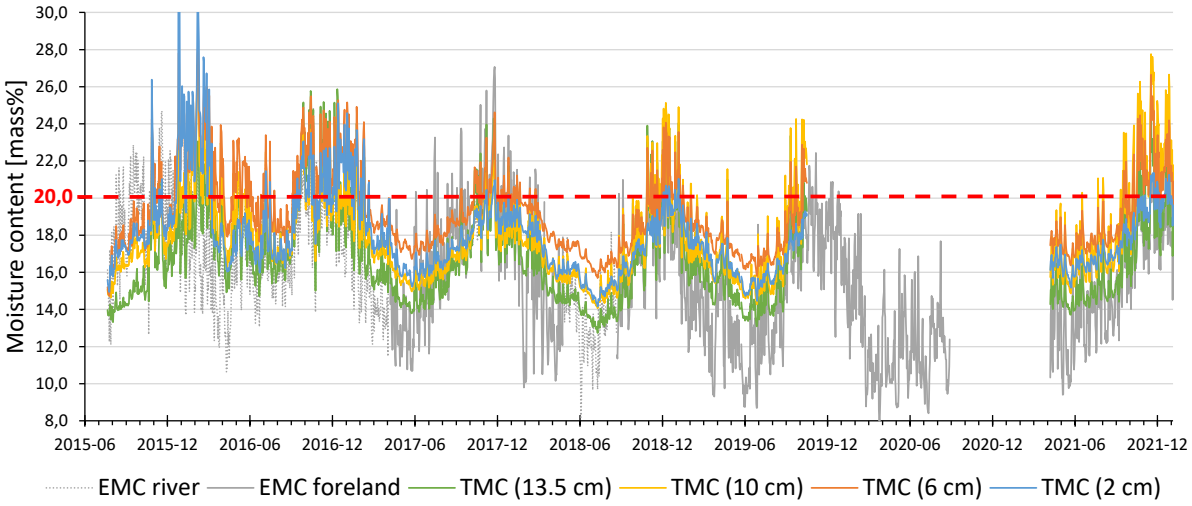


Figure 5: Daily mean values of equilibrium moisture content (EMC) and timber moisture content (TMC) at different measuring depths at the bridge in Lohmar-Höngesberg (measuring area: foreland)

The situation is different at the bridges in Lohmar-Höngesberg and Lörrach. In the first case, a high timber moisture level was already noticed in the first winter of the monitoring in 2015/2016. Specifically, it was then noted that an expansion joint situated above the measuring area had failed. This resulted in rainwater



running over the measuring points, meaning that, in certain cases, the measured timber moisture content reached a high value (Figure 5). As a first act to remedy this, cladding was installed to protect the wood from the rainwater. It is also evident that the moisture content is higher than 20 mass% during some winter months. This contrasts with the results of the measurements at the other two measuring areas above the river. In Figure 6 below, the graph shows shorter periods of moisture contents higher than 20 mass%. It is assumed that the rainwater creates a more humid climate in the measuring area above the foreland. Therefore, it is necessary for the failed expansion joint to be replaced as soon as possible.

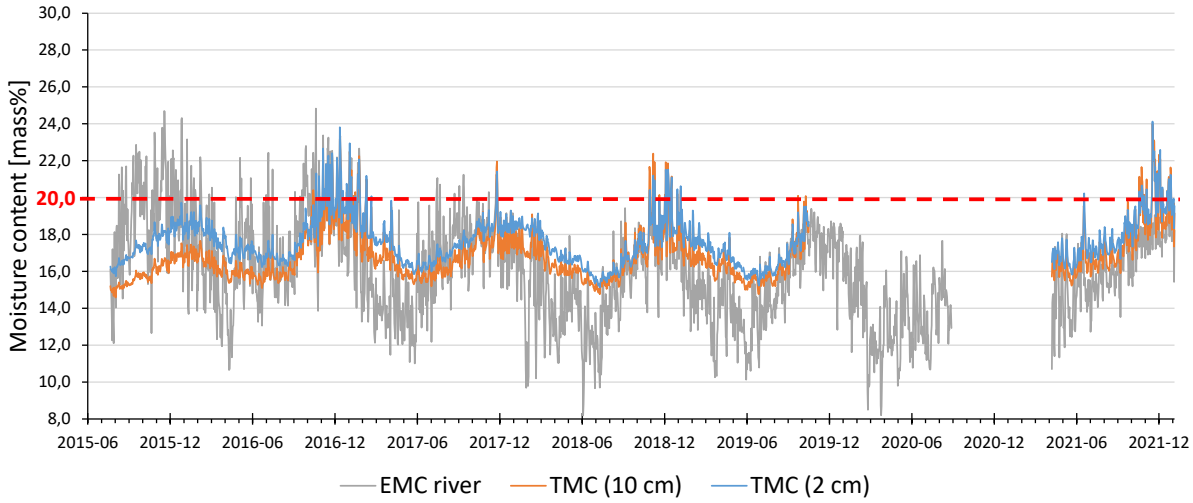


Figure 6: Daily mean values of equilibrium moisture content (EMC) and timber moisture content (TMC) at different measuring depths at the bridge in Lohmar Höngesberg (measuring area: river - arch bridge tension member)

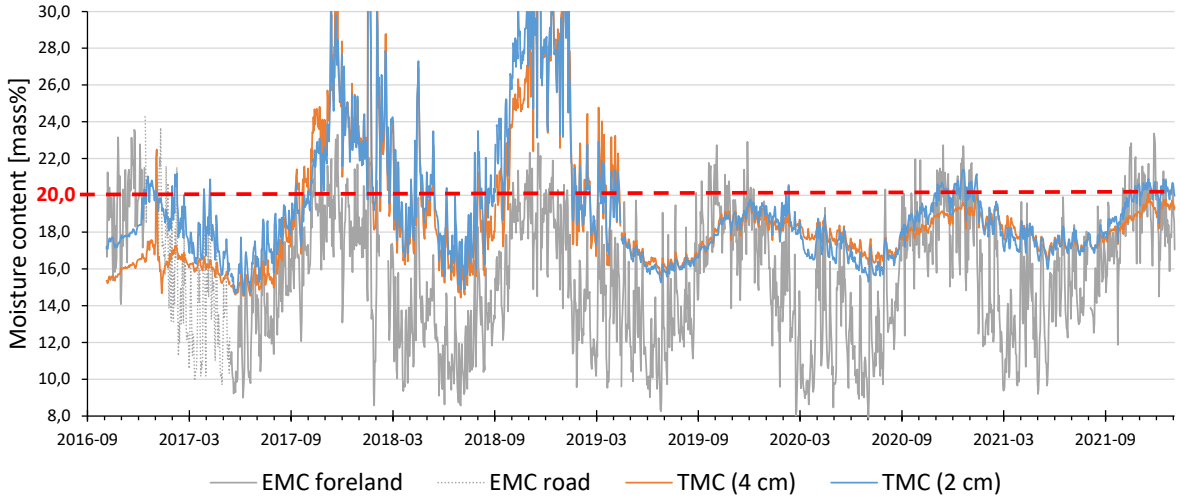


Figure 7: Daily mean values of equilibrium moisture content (EMC) and timber moisture content (TMC) at different measuring depths at the bridge in Lörrach (measuring area: foreland)

It can be noted that moisture monitoring at bridges or other structures can help to explore or monitor neuralgic points in the wood protection or waterproofing concept of a structure. Monitoring also proved to be a benefit for the future of the bridge in Lörrach. As the graph in Figure 7 shows, during the period between October 2017 and April 2019, moisture content reached a high level for a long time, sometimes beyond the fibre saturation point. It was found that the angle of precipitation is sometimes almost horizontal due to an unusual air flow in the valley where the bridge is situated. Despite the carefully-planned wood protection concept in accordance with the current standard specifications (see [8] [16]), the lower load bearing components of the bridge were regularly exposed to weather. Rain and snow penetrated the structure between the roof and the cladding (see Figure 8). This resulted in the lower chord of the truss being wetted. To solve the problem, a number of variants for improving the structural wood protection concept were investigated.

The preferred option was a sensor-controlled curtain that closes the gap between roof and cladding in times of precipitation [17].



Figure 8: View of the bridge in Lörrach

In summary, the structural wood protection measures show positive effects at the observed bridges. Problems only occurred at two of the nine bridges. The failure of the expansion joint at the bridge in Lohmar-Höngesberg should be replaced as soon as possible in order to ensure the full functionality of the structural wood protection concept of this bridge. Only in the case of the bridge in Lörrach was the wood protection insufficient in its original design for the extraordinary exposure. This problem was identified by the monitoring and an innovative solution was developed.

3.2 Moisture exposure of timber bridges spanning waters and roads

All bridges of the monitoring programme span over rivers. They span smaller rivers such as the Agger, the Wipper and the Pleiße, or larger rivers such as the Danube and the Werra. However, at none of the sites was an unusually high moisture level observed that can be associated with the waters.

In Table 1 above, the difference can be seen between the timber moisture content of the measuring areas above the river and the measuring areas above the foreland, which for all bridges is a maximum of 0.7 mass%, except for the bridge in Lohmar-Höngesberg in the period between October 2015 to November 2019. As described above, the difference there is twice as high as a result of the failed expansion joint. Nevertheless, the timber moisture content at all bridges is at a tolerable level.

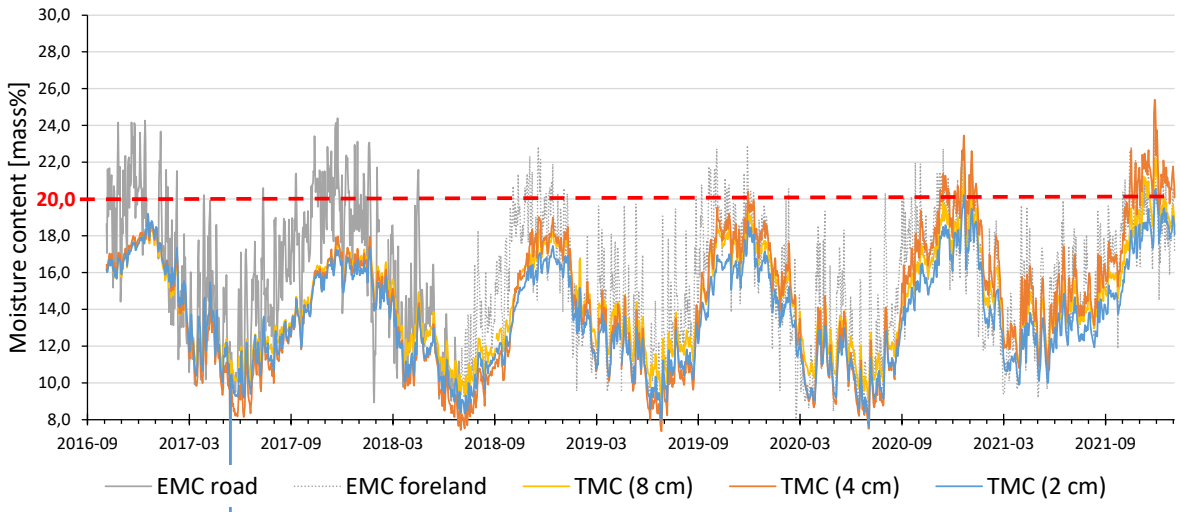


Figure 9: Daily mean values of equilibrium moisture content (EMC) and timber moisture content (TMC) at different measuring depths at the bridge in Lörrach (measuring area: road)



In addition to the fact that the bridge in Lörrach spans the river Wiese, it also spans a highly- frequented federal road. In order to investigate spray exposure from road traffic, an additional measuring area was set up above the road. The results can be seen in Figure 9 above. The mean value of the timber moisture content is 14.2 mass% for the whole evaluation period from November 2016 to January 2022.

Contrary to expectations, the wood moisture content is relatively low and even lower than at the other measuring areas, despite the spray exposure. Therefore, it seems that the spray is not a relevant factor for the moisture load of this structure. This assumption is supported by the results of a Swiss study, which found that the spray is almost irrelevant for the moisture content of timber components located at a distance of about five metres above a road [18]. Nevertheless, it is important to mention that only one bridge spanning a road was investigated in the "ProTimB" monitoring programme. Hence, further investigations should be conducted.

The results of the monitoring show that the moisture content of the components of protected timber bridges does not seem to be influenced to any relevant dimension by the fact that the bridges span water bodies or are influenced by spray resulting from traffic over roads. Therefore, it does not seem to be useful to conduct an expensive and complex main inspection of such bridges every year. Rather, it is suggested that adequate maintenance of the bridges is provided for, and that monitoring in the first few years after construction is carried out so as to be able to identify any unexpected vulnerabilities in the structural wood protection concept.

4 Conclusions

The idea and realisation of an extensive moisture monitoring programme of nine structurally- protected timber bridges in Germany was described in this paper. The results of the monitoring show the effectiveness of structural wood protection measures, but they also demonstrate the benefit of monitoring timber bridges in the first few years after construction. It was found that waters underneath the bridge or spray generated by traffic on roads under the bridges do not affect the moisture content of the bridge construction. Therefore, an annual inspection is not necessary. It is suggested the results of the "ProTimB" monitoring programme will contribute towards overcoming the poor reputation of timber bridge construction in Germany, and furthermore support an increased use of timber in bridge construction.

Acknowledgement

The monitoring programme was part of the research project "Protected Timber Bridges (ProTimB)", which has been supported and funded by the Federal Ministry of Education and Research of Germany, the companies of the Qualitätsgemeinschaft Holzbrückenbau e. V. (Schaffitzel Holzindustrie GmbH + Co. KG, Schmees & Lühn Holz- und Stahlingenieurbau GmbH, Grossmann Bau GmbH) and Setzpfandt Beratende Ingenieure GmbH & Co. KG. The authors thank all partners and supporters for their technical and financial support.

References

[1] Hemmert-Halswick, A. (2012) Nachhaltigkeitsgedanken zum Holz im Brückenbau. in: Forum Holzbau [Hrsg.] 2. Internationale Holzbrückentage (IHB). DE-Bad Wörishofen, 19th and 20th Apr. 2012.
[2] Online source: https://www.fh-erfurt.de/fakultaeten-und-fachrichtungen/bauingenieurwesen-und-konservierung-restaurierung/bauingenieurwesen/projekte/protimb-ergebnisse
[3] Simon, A.; Jahreis, M.; Koch, J (2022) Design, construction and maintenance of structurally protected timber bridges. in: ICTB 2021 plus, CH-Biel, 09th to 12th May 2022.
[4] Bundesministerium für Verkehr und digitale Infrastruktur (2017) Richtlinie zur einheitlichen Erfassung, Bewertung, Aufzeichnung und Auswertung von Ergebnissen der Bauwerksprüfungen nach DIN 1076 (RI-EBW-PRÜF). Feb. 2017.
[5] Graf, E.; Meili, M. (2001) Holzzerstörende Pilze und Insekten – Analyse, Prognose, Bekämpfung. in: Lignum, Schweizerische Arbeitsgemeinschaft für das Holz [Hrsg.] Lignatec: die technischen Informationen der Lignum: EMPA/LIGNUM-Richtlinie 14. Rüschlikon: Schück Söhne AG.
[6] Mohrmann, M.; Wiegand, T. (2015) Holzschutz bei Ingenieurholzbauten. in: Studiengemeinschaft Holzleimbau e.V. [Hrsg.] holzbau handbuch, Reihe 5 Teil 2 Folge 1.
[7] Trendelenburg, R; Meyer-Wegelin, H. (1955) Das Holz Als Rohstoff. Munich: Carl Hanser Verlag.
[8] DIN 68800-1 (2019) Holzschutz – Teil 1: Allgemeines. Berlin: Beuth. June 2019.



[9] Willeitner, H. (2013) Kommentar zur DIN 68800-1:2011-10 – Holzschutz – Teil 1: Allgemeines. in: Marutzky R. [Hrsg.] Holzschutz – Praxiskommentar zu DIN 68800 Teile 1 bis 4. 2. completely revised edition. Berlin: Beuth, p. 9–76.

[10] Koch J., Simon A., Arndt R. W. (2016) Monitoring of moisture content of protected timber bridges. In: CD-ROM Proceedings of the World Conference on Timber Engineering (WCTE 2016), AT-Vienna.

[11] Koch J., Arndt R. W., Simon A., Jahreis M. G. (2017) Moisture monitoring of nine protected timber bridges in Germany. In: 3rd International Conference on Timber Bridges, SE-Skelefteå.

[12] Arndt R. W., Koch J., Simon A., Jahreis M. G. (2018) ProTimB - Monitoring of structurally protected timber bridges. In: NDE/NDT Structural Materials Technology for Highways and Bridges (SMT) and the International Symposium on Non-Destructive Testing in Civil Engineering (NDT-CE), US-New Brunswick.

[13] DIN EN 13183-2:2002-07: Feuchtegehalt eines Stückes Schnittholz - Teil 2: Schätzung durch elektrisches Widerstands-Messverfahren; Deutsche Fassung EN 13183-2:2002.

[14] Hailwood A. J., Horrobin S.: Absorption of water by polymers: analysis in terms of a simple model. Transactions of the Faraday Society, Volume 42B, pp. 84-92, 1946.

[15] Simpson W.T.: Prediction equilibrium moisture content of wood by mathematical model. Wood and Fiber, Volume 5, No. 1, pp. 41-49, 1973.

[16] DIN EN 1995-2/NA (2021) Nationaler Anhang – National festgelegte Parameter – Eurocode 5: Bemessung und Konstruktion von Holzbauten – Teil 2: Brücken. Berlin: Beuth. June 2021.

[17] Schmees, J. (2018) Was heißt schon geschützt – Fachwerkbrücke über die Wiese und die B 317 in Lörrach in: Forum Holzbau [Hrsg.] 24. Internationales Holzbau-Forum (IHF). DE-Garmisch-Partenkirchen, 5th to 7th Dec. 2018.

[18] Finger, A.; Sell, J.: Bewitterungsversuch an Holzfachwerk. Prüfbericht Nr. 414433, EMPA, Dübendorf, 29th Oct. 2002.

Conference Proceedings 4th ICTB (2022)
https://doi.org/10.24451/w5yg-j871

ICTB 2021PLUS
4th International Conference on Timber Bridges
Biel/Bienne, Switzerland, 9 -12 May 2022



Monitoring systems for quality assurance of timber bridges

Steffen Franke[1], Bettina Franke, Marcus Schiere, Sébastien Bonifacio, Andreas Müller

1 Introduction

Wood properly protected and controlled is very powerful and durable.

Continuous monitoring of wood moisture content is a suitable early warning system. The importance of wood moisture in relation to possible damage in timber construction is shown in a study of Frese [1], where 50 % of all investigated objects show damage or failure due to wood moisture changes or low and high wood moisture contents. Another study by Dietsch [2] shows that 30% of these objects are damaged due to seasonal or climate-induced wood moisture changes. Since the distribution of wood moisture is often not constant across the cross-section, internal stresses perpendicular to the grain (moisture-induced stresses, MIS) arise due to the anisotropic moisture-strain behaviour. These stresses can easily exceed the characteristic tensile strength perpendicular to the grain and lead to crack development, [3]. In curved glulam beams, these stresses can also lead directly to the total loss of load-bearing capacity, as shown in [4] or [5].

For structures exposed to the outdoor climate (service class 2), such as wooden bridges, monitoring systems have already been used for many years together with other measures to ensure safety and durability, [6]. Two important aspects are crucial to ensure the safety and functionality of the bridge during the desired lifetime, ASTRA guideline 12002 [7]. First, the design must focus on this goal and second, the condition of the structure must be ensured during the whole operational phase. This is usually done by regular visual checks and inspections combined with control measurements. If the control measurements are carried out continuously by means of a monitoring system, trends in the behaviour, damaging events or even damages can be derived from the data and controls and inspections can be planned more efficiently in time and cost.

Components that are difficult to monitor and concealed are often unavoidable in "protected" wooden bridges. Today, it is possible to monitor a bridge structure by means of point or laminar measurements. The determination of the wood moisture concentrates on the critical points/hazard zones/hot spots, such as connections, roadway transitions, penetrations, and support areas. With a certain amount of experience, it is usually possible to detect significant deviations in the wood moisture content at an early stage by monitoring over a long period of time, [8]. The waterproofing systems can usually not be checked or only with expensive effort. In most cases, this is only done if damage to the deck is already visible, [6]. A laminar leakage detection integrated in a monitoring system can detect irregularities earlier and damage can be avoided.

2 Planning, data management, transmission, and data analysis

For the planning, implementation and evaluation of a monitoring system, an exchange with appropriate experts should take place. At the beginning, the choice of the measured quantity is a first important step next to the definition of the control points and their number. The density of measurement data must be defined individually from object to object or from control point to control point. Specialists in this field can assist and advice in deciding on a suitable system.

The installation of measurement sensors enables the acquisition of measurement data at defined intervals. Data can be transmitted from individual measuring points, e.g., by WLAN, LoRaWan or LPWan to a central module (gateway) and further to a WebPortal, as shown in Figure 1. If the measurement data are stored on a WebPortal, they can be viewed in quasi real time, e.g., from the workplace, and are available worldwide. The server can evaluate the measurement data and trigger warnings or an alarm. Storage and evaluation of the measurement data can also take place directly on the gateway or other measurement/storage units and release warnings or alarms (e.g., via SMS). After commissioning, these systems operate autonomously.

The various components (measuring points, measuring device, gateway and user interface) form the monitoring system. Battery-powered systems can operate maintenance-free for up to several years, depending on the system and the number of measuring points.

[1] Steffen Franke, Professor for Timber Structures, Bern University of Applied Sciences, Switzerland, steffen.franke@bfh.ch

3 Measurement of wood moisture content

3.1 General to the measuring methods

For the measurement of wood moisture content, single point and laminar measuring systems can be used, see overview in Figure 2. For the monitoring of small critical areas, the resistance measuring method, the sorption isotherm method and the passive RFID tag method are available. The principal description of the measurement techniques for wood moisture content is given in the paper "Assessment of wood moisture and its effects", [10]. Specifics for monitoring purposes are added below.

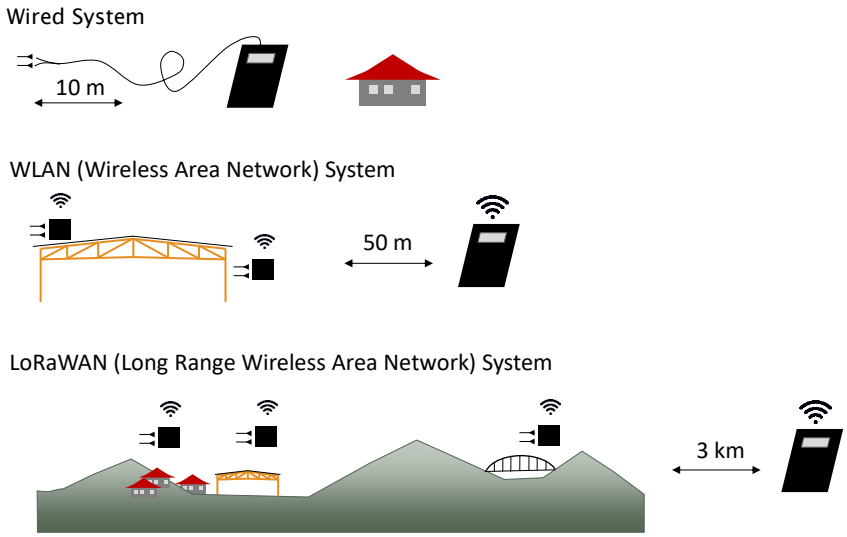


Figure 1: Overview of monitoring system's data management

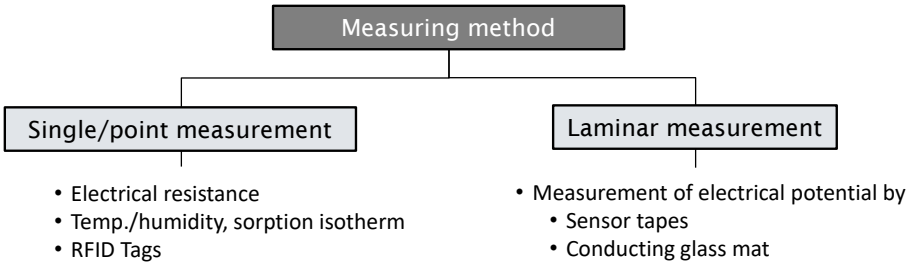


Figure 2: Overview of selected measurement methods for wood moisture content in the monitoring application

The electrical resistance measurement method is technically very simple to implement, easy to install and can be replaced from the outside. The sorption isotherm method provides high accuracy by measuring relative humidity and temperature in an insulated cavity, [9]. An RFID tag measures the humidity in the immediate vicinity of the tag averaged over a certain component depth using the principle of capacitive sensing. The use of RFID tags is inexpensive and wireless. Passive RFID tags do not require an external power supply or battery and can be used in many applications, [11].

Two-dimensional components can be reliably monitored with conductive glass fleece or with tape sensors. Both solutions rely on potential measurements and are mainly used in building construction for monitoring flat roofs, [12]. When the humidity changes or when water is present, the electrical potential of the conductive fabric changes and one can perform a real time moisture monitoring, [11].

In monitoring systems, a distinction is made between two main groups in the sensors, the active and passive sensors. This designation is used to distinguish whether the sensor requires electrical auxiliary power for the measurement or not. Active sensors require a supply voltage and then generate an output signal. This group includes, among others, the sorption isotherm and electrical resistance measurement methods as a point-by-point measurement of wood moisture. Passive sensors, on the other hand, operate without a supply voltage and use the energy in the environment, e.g., of the reader. Passive sensors include some radio frequency identification (RFID) tags.

3.2 Single measurements

3.2.1 Electrical resistance measurement method

The electrical resistance method is the most common non-destructive method to monitor moisture content developments. The method allows measurement of moisture content in different depths from the surface and measured resistances can logged over extended periods of time. The accuracy of the method is about 1 M% [13]. Factors affecting the accuracy concern amongst others the grain orientation, type of electrodes, wood density, and temperature. Resistance between two electrodes roughly ranges between 100 kΩ to 100 GΩ from the fiber saturation point to about 5 M%, respectively. Once resistances are large, electrical currents are extremely small and electrical fields around the monitored structure are considered a possible source of error.

The choice and installation of electrodes should be done carefully, especially for objects subjected to outdoor climate, strong climatic variations, or direct weathering. Due to the shrinkage and swelling of the wood, normal wood screws or nails may have no or poor contact with the wood or the cable. Both lead to falsification of the resistance measurement and mostly indicate lower wood moisture contents than in reality. The use of hanger bolts and a protective box has proved to be successful, cf. Figure 3. The hanger bolts must be insulated with suitable material except for the tip. The cables are fixed directly to the hanger bolt with nut and locknut. The shrinkage and swelling of wood have almost no influence on the required good electrical contact between wood and electrode. All metallic parts of the electrodes should be made of stainless steel, if possible, [11].



Figure 3: Principle sketch and photos of the installation of the hanger bolt electrodes and protective box, [11]

3.2.2 Sorption isotherm method

The sorption isotherm method is most suitable in the presence of glue joints, the influence of salts, the use of protective and impregnating agents, or even in the presence of prolonged temperatures below 5 °C. All these factors do not influence the measurement by means of sorption isotherms. The application and implementation of the measuring probe requires a cavity size of 8 to 10 mm in diameter, whereby the depth of the measuring probe can be controlled as desired, see Figure 4.

The functioning and results of the sorption isotherm method over different component depths are shown as an example in Figure 5 for a solid wood wall. The diagram shows the measured wood moisture content and the calculated equilibrium moisture content (green line) from the room climate over a period of two years. It can be seen very clearly that the sensor near the surface in the wall at a depth of 5 - 10 mm (orange line) reacts very quickly to the room climate with a similar rate of change and amplitude as the calculated compensation moisture. Only in the summer months, when the indoor climate becomes more humid very quickly, there are differences between the orange and green lines. However, these differences quickly equalize. In this construction, for example, plasterboard and abrasion are very diffusion-open materials.

Furthermore, the diagram contains the measured wood moisture contents at depths of 20 - 30 mm, 70 - 80 mm and 95 - 105 mm. Already from a depth of 20 mm (purple line), a "damped" behavior of the wood moisture with respect to calculated equilibrium moisture can be observed. Here, the wood moisture values are lower in summer and higher in winter than the calculated equilibrium moisture. In this case, the sorption isotherm method allows very precise evaluations of the wood moisture content and the interaction between the room climate and the water content in the solid wood wall.

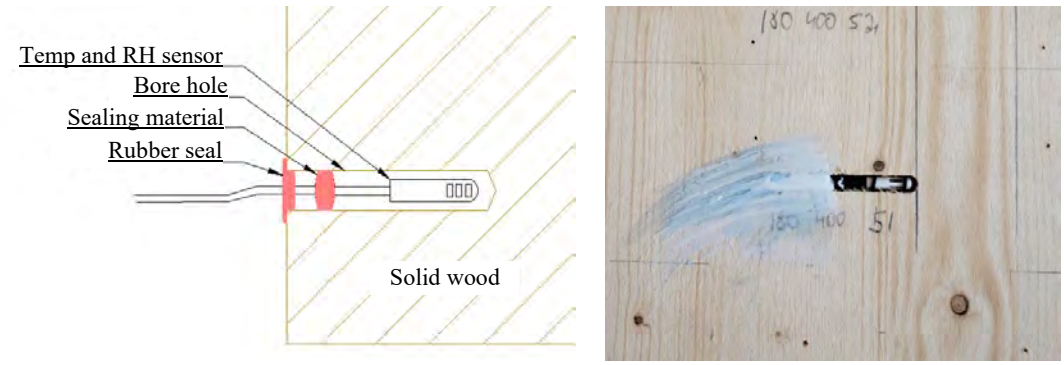


Figure 4: Installation of air temperature and relative humidity sensors in solid wood

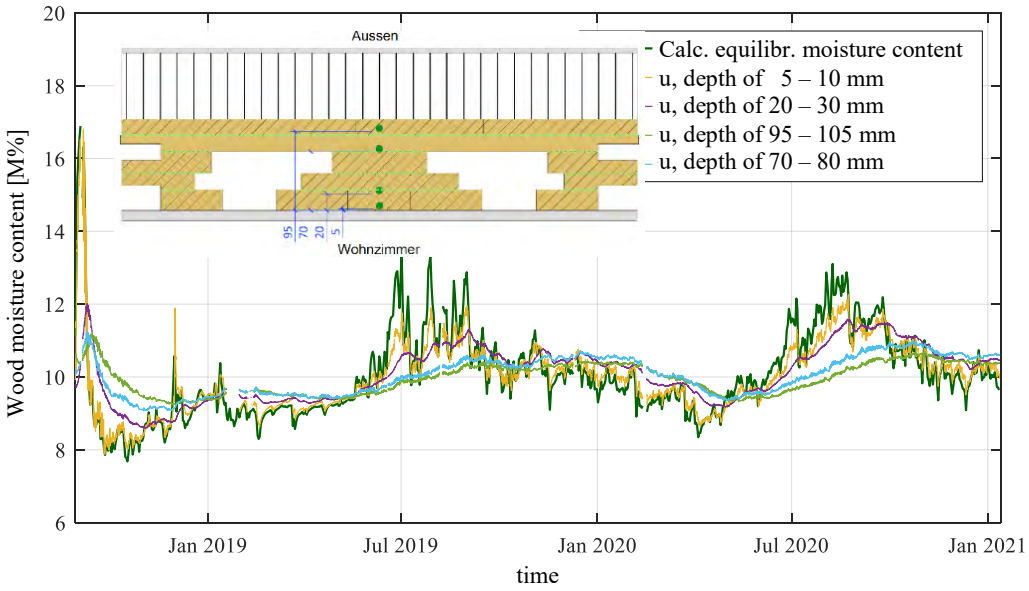


Figure 5: Evaluation of the wood moisture content measured with the sorption isotherm method at different depths in a solid wood wall

3.3 Moisture Sensor developed at BFH

An extra small battery-operated sensor for wood moisture measurement with radio data transmission was developed at the Bern University of Applied Sciences. It is inexpensive and easy to apply, see Figure 6. It measures, among others, the air humidity, and the temperature in a cavity in the material, and transmits it by radio (LoRa) directly to the cloud or to a gateway (Figure 7). The measurement results can then be processed and visualized. The sensor is located at the tip of the pin shaped extension below the electronic facing outwards. The extension which will be screwed into a drill hole. Different extension lengths could be realized to measure in different depths. Measurements up to two years can be made with one battery.

While every node could work and transmit its data individually, the results of several nodes can be synchronized and collected by using a Gateway. It receives the data by LoRaWAN, saves it and transmits them at once via 4G data net. The gateway also provides a remote access for checking the system conditions.



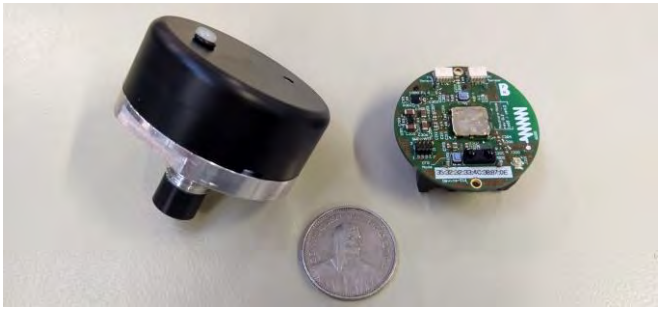


Figure 6: Moisture-Sensor, system with waterproof housing (left), electronic (right).

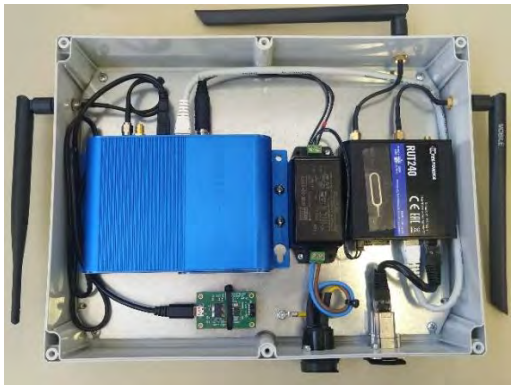


Figure 7: Gateway to use and control several sensor nodes

3.4 RFID tags for local leakage detection

Radio Frequency Identification (RFID) tags are small devices that use low-power radio waves to receive, store, and transmit data to nearby readers (Figure 9). The basic types of RFID tags are passive, active, and semi-passive or battery-assisted passive (BAP), [14].

- Passive RFID tags do not have an internal power source but are powered by electromagnetic energy transmitted from an RFID reader.
- Active RFID tags have their own transmitter and power source on board the tag.
- Semi-passive or battery-assisted passive (BAP) tags consist of a power source integrated into a passive tag configuration.

In addition, RFID tags operate in three frequency ranges:

- Ultra-High Frequency (UHF),
- High Frequency (HF) and
- Low Frequency (LF).

RFID tags can be attached to a variety of surfaces and are available in different sizes and designs. Dimensions vary from a few millimeters to several centimeters. RFID tags are also available in a variety of shapes (dogbone or patch, Figure 8). The Smartrac company or RFMicron are already using passive RFID tags for capacitive measurement of moisture or humidity. These tags have been successfully applied in the fields of construction, energy, but also healthcare.

First applications with RFID tags have also been carried out (Figure 9). The tests have shown that the installation of these RFID tags in the wood allows a punctual measurement of the wood moisture, but with a greater measurement uncertainty than the electrical resistance or sorption isotherm method, which can be seen at the wide band of results in Figure 10 . The RFID tags should be located inside the component and are readable until the overlying material layers do not shield the signal. A comparison of the placement the

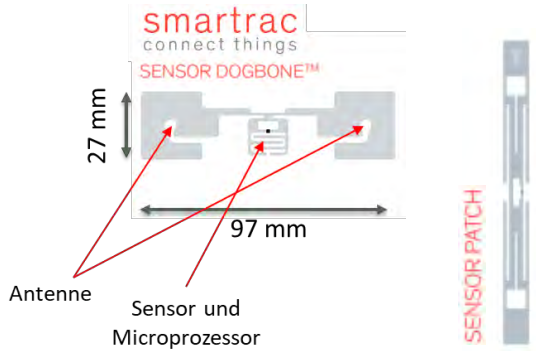


Figure 8: Components of a passive RFID tag from Smartrac without supply voltage



Figure 9: Simultaneous measurement of several RFID tags installed in the wood specimen

ICTB 2021 PLUS
4th International Conference on Timber Bridges
Biel/Bienne, Switzerland, 9 -12 May 2022



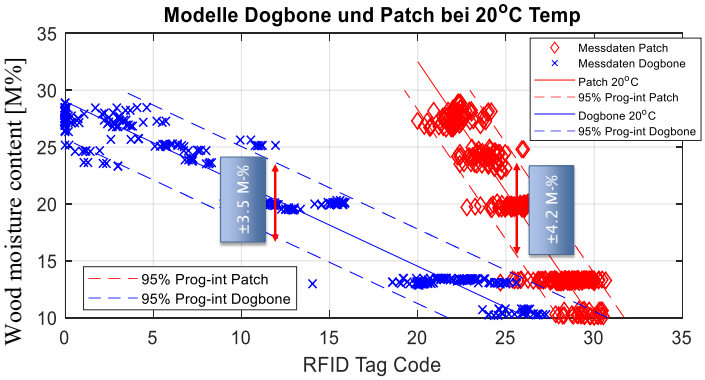


Figure 10: Correlation between RFID tag code vs. wood moisture at 20 °C for the dogbone and patch tag

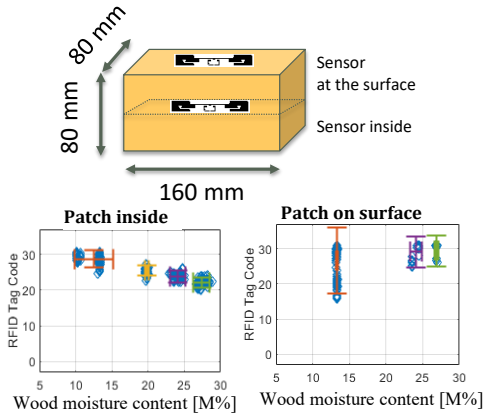


Figure 11: RFID sensor tests at surface and inside, setup (top), correlations (bottom)

RFID tag at the surface or inside was carried out, which showed greater variations of the results for the surface use, cp. Figure 11. This makes it possible to monitor hard-to-reach and invisible components even without a power supply. The RFID sensors are said to have a service life of 50 years.

The correlation between the read-out sensor code and the wood moisture must currently still be determined on the basis of reference checks and is RFID tag-specific. Figure 10 shows an example correlation between sensor code and wood moisture together with the prediction interval. The width of the prediction interval results from the scatter of the measurement data used to derive the correlation. Depending on the application, temperature compensation of the measurement must also be considered. The application range of the model is between 10 M-% and 28 M-% for the wood moisture. The measurement error of the dogbone and patch tag is ± 3.5 M% and ± 4.2 M% respectively, derived from the width of the prediction interval.

Due to the very low price of RFID tags and their small size, several sensors can be installed at each measuring point and an average of the sensor codes can then be calculated. In this way, a higher measurement accuracy can be achieved, and the system is less susceptible to the failure of individual RFID sensors.

3.5 Areal measuring methods

3.5.1 Area leakage detection with sensor tapes

With sensor tapes, it is possible to detect high moisture or wetness in a linear manner, e.g., under a waterproofing layer of flat roofs or road pavements. Band sensors consist of a plastic fabric and stainless-steel wires, see e.g., Figure 12. During monitoring, a potential measurement is made between two wires in the sensor band. The presence of water causes the electrical resistance to drop and can be detected.

This measuring method is mainly used in places where water or moisture can spread under the waterproofing. Depending on the spacing and arrangement of the individual tapes, quasi-area monitoring can be achieved with the sensor tapes. For the application in bridge structures, it must be ensured that for a two-dimensional leakage detection with linear sensor tapes, a roadway structure with a waterproofing without bond is used. This is because, depending on the planned transverse and longitudinal slope of the bridge, any water that has penetrated the separating layer between the waterproofing and the deck slab would flow

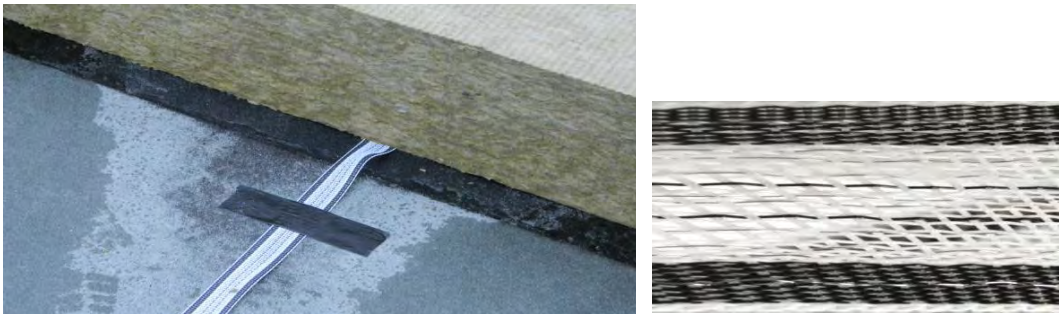


Figure 12: Tape sensor "dm" from ProGeo in a warm roof structure (left) and detail of the tape (right)

in the direction of the slope and could be detected here, e.g., at a bridge edge or deck transition. Point or linear sensors can be used at the slope edges.

The foot and cycle path bridge between Rupperswil and Auenstein was equipped with sensor tapes cf. Figure 13 and Figure 14. The monitoring system monitors the possible leakage of the waterproofing and additionally records climate data, material temperature and wood moisture, Figure 13. The on-site measuring unit evaluates the measurement data and sends it to a cloud so that it can be retrieved worldwide at any time using a browser. Warnings and alarms are triggered when critical values are reached.

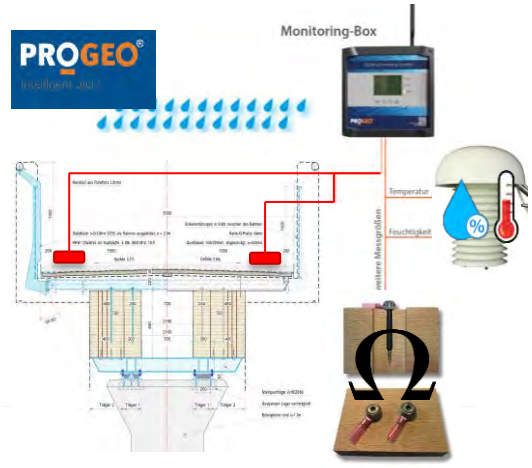


Figure 13: Monitoring system for the foot and cycle path bridge between Rupperswil and Auenstein



Figure 14: Sensors on the wooden panel and laying of the glass fleece and PBD seal

3.5.2 Area leakage detection with conductive fleece

In an intact waterproofing, there is no water flow and therefore no electrical current flow. In case of a leakage in the waterproofing, water penetrates the waterproofing and allows the conduction of electric current in the conductive fleece underneath the waterproofing. Based on this physical principle, areal monitoring of flat roofs or landfills is possible nowadays, [12]. The presence of water in the case of a leakage changes the electrical properties, respectively the measured value, thus leakages can be detected. After drying out, the original values are restored.

Early detection and the detection of hidden water damage are possible. The same functional principle can be used to detect the presence of water in the area of riser zones, installation spaces or interstitial spaces. Various monitoring systems for flat roofs are currently available on the market, e.g., smartex mx from ProGeo (D), Optidry from Ortungstechnik Nachbaur GmbH (A) or RoofProtector from RPM Gebäudemonitoring GmbH (A). These systems measure electrical parameters via conductive mats (laminar) or tapes (linear).

For leakage detection in flat roofs, for example, a conductive glass fleece is installed under the waterproofing and above the insulation. In addition, a grid of flat cables is installed. These form the inner pole of the measuring system. Above the waterproofing, a contact plate is used to set the second pole (Figure 15). During a rain event, the current is conducted from the contact plate over the entire wet surface to the waterproofing. The measuring unit performs a potential measurement between the two points. Using the cable grid, it is possible to display the potential curve in the surface and to determine the position of the leaks.



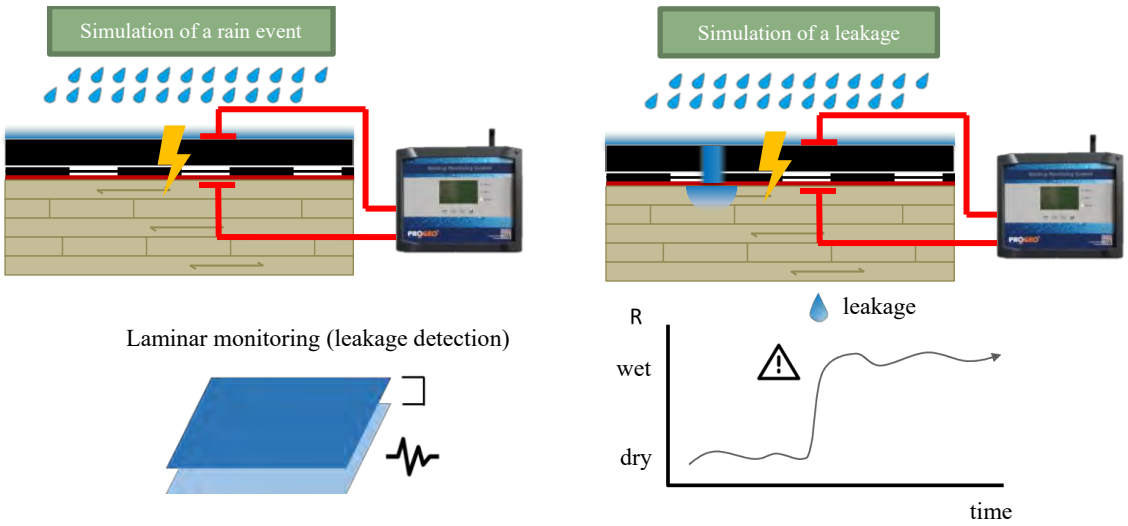


Figure 15: Schematic representation of the measurements on wood panels with conductive glass fleece, PBD waterproofing and mastic asphalt for a full composite structure

4 Measurement of eigenfrequencies for damage detection

Every structure vibrates due to natural excitation or use in its natural frequency, which depends on the mass and stiffness. If damage occurs, the stiffness may change and so does the natural frequency. The constant recording can be used for a systematic gain of knowledge. The constantly occurring measurement data (accelerations, vibrations) must be digitally recorded, filtered, and analysed so that differences in the vibration behaviour, in the natural frequency, can be recognised. In this way, e.g., as a traffic lights principle, authorities can obtain results about the condition and at the same time engineers or researchers can obtain general data sets to improve vibration measurement or design. In timber construction, knowledge is available for the pure vibration assessment of timber ceilings. The application to timber bridge structures for condition assessment is not yet known.

The departments AHB and TI jointly developed a stand-alone vibration measurement system consists of several sensor nodes and a powered HUB, Figure 16. Each sensor node includes the 3-axial acquisition of the accelerations and the wireless data transmission (via BLE - Bluetooth Low Energy - up to 100 m) of the measurands directly to a PC or the HUB. They are battery-operated (runtime 0.5 year) and easy to install and handle. Several nodes can be integrated into one measuring system by the HUB at the same time. The raw data is stored locally and sent to a time series database. The hub controls and monitors the sensor nodes. Problems such as short interruptions in the connection to the sensors are handled correctly, so that long-term use is ensured. A specially developed software is used to control the sensor nodes and visualize the acceleration data. The sensor data can be displayed in the time domain as well as in the frequency domain, Figure 16 right. This makes it possible to determine the natural frequencies.

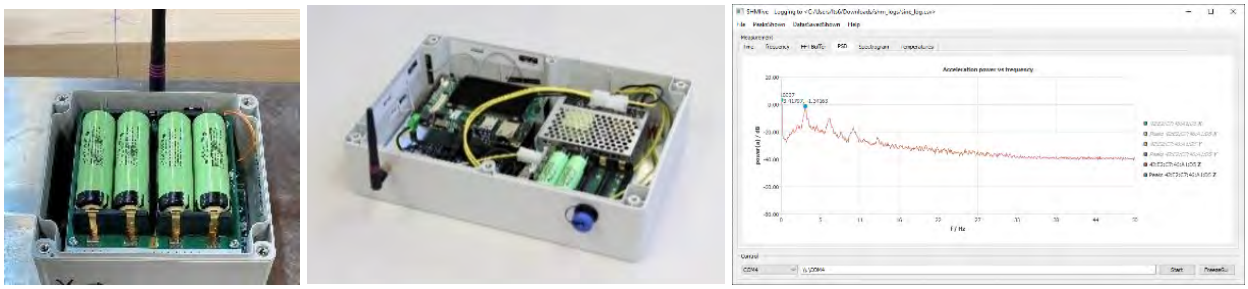


Figure 16: Sensor node with 3-axis acceleration sensor below the battery pack (left), HUB (center) and FFT analyses of the frequencies (right)



5 Case study – Monitoring of a timber bridge

Within the framework of research projects, various road bridges in wood within Switzerland have already been monitored by the Institute for Timber Construction, Structures and Architecture at the Bern University of Applied Sciences. The structures range from beams, arches, trough bridges to log bridges and timber-concrete composite bridges. The locations vary regionally as do the bridge crossings over rivers, valleys or roads. Spans range from 13 to 50 m. More detailed information is summarized in [6] and [15].

Figure 17 shows the course of the air temperatures and relative humidity measured on site together with the calculated equilibrium moisture content on the surface of the wood for the Obermatt bridge in the Emmental valley as an example. Figure 17 contains the measurement locations shown on the bridge cross-section. The other diagrams in Figure 18 show the wood moisture content measured in the supporting cross-section. The wood moisture content was measured near the surface, approx. 20 mm deep, and in the cross-section with a depth of 200 mm. In addition, the calculated equilibrium moisture content was determined for each measuring point; a time delay due to the moisture transport in the wood and the duration of exposure to the climate was not considered. The course of the measured wood moisture content shows a delayed and damped course compared to the calculated compensation moisture content.

On the south side, an increase in wood moisture content for one measurement sensor can be observed from August 2013. This is associated with partial structural leakage, which has since been corrected and the wood is allowed to dry out again. In this case, the installed monitoring system has acted as an early warning system and later serious structural damage could be avoided at an early stage.

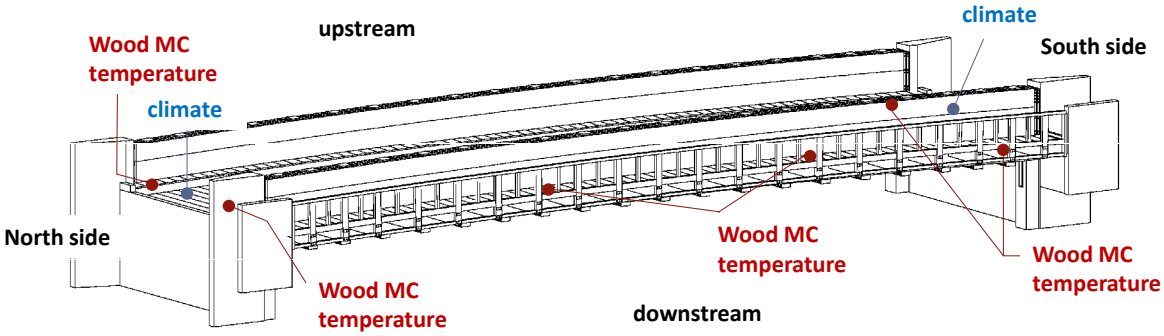


Figure 17: Positioning of the measuring sensors at the Obermatt bridge

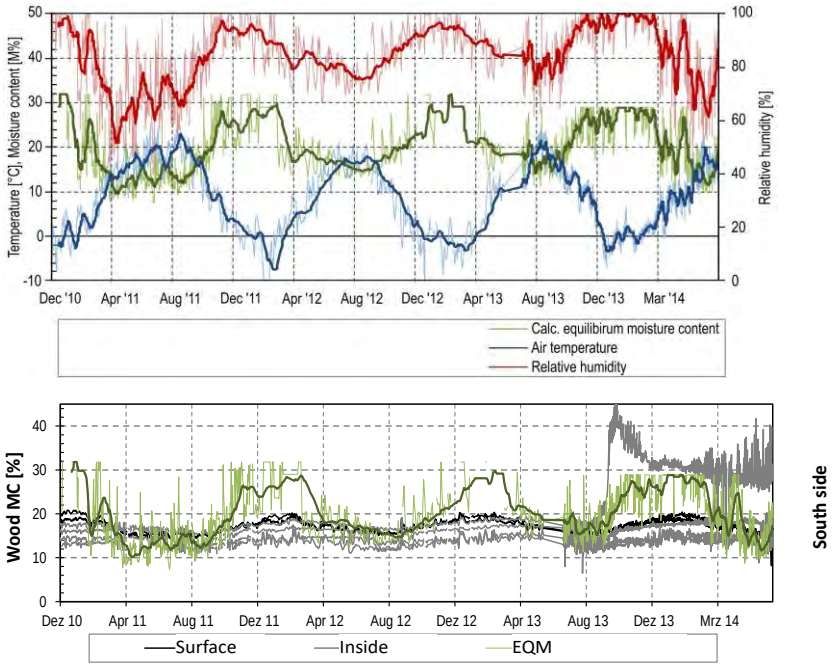


Figure 18: Climate, wood moisture content and calculated equilibrium moisture content for the Obermatt Bridge, after August 2013 Leakage visible in cross-section.



6 SUMMARY

Wood is a living and recognized construction material for the realization of diverse load-bearing structures such as houses, ice, riding and sports halls as well as swimming pools, warehouses, production buildings and bridges. However, wood is also a hygroscopic material and can absorb or release moisture from the surrounding climate. The so-called wood moisture content (MC) influences the material strengths and stiffnesses as well as the long-term load-bearing behavior. As the studies of [1] and 10 show, half of the cause of damage to wood structures is due to a change in wood moisture content or seasonal and climate-related changes in wood moisture content. For this reason, continuous monitoring of wood moisture content is a suitable early warning system to increase the quality of wood structures in the future in a pioneering way and to detect changes in time. The control points in the monitoring should be placed in possible danger zones/hot spots. These can include roadway crossings, support areas, transition areas and penetrations. The various point and area methods presented are suitable for measuring wood moisture content. For the planning, implementation and evaluation of a monitoring system, the number of measuring points, the accuracy and the data storage/transmission should always be defined with a view to the objective. At this stage, an exchange with appropriate subject matter experts can provide positive support.

ACKNOWLEDGMENT

The presented research results have been generated in the projects "Quality Assurance of Wooden Structures" of the Forest and Wood Research Promotion Switzerland (WHFF-CH) of the Swiss Federal Office for the Environment and the "Sealing Systems and Bituminous Layers on Bridges with Pavement Slabs", VSS2016/326 of FEDRO. The funding bodies and accompanying business partners are thanked here for their support.

References

[1] Frese M., Blass H.J. (2011), Statistics of damages to timber structures in Germany, Engineering Structures 33, pp. 2969–2977

[2] Dietsch P., Winter S. (2018), Structural failure in large-span timber structures: A comprehensive analysis of 230 cases, Journal of Structural Safety 71, pp. 41-46

[3] Möhler K., Steck G. (1980), Untersuchungen über die Rissbildung in Brettschichtholz infolge Klimabeanspruchungen, Holzbauforschung, pp. 194-200

[4] Aicher S., Dill-Langer G., Ranta-Maunus A. (1998), Duration of load effect in tension perpendicular to the grain of glulam in different climates, Holz als Roh-und Werkstoff 56, pp. 295-305

[5] Gustafsson PJ., Hoffmeyer P., Valentin G. (1998), DOL behaviour in end-notched beams, Holz als Roh- und Werkstoff 56, pp. 307-317

[6] Franke B, Franke S, and Müller A. (2015) Case studies: long-term monitoring of timber bridges, Journal of Civil Structural Health Monitoring 5, p. 195-202.

[7] ASTRA (2005) Richtlinie 12002, Überwachung und Unterhalt der Kunstbauten der Nationalstrassen

[8] Müller A., Schiere M., Bonifacio S. (2020) Feuchtemonitoringsysteme auf Holzbrücken, Tagungsband 4. Brückenkolloquium, Technische Akademie Esslingen

[9] Bonifacio S. (2020) Untersuchung der Grundlagen zur Messung des Raumklimas in einen Holzgebäude, Berner Fachhochschule Architektur, Holz und Bau, Schweiz

[10] Franke B., Schiere M., Franke S., Müller A. (2021) Bewertung der Holzfeuchte und deren Auswirkungen, in Proceedings: Workshop - Zustandserfassung und Erhaltung von Holztragwerken – Biel/Bienne

[11] Müller A., Angst C., Bueche N., Schiere M., Bonifacio S. (2021) Asphaltbeläge auf Holzbrücken - Synthesebericht der Versuche und Untersuchungen, Forschungsbericht, Berner Fachhochschule

[12] Burger K., Elter P., Holm K. und Kämmer U. (2018), Das dichte Flachdach, Bauphysik-Kalender 2018 Feuchteschutz und Bauwerksabdichtung, 335-360

[13] Dietsch P., Franke S., Franke B., Gamper A., Winter S. 2015. Methods to determine wood moisture content and their applicability in monitoring concepts, Journal of Civil Structural Health Monitoring 5 (2), pp. 115-127

[14] Smiley S. (2019) A Tag, A Label, An Inlay. AtlasRFIDstore, 1 May 2019, www.atlasrfidstore.com/rfid-insider/a-tag-a-label-an-inlay.

[15] Franke B., Müller A., Franke S., Magniere N. (2016) Langzeituntersuchung zu den Auswirkungen wechselnder Feuchtegradienten in blockverleimten Brettschichtholzträgern, Forschungsbericht WHFF 2013.06, ISBN 978-3-9523787-7-9.

Conference Proceedings 4th ICTB (2022)
https://doi.org/10.24451/wd9c-8h83

ICTB 2021 PLUS
4th International Conference on Timber Bridges
Biel/Bienne, Switzerland, 9 -12 May 2022



Wooden bridges enrich the world

Frank Miebach[1]

1 Introduction

Wooden bridges are certainly time-honored exotics among the building types. Thanks to a history that stretches deep into human history, wooden bridges have always reflected the state of the art in the historical context. And surprisingly, the material that has been used for a long time has never gone out of fashion. Even if wooden bridges nowadays only eke out a niche existence, there are good signs of a renaissance. High time for an evaluation and appreciation of this type of construction, taking into account various aspects

2 Technical enrichment

Developments in technology are always visible in buildings. The construction of wooden bridges is particularly interesting, as there are still structures with a service life of over 600 years to be analysed. Here, the technical development can be observed very well: While simple beam structures were originally erected, trusses were later increasingly implemented for larger spans. The relatively small availability of the material wood in the form of solid wood beams was the limiting factor. As a result, however, this type of construction continued to flourish until the last century. Thanks to new production technologies, a new chapter was opened with the invention of glulam. For 100 years now, it has been possible to produce large-format wooden beams, which have culminated in the gluing of log beams for 30 years now.



Figure 1: Trussbridge Kempten (GER)



Figure 2: Stress-Ribbon-bridge Gera-Ronneburg (GER)

3 Socio-cultural enrichment

The coexistence of people becomes very concise and directly tangible, especially in the construction of bridges: bridges serve the exchange and overcoming of obstacles. Pedestrian bridges in particular are more sensitive to the direct interplay of materials, which are intended to accompany people safely in the truest sense of the word. The material wood, which can be experienced with almost all the senses, creates a very harmonious relationship between the building and the user. Numerous identity-creating buildings bear witness to the power of wood as a material.



Figure 3: Cityscape Schwäbisch Hall (GER)



Figure 4: Border bridge Ainring (A-GER)



Figure 5: Landmark Sneek (NL)

[1] Frank Miebach, IB-Miebach, Germany, info@ib-miebach.de



4 Ecological enrichment

The current public debate on climate change is shining a bright light on the timber construction industry in general - and timber bridge construction in particular. The enormous added value of the CO^2 saving capacity will help wood to achieve a new classification. An exemplary comparison of different types of bridge construction shows quite impressively:

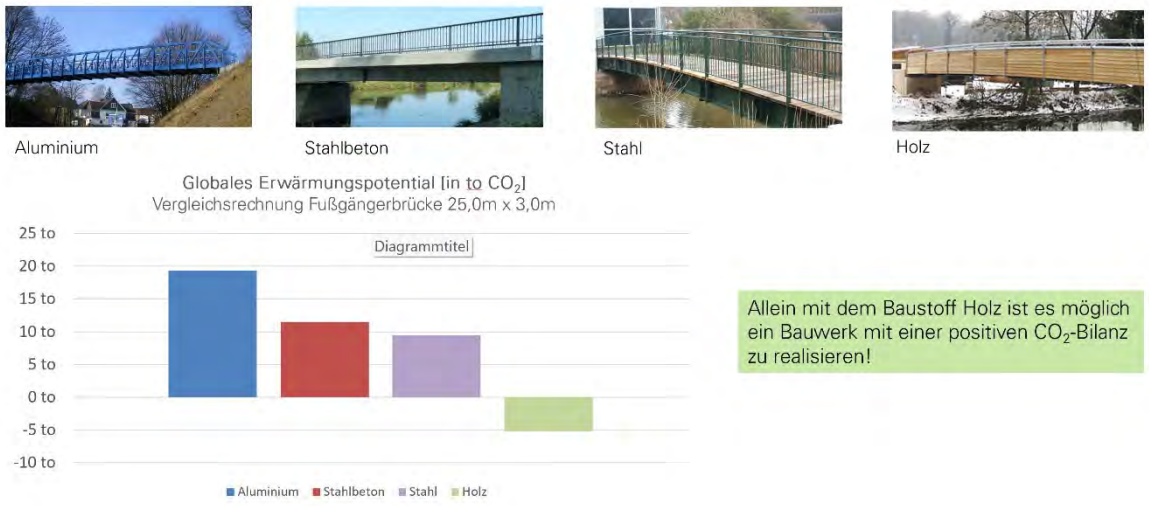


Figure 6: CO_2 Ecobalance timber bridge 25 m long, 3 m wide

The overall context of wood's performance must be assessed: wood is almost the only load-bearing building material capable of storing CO_2.

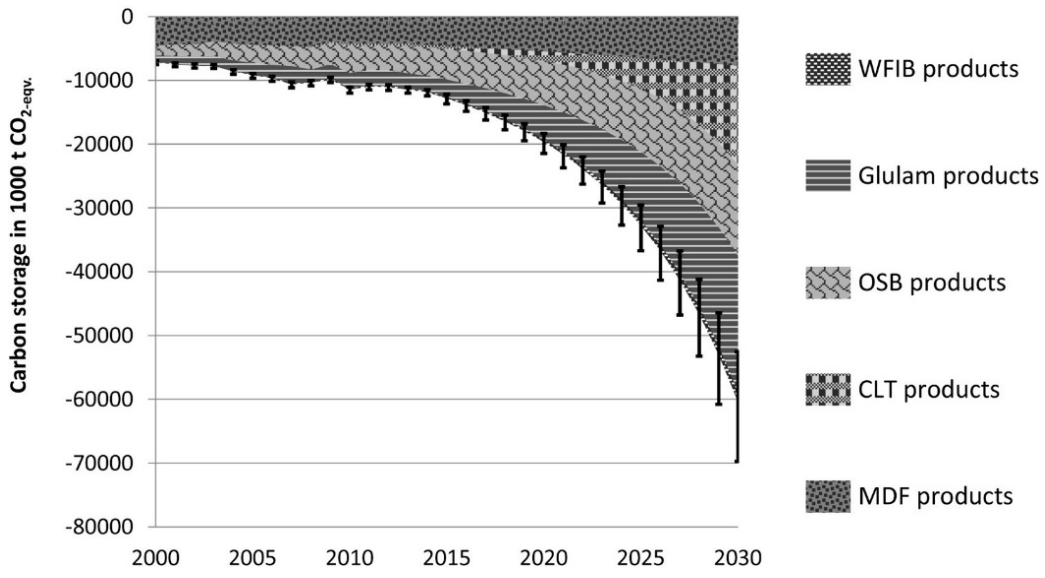


Figure 7: Prediction Carbon storage timber



5 Economic enrichment?

If we look at buildings in terms of their economic benefit, the life span and service life play a central role. Wood as a material is certainly ambivalent in this respect. Wood as a material is not necessarily durable per se if it is exposed to weathering. As soon as moisture is kept out, however, its economic potential becomes apparent: the material ages extremely slowly and can reach a service life of several hundred years.



Figure 8: Bridge Unterregenbach (DE)

With a different approach, the question may be asked why wood is a niche material in bridge construction? The answer is often that timber construction has to be affordable, so the economic viability is doubted.

But isn't it interesting to observe that in Germany, for example, there is a correlation between the timber construction rate and the prosperity of the federal states?

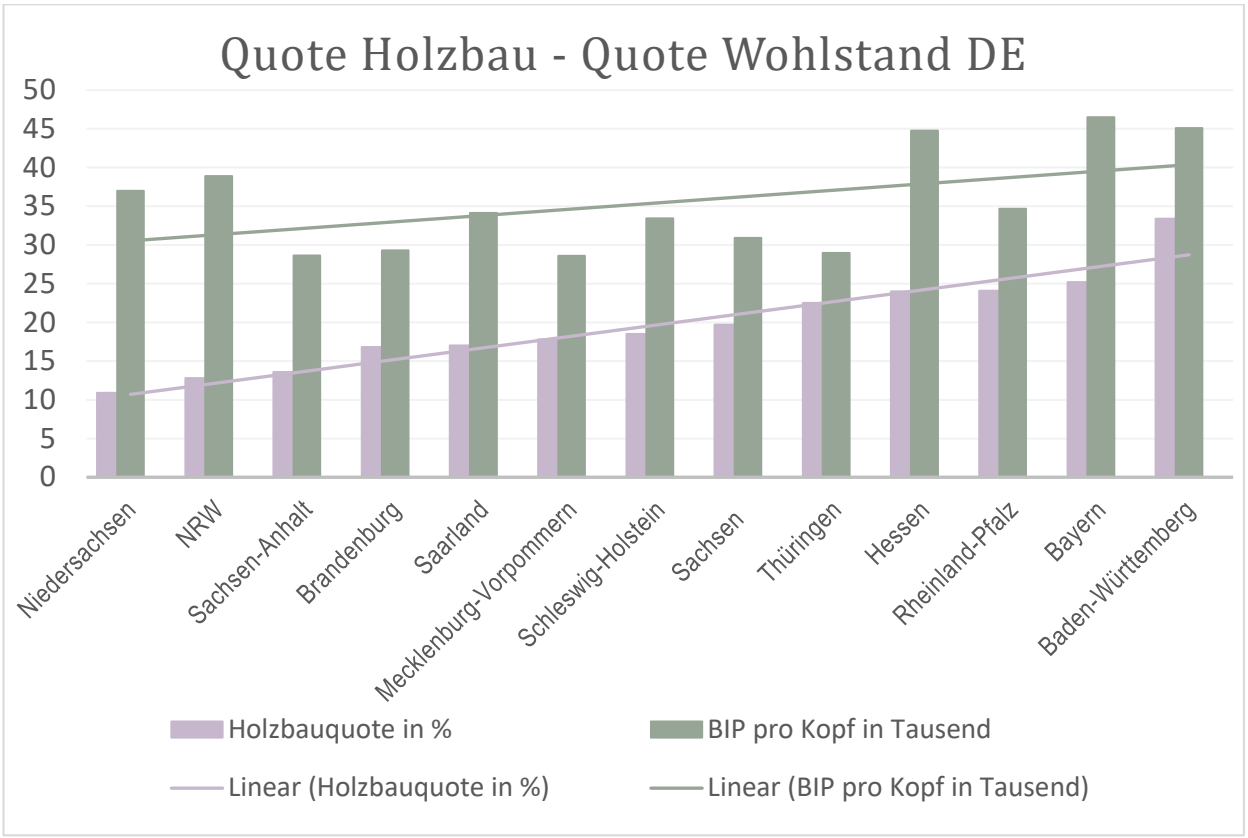


Figure 9: Graph of timber construction rate and income in Germany by federal state (as of 2019)



6 Conclusion

In numerous aspects, timber bridge construction is undoubtedly an enormous asset. The structures can be technically demanding, are often regarded as identity-forming, are ecologically advantageous and sometimes very durable. But beyond that, it seems that the following insight can be gained: In those regions of the world where timber construction is strongly represented, there is increased prosperity. Thus, timber construction enriches in the truest sense of the word!

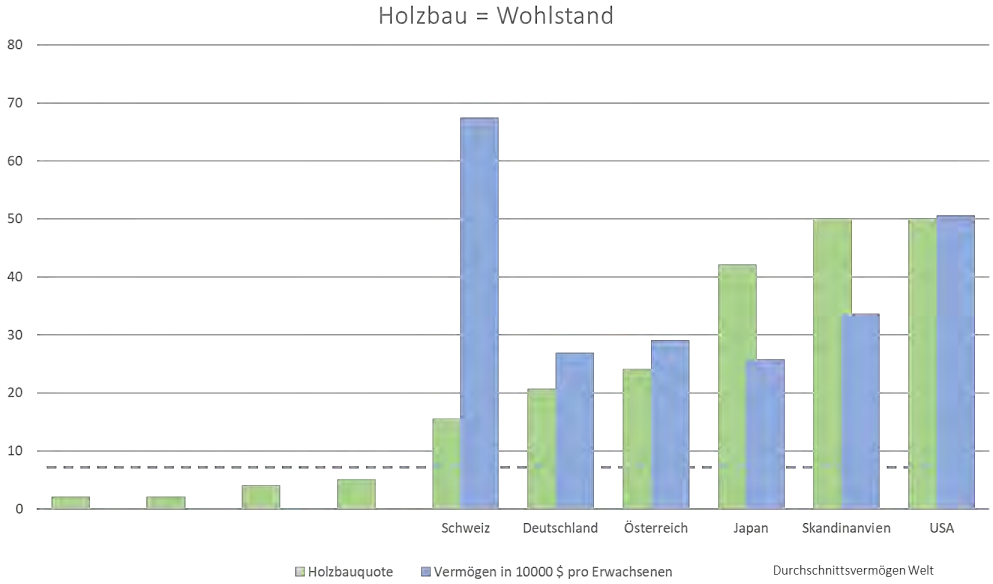


Figure 10: Graphic timber construction rate and income worldwide (as of 2019)

Conference Proceedings 4th ICTB (2022)
https://doi.org/10.24451/y8h3-6087

ICTB 2021 PLUS
4th International Conference on Timber Bridges
Biel/Bienne, Switzerland, 9 -12 May 2022

Modern Timber Bridges

Rune Abrahamsen[1]

1 Introduction

Since the mid 90's Norway has built hundreds of small and large timber bridges. Timber bridges have become viable alternatives to conventional bridges and are regularly proposed by designers and clients for new projects. Increasing focus on carbon storage leads to increased interest in timber bridges. Additionally, most clients seek the benefits of rapid construction, lightweight structures, material efficiency, clever landscape adaptation and good aesthetics.

This paper gives a short introduction to bridges that will be presented at the corresponding keynote lecture in Biel. The emphasis will be on current timber bridge construction in Norway.

2 Pedestrian bridges



Figure 1: Bjørgum bridge, Voss



Figure 2: Built 2015. Spans 38 m



Figure 3: Stela bridge, Brumunddal



Figure 4: Built 2021

[1] Rune Abrahamsen, CEO, Moelven Limtre AS, Norway, rune.abrahamsen@moelven.no



3 Ski bridges



Figure 5: Skei bridge, Skeikampen



Figure 6: Built 2022



Figure 7: Myrkdalen bridge, Myrkdalen



Figure 8: Built 2019

4 Railway flyover bridges



Figure 9: Norsenga bridge, Kongsvinger



Figure 10: Built 2017. Length 94 m.



Figure 11: Drivstua bridge, Oppdal



Figure 12: Built 2019. Length 30 m

5 Highway overpass bridges



Figure 13: Grundset bridge. 1 of 8 bridges crossing Rv3/Rv25



Figure 14: Built 2020. Løten/Elverum



Figure 15: Harpviken bridge. 1 of 3 bridges crossing E6.



Figure 16: Built 2020. Brumunddal



6 Network arch bridges



Figure 17: Steien road bridge, Alvdal. 88 m free span!



Figure 18: Built 2016



Figure 19: Frønes bridge, Åfjord



Figure 20: Built 2021

Acknowledgement

Timber bridges in Norway would have failed if it were not for the persistence of certain individuals in the Norwegian Road Authorities, Industry, Universities, Institutions and designing companies. Thank you all!

References

[1] Moelven Limtre AS (2022) Interactive map of timber bridges in Norway supplied by Moelven. https://www.google.com/maps/d/edit?hl=no&mid=1HlpDAeBMrSE29fhZ9Qz0avQ_Lr4

Conference Proceedings 4th ICTB (2022)
https://doi.org/10.24451/3jpy-3q31

ICTB 2021 PLUS
4th International Conference on Timber Bridges
Biel/Bienne, Switzerland, 9 -12 May 2022



Advanced data logging system for moisture monitoring of timber bridges – background and large-scale application

Kai Simon[1], Jürgen Hezel, Simon Aicher

1 Introduction

Wooden bridges are amongst the oldest structures of man-made infrastructure. While strength and stiffness, processing properties and sizes are assets of wooden members for bridge constructions, the limited natural durability of wood, unless considered adequately, is detrimental. Unfortunately, in the past many wooden bridges were designed without considering the rules for structural wood protection properly [1]. Therefore, the Stuttgart Timber Model Bridge (STMB) incorporating an integral timber-concrete abutment connection was developed on the basis of a wide database of bridge damages. Here, a seamless construction method with a completely gapless waterproofing layer is used. In the course of the construction of the model bridge on the campus of the University of Stuttgart, a system for the long-term monitoring of climate data, wood moisture content, stresses in connection parts and leakage detection was configurated and field-tested. Especially the system for the detection of punctual wood moisture is of high interest in areas of abutments, connections and fasteners to detect and prevent a possible damage development at an early stage.

Although the monitoring system used at the Stuttgart Timber Model Bridge provides very good measurement results there are some drawbacks. To overcome these disadvantages, an optimized system for recording the wood moisture content and climate, among other data, was developed in the context of orders to MPA University of Stuttgart from building owners and engineers for recently built and new timber bridges. Especially for large structures with several supporting areas and an increased number of potential measurement areas, the newly developed data recording system is advantageous.

2 Stuttgart Timber Model Bridge

2.1 Monitoring systems

The detailing of the Stuttgart Timber Model Bridge (STMB) results from an existing research project [1] on damages and related preceding mistakes in the construction of existing timber bridges. The STMB was built in the year 2016 at the Campus of the University of Stuttgart. To ensure and prove the function of the realized construction preservation measures, basically given in EN 1995-2 [5], a monitoring concept with the following components was installed:

- 16 sensors for the punctual moisture content in different depths (electrical resistance method)
- 3 sensors for the climate beside and under the GLT superstructure beam and between the GLT structure and the sealing layer
- 3 sensors for the temperature of the wood
- 11 sensors for a leakage detection at the second sealing layer
- 1 displacement transducer for the temperature and moisture dependent length variation of the GLT
- 5 displacement transducers for the relative displacements at the integral GLT-concrete abutment connection
- 8 strain gauges on the surface of the GLT beam to obtain the stresses at the integral support
- strain gauges on 8 of the glued-in rods at the integral GLT-concrete connection

After six years of monitoring there exists a valuable database which enables to adapt some of the systems for other constructions and buildings. All systems are working and are sending their data in a regular interval wireless to a server. A big challenge of the combination of five different data logging systems is the consolidation and evaluation of the data. For the installed sensors over all five data loggers of different manufacturers are necessary. Every system has its own method to record, transcript and send the data to the web. Some are sending the files via email protocol, others are using the File Transfer Protocol (FTP) to a server hosted by the customer and the last ones are sending the data via FTP to a server of the manufacturer where the customer gets access to read the data. To create a continuously updated health status of the bridge

[1] Kai Simon, Materials Testing Institute, University of Stuttgart, Germany, kai.simon@mpa.uni-stuttgart.de

it represents an enormous effort to gather and host all these different files, formats and accessibilities of data. Due to space limitations of the paper a special attention is given here to the moisture monitoring system only, what is explained below.

2.2 Advantages and Disadvantages of the moisture monitoring system used at STMB

The system used for the moisture content reading of representative points in the GLT beam structure of the STMB is a commercial system for every kind of consumer (Scanntronik Mugrauer GmbH, Germany). The system is well proven at small to medium sized timber bridges and other constructions; valuable results are presented in several publications, e.g. by Dietsch et al. [4], Müller and Franke [9] or Koch et al. [8]. It is possible to install and use the system with almost no knowledge of data processing which makes it appealing to a wide spectrum of users. Most components are just installed by plug and play. The system comes with a more or less intuitive software to ensure data reading and evaluation of smaller monitoring projects. The manufacturer provides a wide range of sensors for e.g. climate, material moisture content or displacements.

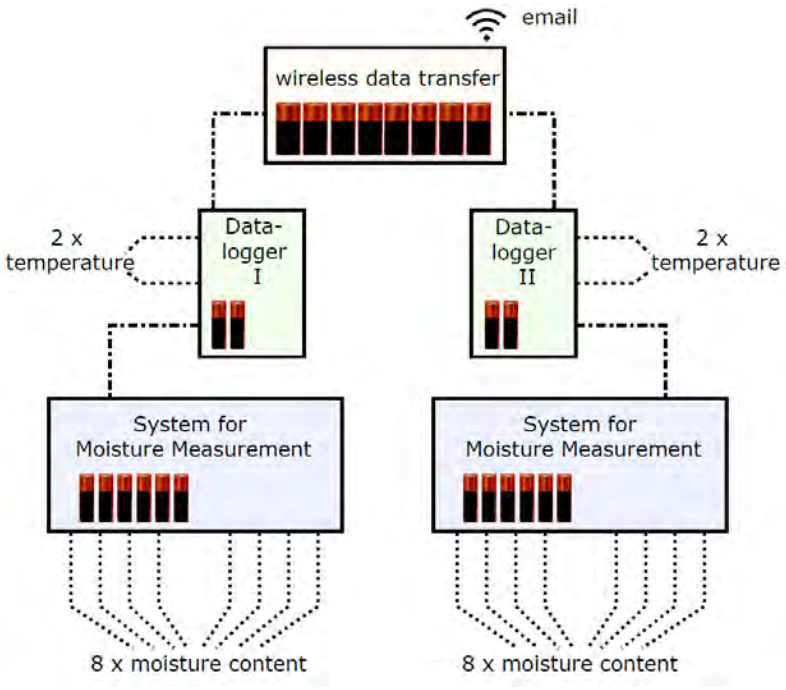


Figure 1: components and battery requirements of the monitoring system at the STMB

The setup principle consists of a modular way. The sensors are connected to each specific measurement unit, which is connected to a data logger. The data logger (optionally) is connected to a wireless data transfer system which can send the measured data via email to the user. The system always sends the complete data set what affords much energy and data traffic. Without this remote system the user is induced to get the data manually with a notebook from the data loggers. For big monitoring systems with a high number of sensors and a small interval of measuring, the data storage reaches the limit after less than one year. An example for a possible setting of then described moisture content reading system is shown in Fig. 1. It is important to mention that this is the maximum number of sensors which can be used with one remote system. In case of a requirement of the double number of sensors, all components of the shown system are needed twice.

A profound disadvantage consists in the limitation of connectable sensors to the different measuring units or data loggers. For any sensor type a separate measurement unit is required. So, for example it is not possible to replace one of the eight moisture content sensors in the configuration shown in Fig. 1 by one displacement sensor. Therefore, a separate data logger together with a displacement measuring unit would be needed. The number of connectable data loggers to one remote system is also limited to two. The greatest handicap noted while using the system was the very large amount of batteries required for the system to run. Every component of the system needs its own quantity of batteries. In the given example configuration 24 batteries are required to supply the monitoring of 16 punctual moisture content sensors. The maximum interval for changing the batteries is about one year. Also, the cable distance between the moisture measuring unit and the sensor, consisting of two electrodes, is limited. In case of long cable distances between the measuring unit and the pair of electrodes this makes the system vulnerable for external radio or electricity signals.

3 Development of a new Moisture Monitoring system

3.1 Setup and functionality

Because of the limitation of the number of sensors, the great energy demand and some other disadvantages some research work was undertaken at MPA University of Stuttgart, Dept. of Timber Constructions, to develop an improved system especially for large timber bridges / buildings. Together with a manufacturer for measurement and sensor technologies a new system for the measurement of the moisture content of timber with the method of the electrical resistance [1] was built up.

The system consists of one central processing and data logging unit, which (optionally) sends the data via FTP to a server of the customer. Sensors are connected to Hubs each gathering up to 11 inputs. From each Hub one data cable connects to the logging unit. The sensors are addressed by a BUS-system (RS-485) which allows to have long cable distances between the logging unit and the HUBs as well as between the HUBs and each sensor. In case of measuring the moisture content or the electrical resistance a small interface near the sensor (2 electrodes) is required to convert the BUS-signal to an electrical measurement signal. From one interface two pairs of electrodes (2 sensors) can be fed.

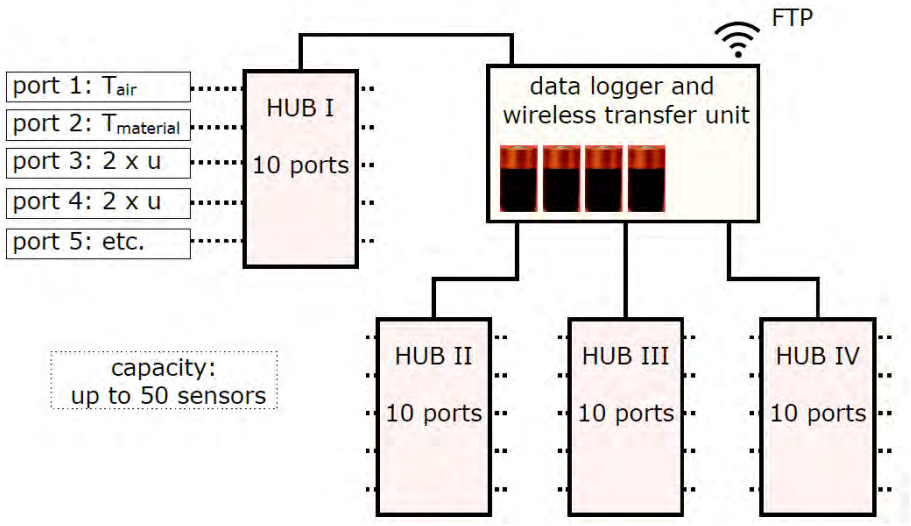


Figure 2: components and battery requirements of the developed monitoring system

Because the data logging system uses an universal BUS-system to address sensor interfaces, it is possible to connect any further sensor types, such as sensors for temperature, relative humidity, leakage/free water detecting, strain gauges, etc.

A schematic system configuration of the system is shown in Fig. 2. The logging unit is able to manage up to 50 sensors or 100 in case of moisture content sensors. Despite the large number of ports, the system gets by with only four mono-type batteries.

3.2 Data processing

The implementation of the data evaluation software was made by MPA University of Stuttgart. The system delivers values for the temperature and the relative humidity in °C and %, respectively, so they can be used as they are. The values from the moisture content sensors are delivered as raw data resistance in MOhm and have to be converted into a moisture content value in %. Several tests in the laboratory with electrodes from stainless steel and timber parts, which were oven dried after the tests to get the moisture content, together with the calculation model from Samuelsson [10] and Forsén and Tarvainen [7] served as a basis for the calibration of the sensor interfaces for spruce. The compilation and verification of different calculation models by Forsén and Tarvainen [7] also deliver a calculation model for the influence of the wood temperature on the electrical resistance which is implemented in the data evaluation.

The script written with the programming language Python© can automatically retrieve the data from the FTP server and save them in a local database. This addresses all further calculations like converting electrical resistance into timber moisture content, summarizing of data sets, exclusion of error measurements from the evaluation or determination of the equilibrium moisture content of the wood surface induced by the surrounding climate according to Avramidis [3]. From the calculated data several diagrams of the monitoring results can be plotted directly, as shown in Fig. 7, or optionally can be embedded on a website. The data form the logging unit is uploaded once a day so then the evaluation software runs once a day and updates the database automatically.

Form every data upload by the data logger the protocol gives the health status of the system. With the script the battery voltage or the signal quality of the remote unit can be read out and documented in form of a health report or an error message to a mail account or a smartphone if for example the battery voltage falls below a critical value.

3.3 Advantages of the system

Although the system still needs to be improved and has some susceptibilities, such like error measurements while there are other electrical signals around or sending problems induced by low GSM quality, there are some advantages compared to the system used at the STMB. First of all, it would be possible to process almost all sensors installed at the STMB by a simple logging unit of the new system. This becomes evident in Table 1, showing a comparison of the two bridges monitored by the established and new systems.

One of the most important advantages consists in the fact that only four batteries are required for the central processing unit. Also, the option to connect several different sensors via the BUS-system to that one unit gives a clear arrangement and a low space requirement.

The logging unit is sending only the new data gathered since the last sending protocol to the FTP-server hereby saving a great amount of data and energy usage. The data is also copied to the local storage which provides 32 Megabytes. The intervals for measurements and data uploading can be chosen separately by the user. The providing of the battery voltage and the sending signal quality at each protocol makes it easy to prevent a data loss or a breakdown of a system. The possibility to connect up to 50 sensors to one unit and to upscale the system as well as the wide range of applicable sensors makes the system attractive for more than just a moisture content monitoring at timber constructions.

4 Large-scale application Bad-Mergentheim

The pedestrian bridge in the spa park in Bad Mergentheim, built in 2020, connects the spa park area with the city over the river Tauber, see also Fig 3. The load-bearing structure of the bridge consists of two parallel block-glued glulam (GLT) superstructure beams with variable height. The bridge girders are supported on a total of 8 RC-abutments; the total length of the bridge is around 90 metres. The largest partial span then crossing the river is 30 m. The deck of the bridge is made of pre-cast concrete slabs resting on cross girders. Fig. 3 shows a view of the bridge structure. Figures 4 and 5 show a side view and the cross-section build-up, respectively, of the GLT superstructure.

A total of 52 pairs of electrodes are installed as sensors for moisture content monitoring. The measuring locations are arranged i) at the end grain faces of the GLT beams at both end abutments (A and B) and ii) at inner supporting pile locations C, D and at the mid-river apex point (C&D). The measuring electrodes at locations C,D and C&D are arranged laterally on the girders to capture the moisture influence area of the river as shown schematically in Fig. 4.



Figure 3: View of the Kurpark Bridge in Bad Mergentheim

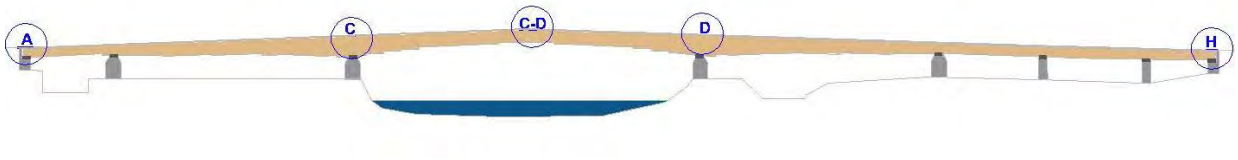


Figure 4: Arrangement of measuring points at the locations A-H

At the two end abutments (locations A and H), each of the superstructure GLT beams has 4 measuring points installed at the end grain face whereby each point includes 2 moisture content sensors measuring at depths of 40 mm and 65 mm. At the abutments on both sides of the river (locations C and D), three measuring points exist, two on the side surfaces of the glulam beams and one on the upper side of the beams, directly below the sealing coat. At the apex of the bridge (area C&D), a further 4 measuring points are placed laterally on the glulam beams on the north side of the structure which is excepted to be the area with the highest moisture input.

Details of the arrangement of the sensors at the cross-sectional end grain face of the beams are shown in Figures 5 and 6. The installation of the sensors was carried out during the production of the bridge elements in the manufacturing plant. This had the advantage that the measuring points could be arranged over the entire width of the cross-section. In the case of subsequent installation of monitoring systems on existing structures, access to the neuralgic component cross-sections is usually no longer possible.

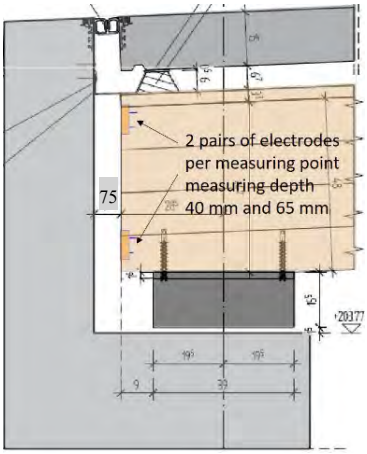


Figure 5: Side view of end abutment (A, H) construction detail, with position of moisture sensors (see Fig 6 also)

A total of 52 electrode pairs for wood moisture measurement, 4 temperature sensors (wood temperature) and one climate sensor are installed. The sensors of each measuring locations A - H are connected to four HUBs. A data cable runs from each HUB to the processing unit, which is installed above the abutment D. The lengths of the 4-wired data cables from the HUBs to the referenced sensors and from the four HUBs to the processing unit add up to a total cable length of 224 m.



Figure 6: Cross-sectional end grain face view of the superstructure GLT block girders with 2x4 measuring points, each with 2 pairs of electrodes for moisture measurement



4.1 Results after two years of logging

The graph in Fig. 7a shows the time dependent evolution of the wood moisture profiles at the end grain face at different cross-sectional depths of 40 and 65 mm in the glulam beams for the measurement period from April 2020 to May 2022. The wood temperature curve is given, too. Fig. 7b reveals the recorded climate data (rel. humidity and air temperature) and the hereon calculated equilibrium moisture content of the wood acc. to [10]. The sensor for the climate monitoring is located in the area next to abutment D at the bottom side of the superstructure GLT beams.

As anticipated for timber structures exposed to service class 2 condition the moisture curves show a seasonal variation of the moisture content. The differences of the moisture measurement at 40 and 65 mm are rather small (about to 1%). A difference between these two sensors would indeed indicate a possible moisture input.

The measurement curves available up to now, show material moisture levels of around 12 - 13 % in the summer months, rising to around 15 % in winter.

In no case a sudden increase of humidity at one measuring point, which would indicate local water penetration into the construction, has been encountered since implementing the monitoring system.

In addition to the continuously evaluated measurement results, which only monitor selected local areas of the structure, an extensive visual inspection of the timber components is carried out once a year as part of the maintenance of the monitoring system.

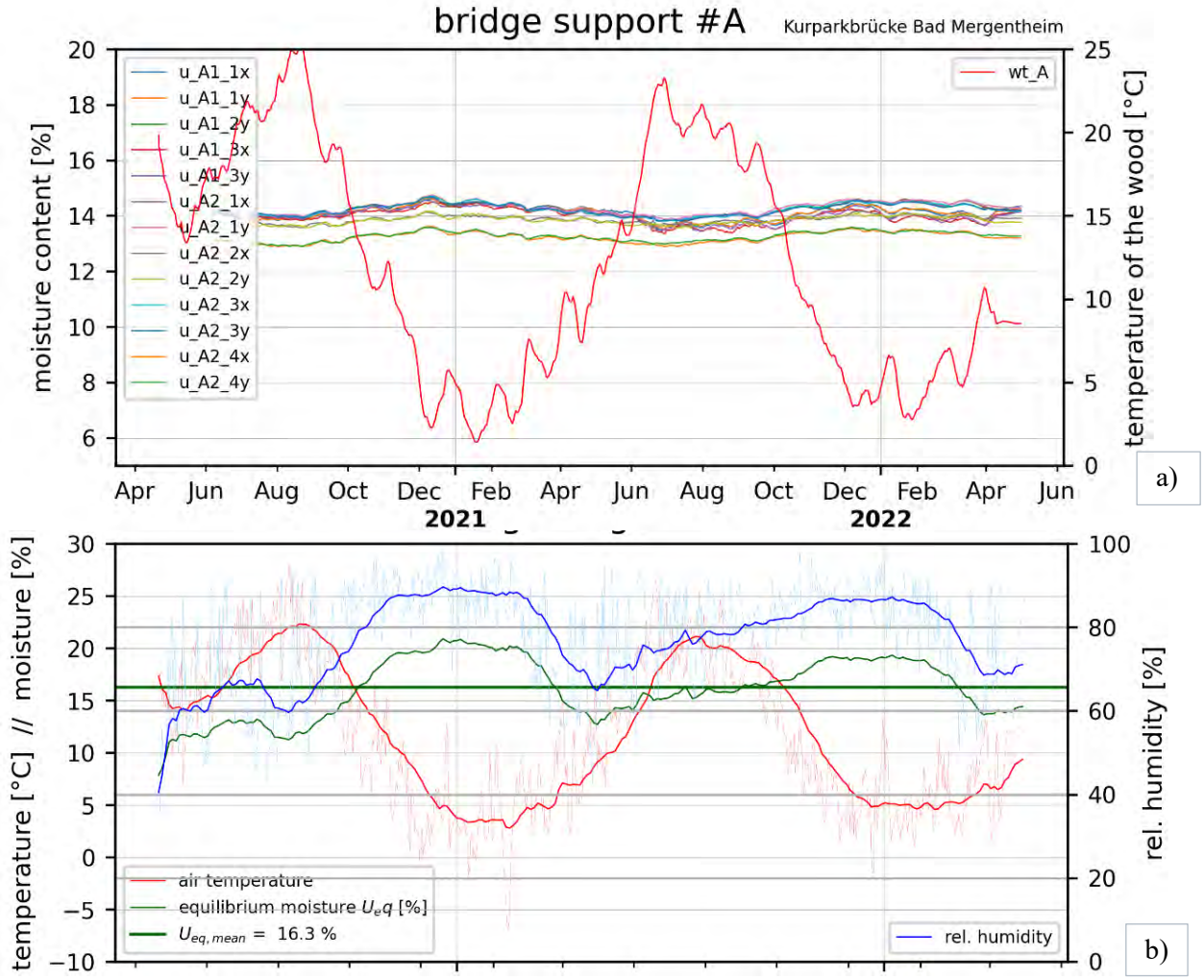


Figure 7: Results of the wood moisture content and climate monitoring over two years measurement time
a) wood moisture content at 2x8 sensors in 45 mm and 60 mm distance to the end grain face at location A
b) climate recording and calculated equilibrium wood moisture content near location D



Table 1: Comparison of the capacity and energy consumption of the established and the new developed system

monitored dimension	systems at STMB	"new" system at Kurpark-bridge
data logging and communication	4 GSM units 7 data loggers 4 SIM cards required	1 processing unit (1 logger and 1 GSM unit integrated) 1 SIM card required
energy requirements	20 AA-type batteries 16 C-type batteries 2 Lithium battery packs	4 D-type batteries
moisture content and climate	16 pairs of electrodes 2 climate sensors 2 wood-temperature sensors	52 pairs of electrodes 1 climate sensor 4 wood-temperature sensors
mechanical (strain gauges / LVDTs)	16 strain gauges 6 LVDTs	possible to connect with no more energy or logger requirements (no long-term experience yet)
leakage detection	11 stripe sensors	

5 Conclusions

The new developed monitoring system incorporates an enhanced capability to evolve smart buildings and check their health status in different dimensions. The system is installed and tested at four timber bridges and could easily be used for other buildings. With the possibility to connect up to 50 different sensors to one processing unit it is possible to install a very flexible system with hardly any limitations. Even for large structures with long distances between observation points the system is able to handle this by distributions of the sensors via HUBs. After gaining some experience it can be summarized that the logging functions as well as the data uploading operates well. Together with a Python written script the data handling and warning systems can transfer results very fast and automatically. The energy usage at the bridge outlined in chapter 4 gets along with 4 D-type batteries for one year while measuring five times a day and uploading the data once a day. Table 1 gives a comparison of the monitoring used at the Stuttgart Timber Model Bridge and the new developed system installed at Kurpark-bridge, where the possibilities and advantages become visible. In summary it can be stated that the developed and field-tested advanced health monitoring system is very well apt, especially for timber buildings in service class 2. The system can be easily combined with other measurement devices (e.g. strain gauges) to monitor interesting mechanical variables, e.g. strains, to assess the long-term mechanical response and the utilization of the structure.

References

[1] Aicher, S. (2016): Dauerhaft Holzbrücken – Schäden, Lösungsansätze, integrale Bauweisen (in German), 4. Internationale Holzbrückentage IHB 2016, Stuttgart, Germany.

[2] Aicher, S; Leitschuh, N (2015): Geh- und Radwegbrücken aus Holz - Ergebnisse und Konsequenzen aus 100 Brückenbegutachtungen (in German), Tagungsband 3. Stuttgarter Holzbausymposium, Stuttgart, Germany.

[3] Avramidis, S. (1989): Evaluation of "three-variable" models for the prediction of equilibrium moisture content in wood, in Wood Science and Technology 23, pp. 251-258, Vancouver, Canada

[4] Dietsch, P., Gamper, A., Merk, M., Winter, S. (2015): Monitoring building climate and timber moisture gradient in large-span timber structures. J Civil Struct Health Monit 5, pp. 153–165, https://doi.org/10.1007/s13349-014-0083-6

[5] EN 1995-2 (2004): Eurocode 5: Design of timber structures - Part 2: Bridges, European Committee for Standardization (CEN), Brussels, Belgium.



[6] EN 13183-2 (2002): Moisture content of a piece of sawn wood – Part 2: Estimation by electrical resistance method. European Committee for Standardization (CEN), Brussels, Belgium.

[7] Forsén, H. and Tarvainen, V. (2000) Accuracy and Functionality of Hand Held Wood Moisture Content Meters. Technical Research Centre of Finland.

[8] Koch, J., Arndt, R., Simon, A., Jahreis, M. (2018): ProTimB - Monitoring von konstruktiv geschützten Holzbrücken (in German), Fachtagung Bauwerksdiagnis 2018, Berlin, Germany

[9] Müller, A. and Franke, B. (2016): Langzeit-Monitoring von Holzbrücken – Erkenntnisse zum Feuchteverhalten im Tragquerschnitt (in German); 4. Internationale Holzbrückentage IHB 2016, Stuttgart, Germany

[10] Samuelsson, A. (1992): Calibration Curves for Resistance-type Moisture Meters, 3rd IUFOR International Wood Drying Conference, Vienna, Austria.

Conference Proceedings 4th ICTB (2022)
https://doi.org/10.24451/cmes-1s31

ICTB 2021 PLUS
4th International Conference on Timber Bridges
Biel/Bienne, Switzerland, 9 -12 May 2022



Characterization and assessment of the mechanical properties of spruce foundation piles retrieved from bridges in Amsterdam

Giorgio Pagella[1], Geert Ravenshorst[2], Wolfgang Gard[3], Jan Willem van de Kuilen[4]

Abstract

Many bridges in Amsterdam are based on timber pile foundations due to the presence of weak soils, where timber piles have proven to be a very good and economic solution over the years. However, aging of the foundations, which can be up to 500 years, implies several challenges for the assessment of the current load carrying capacity and subsequent reliability of bridges. For piles completely below the water table, bacterial decay can occur. Based on the analysis of drill cores retrieved from piles under foundations, the city of Amsterdam concluded that this problem required a more in depth investigation to obtain reliable predictions of the remaining service life of timber foundations. Therefore, 12 spruce (*picea abies*) piles were extracted from foundations of two demolished bridges. Pile segments were sawn from each full-length pile, representing head, middle-part and tip of the pile, and tested in compression in saturated condition. Besides that, micro-drilling measurements were performed to investigate whether the decayed part of a cross section could be predicted with these measurements. On the basis of the results from micro-drilling, the pile segments could be divided in sound and decayed. A soft shell was estimated and the sound remaining cross section was determined for every segment. The load bearing capacity was assigned to the sound remaining cross section and approximately the same stiffness and strength could be observed for the sound parts of both the decayed and sound group. From the 12 assessed whole piles, 6 were assigned to sound and 6 to decayed group. However, also the decayed piles resulted to have a remaining load-bearing capacity. This indicates that for the final assessment of timber pile foundations of a bridge, detailed information about the distribution of decayed piles in relation to the load distribution has to be taken into account. The use of micro-drilling measurements gives promising results to predict the level of decay, and their application could be used for in-situ assessment of wooden piles.

1 Introduction

Many historic bridges in Amsterdam, The Netherlands, are founded on timber piles, but also in cities like Venice [1], Amsterdam, Hamburg, Boston and many others, similar timber foundations can be found. Service life analysis of bridges is complicated [2], since in order to assess the reliability and safety of a bridge, an in-depth analysis of the timber pile foundations is required. A reliable assessment of a bridge is of importance because of the implication on the economic activities in the city. Closing down bridges due to eventual failure of the foundations can cause considerable economical losses [3]. In particular, the city of Amsterdam has many bridges built on wooden foundation piles, which have been in service up to 500 years, and widespread due to their relative cost-efficient application [4]. Given the specificity of the problem, when it comes to characterization and assessment of existing timber foundations, there are many aspects that have to be taken into account; these include analysis of material conditions, age of the structure, assessment of the mechanical properties of wood, inspection techniques and biological degradation [5], [6]. Therefore, the quality of the entire foundation has to be analyzed starting with an assessment of the current state of the timber piles, from both a mechanical as well as a material point of view. Since in Amsterdam the timber piles remain entirely under the water table, the possible degradation is attributed only to bacterial decay, excluding the presence of fungal decay. In order to assess the state of wooden piles with respect to bacterial decay, the current practice in the Netherlands adheres to the F3O guidelines [7] and Dutch standard NEN 8707 [8]. According to these guidelines, drill cores with a diameter of approximately 9 mm and a length of half the pile diameter, are taken under water from the head of the pile. Subsequently, the drill cores are cut in sub-sections and viewed under a microscope to determine the degree of bacterial decay, and then used to determine the maximum achievable moisture content. Using the model from Klaassen

[1] Giorgio Pagella, Bio-based Structures and Materials, Delft University of Technology, The Netherlands, G.Pagella@tudelft.nl
[2] Geert Ravenshorst, Bio-based Structures and Materials, Delft University of Technology, The Netherlands, G.J.P.Ravenshorst@tudelft.nl
[3] Wolfgang Gard, Bio-based Structures and Materials, Delft University of Technology, The Netherlands, W.F.Gard@tudelft.nl
[4] Jan Willem van de Kuilen, Wood Technology, Technical University of Munich, Germany & Bio-based Structures and Materials, Delft University of Technology, the Netherlands, vandekuilen@tum.de



(2008) [9], the compressive strength is estimated from the maximum achievable moisture content. Every subsection with a calculated compression strength lower than 8 N/mm^2 (which was arbitrarily chosen) is defined as being part of a so-called soft shell, to which no strength is assigned. The load bearing capacity of the remaining cross section is then calculated with the compression strength for new piles as determined by van de Kuilen [10] on a limited dataset. Based on the result of a large amount of drill cores retrieved from piles under bridges in Amsterdam, it emerged that a large number of wooden piles could be affected by bacterial decay. However, many uncertainties have to be taken into account, since the model from [9] was calibrated on limited data, based only on pine specimens, and only related to strength values of small specimens. In the light of this, the municipality of Amsterdam decided to set up a research project in which timber piles were retrieved from bridges that were planned to be demolished and replaced. The objectives of this project are:

- The investigation of the material properties of full-size specimens, to gain insight into the remaining strength properties, and the effect of decay on these properties.
- The investigation of the micro-drilling resistance technique for under-water use, as an alternative to the extraction of drill cores, to determine if these measurements could give a more reliable prediction of the soft shell.

To this end, this paper presents the results of the first investigation of timber pile foundations conducted on 12 spruce piles retrieved from two bridges in Amsterdam.

2 Materials and methods

2.1 Materials

In this paper the first results of a large experimental program was presented. This involved the assessment of the mechanical properties of 12 spruce (*picea abies*) foundation piles, driven in 1727, 1886 and 1922. The specimens were retrieved under different locations from the foundation of two bridges that were demolished in the city of Amsterdam (Bridge 30 and 41). The full-length specimens were ranging from 9500 mm to 13500 mm, with an average head diameter of 230 mm and average tip diameter of 145 mm. After in-situ preliminary tests, the full-length piles were subdivided in three parts: head, middle-part and tip, according to the procedure explained in section 2.2.1. From each of the 3 parts of the pile, a segment was sawn for the compression test, depending on the diameter of the average cross-section. The wood species, spruce in this case, was an important aspect to consider, since previous research investigated the properties of pine piles, which have a different distribution of sapwood. However, wooden piles in Amsterdam can be from either pine or spruce species, where, even if always below the water table, the transportation of bacteria through the cross-section could be different depending on the amount of sapwood. Thus, bacterial decay could cause a faster or slower degradation of the material depending on the species but also on different parts of the pile, where its severity had to be analyzed from the head to the tip of a pile, as the tip generally has a larger portion of juvenile wood, and consequently proves to be more vulnerable [11].

2.2 Methods

2.2.1 Mechanical testing

After the extraction of the wooden piles, in-situ preliminary tests were conducted on the 12 full-length specimens at the storage location of the municipality of Amsterdam. All piles were labelled and enumerated by dimensions and weight. At the same time, the dynamic modulus of elasticity parallel to the grain ($MOE_{dyn,wet}$) was evaluated through acoustic frequency response measurements. The $MOE_{dyn,wet}$ was calculated with Equation 1.

$$MOE_{dyn,wet} = 4 \rho f^2 l^2 \quad (1)$$

where ρ = wet density; f = frequency; l = length of the specimen. After these preliminary tests, the specimens were subdivided in three parts: head, middle-part and tip, approximately 4000 mm long, and stored underwater in a container until shipping to the TU Delft was possible. Subsequently, the container was emptied out and the specimens were transported to the TU Delft laboratory for the assessment of the current mechanical properties by mechanical testing. From each of the three parts of the pile, a segment was sawn for the compression test, which length depended on the diameter of the average cross-section. Three categories of length were established: 900 mm, 1350 mm and 1800 mm, according to the standards EN 408 [12] and

EN 14251 [13], which prescribe an axial length of six times the smaller diameter of the cross section for a pile. The cutting procedure was performed with a laser placing system to get the pile in the straight position. After this, a frame-guided chainsaw was used to obtain a parallel plan on the ends, with a laser line indicating the exact position of the cut. Directly after the cut, the moisture content value was determined according to the standard EN 13183 [14] by cutting two 30-mm-thick discs from each side of the selected segment. The discs were dried at a temperature of 103 °C, until a constant mass was achieved. During this process, the moisture content (m.c.) was determined by oven-drying i.e. from the ratio between wet and dry mass. The dry and the wet masses of each pile segment were linked to this moisture content value, therefore any variation of the wet mass of the pile could be related with a dry mass and consequently a precise moisture content value could be estimated. The pile segments were weighted and subsequently submerged for approximately 30 days to achieve the water-saturated condition for the compression test, for aiming a moisture content higher than 70%. Before running full-scale mechanical testing on the pile segments, the specimens were taken out of the water, and the density of each pile was measured by determining volume and wet mass (EN 384 [15]). From this wet mass, the moisture content was calculated. Mechanical testing was performed to determine the short-term strength ($f_{c,0,wet}$) and the static modulus of elasticity ($MOE_{stat,wet}$). In this test campaign, the mechanical properties of 36 pile segments were determined. To this end, a displacement controlled set-up was used (Fig. 1), based on the standards EN 408 and EN 14251, where the specimens were subjected to an axial load in direction parallel to the fibers. The displacement between the two steel plates was monitored with four linear potentiometers placed on four edges of the top plate and connected to the bottom plate. The direct deformation on the specimens was measured with six linear potentiometers screwed on the surface of the piles: four of them were placed on each side of the pile, 90 degrees from each other, with a variable length equal to two-thirds of the length of the specimen; the other two sensors were placed on a knot and on a clear-wood part, in order to evaluate the deformation with and without the influence of a knot. The length of these last two sensors was set at 200 mm. Given the short stroke of the six sensors placed on the pile, they were removed before the peak load to avoid damages. In addition, a hinge, mounted on a steel plate, was placed on top of the specimen to have an uniformly distributed compression load on the pile. The compression test was carried out at a constant speed of 0.02 mm/s until the peak load was reached. The specimens were loaded to failure and the displacement was increased at higher speed until the cracks were visible. This was done to investigate the failure mechanism of water-saturated pile segments.

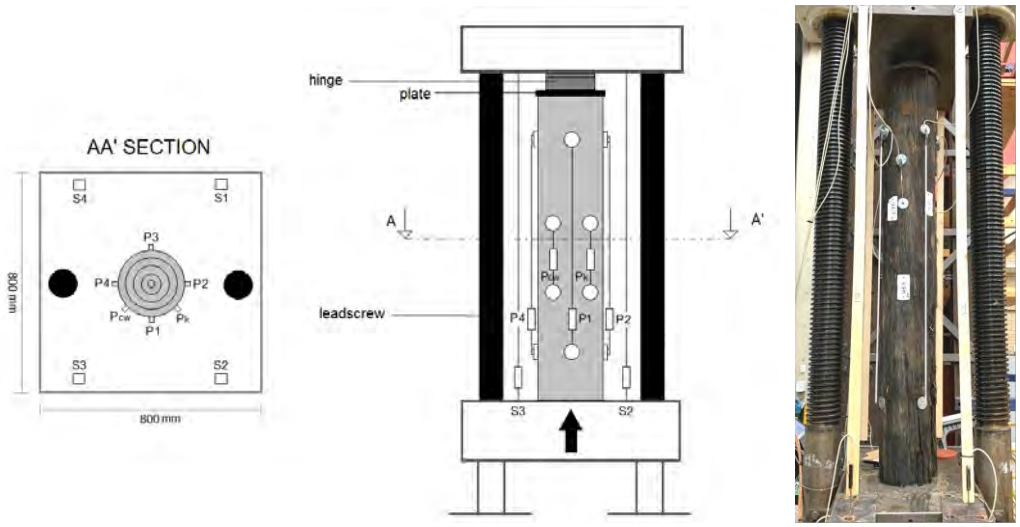


Figure 1: Set-up for mechanical testing of pile segments.

At the end of the test, the global behaviour of the pile was studied with the average stress-displacement curve of four linear potentiometers connected to the compression test machine (Fig. 2a), from which the compressive strength ($f_{c,0,wet}$) was calculated with the ratio between the maximum force, corresponding to the peak of force-displacement curves, and the average cross-sectional area of the pile. The static modulus of elasticity ($MOE_{stat,wet}$) was calculated in Equation 2, with the ratio between stress variation ($\Delta\sigma$) and strain variation ($\Delta\varepsilon$), between 10% and 40% in the slope of the linear elastic portion of the stress-strain curve, resulting from the four linear potentiometers attached on the pile (Fig. 2b).

$$MOE_{stat,wet} = \Delta\sigma/\Delta\varepsilon = (\sigma_2 - \sigma_1)/(\varepsilon_2 - \varepsilon_1) = (\Delta F/\Delta L)/(L_0/A_r) \quad (2)$$

where $\Delta\sigma$ = stress variation between σ_2 and σ_1; $\Delta\varepsilon$ = strain variation between ε_2 and ε_1; ΔF = force variation between $F_2 = 0.4\ F_{max}$ and $F_1 = 0.1\ F_{max}$; ΔL = deformation variation corresponding to points F_2 and F_1; L_0 = length of the linear potentiometers (2/3 of the length of the pile segment); A_r = average cross-sectional area of the pile. At the moment of the test, all the specimens were above fiber saturation, with an average moisture content higher than 70%. In order to study the expected failure mechanisms, the displacement was kept after the peak load reached during compression tests. In general, the failure mechanisms were reported considering a global failure for crushing (Fig. 3a) and a local failure for buckling (Fig. 3b) related to local defects such as knots.

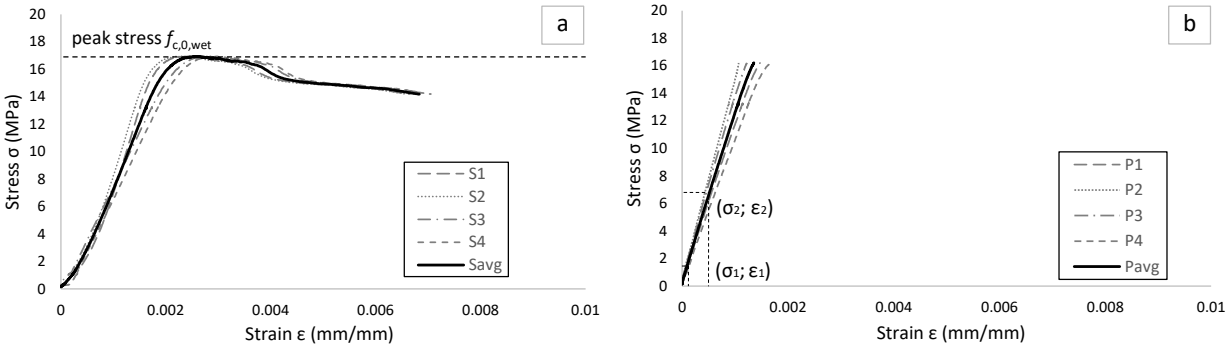


Figure 2: Example of axial compression tests of a water-saturated pile segment: a) global behaviour of the pile with stress-strain curves measured by S1, S2, S3, S4; b) stress-strain curves measured by P1, P2, P3, P4 to determine $MOE_{stat,wet}$.

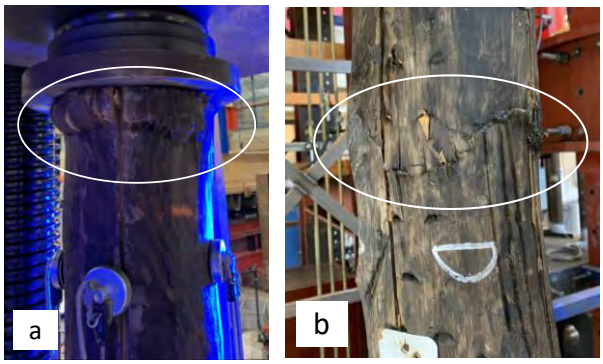


Figure 3: Failure mechanisms of a water-saturated spruce pile in compression: a) crushing; b) localized buckling.

2.2.2 Micro-drilling resistance measurements

Micro-drilling measurements fall within the non-destructive techniques used for wood inspection, commonly used for trees or electrical poles. From the measurements, it is possible to obtain a resistance profile which can give information about the annual rings of a tree and the density of the investigated section [16]. In Amsterdam, micro-drilling was initially used as an innovative inspection method to assess the level of degradation, by performing underwater measurements on the head on wooden foundation piles which were in the soil and completely under the water table. However, a drilling measurement on the head of the pile was not sufficient to predict the status of the material along the length. Therefore, in this study, a IML-RESI PD 400 tool (Fig. 4) was used to assess the level of degradation, performing micro-drilling measurements in different cross-section along the length of 12 extracted wooden foundation piles. For under-water measurements on piles under the bridges, the machine was adjusted by the manufacturer. The acquired data is used to investigate the feasibility to predict the decay in different parts of the pile. The comparison between the measurements carried out in-situ and those performed on extracted specimens is not presented in this paper, since in-situ micro-drilling belongs to a running project that will be subsequently reported. Thus, for the research conducted in this paper, only the IML tool for above-water measurements was used. The measurements were performed in the TU Delft laboratory, allowing to estimate the soft shell by micro-drilling on heads, middle-parts and tips of all the investigated piles. In this way, the decay level along the length of each pile could be studied.



Figure 4: Micro-drilling measurements: a) underwater measurements on wooden piles; b) measurements after piles extraction.



Figure 5: Micro-drilling measurements performed on a pile segment before the compression test.

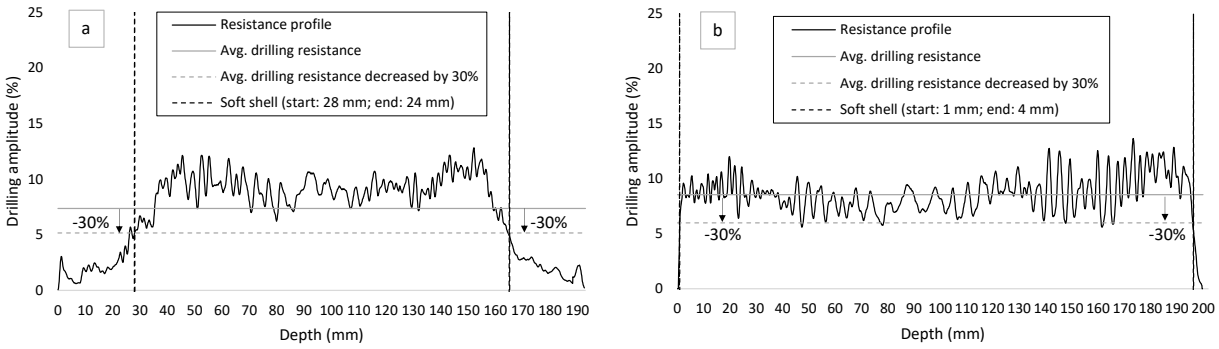


Figure 6: Resistance profile from micro-drilling measurements of a cross section of 2 different pile segments and procedure for the calculation of the soft shell: a) old decayed cross-section; b) old sound cross-section.

During micro-drilling, a drilling needle is pushed into the cross-section with a drill speed of 2500 r/min and a feed speed of 150 cm/min. The drill bit used for the measurements is 400 mm long, with a thin shaft of 1.5 mm in diameter and a 3.1 mm wide triangular shaped cutting part, with hard chrome coating. The acquired data, recorded every 0.1 mm of the drilling depth, was plotted as resistance vs distance, resulting in a wave plot in which amplitude displacements coincided with changes in density and moisture content [17], [18]. Once the 12 piles were subdivided in segments, two micro-drilling measurements were performed through the cross-section of each segment, approximately 90 degrees to each other and 300 mm from the head of the specimen (Fig. 5). These measurements were performed before testing the specimens in compression, therefore it was possible to inspect the material status right before the test. The resistance profile (Fig. 6) was obtained from putting together the two drilling measurements performed through the cross section. By observing the resistance profile, it was possible to distinguish the annual rings, with maximum amplitudes, corresponding to latewood rings, and minimum amplitudes, representing early-wood. Isolated peaks or lower values could be observed in resistance profiles, on the one hand caused by wood knots and other high-density anatomical variations of the material, on the other hand caused by piths and cracks in the cross-section. The possible decay in the cross-section was estimated on the basis of a new definition of the soft shell, defined as the outer decayed layer of the cross section. To this end, an average drilling resistance was determined from the resistance profile. The starting and ending point of the soft shell was manually calculated with the intersection between the average drilling resistance decreased by 30%



and the resistance profile (Fig. 6a). A cross section of a pile was considered as decayed when the soft shell was >15% of the full cross section; it was instead considered sound when the soft shell resulted to be <15% of the full cross section (Fig. 6b). With this method, two categories were established: old sound pile segments and old decayed pile segments, based on the remaining sound cross-section, measured after subtracting the soft shell area to the total cross-sectional area. Pile segments were defined as: old sound piles when the remaining average sound cross-section was higher than 85% of the total cross-section; old decayed piles when < 85%. In order to compare the mechanical properties of old sound and decayed pile segments, an $MOE_{stat,sound}$ and $f_{c,0,sound}$ were calculated with the ratio between the measured $MOE_{stat,wet}$ and $f_{c,0,wet}$ of the segments and the percentage of remaining average sound cross-sectional area, respectively. With these two parameters it was possible to compare if the mechanical properties were correlated with the micro-drilling measurements, and understand if micro-drilling could be used as a predictor for decay. It should be noticed that micro-drilling is a local measurement, thus it can happen that the soft shell measured in a cross section may vary if measured in other positions over the length of the specimen. In order to minimize this effect, all the micro-drilling measurements were performed in positions without visible defects or irregularity of the material.

3 Results

3.1 Basic material properties

Prior to testing, the 12 full-length piles were retrieved from bridge 30 and 41 and tested at the storage location of the municipality of Amsterdam to estimate the basic material properties. Table 1 shows the results of the preliminary tests, listing the 12 full-length specimens by original code and the year in which they were driven in the soil. Each specimen was characterized by dimensions, mass, wet density, and $MOE_{dyn,wet}$ which was determined through frequency response measurements.

Table 1: Material properties of 12 full-length spruce (picea abies) piles tested after the extraction under bridge 30 and 41 in Amsterdam.

Pile ID	Year	Length (mm)	Mass (kg)	Avg. Φ (mm)	Wet density (kg/m³)	$MOE_{dyn,wet}$ (MPa)
BRU0030-PL1 P1.6	1727	9940	147	157	765	8840
BRU0030-PL1 P1.20	1886	10580	250	212	665	13790
BRU0030-PL1 P2.13	1727	10400	156	153	815	15530
BRU0030-PL1 P3.2	1886	11270	378	221	875	10120
BRU0030-PL2 P2.19	1727	9470	197	169	920	7050
BRU0030-PL2 P2.21	1727	10030	183	173	775	5850
BRU0041-PL1 P1.33	1922	13460	363	235	620	11620
BRU0041-PL1 P3.36	1922	13270	297	208	660	9840
BRU0041-PL2 P1.24	1886	13580	283	197	680	10130
BRU0041-PL2 P1.25	1886	12560	260	200	660	8890
BRU0041-PL2 P1.9	1922	11420	318	226	695	11220
BRU0041-PL2 P3.12	1922	11960	300	213	700	7540



3.2 Mechanical characterization of pile segments in relation to decay

The mechanical properties of 36 pile segments, divided in head, middle-part and tip, were characterized in relation to the level of decay estimated with micro-drilling measurements. The load-displacement behaviour of the water-saturated spruce specimens during the compression test was linear up to approximately 80% of the maximum compression load ($F_{c,0,max}$). Out of linearity, a nonlinearity phase was visible until peak load. When softening started, the load gradually decreased showing a quasi-plastic load plateau. In more than 70% of the cases, a failure mechanism for local buckling was observed, where cracks generally started in a section with presence of knots. For the other cases, a failure for crushing was detected, occurred mostly in the top part of the pile, and it was typically observed in pile segments without knots or with knots with diameters lower than 10 mm. The average values of $MOE_{stat,wet}$ and $f_{c,0,wet}$ for the head, middle-part and tip of each pile, were subdivided in two macro categories on the basis of remaining sound cross-section: old sound and old decayed piles (Tab. 2).

Table 2. Mechanical characterization of 36 water-saturated old sound and decayed pile segments tested in compression in relation to the remaining sound cross section determined with micro-drilling measurements.

Material status	Pile segments (number of specimens)	$MOE_{stat,wet}$ (MPa)		$f_{c,0,wet}$ (MPa)		Avg. sound cross-section (%)		$MOE_{stat,sound}$ (MPa)	$f_{c,0,sound}$ (MPa)
		Avg.	SD	Avg.	SD	Avg.	SD	Avg.	Avg.
Old sound	Head (9)	9850	1700	13.8	2.3	95	8	10370	14.5
	Middle-part (8)	9400	2250	13.2	2.1	98	7	9590	13.5
	Tip (5)	8450	2450	11.3	3.4	93	7	9090	12.1
	All segments (22)	9350	2050	13.0	3.0	95	7	9840	13.7
Old decayed	Head (3)	7950	700	9.1	1.8	78	6	10200	11.7
	Middle-part (4)	5400	1550	7.8	2.5	59	11	9150	13.2
	Tip (7)	5600	2350	8.6	3.1	57	14	9820	15.1
	All segments (14)	6050	2050	8.5	2.6	62	14	9760	13.7

More than 60% of the specimens were categorized as old sound material, with a soft shell <15% of the full cross section. Less than 40% of the specimens were classified as old decayed with a soft shell between 15% and 65%. However, only in six piles severe decay was observed, with an average remaining sound cross section lower than 50%. In case of old decayed specimens, it could be observed that the heads of the pile presented an average sound cross-section of 78%, while for middle-parts and tips a lower sound cross-section of 58% was estimated. Besides, the specimens not affected by decay were divided in: 75% heads, 65% middle-parts and 40% tips. This aspect indicates that decay increases progressively from the head to the tip of the pile, possibly because of the progressive decrement of diameter along the pile due to its tapered shape. The calculated values of $MOE_{stat,sound}$ are comparable for head, middle and tip parts of sound and decayed segments. For $f_{c,0,sound}$ this correlation is less clear when looking to head, middle and tip parts, but for all segments the calculated values for sound and decayed wood are similar. Although a more detailed analysis has to be performed. A first conclusion is that micro-drilling measurements have a high potential in the assessment of the level of decay of wooden piles.

3.3 Correlation between compressive strength and static modulus of elasticity

The compressive strength $f_{c,0,wet}$, obtained testing 36 pile segments in compression, was compared with the static $MOE_{stat,wet}$ (Fig. 7a). Heads and middle-parts of the full pile, which often presented a higher diameter and less decay, resulted in a value of $f_{c,0,wet}$ between 10 MPa and 17 MPa, which corresponded to a $MOE_{stat,wet}$ ranging from 7000 MPa to 13000 MPa. In the research of van de Kuilen [10] a mean value of 20 MPa with a standard deviation of 2.2 MPa was found for pile heads of new spruce piles, slightly higher than the values for the sound old piles. However, the research in [10] will be validated on a new series of



tests on new piles. The tips of the pile, characterized by a smaller diameter and a higher level of degradation, presented a significant decrease both in strength and stiffness. A good correlation ($R^2 = 0,9$) can be observed between $MOE_{dyn,wet}$ and $MOE_{stat,wet}$ (Fig. 7b), proving that frequency response measurements can reliably estimate the modulus of elasticity of a wooden pile. Also the good correlation between $f_{c,0,wet}$ and $MOE_{stat,wet}$ (see again Fig. 7a) could be used to have a good prediction of the compressive strength once the $MOE_{stat,wet}$ or $MOE_{dyn,wet}$ is known. Especially the correlation between $MOE_{dyn,wet}$ and $f_{c,0,wet}$ could have in-situ practical implications potential, where by obtaining the $MOE_{dyn,wet}$ from acoustic measurements on the head of the pile, the compressive strength could be estimated.

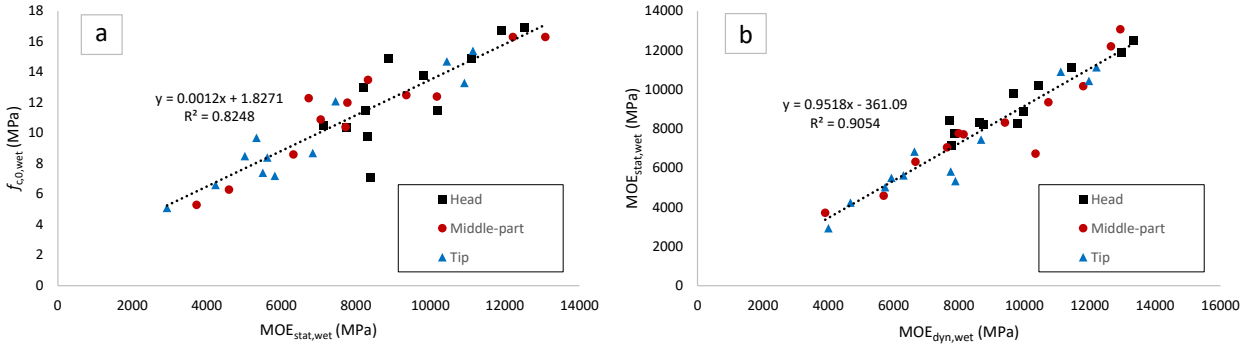


Figure 7: Correlation between: a) $f_{c,0,wet}$ and $MOE_{stat,wet}$; b) $MOE_{stat,wet}$ and $MOE_{dyn,wet}$ of 36 water-saturated spruce pile segments divided in head, middle-part and tip.

3.4 Correlation between wet and dry density, moisture content and mechanical properties

Dry and wet densities of 36 pile segments are presented in relation to moisture content values, to investigate whether the moisture content differs for decayed segments which have been submerged for the same period of time. The moisture content values were subdivided in two categories, again based on old sound and decayed material. Table 3 lists the average wet density (water-saturated condition) and dry density (at m.c. of 0%), by dividing the specimens in head, middle-part and tip. It can be observed that the average dry density value for old sound piles was 350 kg/m^3. For old decayed pile segments, an average dry density of 310 kg/m^3 was calculated. The decrease of density could be attributed to the lower density of the soft shell. An average m.c. of 90% was determined for old sound specimens and an average m.c. of 120% for old decayed specimens, therefore indicating that a higher moisture content is associated to a higher level of decay. Wet and dry densities of each pile segment were compared with $MOE_{stat,wet}$ and $f_{c,0,wet}$ in Figure 8 and 9. A correlation was found between dry density and $MOE_{stat,wet}$ ($R^2 = 0.42$), (Fig. 8b), and between dry

Table 3. Wet and dry densities in relation to moisture content of 36 water-saturated pile segments divided in head, middle-part and tip after the same period of submersion.

Material status	Pile segments (number of specimens)	Wet density (kg/m^3)		Dry density at 0% of m.c. (kg/m^3)		Moisture content (%)	
		Avg.	SD	Avg.	SD	Avg.	SD
Old sound	Head (9)	630	70	350	37	80	16
	Middle-part (8)	650	62	350	32	85	12
	Tip (5)	700	80	350	75	110	30
	Full pile (-)	650	72	350	45	90	20
Old decayed	Head (3)	670	95	310	36	125	60
	Middle-part (4)	650	50	300	38	120	38
	Tip (7)	700	67	320	51	125	52
	Full pile (-)	680	65	310	42	125	46



density and $f_{c,0,wet}$ (R^2 = 0.49), (Fig. 9b). It was not possible to find a correlation between wet density, $MOE_{stat,wet}$ and $f_{c,0,wet}$, since in each specimen the moisture content constantly changes. Similar dry densities were not always associated with the same value of $MOE_{stat,wet}$ and $f_{c,0,wet}$, since the density of a wooden pile could be affected by the natural variation between juvenile wood and mature wood along the length of the pile itself. In tips, a lower density was observed, due to a larger presence of juvenile wood. Moreover, it is often difficult to distinguish from a pile with lower density caused by degradation phenomena or a pile with lower density given by a large presence of juvenile wood. Therefore, further research will be carried out in order to minimise the variability of the data with the goal to obtain a higher correlation between dry densities and the mechanical properties of wooden piles.

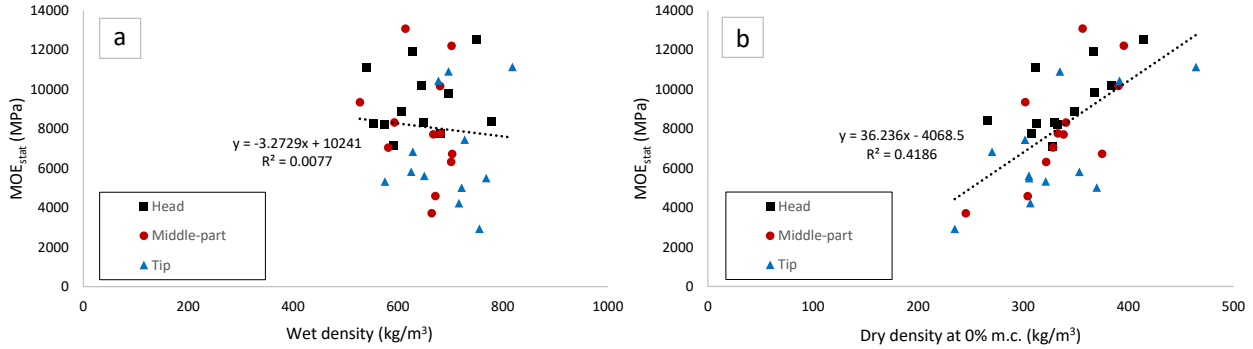


Figure 8: Correlation between: a) $MOE_{stat,wet}$ and wet density; b) $MOE_{stat,wet}$ and dry density (at 0% of m.c.), of 36 pile segments divided in head, middle-part and tip.

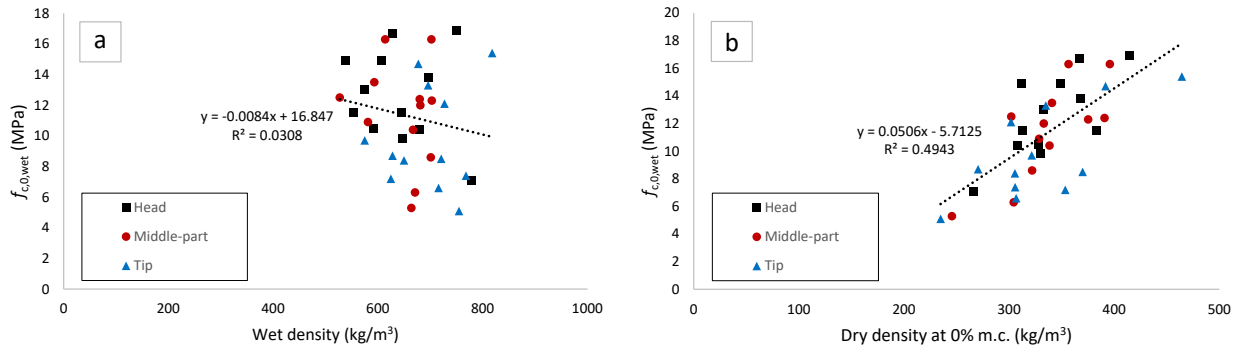


Figure 9: Correlation between: a) $f_{c,0,wet}$ and wet density; b) $f_{c,0,wet}$ and dry density (at 0% of m.c.), of 36 pile segments divided in head, middle-part and tip.

4 Conclusions

The mechanical properties of existing spruce foundation piles retrieved from two demolished bridges in Amsterdam were studied. The study had two objectives: the first was to investigate the material properties of full-size water saturated piles, in order to gain insight in the remaining strength properties and the effect that bacterial decay could have on these properties; the second one was to investigate whether micro-drilling measurements could be used as an alternative to the current practice of extraction and analysis of drill cores from the pile, according to the F3O guidelines [7] and Dutch standard NEN 8707 [8]. To this end, the mechanical properties of 12 full-length wooden piles were investigated, by subdividing the full piles in three segments (head, middle-part and tail) and testing each segment in compression. In addition, micro-drilling measurements were performed on all the segments. On the basis of the results obtained with micro-drilling, it was possible to obtain a reliable prediction of the soft shell, defined as the part of the cross section with no strength. The sound remaining cross section for every segment was estimated, based on the soft shell, and it was possible to distinguish the pile segments in sound and decayed. The load bearing capacity of each segment, measured with mechanical testing, was assigned to the sound remaining cross section, resulting that approximately the same stiffness and strength could be observed in the sound parts of both the decayed and sound group. From all the 12 studied full-length piles, 6 were assigned to sound



and 6 to decayed. However, also the decayed piles resulted to have a remaining load-bearing capacity. Thus, for the final assessment of the pile foundation of a bridge, detailed information about the distribution of decayed piles in relation to the load distribution has to be taken into account. In addition, micro-drilling measurements allow to obtain promising results for the prediction of bacterial decay, opening up the opportunity of a more optimal use of micro-drilling for in-situ assessments of wooden foundation piles.

Acknowledgements

The authors gratefully acknowledge the municipality of Amsterdam for having funded this research project.

References

[1] Biscontin G. et al. (2009) Il sistema delle fondazioni lignee a Venezia, CORILA, Venezia (in Italian).
[2] Van de Kuilen J.W.G. (2007) Service life modelling of timber structures. Mat. & Struct. DOI 10.1617/s11527006-9158-0.
[3] Van de Kuilen J.W.G. (1995) Timber Engineering STEP 2, Lecture E18 Timber Piles, Eds. Blass et al.
[4] Varossieau, W.W. (1949) Opgegraven en aangetast hout vanuit biologisch oogpunt bezien, CIMO Delft (in Dutch).
[5] Van de Kuilen J.W.G., Beketova-Hummel O., Pagella G., Ravenshorst G.J.P., Wolgang G. (2021) An integral approach for the assessment of timber pile foundations, WCTE.
[6] Schreurs, E. (2017) Deterioration of timber pile foundations in Rotterdam. M.Sc. Thesis, TU Delft.
[7] F3O (2011) F3O Richtlijn: Onderzoek en beoordeling van houten paalfunderingen onder gebouwen. Rapportnummer: 978-90-816732-1-1 (in Dutch).
[8] NEN 8707 (2018) Assessment of the structural safety of an existing structure during renovation and rejection - Geotechnical constructions, Nederlands Normalisatie-instituut (NEN).
[9] Klaassen R.K.W.M. (2008) Bacterial decay in wooden foundation piles – Patterns and causes: A study of historical pile foundations in the Netherlands. International Biodeterioration & Biodegradation.
[10] Van de Kuilen J.W.G. (1994) Bepaling van de karakteristieke druksterkte van houten heipalen. Rapportnummer 94-con-RO271. Delft: Toegepast-Natuurwetenschappelijk Onderzoek (in Dutch).
[11] Ibach R.E. (2005) Biological Properties. In Handbook of Wood Chemistry and Wood Composites, CRC Press.
[12] EN 408 (2010) Timber structures – Test methods – Pull through resistance of timber fasteners, CEN.
[13] EN 14251 (2003) Structural round timber - Test methods, CEN.
[14] EN 13183-1 (2002) Moisture content of a piece of sawn timber – Part 1: Determination by oven dry method, CEN.
[15] EN 384 (2016) Structural timber - Determination of characteristic values of mechanical properties and density, CEN.
[16] Gao S., Wang X., Brashaw B.K., Ross R.J., Wang L., (2012) Rapid assessment of wood density of standing tree with nondestructive methods – A review. Proceedings of 2012 International Conference on Bio-based Material Science and Engineering. IEEE.
[17] Gard W.F., Van de Kuilen, J.W.G. (2018) Micro-drilling resistance measurements of dense hardwoods for hydraulic structures. WCTE - World Conference on Timber Engineering, Seoul, South-Korea.
[18] Sharapov E., Wang X., Smirnova E., Wacker J.P. (2018) Wear behavior of drill bits in wood drilling resistance measurements, Wood Fiber Sci 50:154 –166.

Conference Proceedings 4th ICTB (2022)
https://doi.org/10.24451/hqdc-wp58

ICTB 2021 PLUS
4th International Conference on Timber Bridges
Biel/Bienne, Switzerland, 9 -12 May 2022



Climate and moisture induced stresses in block-glued glulam members of timber bridges

Bettina Franke[1], Marcus Schiere[2], Steffen Franke[3]

1 Introduction

Wood as a hygroscopic material interacts with the ambient climate variations of relative humidity and temperature and leads to moisture content (MC) variations across the cross section. The MC affects the physical and mechanical properties as well as the dimensions due to shrinkage and swelling below the fibre saturation point (FSP). Due to constrained volumetric strains, e.g. due to swelling and shrinkage, changes in moisture content impose moisture induced stresses (MIS) which, if exceeding the tensile strength perpendicular to the grain of the material, can cause fractures such as cracks or delaminations. Thus, the correct estimation of the MC is important for the design, quality assurance, and durability of timber bridges.

There was the question especially for large glulam members as produced by block-gluing about the impact of ambient climate variations on the moisture induced stresses and possible failure. Block glulam beams form wide cross-sections by gluing single glulam beams to each other. They are used as, e.g., main structural elements for timber bridges, see Figure 1. Therefore, cross sections of practical dimensions were classified regarding the assumed ambient climate in service by numerical simulations that showed the moisture content and gradient over the cross section. Finally, the moisture induced mechanical response was simulated using a coupled moisture diffusion and mechanical model. The results were summarized to a practical advice for the dimensioning.



Figure 1: Bridge Horen Switzerland, block glued glulam members as main structural elements, Source: BFH, Switzerland

2 Material and method

2.1 Climate impact

The ambient climate depends on the building occupation, their use, on the meteorological conditions, local topography or environment, and altitude. The moisture content of wood follows the variations in ambient climate. The ambient climate and moisture content in timber structures and on timber bridges is being monitored with different objectives, duration, and results by various monitoring campaigns as shown in [1], [2], [3], [4]. Some elements are monitored to investigate moisture gradients, detect leakages, or to obtain equilibrium moisture contents. A large number of various monitoring data from own measurements as well as published data were analysed using the minima and maxima value over one year. They are presented as an envelope of the measurement data for one object, see Figure 2 for timber bridges and/or for other structures and objects in [4].

[1] Bettina Franke, Research Associate, Bern University of Applied Sciences, Switzerland, bettina.franke@bfh.ch
[2] Marcus Schiere, Research carried out at Bern University of Applied Sciences, now: Product Manager, Hupkes Wijma B.V., The Netherlands, mjs@hupkeswijma.com
[3] Steffen Franke, Professor for Timber Engineering, Bern University of Applied Sciences, Switzerland, steffen.franke@bfh.ch



The moisture contents observed close to the surface, in a depth of around 15 mm, was filtered with a moving average filter and analysed for one year. The envelope shown in Figure 2 helps to calculate the difference in moisture content throughout the year, Equation (1).

$$\Delta u_{15\text{mm}} = \max\left(u_{15\,\text{mm}}\right) - \min\left(u_{15\,\text{mm}}\right) \tag{1}$$

A further value called $\Delta u_{\text{Surface}}$ can be obtained from the theoretical equilibrium moisture contents calculated at the surface using temperature and relative humidity of the ambient climate. The relation between the two is then calculated as:

$$r_u = \Delta u_{Surface} / \Delta u_{15\,\text{mm}} \tag{2}$$

This value defines the relation between the moisture content developments. If this value is high, large variations of short duration occur at the surface. If it is small, variations in relative humidity at the surface are smooth and not very large either. For the approximation of the moisture content of timber members and the distribution over the cross sections or the calculation of moisture induced stresses, a simplified climate model over the year was applied. Instead of specific daily or seasonal changes, a model based on the cosines shape (Equation (3)) or a simple step model can be chosen, as shown in Figure 3. The mean equilibrium moisture content was set to 16 M% forcovered timber structures outdoors according to Service Class 2 (SC2), EN 1995-1-1:2004. By using the specified values for the moisture content from Figure 2, variations of $\Delta u_{\text{Surface}} = 4.48$ $r_u =\cdot 3.23$ and $Ø_u = 15.7$ M% could be calculated for the bridges.

$$u(t)_{SC2} = 16 + \frac{\Delta u_{Surface}}{2} \cos\left(2\pi \frac{t}{365}\right) \tag{3}$$

Where:

t Time in Days, $t = 0 \;\hat{=}\; 1^{st}$ of January

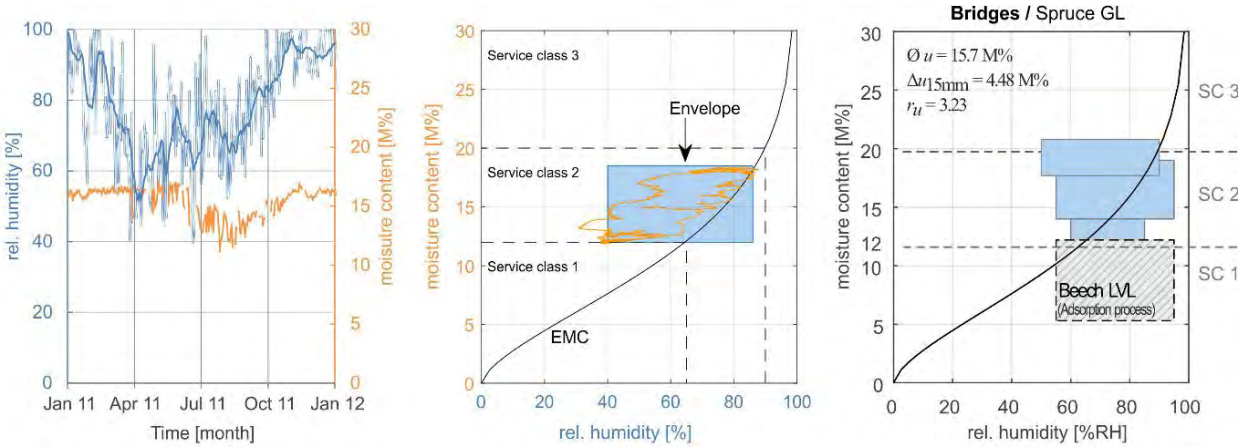


Figure 2: Evaluation of envelope of ambient climate and moisture content for timber bridges, left: moisture content and relative humidity on a specific timber bridge, middle: analyses of data compared with equilibrium moisture content (EMC), right: summary of four analysed timber bridges monitored by BFH

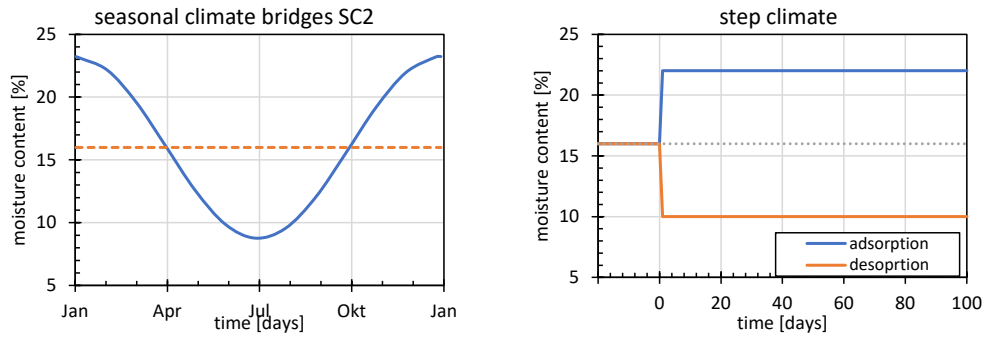


Figure 3: Simplified seasonal climate for bridges (left), stepwise climate change used for numerical simulation (right)



2.2 Numerical model

Numerical simulations were made to predict the effects of the moisture content changes on the structural health as the structures are subjected to ambient climate variations. The numerical finite element model was set up to simulate the moisture diffusion with focus on practical dimensions and applications and considers the calculation of moisture content distribution, deformations, and strain developments. Different numerical models to calculate the moisture content distribution and corresponding moisture induced stresses are available in literature: such as a 1D-model [5], 2D-model [6], and 3D-model [7]. For this research study, simulation of moisture content developments and following stress distributions were enabled through a 1D-model [5] and a 2D-model [6], as described in detail in [8]. Moisture transport was modelled through Ficks' second law observed in Eq. (1), in which u refers to moisture content, D to the diffusion coefficient, and t and x to time and position respectively.

$$\frac{\partial u}{\partial t} = D\frac{\partial^2 u}{\partial x^2} \tag{4}$$

A constant diffusion coefficient of $3.0 \cdot 10^{-10}$ m^2/s [6] was used in all simulations. The dependency of diffusion on moisture content in transverse direction is not as pronounced as in longitudinal direction, so a constant coefficient was assumed to be sufficient. Ambient relative humidity and temperature were used to calculate a theoretical equilibrium moisture content at the surface [9], [10]. This theoretical equilibrium moisture content was used as a driving force at the surface of the cross section. Surface emission factors were not used since the simulations concern sufficiently ventilated structures [6]. A list of the material parameters is given in Table 1.

***Table 1**: List of material parameters used in the numerical model, obtained from [6], [7]*

Parameter	Value	Parameter	Value	Parameter	Value
E_r [N/mm^2]	467	α_r [%/M%]	0.13	m_r [mm^2/N]	0.07e-6
E_t [N/mm^2]	216	α_t [%/M%]	0.32	m_t [mm^2/N]	0.10e-6
G_{rt} [N/mm^2]	42	D [m^2/s]	3e-10	m_{rt} [mm^2/N]	0.40e-6
nu_{rt} [N/mm^2]	0.50	mu_{rt}	0.75	mu_{tr}	0.75

The time dependent stress-strain behaviour was considered by adding the elastic, hygro-expansive, mechano-sorptive and creep strains. Equation (6) and (7) show the total strain ε_t as the sum of the elastic strain ε_E, hygro-expansive strain ε_u, mechano-sorptive strain ε_{ms}, creep strain ε_φ. E represents the anisotropic elasticity matrix, α the vector with the hygro-expansive factors, and m the vector with the mechano-sorptive creep parameters. These are averaged over the cross-section height in the 1D-model, so the extra subscript *eff* (effective) is added to the parameter. In addition to the mechano-sorptive value m in the 1D-model, a parameter β is used to allow for different mechano-sorptive creep during wetting or drying processes. In the 2D-model, only one parameter for the mechano-sorptive creep was used since this concerned only wetting or drying cases. The time dependent creep strains in these dynamic conditions are often neglected, [11].

$$\dot{\varepsilon}_t = \dot{\varepsilon}_E + \dot{\varepsilon}_u + \dot{\varepsilon}_{ms} + \dot{\varepsilon}_\varphi \tag{5}$$

$$\dot{\varepsilon}_t = \frac{\dot{\sigma}}{E_{eff}} + \alpha_{eff}\dot{u} + \left(m|\dot{u}| - \beta\dot{u}\right)\sigma + 0 \tag{6}$$

The moisture distribution numerically modelled was compared with experimental investigations done by Jönsson, [14] as shown in Figure 4. The moisture content of a glued laminated member with a cross section of 90 mm in width and 270 mm in height was increased (wetting process) from 9 M% to 16 M%. Figure 5 shows the resulting stresses for an adsorption process investigated by Jönsson, [14] on the same glued laminated cross section of 90 mm in width and 270 mm in depth. The simulations show a good agreement with the experimental results and validates the model predictions. An influence of the glue lines of glued laminated timber on the moisture diffusion or moisture transport was not considered since the moisture transport took in a direction parallel to the glue lines.

ICTB 2021 PLUS
4th International Conference on Timber Bridges
Biel/Bienne, Switzerland, 9 -12 May 2022

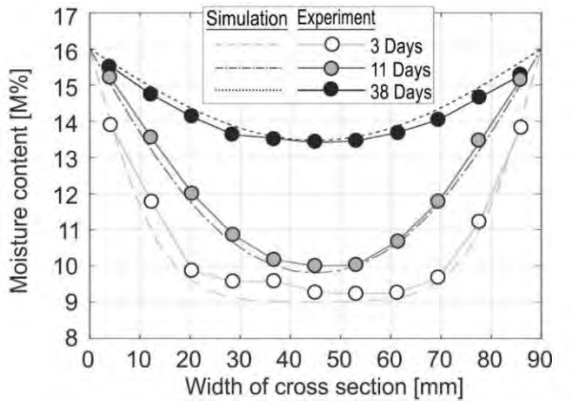


Figure 4: Numerical distribution of moisture content in comparison to experimental results on a glued laminated cross section of 90 x 270 x 16 mm³ under adsorption process from 9 to 16 M% done by Jönsson [13]

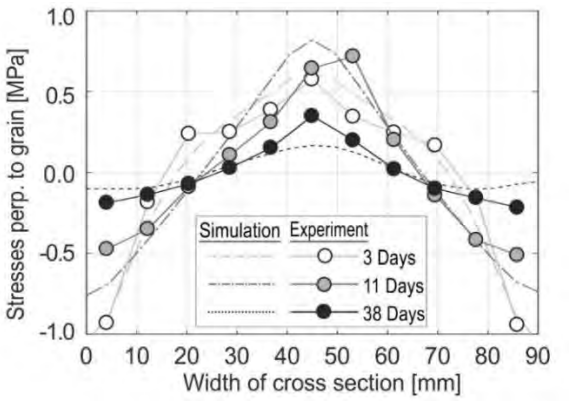


Figure 5: Numerical stress distribution and development in comparison to experimental results on a glued laminated cross section of 90 x 270 x 16 mm³ under adsorption process from 9 to 16 M% done by Jönsson [13]

2.3 Glulam and investigation program

Figure 6 gives an overview of cross section sizes used over the last 50 years in more modern timber bridges. It shows that cross section widths are slowly increasing, until these are finally block glued into very large cross sections with a width of more than 1.5 m. These cross sections can be found in all types of timber bridges: arch bridges, truss bridges, etc. according to the information provided in [14].

The principal layout of one lamella of glulam including the annual ring orientation, pith location and distances are shown in Figure 7 as well as the defined aspect ratio and the sideways assembly of individual beams into a block glulam beam is also illustrated in Figure 7.

Block glulam beams were modelled in which the width over height relation was:

- 160 mm x 800 mm, and as multiple up to 800 mm x 800 mm
- 200 mm x 800 mm, and as multiple up to 800 mm x 800 mm
- 360 mm x 800 mm, in divisions of up to 9 beams

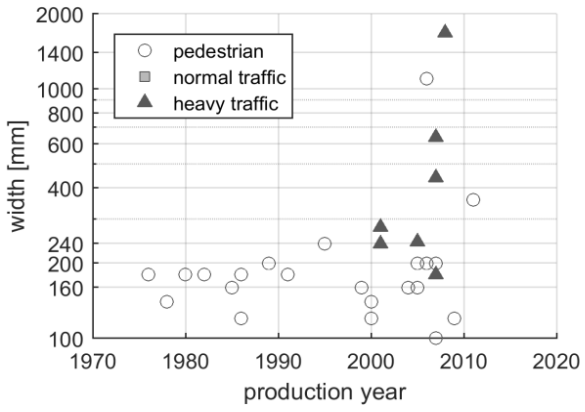


Figure 6: Illustration of increase of width of cross sections used in different types of bridges. Eventually, block glulam beams are used to transfer the high load traffic [14]

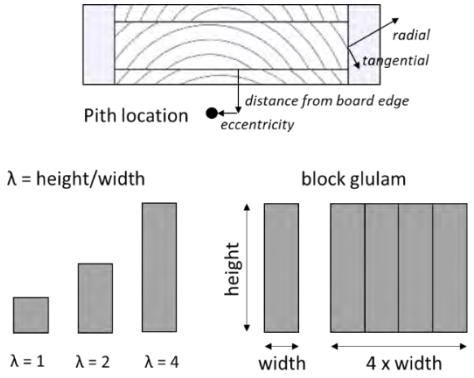


Figure 7: Illustration of a board in a glued laminated beam with the annual ring orientation, pith eccentricity and distance from the board edge (top), aspect ratio and assembly of individual beams into a block glulam beam (bottom).

3 Results

3.1 Moisture content distribution and cross-section deformations

The moisture content distribution and vertical deformations across the width of the two cross sections 160/800 mm and 200/800 mm corresponding to the applied step loads of + 6 M% are shown in Figure 8. The plotted deformations are obtained from the maximum duration of the simulations. This was set to 120 days on the smaller cross-sections and 360 days on the large cross-sections. The smaller cross-sections respond faster to moisture content increases, due to the smaller amount of constraint during swelling, and the faster increase in moisture. It takes a long time until the moisture content reaches equilibrium in the centre of the cross-section. Hence, building with wider cross-sections most likely results in smaller deformations.

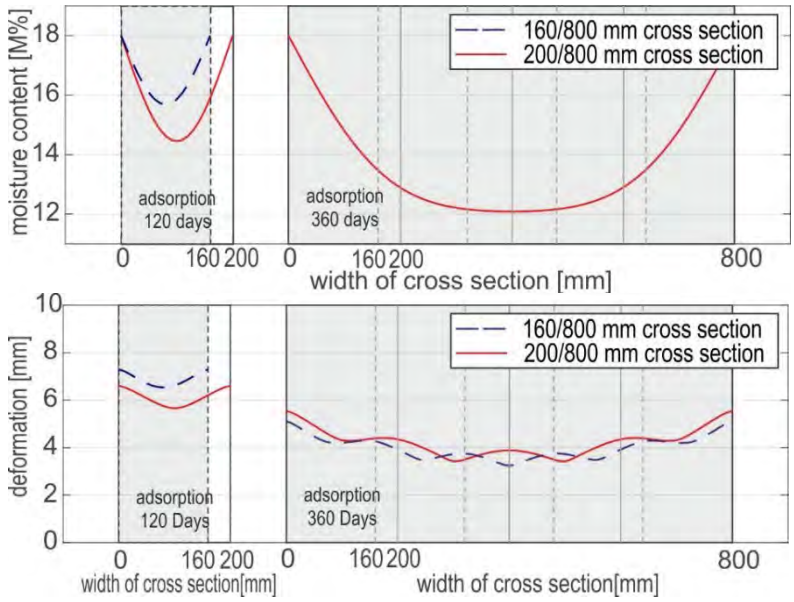


Figure 8: Moisture content distributions (top) and deformation across the width of the timber beams of different widths subjected to a step load of 6 M% moisture content increase. All beams have a height of 800 mm and the duration of the simulations is indicated in the figures.

3.2 Stress situation over the cross section

The magnitude of the climatic variations affects the generated moisture induced stresses in the cross-section. Results showed that the moisture induced stresses are also affected by cross section width. Low aspect ratios showed that the geometry also can affect the generated stress levels. The block glulam beams form wide cross-sections by gluing single glulam beams to each other. This is expected to affect the moisture induced stresses in two ways.

1. The ratio between the areas where the compressive stresses and the tensile stresses are present is different from those in slender beams. The tensile stresses are spread out over a larger portion of the cross section, resulting in smaller values.
2. Since the cross section is not slender anymore, effects of aspect ratio also start playing a role and reduce the total amount of generated stresses in the cross section.

This is however verified by setting up simulations where a stepwise climate is induced of $u = 12 \pm 6$ M%. The cross-section height is always maintained at 800 mm.

The calculated levels of moisture induced stresses in different widths of cross-sections is plotted in Figure 9. The stress distribution is plotted at the point where the maximum tensile stress levels are achieved. Two beam widths were used to calculate stress levels up to total block glulam beam widths of 800 mm:



- four beams of 200 mm were needed to form a block glulam of 800 mm, and
- five beams of 160 mm were assembled to form a block glulam beam of 800 mm.

Figure 9 shows that higher tress levels are found in block glulam beams with an uneven number of single beams when submitted to wetting loads. In the block glulam beams with an even number of single beams, maximum stress levels are lower than in the uneven number of single beams. Converged stress levels remain at around 0.5 MPa. The time needed for each of these beams to develop these stresses is different and all reach a maximum level long after the moisture loads were initially applied.

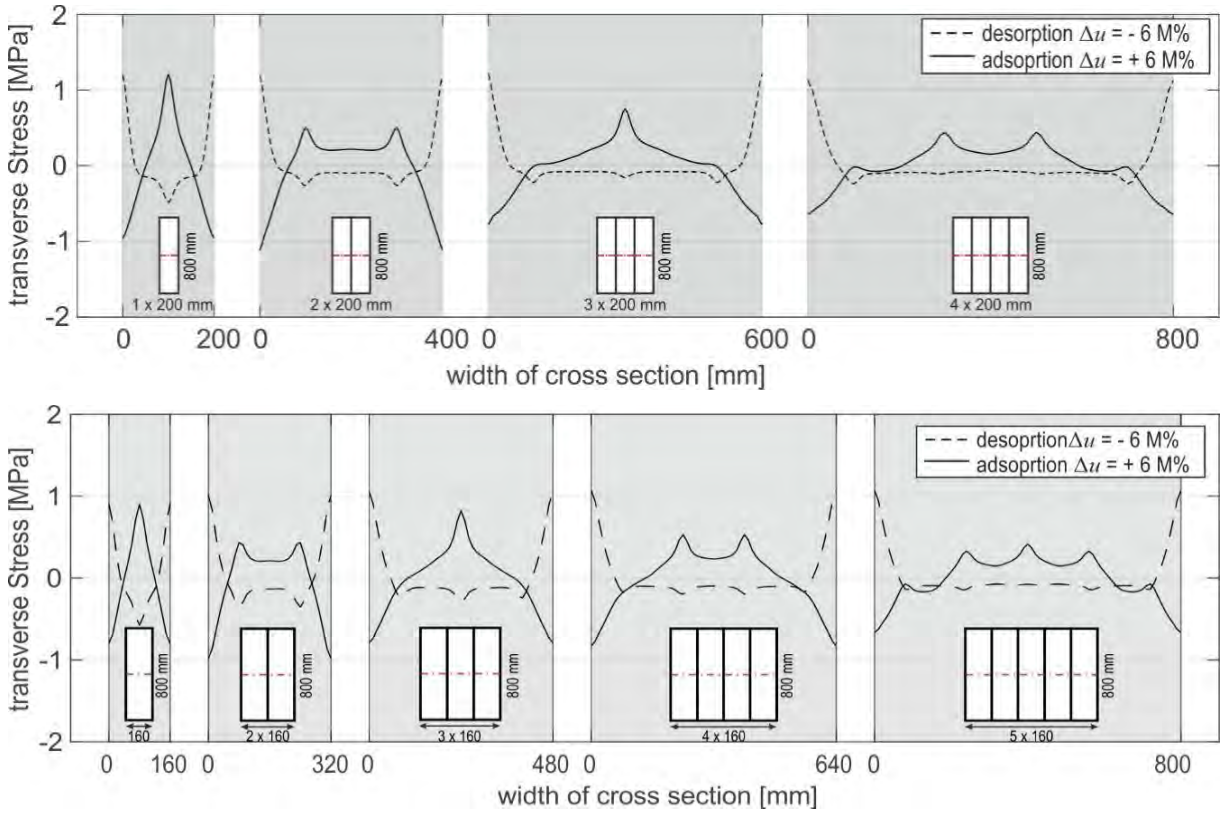


Figure 9: Transverse stresses due to moisture step-loading in block-laminated beams depending on the width of the cross-section

When the beams were subjected to drying loads, the width of the beams or the number of beams used does not affect the level of maximum tensile stresses. These simply occur shortly after the driving load has changed at the surface. This could be an explanation why almost every timber member in a structure shows at least some cracks. It is assumed that these stress levels depend on the angle the annual rings make with the surface of the beam.

To verify if the aspect ratio affected the reduction of strains only a simulation was done where the cross-section width and height were maintained constant, and the number of single beams was varied as shown in Figure 10. A beam with a cross section width of 360 mm is subdivided into two, three, four, six, and nine single beams. Here too, the stress distribution perpendicular to the grain converges once four beams or more are used in the cross section. It is noted that the cross sections simulated here are not necessarily economical for use in practical production lines or construction.

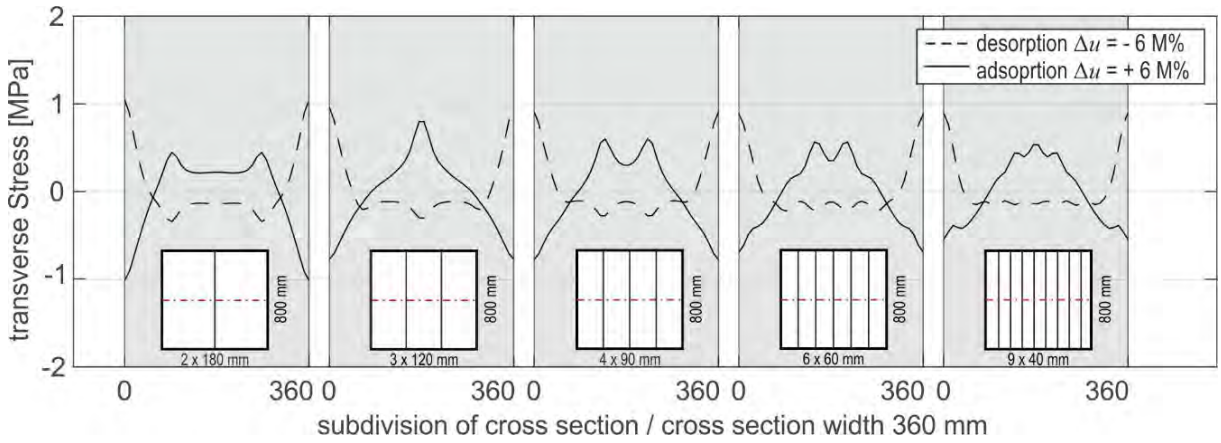


Figure 10: Transverse stresses due to moisture step loading in cross-laminated beams with identical cross-sections but different set-up regarding number of single beams.

4 Discussion and Conclusion

Monitoring results for timber structures and timber bridges are summarized through envelope diagrams that show the moisture content variation and the variation of the surrounding climate during service. The structural elements of bridges are mostly exposed to these variations. A moisture content below 20 M% can be assumed for timber bridges if adequate constructive wood protection is met. The risk of fungi is avoided effectively. Use of timber in bridges is not considered as a problem from the climate point of view, provided that enough ventilation is always available, also around structural details. Design of details, providing protection of structural elements against impact of rain and sun, and keeping a maintenance log is expected to be more important for the durability of the bridge structure. Whether it crosses a water body or road is likely to have an impact, but this is for the moment considered unmeasurable with regards to at least average moisture content, [4].

The numerical investigations concentrate on block glued glulam members. The numerical model includes moisture transport and the resulting stress distributions over various cross sections. The numerical simulations allowed insight in the dependency of moisture load and geometry on the generated moisture induced stresses. The results showed that moisture induced stresses in block-laminated beams depend on moisture load amplitude, geometry, and beam slenderness. Drying loads almost instantly lead to high tensile stresses and visible cracks at the surface, whereas wetting loads lead to gradual increase of tensile stresses in the midplane of the cross section. Cracks generated in the midplane are not visible but have however been observed during the demolition and inspection of timber structures. Drying stresses are much less affected by the geometry. Use of block-gluing shows a positive effect on the development of stresses in the cross-section. The number of glulam members should be two or more than three to reduce the transverse tensile stresses in block glued glulam members for wetting situations.

Acknowledgement

The work was supported by the Federal Office for the Environment (FOEN) under project numbers 2013.06 and 2016.17. Industry partners Roth AG, Makiol Wiederkehr AG, and Tiefbauamt des Kantons Bern, Walt-Garmarini AG, Pirmin Jung Ingenieure AG, Büro für Projektleitungen und Baufragen, Henkel & Cie. AG, SFS Unimarket AG, and Würth AG Schweiz. Research partners Technical University of Munich and Lund University are also acknowledged for their contribution.

References

[1] Gamper A., Dietsch P., Merk M. (2014); Gebäudeklima - Langzeitmessung zur Bestimmung der Auswirkungen auf Feuchtegradienten in Holzbauteilen, Research Report, Technical University of Munich, Germany

[2] Cruz H., Custódio J. (2006) Durability and temperature effects on bond line, Presentation at COST Action FP 1101, Assessment, Reinforcement and Monitoring of Timber Structures, Trento, Italy



[3] Franke B, Franke S, and Müller A., Case studies: long-term monitoring of timber bridges, Journal of Civil Structural Health Monitoring 5, p. 195-202, 2015
[4] Franke B, Franke S, Schiere M, Müller A (2019), Moisture content and moisture-induced stresses of large glulam members: laboratory tests, in-situ measurements and modelling, Volume 14 (4), p. 243-252
[5] Häglund M. (2010) Parameter influence on moisture induced eigen-stresses in timber, European Journal for Wood Products, Vol. 68, pp. 397–406
[6] Angst-Nicollier V.; Moisture induced stresses in glulam - effect of cross section geometry and screw reinforcement, PhD thesis 2012:139, NTNU Trondheim, Norway, 2012
[7] Fortino S., Hradil P., Genoese A., Genoese A., pousette A., Fjellström PA.; A multi-Fickian hygro-thermal model for timber bridge elements under northern europe climates, WCTE 2016 conference proceedings, Vienna, Austria, 2016
[8] Schiere M. (2016): Moisture induced stresses in glulam cross sections, Master Thesis, Bern University of Applied Sciences, Department of Architecture, Wood and Civil Engineering.
[9] Simpson W. (1973) Predicting equilibrium moisture content of wood by mathematical models, Wood and Fiber, 5 (1), 41-49.
[10] Simpson W. (1998) Equilibrium Moisture Content of Wood in Outdoor Locations in the United States and Worldwide. Research Note FPL-RN-0268, Madison, WI: U.S. Department of Agriculture, Forest Service, Forest Products Laboratory
[11] Toratti T., Svensson S. (2000), Mechano-sorptive experiments perpendicular to the grain under tensile and compressive loads. Wood and Science Technology 34, pp. 317–326
[12] Jönsson J. (2004), Internal stresses in the cross-grain direction in glulam induced by climate variations, Holzforschung 58, pp. 154–159
[13] Jönsson, J. Moisture induced stresses in glulam cross sections, CIB Proceedings, CIB-W18/34-12-4, Italy, 2001.
[14] Swiss timber bridges, www.swisstimberbridges.ch, 2017

Conference Proceedings 4th ICTB (2022)
https://doi.org/10.24451/5eyp-2f23

ICTB 2021 PLUS
4th International Conference on Timber Bridges
Biel/Bienne, Switzerland, 9 -12 May 2022



Vibration serviceability of timber pedestrian bridge based on field test and analysis

Shingo Kato[1], Hideyuki Honda[2], Atsushi Toyoda[3]

1 Introduction

Investigation of vibration serviceability for pedestrian bridges is an important issue in de-sign and maintenance. The vibration serviceability of pedestrian bridges has been studied for many pedestrian bridges made by concrete and steel, for example (Kajikawa, 1979), (Kobri, 1990), (Tanaka, 1994), (Obata, 1997) and (Yoneda, 2003). However, the study on vibration serviceability for timber pedestrian bridges is almost never carried out, except by (Yamada, 2003) and (Kusaka, 2006).



Figure 1. Tokiwa Bridge; subject of this study

The purpose of this study is to evaluate vibration serviceability of timber pedestrian bridges based on experiment and analysis. The subject bridge is Tokiwa Bridge, a large scale three spans continuous girder made by bongossi wood material and constructed at 1995 in Kitakyushu City in Japan as shown in Fig.1. The design geometry is: bridge length: 84.4 m, maximum span length: 31.0 m and clear width: 6.0 m.

The dynamic field test of Tokiwa Bridge was carried out in 2007. The vibration characteristics and dynamic behavior were investigated, and then vibration serviceability of the bridge was verified by the measured response velocity. Next, a three dimensional dynamic response analysis due to walking of pedestrian on the bridge was also carried out, and then the experimental and analytical results were compared. Furthermore, the investigation of the dynamic response characteristics by the dynamic response analysis and evaluation of vibration serviceability were carried out, and vibration serviceability was finally verified from both results of the experiment and the analysis. As a result, this study verified that it is possible to evaluate vibration serviceability of the timber pedestrian bridge analytically.

2 Subject Bridge and Vibration Limit for Vibration Serviceability

2.1 Subject bridge

The general drawing of Tokiwa Bridge; the subject of this study is shown in Fig. 2 to Fig.4. The bridge length is 84.4 m, and the maximum span length is 31.0 m. Each main girder with the cross section of 1200 x 265 mm is 3 spans continuous girder laminated by bongossi material of 5 layers. For this lamination method, drift pins driven in 25 cm interval are used. Fig. 5 and Fig. 6 show the outside and inside of joint part. The reinforce steel element shown in Figure 6 was newly installed in reinforcing work at 2005. Table 1 shows the design condition of the bridge.

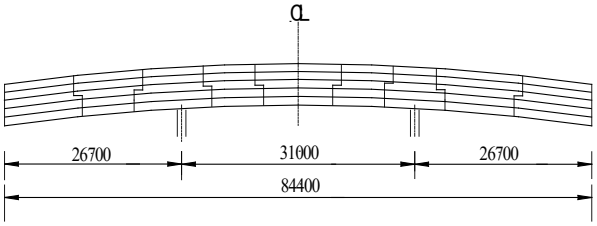


Figure 2. General drawing of Tokiwa Bridge

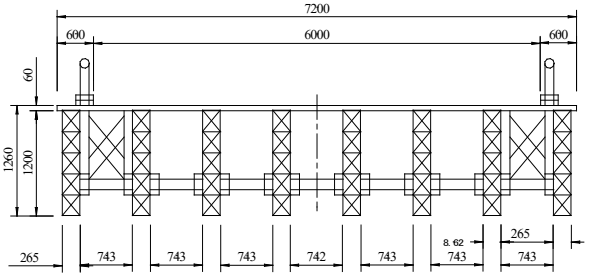


Figure 3. General drawing of Tokiwa Bridge

[1] Tokyo Electric Power Services Co,.Ltd. Japan, E-mail: shingo.kato@tepsco.co.jp
[2] Kanazawa Institute of Technology, Japan, E-mail: honda@neptune.kanazawea-it.ac.jp
[3] Geotech Consultants Inc. Japan, E-mail: atsuminopapa@yahoo.co.jp

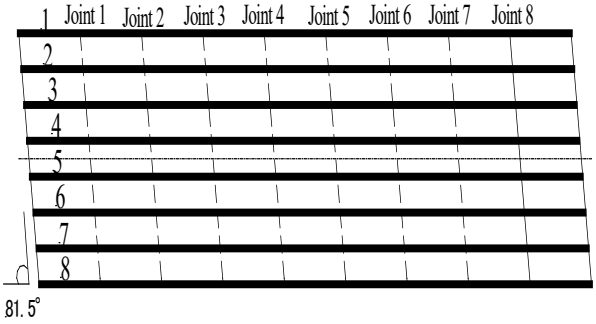


Figure 4. General drawing of Tokiwa Bridge

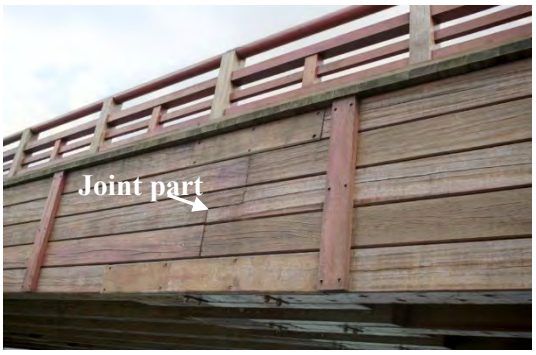


Figure 5. Outside of joint part

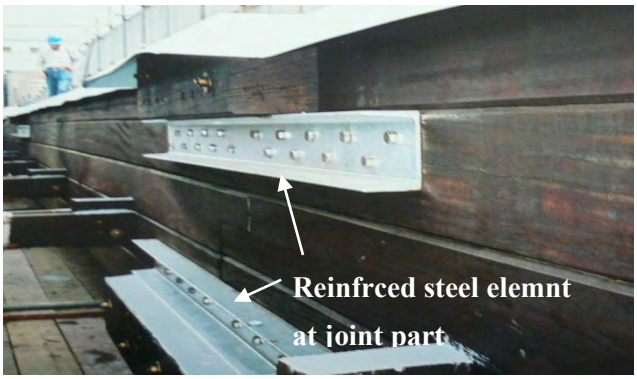


Figure 6. Inside of joint part

Table 1. Design condition of the subject bridge

Constructed Place	Fukuoka, Japan (1995)
Bridge class	Timber pedestrian bridge
Bridge type	3 span continuous girder laminated in 5 layers
Bridge length	85.0m
Span, length, width	26.75+31.0+26.75m
Main timber kind	Bongossi

2.2 Vibration limit for vibration serviceability

Some international specifications and codes such as British Standard (BS5400), Eurocode 5 and Ontario Code in Canada specify vibration limit for vibration serviceability of pedestrian bridges. These vibration limits are based on the evaluation of response acceleration.

In Japan, the design guideline of pedestrian bridges was instituted in 1967. The design code on vibration serviceability has been revised in 1979, with some revision carried out afterwards. The present vibration limit of pedestrian bridges which is more strict than the design specification of highway bridges has been adopted as the code on vibration serviceability. In present code, the maximum deflection of main girder by live load is forbidden to exceed 1/600 of span length. However, when the vibration effect of pedestrian is considered in design, deflection limit is relduced to 1/400 . To consider the vibration effect of pedestrian means to exclude natural frequency of 1.5-2.3 Hz in the design of pedestrian bridges. The code on deflection and vibration has been adopted in the design method that the discomfort of pedestrian may not occur in waking on pedestrian bridges.

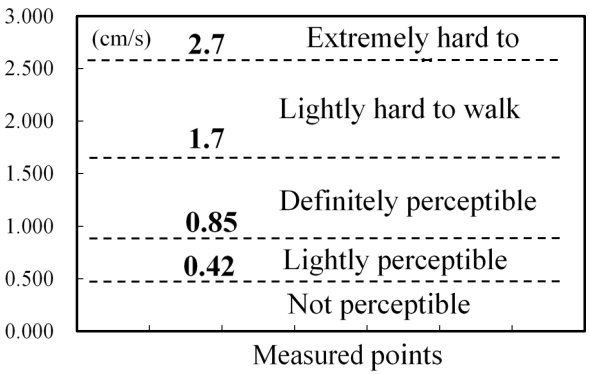


Figure 7. Vibration limit by maximum value of response velosity

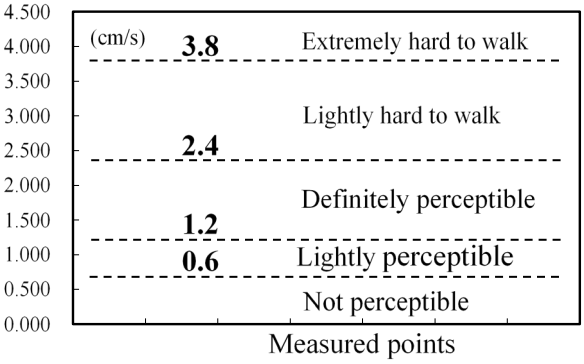


Figure 8. Vibration limit by root mean square (rms) value of response velosity



In Japan, the vibration limit on discomfort of pedestrian is based on the evaluation of response velocity. The studies by Kobori and Kajikawa (1974), and Kajikawa (1982) greatly contribute for the vibration limit. There are 2 methods to evaluate vibration serviceability by response velocity. Fig. 7 shows the vibration limit by maximum value of response velocity for vibration serviceability. The response velocity of 2.4 cm/s with the sense that pedestrian reacts with a lightly hard to walk feeling is evaluated as a vibration limit value for vibration serviceability of pedestrian bridges. Fig. 8 shows the vibration limit by root mean square (rms) value of response velocity for vibration serviceability. The response velocity of 1.7 cm/s with the sense that pedestrian reacts with a lightly hard to walk feeling evaluated as a vibration limit value for vibration serviceability of pedestrian bridges.

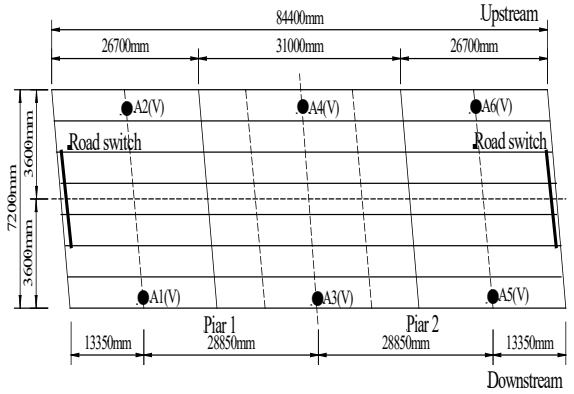


Figure 9. Measurement points of resnant waking and running tests

3 Field Dynamic Test

3.1 Testing method

The field dynamic test was conducted in order to investigate dynamic characteristics of Tokiwa Bridge in 2007. The dynamic test was done by tests such as (1) ambient vibration test, (2) impact loading test by dropping of sand bag with weight 0.3 kN and (3) resonant waking and running tests of pedestrians. The measured data is checked and stored in digital recorder and personal computer, and then the dynamic behaviour and characteristics of the bridge are analyzed in monitoring system of field test. In resonant waking and running tests, the 1-2 pedestrians walked and ran in a pace equal to vertical flexural first natural frequency of 2.25 Hz of the bridge obtained by the ambient vibration and impact loading tests, and then the response velocity and acceleration were measured. This is a critical experimental method in which the bridge becomes in resonant state by the external force of pedestrian with 2.25 Hz. Fig. 9 shows the measurement points of resonant waking and running tests. The symbol of V in this figure indicates the vertical direction of the bridge. The signal of In and Out on transfer of pedestrian is measured by the load switch shown in this figure. The transfer cases of pedestrian are walking and running at edge part of upstream.

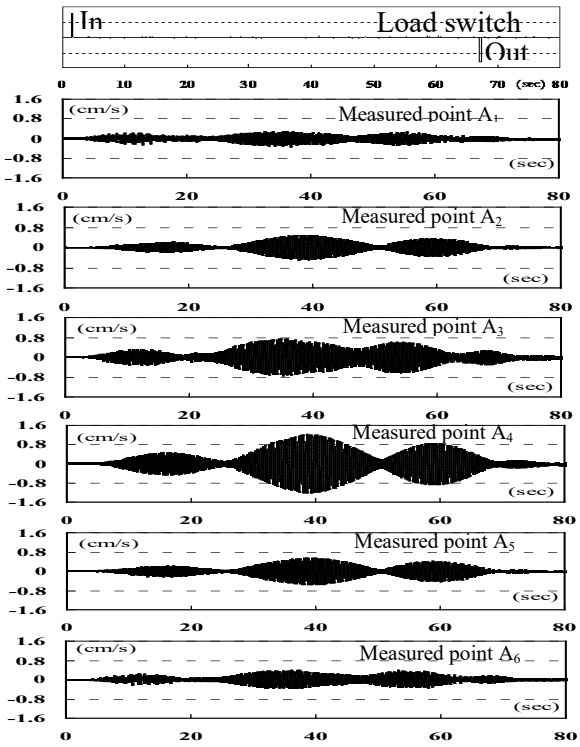


Figure 10. An example of response velocity in one person walking test with resonant pace of 2.25Hz at edge p art of upstream



3.2 Result of dynamic test

Fig. 10 shows an example of response velocity in one person walking test with resonant pace of 2.25Hz at edge part of upstream. The structural characteristics of three spans continuous girder has appeared clearly from this vibration response wave. In the walking test of one pedestrian, the maximum value of response velocity was 1.23 cm/s at measured point of A4. That value was 1.63 cm/s at A4 in the walking test of two pedestrians. In the running test of one pedestrian, that value was 4.25 cm/s at A4. In the walking test of one pedestrian, the rms value of response velocity was 0.44 cm/s at A4. That value was 0.51 cm/s at A4 in the walking test of two pedestrians. In the running test of one pedestrian, that value was 1.69 cm/s at A4.

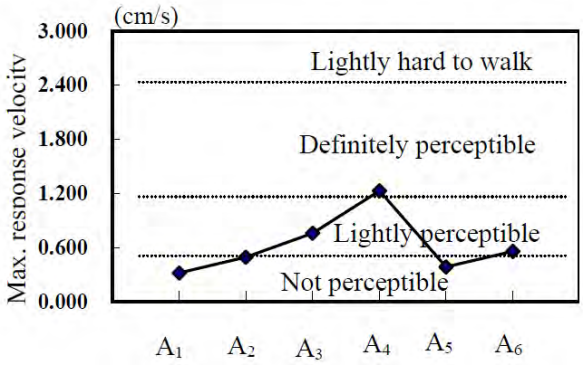


Figure 11. Evaluation of vibration serviceability

Fig. 11 shows an example for evaluation of vibration serviceability by maximum response velocity in the walking test of one pedestrian. Pedestrian may have vibration sense of lightly perceptible, when one person walks in the resonant state. Fig. 12 shows an example for evaluation of vibration serviceability by maximum response velocity in the running test of one pedestrian. Pedestrian may have vibration sense of extremely hard to walk, when one person is running in the resonant state.

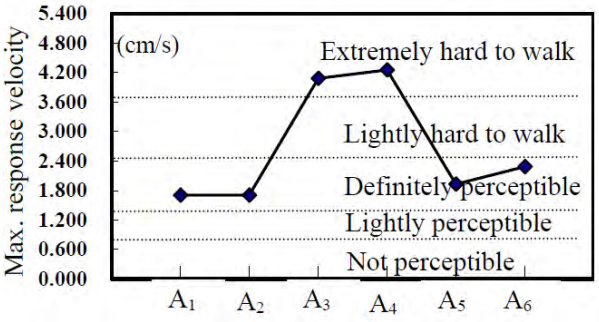


Figure 12. Evaluation of vibration serviceability

Spectral analysis using FFT was conducted with data measured by the dynamic test. The experimental and analytical dynamic characteristics are shown in Table 2 until vibration of the 4th degree. The vibration modes and natural frequencies of the bridge were also computed by three dimensional eigenvalue analysis using MSC/NASTRAN. There is good agreement between experimental and analytical results.

Table 2. Dynamic characteristics of the objected bridge

No.	Mode types	Natural frequencies f_i (Hz)		Damping coefficients h_i
		Measured	Analyzed	
1	Horizontal 1st	1.37	1.40	0.0050
2	Vertical 1st	2.25	2.27	0.0145
3	Vertical 2 nd	3.10	2.85	0.0128
4	Torsional 1st	3.71	3.69	0.0154

ICTB 2021 PLUS
4th International Conference on Timber Bridges
Biel/Bienne, Switzerland, 9 -12 May 2022



4 Dynamic Response Analysis

4.1 Analysis method

In the three dimensional dynamic response analysis of the bridge due to walking and running of pedestrian, Fig. 13 shows the coordinate system of x, y and z axis on node displacement and node force of element member. The ui and uj in this figure are axis displacement in x direction at node i and j. The vi and vj are axis displacement in y direction. The wi and wj are axis displacement in z direction. The θxi and θxj are rotational angle in x axis. The θyi and θyj are rotational angle in y axis. The θzi and θzj are rotational angle in z axis. The xi and xj are axis force in x direction at node i and j. The yi and yj are axis force in y direction. The zi and zj are axis force in z direction. The Mxi and Mxj are bending moment with respect to x axis at node i and j. The Myi and Myj are bending moment with respect to y axis. The Mzi and Mzj are bending moment with respect to z axis.

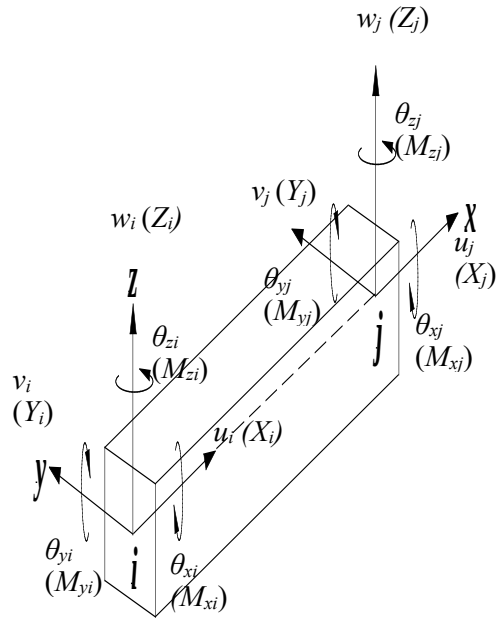


Figure 13. Coordinate system of element member

In the dynamic response analysis method, there are modal analysis method and direct integral method. In this study, the analysis shown in the following was carried out using direct integral method. The equation of motion on vibration system of pedestrian and bridge is given by:

$$[M]\{Z\&\&\}+[C]\{Z\&\}+[K]\{Z\} =\{F\} \tag{1}$$

where: [M] - mass matrix; [C] - damping matrix; [K] - stiffness matrix;
{F} - external force vector by pedestrian.

As numerical integration method, Newmark's β method was used to solve the equation (1) in this study. The integral time interval Δt is 0.05 seconds. The arbitrary constant γ is 1/2. The parameter β is 1/4. The convergence accuracy of acceleration is 1/1000 in Δt.

The damping matrix in this study is assumed by Rayleigh damping. The parameters of α and η on damping are obtained from natural frequency fi and damping coefficient hi in vertical vibrations based on experimental values as shown in Table 2. The Rayleigh damping is given by

$$[C] = \alpha[K]+\eta[M] \tag{2}$$

where: α=(h1 f1-h2 f2)/(π(f12-f22)); η=4π f2 (h2-πf2 α).

The external force by pedestrian is given by

$$\{F\} = F(t)=\{mg + mg\xi \sin(2\pi p_s t)\}\vartheta(t) \tag{3}$$

where: mg - body weight of pedestrian; ps – pace of pedestrian (Hz); ξ- impact force ratio; θ(t) - coefficient vector done proportional distribution at both nodes of element in which pedestrian loads.



The field experiment at the subject bridge and laboratory experiment which changed body weight, pace and step size of pedestrian were conducted in order to calculate the impact force ratioξwith four load cells of plate type. Fig. 14 shows the result obtained by those experiments. There are many cases in which pedestrian generally does walking and running in 2.0 - 2.5 Hz pace. The external force of pedestrian in this study improved the method by using sine wave which Kajikawa (2000) proposed. As it is shown in Fig. 15, the method where half sine wave removed negative load part (load to top from under floor system) of input sine wave was used.

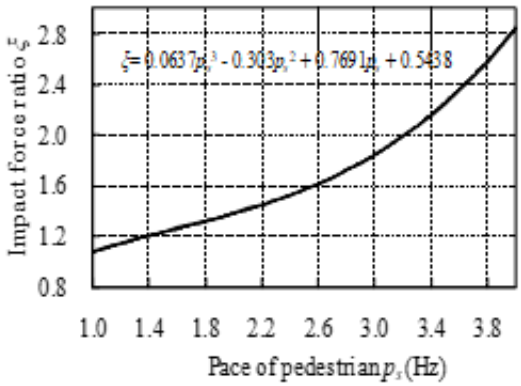


Figure 14. impact force ration of pedestrian

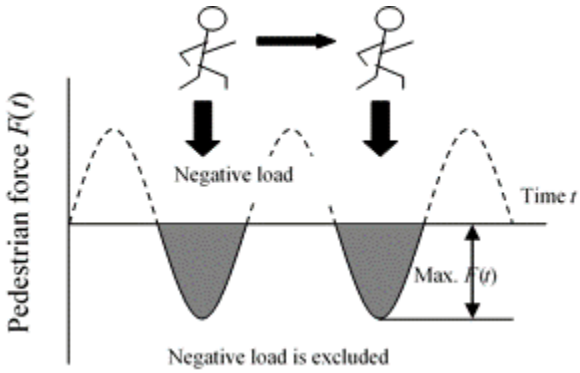


Figure 15. Half sine wave of external force



Figure 16. Structural girder model of 5 layers



Figure 17. Structural girder model of 2 layers

The partial structural models in case with joint and in case without joint were made, and the effect of joint part was investigated from static and eigenvalue analyses. As a result, there was no difference by both structural models from both sides of natural frequency and static deflection. From this fact, the structural analysis model in this study has been modelled as without joint part. At the beginning of structural modelling, the structural analysis model of this bridge was made as faithful model of 3 spans continuous girder laminated in 5 layers shown in Fig.16, and then eigenvalue analysis using the subspace method was carried out in order to confirm the validity of three dimensional structure analytical model. As a result, the vertical first vibration was 2.19 Hz, which is a value that was an approximation of the experimental value.

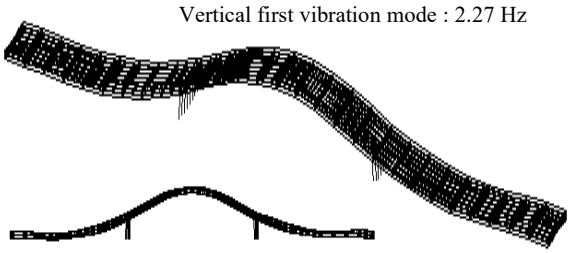


Figure 18. Analyzed vibration mode

However, it was proven that three dimensional dynamic response analysis was difficult on this structural model, because the node number is enormous. From this fact, the structural analysis model was improved again, and a structural model of 3 spans continuous girder laminated in 2 layers which considered the effect of bracing member was made. This structural model is shown in Fig. 17. The eigenvalue analysis was carried out for this structural model. The results are shown in the analyzed natural frequencies of Tables 2. The vertical first vibration mode analyzed is shown in Fig. 18.



4.2 Dynamic response Analysis

Three dimensional dynamic response analysis of this bridge due to walking of one pedestrian was carried out using the girder model laminated by 2 layers shown in Fig. 17. The response velocity waves at each analyzed point in resonant walking are shown in Fig. 20. As well as measured wave in Fig. 12, the vibration behaviour of three spans continuous girder has appeared clearly from this analyzed wave. The maximum value of measured point and analyzed point which is close to walking lane increases from other values, when analyzed wave in Fig. 20 and measured wave in Fig. 12 are compared. It is shown that lateral load sharing is clearly small, though the simple bracing member between each main girder has been installed. The maximum values and wave shapes based on experiment and analysis almost agree.

Power spectrum density function (PSD) was also required from spectrum analysis by FFT in order to examine frequency of response wave obtained the experiment and the analysis. As a result, the experiment wave became 2.25Hz, and the analysis wave became 2.24Hz. The validity of this three dimensional dynamic response analysis can be confirmed, because both peek spectra agree.

5 Vibration Serviceability

The evaluation of vibration serviceability may become less for rms value which has meaning of mean value for variational data. From this fact, vibration serviceability in this study was evaluated by maximum value of response velocity. Fig. 21 shows evaluation of vibration serviceability for the subject bridge by maximum response velocity obtained by the experiment and the analysis due to resonate waking of one pedestrian at edge part of up-stream. From this figure, it is proven that the measured and analyzed values cause both reactions of "not perceptible for vibration" or "lightly perceptible" on vibration serviceability of this bridge. It is also proven that that analyzed and measured values agree well and that the shape of response velocities resemble. From this fact, they seem to be able to evaluate vibration serviceability of the subject bridge analytically, even if dynamic testing of the actual bridge is not done, when the vibration characteristic of the subject bridge has been proven.

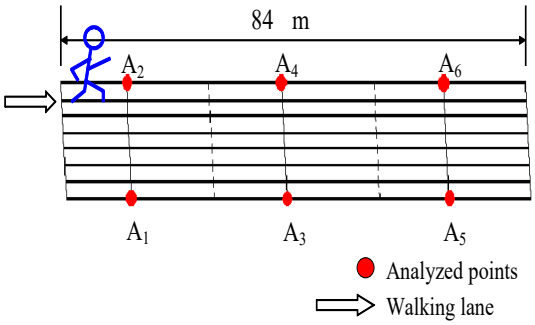


Figure 19. Analyzed point and walkin lane

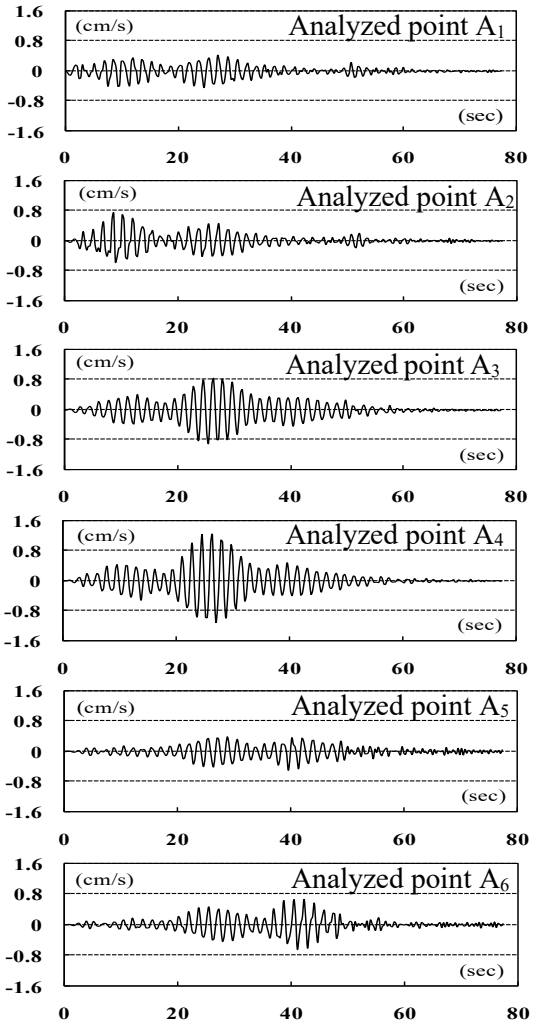


Figure 20. An example of response velocity analyzed by waking of one person with resonant pace of 2.25Hz at edge part of upstream



As an example, vibration serviceability of the subject bridge was investigated by maximum value analyzed and measured response acceleration using the vibration limit of Canadaian Ontario Code and BS5400. The result is shown in Fig. 22. The measured and analyzed values are proven of becoming very close values, and both values are also within the permission region of the Ontario Code.

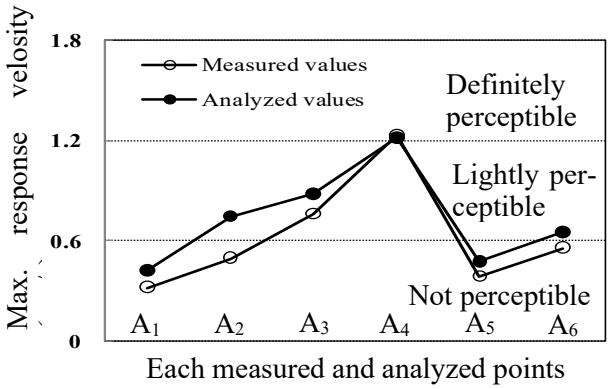


Figure 21. vibration serviceability of this bridge

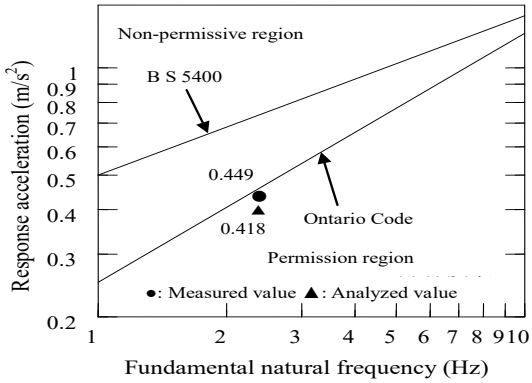


Figure22. An example on vibration serviceability of the objected bridge by maximum acceleration values using Ontario code and BS5400.

6 Conclusions

This study is done on a pedestrian bridge with large scale three spans continuous girder made by bongossi wood material. It investigated vibration serviceability of the timber pedestrian bridge based on experiment and analysis. The three dimensional dynamic response analysis of bridge due to walking and running of pedestrian was originally developed by FORTRAN program. The investigation of the dynamic response characteristics by the dynamic response analysis and evaluation of vibration serviceability were carried out, and vibration serviceability was finally verified from both sides of the experiment and the analysis for the bridge. The validity of this analysis was verified because measured and analyzed value agreed well. It seems that vibration serviceability of this bridge is the degree at which pedestrian senses “lightly perceptible” vibration, which causes no problem. As the result, this study verified that it is possible to evaluate vibration serviceability of the timber pedestrian bridge analytically.

7 References

[1] Kajikawa, Y. (1979): The Study on Vibration of Highway Bridges and Effect on Vibration Serviceability, The doctoral dissertation by Kyoto University (in Japanese).
[2] Kobori, T. And Yoshida, M. (1990): Analysis and Measurement of Natural Frequency for Pedestrian Bridges, Journal Structural Engineering, Vol.36A, 671 + 678 pp. (in Japanese).
[3] Tanaka, S. (1994): The Study on Vibration Characteristics and Design Method of Vibration Serviceability for Pedestrian Bridges, The doctoral dissertation by Nagoya University (in Japanese).
[4] Obata, T. (1997): The Study on Vibration Serviceability of Pedestrian Bridges based on Human Sense of Vibration, The doctoral dissertation by Hokkaido University (in Japanese).
[5] Yoneda, M. (2003): A Simplified Method to Evaluate Maximum Lateral Response of Pedestrian Bridges due to Synchronized Walking by Pedestrians, Journal Structural Engineering, Vol.49A, 263 + 273 pp. (in Japanese).
[6] Yamada, M., Honda, H. and Furumura, T. (2003): Vibration Serviceability and Structural Characteristics of Pedestrian Timber Arch Bridge, Proc. of The 2nd Symposium on Timber bridges, 59 + 64 pp. (in Japanese).
[7] Kusaka, M. and Honda, H. (2006): Three dimensional dynamic response analysis for vibration serviceability of timber pedestrian bridges, Proc. of The 5th Symposium on Timber bridges, 37 + 44pp. (in Japanese).
[8] Kobori, T. and Kajikawa, Y. (1974): Ergonomic Evaluation Methods for Bridge Vibration, Proc. of the JSCE, No.230, 23 + 31 pp. (in Japanese).
[9] Kajikawa, Y. (1982): Some Considerations on Ergonomical Serviceability analysis of Pedestrian Bridge Vibrations, Proc. of the JSCE, No.325, 23 + 33 pp. (in Japanese).
[10] Kajikawa, Y. (2000): Guidelines for Bridge Vibration Monitoring, Subcommittee on Bridge Monitoring of JSCE, 121+125, 165+167 pp. (in Japanese).
[11] British Standards Institution 2022 :BS 5400 - Steel, concrete and composite bridges. Bridge bearings
[12] European Standed: Eurocode 5 (1995) Design of timber structures
[13] Ontario ministry of transport and communications: Ontario Highway Bridge Design Code (1992)

Conference Proceedings 4th ICTB (2022)
https://doi.org/10.24451/gak8-4k79

ICTB 2021 PLUS
4th International Conference on Timber Bridges
Biel/Bienne, Switzerland, 9 -12 May 2022



Study of the dynamic response of a timber pedestrian bridge during different construction stages

Jens Bergenudd[1], Jean-Marc Battini, Roberto Crocetti, Costin Pacoste

Abstract

The objective of this article is to study the dynamic behaviour of a timber pedestrian bridge by performing in-situ tests at four different construction stages: 1) on only the timber structure 2) on the timber structure with the railings 3) on the timber structure with railings and an asphalt layer during warm conditions and 4) same as stage 3 but during cold conditions. The study included numerical calculations with a 2D finite element model. Two modal parameter extraction methods were implemented during the post-processing. The modes of vibration were analysed with the modal assurance criterion (MAC) to ensure their validity. The results show that the presence of the railings during stage 2 increases the resonance frequencies with 0-2 % compared to stage 1, despite an approximately 5 % increase of the total mass of the bridge. The vertical resonance frequencies decreased 12-22 % when the asphalt was installed at stage 3 compared to stage 2, due to an approximately 70 % increase of the total mass and the asphalt's low stiffness due to a high temperature. The resonance frequencies increased 14-27 % during cold conditions at stage 4 compared to stage 3. This was mainly due to an increased stiffness of the asphalt layer due to a low temperature. Adding railings therefore resulted in a higher overall stiffness of the bridge, whereas asphalt essentially only added mass to the bridge at warm conditions but increased the stiffness at cold compared to warm conditions. The damping ratios increased for each construction stage and were approximately 2-3 % for the finished bridge. The two modal parameter extraction methods produced similar results which ensures that reliable results are obtained. The auto-MAC indicated well-separated modes and the cross-MAC ensured comparison of the same modes. The finite element model showed that some stiffness was lacking for the first bending mode. This stiffness could be due to shear deformation of the plastic pads at the bridge supports.

1 Introduction

Timber is a sustainable construction material and is suitable for short and medium span bridges, particularly pedestrian bridges. This is beneficial in areas with high availability of timber and with fairly short transports. Parts of the bridges can also be assembled in a factory and lifted in place on-site which reduces the construction time [1]. Problems with vibrations can however be a problem for these bridges since they can be made quite slender [2]–[5]. Therefore, it is important to have adequate calculation models in the design phase.

As a way to reach more refined finite element (FE) models for timber pedestrian bridges, a research project has been initiated where a number of bridges will be dynamically tested during different construction stages and at different seasons to study temperature effects. In this way, the influence of the different parts of the bridge, such as railings and an asphalt layer, can be identified. The asphalt stiffness is for example highly temperature dependent and has been reported to lower the resonance frequencies at warm temperatures and vice versa. Asphalt also increases damping which is mainly due to friction at the interface between timber deck and asphalt as well as internal viscous friction [6], [7].

A timber pedestrian bridge in Växjö, Sweden, has been investigated during four different construction stages. The main objective was to study the difference of the resonance frequencies and damping ratios. The modes of vibration were also compared and investigated for the different construction stages. Two modal parameter extraction methods were implemented during the post-processing to achieve reliable results and to investigate their interchangeability.

[1] Jens Bergenudd, PhD student, Department of Civil and Architectural Engineering, KTH, Royal Institute of Technology, Stockholm, Sweden, jbergenu@kth.se



2 Material and method

This section describes the bridge, the experimental tests and the methods to post-process the experimental data.

2.1 The bridge

The bridge is a single-span pedestrian timber bridge situated in Växjö, Sweden, see Figure 1. The bridge is 26.1 m long in total with a span of 25 m. The loadbearing structure consists of five longitudinal glulam beams (165x1170 mm) with a top flange made of a stress-laminated timber (SLT) deck with a thickness of 315 mm and total width of 4005 mm, see Figure 2. The connection between the SLT deck at the top flange and the longitudinal beams is achieved with friction due to the pre-stressing force from 43 steel bars running through the deck. Five crossbeams (115x540 mm) are installed at 5 locations between the longitudinal beams with a c/c of 6 m along the bridge. The crossbeams are connected to the longitudinal beams with angle irons. Steel bars also are installed at the lower flange of the longitudinal beams at the same locations as the crossbeams to prevent lateral deflection of the longitudinal beams. All the structural timber parts of the bridge are made of glulam with strength class GL30c. The finished bridge have railings which extend 7.65 m from the bridge deck boundary edges as well as an asphalt layer with a constant thickness of 75 mm. The asphalt layer is a preliminary layer without the final camber with a 2 % slope seen in Figure 2. The asphalt is termed PGJA 11 in the Swedish norm which consists of mastic asphalt (MA) with a nominal maximal aggregate size of 11 mm and polymer modified bitumen (PMB).



Figure 1: An overview of the finished bridge.

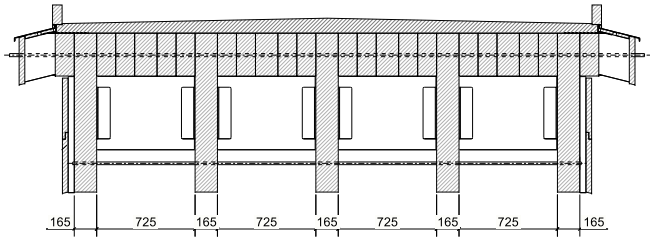


Figure 2: The bridge cross-section. Dimensions are in mm.

2.2 Equipment

Nineteen accelerometers of type PCB 393a03 with a sensitivity of 1 V/g were placed on the bridge deck and two accelerometers of type PCB 393b31 (10 V/g) were placed at the bridge supports. Two types of excitation sources were applied during the experiments: impulse and slow sine excitation. A Dytran impulse hammer model 5803A was used to provide a transient impulse force of around 10 kN. The subsequent free vibration of the bridge was thereafter recorded. A soft hammer tip was chosen in order to excite frequencies in the low frequency range. In order to reduce the influence of noise, approximately 10 hits were recorded at each excitation point in order to perform an average when producing frequency response functions and achieve good coherence. Slow sine testing with a force of 75 N and a linearly increasing speed of around 0.01-0.02 Hz/s was achieved with an electrodynamic shaker of type BD-5 from Wölfel Monitoring Systems. Two accelerometers were placed on the shaker: one PCB 393a03 at the platform and one PCB308B (0.1 V/g) on the moving mass. The amplification of the signals and conversion from analogue to digital signals was achieved with the data acquisition system QuantumX by HBK (former HBM) with one MX1601B and two MX840B modules. The accompanying software Catman®Easy version 5.3.1 was used to store the data. In order to determine the average temperature of the asphalt layer, an infrared thermometer

of type Testo 830-T2 was utilized. The surface temperature was measured at a few points on the bridge deck and at a couple of time instants during the measurements.

2.3 Instrumentation

The bridge was experimentally tested during four different construction stages, see Figure 3:

Stage 1) Timber structure including longitudinal beams, SLT deck and crossbeams.
Stage 2) Timber structure and railings.
Stage 3) Timber structure, railings and asphalt during warm conditions.
Stage 4) Timber structure, railings and asphalt during cold conditions.



Figure 3: The bridge during and after construction. Left: Stage 1 with only the timber structure. The vertical flat bars for the railings were present on the bridge. Right: Finished bridge (stage 3 and 4) with timber structure, railings and asphalt.

The instrumentation setup for the measurements, see Figure 4, were identical for the different construction stages with 14 vertical (a_{V1}-a_{V14}) and 5 lateral (a_{L1}-a_{L5}) accelerometers on the bridge deck as well as 2 axial (a_{A1}-a_{A2}) accelerometers at the bridge supports. Six excitation points were chosen on the bridge in order to obtain a sufficient number of vibration modes. Hammer excitation was applied at each excitation point. Slow sine tests were applied at positions E2 and E5 in order to excite the first bending and torsional mode.

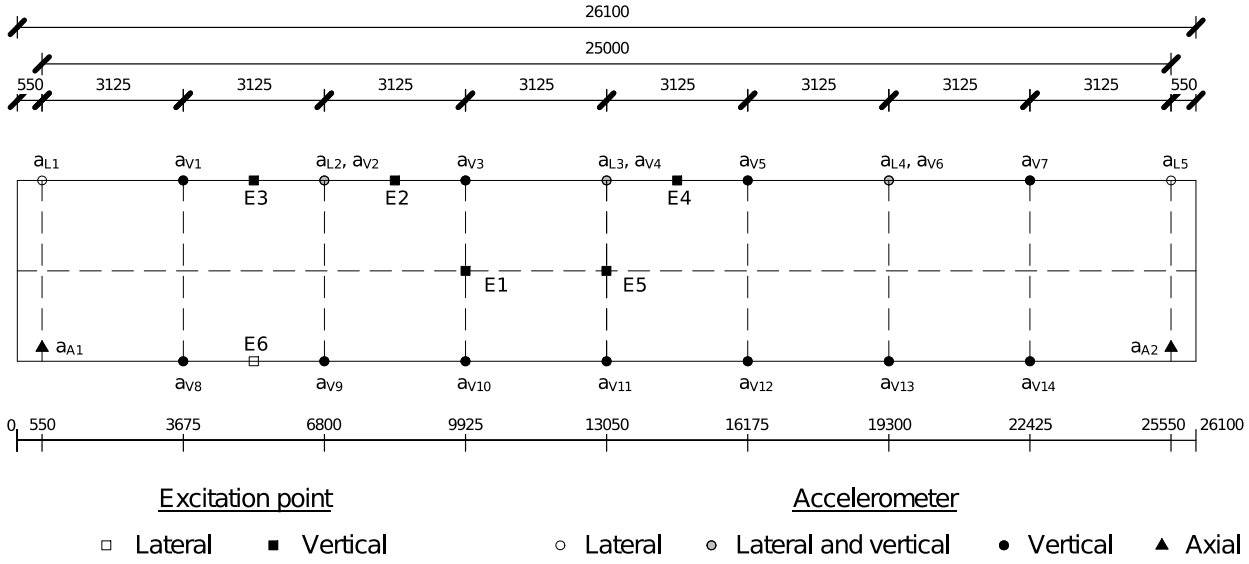


Figure 4: Instrumentation setup for the experiments. The white, grey and black circles indicate if a vertical, lateral or both lateral and vertical accelerometer exist on the position. The black triangles indicate the locations of the axial accelerometers at the bridge supports. The white and black boxes indicate if it is a lateral or vertical excitation point.



2.4 Post-processing

This section describes the post-processing which includes frequency response functions as well as the coherence function, mode indicator function and modal assurance criterion.

2.4.1 Frequency response function

The frequency response function (FRF) was calculated as the H_1-estimator in Equation 2-1, which assumes that the input signal is known and that only the output signal contains noise. It is determined by applying fast Fourier transform (FFT) on both input and output signals, resulting in $X(f)$ for the input and $Y(f)$ for the output signal. Both results are thereafter multiplied with the complex conjugate of the input signal's FFT, $X^*(f)$. Averaging these quantities for N measurements results in $\hat{S}_{yx}(f)$ and $\hat{S}_{xx}(f)$ in Equation 2-1, which are the averaged cross- and auto-spectral densities respectively. The H_1-estimator assumes that enough averages are made such that the uncorrelated noise in the output signals becomes small enough to neglect [8].

$$\widehat{H}_1(f) = \frac{\frac{1}{N}\sum_{i=1}^{N} Y_i(f)X_i^*(f)}{\frac{1}{N}\sum_{i=1}^{N} X_i(f)X_i^*(f)} = \frac{\hat{S}_{yx}(f)}{\hat{S}_{xx}(f)} \qquad 2\text{-}1$$

2.4.2 Coherence function

To validate the quality of the FRFs, the coherence function ($\hat{\gamma}_{yx}^2$) in Equation 2-2 can be applied.

$$\hat{\gamma}_{yx}^2(f) = \frac{\widehat{H}_1(f)}{\widehat{H}_2(f)} = \frac{\left|\hat{S}_{yx}(f)\right|^2}{\hat{S}_{xx}(f)\hat{S}_{yy}(f)}, \qquad 0 \le \hat{\gamma}_{yx}^2(f) \le 1 \qquad 2\text{-}2$$

The coherence function calculates the ratio between the H_1- and H_2-estimator. The H_2-estimator assumes, contrary to the H_1-estimator, that noise is only present in the input signal. The average $\widehat{H}_2$-estimator based on N measurements can be seen in Equation 2-3.

$$\widehat{H}_2(f) = \frac{\frac{1}{N}\sum_{i=1}^{N} Y_i(f)Y_i^*(f)}{\frac{1}{N}\sum_{i=1}^{N} X_i(f)Y_i^*(f)} = \frac{\hat{S}_{yy}(f)}{\hat{S}_{xy}(f)} \qquad 2\text{-}3$$

Since H_1 contains noise in the numerator and H_2 in the denominator, the true function H must exist somewhere in the range stated in Equation 2-4. A value of $\hat{\gamma}_{yx}^2 = 1$ indicates therefore that $\widehat{H}_1 = \widehat{H}_2$ and that there is no noise present in the signals [8].

$$\left|\widehat{H}_1(f)\right| \le |H(f)| \le \left|\widehat{H}_2(f)\right| \qquad 2\text{-}4$$

2.4.3 Mode indicator function

To determine the resonance frequencies correctly, the mode indicator function (MIF) in Equation 2-5 can be established. There exists several MIFs, and in this work the "normal MIF" or "MIF 1" is utilized. The MIF for n accelerometers is defined as a sum of the real part of the FRFs divided by the magnitude of the FRFs at each frequency. Since the FRF is mainly real-valued except at an undamped eigenfrequency where it is imaginary, the MIF will be approximately 1 for all frequencies except at an eigenfrequency where it dips towards zero [8].

$$\mathrm{MIF}(f) = \frac{\sum_{i=1}^{n}\left|\mathrm{Re}\left[\widehat{H}_{1,i}(f)\right]\right|^2}{\sum_{i=1}^{n}\left|\widehat{H}_{1,i}(f)\right|^2}, \qquad 0 \le \mathrm{MIF}(f) \le 1 \qquad 2\text{-}5$$



2.4.4 Modal assurance criterion

To validate the modes of vibration, the modal assurance criterion (MAC) in Equation 2-6 can be implemented. This method compares the similarity between two mode vectors and produces a value between 1 and 0. A value closer to 1 indicates a greater similarity and vice versa. When comparing more than one mode a MAC matrix is produced where the value $\mathrm{MAC}(m,n)$ is the comparison of mode vector ϕ_m and ϕ_n at row m and column n.

$$\mathrm{MAC}(m,n) = \frac{|\{\phi_m\}^T\{\phi_n\}|^2}{(\{\phi_m\}^T\{\phi_m\})(\{\phi_n\}^T\{\phi_n\})} \qquad 2\text{-}6$$

The auto-MAC is a comparison between the same set of modes, which is an indicator of how well separated they have been established from the measurements. The degree of separation depends greatly on the number of measurement positions during the experiments. The cross-MAC is a comparison between two different sets of mode, for example numerical and experimental modes [8]. In this work auto-MAC is established for the individual experiments and cross-MAC between modes for stage 1 and stages 2-4 to ensure that the same modes are compared and evaluated.

2.5 Modal parameter extraction

The FRFs were thereafter analysed with two different modal parameter extraction methods: the complex exponentials method and a single degree of freedom method. Resonance frequencies and damping ratios were retrieved with both methods, whereas the mode shapes were only retrieved with the complex exponentials method.

2.5.1 Complex exponentials method

The complex exponentials (CE) method expresses the FRF on pole-residue form, see the receptance based on displacement $X(s)$ with the Laplace variable s in Equation 2-7. A summation of P number of poles is expressed in the equation and out-of-bounds modes are not considered. The subscripts i and j denotes accelerometer i and excitation point j. The real part of the poles (s_n) represents the damping and the imaginary part represents the resonance frequency. The real part of the residues ($_nR_{ij}$) represent the phase angle and the imaginary part represents the amplitude for the mode of vibration. Poles and residues come in complex conjugate pairs to represent both the negative and positive imaginary axis. Derivations of the CE method can be found in literature [9].

$$H_{ij}(s) = \frac{X_i(s)}{F_j(s)} = \sum_{n=1}^{P}\left(\frac{{}_nR_{ij}}{s-s_n} + \frac{{}_nR_{ij}^*}{s-s_n^*}\right) \qquad 2\text{-}7$$

2.5.2 Single degree of freedom method

The single degree of freedom (SDOF) method assumes that each resonance peak can be approximated as an oscillating mass-spring-damper system with a single degree of freedom. The accelerance function based on acceleration $A(\omega)$ expressed with the stiffness k, angular frequency ω and natural frequency ω_n is presented in Equation 2-8 [8]. A curve-fitting procedure estimating the coefficients in the denominator polynomial in Equation 2-8 for each resonance peak individually gives an approximation of the modal parameters.

$$|H(\omega)| = \left|\frac{A(\omega)}{F(\omega)}\right| = \frac{\omega^2/k}{\sqrt{\left(1-\left(\frac{\omega}{\omega_n}\right)^2\right)^2 + \left(2\zeta\frac{\omega}{\omega_n}\right)^2}} \qquad 2\text{-}8$$

3 Results

This section presents the experimental results, i.e. the modes of vibration, resonance frequencies and damping ratios. Numerical results from an FE model are also presented.

3.1 Experimental results

The average air temperature during the construction stages were: 1) 12.6 ºC, 2) 5.5 ºC, 3) 21.4 ºC and 4) -0.8 ºC. The average relative humidity was: 1) 57 %, 2) 48 %, 3) 58 % and 4) 70 %. The average temperature of the asphalt layer was 41.9 ºC during stage 3 and 0.6 ºC during stage 4. The mechanical properties of timber are not significantly affected by temperature in the normal range of -30 ºC to 90 ºC [1]. The asphalt stiffness is however largely affected by temperature. The varying stiffness of asphalt can be found in several other previous studies with a value of the modulus of elasticity (MOE) of around 0.5-1.5 GPa at 40 ºC and 15-20 GPa at 0 ºC [10]–[12].

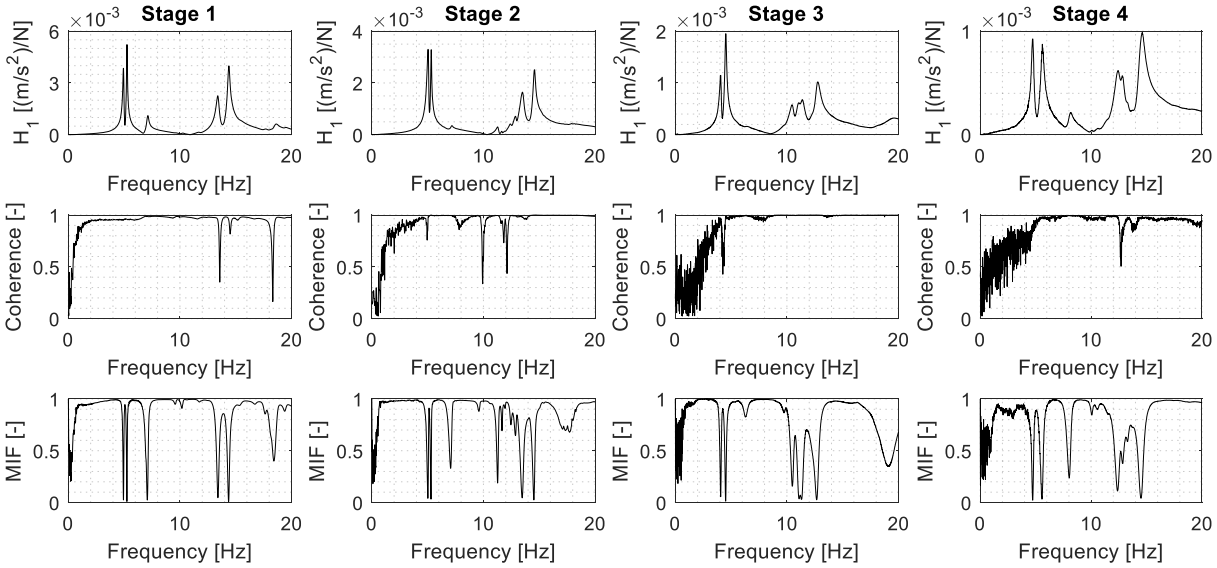


Figure 5: Hammer excitation at excitation point E2. H_1-estimator, coherence and MIF between 0-20 Hz for accelerometer a_{V3} at construction stages 1-4.

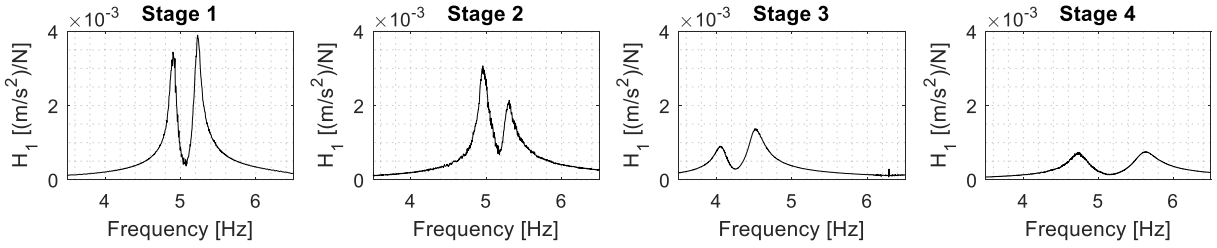


Figure 6: Slow sine excitation at excitation point E2. H_1-estimator between 3.5-6.5 Hz for accelerometer a_{V3} at construction stages 1-4. The resonance peaks for the first bending and torsional mode are well-defined.

The H_1-estimator, coherence and MIF for construction stages 1-4 are presented in Figure 5. The excitation point is E2 with impulse hammer and accelerometer a_{V3} is evaluated for the FRF and coherence. The MIF is however evaluated for all accelerometers in order to determine the resonance frequencies correctly. The coherence indicate well-established FRFs with a value close to 1 at the resonance peaks. The FRFs at stages 1-4 for accelerometer a_{V3} from slow sine excitation at excitation point E2 between 3.5 to 6.5 Hz are presented in Figure 6. The first bending and torsional mode are excited.



3.1.1 Modes of vibration

The first six modes of vibration for the bridge can be seen in Figure 7. The modes are abbreviated according to their shape with bending (B), torsion (T) and lateral (L). They are also ordered numerically (1, 2 …) within their category.

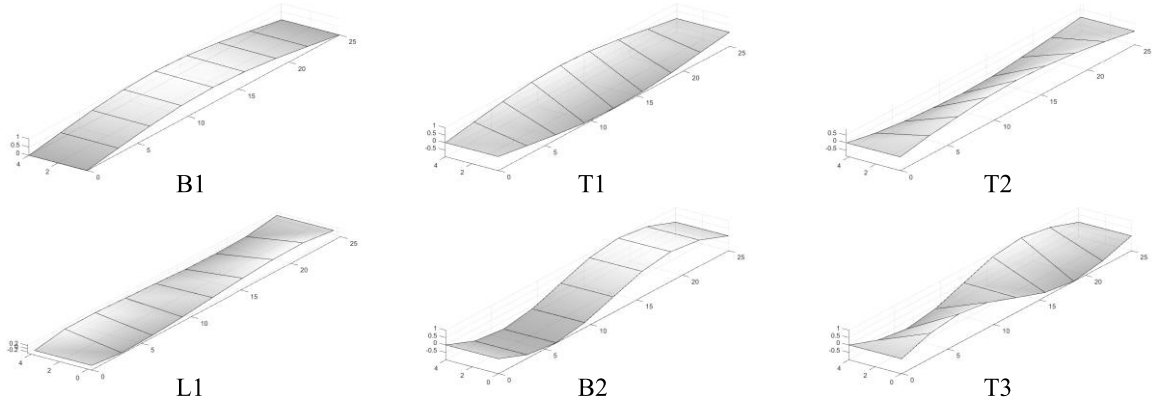


Figure 7: The first six vibration modes for the bridge.

The auto-MAC was established for the individual experiments in order to distinguish how well separated the modes are, see Figure 8. All diagonal values are 1 since the mode is compared with itself. T1 and T2 as well as L1 and T3 are quite similar but the lateral components for T2 and L1 are much larger than for T1 and T3. An increased number of measurement points would be needed to separate them more. It is however assumed that they are sufficiently separated to be able to compare them with numerical modes for example. The cross-MAC, i.e. comparison between two different set of modes, is established to verify that the same modes are chosen for all experiments, see Figure 9. The modes for stage 1 are therefore compared with the modes for construction stages 2-4. It can be seen that the current cross-MAC values are between 0.74-1 on the diagonals which provides a good validation.

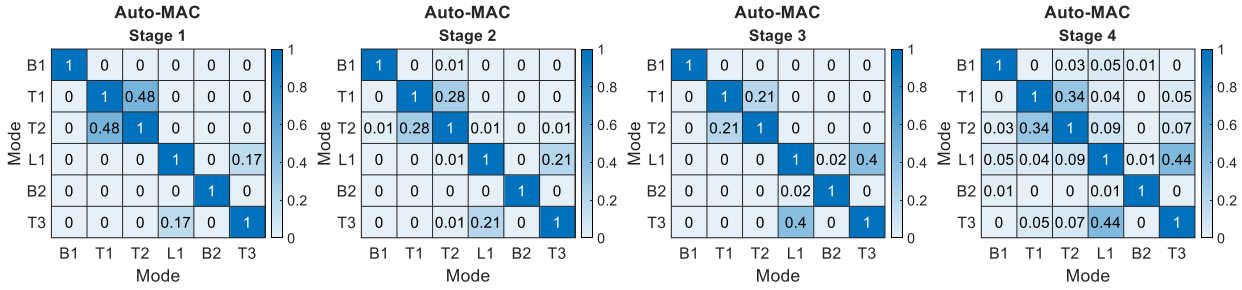


Figure 8: Auto-MAC for construction stages 1-4.

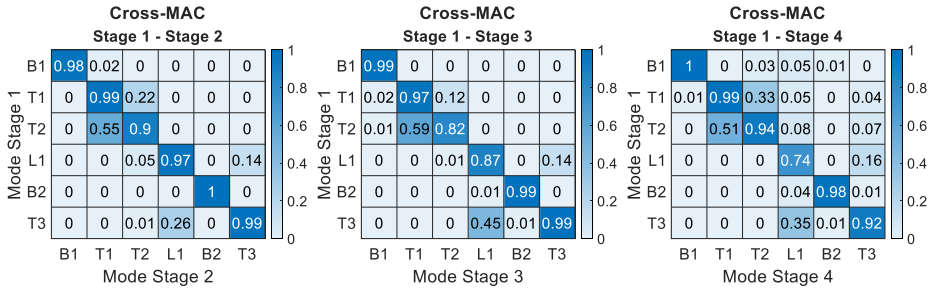


Figure 9: Cross-MAC between construction stage 1 and stages 2-4.



Table 1: Resonance frequencies for the construction stages.

	Resonance frequencies [Hz]					
Stage	**B1**	**T1**	**T2**	**L1**	**B2**	**T3**
Stage 1	4.93	5.24	7.11	9.65	13.41	14.37
Stage 2	5.03	5.31	7.16	9.65	13.52	14.56
Stage 3	4.07	4.52	6.33	9.81	10.52	12.72
Stage 4	4.74	5.58	8.05	11.45	12.37	14.54

3.1.2 Resonance frequencies and damping

The resonance frequencies for each construction stage can be seen in Table1. The resonance frequencies are increased with 0-2 % at stage 2 when railings are present on the bridge. This is most likely due to an overall higher stiffness compared to its mass as well as the continuity of the railings beyond the bridge deck boundaries. If only the mass of the railings is considered, which is around 5 % of the bridge's total mass (10 % if the vertical flat bars for the railings from stage 1 is included, see Figure 3), B1 would be decreased to around 4.81 Hz. The increase to 5.03 Hz with railings must therefore mean that the stiffness is increased with around 10 % for B1. L1 is not changed however which means that the added mass and stiffness cancel each other out laterally. Adding an asphalt layer on the bridge at stage 3 can be seen to lower all vertical resonance frequencies with 12-22 %, which is expected since the temperature of the asphalt layer was around 41.9 ºC. The asphalt is expected to mainly increase the mass of the bridge and not the stiffness since asphalt has a low MOE at high temperatures. However, L1 is increased with 2 % at stage 3 compared to stage 2. This is probably due to the asphalt layer's second moment of area which is approximately $3 \cdot 10^3$ larger in the lateral direction compared to the vertical direction. The resonance frequencies increased with 14-27 % at stage 4 compared to stage 3. This is probably due to the asphalt's higher stiffness at a low temperature of around 0.6 ºC. B1 and B2 at stage 4 are not larger than B1 and B2 at stage 2. However, T3 is similar and both T1 and T2 are larger at stage 4 as compared to stage 2. This indicates that the asphalt increases the torsional stiffness of the bridge substantially. A larger decrease in the resonance frequencies for bending modes compared to torsional modes can also be seen between stage 2 and 3.

The damping ratios for the different construction stages depending on type of excitation and modal parameter extraction method are presented in Table 2. They are evaluated for all excitation points when applicable and the average (μ) damping ratios and standard deviations (σ) are presented. Average values based on both modal parameter extraction methods and excitation types are also presented. The damping ratios for the finished bridge with asphalt are around 2-3 %, which fall in the normal range of pedestrian bridges of around 1-3 % [2], [3], [5], [13]. The damping ratio for timber bridges is set to 1-1.5 % in EN-1995-2, which may be regarded as conservative [14]. Both railings and asphalt increase the damping ratio. The damping with an asphalt layer is increased during cold compared to warm conditions which could be due to increased friction at the interface between timber deck and asphalt. An effective way of adding damping to the bridge is therefore to add asphalt, which is confirmed by previous studies [6], [7]. The values of the standard deviations can be seen to be quite small which reinforces the reliability of the damping ratios, except when the damping is only evaluated for one excitation point. The two different modal parameter extraction methods can be seen to produce similar values which ensures their reliability. The two types of excitation, i.e. impulse and slow sine excitation, also produce similar values.

*Table 2: Damping ratios in percent for the construction stages. The values are presented as "μ (σ)", where μ is the mean value and σ is the standard deviation. All excitation points are included in the results when applicable. * σ is only based on one value due to limited ability for parameter extraction in this particular case. The rows with "Average" presents the average values based on both modal parameter extraction methods and excitation types.*

			Damping ratios [%]					
Stage	**Excitation**	**Method**	**B1**	**T1**	**T2**	**L1**	**B2**	**T3**
Stage 1	**Hammer**	**CE**	1.09 (0.12)	0.88 (0.02)	1.47 (0.01)	1.14 (0.00*)	1.20 (0.13)	0.84 (0.04)
		SDOF	1.04 (0.10)	0.84 (0.02)	1.47 (0.02)	1.17 (0.00*)	1.13 (0.09)	0.85 (0.01)
	Sweep	**CE**	0.94 (0.18)	0.87 (0.09)				
		SDOF	1.01 (0.14)	0.97 (0.10)				
		Average	1.04	0.88	1.47	1.16	1.17	0.84
Stage 2	**Hammer**	**CE**	1.54 (0.13)	1.07 (0.14)	2.05 (0.09)	1.24 (0.00*)	1.63 (0.15)	0.84 (0.05)
		SDOF	1.42 (0.16)	1.03 (0.01)	1.87 (0.07)	1.30 (0.00*)	1.51 (0.09)	0.91 (0.01)
	Sweep	**CE**	1.07 (0.08)	1.09 (0.01)				
		SDOF	1.15 (0.02)	1.27 (0.14)				
		Average	1.37	1.10	1.96	1.27	1.57	0.88
Stage 3	**Hammer**	**CE**	1.81 (0.06)	1.86 (0.08)	5.07 (0.00*)	2.01 (0.00*)	1.63 (0.02)	1.89 (0.06)
		SDOF	1.93 (0.18)	1.90 (0.01)	4.62 (0.00*)	1.93 (0.00*)	1.73 (0.11)	1.91 (0.01)
	Sweep	**CE**	2.06 (0.03)	2.14 (0.02)				
		SDOF	2.06 (0.00)	2.33 (0.00*)				
		Average	1.96	2.03	4.85	1.97	1.72	1.90
Stage 4	**Hammer**	**CE**	2.72 (0.15)	2.78 (0.21)	2.85 (0.29)	2.74 (0.00*)	2.53 (0.10)	2.16 (0.24)
		SDOF	2.60 (0.15)	3.17 (0.20)	2.57 (0.11)	2.29 (0.00*)	2.65 (0.24)	2.07 (0.01)
	Sweep	**CE**	2.48 (0.03)	2.95 (0.00*)				
		SDOF	2.80 (0.07)	3.05 (0.03)				
		Average	2.65	2.97	2.66	2.52	2.59	2.12

3.1.3 Boundary conditions

A figure of the bridge supports is presented in Figure 10. The bolt hole is circular at accelerometer a_{A2} whereas it is oval at accelerometer a_{A1} to allow for expansion of the timber due to temperature and moisture.

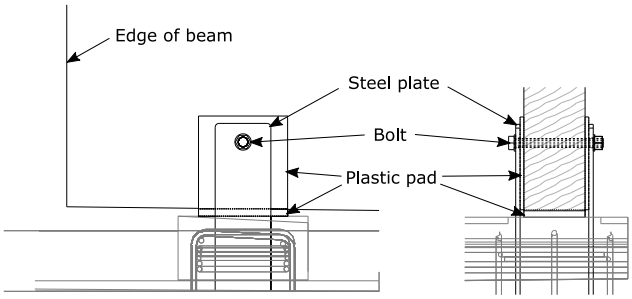


Figure 10: Bridge support. Left: View from the side. Right: Cross-sectional view.

Accelerometers a_{A1} and a_{A2} show that the bridge bolts have free axial translation for bending modes, whereas a_{A1} have free and a_{A2} have restricted translations for torsional modes due to the differences of the bolt holes, see Figure 11.

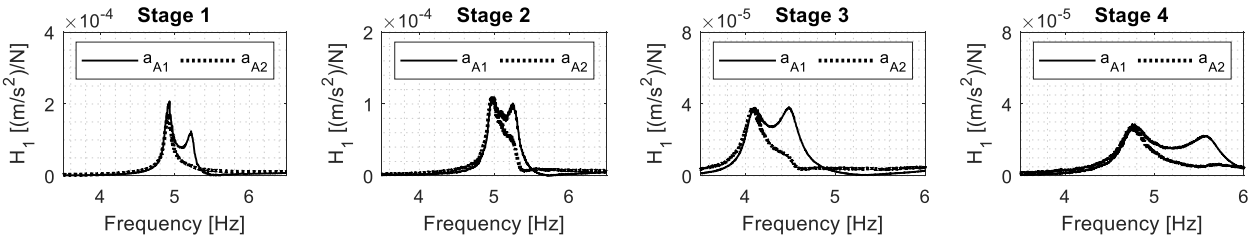


Figure 11: Slow sine excitation at excitation point E2. H_1-estimator between 3.5-6.5 Hz for accelerometers a_{A1} and a_{A2} at the bridge supports. The resonance peaks for the first bending and torsional mode can be seen for a_{A1} but only the first bending mode for a_{A2}.

3.2 Numerical results

An FE model is made in MATLAB with 2D Euler-Bernoulli beam elements with isotropic material elasticity. The length of the beam is increased from 26.1 to 26.2 m to simplify the modelling, has supports at 0.6 m from the beam edges and a beam element length of 0.2 m, see Figure 12. The vertical translations are restricted and the axial translations are free at the bridge boundary conditions in accordance to Section 3.1.3. Since the bridge supports are at the bottom edge of the longitudinal beams, the degrees of freedom are translated a distance e from the centre of gravity to this position in the model. The timber MOE is set to 12500 MPa and the density is set to 475 kg/m^3. The values are retrieved from two studies: one by the Scandinavian company Moelven and another by Jockwer [15]. Both studies performed tests on samples of class GL30c or equivalent with a moisture content of 12 %. Both values are close to the ones found in EN-14080, but the applied values could be more reasonable based on experience gained by the authors' previous research. The asphalt density is set to 2450 kg/m^3 since normal values are between 2400-2500 kg/m^3 [1]. It is also noted that the results only differ around 1 % within this range. The value of 2450 kg/m^3 is similar compared to previous experimental studies [16]–[18]. The asphalt MOE is estimated to 1 GPa during warm and 17 GPa during cold conditions from previous studies such as [10]–[12]. The asphalt and timber deck is assumed to act as a beam with full composite action where the asphalt cross-section is transformed to an equivalent timber cross-section. The railings are neglected in the model.

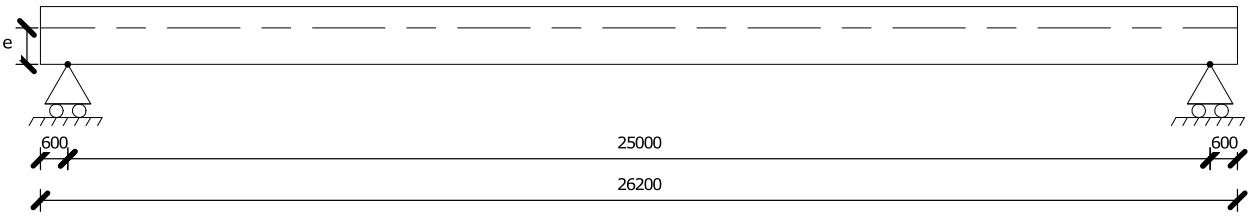


Figure 12: 2D beam model of the bridge with supports at the bottom of the beam at a distance e from the centre of gravity (dashed line). Dimensions are in mm.

The results for the first two bending modes for stage 1, 3 and 4 are presented in Table 3. Stage 2 is not included since there is only a slight difference in the experimental results between stage 1 and 2. The numerical results for B1 are lower than the experimental results and no reasonable change in the material parameter values can be applied to come closer to the experimental values. This indicates that there is a lack of stiffness for B1 in the FE model which could be explained by shear deformation of the plastic pads underneath the longitudinal beams which is neglected in the model. In fact, introducing a spring at both supports in the FE model increases B1 but not B2.

Table 3: Experimental and numerical results for the first two bending modes for stages 1, 3 and 4. All values are in hertz (Hz).

	Stage 1		**Stage 3**		**Stage 4**	
	Exp.	**Num.**	**Exp.**	**Num.**	**Exp.**	**Num.**
B1	***4.93***	4.19	***4.07***	3.17	***4.74***	3.53
B2	***13.41***	16.77	***10.52***	12.66	***12.37***	14.12



4 Conclusions

This article evaluates the dynamic properties of a timber pedestrian bridge. Dynamic tests were performed at four different construction stages: 1) on only the timber structure 2) on the timber structure with the railings 3) on the timber structure with railings and an asphalt layer during warm conditions and 4) same as stage 3 but during cold conditions. The modes of vibration, resonance frequencies and damping ratios were retrieved by modal parameter extraction for all stages. A 2D FE model was thereafter implemented and numerical results were retrieved for stage 1, 3 and 4. The following conclusions can be derived:

- The stiffness of the railings contribute more than the railing mass to the resonance frequencies at stage 2 compared to stage 1. The first bending mode is increased from 4.93 to 5.03 Hz and would theoretically be decreased to around 4.81 Hz if only the railing mass would be considered. This means that the railings increases the stiffness of the first bending mode with around 10 %.
- The effect of the asphalt during warm conditions is mainly to add mass to the vertical bending and torsional resonance frequencies which are lower in stage 3 compared to stage 2. This is the opposite for the first lateral mode where the resonance frequency is higher in stage 3 compared to stage 2. This is probably due to a large increase in the second moment of area in the lateral direction due to the presence of the asphalt layer.
- The resonance frequencies at stage 4 (cold conditions) are higher compared to stage 3 (warm conditions). This is probably due to the increase of the asphalt stiffness at cold conditions. It can also be observed that the resonance frequencies are lower for the bending modes but higher for the torsional modes at stage 4 compared to stage 2.
- Damping is increased for each construction stage and the final values are in the normal range of approximately 2-3 %. The asphalt increases the damping and is a good way to increase the damping of pedestrian bridges. The damping is also increased during cold (stage 4) compared to warm conditions (stage 3).
- Both the auto-MAC and cross-MAC values are consistent for the modes of vibration for all construction stages.
- The CE and SDOF method produce similar results and the results are therefore reliable. It should therefore be possible to achieve results for resonance frequencies and damping ratios with only one of these methods.
- The FE model shows large differences from the experimental results. It appears that some stiffness is lacking for the first bending mode. This stiffness could be due to shear deformation of the plastic pads at the bridge supports. Further modelling with a 3D orthotropic numerical model is suggested.

Acknowledgement

This project is funded by the Swedish Transport Administration and the J Gustaf Richerts foundation. The authors gratefully recognize these contributions. The authors also want to thank the companies Moelven and Skanska for all help with the dynamic measurements on-site and for providing constructional drawings of the bridge. The authors also want to thank the municipality in Växjö, Sweden, for providing information and help.

References

[1] Swedish Wood, *Design of timber structures. Volume 1 - Structural aspects of timber construction*. Swedish Wood, 2019.

[2] J. H. Neilson *et al.*, “Experimental and Numerical Dynamic Properties of Two Timber Footbridges Including Seasonal Effects,” *Int. J. Civ. Eng.*, vol. 19, no. 10, pp. 1239–1250, 2021.

[3] R. Castro-Triguero, E. Garcia-Macias, E. S. Flores, M. I. Friswell, and R. Gallego, “Multi-scale model updating of a timber footbridge using experimental vibration data,” *Eng. Comput. (Swansea, Wales)*, vol. 34, no. 3, pp. 754–780, 2017.

[4] A. Gheitasi, O. E. Ozbulut, S. Usmani, M. Alipour, and D. K. Harris, “Experimental and analytical vibration serviceability assessment of an in-service footbridge,” *Case Stud. Nondestruct. Test. Eval.*, vol. 6, pp. 79–88, 2016.



[5] C. Heinemeyer and M. Feldmann, "European design guide for footbridge vibration," *Footbridge Vib. Des.*, pp. 13–30, 2009.
[6] S. Schubert, D. Gsell, R. Steiger, and G. Feltrin, "Influence of asphalt pavement on damping ratio and resonance frequencies of timber bridges," *Eng. Struct.*, vol. 32, no. 10, pp. 3122–3129, Oct. 2010.
[7] Glauco Feltrin, Sandy Schubert, and René Steiger, "Temperature effects on the natural frequencies and modal damping of timber footbridges with asphalt pavement," 2011.
[8] A. Brandt, *Noise and vibration analysis signal analysis and experimental procedures*. Chichester, West Sussex, U.K. ; Hoboken, N.J.: Wiley, 2011.
[9] N. Maia, "Extraction of valid modal properties from measured data in structural vibrations," 1989.
[10] Y. Zhao, J. Tang, and H. Liu, "Construction of triaxial dynamic modulus master curve for asphalt mixtures," *Constr. Build. Mater.*, vol. 37, pp. 21–26, 2012.
[11] P. Pokorski, P. Radziszewski, and M. Sarnowski, "Rheological properties of asphalt mixtures for bridge pavements," *Procedia Eng.*, vol. 111, no. TFoCE, pp. 637–644, 2015.
[12] M. Halle, T. Rukavina, and J. Domitrovic, "Influence of temperature on asphalt stiffness modulus," *5th Eurasphalt Eurobitume Congr. 13-15th June 2012, Istanbul*, no. June 2012, pp. 13–15, 2012.
[13] K. Van Nimmen, "Numerical and Experimental Study of Human-Induced Vibrations of Footbridges." 2015.
[14] Swedish Standards Institute, "Swedish standard SS-EN 1995-2:2004. Eurocode 5: Design of timber structures – Part 2: Bridges," Stockholm, 2009.
[15] R. Jockwer, "Structural behaviour of glued laminated timber beams with unreinforced and reinforced notches," 2014.
[16] A. Baltrušaitis, A. Vaitkus, and J. Smirnovs, "Asphalt layer density and air voids content: GPR and laboratory testing data reliance," *Balt. J. Road Bridg. Eng.*, vol. 15, no. 3, pp. 93–110, 2020.
[17] C. E. Sengul, S. Oruc, E. Iskender, and A. Aksoy, "Evaluation of SBS modified stone mastic asphalt pavement performance," *Constr. Build. Mater.*, vol. 41, pp. 777–783, 2013.
[18] A. Chegenizadeh, B. Peters, and H. Nikraz, "Mechanical properties of stone mastic asphalt containing high-density polyethene: An Australian case," Case Stud. Constr. Mater., vol. 15, no. May, p. e00631, 2021.

Conference Proceedings 4th ICTB (2022)
https://doi.org/10.24451/WHFN-BP29

ICTB 2021 PLUS
4th International Conference on Timber Bridges
Biel/Bienne, Switzerland, 9 -12 May 2022



New concepts for timber bridge decks without cross beams: Stress laminated decks and interlocked laminated decks

Tormod Dyken[1], Hauke Burkart[2]

1 Introduction

Timber bridge decks have been built for long period of time with transversal planks. In the US, nailed laminated decks were built from the 1920's to mid 1960's. Flat laying glulam beams sometimes connected with dowels were used before the stress-laminated timber decks were introduced in the Ontario Highway Bridge Design Code in 1976 [5].

The introduction of the stress lamination technique in the 1970's represented a significant renewal of timber bridge building. Since then, significant improvements have been made with respect to materials and structural protection. However, little progress has been made in the area of structural design. In this paper two attempts to introduce new ideas in the structural design of timber bridges are presented: one with the purpose to eliminate the losses of stress by using unstressed bars and one with the purpose of reducing the amount of steel and increase clearance below the bridge by omitting cross beams.

2 Evolvement of stress laminated timber decks in Norway

Stress laminated timber bridge decks evolved in the 70th in Canada and the US. In Norway these have been built since the 90s. Before about 2005 most bridges were built using planks of 233 mm depth, typically stressed with 18 mm high-strength steel bars. Since 2005 new load models introduced by the Eurocodes made it difficult for road bridges to handle the loads using planks and thus glulam beams were introduced instead. Greater spans were, hence, possible and glulam beams are now dominating pedestrian bridges as well.

Because of issues with corrosion, grease incapsulated steel strands have been introduced instead of bars and have been used on several bridges lately. The stressing system should ideally be with a low E-modulus and high strength to ensure little stress loss by later shrinkage and creep effects. Steel strands have some advantages here, but other materials such as fibre composite rods have been tried and reportedly also so in Canada. Up to this date these are however still in development.

The deck structure is most often a secondary superstructure connected through cross beams to a primary superstructure. In the design of Evenstad Bridge, back in the start of the 90's, various systems for lateral support of arch girder were investigated. Case studies were made of both a sideways stiffening system at the supports and by a stiff connection to the cross beams. Evenstad Bridge was at the time the first large road bridge constructed in Norway for several decades, comprising of 5 equal spans of bow trusses with a total length of 180 m. The use of cross beams of steel was found to be the most efficient solution, though the wish to use more timber was strong. Cross beams of steel could be made reasonable small in depth and also function as transversal stiffening of the truss. Using timber for cross beams would make it difficult to protect the top-down connection needed, and also to achieve sufficient flexural stiffness for the connection to the superstructure. Using steel beams has since been state of the art for all corresponding projects.

The concept with simply supported timber decks on cross beams has some disadvantages when it comes to clearance below the bridge. The cross beams of road bridges are typically 500-1000 mm deep. With increased focus on gradients of the bridge approaches, solutions placing the cross beams in-between carriageways (typically on highways) or between railway tracks has been done on several projects, though with the downside of none-optimal spacing and even using beams with various angles to the deck. Using such simple static solutions may result in more complex design [4].

Another focus on timber deck structures in Norway has been on the need for re-stressing bars, which at times may be difficult due restrictions to access. Designing bridges that have such planned maintenance has been disputed as alternatives with other materials do not require this. Furthermore, the long-term stress levels of stress laminated decks and their rest-capacity has never really been explored being a momentum of unknown. It must also be said that even with these unknowns stress laminated decks have proven to work well on public roads where axel loads of 10 tons are common.

[1] Tormod Dyken, Consulting Engineer, Dyken AS, Norway, tormod.dyken@gmail.com
[2] Hauke Burkart, Standards Norway, hauke@burkart.no



3 Laminated decks without cross beams

3.1 General

Traditional timber bridges were provided with cross beams of timber, but modern traffic loading with heavy wheel loading required cross beams of significant depth with respect to the shear force capacity. Cross beams made of steel, however, showed to be far more efficient, and today steel material is the primary option for cross beams on timber bridges on roads with vehicle traffic.



Figure 1: Hot dip galvanized cross beams with fixing lugs for suspension post attachment

A frequent plea raised against today's timber bridges is that they contain as much steel as timber, and that the designation "timber bridge" is hardly justified. In addition, today's focus on environmental foot print has given reason to try to reduce the amount of steel as timber normally is the more environment friendly material. In this context the omission of cross beams is an obvious issue to investigate.

A stress laminated bridge deck without cross beams requires significantly more timber than with cross beams. The costs of the required additional timber will, normally, amount to a higher cost than the steel beam. It is, thus, not surprising that a concept without cross beams in most cases will be more expensive than a traditional solution. However, in an environmental and global warming context the increased use of wood instead of steel may be favourable. Another advantage by omitting the cross beams is that it will – in most cases – reduce the effective construction depth, i.e. the distance from the top surface of the deck to the lowest point of the deck. This may be of importance by bridges crossing rivers exposed to flooding. True, increased depth of the timber deck will be unfavourable, but in most cases the required depth of cross beams will increase more than the depth of the timber deck.



Figure 2: Stress laminated deck of sawn timber on steel cross beams (Måsørbrua)

As stress laminated plates are extremely orthotropic with one strong and stiff direction and one very weak direction it may seem strange to consider the transverse and weak direction for load carrying purpose. However, a local concentrated load will, to a certain extent, be carried in both directions. The distribution of load in the two main directions will depend on the main static system of the bridge. In case of, e.g., an arch bridge the load on the bridge deck may be transferred to an edge beam, while in another case, where the bridge deck constitutes the whole static system, the entire load has to be transferred in the longitudinal direction.

Arch bridges, suspension bridges and stay cable bridges may be provided with edge girders. The bridge deck will then span between the edge girders. The governing sectional forces will be the bending moment in transverse direction and shear along the edge girder. By concentrated loads like wheel loads the larger stiffness in longitudinal direction will provide a significant load distribution in that direction and a substantial reduction of the peak moment and a corresponding reduction of the shear force at the edge girder.

In case of evenly distributed load along the bridge deck this favourable effect will not be present, but there are other possibilities. The tie bars may be placed below the centre of the deck slab in order to impose a negative moment to counter the governing moment in case of stress lamination and in order to obtain an increased lever arm of internal forces in case of interlocked lamination. In addition the depth of the bridge deck may be varied such that the maximum depth will be in the middle of the deck and the required cross slope will be obtained without increasing the the non-structural dead weight of the slab.

3.2 Design principles of stress laminated bridge decks without cross beams

Bending in transverse direction, i.e. in the weak direction, will require an increased depth of the deck as well as more prestressing. One requirement for prestressing is that there shall be no tension between the laminations on the one hand and on the other hand the maximum compression transverse to fibres has to be limited. In addition, the prestressing shall be sufficient to ensure transfer of shear across the intersection between laminations.

It should be noticed that the increased depth of the deck will increase the the bending capacity in longitudinal direction as well as in transverse direction. This means that the timber is utilized for load carrying purposes in both directions, and that the increased depth of the deck allows larger spans in longitudinal direction.

The lack of cross beams may represent a problem for the erection of the bridge deck. However, it may be overcome by e.g. the use of temporary supports, scaffolding, skidding or by use of cranes.

3.3 Hemsila Footbridge in Hemsedal, Norway

A prototype bridge is designed as a footbridge crossing the river Hemsila in Hemsedal in order to demonstrate the applicability of the concept of omitting cross beams. As the valley floor is quite flat at the bridge site and the bridge had to be designed for a 200 years inundation where most of the adjacent area is flooded. Consequently, it was important to raise the road surface as little as possible while still keep the required clearance above the water level. The concept showed to be ideal in such cases.

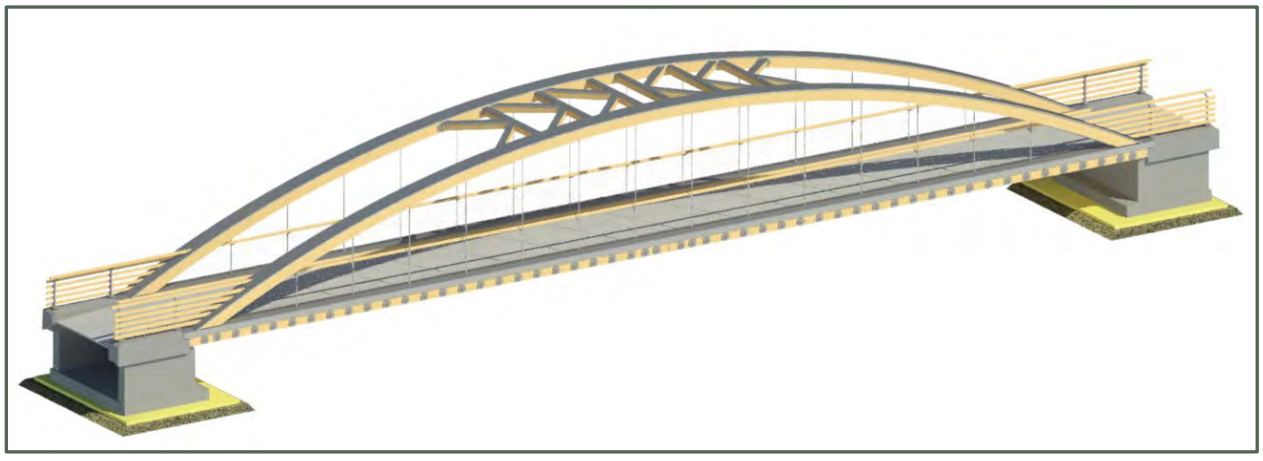


Figure 3: Hemsila Bridge, Hemsedal, Norway

The span of the arch bridge is 33,7 m and the span of the bridge deck between suspension ties is 3,67 m. The width of the footway is 3,0 m allowing for a service vehicle. The structural design is according to Eurocode.

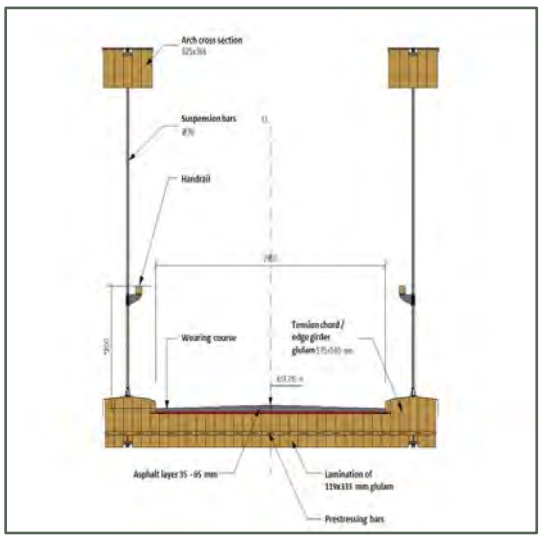


Figure 4: Cross section of Hemsila Bridge

As can be seen from the figure the possibility of increasing the depth of the lamination towards the centre of the deck in order to form the surface slope was not utilized in this case.

Structural design was performed by Sweco, Norway more than two years ago, based on a bridge concept of Dyken AS, and production of the superstructure were commenced at Moelven. However, the awarding authority got some financial problems and it was decided to complete the production of the superstructure and put the bridge project on ice. The complete superstructure is now stored at Moelven, and hopefully, the bridge may be completed this year.

Due to poor soil conditions a bowstring arch system was considered the best solution. In this particular bridge concept the edge girder was chosen to be an integrated part of the bowstring arch, acting as the tension chord. This means that the horizontal truss from the arches is taken as tension in the glulam truss and the abutments are exposed to vertical forces only.

In the case of Hemsila Footbridge the superstructure is presupposed to be assembled on a temporary rig on shore alongside the river and then turned 90 degrees and lifted in place by a mobile crane.

3.4 Road bridges without cross beams

The Hemsila Footbridge concept showed to be promising, and the idea of investigating the possibility of designing a similar road bridge without cross beams suggested itself. Test calculations on a two lane road bridge were carried out based on the Eurocode. A challenge in this context showed to be the optimization of prestressing versus the depth of the timber deck.

The design starts in transverse direction with determination of the necessary depth of the deck plate and the corresponding amount of prestressing which fulfils the requirements with respect to cracking between laminations and maximum compression transverse to fibres. When the geometry of the cross section is determined, the maximum span of the deck has to be calculated in order to utilize the timber material in both directions. It is a good design principle to utilize the material twice – if possible. However, for design criteria, such as comparison strength for two dimensional stress, and for bending stress transverse to fibre Eurocode offers no rules. The test design had to be based on simplified and conservative assumptions.

Figure 3 shows a schematic diagram of a cross section. The cross section is independent of the overall structural system. The edge girders are stressed together with the lamellas to form one unit. The edge girders are, thus, an integral part of the deck structure. The span in longitudinal direction is approximately the distance between supports by e.g. pillars or suspension rods.

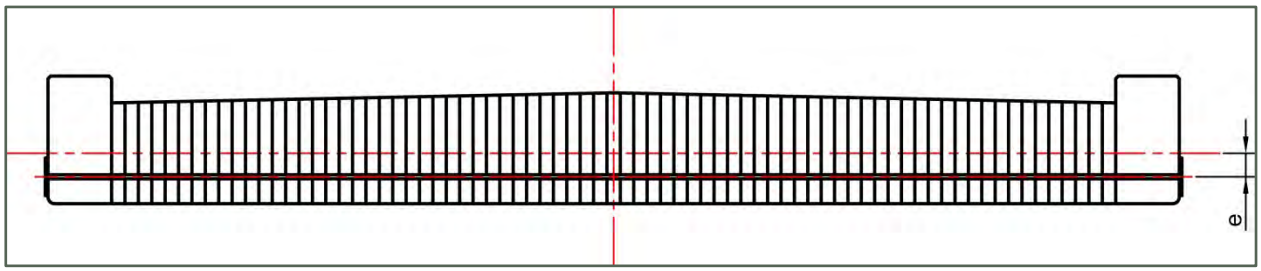


Figure 5: Cross section of a bridge deck without cross beams

3.5 Considerations regarding loss of prestress

Loss of prestress will always be an effect which has to be considered for designs that rely on prestressing. In some cases the loss of prestress may lead to a total collapse in other cases the loss may cause local damage only or violation of serviceability requirements. It is also important distinguish between if the failure of one prestressing tendon may cause failure of the entire structure or if there are some redundancy in the system. In most cases the problem is only that the prestressing force slowly diminishes over a long period of time. In that case minor visible effects may be observed and the problem solved by restressing.

For stress laminated decks there is no serious problem if some single tendons fail as the overall integrity of the deck is not depending on a few tendons, and the broken tendons may be replaced. By a general loss of prestress due to e.g. creep and shrinkage and missing re-stressing of the tendons increased deflection or slipping between the laminations may be observed and the damage be mended relatively easy.

One may query what the effect of prestressing loss will be for a stress laminated deck without cross bars. The general effect will be about the same as for ordinary stress laminated decks. Bending in transverse direction will cause cracks to open up between the laminations at the underside of the deck and at the edge girders slip due to shear force may occur. The cracking at the underside of the deck will of course cause increased compression transverse to fibres at the top surface of the deck and possible permanent damage by local crushing.

By loss of prestress some problems may arise at butt jointed lamination. When the lamination is consisting of large glulam beams a significant amount of prestress is required in order to maintain the full bending capacity at the cross section with the butt joint. If it is considered a problem the application of slotted in gusset plates and dowels may increase the bending stiffness and capacity.

4 Interlocked Laminated Decks

Transferring shear stresses between lamellas through an interlocking shape of elements could reduce the need for pre-stressing. In order to investigate the concept, tests were conducted by a student group making hexagonal shaped elements from square timber elements /1/, having the pith close to the centre of each element. The depth of each element after sawing was 76 mm. The elements were afterwards glued together in the vertical direction. For the tests the depth was limited to two elements, or 2 half's and one in centre, total depth of 152 mm.

Tests have shown that if using hexagonal shapes as shown in figure 4 the failure mechanism was very much ductile and no brittle shear failure was observed on any tests. In the tests the lamellas were totally restrained sideways, which might impact especially the friction between lamellas. Still, the failure mode was clearly compression perpendicular to grain from the loading block. Only after considerate deformations flexural stresses perpendicular to grain resulted in tension stresses. This came to some surprise since interlocking in shapes often has been said to be doomed due to the low rolling shear capacity of timber. This is probably dependent on the angle of the interlocking, but for the hexagonal shape clearly not an issue.



Figure 6: Shear test failure of oblique interlocked lamellae [2]

Tests were also done with a small deck to find system parameters such as the relation between transversal and longitudinal stiffness E_{90}/E_0. A deck of 0,815 m width, 3 m length and 0,152 m depth was tested with



a point load in the middle. The elements were hand-tightened together by steel rods. The deflection was measured at several points and afterwards the corresponding E-modulus was calculated by numerical software.

The tests proved transversal bearing, however with only a small relation of E_{90}/E_0 of 0,004. This might be due to several reasons. One is that the transversal stiffness is known to vary with stress level of pre-stressed decks [3]. Therefor it was no surprise that just hand-tightening did not give a stiff deck. Secondly voids between the elements probably also has a large impact on the results. However, a plate effect was proven being able to transfer shear loads corresponding to a pre-stressed deck, just not being pre-stressed.

In case of large deformations, the steel bars could experience contact pressure to the timber deck. In such cases the real load bearing strength would be increased which for accidental load situations would be positive. As is the case for pre-stressed decks, though to our knowledge not being argued for in design. By using ordinary low-strength steel this effect might be easier to design with.

Advantage of this concept is that it only requires restraining, not pre-stressing, though some pre-stressing probably has advantages when it comes to the stiffness of the deck. For instance, local unevenness's may be smoothed out. From inspection experience the prestressing of decks seem to stabilize at around 0,10-0,15 MPa which probably should be sufficient. The bars holding the deck together should not be of high-strength steel, but rather normal steel being more stiff and less flexural as there probably wouldn't be a problem of stress loss over time. Using normal steel would also ease coating protection which at times has been an issue in Norway on stressing rods.

5 Conclusive remarks

It has been proven by calculation that using the deck structure in transversal direction instead of cross beams is possible. It has also been shown by tests that interlocking shapes of deck lamellas is possible for transferring shear loads. A combination of the two might be beneficial to some projects.

References

[1] Aas E., Bentdal S., Pettersen D.A. (2017) Tverrholdt dekke, et nytt brudekkekonsept. Bachelor thesis NTNU Gjøvik, Norway 2017

[2] Burkart H., Dyken T. (2018) Rapport 420 Tverrholdt dekke i tre (Oblique Interlocked Laminated Timber Deck) Oslo. Norwegian Public Roads Administration (NPRA) 2018. https://hdl.handle.net/11250/2617209

[3] Ekholm, K. (2013), Performance of Stress-Laminated-Timber Bridge Decks, PhD Thesis, Chalmers University of Technology, Gothenburg, Sweden

[4] Dyken et al (2017). Rapport 422 Trebruer (Timber bridges). Oslo. Norwegian Public Roads Administration (NPRA) 2017. https://hdl.handle.net/11250/2670309

[5] Ritter, M (1990), Timber Bridges: Design, Construction, Inspection, and Maintenance, Washington, DC, USA

Conference Proceedings 4th ICTB (2022)
https://doi.org/10.24451/g05z-ve83

ICTB 2021 PLUS
4th International Conference on Timber Bridges
Biel/Bienne, Switzerland, 9 -12 May 2022



Details for timber bridges with asphalt wearing surfaces

Andreas Müller[1], Marcus Schiere[2]

Abstract

Timber bridges for road traffic are built out with an asphalt wearing surface on the timber deck so vehicles can cross with high velocity (>50 km/h). The application of the asphalt layer on the majority of the surface is usually unproblematic, but is challenging along the edges. Engineers and practitioners often find themselves using their own creativity as constraints, geometry, and design of new timber bridges does not allow a direct copy of details of existing bridges. This paper presents base details along with recommendations listed by experienced timber bridge designers and experts from the field of detailing of concrete bridges. Furthermore, the advantages and disadvantages of existing details are discussed, and new details are presented. This forms a basis for new bridge designs, as the details from a basis for economic and robust construction of timber bridges and, hence, increases their longevity.

1 Introduction

The construction of road layup and especially that of the watertight layer can be produced in a high quality. It is generally unproblematic on majority of the bridge's wearing surface. However, experience won during inspection and repair of existing timber bridges shows that the expansion joints, side edges along curbs and details around drains are often weak and prone to damage. Leakages are often difficult to detect and can lead to uncontrolled water ingression. Until now, secure standard solutions have not been documented, yet. Although many bridges have been built already, engineers design new solutions, or variations to existing ones every time they design a new bridge. Secured standard details would substantially simplify the design process and improve the quality every time a new bridge is designed.

This objective was pursued in the research project VSS2016/326 [1]. During several meetings and workshops (Figure 1), experienced timber bridge designers gathered, discussed, and documented details that were based on their experience with design of different bridges. In the discussions, the specific requirements to details around expansion joints, curbs, and drains were agreed on. These are listed and detailed in this paper, along with the corresponding sketches and form a basis for future traffic bridge designs.



Figure 1: Workshop on detailing of timber bridges with engineers visiting the Obermatt bridge, Canton of Bern, Zwitzerland

[1] Andreas Muller, Berner Fachhochschule, Institute of Timber Construction, Structures and Architecture, Biel, Switzerland, currently at Holzbauexperten, Biel, Switzerland: andreas.mueller@holzbauexperten.ch
[2] Marcus Schiere, Research Collaborator, Bern University of Applied Sciences, Institute of Timber Construction, Structures and Architecture, Biel, Switzerland



2 Designs found in literature

2.1 Detailing in timber bridge design

Details for timber bridges have been documented and published already. They show details and simultaneously show an overview of the state of the art. Traditionally, there are differences between countries. In Scandinavia and Switzerland, details are often published on a high level in which only principles of designs are shown, and leave room for own interpretation by the designing engineer. On the other hand, in Germany for instance, detailed designs and solutions are offered that leave little room for alternatives or variation.

Differences between countries are also found in the layup of bridge decks. In Switzerland and in Scandinavian countries, the asphalt wearing surface is applied directly on the load bearing bridge deck. This can be a stress laminated deck (SLT), cross laminated deck (CLT) or a laminated veneer lumber deck (LVL). This timber deck is relatively thick, order of magnitude of 160 mm to 600 mm, compared to the asphalt layer. Hence, the bridge deck provides a dual function: that of load bearing structure and support of the watertight wearing surface like asphalt. In Germany, the asphalt wearing surface is applied on a separate timber panel which is thin, in the order of a couple of cm. This LVL or laminated wood panel is separated from the load bearing timber deck by timber battens, thus creating a control and ventilation layer between road structure and timber structure [2][3]. In other words, two timber decks are built, a first one which supports the wearing surface and the second, which supports the first deck and has a load-bearing function.

In literature, the following details for timber bridges with asphalt wearing surfaces are found:

- Two details for side edges are found [4] from Scandinavia where the water proof polymer bitumen membrane (PBM) is used between the SLT deck and the asphalt wearing surface. This PBM is led upwards from the timber deck along the curb, thus, consisting a corner where water cannot be drained once the wearing surface leaks. Two other details are also shown where the PBM remains straight on the timber deck until the bridge deck's edge. In the latter, water on the wearing surface can flow off the sides of the bridge. In Scandinavia, SLT decks are commonly used in timber road bridges.
- Milbrandt and Shellenberg [5] (Germany) published several details for expansion joints and side edges. The side edge details without curbs consist of steel profiles. Details with curbs, in hardwoods, are suggested, too. In all the details, the PBM is consistently continued horizontally towards the edge of the bridge's timber deck. Along curbs or steel profiles used along the side edges, an extra layer of PBM is added and melted on the first, and subsequently led upwards over the edge of the curb. In all details a fugue grouting is drawn, too. On details of expansion joints, sufficient room to optimally stimulate air circulation is suggested.
- In the sketches published by Harrer engineers from Karlsruhe [2], the timber panel and load bearing bridge deck is separated by an air ventilation layer. Details for open connections and closed expansion joints are very detailed. In the steel profiles at all edges, drainage holes are drilled along the fugue grouting. This allows water to flow away, thus, preventing it from flowing onto the timber deck. Along the edges, drains along curbs are suggested, too.
- In the Holzbau Handbuch [3], details from the Protimb project [6] and Harrer engineers [2] are published. The handbook offers an overview of the state of the art for german bridge design practices. It even introduces one detail in which a drag plate is used to create a closed expansion joint.

2.2 Detailing in concrete bridges

Lehmann and Bernard [7] (Switzerland) published details for curbs in concrete bridges in 'Forschungspaket Brückenabdichtungen: EP6 Anschlüsse von Brückenabdichtungen'. In these details, a combination of use of PBM and liquid plastics like Polymethylmethacrylate (PMMA) is suggested. Contrary to what is often seen in details for timber bridges, PBM is led upwards from the bridge deck along the curb. The PBM layer on the side of the curb is fixed mechanically to the curb using steel strips. This detail, where transition from bridge deck to curb needs to be made, liquid plastics are also often used.

3 Creation of new details for timber bridges

3.1 General structure

Most of the details from German literature cannot be used directly, as these contain the principle that the road deck and the supporting timber load bearing deck structure are separated. As mentioned in the



introduction already, these are traditionally combined in one single deck structure in Switzerland (and Sweden). The type of details are structured according to the following list.:

1. Expansion joint (abutment)
    a. Open
    b. Closed
2. Side-edges
    a. With curb
    b. Without curb, usually just a steel profile
    c. With guiding rail
3. Other drains
    a. In the asphalt surface
    b. At the edge

Although the focus lies on road bridges, the details can of course also be used for pedestrian and cyclist bridges, on which lighter traffic loads need to be born. This structure presented above is used in the following chapters to present the types of developed details.

3.2 Purpose and goals of the definition of details

In the following sketches are those of base details that can be used for new designs. When a dimension is not given, it means it can be adjusted to the requirements set by the bridge and its structure: traffic loads and frequency, specific constraints of the project, geometry, etc., and can be adjusted accordingly.

The timber bridge deck, the watertight membrane, and the asphalt wearing surface are sketched in a setup that can be used both for connected layup and the unconnected layup, such as given in the VSS 40 451 [8]. The listed details can be made under large constraints and set by time and costs found on the building site.

The details suggest robust solutions. It is, however, still necessary that bridge owners perform regular maintenance and inspect the structure regularly.

A drainage concept that prescribes the amount of needed drains, can be made, such as proposed by the ASTRA guideline 12004 [9]. In case of rainfall, sufficient drainage capacity over the bridge's surface has been planned.

3.3 Methodology

As mentioned in the introduction, the details were created in a combination of several meetings and workshops where engineers gathered, worked together, discussed and documented details, based on their experience with design of different bridges. During the discussions, the specific requirements, advantage, and disadvantages to details around abutments, curbs, and drains were agreed on.

4 Details for expansion joints

4.1 General

Experience shows that of all elements of the timber bridge, expansion joints require most maintenance and repair of the bridge. These need to be designed and built with utmost care to mitigate risk of water entry on the timber deck. The expansion joints are highly loaded by traffic which cause impact loads. These need to fulfill the following requirements according to the ASTRA guideline 12004 [9]:

- load bearing strength
- fatigue resistance
- functionality (deformation and elasticity)
- robustness for all traffic types, no matter what the weather conditions are
- traffic safety
- low noise emission
- good premises for inspection and repair.

The following recommendations are listed:

- The road and bridge-structure around the expansion joint should have a similar vertical stiffness. This prevents large relative deformations between the two systems every time a vehicle crosses.



- The maximum vertical deformations recommended by ASTRA guideline 12004 are to be maintained. A low vertical deformation reduces wearing of the asphalt layer and increases the longevity of details.
- Timber decks that are not stiff enough can be reinforced with steel beams around the expansion joints. These need to be connected in such a way that they do not lead to fatigue failure of any elements either. This can subsequently cause to leakage of water onto the timber deck.
- Apart from large relative deformations in the expansion joint, weak transitions lead to rotations in timber deck, supporting steel beams, and fugue grouting. These can eventually lead to leakages.
- The asphalt types, layer thicknesses and layup used on the bridge and road should be similar, at least for one meter around the expansion joint. For instance, thickness of the mastic asphalt on both sides of the expansion joint should equal. It can even be increased locally, like done around expansion joints of concrete bridges, where the thickness is increased from 80 mm to for instance 120 mm in the first meter next to the expansion joint.
- The inclination of the road on abutment and bridge around the expansion joint should be equal. A vehicle crossing a bridge will thus not create additional (vertical) impact loads which can damage the bridge deck on the long run.
- The connection of PBM to the steel edge-profiles can additionally be sealed with PMMA.
- Water leaking into the fugue grouting close to the edges around the expansion joints, should be drained using tubes and Omega-type profiles (ETADRAIN). In case of leakage, water can be led to a drain through the timber deck.
- In the vicinity of the expansion joint, both on the abutment and bridge structure, ventilation must be encouraged. This improves the drying capacity of the timber elements. In addition, the end grains of the timber elements can be covered by any watertight material.

4.2 Closed expansion joints

- Closed expansion joints are generally to be carried out using a ‘trough filling’, see Figure 2.
- Trough fillings are suited to obtain silent expansion joints in busy bridges or in bridges located in residential areas
- When using trough fillings, substantial braking or other horizontal loads are generated too an need to be led into the bridge or abutment.
- Although trough fillings can be used to overcome relative displacements between bridge and abutment (up to 1.5 mm vertically and 5 mm horizontally), it is still recommended to create a stiff structure around the expansion joint.
- Alternatively, closed expansion joints can also be made using solutions like the elastomeric sealing profiles, Figure 3, that allow movement up to 100 mm (manufacturer mageba “Tensa-Grip“ or similar)
- Elastomeric sealing profiles like the “Tensa Grip” can be used to create the expansion joints, but must be connected/welded to steel beams that are fixed to the bridge structure.
- Expansion joints using drag plates are not recommended over traffic speeds of 50 km/h as they can produce too much noise pollution.

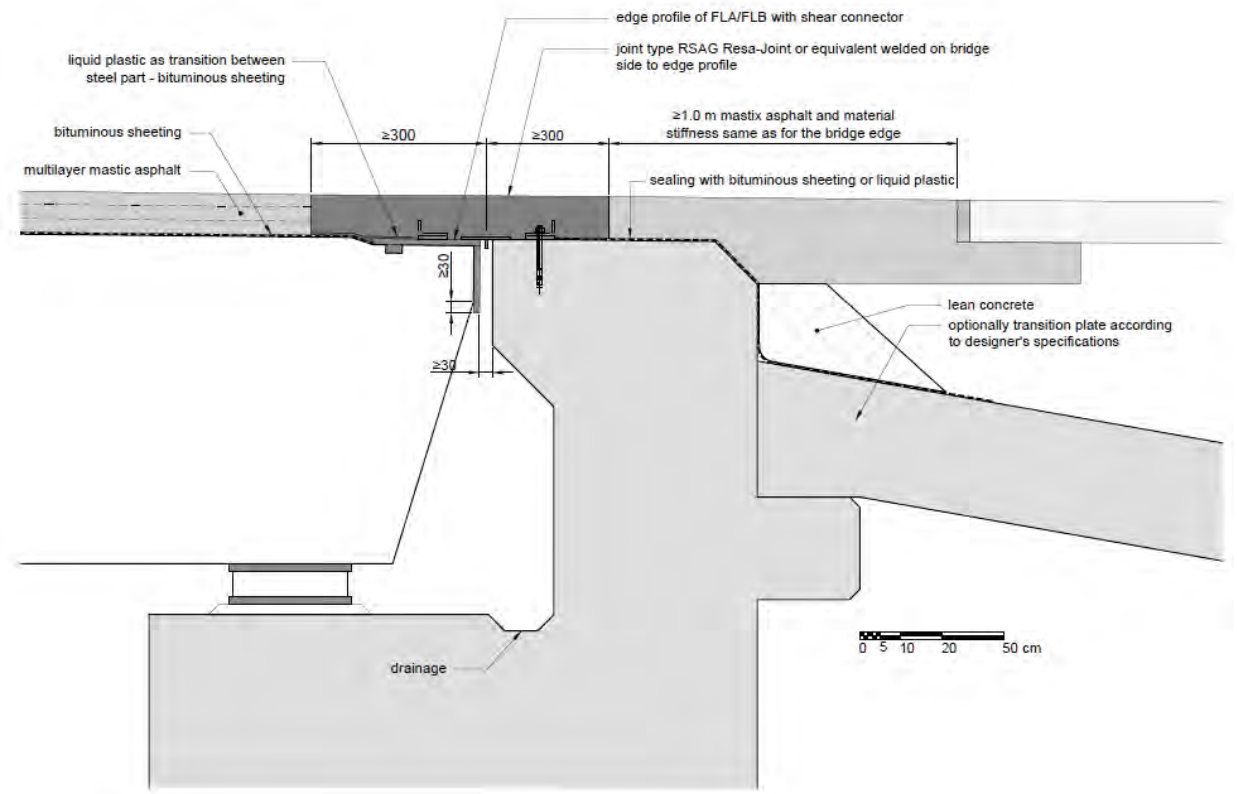


Figure 2: Closed expansion joint created with a trough filling

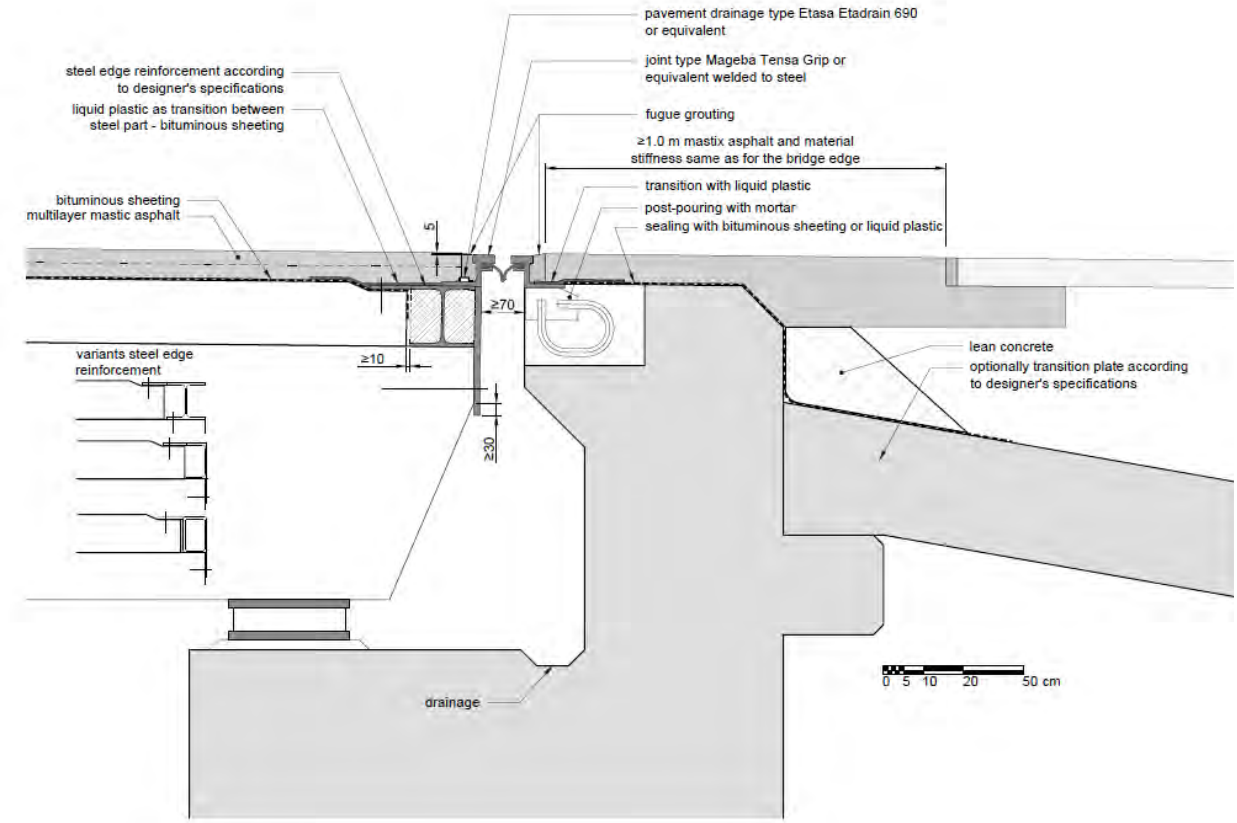


Figure 3: Closed expansion joint created with a elastomeric sealing profiles

4.3 Open expansion joints

- Open expansion joints, like seen in Figure 4, are to be used in exceptional cases. This is due to the low constructional protection of wood: water can, in principle get close to the timber structure. Any dirt, twigs, leaves, or gravel that gets stuck between bridge and abutment can prevent drainage of the joint.
- Open joints can however be used in pedestrian and cyclist bridges, or in bridges with a very low frequency of traffic.
- The open expansion joints lead to large noise pollution at traffic speeds above 50 km/h.
- Open expansion joints should offer sufficient possibility to drain water, clean, inspect, etc.
- Elements with dripping edges can be used to lead water away from the end grain of timber elements
- A sufficiently large space in the abutment encourages the air circulation, improves the drying capacity, and facilitates inspection. The condition of the expansion joint can be better monitored, too
- Optimal drainage of water below the expansion joint should be facilitated during a planning phase
- Open expansion joints are generally not wider than 20 mm
- Edges of steel beams or profiles should be to be located about 5 mm to 10 mm lower than the asphalt wearing surface to prevent damage caused by impact of snow ploughs.

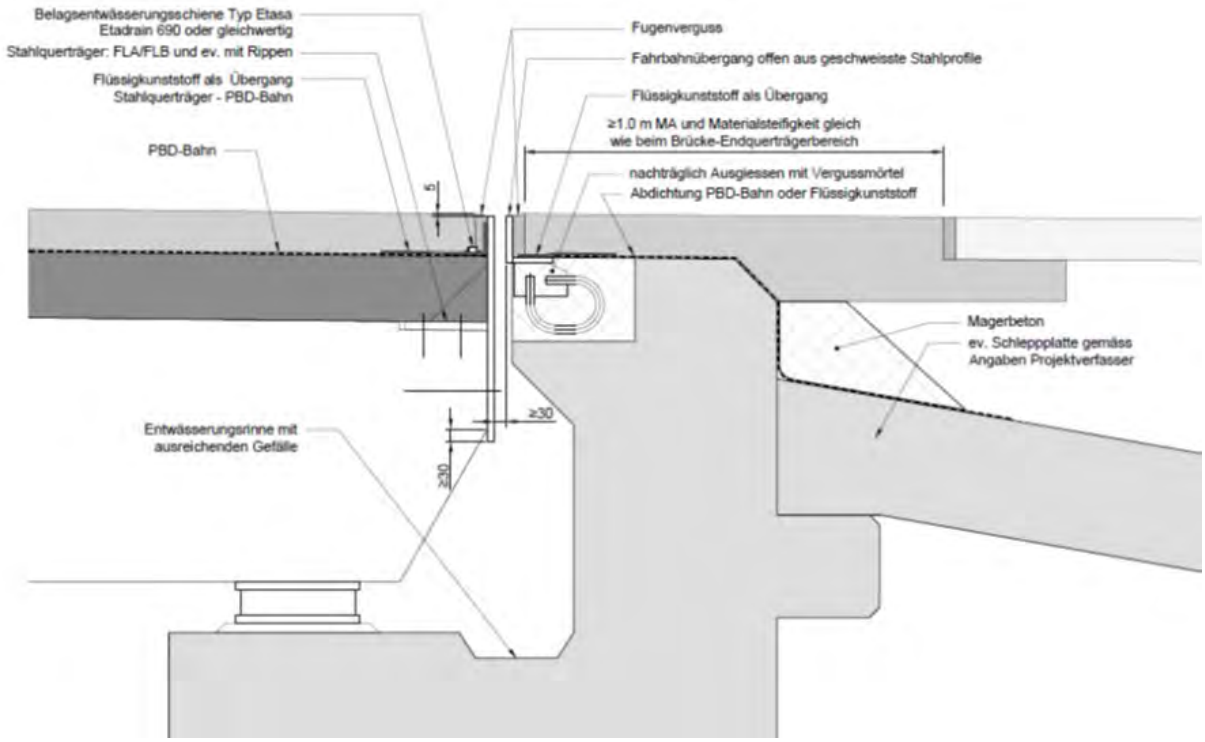


Figure 4: Open transition joint for pedestrian bridges or low frequent traffic

5 Details for side edges and curbs

5.1 General

The auxiliary drain in the fugue grouting along the edge profiles is best made using drainage pipes of Ø15 mm, located on the bridge deck, or like the so-called Omega profiles (e.g. ETADRAIN). both can be used to lead water away to drainage holes.

Bending or folding the PBM in corners is to be avoided it should not be led upward along the side edges. It can be melted on a steel profile, and an additional watertight sealing is best made using PMMA. Sharp edges and corners in the watertight membrane should be avoided as these tend to be weak in timber bridges, and subsequently, PBM or PMMA membrane can tear due to material fatigue.

5.2 Side-edges without curbs

- It is recommended to use a guide rails or timber lattice (sacrificial element) on the edges to prevent that snow ploughs, or any other vehicle or object, to damage edges or exposed watertight membranes.
- The edge between asphalt and edge profile can additionally be protected using a plastic profile 'Kitt-teil' that additionally protects the fugue grouting and increases longevity of the detail.
- When using steel edge profiles, a dilatation joint of about 8 mm should be made every six meters. This allows thermal strains to develop. These steel elements should be made using standard profiles. Welded profiles can bend/deform during a hot dipped galvanization process. Welding stresses are released.
- Along the edges of the timber deck, the watertight PBM membrane should be connected to the steel profile and additionally be sealed using PMMA. Application of PMMA on hot dipped galvanized steel profiles is unproblematic. On painted profiles however, application of PMMA has proven to be problematic.

5.3 Side edges with curbs

- It is recommended to make curbs using either pre-cast or cast in place concrete.
- Timber curbs can be made too, but it is recommended to leave an air gap to asphalt wearing surface. Water from the wearing surface can flow underneath the curb. Similar detailing as on edges with steel profiles should be made in those cases. Larger curbs may be required.
- The waterproofing membrane should be continued under the curbs too, so that standing water is avoided in case of leakage
- In case of impact, the shear displacement of the curb should best be prevented using heel-type connections to the timber deck. Horizontal shear loads are not easily transferred using screws or other mechanical fasteners. In addition, screws and mechanical fasteners would penetrate the watertight membrane and potential leakages cannot be detected as the details are inaccessible. They cannot be opened easily during an inspection.

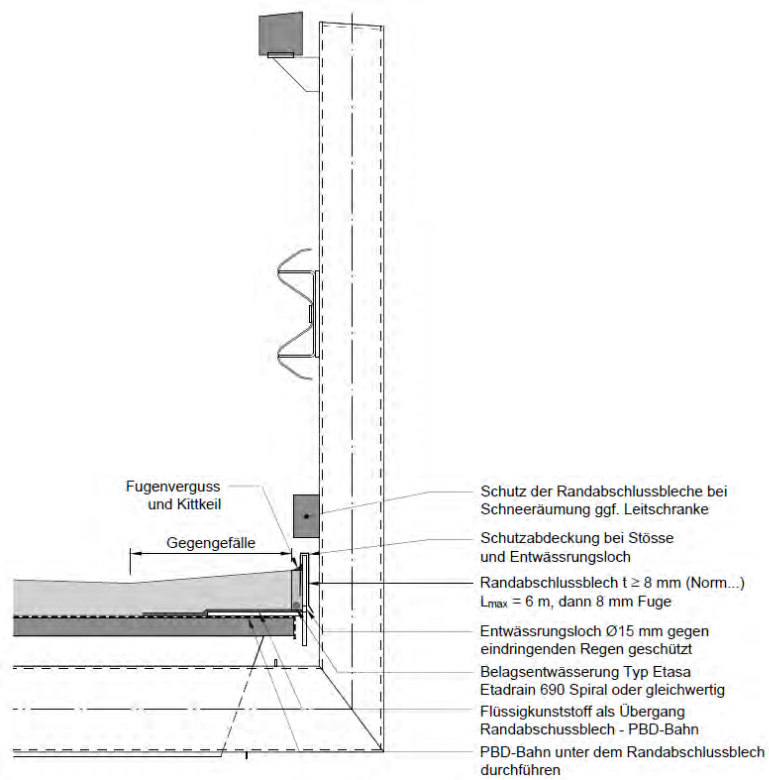


Figure 5: edge detail without curb, primarily with steel edge profile

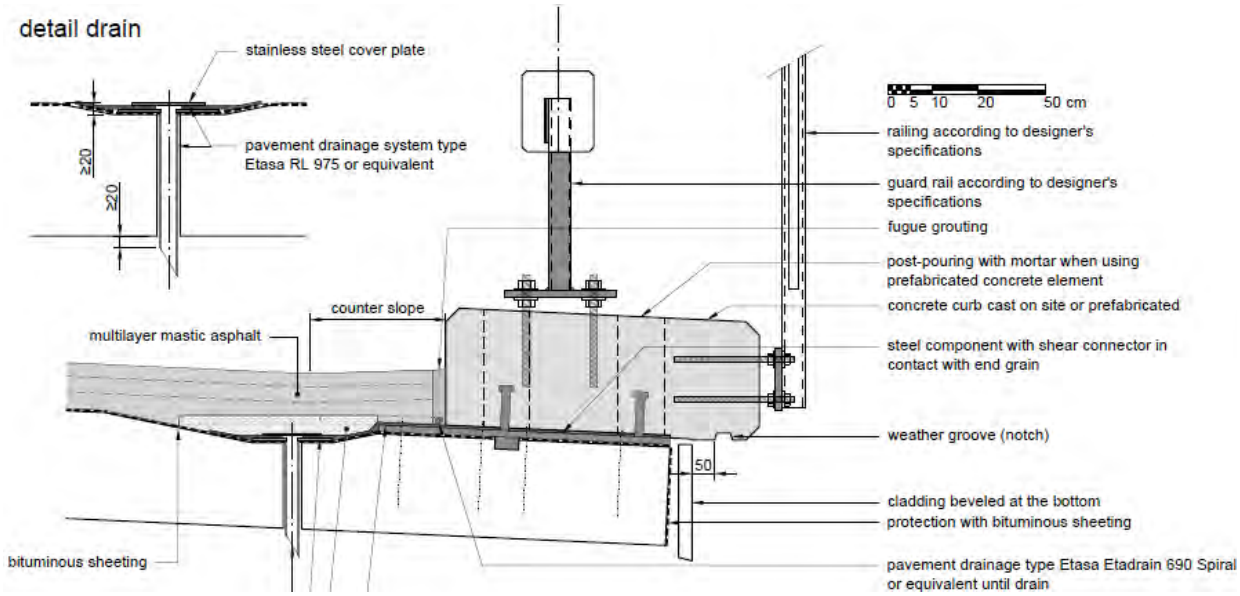


Figure 6: Edge detail with curb of concrete elements with guide rail

6 Drains in the asphalt wearing surface

In large bridges, water cannot always be led over the sides and drains in the middle of the deck are required. Standard details and products for drains can be obtained from details and solutions developed for concrete bridges. These have often proven to work well.

7 Discussion and conclusions

Experience gained during inspections and during repair of existing bridges show that apart from a robust layup of the wearing surface, the detailing along the edges of expansion joints, sides like curbs, and drains are essential for the longevity and durability of timber bridges. That means that they are important for correct and efficient maintenance of the bridges, too.

Leaks along these edges are often not detected timely and can lead to uncontrolled ingression of water onto timber decks in a short period of time.

The presented details are created using the expertise of experienced engineers and create a solid starting point for individual planning efforts for bridges with timber decks. This will significantly increase the economic aspects, efficient planning of construction process, and improve quality of future bridges. It still is, however, important that bridge owners realize that regular inspection and maintenance is carried out, too.

In all the listed details, polymer bitumen waterproofing membranes are used as a system structure on wooden roadway decks, both with and without bonding in the surface, and mastic asphalt is used for the protective layer and sealing. The creation of the asphalt road layups is usually unproblematic when robust components are used and can be made in high quality [10].

Acknowledgement

The research was performed in the scope of grant VSS 2016/326 ‘Abdichtungssysteme und bitumenhaltige Schichten auf Brücken mit Fahrbahnplatten aus Holz’ by the Swiss Highway Authority ASTRA.

The steering committee headed by Fred Stalder-de Marco is also gratefully thanked for their input. The input of experience of practitioners was vital to the success of the project. Within the project, the working group for the details consisted of Fred Stalder-de Marco, Heinz Aeschlimann, Kurt von Felten, Lukas Rüegsegger, Andrea Bernasconi, Martin Adam, Sébastien Bonifacio, and the authors. The Road Authority of the Canton of Bern, Region IV, is thanked for hosting the group’s workshop.



References

[1] Müller A., Angst C., Bueche N., Schiere M., Huber L., Bonifacio S., Maurer J. (2021), VSS2016/326 Abdichtungssysteme und bitumenhaltige Schichten auf Brücken mit Fahrbahnplatten aus Holz, Bern University of Applied Sciences, Institute of Timber Construction, Structures and Architecture, Biel, Switzerland

[2] Matthias Gerold, 2006: Musterzeichungen als Grundlage zur ZTV-ING 9.3 Holzbrücken. Abschlussbericht Forschungsvorhaben, DGfH Innovations- und Service GmbH, München. (Sample drawings to the German standard ZTV-ING 9-3 Timber Bridges. Final research report, DGfH Innovations and Service Ltd., Munich.

[3] Seidel, A., Miebach, F. and Osterloff, L. (2019) Entwurf von Holzbrücken, Holzbau Handbuch (Series 1, Part 9, Issue 1). Informationsdienst Holz (Bonn, Germany).

[4] Pousette A. (1997), Wearing surfaces for timber bridges, Nordic Timber Council, ISBN 91-89002-12-1

[5] Milbrandt E. and Schellenberg K. (1998) Eignung von bituminösen Belägen für Holzbrücken – Schlussbericht. Forschungsauftrag E96/7, Entwicklungsgemeinschaft Holzbau (GH) in der Deutschen Gesellschaft für Holzforschung e. V., München, Germany

[6] Protected Timber Bridges (ProTimB) (2019), Entwicklung einheitlicher Richtlinien für den Entwurf, den Bau, die Überwachung und Prüfung geschützter Holzbrücken, Fachhochschule Erfurt, Germany Lehmann and Bernard (2014)

[7] Bernard and Lehmann (2014), Forschungspaket Brückenabdichtungen: EP6 - Anschlüsse von Brückenabdichtungen, Forschungsprojekt VSS 2006/516, Schweizerischen Verbands der Strassen- und Verkehrsfachleute, Switzerland

[8] VSS 40 451 (2019) Abdichtungssysteme und bitumenhaltige Schichten auf Brücken mit Fahrbahnbelägen aus Holz, Schweizer Verband der Strassen und Verkehrsfachleute VSS, Switzerland

[9] ASTRA guideline 12004, Richtlinien für konstruktive Einheiten von Brücken, Bundesamt für Strassenbau, Bern, Switzerland

[10] Schiere, M., Müller, A., Bueche, N., Angst, C. (2022), Creating a connecting between asphalt wearing surface and timber bridge decks, International Conference of Timber Bridges proceedings, Biel, Switzerland

Conference Proceedings 4th ICTB (2022)
https://doi.org/10.24451/pe83-p237

ICTB 2021 PLUS
4th International Conference on Timber Bridges
Biel/Bienne, Switzerland, 9 -12 May 2022



Direct trafficable waterproofing and wearing courses for timber decks

Dirk Uebelhoer[1], Mareike Vogel, Thomas Volkmer, Adrian Willi Wick

1 Introduction

Sustainability is becoming a more and more important topic in the construction industry. Climate change is the most important environmental global threat, so the use of environmentally friendly products with a low carbon footprint gets very popular [1].

The use of timber in the bridge construction is common for more than 3000 years. After using step stones, to cross small rivers approx. 6000years back the next step was using felled trees to cross rivers. One of the oldest piled timber bridges has been found in the Zurich Lake/ Switzerland, dated back to approx. 1500 BC [2].

Timber, a natural renewable construction material, requires less energy than other construction materials, i.e. concrete and stores CO_2.

Timber decks made of planks have space between the planks and a certain slope to get the water running off, so the deck can dry easily. This deck design is often used for pedestrian and bicycle bridges.

Decks exposed to vehicular traffic are often made from Cross-Laminated-Timber (CLT) because of the flat and uniform surface. The closed deck protects the load beams underneath the deck from moisture and ensures a dry supporting structure. The state of the art is to apply bitumen sheets as a waterproofing layer followed by an asphalt overlay. Because of the movement of the timber structure this waterproofing technology has been proven as in-adequate due to crack forming, which allows the ingress of water to the timber deck. This happens due to the lox flexibilty of bituminous deck waterproofing system that can´t cope with the movement of the structure. Sometimes the hairline cracks are not visible, and the ingress of water remains unremarked This leads to a permanent humid environment at the timber structure, which leads to deterioration caused by attack of microbes and growth of fungi. This could be prevented using a loose laid waterproofing system, but this would not work well with shear foces applied to the deck by breaking and accelerating vehicles and slide on the deck panels.

2 The idea

Due to the movement of timber beams and panels under dynamic load the currently used solution for deck waterproofing and wear protection does not provide satisfactory results. A more flexible system, providing sufficient wear resistance should perform better on the CLT-deck. The system shall be fully bonded to the substrate to prevent ingress of moisture and water caused by delamination. An already approved and used system for concrete decks, based on hot-spray-applied Polyurea, has been detected as a promising solution.

An additional advantage of this technology would be a reduction of the deck load. An asphalt pavement with thickness of 7cm has a weight of approx. 168kg/m², the waterproofing and wearing course made of Polyurea counts for approx. 5kg/m². This would allow more filigree bridges design and will reduce the carbon footprint of the structure notably. Possible necessary repair works on the deck will be much easier using the spray applied technology, compared to ashpalt pavement.

3 Test programme

Adhesion and shear strength are important measurements when it comes to Bridgedeck waterproofing. The protective system must develop a good bond to the substructure to prevent delamination and ingress of water. High shear strength ensures, that the waterproofing and protection layer doesn´t delaminate from the deck when vehicles break and accelerate. Water vapour diffusion and change of physical properties, after artificial weathering are also important indicators for the suitability of the chosen system.

Wood has the nature, that wood moisture is not constant and changes frequently due to ambient conditions, therefore the applied system needs to develop perfect adhesion to the substrate at different levels of wood

[1]Dirk Uebelhoer, Sika Services AG, Switzerland, uebelhoer.dirk@de.sika.com



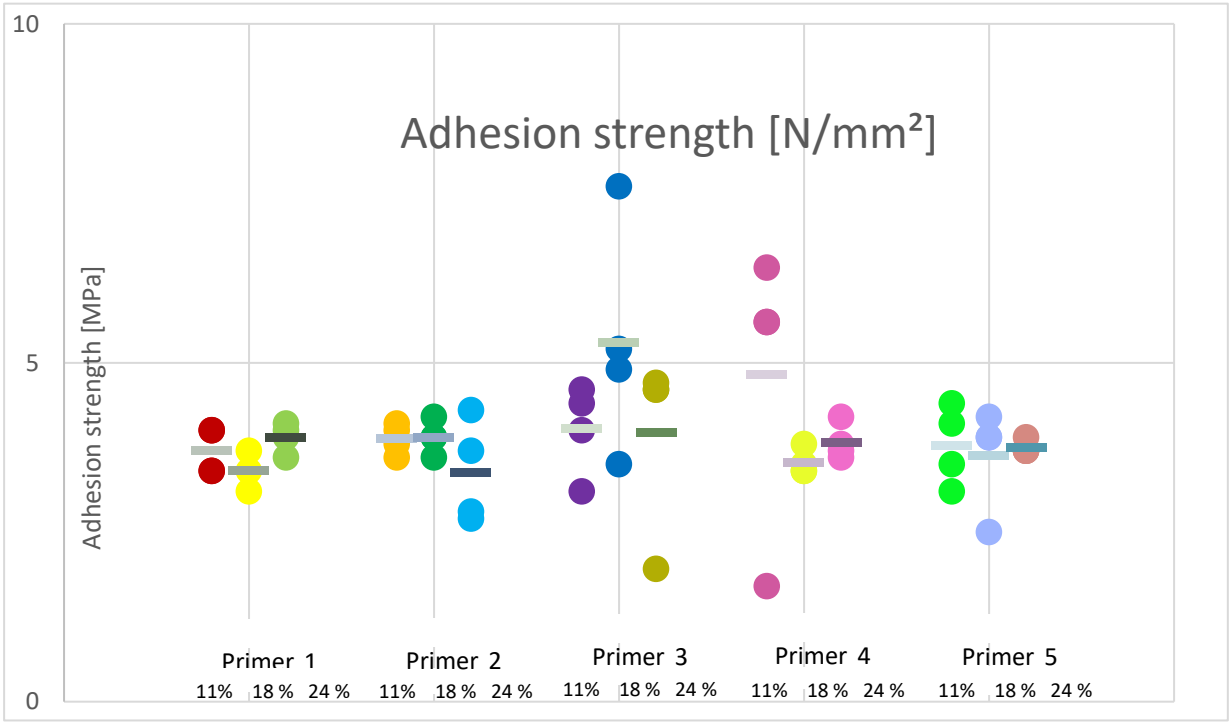
moisture. For the preliminary testing 3 levels of moisture have been agreed, approx. 11%, approx. 18% and approx. 25%.

3.1 Primer testing, tensile adhesion strength

The test series has been started with a prelimary primer testing program to reduce the possible systems for testing.

Table1: Primer Overview

Primer 1:	epoxy resin, solvent free, unfilled, 2nd generation
Primer 2:	epoxy resin, solvent free, pre-filled, 2nd generation
Primer 3.	epoxy resin, solvent free, unfilled, 1st generation, approved for bridge application on concret
Primer 4:	epoxy resin, solvent free, unfilled, fast curing, 1st generation, approved for bridge application onconcret
Primer 5:	epoxy resin, solvent free, pre-filled, low odour



Graph 1: Adhesion strength, primers, acc. EN ISO 4624, 20mm dolly

Due to the thin layer resulting for the primer the determination of shear strength, according to SIA 281-2:2011 was not possible. The test has been postponed to the system testing part.

3.2 System testing

All tested primers worked well and fulfilled the requirements. Having a closer look at the result the variation in adhesion values for Primer 1 was less than others. To reduce workload the involved parties decided to perform system testing only with Primer 1, an unfilled solvent free epoxy resin. Testing was agreed for four systems to screen possible combinations of product. The four systems are described in the table below:



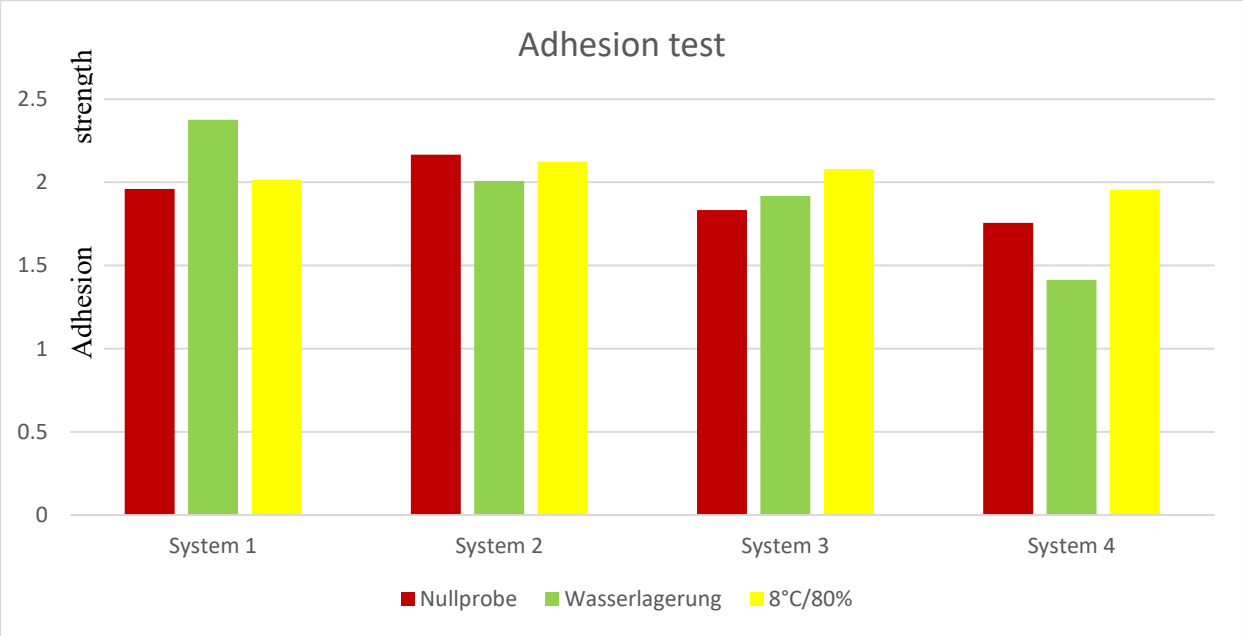
Table2: System Overview

Technology	System 1	System 2	System 3	System 4
Primer, epoxy solvent free, unfilled	X	X	X	X
Membrane pure Polyurea	X	X		
Membrane Polyurea- Polyurethane-Hybrid			X	X
Topcoat, solvent based aliphatic Polyurethane	X		X	
Topcoat, solvent free, aliphatic Polyaspartic		X		X

3.2.1 Adhesion test

All four systems have been applied on CLP-Panels with the dimension 300 x 300 x 26mm. The adhesion strength has been determined under 3 different conditions,

1. Wood moisture approx. 12%
2. Stored 14 days under water after application, before testing
3. Stored in +8°C/ 80% relative air humidity before application



Graph 2: Adhesion strength, systems with different stress, 50mm dolly

System 2 and 4 showed failure between wearing layer and topcoat, after strorage in water. Systems 1 and 3 had the failure level in the CLT.



Pic.1: Adhesion test sys-

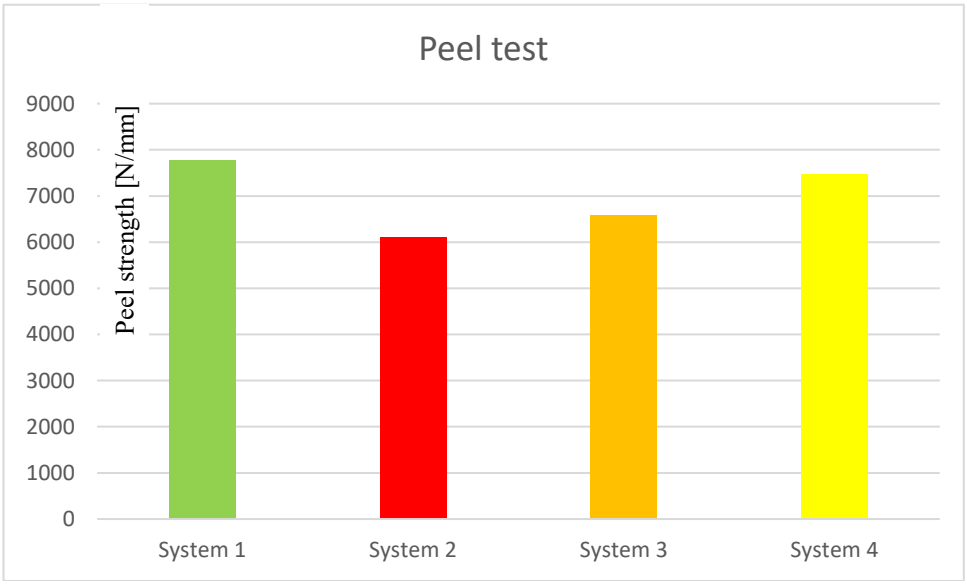


Pic.2: Adhesion test sys-

The preferred failure level is in the substrate. This indicates that the adhesion strength and the cohesion strength of the protective system is higher than the cohesive strength of the substrate.

3.2.2 Peel test

The peel test had been performed in accordance with the Swiss Standard SIA-281-2:2011, method B. Peel resistance gives a good indication to the shear force resistance of the applied waterproofing and protection system, especially when vehicles brake or accelerate on the bridge. The measured values can be found in graph 3.



Graph 3: Peel resistance, system performance

Also with the peel test the preferred failure level is failure in the substrate. If the failure level is between protective system and substrate the system shear strength needs to be evaluated as inadequate.



Pic.3: Peel test, System 1

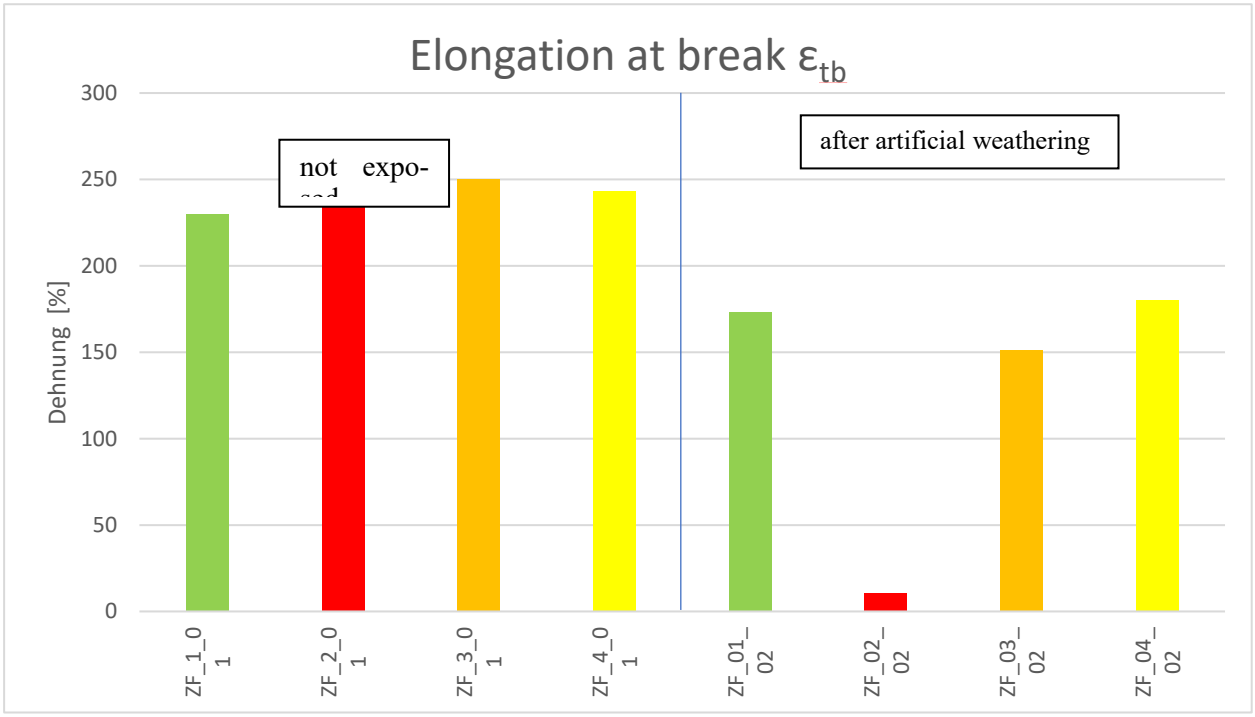


Pic.3: Peel test, System 4

Even if both systems show almost the same peel resistance System 1 is the preferred technology, due to the failure level in the CLP plate.

3.2.3 Elongation at break

Elongation at break is an indicator of the flexibility of the used system. The target is to find a system, which is flexible enough to handle the movement of a timber structure, caused by temperature and variation of wood moisture over the year. The waterproofing and protection system will be exposed to weathering; therefore a comparison has been made with unstressed samples and test specimens exposed to artificial weathering. Testing has been in accordance with EN 527-1.



Graph 4: Elongation at break before and after weathering

System 1 has the lowest difference between the two test results. System 1 is less affected from artificial weathering than the other 3 systems. System 2 has lost almost the whole flexibility, degraded under the weathering exposure, and had the strongest impact.

3.2.4 Water vapour Diffusion

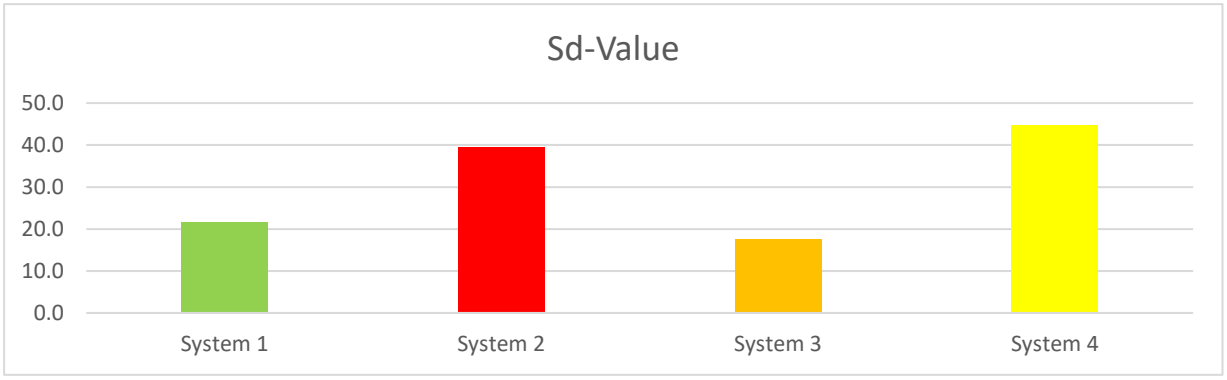
Moisture control is the simplest, most economical method of reducing the decay in timber bridge structures [3]. To prevent ambient relative moisture to penetrate the timber and to keep the construction dry, the protective system needs to block water vapour diffusion. DIN EN ISO 10456 contains tables with the µ-value of most used construction materials. Multiplication of the µ-value by the thickness of the related layer [m] leads to the s_d-Value. The classification in accordance to DIN 4108-3 is:

Table 3: evaluation scheme water vapour diffusion acc. DIN 4108-3

s_d-value	**evaluation of tightness**	**Resistance to water vapour diffusion**
$s_d \leq 0.5$m	open to water vapour diffusion	Low
$0.5 < s_d < 1500$	inhibitive to water vapour diffusion	middle
$s_d \geq 1500$	blocking water vapour diffusion	high



The following results have been optained:



Graph 5: Water vapour diffusion; s_d-value

All systems are in the same range, to be classified as inhibitive to water vapour diffusion.

4 Summary

The results shown above are an overview of test performed to determine the most promising waterproofing and protection system for timber bridges with the approach to be directly exposed to pedestrian, bicycle and car traffic at low frequency. The rating was made by evaluating the test results with numbers 1 (best in class) to 4. The system with the lowest overall number is the best performing and shall be used for further evaluation and for field test applications on real projects.

System 1, made of a solvent free epoxy primer, a pure polyurea waterproofing membrane, a pure polyurea wearing course and a solvent borne PU topcoat had the best performance and is the system which is already often used for the waterproofing and protection of concrete bridges.

Currently the project team is in process to finish the planned testing, find a trial bridge for the system application, which will be necessary to make a step forward with the project.

Acknowledgement

The author acknowledges the following individuals, universities, and companies for the substantial contribution they made to this publication:

- Prof. Dipl. Ing Andreas Müller; University of Applied Science Bern of Architecture, Timber and Construction, Project Initiator and Senior Consultant
- Thomas Volkmer; University of Applied Science Bern of Architecture, Timber and Construction, Project Co-Lead and Senior Consultant
- Dipl. Ing. Mareike Vogel, University of Applied Science Bern of Architecture, Timber and Construction, Project Co-Lead and Documentation for Innosuisse Program
- B.Sc. Adrian W. Wick, University of applied Science Bern of Architecture, Timber and Construction, Test planning, Testing and Evaluation
- Patrik Barmettler and Conradin Huerlimann, Sika Schweiz AG, Project partner and Sponsoring Roland Jaeggi, Sika Schweiz AG, peel testing
- Christoph Goy, Sika Services AG, application of est specimen and pull-off testing

References

[1] Timber: Trends in Availability, Sustainability and Durability for Bridges Mick Stephens*, Chief Executive Officer, Timber Queensland, 30 Boothby Street, Kedron, Queensland 4031 Rob McGavin, Queensland Department of Agriculture and Fisheries, Horticulture and Forestry Science, Salisbury Research Facility, 50 Evans Road, Salisbury, Queensland 4107
[2] Ritter, Michael A., 1990, Timber Bridges: Design, Construction, _Inspection, and Maintenance; Washington, D.C. 944.
[3] EM-7700-8, AASTHO 1996.

Conference Proceedings 4th ICTB (2022)
https://doi.org/10.24451/h7yr-4817

ICTB 2021PLUS
4th International Conference on Timber Bridges
Biel/Bienne, Switzerland, 9 -12 May 2022



Creating a connection between asphalt wearing surface and timber bridge decks

Marcus Schiere[1], Andreas Müller[2], Nicolas Bueche[3], Christian Angst[4]

Abstract

Timber bridges are increasingly popular again in infrastructure networks nowadays. Protection of timber structural elements from direct exposure to rain and sun is essential to prevent biological degradation of the wood material when using softwoods. In case of a timber deck, the asphalt wearing surface must be watertight. Creating connected layups has advantages over layups where the asphalt is not connected as traffic loads are transmitted directly to the bridge deck: asphalt surfaces can be loaded with heavier traffic, slopes of bridges can be higher, breaking and acceleration loads are directly transmitted to the bridge deck, and fatigue life of the asphalt is improved. The Swiss standard VSS 40 451 standardized an unconnected mastic asphalt surfacing on timber bridges. Research project VSS 2016/326 was performed to investigate road layups where asphalt wearing surfaces were connected to the bridge deck. This work presents only a part of the results, focused on the bonding issues. Results show that such a layup proves to deliver satisfactory performances, and that shear capacity is comparable to that of concrete and steel decks. Good surface quality of the timber deck is important before application of the bonding agent to avoid short term blistering of the asphalt.

1 Introduction

Timber bridges know a long tradition within Europe and the rest of the world [1]-[5]. Use of raw materials continues to become more efficient, new timber products are developed and load bearing systems are developed. Timber is now recognized next to steel and concrete as a main structural material [6]-[9]. The development of Glued Laminated Timber (GLT), Cross Laminated Timber (CLT), and Stress Laminated Timber (SLT) has contributed to this regained interest [10]-[14].

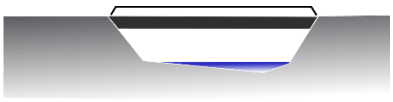
Along with the introduction of the motorized vehicles, so have the requirements to the wearing surface, not only on timber bridges. Use of Mastic Asphalt (MA) or Asphalt Concrete (AC) became an important research topic in the development of new timber bridges [15]-[17]. The asphalt not only serves as a skid resistance, but it is also offers a water-proof layer for the timber [9][17][19]. This is essential for the longevity of softwood timber decks [20]-[22]. The asphalt wearing surface can be separated from the supporting timber deck or connected to it, thus establishing a shear bond or a composite layup in the bridge deck (Figure 1). The shear bond is used on concrete and steel bridge decks, and it is standardized in the EN 12970 [23] or SN 640 450 [24]. Despite the performed research on connected layups for timber bridges [15][16][17][25], the authors are only aware of standardized unconnected layups in VSS 40 451 [26].

When the road layup is connected, it typically consists of the (timber) road deck, a bonding agent, a modified polymer bitumen membrane (PBM) and the asphalt wearing surface. In a floating layup, the bonding agent is replaced by a glass-fiber mat or oil-paper to separate the timber deck from the PBM and thus from the asphalt wearing surface, too [15]-[17][24][26]. In a connected layup, the service life of the asphalt on concrete and steel bridges is longer: in the order of 40 years in connected layup compared to 20 years in unconnected condition [27]. When asphalt and bridge deck are connected, the asphalt is loaded primarily in compression and less in bending, which is better for the fatigue life of the asphalt surface every time a

[1] Marcus Schiere, Research Collaborator, Bern University of Applied Sciences, Institute of Timber Construction, Structures and Architecture, Biel, Switzerland, currently Hupkes Wijma B.V, Kampen, the Netherlands: mjs@hupkeswijma.com
[2] Andreas Muller, Berner Fachhochschule, Institute of Timber Construction, Structures and Architecture, Biel, Switzerland
[3] Nicolas Bueche, Berner Fachhochschule, Institute for Urban Development and InfrastructureBurgdorf, Switzerland
[4] Christian Angst, IMP Bautest, Oberbuchsiten, Switzerland



bridge deck with asphalt wearing surface



	connected layup	floating layup
wearing layer binding layer base/protection layer	asphalt wearing surface of Mastic Asphalt or Asphalt Concrete	
waterproofing membrane	Polymer Bitumen Membrane or liquid plastic	
bonding agent	primer or sealant	glass fiber mat or oil paper
substrate/bridge deck	bridge deck of concrete or wood based material like CLT/SLT/GLT/LVL	

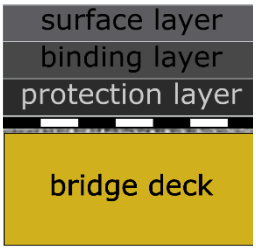


Figure 1: Bridge deck layup as described in the SN 640 450 and VSS 40 451[24][26]

vehicle crosses. The need for a connection between the supporting wooden deck and asphalt layer is further recommended for the following cases [16]: (1) For bridges that are designed for heavy traffic, (2) In bridges with road inclinations of more than 6%, (3) In bridges located in curves, close to traffic lights or locations where traffic is expected to accelerate or to decelerate.

During and after the application of mastic asphalt (MA), there is a risk of blistering that can result in damage of the asphalt layer [28]-[30]. Any (leftover) water in the substrate is potentially transformed into vapour (short term blistering). Blisters formed shortly after application of the base layer can continue to grow in the continuing years due to heating and cooling of the asphalt due to solar heating (long term blistering). The formation of the latter type is often a consequence of weak quality procedures due to tight, weather affected, building schedules.

In 2007, the Obermatt bridge (30 meter and 40 tons, Lauperswil CH) was equipped with such a system [31], just like the Isalas (20 meter and 10 ton traffic load, Celerina CH) and the Ova da Bernina (22 meters and 40 ton traffic load, Pontresina CH) built in 2020 [32]. Until now, good long-term experience has been obtained using the composite system in the Obermatt bridge.

The presented research aims at examining the composite layup and its different aspects: used substrate materials (bridge decks) and bonding agents, development of temperature in different layers during application of the base layer of the MA, blistering under different thicknesses of the base layer (MA8 and MA11), and mechanical aspects such as shear and adhesion capacity [18].

2 State of the Art

2.1 Connected layup on timber bridges

As mentioned in the introduction, GLT, SLT, and CLT are popular materials when it comes to the bridge deck, so is Laminated Veneer Lumber (LVL). GLT beams are used in stress laminated bridge decks [12] [31]. Relatively new to the wood products market is the CLT.

SLT is a relative stiff material for the road deck. This was used with bonding agent (Isoglasyr 11P) and PBM (SBS) to determine the bonding quality of the road layup [15]. Whether the boards in the SLT where rough sawn, planed, or sanded did not affect on the adhesion strength. Secondly, blisters in the PBM were also seen to occur already before the application of asphalt due to heat from solar radiation.

Optimal properties of MA for timber decks we investigated [16]. An inert oil coating was one of the main bonding agents before waterproofing with MA (10 mm thick), PBM (5 mm thick), and bitumen B80 (2 mm thick). Specimen sizes were 0.2 m x 0.2 m and wood-based panels (amongst others LVL) were used, many only several cm thick. Moisture in the wood increased the risk of blistering of the asphalt base layer, even if the moisture content was below 13%-m. Authors also stated that the thinner the base layer (MA8 instead of MA11), the better the blistering could be mitigated.

Timber deck layups similar to those for concrete (SN 640 450) were also made [17]. Both LVL and CLT were used as substrate and compared to references on steel and concrete. Epoxy (EP) as bonding agent together with PBM and liquid plastics were used as a waterproofing membrane, too. The test specimen size



was 0.2 m x 0.2 m, however significantly thicker panels were used than in [16]. The road structure layup consisting of wood, EP, PBM and MA could be made without any short-term blistering. However, blistering could occur in sealings made with liquid plastics. Shear capacities with connected layups on CLT and LVL led to equal values as on steel and concrete substrates.

2.2 Asphalt wearing surfaces

MA has a higher content of binding agent of 6.5 - 8.5%-m, compared to conventional AC and proved to be very stable and resistant to aging. It is generally heated to 230 °C to obtain a good workability for the laying phase. The working temperature can be reduced to 190 °C when using additives as for instance wax.

MA is self-compacting whereas (AC) must be compacted. The compacting can lead to high vibrations of the bridge deck. AC is not recommended either on bridge decks, as the timber deck is often believed to be too flexible and the required compaction energy, up to a void content of 3%-Vol, cannot be introduced with common asphalt mixtures [16]. Examples where AC was used, have varying success [16][17][25].

2.3 Bonding agent/sealing

The bonding or sealing agent enhances the connection between the bridge deck and the PBM. For instance, after the casting of concrete, lighter fine material is left on the upper surface. This is removed by sand or shot blasting [33], simultaneously removing smaller air bubbles which might have formed just below the upper surface. The bonding or sealing agent is then applied which fills smaller cracks and holes during its curing, thus creating a strong top layer in the bridge deck to which the PBM can be melted. The SN 640 450 mentions minimum requirements to the quality of the bridge deck before applying a bonding agent.

Examples of modern bonding agents on concrete and steel are bituminous lacker, EP or liquid plastics such as Polymethyl Methacrylate (PMMA) or Polyurea (PUA) [24][33]. PMMA has gained in popularity due to its short curing times, reducing time of construction and dependency of weather in comparison to the EP bonding agent.

In practice, EP is preferred over inert oil as it solvent free, is easy to apply, quality is better controlled and has an excellent adhesion to concrete, higher than 1.5 N/mm^2. It is often applied in two layers, and sand is used to roughen the surface of the bonding layer and to improve shear capacity once the PBM is melted [34].

2.4 Adhesion strength tests

The adhesive tensile strength of the PBM membrane is temperature related [24]. Adhesive tensile capacity of the seals were tested for both PMMA and EP/PBD [17]. Similar tests were also performed with PBM on different bonding agents, mainly inert oil [16]. The adhesive strength of the layup with PMMA was better than that of EP/PBM. Published results mentioned above are compared to experiments performed in this research project (Table 1).

2.5 Shear strength

Shear tests that can prove the suitability of the road layup over the entire service life are not available yet [35]-[37], however, relative comparisons can be made. The most common methods to test the shear strength are based on monotone loading like the Leutner test or the related Advanced Shear Test (AST). Dynamic test methods have been developed but have not found their way yet into international standardization, yet [38].

Shear capacities between SLT timber decks and asphalt wearing surfaces were tested using specimens of 115 mm x 175 mm (square specimens) [15]. These were simultaneously loaded by a normal load. Similar tests, without normal load, were performed with samples of 200 mm x 200 mm, both on substrate materials of LVL and CLT [17]. Specimens with PMMA waterproofing membrane were stiffer in shear than those with PBM seals, but also showed a brittle fracture behavior, too. There were no measurable differences between the shear response of the MA on concrete, steel, and wooden panels when a PBM waterproofing membrane was used. The Leutner test (150 mm and test at speed of 50 mm/min) was used to test the shear strength of MA on concrete using different types of PBM membranes [35]. Published results from both sources are presented in Table 2, together with experimental results from tests performed in this research.



3 Material and methods

3.1 Variants

CLT, GLT (resembling the setup for SLT), and LVL were selected as representative materials for a timber bridge deck in these experiments. The CLT and GLT were ordered using C24 strength calss boards of spruce and pine. The surface qualities differed from: (1) Quality D/Industry: material failures are visible and not sealed (CLT and GLT). (2) Quality C/Industry+Visible: smooth planed and sanded surface. Material failures are filled and leveled out (CLT). To simulate cases where bridges decks had higher moisture content, for instance if repair work needed to be carried out, some panels were climatized to achieve humidity of 18%-m and 24%-m instead of the more common 12%-m. The panel size was 1.0 m x 1.0 m x 100 mm (length x width x thickness). The moisture of the panels was measured before application of the bonding layer using a GANN Hydromette M4050.

Four concrete slabs with dimensions of 0.8 m x 0.8 m x 100 mm were produced to do reference test.

Wood and concrete panels were sealed with EP (Sikadur® -188) [34] and PMMA (ALSAN REKU P70 [39] and Eliminator Par1 [40]). The EP was applied in two layers of about 500 g/m^2 each, and sand was mixed into the first layer. The PBM was the SOPRALEN IMPACT MA/AC Flam with a thickness of 5 mm. The PMMA waterproof sealings were applied on the PMMA bonding agents too [41]. MA8 and MA11 was applied in layers of 25 mm and 40 mm, respectively. Only in one case, the MA11 was applied with 230 °C, in all other cases between 190 °C and 200 °C.

3.2 Adhesive bonding test

The adhesive bond was tested according to the SN EN 1542 [42], using stamps of 50 mm in diameter per variant. The adhesive bonding test was performed on (1) the primer, (2) the combination of primer and waterproofing membrane, and (3) the combination of primer, waterproofing membrane, and base layer of asphalt. In each test, the weakest layer was expected to fail. The standard requires that the average capacity of three tests must be higher than 1.5 N/mm^2 on the bonding agent, but is temperature dependent on the waterproofing membrane, for instance 0.46 N/mm^2 at 20 °C.

3.3 Leutner and Advanced Shear Test

Leutner and AST tests are performed using cylinders cut from the road of 150 mm diameter. In the AST, a normal load is applied to the road surface, too, to realistically simulate the forces of a braking vehicle on the road layup [33][35] (Figure 2). The normal load during execution of the AST is applied using loaded springs, so the normal load decreases or increases as the surface deforms in normal direction. Experiments were performed with a 10 kN normal load.

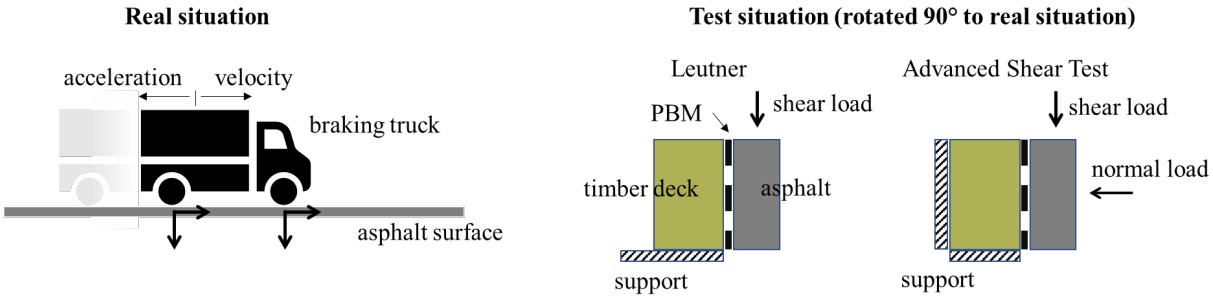


Figure 2: Illustrated difference between real situation and simplified situation and load application during Leutner and ADS test

3.4 Temperature measurements

The temperature levels in different layers of the timber panels during application of the MA are unknown. The temperatures in multiple layers of the road layup and timber panel were measured in both P31 and P32, where MA8 and MA11 were applied, respectively. Figure 2 shows the position of the sensors on the PBM waterproofing layer, in the EP bonding agent, and in the middle of the four upper layers of the CLT panel (five layers 20 mm thick). Before application of the asphalt, the temperature in the asphalt heater was measured using a Metra© Asphalt Thermometer.

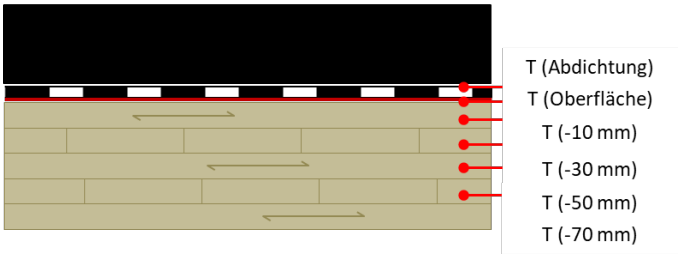


Figure 3:Instrumentation of panels P31 and P32 with temperature thermocouplee type K-sensors.

3.5 Glass transition temperature

The glass transition temperature T_g helps to determine the temperature when the phase of materials changes, e.g., from solid to liquid. The method measures the difference in the amount of heat required to increase the temperature of a sample. This point was determined for both the EP and PMMA using the Differential Scanning Calorimetry (DSC) method.

4 Results

4.1 Climate conditioning of the timber panels

Panel P03 and P11 were obtained straight from the production line and had a moisture content below 12%-m. The rest of the panels were climatized and humidity was achieved to a satisfactory level of the target values of 12%-m, 18%-m and 24%-m. The humidity of the concrete panels was higher than targeted (3%-m), but within the limits of application of the bonding agents (Table 1).

Table 1: Average values of the adhesive bonding tests on the primer, the membrane, and asphalt with panel humidity and testing temperature (where relevant and available)

panel	primer/ waterproofing	humidity	adhesive capacity primer	adhesive capacity membrane (temperature)	adhesive capacity asphalt (temperature)
P11 (CLT) P31 (CLT) P51 (SLT) K6 (LVL)	EP/PBM	9.8%-m 13.9%-m 12.4%-m 16.1%-m	3.5 N/mm² 3.9 N/mm² 3.5 N/mm² 1.7 N/mm²	1.17 N/mm² (13.0 C) 1.21 N/mm² (21.7 C) - 1.21 N/mm² (22.0 C)	0.97 N/mm² (15.0 C) 1.03 N/mm² (23.9 C) - 1.00 N/mm² (23.8 C)
P41 (CLT) K2 (LVL)	EP/PBM	19.4%-m 18.1%-m	4.9 N/mm²	1.25 N/mm² (21.4 C)	1.07 N/mm² (24.0 C) 1.03 N/mm² (24.1 C)
P1 (CLT) K1 (LVL)	EP/PBM	21.2%-m 24.1%-m	2.3 N/mm² -	0.64 N/mm² (21.3 C) -	- 1.00 N/mm² (24.2 C)
P03 (CLT) P38 (CLT) K3 (LVL)	PMMA/PMMA	8.8%-m 13.7%-m 16.4%-m		3.3 N/mm² 4.0 N/mm² 1.8 N/mm²	
P22 (C)	EP/PBM	3.8%-m	4.25 N/mm²	1.28 N/mm² (13.0 C)	
P24 (C)	PMMA/PMMA	4.0%-m		4.25 N/mm²	
Different [15]				Between 0.40 N/mm² and 0.55 N/mm²	
CLT [17] LVL [17]	EP/PBM			0.33 N/mm² 0.43 N/mm²	
CLT [17] LVL [17]	PMMA/PMMA			1.41 N/mm² 1.12 N/mm²	

4.2 Adhesive bond

The adhesive tensile capacities of the different layers are observed in Table 1. The table lists the panel number, the material, the humidity and average adhesive capacity of the different layers. Wherever relevant, logged temperatures of the panels, are listed, too.

The following results are formulated: (1) All the minimum capacities (of bonding agent, membrane, and MA) were met, (2) the panel humidity has little effect on the capacity of the bonding agent, (3) the tensile capacity of the bonding agent on LVL panels is systematically lower than that of the CLT and SLT panels, and (4) capacity on the timber panels and on the concrete panels is similar.

During the testing of the adhesive capacity of the primer, the glue between stamp and primer sometimes failed instead of the bond between primer and substrate itself. Adhesive bonding values for the combination of EP/PBM are better than those measured by [17] (temperature unknown). For the PMMA waterproofing membranes, values are similar.

4.3 Shear capacity

The shear capacity of six different layups is shown in Figure 3. The comparison of the results to values found in literature and mentioned in the state of the art is made in Table 2. From the six diagrams, two important conclusions can be drawn:

- Whether the panel is made of CLT, SLT/GLT, LVL, or concrete, the resistance is determined by the combination of bonding agent and waterproofing membrane. No dilitation of any layers in the layups was observed, i.e. EP/PBM connected exellent to the substrate or MA even though it was applied with low temperature (190 °C)
- Using either EP/PBM or PMMA determines the properties of the development of shear resistance, hence weak and plastic or strong and brittle, respectively.

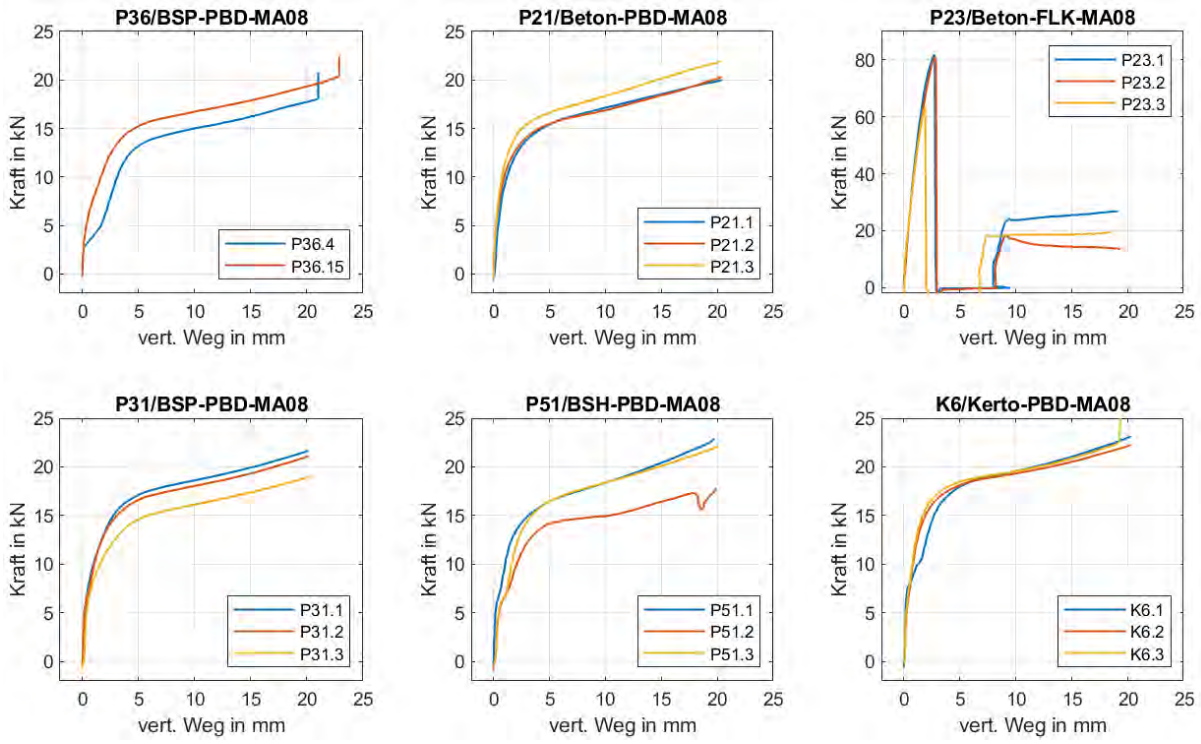


Figure 4: load displacemnt diagrams of different road layups



Table 2: Measured capacity of shear bond

	Pousette (1998)	**Müller und Scharmacher (2013)**	**Raab und Partl (2014)**	**AST (deformation 10 mm)**	**AST (deformation 10 mm)**
	literature	**literature**	**literature**	**experiment**	**experiment**
Specimen size	115 mm x 175 mm	200 mm x 200 mm	Ø 150 mm	Ø 150 mm	Ø 150 mm
Load application	10 mm/min	5 mm/min	50 mm/min	1 mm/min	50 mm/min
Normal load (perp. to layup)	0.7 N/mm^2	no	no	10 kN	10 kN
Substrate	Timber	Timber	Concrete	Concrete	Timber
Capacity [kN]			10.6 kN	5 kN	15.9 kN to 18.0 kN
Capacity [N/mm^2]	0.17 to 0.23 N/mm^2	0.2 N/mm^2	0.60 N/mm^2	0.28 N/mm^2	0.90 to 1.26 N/mm^2

The shear strengths obtained in experiments compare well with the results of Raab and Partl [36], with shear strengths between 0.4 N/mm^2 and 0.7 N/mm^2 (SBS-PBM). However, those drill cores were tested without any normal load (Leutner test). Results depend on speed of load application too, those with low speed (1 mm/min) have about 3.6 lower resistances than those at high speed.

4.4 Blistering of the MA after application of the base layer

Most of the MA was applied with target temperature of 190 °C. Nevertheless, blistering could not be avoided, and was sometimes even provoked on purpose. The extent of the blistering was determined visually. They usually appeared within 10 minutes after application of MA. The following conclusions apply to these tests:

- on the concrete panels, regardless of EP/PBM and PMMA waterproofing system, no blisters appeared.
- In CLT and LVL panels with PMMA waterproofing systems blisters appeared in panels with the eliminator® and ALSAN® products.
- The CLT panels sealed with bituminous products and PBM, very large blisters developed.
- The CLT panels with poor surface quality (industry) and EP/PBM sealing systems, several larger blisters appeared.
- In the CLT panels with good surface quality (industry visible) and EP/PBM sealing systems being, no blisters appeared using either MA08 or MA11 below 200 °C.
- In the SLT panels with industry quality and EP/PBM sealing systems no blisters appeared in the panels with MA08, and only small blisters appeared in the panel with MA11. These could theoretically be repaired on-site.
- In the LVL panels with normal quality and EP/PBM sealing systems, no blisters appeared.

Summarizing, this means that although PMMA systems function well on concrete, these do not work well on timber. EP/PBM systems work on wood, but only if a good surface quality is used. Moisture of the timber panels did not show a visible difference in blistering: on the LVL panels no blisters were visible whereas these were on all the CLT panels. Finally, there was a tendency of panels with MA11 (40 mm) had more blisters than those with MA08 (25 mm).

4.5 Temperature developments in P31 and P32

Temperature measurements in panels P31 and P32 during and after application of the asphalt are seen in presented in Figure 4. The measurements made in the different layers during the application of MA8 (P31, MA temperature 188 °C) and MA11 (P32, MA temperature 194 °C). The temperature of the panels right before application of the asphalt was. The following observations are made.



- The maximum temperature in the sealing of both panels lies at 105 °C (P31) and 109.5 °C (P32). It is noted that the temperature of the panels was nearly equal (22 °C and 21 °C, respectively) and that of the MA11 asphalt was only 6 °C higher than that of the MA08.
- The development of the temperature in both panels is similar, although stretched in P32 (MA11) compared to P31 (MA8).
- The differences between the temperatures measured in the sealing and 10 mm deeper into the wood panel are 30 °C (3.5 °C/mm in the P31 and 4.0°C/mm in P32). Shortly after application of the MA, these are higher because the development of heat in the wood material is delayed.

4.6 Glass transition temperature

The *Tg* for both tested bonding agents was difficult to determine, as the energy required for the phase change was very small. For the PMMA (3% Catalysator), a Tg (at 139°C) and with the EP, a *Tg* of 94 °C, was measured.

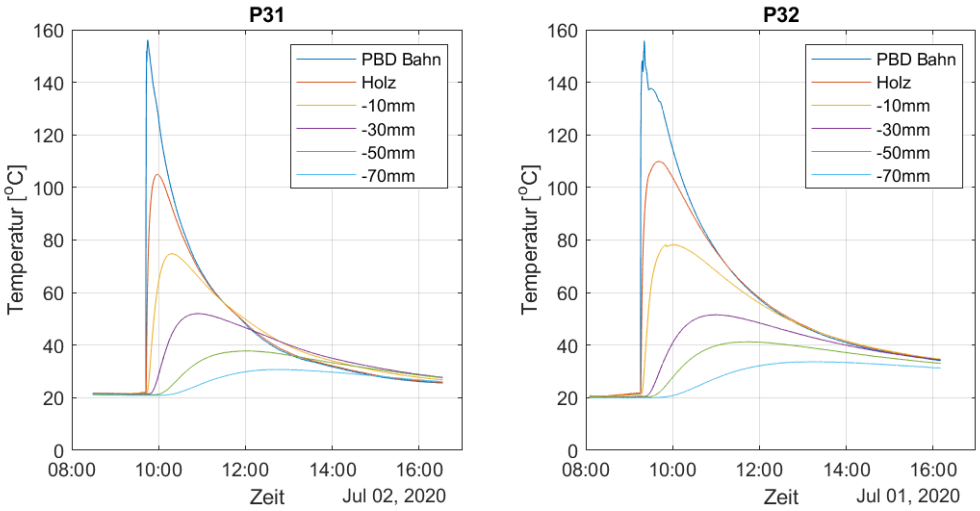


Figure 5: Developement of temperatures in different layers of panels P31 and P32 during the application of asphalt MA8 (25 mm) and MA11 (40 mm).

5 Discussion

5.1 Adhesion capacity

The adhesion capacity of different sealing systems met requirements set by standards and compared well with values found in literature. Above 18%-m a slight reduction in adhesion strength was observed, but not to the extent that values failed the minimum requirements. This suggests that the connected layup can also be applied on existing timber bridges where moisture contents are higher than during construction. The adhesion strength of the bonding agent on LVL was lower than that on CLT, plausibly be due to the peeling of the veneers in the production of LVL where small micro-cracks develop in the wood.

Whether set by standard or found in literature, tensile capacity is higher than the characteristic tensile strength perpendicular to the grain 0.45 N/mm^2 set by the SN 14080 [43] or the design strength perpendicular to the grain of 0.15 N/mm^2 set by the SIA 265 [44]. It is reasonable to assume that there is a volume effect. The above-mentioned values are used for a reference volume of 1 dm^3, whereas the diameter of the stamp is in only 50 mm and the tested volume is at best a tenth of that (0.1 dm^3, 50 mm diameter and 50 mm depth).

5.2 Shear capacity

Although brittle, the shear capacity of PMMA showed outstanding results on concrete panels, up to 70 kN with a cylinder of 150 mm diameter. On either CLT or LVL, these layups could not be produced due to extensive blistering. On sealing systems using EP and PBM, the shearing behavior on CLT, SLT/GLT, and LVL panels was equal to that observed on concrete panels. There seems to be no reason for concern in shear capacity of the bond.



5.3 Temperature

Earlier work recommends base layers of MA8 (25 mm) only, because MA11 (40 mm) base layers lead to significantly higher input of energy and temperature. It is relevant to note that inert oil was used as a bonding agent in those tests [16]. However, a comparison of the temperature developments measured in P31 and P32, only showed a couple degrees difference in maximum temperatures in the bonding agent. Such temperature measurements have not been made up to now.

A comparison of the measured temperatures with the glass transition temperatures is perhaps more interesting. At a *Tg* of 95 °C, EP already enters the liquid phase. However, during experiments, only a softening of the EP was visually observed on chips of material left around the panels after application of the bonding agent. The question is raised if the 4.5 °C (105 °C MA8 and 109.5 °C at MA11) difference is really decisive for the EP, in such a way that it is absolutely not recommended to use MA11. The transition from the solid to the liquid phase is smooth, perhaps so smooth that the determination of the *Tg* here is probably more of an estimate. The *Tg* on the concrete panels is perhaps never passed.

In measurements which were not presented here, the *Tg* of PMMA are almost reached as well. The temperatures in the bonding layers were at least 35 °C higher than on the EP/PBM layup. It is reasonable to assume too, that the pressure of vapour gas developed in the top layer of the wood was higher, too.

Calculated temperature gradients were around 3.5 °C/mm, meaning that that the high temperatures only develop in the first couple of millimeters of the wood panel.

5.4 Blistering

Blisters always appeared on wood panels with poor surface quality, regardless of the type of bonding agent. It is recommended to use CLT panels with high surface quality where the edges of the boards are glued to each other too. Using SLT or LVL, production quality was sufficient, but still, it is recommended to monitor the presence of cracks, knots, holes, etc., and if necessary seal these before application of the EP primer.

On concrete, long-term blistering is often observed after two or three years [29][30]. This was also observed in timber bridges in Sweden [25] where other bonding agents were used. No blisters are yet observed on the Obermatt bridge, even after 13 years where an EP primer and PBM was used.

5.5 Compatibility of PMMA with resin

PMMA would not cure when terpenes (resin pockets and knots), were present in wood. This makes it practically impossible to use PMMA, unless a primer or method can be found to bind or fix these terpenes before the PMMA is applied.

6 Conclusions

MA surfacing on timber wood panels can be made under the following conditions:

- Good wood-panel surface quality. On CLT, this means that Quality C is a minimum, in SLT/GLT or LVL, production quality (D) is generally sufficient.
- Only EP as a bonding agent, applied in two layers, as prescribed by the SN 640 450 can be used.
- Adhesive bond test showed that a minimum average value of 1.5 N/mm^2 per three stamps can be expected, although it exceeds the characteristic tensile capacity perpendicular to grain.
- The adhesive bonding properties of EP are not affected by moisture below 18%-m and only minimally reduced above 18%-m. Hence, EP can also be applied on existing bridges when repair work is needed.
- Equal shear resistances are obtained when using wood or concrete bridge decks in the above-mentioned layups.
- Temperature in the bonding agent needs to be kept low. MA is to be applied with a temperature below 200 °C, both in MA8 or MA11. Risk for blistering can slightly be reduced, for instance on warm days, with MA8 in a base layer of 25 mm thickness. Any surface irregularities in the first layer of the MA are eliminated once the intermediate or top layer is applied again.

Further development of PMMA systems is recommended. Application could alternatively be used if upper layers of bridge decks are made in hardwood for instance, where no terpenes are present. The system with the highest potential for application on wood was the ELIMINATOR® system. Apart from short curing



time, the sealing of PMMA is much harder than that of PBM, which increases service life of frequently crossed bridges such as in highways (>50000 vehicles a day).

During application of the base layer of MA, the maximum temperatures achieved in the bonding agent are slightly higher than the *Tg*. The extent of the softening of the bonding agent is to be investigated further.

To reduce the risk of delays on the construction site due unfavorable weather, it is recommended to seal bridge decks already in a production hall. Joints can be sealed on site.

Experience with asphalt surfacing on timber bridges is gained by building an applying these systems in real bridges. Roadway authorities are asked to provide objects where these systems can be applied and monitored. This also allows to investigate the properties of long-term blistering and compare these to bridges made in concrete for instance.

7 Acknowledgement

The research was performed in the scope of grant VSS 2016/326 ‘Abdichtungssysteme und bitumenhaltige Schichten auf Brücken mit Fahrbahnplatten aus Holz’ by the Swiss Highway Authority ASTRA.

The steering committee headed by Fred Stalder-de Marco is also gratefully thanked for their input. The input of experience of practitioners was vital to the success of the project.

The employees of Aeschlimann AG, especially Kurt Andres, Peter Schmid, and Roman Schaerer, are thanked for their contribution of material, their patience in responding the many questions posed by the project team.

8 References

[1] Kleppe, O. and Aasheim E (1996), Timber Bridges in the Nordic Countries, National Conference on Wood Transportation Structures, Madison, USA, 23 October 1996

[2] Buholzer H, and Fuchs D. (2018), Historische Holzbruecken der Schweiz bis 1850, Edition Salus, Switzerland, ISBN 978-3-03-3-7490-3

[3] Quartier, C. (2013), Ce qui racontent les ponts couverts en Suisse (et d’ailleurs), Favre, Switzerland.

[4] Stalder F. And Meyer HU (2000), Neue Holzbruecken, Wettbewerb fuer die Erneuerung von Vier olzbruecken im Oberen Emmental, Tiefbauamt des Kantons Berns, Oberingenieurkreis IV, Burgdorf, Switzerland

[5] Bachofer, R. and Conzett J. (2013) Brucken in Holz: MOeglichkeietn und Grenzen, Forschungsprojekt AGB 2003/012, Schweizer Verband der Strassen – und Verkehrsfachleute VSS, Switzerland.

[6] Hosteng T., Wacker J., Phares B. (2013) Condition Assessment of Iowa Timber Bridges Using Advanced Inspection Tools, International Conference on Timber Bridges, Las Vegas, Nevada USA

[7] Pousette A., Malo KA., Thelandersson S., Fortino S., Salokangas L., Wacker J. (2017) Durable Timber Bridges, Final Report and Guidelines, Research Institute of Sweden, SP report 2017:25

[8] Protected Timber Bridges (ProTimB) (2019), Entwicklung einheitlicher Richtlinien für den Entwurf, den Bau, die Überwachung und Prüfung geschützter Holzbrücken, Fachhochschule Erfurt, Germany

[9] Mahnert K.C., Hundhausen U. (2018) A review on the protection of timber bridges, wood material science and engineering, Vol. 13, pp. 152–158

[10] Oliva, M., Dimakis, A., Ritter, M., Tuomi, R., (1990) Stress-laminated wood bridge decks: experimental and analytical evaluations. Res. Pap. FPL-RP-495. Madison, WI: U.S. Department of Agriculture, Forest Service, Forest Products Laboratory.

[11] Miebach. F. (2018) Design ideas for solid timber bridges, Wood Material Science & Engineering, 13:3, 184-189,

[12] Crocetti R., Ekholm K., Kliger R. (2015) Stress-laminated-timber decks: state of the art and design based on Swedish practice, Eur. J. Wood Prod.

[13] Massaro F., Malo KA. (2020) Stress-laminated timber decks in bridges: Friction between lamellas, butt joints and pre-stressing system, Engineering Structures 213

[14] Seidel, A., Miebach, F. and Osterloff, L. (2019) Entwurf von Holzbrücken, Holzbau Handbuch (Series 1, Part 9, Issue 1). Informationsdienst Holz (Bonn, Germany).

[15] Pousette A. (1997), Wearing surfaces for timber bridges, Nordic Timber Council, ISBN 91-89002-12-1

[16] Milbrandt E. and Schellenberg K. (1998) Eignung von bituminösen Belägen für Holzbrücken – Schlussbericht. Forschungsauftrag E96/7, Entwicklungsgemeinschaft Holzbau (GH) in der Deutschen Gesellschaft für Holzforschung e. V., München, Germany

[17] Müller A. and Scharmacher F. (2012) Asphaltbeläge für Strassenbrücken aus Holz, Conference Proceedings IHB, Bad Wörishofen, Germany



[18] Müller A., Angst C., Bueche N., Schiere M., Huber L., Bonifacio S., Maurer J. (2021), VSS2016/326 Abdichtungssysteme und bitumenhaltige Schichten auf Brücken mit Fahrbahnplatten aus Holz, Bern University of Applied Sciences, Institute of Timber Construction, Structures and Architecture, Biel, Switzerland

[19] Simon A., Jahreis, M., Koch. J., and Arndt R. (2017), New design guidelines for structural protected timber bridges, 3rd International Conference on Timber Bridges 2017- Skellefteå, Sweden

[20] Franke, B., Franke, S. and Müller, A. (2014) Case studies: long-term monitoring of timber bridges. Journal of Civil Structural Health Monitoring, 5, 195–202.

[21] Franke, B., Franke, S., Schiere, M., Müller, A. (2019) Quality assurance of timber structures – research report, Bern University of Applied Sciences, Switzerland, ISBN 978-3-906878-04-1.

[22] Augenstein, M., Dittrich, W. and Goehl, J. (2000) Details für Holzbrücken. In Holzbau Handbuch (Series 1, Part 9, Issue 2). Informationsdienst Holz (Bonn, Germany).

[23] EN 12970 (2000) Mastic asphalt for waterproofing. Definitions, requirements and test methods, European Committee for Standardisation, Brussels, Belgium

[24] SN 640 450 (2017) Abdichtungssysteme und bitumenhaltige Schichten auf Brücken mit Fahrbahnbelägen aus Beton, Swiss Association for Standardization, Switzerland

[25] Pousette A. (2016) Tätskikt och kantlösningar på tvärspända brobaneplattor av trä, SP Rapport 2016:90, SP Sveriges Tekniska Forskningsinstitut

[26] VSS 40 451 (2019) Abdichtungssysteme und bitumenhaltige Schichten auf Brücken mit Fahrbahnbelägen aus Holz, Schweizerischen Verbands der Strassen- und Verkehrsfachleute (VSS)

[27] Fritz H. and Zolliker J (1996) Brueckenabdichtungen und Bodenlage, Untersuchung verschiedener Systeme in der Schweiz, FA 26/79, Schweizerischen Verbandes der Strassen-und Verkehrsfachleute (VSS)

[28] Hailesilassie B. and Partl M. (2013) Adhesive blister propagation under an orthotropic bituminous waterproofing membrane, Construction and Building Materials 48, p. 1171–1178

[29] Partl M. and Hailesilassie B. (2014) Research Package on Bridge-deck Waterproofing Systems: EP5-Mechanisms of Blister Formation, research report VSS 2006/515, Schweizerischen Verbandes der Strassen-und Verkehrsfachleute (VSS)

[30] Hailesilassie B., Hean S. and Partl M. (2013) Testing of blister propagation and peeling of orthotropic bituminous waterproofing membranes, Materials and Structures (2015) 48:1095–1108

[31] TBA Bern (2007), Projektdossier

[32] Nievergelt A. (2020) Personal correspondance M. Schiere, 22/12/2020

[33] Hean S. And Partl M. (2006), Erfassung massgebender Einflussfaktoren bei Brueckenabdichtungssysteme mit Bitumenbahnen, Forschungsauftra AGB 1998/201, Schweizerischen Verbandes der Strassen-und Verkehrsfachleute

[34] Sikadur® -188 Product data sheet, www.sika.com, accessed 12/5/2021

[35] R. Leutner (1979): Untersuchungen des Schichtenverbunds beim bituminösen Oberbau. Fachartikel. Bitumen 3/1979

[36] Raab C und Partl M (2014) Forschungspaket Brückenabdichtungen: EP1. Standfester Gesamtaufbau, Prüfung und Bewertung, Forschungsprojekt VSS 2006/511, Schweizerischen Verbandes der Strassen-und Verkehrsfachleute

[37] Zofka A., Maliszewskia M., Bernier A, Josen R., Vaitkus J, and Kleizienė R (2015) Advanced shear tester for evaluation of asphalt concrete under constant normal stiffness conditions, Road Materials and Pavement Design, DOI: 10.1080/14680629.2015.1029690

[38] Angst C. (2015) Forschungspaket Brückenabdichtungen: EP3 – Langzeitverhalten des Verbundes, Forschungsprojekt VSS 2006/513, Schweizerischen Verbands der Strassen- und Verkehrsfachleute (VSS)

[39] ALSAN REKU P70 product data sheet, www.soprema.com, accessed 12/5/2021

[40] Eliminator® product data sheet, www.gcpat.com, accessed 12/5/2021

[41] ALSAN P773 product data sheet, www.soprema.com, accessed 12/5/2021

[42] EN 1542 (1999), Products and systems for the protection and repair of concrete structures - Test methods - Measurement of bond strength by pull-off, European Committee for Standardisation, Brussels, Belgium

[43] SIA 265 (2021), Holzbau, Swiss Association for Standardization, Switzerland

[44] EN 14080 (2013), Timber structures – glued laminated timber und glued solid timber - requirements, European Committee for Standardisation, Brussels, Belgium

Conference Proceedings 4th ICTB (2022)
https://doi.org/10.24451/1pdk-8v72

ICTB 2021 PLUS
4th International Conference on Timber Bridges
Biel/Bienne, Switzerland, 9 -12 May 2022



Setting the Standard – Advancements in Wood Bridge Design in the Canadian Highway Bridge Design Code

Andrew Lehan[1], David Moses

1 Abstract

The Canadian bridge design standard is being updated to account for the growing interest in mass timber construction and to allow for evolving and emerging wood bridge technologies. Governments and technical bodies are responding to this interest through the provision of funding and improvements to design standards. The Ontario Wood Bridge Reference Guide was recently published to promote the use of wood in bridges. The CAN/CSA-S6-19 Canadian Highway Bridge Design Code (CHBDC) governs the design of vehicular and pedestrian bridges in Canada. Section 9 of the CHBDC covers the design of wood bridges. The technical subcommittee for Section 9 is working to advance the code to reflect the state-of-the-art in wood bridge design. Initial advancements were made to the current 2019 edition of the CHBDC. The subcommittee is actively working on advancements for the forthcoming 2025 edition in the areas of shear design for glued-laminated timber beams, the load-sharing factor, glued-laminated timber deck panels, wood-concrete composites, camber requirements for glued-laminated timber beams, and pedestrian contact with preservative-treated wood. These advancements are expected to encourage further use of wood in bridges by providing guidance on evolving and emerging wood bridge technologies. This paper presents the on-going work of the subcommittee.

2 Introduction

After years of waning popularity, there is once again an interest in wood bridge construction in Canada, particularly where mass timber technologies are utilized. These technologies have seen markedly increased usage in construction applications in recent decades, including wood bridge construction, due to reasons of environmental sustainability and local economic development opportunities [1]. Canadian governments and technical bodies have helped perpetuate this increased usage through provision of project-specific funding and research funding, the creation of educational materials, and improvements to design standards.

Natural Resources Canada (NRCan), which is responsible for natural resources at the Canadian national level, has helped lead the way with respect to project funding. In 2017, they created the "Green Construction Through Wood" (GCWood) program to provide $39.8 million in industry funding to promote a "more wood-inclusive construction industry" [2]. Some of this funding was aimed at promoting wood bridge demonstration projects for spans over 20 m [3]. NRCan published their State of Mass Timber in Canada report in 2021 [4]. It included an online database to track planned, on-going, and completed mass timber bridge projects. Per the database, a total of 28 wood bridge projects had been undertaken, with almost all of them complete [5].

In 2017, Ontario Wood WORKS!, the Canadian Wood Council (CWC), and the Ontario Ministry of Natural Resources and Forestry collaborated to commission the Ontario Wood Bridge Reference Guide (OWBRG) [6]. The guide was co-authored by practicing consulting engineers with wood bridge expertise from both Moses Structural Engineers and Entuitive. It contains three sections concerning design best practices for wood bridges, current opportunities and limitations of wood bridges, and two fully worked wood bridge superstructure design examples. The purpose of the guide was to promote new wood bridge construction in Canada through design education, noting that Canadian engineering educational programs tend to be much stronger in teaching steel and concrete design than wood design. The guide was also seen as a modern augmentation of the Canadian Institute of Timber Construction's 1970 "Modern Timber Bridges" publication [7] and the CWC's 1992 "Wood Highway Bridges" publication [8]. These documents, while popular at one time, were no longer reflective of mass timber technologies and advancements in wood bridge design. Staff from the United States Forest Products Laboratory were particularly helpful in communicating advancements in timber bridge design when it came to authoring the design examples for the guide.

To compliment the OWBRG, NRCan and the CWC have commissioned Wood Research and Development (WRD), a wood engineering design and inspection firm, to author the Timber Bridge Maintenance and

[1] Andrew Lehan, Senior Engineer, Entuitive, Canada, andrew.lehan@entuitive.com



Restoration Detailing Guide. This forthcoming publication will provide guidance on the inspection, maintenance, and restoration of existing timber bridges. This guide, along with the OWBRG, are intended to provide the necessary engineering design knowledge for brownfield and greenfield wood bridge sites, respectively.

In response to the renewed interest in timber bridges, the CAN/CSA-S6-19 Canadian Highway Bridge Design Code (CHBDC) [9] and its accompanying commentary [10] are being updated to reflect the state-of-the-art in wood bridge design. The CHBDC is the national design standard for new and existing bridges in Canada. It has been adopted by all Canada's provinces and territories, except for Manitoba, which instead uses the AASHTO LFRD Bridge Design Specifications [11]. The CHBDC is a limits states design code. It covers design loadings, load combinations, structural analysis, and detailed design criteria for bridge engineering materials and components. The current format of the code followed from the amalgamation of the CAN/CSA-S6-88 Design of Highway Bridges standard and the OHBDC-91-01 Ontario Highway Bridge Design Code in the year 2000. The current format has been published in 2000, 2006, 2014, and most recently in 2019. The next publication is intended for 2025.

Section 9 of the CHBDC is dedicated to wood structures. This section is maintained by a technical subcommittee comprised of subject matter experts ("the subcommittee"). Members include representatives from various levels of government, academia, consulting, and industry. The subcommittee membership has entirely turned over in the past decade, with no members remaining from the 2006 edition of the code and only three members remaining from the 2014 edition of the code. The previous membership had remained relatively stable for decades, with that membership ("the previous subcommittee") having contributed to the CHBDC the state-of-the-art in wood structures design from the 1970s through to the 1990s. The current membership is currently working to reflect modern advancements in wood design and mass timber technologies for the forthcoming 2025 edition of the code. Areas of primary focus include shear design for glued-laminated timber (glulam) beams, the load sharing factor, glulam deck panels, wood-concrete composites, camber requirements for glulam beams, and pedestrian contact with preservative-treated wood. The purpose of this paper is to communicate the technical content advancements that the subcommittee is pursuing in these topic areas for the 2025 edition of the code.

3 The 2019 Code Cycle

Before 2019, Section 9 of the CHBDC had remained relatively unchanged since the CHBDC was adopted in its current format in 2000. With the Section 9 subcommittee membership having turned over largely during the 2019 code cycle, there was opportunity for updating and introducing new content into Section 9. The following advancements were made during that code cycle:

- Specified material properties and resistance equations were revised to be consistent with CSA O86-19 Engineering Design in Wood standard [12] (CSA O86);
- New glulam material properties were introduced;
- Preservative treatment requirements were updated to reflect current industry standards;
- Structural composite lumber properties were deleted; and,
- Provisions were introduced for glulam deck panels.

Canadian structural engineers are typically taught wood design based on CSA O86, which is the wood design standard for buildings and associated structures. Very few engineers are taught wood design per the CHBDC. As such, the subcommittee sought to make the specified materials properties for sawn wood and glulam timber in the bridge code consistent with main wood design standard CSA O86. For unknown reasons, the previous subcommittee had long ago published specified material properties in the CHBDC that had implicitly been modified for service condition, a factor that accounts for strength and stiffness reduction as a function of wood moisture content. The resistance equations in CSA O86 account for service condition using an explicit factor that the designer can select. To avoid confusion between codes, the subcommittee decided to extract the implied service condition factor from the specified material properties published in the CHBDC so that the properties would be the same as published in CSA O86. In doing so, the service condition was introduced to several resistance equations in the CHBDC. Furthermore, some of the symbols and variables in the CHBDC resistance equations were modified to be consistent with CSA O86. The idea was to make the CHBDC a more comfortable code to use for wood designers who would be accustomed to CSA O86.

The 2019 CHBDC saw the introduction of material properties for glulam comprised of spruce, lodgepole pine, and jack pine. These species are common in the interior of Canada. Including material properties for



their use in glulam members was intended to promote further use of glulam, and to provide new economic development opportunities for locales with an abundant supply of those species. The superstructure design example included in the 2017 OWBRG were based on these properties for the same reasons.

Minor changes were made to the preservative treatment requirements in the 2019 CHDBC. In particular, different types of alkaline copper quaternary (types A, C, and D) were permitted for use. The more important changes were in the CHBDC commentary, where a greater explanation was given regarding the function of preservatives, the relationship between wood moisture content and decay, environmental considerations when selecting a preservative treatment, and the impact of climate change on the rate of decay and likelihood of insect attack by termites.

Until 2014, the Section 9 of the CHBDC had included material properties for structural composite lumber (SCL). After review of this technology, the subcommittee decided to delete the SCL material properties from the code because SCL is often proprietary and material properties tend to vary between manufacturers. Going forward, a designer will have to select an SCL product upon which to base their design. Doing so will ensure that correct material properties are used.

Glulam deck panels were introduced into the CHBDC in 2019. These decks were invented in the 1970's at the United States Forest Product Laboratory in Madison, WI [13] [14]. Despite their popularity in American wood bridge applications, their use had been rare in Canada until the past decade. In the 1970's and 1980's, Canadian wood bridge research efforts had been focussed on the invention and development of stress-laminated wood decks [15] [16] [17] [18] [19]. At present, increased glulam production and ease of installation relative to nail-laminated and stress-laminated wood decks have made glulam deck panels an attractive decking solution. To reflect this shift in popularity, the subcommittee introduced provisions to assist designers with glulam deck panel design. The changes were not completed in time for the 2019 code cycle. Consequently, further provisions are expected for the 2025 code, as explained below in section 4.3.

4 Forthcoming Advancements to the CHBDC

This section of the paper explains in detail the technical topics that the subcommittee is investigating for inclusion in the 2025 edition of the CHBDC. References are made to other national-level wood design standards including CSA O86, the AASHTO LFRD Bridge Design Specifications [11] (AASHTO), the American Wood Council's National Design Standard for Wood Construction [21] (NDS), the Eurocode 5: Design of Timber Structures standard [22] (Eurocode 5), the Australian AS 5100.9:2017 Bridge Design Part 9:Timber standard [23] (AS 5100.9:2017), and the American Railway Engineering and Maintenance-of-Way Association's Manual for Railway Engineering [24] (AREMA).

4.1 Shear Design of Glulam Beams

At the conclusion of the 2019 code cycle, the subcommittee identified the shear design of glulam beams as a topic to be improved upon for the 2025 code. Issues with respect to the specified shear stress for Douglas-fir, the volume shear effect, and the size effect factor applied for in-situ evaluation of glulam beams were identified as particular topics for improvement. The following sections explain the forthcoming improvements.

4.1.1 Specified Shear Strength

As aforementioned, before the 2019 CHBDC, the specified material properties for glulam beams included an implied service condition factor. The previous subcommittee had embedded this factor into the material properties to account for strength and stiffness reductions due to wet service conditions. The limits states editions of CSA O86 historically featured this factor as well, but it had always been an explicit factor that was part of all resistance calculations. For unknown reasons, the previous CHBDC Section 9 subcommittee decided in 2000 to present specified material properties that were already modified for service condition. For glulam beams, the service condition factors had been applied for "semi-wet" service, an intermediate condition between wet and dry services that was unique to the CHBDC. The semi-wet service condition factor was the average of the wet and dry service condition factors defined in CSA O86. No definition of semi-wet service had been given. The current subcommittee's understanding is that the previous subcommittee believed that the relatively large volume of a glulam beam prevented the beam's moisture content



from becoming increasingly high enough to the point of wet service, implicitly supposing that a designer had suitably detailed the bridge to protect the girders from repeated exposure to direct moisture.

During the 2019 code cycle, the subcommittee elected to adjust all the specified material properties and member resistance equations, symbols, and variables to reflect those in CSA O86. In doing so, the implied service condition factor was removed, thus reverting the specified material properties back to the values presented in CSA O86. However, in removing the implied semi-wet service condition factor for Douglas-fir glulam beams, it was observed that the specified shear strength remained less than what is reported in CSA O86. In CSA O86, that specified shear strength was 2.0 MPa. After removing the implied semi-wet service condition factor of 0.94, the specified shear strength in the CHBDC increased from 1.4 MPa to 1.5 MPa. This difference puzzled the subcommittee during the 2019 code cycle. It was of great interest because the resulting specified shear strength was 75% of the CSA O86 shear strength, a problem that was even more problematic given that the sizing of glulam beams in bridges is often governed by their shear capacity. A sufficient explanation of this difference was not available when the 2019 code was finalized, so the committee decided to keep the 1.5 MPa value on an interim basis until a full review could be conducted and a rational explanation identified.

Significant effort was put into addressing this issue during the 2025 code cycle. A careful review of all previous versions of the CHBDC, CSA O86, and their commentary documents was undertaken. It was ultimately concluded that the lower specified shear strength value used in the 2000, 2006, 2014, and 2019 editions of the CHBDC was the result of this shear stress value not being kept in calibration with advancement made to the shear stress values in CSA O86. It is believed that a 0.75 shear reduction factor may have still been incorporated from the time of working stress design codes, which was before 1984 for CSA O86 and before 1979 for the OHBDC that preceded the CHBDC. It is believed that this shear reduction factor was an outdated empirical factor used to account for reductions in shear strength that were at the time believed to be caused by the presence of knots along the critical shear plane [25]. As demonstrated by Gupta et al. [26], the shear strength of Douglas-fir members is in fact not statistically significantly affected by the presence of knots, therefore rendering the empirical 0.75 times shear reduction factor redundant. Accordingly, the specified shear strength for Douglas-fir glulam beams is intended be increased from 1.5 MPa to 2.0 MPa in the 2025 CHBDC. The subcommittee assessed the impact of this change by comparing the demand-to-capacity ratios for several beams loaded with concentrated loads, with ratios calculated per the CHBDC, CSA O86, AASHTO, AREMA, and NDS. The results using the CHBDC shear resistance equation for a specified shear strength of 2.0 MPa were considered acceptable [25].

The correction of the specified shear strength is of great significance because glulam beams are the most popular mass timber technology used in Canadian wood bridge engineering, and the design of these beams is often governed by their shear capacity. By increasing the specified shear to its proper value, significant economy will be afforded to future designs, allowing them to better compete with steel and concrete alternatives. While the subcommittee is proposing this change, this item has yet to be balloted for approval in the 2025 code.

4.1.2 Shear Resistance

The calculation of glulam shear resistance in CSA O86 is based on the influence of beam volume and loading pattern, as was identified by Foschi and Barrett in the 1970's for Douglas-fir glulam beams [27] [28]. Their research was distilled into a practical design approach in CSA O86 in the form of the "total factored shear resistance" , W_r, which is unique for glulam beams. This resistance accounts for shear stresses along the critical horizontal plane over the entire length of the beam using a variable called the shear-load coefficient, C_v. It is compared to the summation of all vertical loads acting on the member to determine a safe design. This approach is unlike traditional beam design, wherein the maximum factored shear force determined by traditional structural analysis is compared to a shear resistance calculated using elementary beam theory.

When the CHBDC was created in 2000, the previous subcommittee took a different approach of addressing the influence of beam volume and loading pattern on the shear resistance of a glulam beam. Instead of accounting for this influence in the resistance equation like CSA O86, the previous subcommittee instead accounted for it in the demand using a concept referred to as the "shear load". The shear load, V_f, involved integrating the shear force diagram over the entire length of the beam, L, per equation (1),



$$V_f = 0.82\left[\frac{1}{L}\int_0^L |v(x)|^5 dx\right]^{0.2} \quad (1)$$

where $|v(x)|$ is the absolute value of the factored shear force at a section at distance x along the beam. Physically, the shear load is the total horizontal shear force over the entire length of the beam resulting from the applied vertical loading. By using the shear load, the previous subcommittee enabled the glulam shear resistance to be calculated the same as for a sawn wood beam. In essence, by introducing the shear load to the CHBDC, the previous subcommittee reduced the difficulty of the shear resistance calculation relative to CSA O86 but increased the difficulty of the shear demand calculation.

The response to the shear load from the engineering community was generally one of confusion. In our experience, few engineers understood the physical meaning of the shear load and were deterred from undertaking its cumbersome calculation.

To eliminate any confusion surrounding the shear load, the current subcommittee is intending to eliminate the shear load and to implement the shear design approach used by CSA O86 for glulam beams. CSA O86 includes tables of precalculated values of the shear-load coefficient to reduce the difficulty of glulam shear resistance calculations. Table 7.12 of CSA O86, which is for this purpose, specifically includes a series of concentrated loads intended to represent a moving truck load. Unfortunately, the magnitude and relative position of the concentrated loads are different than the design truck loading mandated by the CHBDC. The S9 subcommittee is considering publishing a similar table in the commentary of the 2025 CHBDC to assist designers with the discrete point loads of the CL-625 and CL-625-ONT design trucks that form the basis of live load design in the CHBDC.

4.1.3 Size Effect Factor for Shear

Section 14 of the CHBDC concerns the evaluation of existing bridges. This section contains clauses concerning the resistance of wood members in existing structures. The Section 9 subcommittee was asked by the Section 14 subcommittee to review all Section 14 clauses pertaining to wood. Clause 14.14.1.7.2 concerns the size-effect factor for shear resistance calculations. The factor, k_{sv}, is defined in equation (2),

$$k_{sv} = \frac{75}{\sqrt{d}}\frac{1}{(1+2a/d)} \leq 2.5 \quad (2)$$

where d is the member depth and a is the distance measured from the centreline of the support to the end of a split, if any split were to be present. The intent of this formula was to provide a means of assessing the effect of end splits observed in an existing wood member during a tactile inspection of the structure. The formula was carried over the OHBDC [10] and was first introduced in 1979 [25]. The formula was intended for sawn wood members. It was introduced at a time when glulam usage was rare in Canadian bridges. Sawn wood members are typically installed with high moisture contents. It is understood that they tend to develop end splits and checks as their moisture content reduces through in-situ seasoning. By using the formula, a designer that has physically inspected a sawn wood member can more accurately assess the shear resistance in the presence of any end splits.

The problem with the size effect factor in clause 14.14.1.7.2 is that it is only valid for beam and stringer grade and post and timber grade sawn wood members of Select Structural or No. 1 grade quality. No formula is provided for glulam members. This had led to some confusion amongst engineers. The Province of British Columbia published a supplement to the CHBDC in 2016 [29]. This supplement is intended to augment or override the CHBDC. This supplement overrides clause 14.14.1.7.2, indicating that the size-effect factor is also applicable to glulam members, which the subcommittee has observed to be problematic. The upper limit of 2.5, while appropriate for sawn wood members, produces excessively large shear resistances for glulam members. Accordingly, the Section 9 subcommittee is thinking of providing a size effect formula in clause 14.14.1.7.2 for glulam members, but with a lower upper limit. After review of the formula and comparison with a similar clause in AREMA, the subcommittee found an upper limit of 1.3 to be appropriate for glulam members. This proposed change is being considered by the subcommittee and has yet to be balloted for approval in the 2025 code.



4.2 Load-Sharing Factor

The member resistance equations in the CHBDC feature a variable called the "load-sharing factor", K_m. This factor is an augmented version of the "system factor", K_H in CSA O86. The system factor affords an increase in resistance for member arrangements in which it is unlikely that multiple members have a strength-reducing defect in the same cross-sectional plane. The load-sharing factor in the CHBDC also includes the beneficial effect of a member within a multiple member system to shed load to adjacent members when the individual member is nearing its ultimate failure. This benefit is based on the work of Sexsmith et al. [30] conducted at Forintek in 1979. For that research, laminated beams consisting of multiple 2x10 rough sawn dimension lumber laminations were transversely prestressed using prestressing bars and were tested to failure in four-point bending. The main finding was that the modulus of rupture for the laminated beams was greater than that observed for individual laminations tested to failure, implying non-linear material behaviour. This finding was used by Bakht and Jaeger [31] to develop an analytical procedure that became the calculation of the load-sharing factor in the CHBDC [10].

Table 9.5 of the CHBDC provides intermediate variables that allow for the calculation of the load-sharing factor for various wood systems, including nail-laminated decks, stress-laminated decks, wood-concrete composite decks, and sawn wood stringers. Of note, it does not provide guidance for glulam deck panels nor glulam beams. At present, it is known that some designers are calculating the load-sharing for glulam beams using the approach for sawn wood stringers. This practice is believed to be unconservative because the lesser variability in material properties for glulam relative to sawn wood is likely to limit any strength benefits arising from the presence of defects.

The subcommittee is currently working to develop the load-sharing factor for glulam deck panels and glulam beams. A large testing program is being undertaken by WRD to assist this process. The program is being co-funded by WRD and NRCan. The program will consist of testing 58 glulam beams to failure in four-point bending. Twenty-eight of the beams will be tested as individual beams to establish the 5th percentile lower exclusion limit. The remaining 30 beams will be used to construct five full-scale wood bridges. Each bridge will be comprised of five glulam beams spanning 40 ft (12.192 m) and spaced at 1200mm centres. The bridges will feature 130 mm thick transverse glulam deck panels and blocking. These bridges will all be tested to failure. The intent of the tests is to establish the load-sharing factor for glulam beams. Testing is anticipated to be undertaken in the spring of 2022, with the results published by the end of 2022. This testing program is believed to be the first of its kind internationally.

4.3 Glulam Deck Panels

The subcommittee is working to develop additional clauses to aid in the design of glulam deck panels. The intent is to provide at least a similar level of guidance to that provided in AASHTO.

At present, CSA O122 [32], the Canadian national standard for the manufacture of structural glulam members, prescribes glulam layups to achieve reliable material properties for glulam beams only. It does not address glulam deck panels. The experience of our subcommittee is that Canadian designers are sourcing deck panels from the United States and using the reference design material properties provided by the NDS. This practice presents a concern with respect to the NDS material properties and the calibration of the CHBDC. The subcommittee is intending to work with Canadian glulam manufacturers to obviate this concern by developing Canadian material properties for glulam deck panels for use with the CHBDC and CSA O86.

The subcommittee is also looking to advance clauses regarding live load distribution in glulam deck panels under discrete wheel loads. Bakht [33] developed design curves for this purpose in 1988. These curves were found to be applicable to stress-laminated decks as well. They were developed based on the work of McCutcheon and Tuomi [13] [14]. The curves were developed into closed-form equations in clause 5.7.3.2 in Section 5 of the CHBDC. Section 5 covers structural analysis. Unfortunately, clause 5.7.3.2 only speaks to stress-laminated decks and does not mention glulam decks. The Section 9 subcommittee is working with the Section 5 subcommittee to correct this issue. Furthermore, these subcommittees are working together to investigate the possibility of new equations that would reflect improved live load distribution. During the development of the OWBRG, it was observed that the live load distribution equations in AASHTO yielded much better distribution than the equations in clause 5.7.3.2 of the CHBDC. This effort is not expected to be completed quickly and may require an additional code cycle to complete.



The braking load calculation in the CHBDC provides the braking force for an entire bridge as a function of the total bridge length. This approach is sufficient for bridges with concrete decks, wherein the deck acts as a large diaphragm to distribute the load amongst the primary load carrying members. No guidance is provided, however, for discrete deck elements such as glulam deck panels. The Section 9 subcommittee has reached out to the Section 3 (loads) subcommittee for assistance on this matter, so that appropriate provision can be made for designing glulam deck panels for the in-plane shear forces and bending moments arising from braking loads. The OWBDG provides an interim design approach for calculating the braking load applied to a single deck panel.

4.4 Wood-Concrete Composites

Wood-concrete composites (WCCs) offer great potential to increase the span ranges of wood bridges. They have been the subject of significant research over the past decade. The CHBDC has historically included language on WCCs, but for a very specific pair of systems. Both systems consist of a longitudinal nail-laminated deck with a cast-in-place concrete topping. The difference lies in the wood-concrete interface. The first system features a series of grooves and daps fabricated in the tops of the wood laminations. The second system features a series of transverse grooves in the tops of the wood laminations with battered common spikes driven into the grooves. These systems were developed in the 1950's [34] and late 1970's [35] [36], respectively. They were rarely used in Canada, and few remaining examples exist in practice. The problem with these systems is that they rely on following a very narrow, prescriptive set of parameters, resulting in both systems having maximum span capabilities of about 6 m. This limitation has left them with little opportunity for use, other than for very short bridges, or as floor systems in truss bridges. The subcommittee is currently interested in retiring these designs to the code commentary and introducing new, flexible clauses for WCCs that is in line with modern research and design codes.

The subcommittees for CSA O86 have developed draft clauses for WCCs. These clauses reflect the state-of-the-art in WCC design. They are primarily based the approach provided in Annex B of Eurocode 5 for mechanically jointed beams and are intended for indoor structures. The Section 9 subcommittee is currently awaiting approval of these clauses by CSA O86. It is anticipated that they will be eventually adopted by the CHBDC, with modifications and additions as necessary to account for the additional challenges presented for outdoor structures such as large changes in temperature and moisture content.

4.5 Camber Requirements for Glulam Beams

The CHBDC currently requires glulam beams to be cambered for twice their unfactored dead load plus an additional one six-hundredth of the span length. The first component of the camber requirement implies a creep coefficient of 1.0. The second part of the camber requirement was added to provide additional protection against unsightliness resulting from excessive deflections [10]. Essentially, the one six-hundredth term was a conservative factor applied to correct for any design errors. Leading up to this current code cycle, requests were made to eliminate this one six-hundredth term because it further complicates the fit-up of connections caused by camber. The subcommittee is investigating this possibility, acknowledging that other codes, such as AASHTO, Eurocode 5, and AS 5100.9:2017 do not have such a requirement. In addition, the subcommittee is considering updating the 2025 CHBDC commentary clause for glulam camber to remind designers and fabricators of the need to adjust cambers to reflect other sources of deflection including connection stiffness, connection slip, changes in moisture content, and concrete creep and shrinkage for the case of WCCs.

4.6 Pedestrian Contact Preservative-Treated Wood

The CHBDC mandates the use of wood preservatives for all wood bridges. The code prescribes a list of permitted preservatives. It limits that list to a select of waterborne preservatives when the treated wood component is expected to receive "pedestrian contact". The definition of pedestrian contact has been a historically confusing term in the CHBDC, having never been defined in the code due to the difficulty in doing so. The subcommittee is currently working to define pedestrian contact so that the implications of its definition are in line with similar codes, particularly the AASHTO code. Of interest, glulam members are rarely treated with waterborne preservatives because of the resulting high moisture content and dimensional changes that typically ensue. Instead, they are usually treated using oil-borne preservatives. At present, a glulam member, such as a deck panel or a girder rising above the deck to also act as a barrier would effectively not be permitted for use in pedestrian bridges because of the possibility of direct



pedestrian contact, unless the glulam member was made of an untreated naturally durable species. By defining pedestrian contact, there exists the possibility that glulam members could see increased usage in pedestrian bridges without having to be made of an untreated naturally durable species.

5 Conclusions

The Section 9 subcommittee of the CHBDC is working to update the code to reflect state-of-the-art advancements in wood bridge design. Advancements are being made with respect to the shear design of glulam beams, the load-sharing factor, glulam deck panels, wood-concrete composites, camber requirements for glulam beams, and pedestrian contact with preservative-treated wood. While the subcommittee has yet to affirm these advancements, many of them are anticipated to be balloted for approval for inclusion in the forthcoming 2025 edition of the CHBDC.

6 Acknowledgement

The authors would like to thank their colleagues on the Section 9 subcommittee for their continued efforts in advancing the CHBDC and informing this paper. We would also like to thank NRCan and WRD for providing input on the full-scale testing program that will be conducted on a family of glulam beams to help determine the load-sharing factor for glulam beams, as well as their input regarding the forthcoming Timber Bridge Maintenance and Restoration Detailing Guide.

7 References

[1] Ontario Ministry of Natural Resources and Forestry (2016) Ontario's Crown Forests: Opportunities to Enhance Carbon Storage? A Discussion Paper, Ontario Ministry of Natural Resources and Forestry, Sault Ste. Marie, ON, Canada.

[2] Natural Resources Canada. "Green Construction Through Wood (GCWood) Program", Last accessed March 12, 2022, https://www.nrcan.gc.ca/science-and-data/funding-partnerships/funding-opportunities/forest-sector-funding-programs/green-construction-through-wood-gcwood-program/20046

[3] Natural Resources Canada (2019) Green Construction Through Wood (GCWood) Program: A Request for Ex-pressions of Interest to Design and Construct Timber Bridge Demonstration Projects in Canada, Natural Re-sources Canada, Ottawa, ON, Canada.

[4] Natural Resources Canada (2021) The State of Mass Timber in Canada 2021, Natural Resources Canada, Ottawa, ON, Canada.

[5] Natural Resources Canada. "SMTC Database", Last accessed March 12, 2022, https://nrcan-rncan.maps.arcgis.com/apps/dashboards/041e338d2a4d4b3a82ff2c238a9f0f93.

[6] Moses Structural Engineers and Brown & Co. Engineering Ltd. (2017) Ontario Wood Bridge Reference Guide, Ontario Wood WORKS!, North Bay, ON, Canada.

[7] Canadian Institute of Timber Construction (1970) Modern Timber Bridges: Some Standards and Details, 3rd edition, Canadian Institute of Timber Construction, Ottawa, ON, Canada.

[8] Taylor, R.J. and Keenan, F.J. 1992. Wood Highway Bridges. Canadian Wood Council, Ottawa, ON, Canada.

[9] Canadian Standards Association (2019) CSA S6:19 Canadian Highway Bridge Design Code, CSA Group, To-ronto, Canada.

[10] Canadian Standards Association (2019) CSA S6.1:19 Commentary on S6:19, Canadian Highway Bridge Design Code, CSA Group, Toronto, Canada.

[11] American Association of State Highway and Transportation Officials (AASHTO) (2020) AASHTO LFRD Bridge Design Specifications, 9th Edition, Washington, DC, USA.

[12] Canadian Standards Association (2019) O86-19 Engineering Design in Wood, CSA Group, Toronto, Canada.

[13] McCutcheon W.J., Tuomi R.L. (1973) Procedure for Design of Glued-Laminated Orthotropic Bridge Decks, Research Paper FPL 210, United States Department of Agriculture, Forest Service, Forest Products Laboratory, Madison, WI, USA.

[14] McCutcheon W.J., Tuomi R.L. (1974) Simplified Procedure for Glued-Laminated Bridge Decks, Research Paper FPL 233, United States Department of Agriculture, Forest Service, Forest Products Laboratory, Madison, WI, USA.

[15] Taylor R.J., Csagoly P.F. (1979) Transverse Post-Tensioning of Longitudinally Laminated Timber Bridge Decks, R&D Branch Report RR-2200, Ontario Ministry of Transportation, Toronto, ON, Canada.

[16] Batchelor B. deV., Van Dalen K., Hachborn A., Lee E. (1980) Report on Structural Specifieds of Transversely Prestressed Laminated Wood Bridge Decks, OJT & CRP Project No. 8305 (Parts I and II), Department of Civil Engineering, Queen's University, Kingston, ON, Canada.

[17] Batchelor B. deV., Van Dalen K., Morrision T., Taylor R.J. (1981) Structural Specifieds of Red Pine and Hem-Fir in Prestressed Laminated Wood Bridge Decks, OJT & CRP Project No. 23122, Department of Civil Engi-neering, Queen's University, Kingston, ON, Canada.



[18] Batchelor B. deV., Van Dalen K., Morrison T., Taylor R.J. (1981) Relaxation Specifieds of Prestressed Laminated Wood Decks, OJT & CRP Project No. 23123, Department of Civil Engineering, Queen's University, Kingston, ON, Canada.
[19] Morrison T. (1981) Orthotropic Plate Parameters of Prestressed Laminated Wood Systems, Department of Civil Engineering, Queen's University, Kingston, ON, Canada.
[20] Taylor R.J. (1981) Inter-Laminate Shear Strength in Post-Tensioned Laminated Wood Systems, Thesis Report, Department of Civil Engineering, Queen's University, Kingston, ON, Canada.
[21] American Wood Council (2019) National Design Specification (NDS) for Wood Construction, 2018 Edition, American Wood Council, Leesburg,VA, USA.
[22] ENV 1995-1-1:2004 (E) (Eurocode 5): Design of Timber Structures, Part1-1 General Rules and Rules for Buildings, 2004
[23] Standards Australia (2017) Bridge Design, Part 9: Timber, AS 5100.9:2017, Standards Australia, Sydney, NSW, Australia.
[24] American Railway Engineering and Maintenance-of-Way Association (AREMA) (2020) Manual for Railway Engineering, Volume 2, Part 7 – Timber Structures, AREMA, Lanham, MD, USA.
[25] Tingley D.A., Hoger C.B. (2021) Investigation into Horizontal Shear Design Values for Glulam Beams and Solid Sawn Timber, Discussion Paper for Committee 9 S6, Wood Research and Development, Jefferson, OR.
[26] Gupta R., Basta C., Kent S.M. (2004) Effect of Knots on Shear Strength of Douglas-fir Using Shear Blocks, Forest Products Journal, 54(11): 77-83.
[27] Foschi R.O., Barrett J.D. (1975) Longitudinal Shear Strength of Douglas Fir, Canadian Journal of Civil Engineering, 3(2): 198-208.
[28] Foschi R.O., Barrett J.D. (1977) Longitudinal Shear in Wood Beams: A Design Method, Canadian Journal of Civil Engineering, 4(3): 363-370.
[29] British Columbia Ministry of Transportation and Infrastructure (2016) Bridge Standard and Procedures Manual, Volume 1, Supplement to CHBDC S6-2014, British Columbia Ministry of Transportation and Infrastructure, Victoria, BC, Canada.
[30] Sexsmith, R.G., Boyle, P.D., Rovner, B., Abbott, R.A. (1979) Load Sharing in Vertically Laminated Post-Tensioned Bridge Decking, Forintek Canada Corporation, Vancouver, BC, Canada.
[31] Bakht B., Jaeger, L. (1991) Load Sharing Factors in Timber Bridge Design, Canadian Journal of Civil Engineering, 18: 312-319.
[32] Canadian Standards Association (2016) O122-16 Structural Glued-Laminated Timber, CSA Group, Toronto, Canada.
[33] Bakht B. (1988) Load Distribution in Laminated Timber Decks, Journal of Structural Engineering, 114(7): 1551-1570.
[34] May T.K. (1955) Composite Timber-Concrete Construction. Report of Committee 7 – Wood Bridges and Trestles, American Railway Engineering Association, 56(520).
[35] Chlopecky J.O. (1980) An Experimental Investigation of Composite Wood-Concrete Bridges, Master's thesis report, Department of Civil Engineering, University of Toronto.
[36] Thompson J.A. (1980) An Experimental Investigation of Composite Wood-Concrete Bridges, Master's thesis report, Department of Civil Engineering, University of Toronto.

Conference Proceedings 4th ICTB (2022)
https://doi.org/10.24451/3zd7-ar34

ICTB 2021 PLUS
4th International Conference on Timber Bridges
Biel/Bienne, Switzerland, 9 -12 May 2022



Fatigue strength of axially loaded steel rods bonded in European ash glulam

Bruno Maurer [1], Ernst Gehri, Thomas Strahm, René Steiger, Christian Affolter

Abstract

Bonded-in profiled rods are among the most efficient fasteners in modern timber construction. Especially under axial loading, they are characterised by high load-carrying capacity and high stiffness. In addition, connections with steel rods can be designed to exhibit ductile failure, so that the brittle failure modes of wood in connections and reinforcements are excluded. For bridges, fatigue can be a critical ultimate limit state. Starting from the desired design value of a rod in practice, in this paper the required load level for the typical connection configuration is derived. Based on experiments, it is shown how the undesired mixed failure modes can be avoided. The effect of the loading frequency and the corresponding temperature rise in the specimen are presented and discussed. The results of the experimental campaign confirm the appropriate performance of the bonded-in rod system under the tested conditions.

1 Introduction

1.1 Background

The GSA Technology is a practice-proven system for bonding steel rods with metric thread into timber members. The German Technical Approval (Z-9.1-778) as well as the European Technical Assessment (ETA-19/0752) confirm the suitability of the applied epoxy adhesive (EPX) and provide confidence in the practical application of these high-performance joints to all parties involved in a project. Both approval documents mention softwoods as substrates and load-bearing structures with mainly static loading as the scope of application. The reason for these restrictions is that no fatigue tests had been carried out during the development of these approvals and fatigue design rules for such type of connections are missing in the currently applicable standards (e.g. EN 1995).

For structures or structural components that are frequently exposed to cyclic loading with large amplitudes, fatigue verifications are required. It shall be verified that no failure or major damage occurs due to fatigue, i.e. the weakening of the bond or any component caused by cyclic loading. Various verification methods are described in literature and some of them have found their way into standardisation, for example into the Swiss standard SIA 265:2003 [1] and into Eurocode 5 (EN 1995-2:2004 [2] and later versions). The methods differ considerably, especially with regard to involving different parameters in the design equations: For instance, the verification method in SIA 265 is based on the stress range whereas the one in EN 1995-2 uses stress ratios and maximum stresses. The latter procedure is nowadays, considered more suitable and reliable for timber structures [3]. An overview of this verification method can be found in the papers of the recent ICTB [4]. For the interested reader, publications [5] and [6] (in German) are also recommended. In the current version of Eurocode 5 [2], the fatigue coefficients (a and b) are specified only for connections with dowel-type fasteners. From published work within the project "TACITUS" it can be concluded that an extension of the verification method to bonded-in rods is possible [7].

In December 2019, the first fatigue tests on specimens with bonded-in rods applying the GSA Technology were successfully conducted at the Structural Engineering Research Laboratory of the Swiss Federal Laboratories for Materials Science and Technology, Empa. Specimens with identical end grain connections made of 2 steel rods with metric thread M16 bonded into European ash (*Fraxinus excelsior*) glulam were tested in a pull-pull setup. In this first test series, the rods were pre-stressed against the end grain with a controlled torque. With this procedure and by using duplex stainless steel threaded rods, the specimen could be subjected to $2 \cdot 10^6$ stress cycles without occurrence of fatigue failure. The frequency of the sinusoidal loading was increased step by step starting from 5 Hz. Finally, most of the cycles were tested at a frequency of 12 Hz, which led to a welcome reduction of the test duration. One specimen was even subjected to 50'000 stress cycles both at frequencies of 15 and 20 Hz. The four temperature sensors installed in the bond lines (one on each rod) recorded only moderate temperature rises of less than 2 °C throughout the test duration. In the summer of 2021, further specimens were tested at the Empa. Besides the omission of the pre-stressing, the edge distances and spacings were slightly reduced. The objective of these tests was to investigate the performance of the GSA adhesive and to compare it with test results published in literature.

[1] Bruno Maurer, R&D Engineer, neue Holzbau AG, Lungern, Switzerland, bruno.maurer@neueholzbau.ch



1.2 Failure modes

The design approach in EN 1995-2:2004 is considered appropriate to design for fatigue of wood itself. Difficulties are encountered, however, in the case of combined wood and steel configurations. Depending on the failure mode - wood failure or steel failure - different types of verification apply (Figure 1). In the given example, the failure mode changes from wood to steel failure in the range of 10^4 to 10^5 stress cycles.

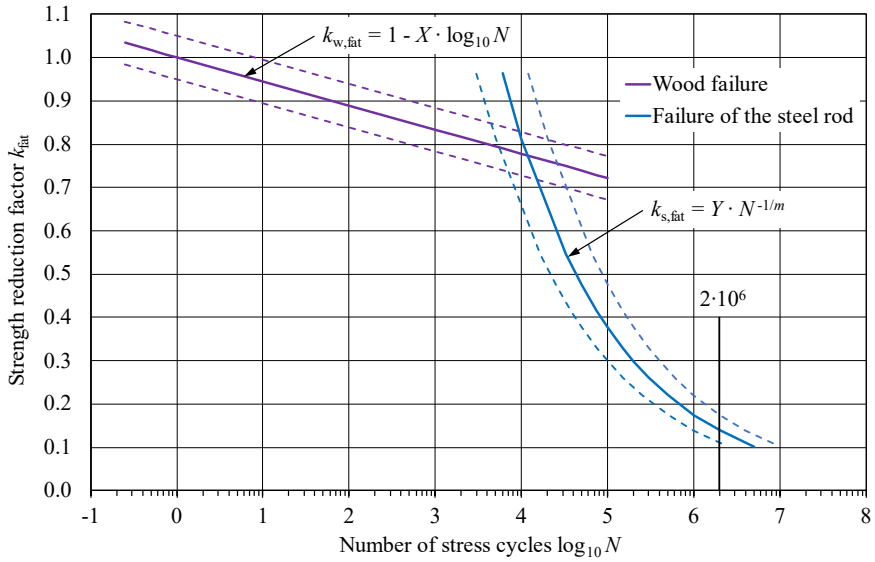


Figure 1: Strength reduction factor for fatigue loading k_{fat} considering two different failure modes

For lower numbers of stress cycles, **pull-out failure of the bonded-in rod** occurs; with EPX bonding, i.e. shear failure in the wood. According to the design approach in EN 1995-2:2004, the decrease in load-carrying capacity can be described as a linear function of the logarithm of the number of stress cycles (Figure 1). The parameter X is a function of the stress ratio R ($= F_{min,fat} / F_{max,fat}$), of the configuration of the structural element or connection and of the wood species. Its definition is identical with the slope parameter A according to [4].

With higher numbers of stress cycles, a **fatigue fracture occurs in the threaded steel rod**; the decrease in load-carrying capacity can be described here as a function of the difference in force or stress $\Delta\sigma_{fat}$, which is also called the stress range. The common approach for fatigue design of steel members is adopted here. In this case, the parameter Y is a function of the shape of the thread i.e. the sharpness of the indentation (which is different for cut threads, and cold-rolled or warm-rolled threads), the configuration of the structural element or connections, as well as the mechanical properties of the steel (grade). In steel design (e.g. [8]), usually a value of 3 is adopted for the parameter m in stress ranges below $5 \cdot 10^6$ stress cycles.

By optimising the connection and test parameters, the range of stress cycles where wood failure changes to steel failure can be shifted, e.g. up to about 10^7 stress cycles. This makes a separate evaluation of the two failure modes possible.

1.3 Target values

The design of the specimens was based on the characteristic withdrawal resistance $F_{w,k}$ of 100 kN for a GSA fastener M16 bonded in hardwood parallel to the grain. Hardwood was chosen because with an identical configuration, significantly higher forces can be applied here than in softwood and thus the bond line is subjected to higher stresses. The high strength of the rod material used requires a substantial reduction of the cross-section to ensure ductility in the ultimate limit state. Based on the rod's tensile strength of f_u = 1000 N/mm² determined in tests, a reduced diameter of 11.5 mm (A_C = 104 mm²) would be chosen for practical applications. According to standard SIA 263 [9], this would result in a design load-carrying capacity of $F_{t,Rd}$ = 74.8 kN of the steel rod. The design value of the withdrawal resistance would therefore still be decisive with 100/1.5 = 66.7 kN and a smaller steel cross-section would therefore be possible. Assuming a partial factor of γ_Q = 1.5, the rod could be expected to be able to carry a variable live load of almost 45 kN. For the configuration to be tested, this results in the target load value of 45 kN per rod. For



the stress ratio R a value of 0.1 was chosen. This ratio is considered to be relevant in practice for a light-weight structure with a large cyclic live load. In addition, this choice allows a comparison with results from literature [7]. The target value for the test duration was fixed at $2 \cdot 10^6$ stress cycles, because steel design codes also refer to this number for defining their detail categories [8], usually.

2 Material and method

2.1 Tests on steel rods and internal threads

By previously determining the factor Y (Figure 1), mixed mode failures in the main test series should largely be avoided. Therefore, a first test series was carried out on pure steel specimens without adhesive bonding. In order to determine the fatigue strength, the "Mechanical Systems Engineering" laboratory at the Empa carried out single-step fatigue tests and load increase tests on M16 threaded rods and their connection to a steel part. (Figure 2).



Figure 2: Steel specimens; connection with internal thread (top) and machined threaded rods (bottom)

For the connection, a metric internal thread was chosen, which was cut into the narrow side of a 30 mm thick plate made of steel S355J2. The threaded rods made of duplex stainless steel were machined to a defined diameter over a certain length in accordance with the building practice when bonding-in according to the standard of the GSA Technology [10]. This zone, called "constriction zone" was 110 mm long with linear transitions to the full rod diameter over a length of 15 mm on both sides. Specimens with constriction zones of three different diameters (11.5 mm, 12.0 mm, 12.5 mm) were prepared. Finally, only the specimens with the smallest constriction diameter were tested because these three specimens already exceeded all expectations. Also in terms of connections, four different variants were planned to be tested. But even here, the most economical option already provided satisfying results.

For the fatigue tests, an electrodynamic high-frequency resonance testing machine ("HFP") of type Russenberger, *Rumul Testronic 8601.11-1* (150 kN) was employed. The machine has hydraulic grips ("Hydrogrip") in which the ends of the threaded rods of the specimens were clamped directly. Stainless steel shims were used to apply the external load evenly via shear to the threads of the M16 threaded rod. The free length between the 80 mm long grips was 270 mm. Figure 3 shows three different specimens during the fatigue tests under cyclic tensile loading.



(a) *(b)* *(c)*

Figure 3: Installed specimens; (a) threaded rod machined to ø11.5 mm, (b) connection "S-03b-1", (c) connection "S-05a-1"



Three threaded rods with a machined centre zone were tested. The stress ratio R (= F_{min} / F_{max}) was kept constant at a value of 0.2 and the frequency was about 72 Hz for all specimens of this series. For the first specimen, the maximum load F_{max} was increased by 5 kN every 10^6 stress cycles (block programme). A total of $4 \cdot 10^6$ stress cycles with a final maximum load F_{max} of 65 kN were imposed to this specimen. The two other specimens were tested at this highest load level up to $5 \cdot 10^6$ stress cycles. The duplex stainless steel of these threaded rods thus carried a tension-tension stress range $\Delta\sigma$ of 500 N/mm².

The first connection tested was specimen "S-03b-1" with a conservative thread length. After this specimen had survived 10^6 stress cycles to F_{max} = 65 kN with R = 0.2, the specimens detailed as considered optimal were installed. Three specimens were tested to 10^6 stress cycles under identical loading. As the threaded rods no longer had any constriction, the load can be related to the stressed cross-section A_s of 157 mm², resulting in a stress range $\Delta\sigma$ of 255 N/mm². Here, the frequency was around 80 Hz.

Another specimen was successfully tested during $5 \cdot 10^6$ stress cycles with F_{max} = 50 kN and a reduced stress ratio of R = 0.1. Finally, again a block programme was defined for specimen "S-05a-1". This started with F_{max} = 55 kN. Again, the maximum load was increased by 5 kN every 10^6 stress cycles, at a constant stress ratio R of 0.1. After a total of $5 \cdot 10^6$ stress cycles with a stress range in the last block of $\Delta\sigma$ = 430 N/mm², this test was also completed without failure.

During these tests, the temperatures of the specimens were monitored periodically with an infrared thermometer (especially in the clamping area and at the internal threads). A temperature rise could have been an indication of frictional fatigue or friction corrosion. The temperatures generally remained below 50 °C. The maximum of 56 °C was measured during the second test on a machined rod.

2.2 Tests on rods bonded in European ash glulam

For the tests on bonded-in rods, four identical specimens were designed and produced. They were made of European ash glulam of strength class GL40h. The ash (*Fraxinus excelsior*) lamellas were graded with the Timber Grader MTG (device for strength grading of wood based on the determination of the dynamic modulus of elasticity from the measurement of the eigenfrequency and the density) in such a way that the moduli of elasticity and the densities of the specimens had a uniform distribution. Two threaded rods M16 were bonded in parallel to the grain direction of the wood, according to the standard of the GSA Technology into both end faces of the glulam members, each consisting of four bonded lamellas. The adhesive used was a 2-component EPX resin and the drill hole diameter was 18 mm. The bond length was 290 mm (i.e. $16.1 \cdot d_{drill}$) with a recess (not bonded length) of 70 mm. To apply the force from the testing machine to the specimen, 30 mm thick steel plates of grade S355J2 were used. The connection detail to the two threaded rods corresponded to the previously tested variant (see section 2.1). In addition, the specimens had two holes each, which allowed the installation of temperature sensors into two bond lines. The geometric dimensions of the specimens are shown in Figure 4.

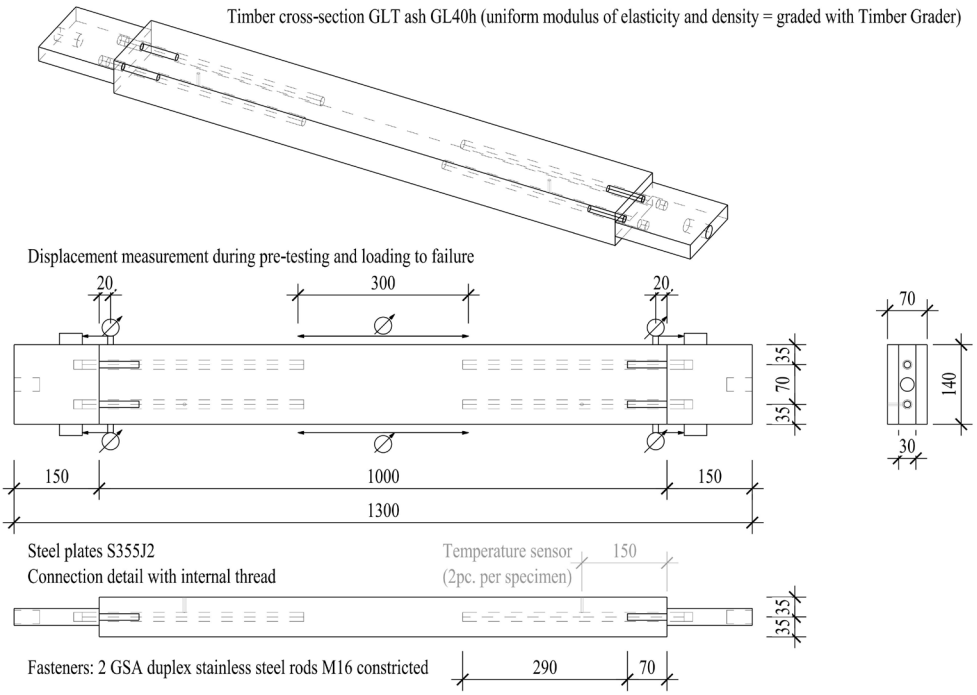


Figure 4: Design and dimensions (in mm) of the four timber specimens subjected to fatigue testing



The specimens were produced by the neue Holzbau AG (n'H) and then proof-loaded almost to their characteristic withdrawal resistance (185 kN) in order to confirm proper production and curing. In this pre-testing, the displacements depicted with a ∅ symbol in Figure 4 were measured. The static modulus of elasticity of the timber was determined based on the measurement in the centre of the member. Then the Structural Engineering Research Laboratory of Empa carried out the main series of tests. For this purpose, a servohydraulic fatigue testing machine of type Walter & Bai, *LFV-500* (500 kN) was used. The machine has hydraulic grips in which the steel plates are directly clamped over a length of 90 mm. The displacements in the direction of the longitudinal axis of the specimens were recorded by the crosshead gauge installed in the testing machine (stroke). In addition to the readings of the climate logger in the hall (air temperature and relative humidity), a third temperature sensor was placed near the testing machine.

Of the four test specimens, three could be tested within the available (time) budget. Initially, each specimen was statically loaded in tension up to the maximum load F_{max} of 100 kN (loading rate 2 kN/s, force-controlled) in order to determine the stiffness of the system. For the following fatigue tests, a sinusoidal waveform with constant amplitude and a stress ratio R of 0.1, with force-controlled loading was applied. Looking at the cross-section area of the constriction zone ($2 \cdot A_C = 265$ mm²), this resulted in a tension-tension stress range $\Delta\sigma$ of 340 N/mm². The specification for the frequency was: As high as possible without however, provoking the temperature in a bond line to exceed 55 °C.

After successful fatigue testing, one specimen was finally tested to static tension failure by the n'H at their own laboratories. The specimens "H-01" and "H-03" were cut open after the fatigue test to evaluate the state of the bond lines. Based on the central part of each specimen, the density was determined and two samples were taken to assess the moisture content of the wood using the kiln-drying method.

3 Results and discussion

3.1 Frequencies and temperatures

For the first specimen "H-01" with GSA rods bonded in ash glulam, the loading frequency was initially set to 12 Hz. However, as shown in Figure 5a, within short time (i.e. 30 minutes) a considerable temperature rise occurred in the bond lines, and hence, the frequency was halved for the next phase (i.e. 6 Hz). After a total of about 455'000 stress cycles, the frequency was increased to 9 Hz. In this phase, a ventilator was placed on the floor next to the testing machine in order to cool the specimen. Since the desired effect did not occur and the temperatures continued to rise, the ventilator was removed after a while. Due to a new excessive rise of the temperature in the bond lines, the frequency was set to 8 Hz after a total of approximately 505'000 stress cycles.

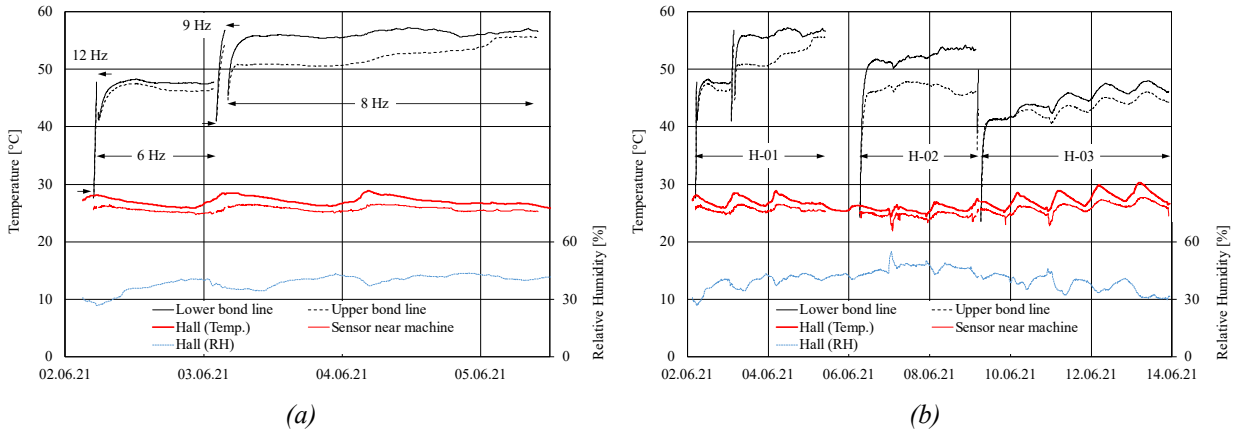


Figure 5: Temperatures in the bond lines and in the ambient air, as well as the relative humidity of the air in the testing hall as a function of time; (a) specimen "H-01", (b) compilation of all specimens

For the specimen "H-02", the frequency of 8 Hz was adopted and maintained throughout the $2 \cdot 10^6$ stress cycles. The fatigue test had to be restarted shortly before its end because a breakdown of the power supply of the hydraulic pumps had occurred. The curves of the temperature measurements in the bond lines therefore show a second rise. Because these values in the second specimen were around 50 °C, a frequency of only 5 Hz was chosen for testing specimen "H-03". Here, the variation in ambient temperature was clearly visible in the temperatures measured in the bond lines. Reducing the loading frequency by 3 Hz led to a



5 °C lower average bond line temperature (48.3 °C in H-02, 43.3 °C in H-03), although the ambient temperature was considerably higher during the third test. The temperatures recorded by the sensor next to the machine were on average 1.2 °C higher, the testing hall was on average 1.8 °C warmer. These differences, however, are in the range of the precision in temperature measurements.

3.2 Ultimate resistance and stiffness

The moduli of elasticity derived from the displacement measurements in the preliminary tests are shown in Table 1. The determination of the ultimate tensile force F_u after the fatigue test showed no change in the measured static modulus of elasticity of the timber E_{timber}. The specimen failed in a brittle mode at a force of 246 kN, which is 23 % above the characteristic value found in static short-term tests of GSA rods bonded in hardwood. Since the constriction diameter of 13.0 mm chosen for the fatigue tests was intentionally not designed to get ductile failure, the observed failure mode, i.e. pull-out failure and splitting of timber, was as expected.

Table 1: Properties and number of stress cycles in fatigue testing for the specimens made of European ash glulam

Label	Density [kg/m³]	MC [%]	E_{timber} [N/mm²]	Number of cycles, N	F_u [kN]
H-01	702	8.0	15'000	2'054'712	not determined
H-02	679	7.7	13'000	2'010'000	246
H-03	696	8.2	16'900	2'010'000	not determined

The crosshead stroke rose with increasing number of stress cycles, whereas the measured displacement developed consistently with the temperature of the bond lines. The effect of the temperature is superposed by the different stiffnesses of the timber members (Figure 6).

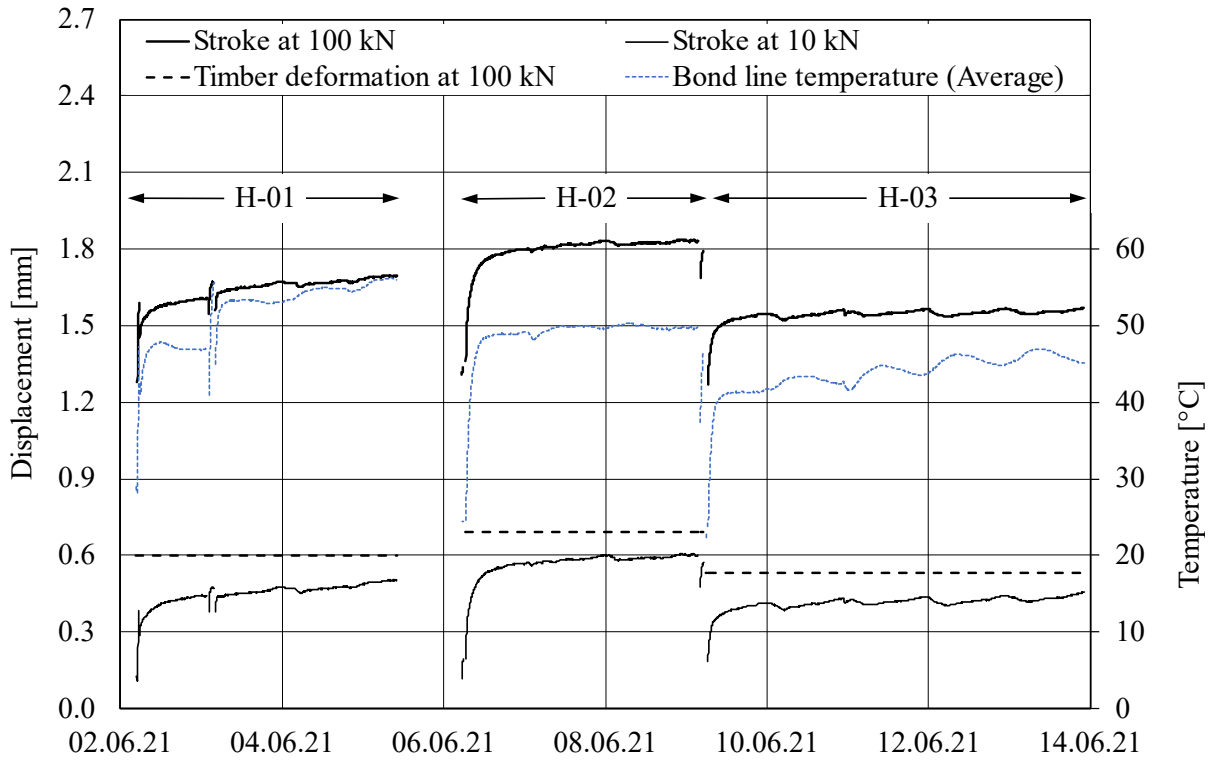


Figure 6: Crosshead stroke and average of the bond line temperature as a function of time; all specimens with displacement share of the timber member

These differences are not large enough to explain the differences between the specimens. Therefore, an attempt was made to model the measured crosshead strokes by shares of linear-elastic displacement in steel and timber. In addition, the temperature rise of the threaded rod was taken into account with a constant thermal expansion coefficient. Figure 7 shows that this worked well for the specimen "H-03". On the other hand, the specimen "H-02" shows a difference between the measured values and the analytical model, which is similar for the minimum and the maximum load. Heating the bond lines to about 50 °C seems to cause an additional, small, but irreversible displacement share. This displacement very likely originates from the adhesive.

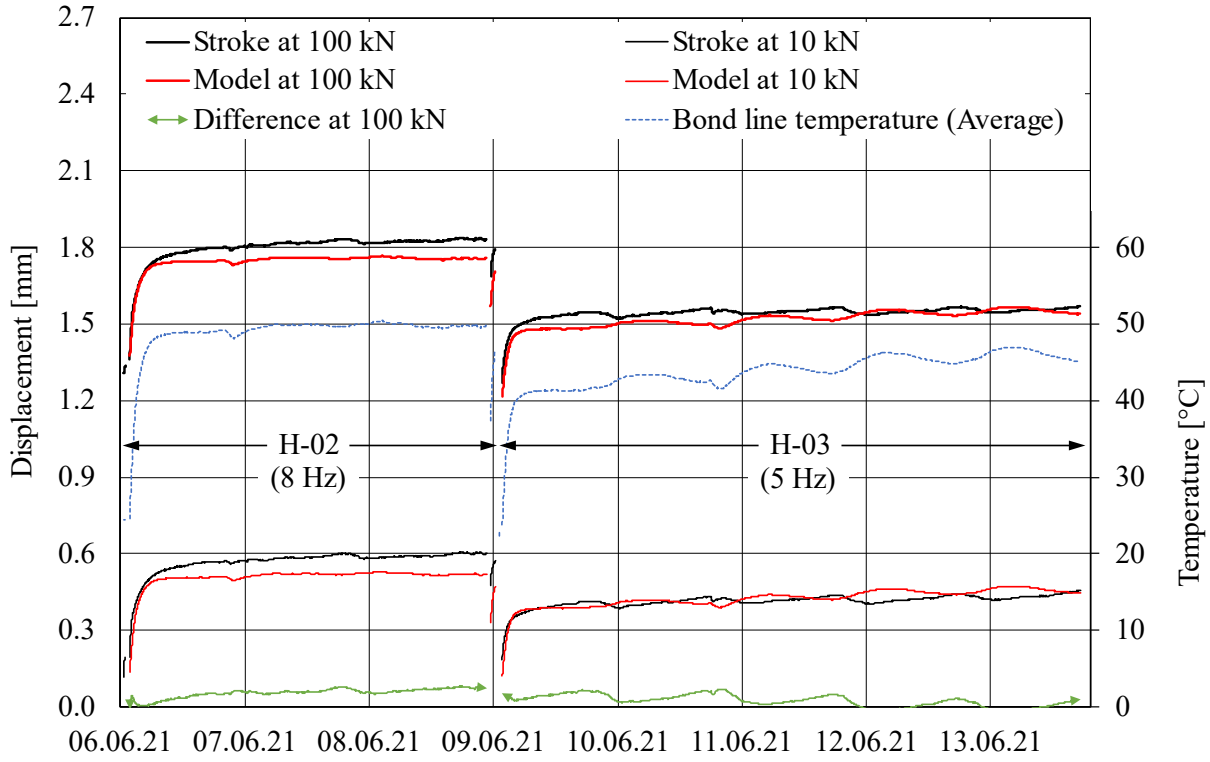


Figure 7: Crosshead stroke and average of the bond line temperature as a function of time; specimens "H-02" and "H-03" with analytical stiffness model

In the visual inspection of the specimens after the fatigue test, a gap between the steel plate and the end grain was noticed on specimen "H-02". On the third specimen, such a gap was only barely apparent.

3.3 Fatigue strength

The tests carried out on machined threaded steel rods, internal threads and rods bonded in European ash glulam did not lead to fatigue failure in any case. Because only one load level with one stress ratio was tested, a relationship valid for design can hardly be derived from this investigation. However, a comparison with the "Inoxripp" proposal according to Myslicki et al. [7] shows that the performance of the tested system is well within the range of other test results (Figure 8). In the past, comparisons of fasteners were made based only on the slope of the curve describing the strength reduction factor k_{fat} [4]. Graphing the test data in form of axial load-carrying capacity per rod reveals that the slope parameter X should always be rated in conjunction with the quasi-static resistance $F_{w,k}$. In addition, the various differences in the connection configuration, such as the area of the bonding surface A_b, have to be taken into account. The question might be raised if the extrapolation based on a tested bond line shear strength as usually done in common design methods is conservative enough with regard to fatigue. The results of the present investigation are considered to be more reliable in this respect, because the tested configuration (bond length, edge distance, etc.) and the chosen pull-pull setup correspond very closely to the actual reality in building practice.

Figure 8 also shows possible fatigue resistance curves of the steel components in the connection. To represent the threaded rods made of duplex stainless steel, a value of 5 was chosen for the parameter m. For comparison, a curve is drawn as it could apply for a threaded steel rod of grade 8.8. This curve corresponds to the detail category 50 according to Eurocode 3 [8]. For the GSA Technology, the stress cross-section of the threaded rod A_s is replaced by the cross-section area of the constriction A_C. For both rod types, a value for A_C was assumed that is deemed a realistic value for building practice.



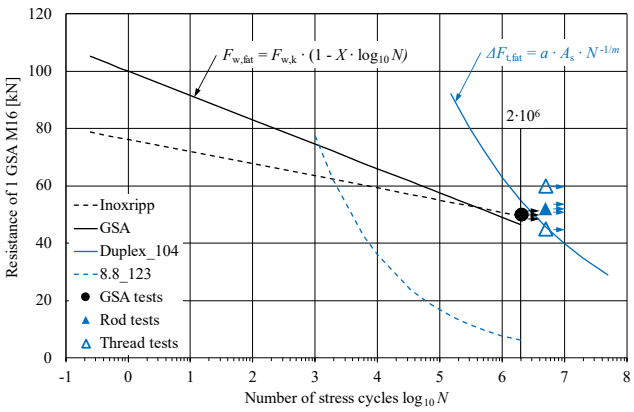


Figure 8: Fatigue resistance of an axially loaded GSA M16 in hardwood also considering the steel components (R = 0.1)

Table 2: Parameters of the curves describing the fatigue resistance

Curve	$F_{w,k}$ [kN]	X [-]	A_b [mm²]
Inoxripp	76.16	0.056	10'050
GSA	100.00	0.085	16'400
	a [-]	A_C [mm²]	m [-]
Duplex	9.62	104	5
8.8	6.30	123	3

4 Conclusion

The experimental investigation presented in this paper was intended as a contribution to the development of a practical verification method for connections with bonded-in profiled rods in timber structures subject to fatigue loading. Suitable threaded rods and an appropriate connection detail with regard to the steel part could be found, allowing passing fatigue tests with more than $2 \cdot 10^6$ stress cycles without failure. Loading frequencies exceeding 5 Hz caused the bond line temperatures to rise above 45 °C. This is considered unfavourable because it resulted in irreversible displacements suggesting assuming that changes in the adhesive occurred due to elevated temperatures. Nevertheless, the stiffness of the connections remained very high during the entire tests. The final loading to failure in a static test also indicated a high consistency of the load-carrying capacity. The results of this investigation provide additional arguments that the GSA Technology is very suitable for the realisation of reliable and durable structures also in the case of fatigue loading.

5 Acknowledgement

This work was financed by the neue Holzbau AG. The support by Empa - Materials Science and Technology (Laboratories for Mechanical Systems Engineering and for Structural Engineering) and by Professor Gehri is gratefully acknowledged.

6 References

[1] SIA, Swiss Society of Engineers and Architects (2003) SIA 265: Timber Structures, Zurich, Switzerland.
[2] CEN, European Committee for Standardization (2004) EN 1995-2: Design of timber structures. Part 2: Bridges, Brussels, Belgium.
[3] Malo K. A., Holmestad A., Larsen P. (2006) Fatigue Strength of Dowel Joints in Timber Structures. In: Proc. of the World Conference on Timber Engineering WCTE, Portland, USA.
[4] Stamatopoulos H., Malo K. A. (2017) Fatigue strength of axially loaded threaded rods embedded in glulam at 45º to the grain. In: 3rd International Conference on Timber Bridges ICTB, Skellefteå, Sweden
[5] DIN, German Institute for Standardization (2016) DIN 50100: Load controlled fatigue testing - Execution and evaluation of cyclic tests at constant load amplitudes on metallic specimens and components, Berlin, Germany
[6] Aicher S., Christian Z. (2015) Fatigue behaviour of wood and glued wood components (German), In: 21st International Forum Wood Building IHF, Garmisch, Germany
[7] Myslicki S., Bletz-Mühldorfer O., Diehl F., Lavarec C., Vallée T., Scholz R. & Walther F. (2019) Fatigue of glued-in rods in engineered hardwood products - part I: experimental results, The Journal of Adhesion, 95:5-7, 675-701, DOI: 10.1080/00218464.2018.1555477.
[8] CEN, European Committee for Standardization (2005) EN 1993-1-9: Design of steel structures - Part 1-9: Fatigue, Brussels, Belgium.
[9] SIA, Swiss Society of Engineers and Architects (2003) SIA 263: Steel Structures, Zurich, Switzerland.
[10] neue Holzbau AG, (2021) GSA Technology - characteristics, [Online], Available: gsa-technologie.ch/en/gsa-technologie/gsa-grundlagen-2.

Conference Proceedings 4th ICTB (2022)
https://doi.org/10.24451/ggxv-h219

ICTB 2021 PLUS
4th International Conference on Timber Bridges
Biel/Bienne, Switzerland, 9 -12 May 2022



Exploring fatigue rules for timber structures in Eurocode 5

Kjell Arne Malo[1], Francesco Mirko Massaro and Haris Stamatopoulos

Abstract

The next generation of Eurocode 5 "Design of timber structures" is currently planned with normative rules for prevention of fatigue failures in timber structures. Probably only a few building structures like windmill towers will need evaluation with respect to high numbers of cyclic loading, and the proposed rules will most likely be used in timber bridge design. The proposed rules for fatigue in the second generation of the timber Eurocode are almost identical to the informative rules found in an annex to the current Eurocode 5 for timber bridges; EN1995-2. Although few new fields of applications or more comprehensive rules are brought into the new normative rules of the second generation, it is nevertheless worth to explore what is incorporated in the rules, and their possible limitations.

In the present paper, the rules limiting the applicable stress, or the number of cycles to failure, are mainly presented and commented. It is shown how experimental results have been used for calibration of expressions, using dowel type connections with slotted-in steel plates as case. Other effects of the formulations and calibrations will also be explored and commented.

1 Introduction

The second generation of Eurocodes is currently under development. A large amount of new design rules as well as fields of applications have been proposed and are under investigation. However, for timber structures exposed to loading with relatively low-intensity but high number of cycles, as for example traffic loading on road bridges, the existing informative annex (Annex A EN1995-2:2004) [1] is proposed to be kept approximately as it is without any major changes. The most significant changes are that the fatigue provisions are proposed to move to the main part of Eurocode 5 (EN1995-1-1) [2], and to make them normative. The proposed normative status in the Eurocode makes it more intrusive to explore the implications of the fatigue provisions. An approach for fatigue regulations based on integration of rate and time dependent effects is not relevant for the Eurocodes, as the time dependency of loading and loading models are absent in EN1990 and EN1991. Consequently, possible effects of time dependency or order of load appearance must be incorporated in an implicit way.

So far, no satisfactory analytical model for the prediction of the fatigue life of wood or other composites is known to the authors. The knowledge on fatigue behaviour of wood and connections in timber structures comes from experimental testing at various scales. Most experimental fatigue results have been derived from constant stress amplitude loading until failure. The parameters are commonly the maximum and minimum stress levels, and the experimental result is the number of cycles until failure. The experimental results are usually presented by use of Wöhler-curves (SN-curves), relating the stress level to the logarithm of the number of cycles to failure.

For most composites, wood included, the experimental results show a clear dependency of the mean stress level on the fatigue life. The approach used for components in steel, considering only the stress range (the variation in stresses), is therefore probably not satisfactory for wooden components. Moreover, there is a general agreement that increased moisture content and long duration of load interact with the fatigue life, making it shorter, but the experimental results are so sparse that hardly any general quantification can be made.

[1] Kjell Arne Malo, Professor, NTNU Norwegian Univ of Sci and Technology, Dep of Structural Engineering. Norway, Kjell.Malo@ntnu.no



2 Method

2.1 Fatigue loading

2.1.1 Load combinations

The proposed second generation of EN 1990, specifies the load combination for fatigue actions by:

$$\sum F_d = \sum_i G_{k,i} + \sum_j \psi_{2,j} Q_{k,j} + (P_k) + Q_{fat} \tag{1}$$

where Q_{fat} is the relevant fatigue load, giving cyclic stresses in a building structure. Note that the quasi-permanent part of the live load $\sum_j \psi_{2,j} Q_{k,j}$ shall probably not have a spatial variation between the load cases, it is merely an addition to the self-weight of the structure. For timber structures it might be recommended to evaluate several levels of density and quasi-permanent load levels, depending on the mean stress sign and level.

Note also that all load factors shall be set to unity ($\gamma_f = 1.0$), which indicate that all safety measures must be dealt with on the resistance side.

2.1.2 Stresses

The fatigue strength of wood is dependent on both mean stress σ_{mean} and alternating stress σ_a. All stress components have contributions from both quasi-static loading and cyclic loading.

The alternating stress from stress cycles can be determined by:

$$\sigma_a = \frac{1}{2}\Delta\sigma = \frac{1}{2}(\sigma_{max} - \sigma_{min}) \tag{2}$$

where σ_{max} is the numerical largest stress and σ_{min} the numerical smallest in representative stress cycles. Note that tensile stresses are defined positive, while compressive stresses are defined negative. The alternating stress amplitude σ_a corresponds to half of the stress range $\Delta\sigma$ and any effect of quasi-static loading is here cancelled out. Furthermore, the alternating stress σ_a is, by definition, positive.

The mean stress from stress cycles is calculated by:

$$\sigma_{mean} = \frac{1}{2}(\sigma_{max} + \sigma_{min}) \tag{3}$$

As an alternative to the use of mean stress and amplitude, the stress ratio R is commonly used in fatigue evaluations to characterize the stress situation, where R is defined by

$$R = \frac{\sigma_{min}}{\sigma_{max}} \tag{4}$$

Note that the stresses can have any value and sign, and consequently R also can take on any value. For a pure alternating load with zero mean stress $R = -1$, while $R = 1$ indicates a pure static load without any change in stress. The use of the stress ratio R together with the maximum stress, or the use of alternating and mean stresses are two sides of the same story, i.e. they are interrelated in the following way:

$$\sigma_a = \tfrac{1}{2}\sigma_{max}(1 - R) \text{ and } \sigma_{mean} = \tfrac{1}{2}\sigma_{max}(1 + R) \tag{5}$$

When stress resultants, i.e. forces or moments, are used in fatigue strength evaluations, the stresses in the expressions above can be replaced by the corresponding stress resultants.

2.2 Constant life diagrams

For the evaluation of fatigue strength experimental results, it is very convenient to use constant life diagrams, confer for example [3] and [4]. For an easy understanding of the concept, we reformulate the maximum and minimum stresses to

$$\sigma_{max} = \sigma_a + \sigma_{mean} \text{ and } \sigma_{min} = -\sigma_a + \sigma_{mean} \tag{6}$$

Both static loading by σ_{mean} and cyclic loading by σ_a can independently lead to failure in a material. For most composites, also wood, it is generally found that the absolute stresses are more important for the



fatigue life than the stress range $\Delta\sigma$. Considering Eq. (6), it is obvious that an increase in σ_{mean} will reduce the strength margin in case of tension (σ_{max}), while for compression (σ_{min}) a reduction of mean stresses will reduce the compressive strength margin. To take the combined effect into account, we can estimate the combined strength by, conservatively, applying a linear interaction between the two different failure modes, leading to

$$\frac{\sigma_a}{f_a} + \frac{\sigma_{mean}}{f_{mean}} = 1 \tag{7}$$

Note that the strength for alternating stress f_a is dependent on the number of cycles, and that the static strength can be the positive tensile strength, or the negative compression strength, for positive and negative mean stresses, respectively. A graphical representation of Eq. (7) for a given number of cycles is usually called a Goodman diagram. Since the alternating stress σ_a is, by definition, positive, we have only two quadrants in the stress space, one for positive and one for negative mean stresses; see visualization in Figure 1. A stress combination inside the triangle enclosed by Eq. (7) and the horizontal axes for mean stresses is considered safe, while the domain outside the triangle is considered unsafe. The Goodman constant life diagram is usually found either close to experimental results, or slightly conservative. More accurate results have been reported for some cases by letting the ratio σ_{mean}/f_{mean} be raised to the power $c \geq 1$, see Eq. (8), making the interaction curves slightly convex.

$$\frac{\sigma_a}{f_a} + \left(\frac{\sigma_{mean}}{f_{mean}}\right)^c = 1 \tag{8}$$

Letting the parameter $c = 2$ is known as a Gerber type diagram. Usually, timber structures will have c values somewhere in between 1 and 2. However, it is not possible that the slope of the strength interaction curve, Eq. (8), is positive for positive mean stress (or negative for negative mean stress), since this would imply that the strength limit increases for an increase of maximum stress.

The alternating stress σ_a and the mean stress σ_{mean} can also be related by use of the stress ratio R giving

$$\sigma_a = \frac{1-R}{1+R} \cdot \sigma_{mean} \tag{9}$$

In the stress space, this is the equation of a straight line from the origin with a slope given purely of the stress ratio R. Note that $R = +1$ corresponds to the horizontal axes for σ_{mean}, while $R = -1$ corresponds to the vertical axes for σ_a. An example (with units MPa) of a Goodman diagram using tensile static strength of 30, compression strength of -20, and alternating strength (depending of number of cycles) equal 10 is visualized in Figure 1. For a given stress ratio R, the combined strength can be estimated from the interception of the strength line given by Eq. (7) and the stress combination given by Eq. (9).

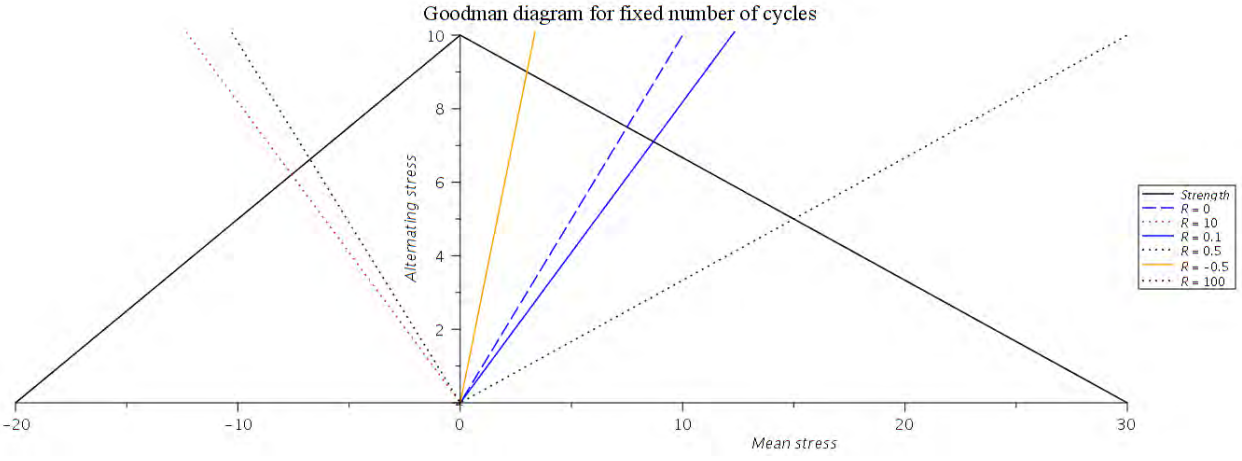


Figure 1: Example of a constant life diagram for a given number of cycles.



2.3 Fatigue strength and Eurocode 5

The degradation of strength due to cyclic stresses in wood is commonly represented by letting the strength level (SL) be reduced linearly with the base 10 logarithm of the number of cycles N (SN-curves).

$$SL = B - A \cdot Log_{10}(N) \tag{10}$$

The slope of the SN-curve is given by parameter A. The parameter A must be calibrated by experimental testing. The parameter B is the interception of the fitted straight line $A \cdot Log_{10}(N)$ with the stress axes (SL). The stress level can be either real stresses or dimensionless stress levels by scaling the stresses by some representative stress level.

In the annex A of EN 1995-2 (2004) [1] the design stress level is given by the parameter k_{fat}, where

$$k_{fat} = 1 - \frac{1-R}{a(b-R)}\mathrm{Log}(\beta \cdot N_{obs} \cdot t_L) \geq 0 \tag{11}$$

and the product $(\beta \cdot N_{obs} \cdot t_L)$ is the number of cycles to be used in the design [1]. This corresponds to a scaling of Eq. (10) by the static design strength, since

$$f_{\mathrm{fat,d}} = k_{\mathrm{fat}} \frac{f_{\mathrm{k}}}{\gamma_{\mathrm{M,fat}}} \tag{12}$$

A comparison of Eq. (10) to (11) gives $B = 1$ and implies that the design static strength is achieved for one full cycle. However, strictly speaking the static strength is determined at one quarter of a stress cycle, and hence B equal unity should correspond to $\mathrm{Log}(0.25) = -0.6$. The assumption $B = A \cdot Log_{10}(1) = f_{fat,d}$ is a convenient choice but does not necessary match experimental results. Usually, the slope of an SN curve is determined based on experimental mean values. Forcing a SN curve to pass through the point $(Log(1), f_{mean})$ puts a restriction on the determination of the slope of the SN curve.

By fitting the slope of the SN curve to experimental mean values both from static and cyclic results, and thereafter scaling the vertical axes of the SN curve by the ratio between the static design strength to mean experimental values, is the same as to rotate the whole SN curve about the point of interception between the SN-curve and the horizontal axes for number of cycles to failure with respect to absolute stresses. Hence, the characteristic values for low cycle fatigue strength are matching the static values, but it is implied that the standard deviation of the fatigue strength is linearly decreasing with the logarithmic number of cycles and ends up with zero standard deviation at the interception point. If this assumption is valid is not known to the authors.

The informative annex A in EN1995-2 [1] has in principle separate curves for each type of stress/or connection type and value of the ratio of min and max stresses (R-values).

By comparison of Eqs. (10) and (11), the slope A of the SN curves is given by

$$A = \frac{1-R_T}{a \cdot (b-R_T)} \tag{13}$$

Note that the informative annex A in EN1995-2 has a special interpretation of the stress ratio R. To distinguish it from the usual definition given by Eq. (4), it is here (and in a proposal for new EN1995-1-1) denoted R_T. The use of R_T requires that the absolute values of the stresses govern what is used as minimum and maximum stresses. Here it is required that $\sigma_{d,min}$ is determined such that

$$|\sigma_{d,min}| \leq |\sigma_{d,max}| \tag{14}$$

Consequently, the value of R_T is limited to the range $-1 \leq R_T \leq +1$. Note that this choice also necessitates that the total variation of stresses must be subdivided into separate cases dependent on the mean value of σ_{mean}, i.e. a separate case for tensile stresses $\sigma_{mean} \geq 0$, which is different from the case of compression stresses where $\sigma_{mean} \leq 0$.

This is reflected in the various cases in EN 1995-2 with different sets of parameters for a and b in Eq. (13). The tabulated parameter values proposed for new EN1995-1-1 are given in Table 1. By the separation into two separate cases based on the mean stresses, only one quadrant of the stress space is needed for each case.



Table 1: Proposed values for SN curves in the new EN 1995-1-1

Stress type	**Stress σ_d**	**Mean stress $\sigma_{d,mean}$**	***a***	***b***
Normal; compression	$\sigma_{d,c,0}$, $\sigma_{d,c,90}$	≤ 0	2.0	9.0
Normal; tension parallel	$\sigma_{d,t,0}$	≥ 0	9.5	1.1
Normal; tension perpendicular	$\sigma_{d,t,90}$	≥ 0	4.7	2.1
Shear	τ_d		6.7	1.3
Connection, dowels 12 mm		≥ 0 or ≤ 0	6.0	2.0
Connection, nails		?	6.9	1.2

By applying the parameters in Table 1 and a stress ratio of $R_T = 0.1$, the SN-curves plotted in Figure 2 are obtained. For this stress ratio, tension parallel and perpendicular to the grain direction have practically the same relative strength reduction due to fatigue loading, see the two dotted lines in Figure 2.

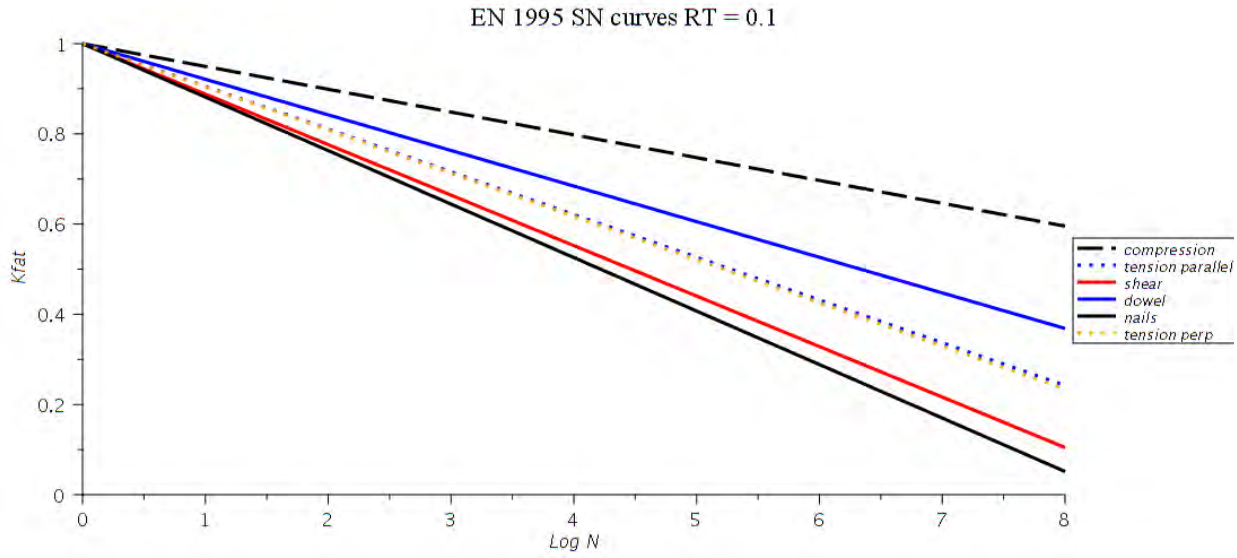


Figure 2: Proposed S-N curves for various cases with $R = 0.1$ for new EN1995-1-1.

The slopes of the curves are given by the value of A, Eq. (13), and a plot of A for the range of R_T shows considerable variation for the various values of R; confer Figure 3. From this plot we also see that the only value of the stress ratio giving equal strength reduction for tension parallel and perpendicular to the grain is approximately the value $R_T = 0.1$. The curves for compression and tension parallel to grain end up with the same value for $R_T = -1$ which is correct, since this is the same stress situation in both cases, having $\sigma_{max} = -\sigma_{min}$. For tension and compression perpendicular to grain, the curves do not end up with the same value for $R = -1$, and this is not satisfactory.

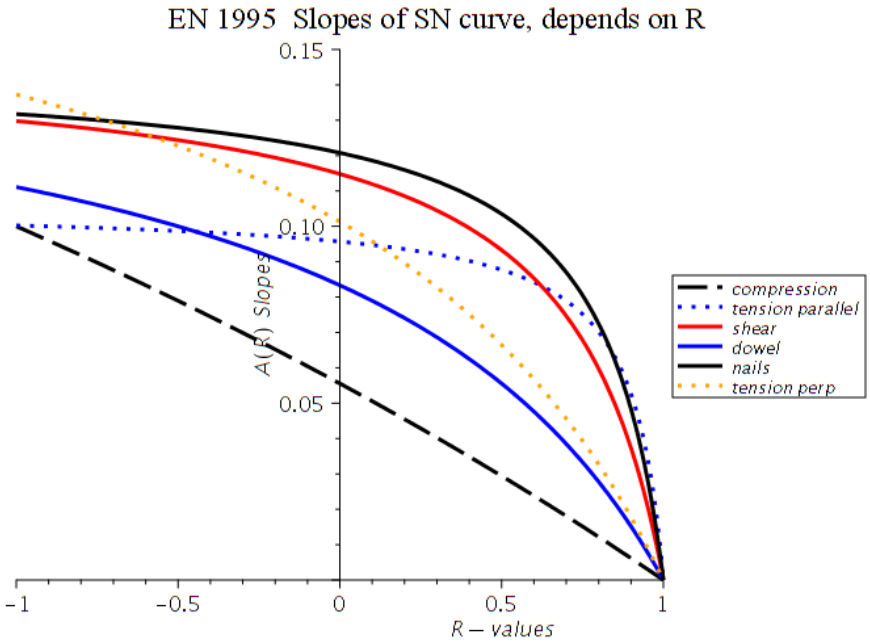


Figure 3: The slope parameter A for the EN 1995 S-N curves for various values of $R = R_T$.

2.4 Calibration of fatigue model for dowel connection

In Figure 4, the SN curves from EN 1995 for dowel connections for various R ratios are plotted. By reading the values for the various R ratios at a given number of cycles, for example 1 million cycles ($Log(N) = 6$), and plotting them in a constant life diagram, it will be visible how well they fit into a linear or nonlinear interaction between alternating and mean stresses.

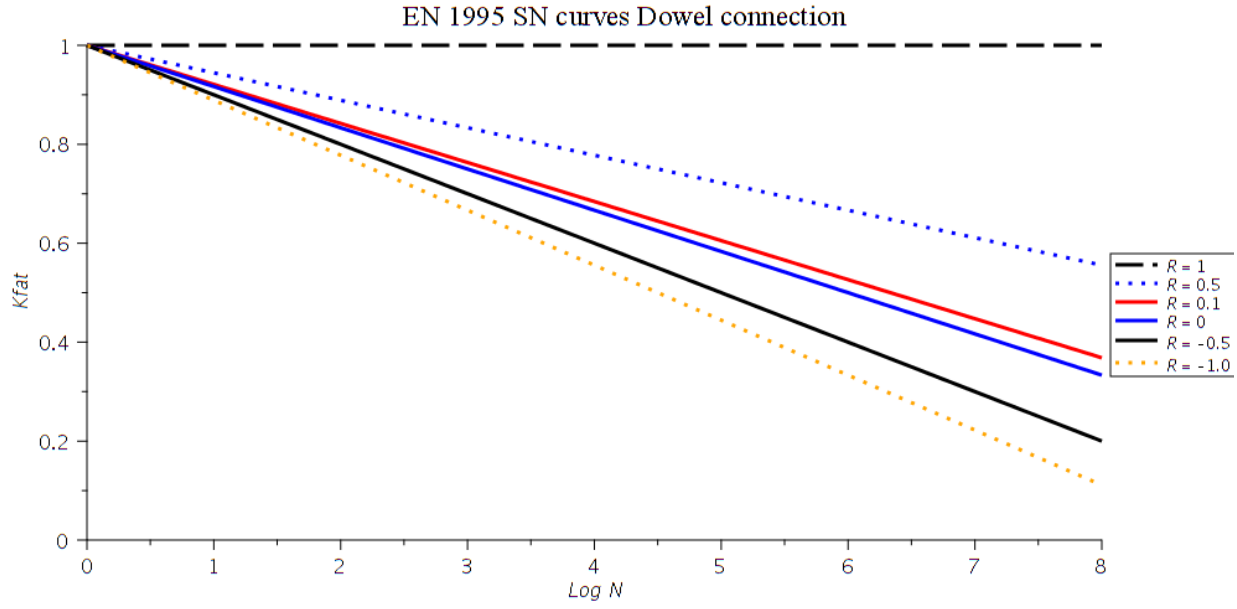


Figure 4: S-N curve for dowel connection

Few experimental test series have enough experimental results to cover the whole field of R values. For dowel connections with slotted-in steel plates, the experimental data used in the calibration are published in refs. [5] to [8], and depicted in Figure 5 and Figure 6. The slopes of the SN curves were determined to $A = 0.079$ and $A = 0.111$ for $R = 0.1$ and $R = -1$, respectively. Note that f_{max} is the available maximum relative strength based on mean values and has the same meaning here as the symbol k_{fat} used in EN 1995.

The maximum strength f_{max} (and k_{fat}) is a dimensionless parameter which relates the fatigue strength to the corresponding static strength and this strength should be compared to the maximum stress σ_{max}.

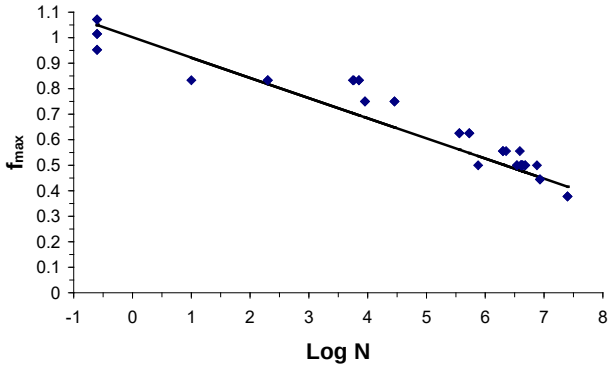


Figure 5: Maximum stress vs. cycles to failure, $R = 0.1$, EC5 compared to test results.

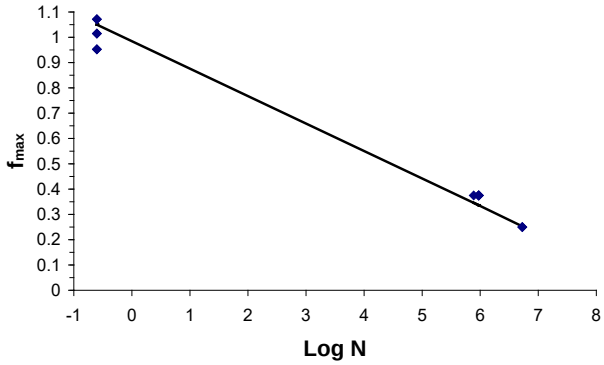


Figure 6: Maximum stress vs. cycles to failure, $R = -1$, EC5 compared to test results.

As an example on calibration, 1 million cycles ($Log(N) = 6$) will be used. For reversed loading $R = -1$, this gives

$$f_{max} = \frac{\sigma_{max}}{f_{mean}} = \frac{\sigma_a}{f_{mean}} \quad = 1 - 0.111 \cdot 6 \approx 1 - \frac{6}{9} = \frac{1}{3} \tag{15}$$

For loading with $R = 0.1$ is the following obtained

$$f_{max} = \frac{\sigma_{max}}{f_{mean}} = 1 - 0.079 \cdot 6 \approx 0.526 \tag{16}$$

and by use of Eq. (5):

$$\frac{\sigma_a}{f_{mean}} = 0.526 \cdot \frac{1}{2}(1 - 0.1) = 0.236 \text{ and } \frac{\sigma_{mean}}{f_{mean}} = 0.526 \cdot \frac{1}{2}(1 + 0.1) = 0.289 \tag{17}$$

Plotting this data into a linear constant life diagram (Goodman), the results show that a linear constant life diagram in this case fits the experimental results well.

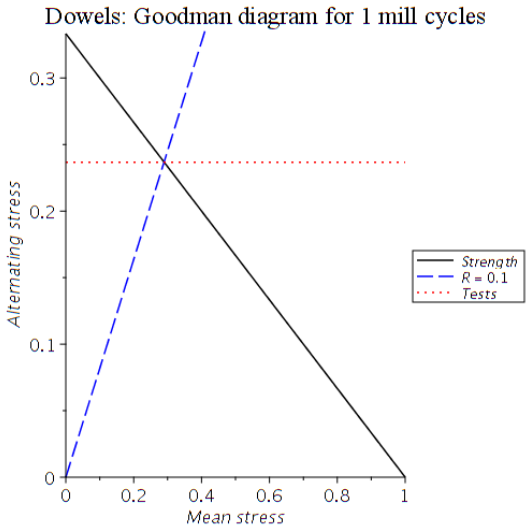


Figure 7: Constant life diagram for 1 million cycles for dowel connection



To generalize the results for other stress ratios $R = R_T$, we combine Eqs. (5) and (7), giving

$$\frac{\frac{1}{2}\sigma_{max}(1-R)}{f_a} + \frac{\frac{1}{2}\sigma_{max}(1+R)}{f_{mean}} = 1 \tag{18}$$

The strength for purely alternating load f_a is found by letting $R = -1$ and is determined by

$$f_a = f_{mean} \cdot (1 - A^* Log(N)) \tag{19}$$

where A^* means the slope of the SN-curve determined for $R = -1$. The maximum allowed stress σ_{max} is governed by

$$\sigma_{max} = f_{mean} \cdot (1 - A \cdot Log(N)) \tag{20}$$

Combining Eqs. (18), (19) and (20), the resulting equation is solved for A giving

$$A = \frac{(1-R) \cdot A^*}{2 - (1+R) \cdot A^* Log(N)} \tag{21}$$

Considering the expression for the generalized slope A, it is observed that it will not be possible to do this type of calibration independent of which number of cycles the calibration is made at. The slope A will always be dependent of the number of cycles used for calibration. If we choose to calibrate dowel connections at 1 million cycles, we will have $\mathrm{Log}(N) = 6$ and $A^* = 0.111 \approx 1/9$, giving

$$A = \frac{(1-R)}{6(2-R)} \tag{22}$$

This result is identical with the use of Eq. (13) and the parameters for dowels in Table 1 and is the basis of the calibration performed for annex A in EN 1995-2 [1].

3 Results

In the following all calibrations given in EN 1995 are explored for various values of the stress ratio in the domain $-1 \leq R_T \leq 1$, and for various number of cycles to failure. The maximum stress σ_{max} is set equal to the fatigue strength and the alternating and mean stresses are calculated by Eq. (5) and plotted in a constant life diagram format.

3.1 Dowel connections

Considering Figure 8, the interaction line is straight for 1 million cycles, as it should be as this is the value used for the calibration. The calibration is probably satisfactory up to 10 mill cycles, but above it is obviously not working for all R_T ratios as the slope of the strength line then becomes positive. For smaller number of cycles, the calibration probably gives slightly conservative results as the curves appear somewhat concave.

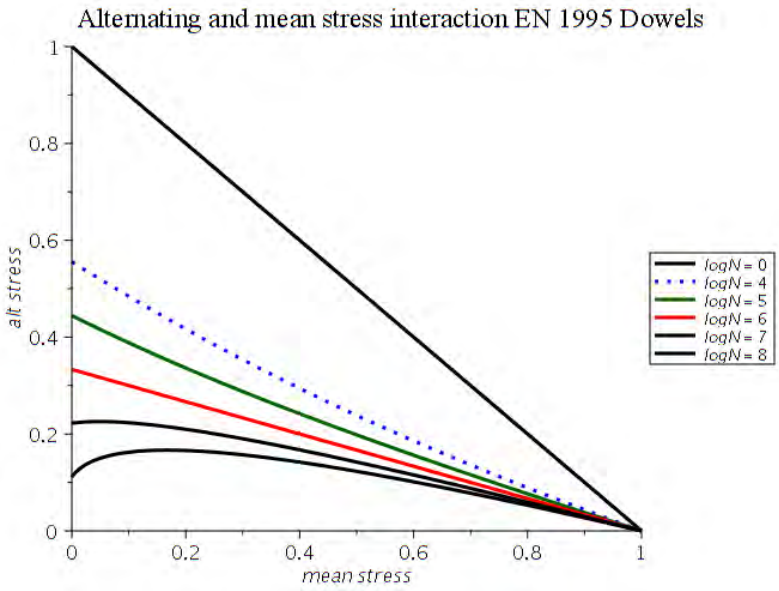


Figure 8: Constant Life diagrams for dowel connections

3.2 Compression parallel and perpendicular to grain

The calibration made for compression parallel and perpendicular to grain, see Figure 9, gives only a straight line for one cycle, while more cycles lead to convex curves. The calibration might be acceptable up to 100000 cycles for the full range of R_T, but above the calibration does not seem to work, at least not for the full range of the stress ratios.

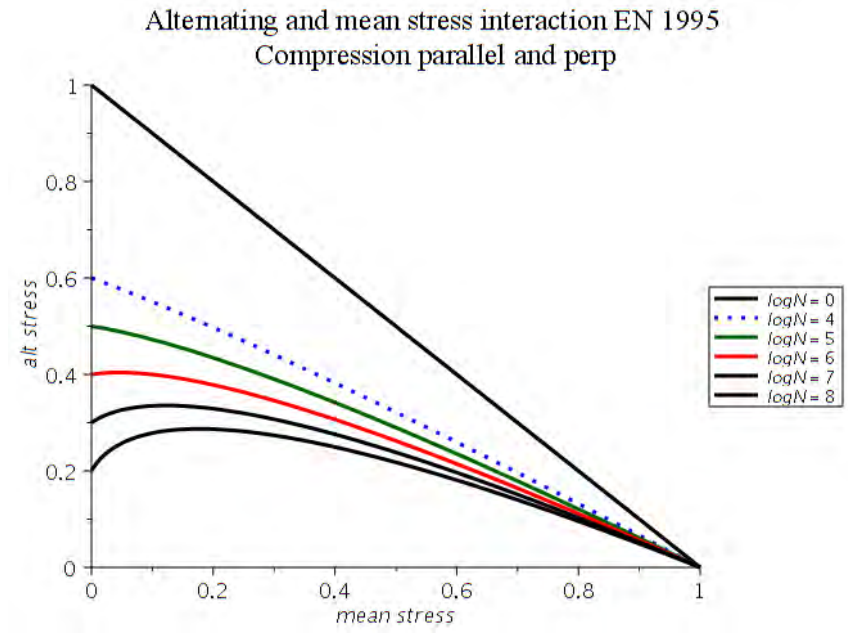


Figure 9: Constant Life diagrams for compression parallel or perpendicular to grain



3.3 Tension parallel to grain

The strength interaction curves are all strongly concave (except for one cycle) for tension parallel to grain, see Figure 10. It is noted that the calibration gives the same values as for compression parallel to grain for purely alternating loads ($R_T = -1$), as it should, as this loading situation is identical both for compression and tension. This property is also visual from the SN-curve plots for alternating loads ($R_T = -1$) in Figure 11, where the compression and the tension parallel curves practically coincide. However, it is hard to find any physical reason for the excessive concave shape of the strength curves in Figure 10 and this effect is likely to be caused by improper calibration or experimental data.

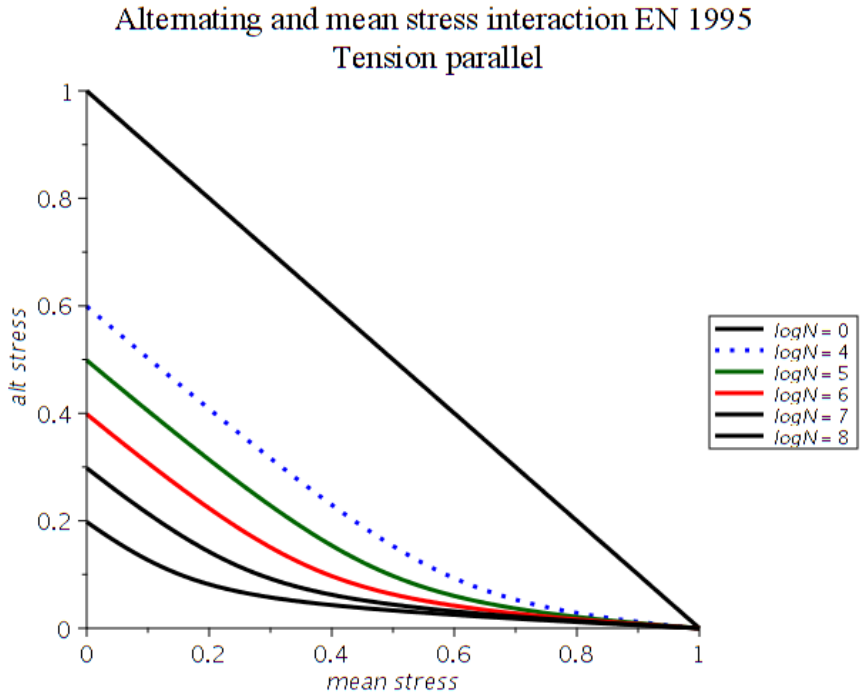


Figure 10: Constant Life diagrams for tensile stresses parallel to grain

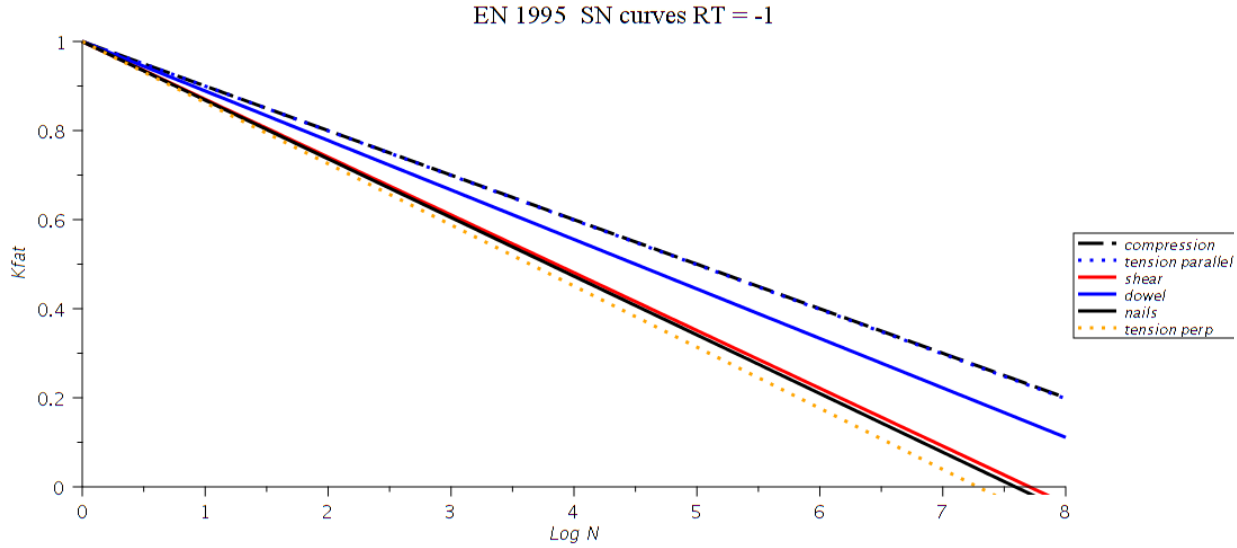


Figure 11: S-N curves for alternating loads $R_T = -1$ in EN 1995

3.4 Tension perpendicular to grain

By comparing the SN-curves for alternating loads ($R_T = -1$) in Figure 11, it is obvious that either the compression curve is not valid for $R_T = -1$, or the tension curve is not valid for $R_T = -1$, as purely alternating loads have the same stresses regardless of whether the stress quadrant is denoted compression or tension. Considering the strength curves in Figure 12, they are hardly valid for cycles above 100000 cycles, at least not for R_T values less than 0.5.

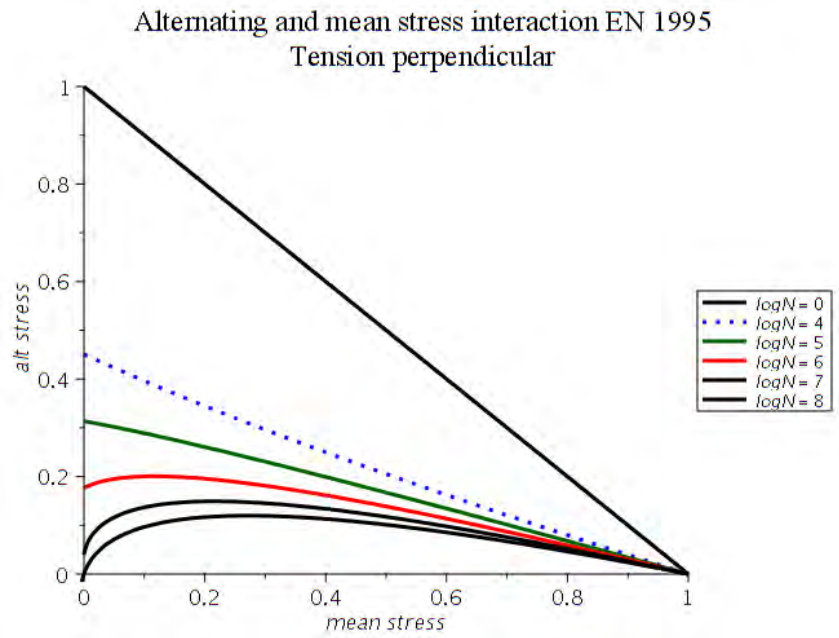


Figure 12: Constant Life diagrams for stresses perpendicular to grain

3.5 Shear

The strength curves for shear are presented in Figure 13. The calibration of fatigue shear strength seems inconsistent as they are strongly concave up to one million cycles. Probably, the calibration suffers from lack of consistent experimental results.

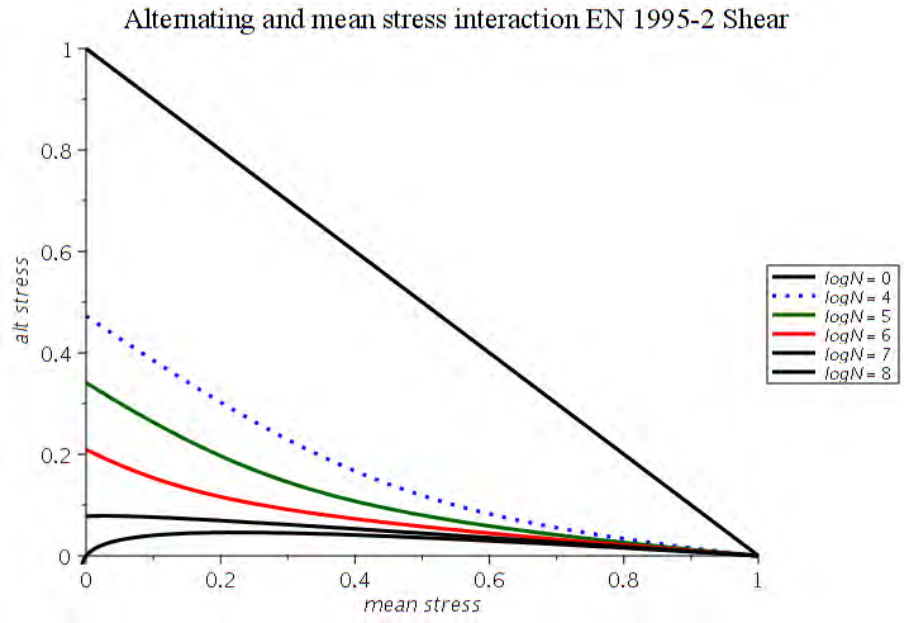


Figure 13: Constant Life diagrams for shear stresses



3.6 Nails

The strength curves for nails are presented in Figure 14. This calibration has approximately the same parameters as shear, and no further comments are made here.

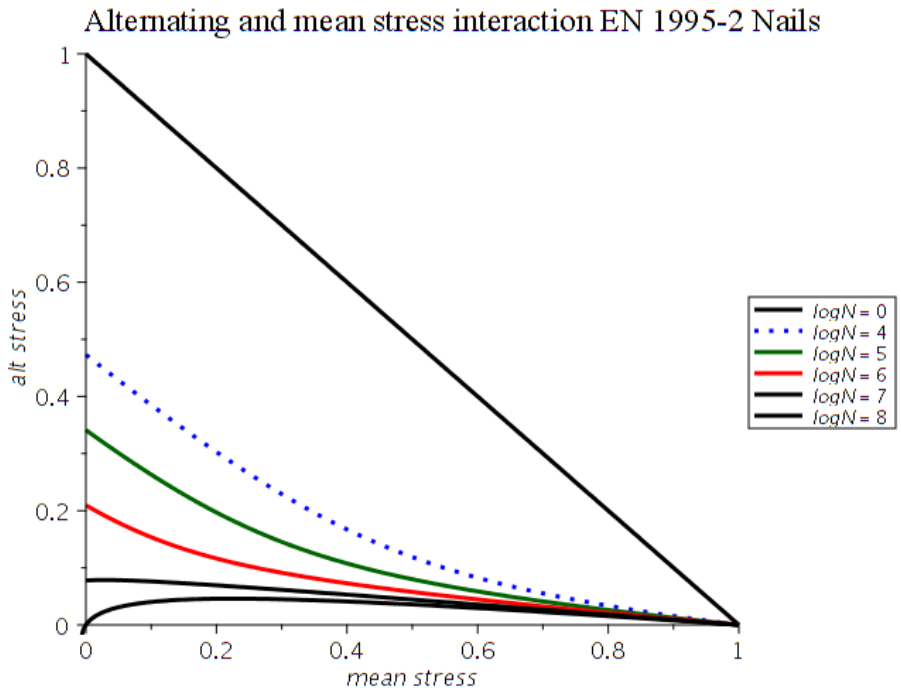


Figure 14: Constant Life diagrams for dowel connections

4 Concluding Remarks

Some aspects of the predictive rules for fatigue life of wooden structures in the present and future version of the Eurocode EN1995 have been explored and commented in the present paper. It has been shown that the general expression for determination of the slopes of the SN curves has limited generality and gives values which are obviously erroneous in some ranges. Especially for stress ratios R_T less than 0.5 and high number of cycles the fatigue strength appears to be wrongly estimated. Possible causes for this defect might be lack of experimental data, or calibration based on only a narrow band of stress ratios. A re-evaluation and possibly a recalibration of the strength parameters are recommended.

References

[1] European Committee for Standardization (2004) Eurocode 5 – Design of timber structures – Part 2: Bridges, Annex A, EN 1995-2: 2004.

[2] European Committee for Standardization (2005) Eurocode 5 – Design of timber structures – Part 1-1: General rules and rules for buildings, EN 1995-1-1: 2005.

[3] Smith, I., Landis, E, Gong, M. (2003) Fracture and Fatigue in Wood. John Wiley & Sons, England.

[4] Ansell, M.P. (1995) Fatigue design for timber and wood-based materials. In: Timber Engineering, STEP 2, lecture 22, STEP/EUROFORTECH, 1. ed. Centrum Hout, The Netherlands.

[5] Malo, K.A. (1999) Fatigue Tests of Dowel Joints in Timber Structures, Nordic Timber Bridge Project, ISBN 91-89002-24-5. Nordic Timber Council AB, Stockholm, Sweden.

[6] Malo, K.A., Holmestad, Å and Larsen, P.K. (2001) Fatigue Tests on Dowel Joints in Timber Structures. IABSE Conference "Innovative Wooden Structures and Bridges", August 29-31, Lahti, Finland.

[7] Malo, K.A (2002) Fatigue Tests of Dowel Joints in Timber Structures, Part II: Fatigue Strength of Dowel Joints in Timber Structures. Nordic Timber Bridge Project, ISBN 82-7120-035-6. Nordic Timber Council AB, Stockholm, Sweden.

[8] Malo, K.A., Holmestad, Å and Larsen, P.K. (2006) Fatigue Strength of Dowel Joints in Timber Structures. 9th World Conference of Timber Engineering, August 6 – 10, Portland, OR, USA.

Conference Proceedings 4th ICTB (2022)
https://doi.org/10.24451/2xwb-rt40

ICTB 2021PLUS
4th International Conference on Timber Bridges
Biel/Bienne, Switzerland, 9 -12 May 2022



Assessment of glulam structures: moisture monitoring and investigation on the effect of climatic conditions on durability

Placide Uwizeyimana[1], Marianne Perrin[2] and Florent Eyma[3]

Abstract

Glulam is currently an interesting solution to build economical, environmentally friendly and mechanically strong timber bridges. Nevertheless, the durability of these bridges is influenced by the climatic wetting/drying (W/D) cycles to which they are exposed. This experimental study is aimed at setting up a technique for continuous moisture content (MC) monitoring of glulam beams over time (structural health monitoring), and to study the impact of W/D cycles on their mechanical properties. For this purpose, patch-type sensors were embedded between the lamellae, thus allowing local MC to be monitored. A system based on continuous resistive measurements was developed in the laboratory. Durability tests were carried out to expose the glulam specimens to accelerated W/D cycles in order to highlight the impact of variable climatic conditions, generally encountered in timber bridges, on the mechanical properties of glulam beams in bending. The results showed that the patch sensors and the developed measurement system will be able to be useful and functional for the continuous MC monitoring in glulam beams used in timber bridges. In addition, the exposure of glulam beams to these moisture variations has a significant influence on the bending strength whereas it does not seem to have one on the modulus of elasticity. These results also enabled to propose an experimental model for predicting the bending strength as a function of W/D cycles.

1 Introduction

In bridges construction, timber structures are economical, easy to build and use renewable materials providing solutions to current sustainable development issues. In order to increase the structural capacity of this material, glulam is increasingly used as a load-bearing element in these structures [1]. However, for a few years, durability problems have been observed in these structures, limiting their development [2-4]. Degradations related to excessive (often local) moisture in the material, and more particularly to climatic wetting/drying (W/D) cycles have been observed and can lead to severe structural damage. Moreover, little is known about the effects of these W/D cycles on the mechanical strength of these structures. It is therefore essential to associate to these timber bridges a continuous monitoring system of the local MC in order to quickly identify the zones likely to present risks of pathologies. So, this work aims firstly to propose a technique for continuous monitoring of local moisture content (MC) via the use of resistive sensors embedded into glulam beams. To do this, resistive patch-type sensors were integrated between the lamellae. The data were collected using a continuous measurement and recording system developed in our laboratory. The MC values were obtained using an equation relating MC and electrical resistance [5].

Then the effect of W/D cycles on the structural durability of glulam beams was studied. According to the literature, the study of durability under natural conditions is usually conducted by exposing the material to an outdoor environment, which requires a relatively long test duration [6]. As a result, it is often necessary to carry out durability tests with accelerated ageing cycles. These are usually based on exposing the material to controlled relative humidity and temperature conditions [7]. Indeed, moisture is an ageing factor that strongly impacts hydrophilic materials like wood. These hydric ageing induce a progressive mechanical degradation most often linked to heterogeneous shrinkage/swelling mechanisms in the wood [8]. Although some works have focused on accelerated ageing tests, no study refers to the actual ageing cycles encountered in timber bridges that could be used to study the durability of these glulam beams. Following this observation, the conditions of an accelerated W/D cycle were defined in order to come as close as

[1] Assistant professor, Institut Clément Ader (ICA), CNRS UMR 5312, University of Toulouse, France, placide.uwizeyimana@iut-tarbes.fr
[2] Institut Clément Ader (ICA), CNRS UMR 5312, University of Toulouse, France, marianne.perrin@iut-tarbes.fr
[3] Institut Clément Ader (ICA), CNRS UMR 5312, University of Toulouse, France, florent.eyma@iut-tarbes.fr

possible to the reality encountered in the field, i.e. to obtain MC values equivalent to those present in timber bridges exposed outdoors, i.e. between 10% and 30% MC according to the literature [3,9,10]. Then, glulam specimens were exposed to accelerated cycles defined in the laboratory in order to highlight the impact of varying moisture and temperature conditions on the bending mechanical properties of glulam beams. The final objective is to establish models for predicting the residual life of these structures in order to optimise preventive maintenance operations.

2 Materials et methods

2.1 Specimens used, ageing conditions and moisture monitoring protocol

66 glulam beams made of Douglas fir were used. Douglas fir (*Pseudotsuga menziesii*) was chosen because it is very commonly used in the construction of timber bridges [2]. Each glulam beam was made of three lamellae and was 480 mm in length (L) with a cross-section 30 mm (R) x 30 mm (T), dimensions defined according to the standard EN 408 [11]. These beams were exposed to accelerated W/D cycles and the evolution of the mechanical properties in bending was evaluated. An accelerated W/D cycle is defined in three phases in order to obtain variable moisture between 10% and 30% MC (Figure 1). The first phase (AB) consisted of humidifying the specimens in a climatic chamber at 98% RH and 35°C until the mass was stabilised, thus achieving 20.8% MC. In the second phase, the specimens were immersed in water at room temperature (20°C) for 24 hours to simulate the presence of free water found in the wooden elements of the bridges [12]. This step allowed 30% MC to be obtained. The final drying phase consisted of returning the specimens to a climatic chamber at 50% RH and 35°C until the mass had stabilised, thus allowing the wood to return to 10% MC.

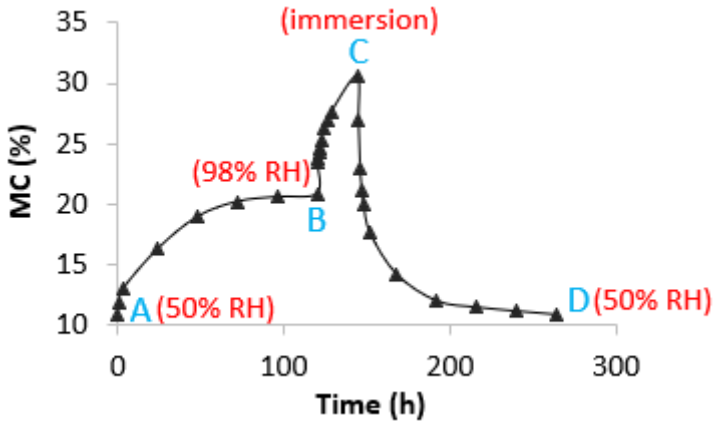


Figure 1: Wetting/drying cycle used for ageing glulam specimens

On the whole, seventeen accelerated W/D cycles were performed. Moisture content were monitored on six control specimens instrumented with three resistive patch-type sensors (MC1, MC2 and MC3) embedded between the lamellae (Figure 2). The instrumentation and measurement protocol are given in [5].

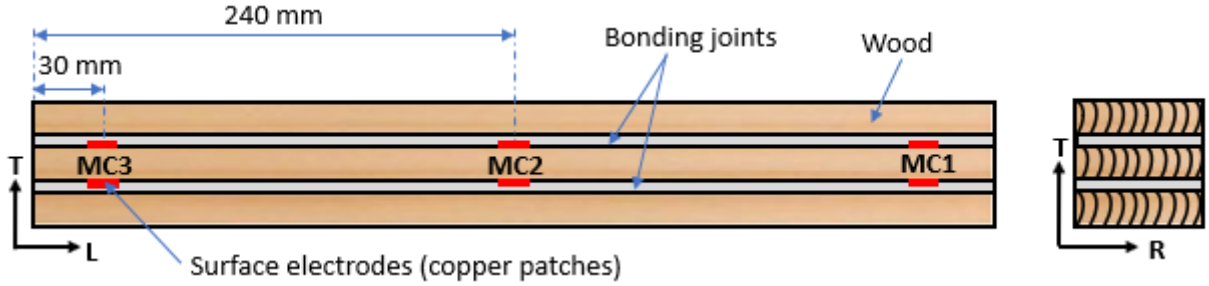


Figure 2: Representation of a glulam specimen instrumented with resistive patch-type sensors between the lamellae for moisture content monitoring

2.2 Mechanical characterization in bending

In order to identify the effect of moisture variations on the mechanical strength of glulam beams, four-point bending tests (Figure 3) were conducted during the different W/D cycles, in 11 sequences presented in Table 1. Before each bending test, the specimens were conditioned in a climatic chamber at 65% RH and 20°C until their masses were stabilised according to standard EN ISO 12571 [13]. The specimens had an average density of 558 ± 26 kg/m3 at 12 ± 1% MC. The bending tests were then conducted with an imposed displacement speed of 5.4 mm/min. The deflection was measured using a Solartron AX5S LVDT displacement sensor. The bending strength and modulus of elasticity were determined after each sequence, according to standard EN 408 [11].

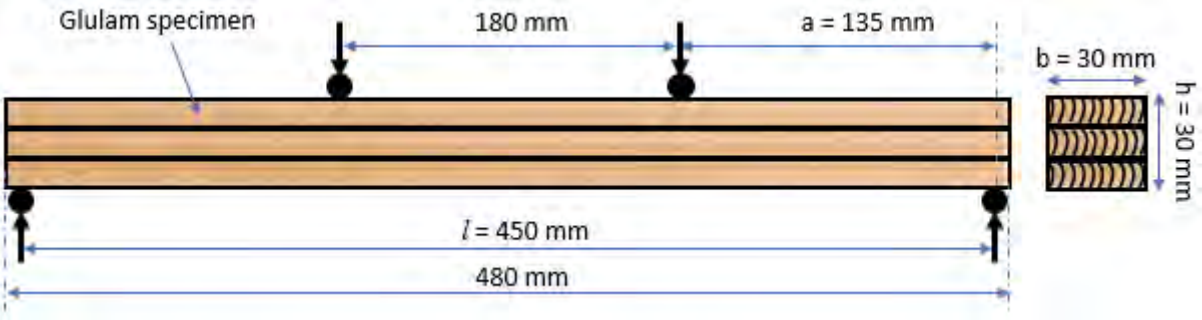


Figure 3: Four-point bending tests performed according to standard EN 408 [5]

Table 1: Sequencing of bending tests during W/D cycles

Number of cycles	0	1	2	3	5	7	9	11	13	15	17
Sequence number	1	2	3	4	5	6	7	8	9	10	11
Number of specimens	10	5	5	5	5	5	5	5	5	5	5

3 Results and discussion

3.1 Moisture evolution in glulam specimens during ageing

The Figure 4 shows the MC evolution of one specimen (all specimens having similar trends), monitored as a function of time for 17 W/D cycles. It can be seen that the wood MC measured in the climatic chamber are quite similar (phase AB) for all cycles. However, some variability between cycles in the immersion phase (BC) is noticed. According to the additional tests carried out, this variability can be explained by the change in conditioning when the specimens are moved from the climatic chamber to the immersion tank (and vice versa), which induces a sudden change in electrical resistance due not only to the electrolytic substances present in the water but also to the temperature change.

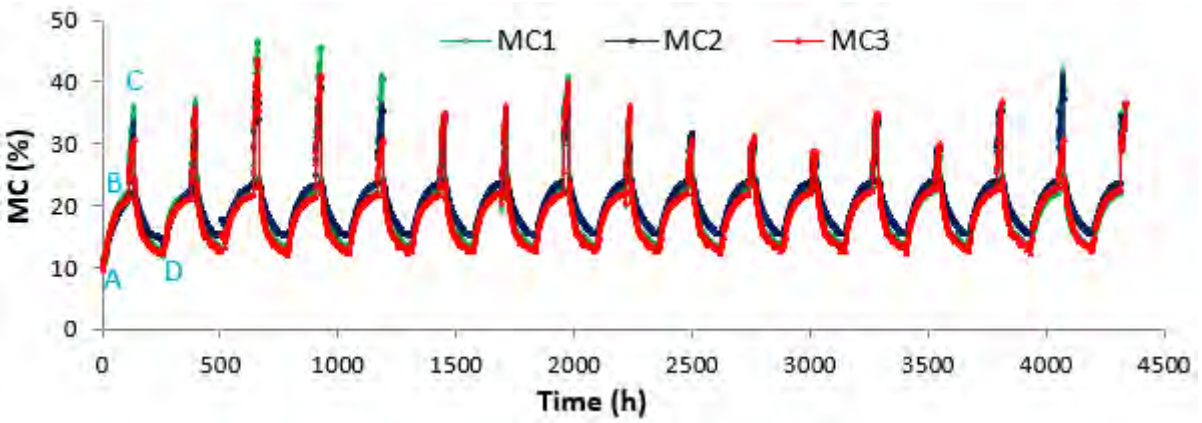


Figure 4: Evolution of the MC monitored by the three sensors MC1, MC2 and MC3 in glulam specimen



The MC curves (Figure 4) also enabled to show a difference in moisture between the edges (MC1 and MC3) and the centre (MC2) of the specimen during the W/D cycles. This allows to appreciate the ability of the embedded sensors to perform local MC monitoring, thus allowing to estimate the moisture gradients between the edges and the centre of the glulam beam.

Figure 5 shows the moisture gradients at points B, C and D of each W/D cycle for the three conditions (98% RH, immersion and 50% RH) between the edge and the centre of the specimen (average moisture (MC1 and MC3) - MC2). At the first sight, the moisture gradients are globally positive during the wetting phase (98% RH in the climatic chamber and in immersion), whereas they are negative in the drying phase (at 50% RH). This can be explained logically by the fact that during the wetting phase, the MC remains higher at the edge of the specimen (MC1 and MC3) than at its centre (MC2). Then the situation is reversed when the specimen is dried. It was also noted that the moisture gradients are very variable from one specimen to another with sometimes significant standard deviations, which can be explained by the heterogeneity between the specimens. Furthermore, these moisture gradients can generate internal stresses in the wood and create cracks in glulam wood structures [1,3,14]. The impact of these damage mechanisms created by cyclic moisture ageing is analysed in the next section.

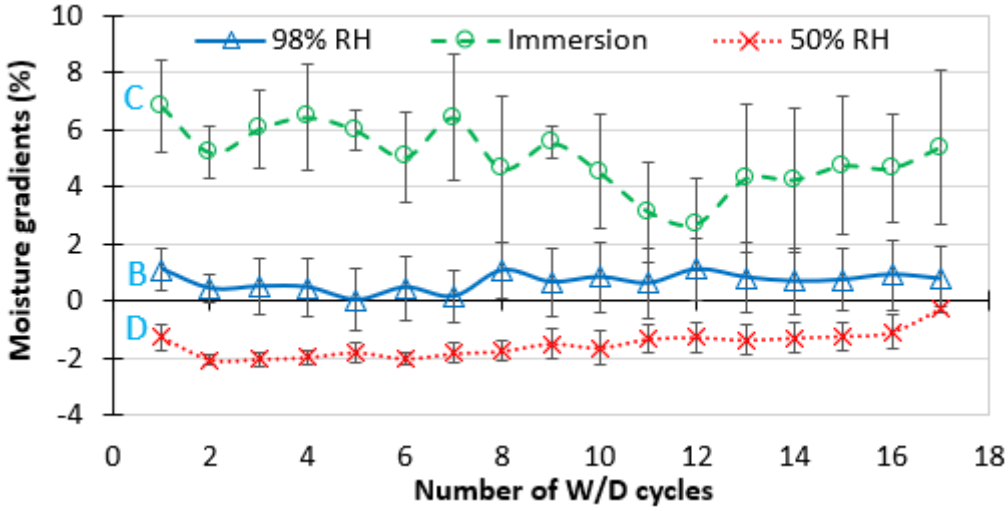


Figure 5: Moisture gradients measured between the edge and the centre of the specimen at points B, C and D of the W/D cycle

3.2 Influence of wetting/drying cycles on the mechanical strength of glulam

3.2.1 Mechanical behaviour in bending

Figures 6a and 6b show the load-displacement curves of specimens respectively before ageing and specimens exposed to 17 W/D cycles. In general, whatever the cycle, the curves show a linear part at the beginning of the load, where the load seems to be less than 50% of the maximum load. Then the curve becomes slightly non-linear until the load reaches its maximum value followed by specimen failure. This corresponds classically to the static bending behaviour of wood [15,16]. However, unlike the aged specimens after 17 cycles, it can be observed that the majority of the unaged specimens (at 0 cycles) shows a more pronounced load recovery even after a significant load drop in the non-linear zone. Furthermore, after 17 cycles, the material seems to lose its ability to deform in the non-linear zone, i.e. it loses its "ductility" after cyclic moisture ageing. A decrease of failure load of 2990 N (i.e. 43.5%) after ageing can also be observed as can be seen in Figure 6b by comparing the average values failure load at 0 and 17 cycles.

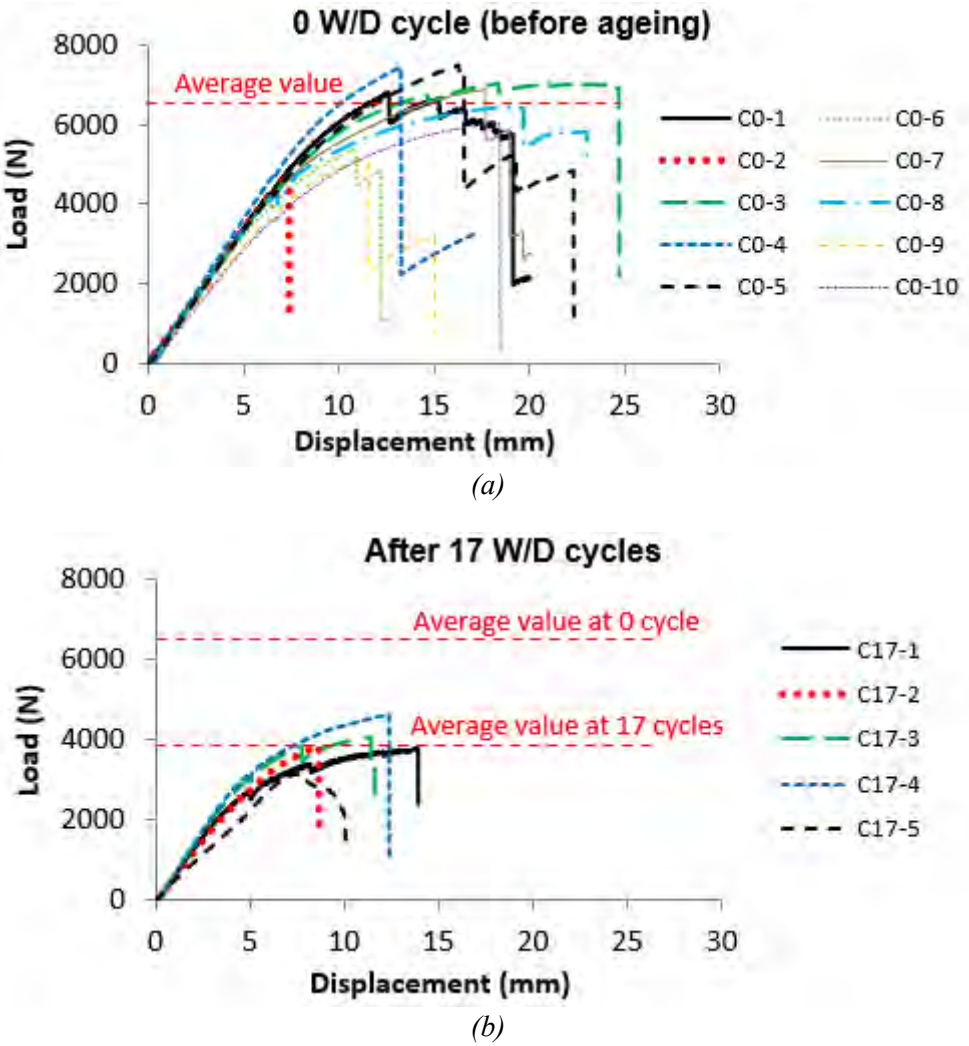
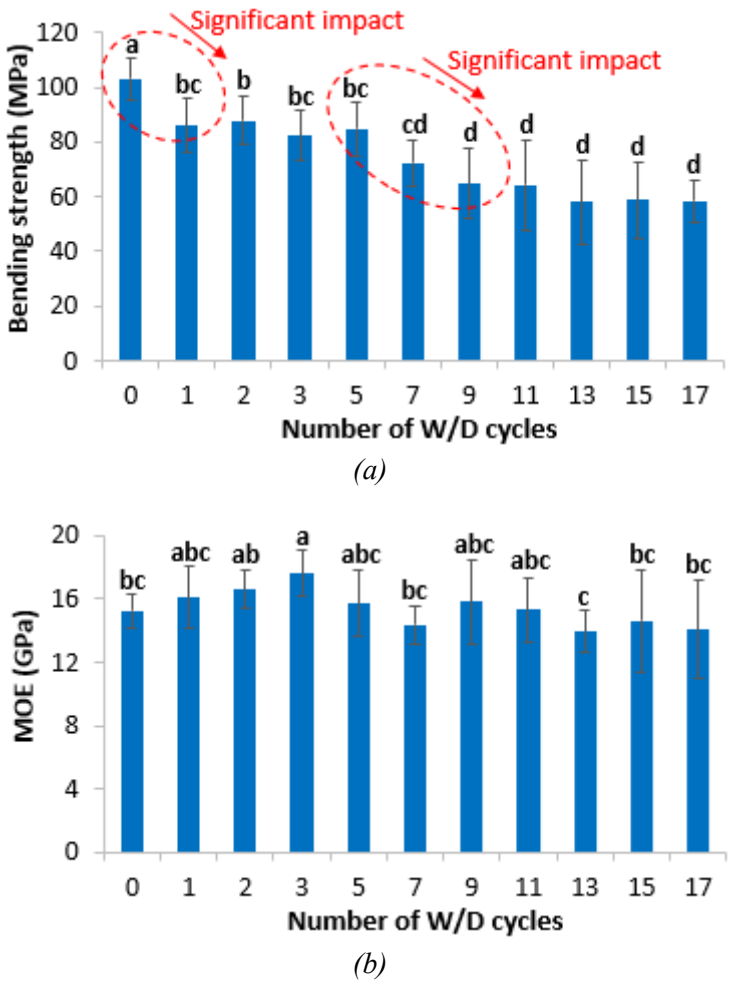


Figure 6: Load-displacement curves of the specimens tested in bending: (a) before ageing (0 W/D cycle); (b) after ageing (after 17 W/D cycles)

3.2.2 Influence of wetting/drying cycles on bending strength and modulus of elasticity

Figures 7a and 7b show the evolution of the bending strength and the modulus of elasticity respectively as a function of the number of W/D cycles. To determine whether there is a significant difference between the calculated average values as a function of the cycles, an analysis of variance at 95% confidence was performed using XLSTAT software. The results of this analysis for the 17 cycles are presented in Figure 7 by the letters "a, b, c, d". It can be seen that the bending strength of the unaged specimens (0 cycle) and those of the aged specimens (after 17 cycles) are significantly different. It can also be seen that the decreases in strength are much more pronounced after the first cycle and after the seventh cycle. This weakening of the bending strength can be explained by microstructural changes of the wood material under cyclic moisture stress [17,18]. Indeed, during the W/D cycles, some microcracks were observed in the material that caused irreversible damage and thus the weakening of the bending strength. Besides, from Figure 7b, it can be observed that no significant influence of the W/D cycles was found on the modulus of elasticity.



(a)

(b)

Figure 7: Evolution of the mechanical properties in bending of the specimens during the W/D cycles: (a) case of the bending strength; (b) case of the modulus of elasticity (MOE)

By considering the percentage decrease in strength caused by each W/D cycle, the loss of bending strength as a function of cycles can be calculated using equation (1).

$$\Delta\sigma_{max}(\%) = \frac{\sigma_N - \sigma_0}{\sigma_0} \text{x } 100 \quad (1)$$

where $\Delta\sigma_{max}(\%)$ is the loss of bending strength,
σ_N(MPa) is the bending strength after N cycles,
σ_0(MPa) is the bending strength of the specimens before ageing.

Figure 8 shows the loss of bending strength as a function of the number of cycles. Overall, the 17 W/D cycles cause an average 43.5% loss of the bending strength of the unaged specimens (i.e. an average decrease of 44.8 MPa). The trend analysis enabled the predictive experimental model presented in Figure 8 to be proposed. This model allows to estimate the bending strength (**σ**max) as a function of the number of cycles (N) with a coefficient of determination (R^2) of 93%.

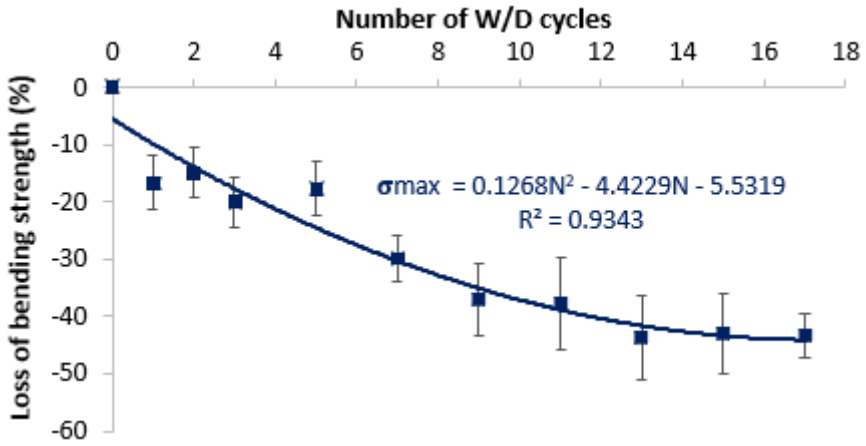


Figure 8: Experimental model of bending strength loss as a function of W/D cycles (N: number of cycles)

4 Conclusion

Within the framework of structural health monitoring of timber bridges, the objective of this study was to set up a system for continuous monitoring of local moisture content (MC) in glulam beams, and to highlight the impact of wetting/drying (W/D) cycles on the durability of glulam timber elements. The experimental results show that the developed measurement system allows to monitor in real time and continuously the MC of glulam beams. The resistive patch-type sensors embedded in glulam beams allow to trace the local MC in a lamella, to discretize different moisture areas in a beam, and thus to have an estimation of the moisture gradients between the edges and the centre of a glulam beam.

Regarding the impact of W/D cycles, the results showed that the exposure of glulam to moisture variations had a significant influence on the bending strength with an average decrease of 43.5% after 17 W/D cycles. The evolution analysis of the values allowed to propose a predictive model for the evolution of the bending strength as a function of the W/D cycles. Furthermore, no significant effect of W/D cycles was observed on the modulus of elasticity of the specimens.

Other works are currently underway in the laboratory to evaluate the durability of these structures under real conditions, i.e. outdoors. In addition to highlight the impact of natural whether conditions on the mechanical strength of timber beams used in bridges, this will enable to validate the reliability of the accelerated W/D cycle developed in the laboratory. Afterward, a model for predicting the residual life of glulam structures will be established in order to optimise maintenance operations on timber bridges.

Acknowledgement

This work was financed by the Occitanie Region, the Communauté d'Agglomération Tarbes-Lourdes-Pyrénées and the Institut Universitaire de Technologie de Tarbes. The authors would also like to thank the GEII department (Electrical Engineering and Industrial IT), in particular Emmanuel Laügt for his contribution to the development of the MC monitoring system. Thanks also to Pierre Larricq and Frédéric Leroy for their contribution to the achievement of the test set-ups.

References

[1] Franke B., Schiere M., Franke S. (2018) Stress developments in large timber cross sections in relation to geometry and encountered climate. In: World Conference on Timber Engineering, August 20-23 in Seoul, Korea.

[2] SETRA (2006) Timber bridges how to ensure their durability. SETRA (Service d'Etudes Technique des Routes et Auto-routes), France.

[3] Franke B., Franke S., Schiere M., Müller A. (2019) Moisture content and moisture-induced stresses of large glulam members: Laboratory tests, in-situ measurements and modelling. Wood Material Science & Engineering 14: 243–252.

[4] Pousette A., Malo K., Thelandersson S., Fortino S., Salokangas L., Wacker J. (2017) Durable timber bridges—final report and guidelines, pp 142–149. SP Report 25. Research Institutes of Sweden RISE, Skellefteå.



[5] Uwizeyimana P., Perrin M., Eyma F. (2020) Moisture monitoring in glulam timber structures with embedded resistive sensors: study of influence parameters. Wood Sci. Technol. 54: 1463–1478.
[6] Brischke C, Rapp A.O. (2010) Service life prediction of wooden components - Part 1: Determination of dose-response functions for above ground decay. In: The International Research Group on Wood Protection, IRG/WP/10-20439, Stockholm.
[7] Follrich J., Teischinger A., Müller U. (2011) Artificial ageing of softwood joints and its effect on internal bond strength with special consideration of flat-to-end grain joints. Eur. J. Wood Prod.69:597–604.
[8] Nguyen S.L. (2016) Modélisation hydromécanique du bois : application au sapin blanc du Massif Central. Thèse de doctorat, Université Blaise Pascal-Clermont-Ferrand.
[9] Koch J., Simon A., Arndt R.W. (2016) Monitoring of Moisture Content of Protected Timber Bridges. In Proceedings of WCTE 2016 (World Conference on Timber Engineering), Vienna, Austria.
[10] Dietsch P., Gamper A., Merk M., Winter S. (2014) Monitoring building climate and timber moisture gradient in large-span timber structures. J Civil Struct Health Monit 5(2): 153–165.
[11] EN 408 (2012) Timber structures - structural timber and glued laminated timber – determination of some physical and mechanical properties, AFNOR editions.
[12] Björngrim N., Hagman O., Wang X. (2016) Moisture Content Monitoring of a Timber Footbridge. BioResources 11 :3904–3913.
[13] EN ISO 12571 (2000) Hygrothermal performance of building materials and products determination of hygroscopic sorption properties.
[14] Fortino S., Hradil P., Metelli G. (2019b) Moisture-induced stresses in large glulam beams. Case study: Vihantasalmi Bridge. Wood Mater Sci Eng. 14 (5): 366–80.
[15] Kubojima Y., Okano T., Ohta M. (2000) Bending strength and toughness of heat-treated wood. J Wood Sci. 46: 8-15.
[16] Yahyaoui I. (2017) Contribution au suivi par émission acoustique de l'endommagement des structures multi-matériaux à base de bois. Thèse de doctorat, Université de Toulouse.
[17] Murata K., Masuda M. (2001) Observation of the Swelling Behavior of Coniferous Cells Using a Confocal Scanning Laser Microscope and a Digital Image Correlation Method. Materials Science Research International 7 (13): 200-205.
[18] Almeida G., Huber F., Perré P. (2014) Free shrinkage of wood determined at the cellular level using an environmental Scanning Electron Microscope. Maderas. Ciencia y tecnologia. 16(2) : 187-198.

Conference Proceedings 4th ICTB (2022)
https://doi.org/10.24451/sxp0-fx66

ICTB 2021 PLUS
4th International Conference on Timber Bridges
Biel/Bienne, Switzerland, 9 -12 May 2022



Defect Identification Coupled with Grayscale Image Enhancement Technology

Junwon Seo[1], Euiseok Jeong, James Wacker

Abstract

The goal of this study was to improve the visibility of defects within inspection images obtained by drones using image enhancement technologies. In recent years, drones have been applied to bridge inspections as reported by several studies as a result of the drones' abilities such as providing improved accessibility along with high image resolution. However, poor-quality inspection images frequently hamper the process of efficient defect identification and quantification with low visibility caused by brightness and/or contrast inconsistencies. To resolve such issues, a grayscale image enhancement algorithm in MATLAB and image property adjustment were considered for this study. The visibility of representative images, collected from a drone-aided inspection on an existing timber slab bridge located in the state of Minnesota in the United States, was improved through the use of an Adaptive Histogram Equalization algorithm available within MATLAB and image property adjustment algorithm. To evaluate the accuracy of the algorithms with the drone inspection images, defect area quantification for the weathering identified during the inspection was conducted using an unfiltered drone image (0.097 m²), grayscale image (0.078 m²), the enhanced image visibility (0.118 m²) with the adaptive histogram equalization algorithm, and the filtered image (0.085 m²) using image property adjust algorithm. From this work, it was concluded that the adaptive histogram equalization algorithm applied to the drone imagery is capable of improving the image visibility to better quantify the defect areas.

1 Introduction

According to America's Infrastructure report cards [1,2], the grades of bridges in the United States (U.S.) were down from C+ to C between 2017 and 2021. 267,316 U.S. bridges were under the fair condition in 2017, and the number of fair bridges gradually increased to 291,339 in 2019, while the number of bridges in good condition decreased from 288,126 in 2017 to 279,582 in 2019. In particular, the number of bridges in fair condition has exceeded the number of bridges in good condition in 2019, the first time since 2009 [2]. Furthermore, approximately 260,000 bridges (42% of all U.S. bridges) are evaluated as deteriorating bridges, which have been in service for 50 years old or more. With these concerns, bridge maintenance will gain more interest from bridge engineers and owners. For appropriate bridge maintenance, periodic bridge inspections with high accuracy and cost-efficiency shall be one of the most important priorities. As the periodic bridge inspections, conventional bridge inspections with direct measurement have been conducted to date but are increasingly a higher cost and riskier work task. For example, when critical defects to the bridge exist at an inaccessible location by inspectors, the conventional inspections shall be carried out through rope access or by use of specialized vehicles such as under-bridge inspection vehicles, e.g., snooper trucks or boom lift trucks. During these inspections, some accidents have occurred with rope access [20] or specialized vehicles [3,12]. The risk of these accidents can be prevented or greatly reduced with drone-aided bridge inspections. With the merits of drone-aided bridge inspections, the cases of drone use in bridge inspections by the U.S. State Departments of Transportation (DOTs) increased from 6% to 21% [13]. Many studies on bridge inspections using drones considered that such bridge inspection approaches can be a proper alternative to conventional inspections [14,15,24].

With drones, inspectors can acquire inspection images and identify defects to generate results of the bridge inspections. For such an endeavor, the quality of the drone inspection images is most critical to bridge evaluation. However, these inspection images are significantly influenced by the surrounding environments of the bridges. For instance, defects on bridges are not able to be identified in images with inadequate light exposure, such as images taken underneath the bridge having low light exposure. To improve visibility of low-quality images, inspectors can consider image processing methods, e.g., edge detection [4], k-means clustering [5], Grayscale image processing [16,19], and brightness-contrast-sharpness adjustment [17,25]. Among them, grayscale image processing is efficiently capable of converting an existing color image to

[1] Junwon Seo, Associate Professor with Tenure and Chairman of ASCE Timber Bridges Committee, South Dakota State University, United States, Junwon.Seo@sdstate.edu

grayscale and adjusting the pixel's contrasts to enhance the visibility of inspection images. In a past study [16], grayscale image processing was applied to bridge inspection images obtained by drones. It was found that the quality of drone inspection images was improved with the grayscale image processing and the boundaries of defects due to efflorescence, water leakage, discoloration, and so on were detected effortlessly. Specifically, the clear boundaries of defects (i.e., water leakage and efflorescence) were identified through grayscale image-based adaptive histogram equalization [16]. The adaptive histogram equalization [19] was ordinarily used to separate images into small regions, to amend contrast for each small region to increase visibility, and to combine the small regions into the image for the prevention of undesired boundaries in the image.

The goal of this study is to improve the accuracy and efficiency of defect identification and quantification using the images obtained through drone-aided bridge inspections. To achieve this goal, grayscale image processing technology was implemented into images acquired from drone-aided inspections for an in-service bridge in the U.S. This paper consists of three sections, including this section, methodology, and results and discussions.

2 Methodology

In recent years, drone technology has gained traction in several studies [6–8, 14–17, 21–29] as a supplementary bridge inspection approach. Despite a burgeoning interest in using drones in bridge inspections, some issues have arisen related to the image quality during drone-aided inspections. To address this image quality issue, the grayscale image enhancement algorithm in MATLAB [18] and image property adjustment technology [17, 25] were applied. For evaluation of the algorithms, DJI Matrice 210 inspected an existing timber slab bridge located in Minnesota on August 20, 2019. The inspected bridge was built in 1987, and the type of bridge is a three-span, timber slab bridge having a structure length of 31.1 m and a deck width of 10.36 m. According to the NBI condition rating system, the deck, superstructure, and substructure were recently evaluated to be in good condition exhibiting minor defects but with no structural issues [9–11]. The bridge inspection was performed on the east side, west side, and underneath the deck, as shown in Figure 1a. A representative defect due to weathering observed on the east side of the bridge can be depicted in Figure 1b. Although the defect on the bridge element is observed using inspection images obtained from the drone, the defect measurement may be impeded due to unclear boundaries with some type of deterioration such as weathering. To resolve this issue, two image processing technologies, grayscale image enhancement technologies available in MATLAB [18, 19] and image property adjustment technology [17, 25], were considered. Adaptive histogram equalization technology among the grayscale image enhancement technologies adjusts the contrast on specific small regions, known as tiles, in the image. During this processing, the histogram of the tile approaches a specified contrast histogram. In the last step of processing, bilinear interpolation is performed on neighboring tiles to remove the tile boundaries. On the other hand, the image property adjustment technology can improve the visibility of inspection images with adjustment of various image properties including brightness, contrast, and sharpness.



(a) (b)

Figure 1: Bridge inspection: (a) drone-aided bridge inspection and (b) inspection images captured by DJI Matrice 210.



3 Results and discussions

The results of two technology applications, including image property adjustment technology and grayscale image enhancement technology, will be discussed in the following sections. To compare the results, the technologies amend and improve the same raw inspection image (refer to Figure 1b).

3.1 Application of grayscale image enhancement technology

The proposed image enhancement methodology was applied to the drone captured image shown in Figure 1b. In this methodology, the original color drone image (refer to Figure 1b) is converted to a grayscale image as depicted in Figure 2a and the corresponding contrast histogram as shown in Figure 2b. In Figure 2a, the weathering area marked yellow boundaries is not visibly observed. Note, the dark areas marked by a white dashed box are not detected due to low visibility. The adaptive histogram equalization algorithm was employed to enhance the visibility of the image as depicted in Figure 2c and relevant contrast histogram (see Figure 2d). In a comparison of histograms, Figure 2d shows the uniform distribution compared to Figure 2b. With a contrast adjustment, the weathering area changed and it can be observed underneath the deck compared to the grayscale image (refer to Figure 2a) and original image (see Figure 1b). The measured weathering areas are 0.097 m² for Figure 1b (original color drone image), 0.078 m² for Figure 2a (converted grayscale image), and 0.118 m² for Figure 2d (application of grayscale image enhancement). It was revealed that the adaptive histogram equalization can improve the visibility of images to more efficiently identify the defects through this methodology.

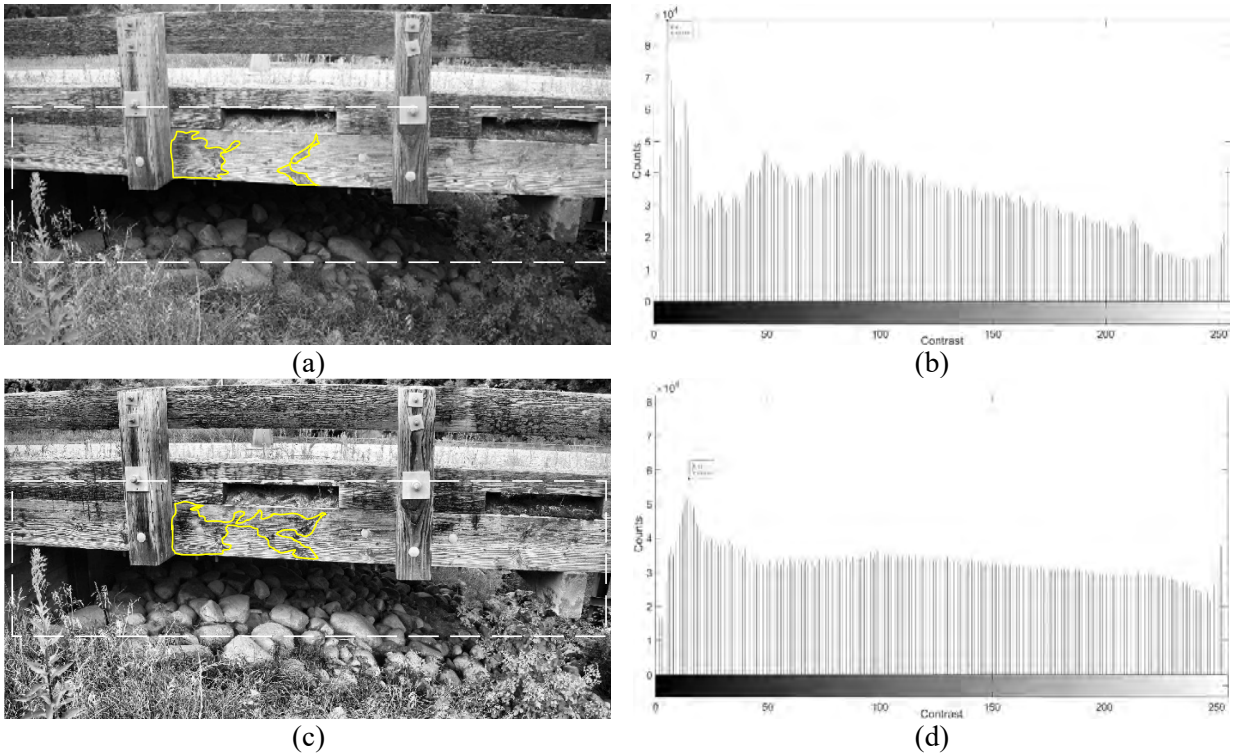


Figure 2: Grayscale image enhancement applications using inspection image (Figure 1b): (a) grayscale image conversion; (b) histogram of Figure 2a; (c) adaptive histogram equalization algorithm application; and (d) histogram of Figure 2c.

3.2 Application of image property adjustment technology

To improve the visibility of the inspection image (see Figure 1b), image property adjustment technology is applied to this image. This technology amends the image properties (brightness, contrast, and sharpness) as shown in Figure 3. All properties can be adjusted from -100% to 100% and the default value of each property is 0%. The negative values of properties indicate darkness, low contrast, and blurriness in the adjustment of brightness, contrast, and sharpness, respectively. The inspection image (Figure 1b) was adjusted with brightness -10%, contrast 30%, and sharpness 20% as depicted in Figure 3. The defects due to wearing on the side of the bridge are detected obviously as marked with red boundaries in Figure 2. The measured area of weathering is 0.085 m².

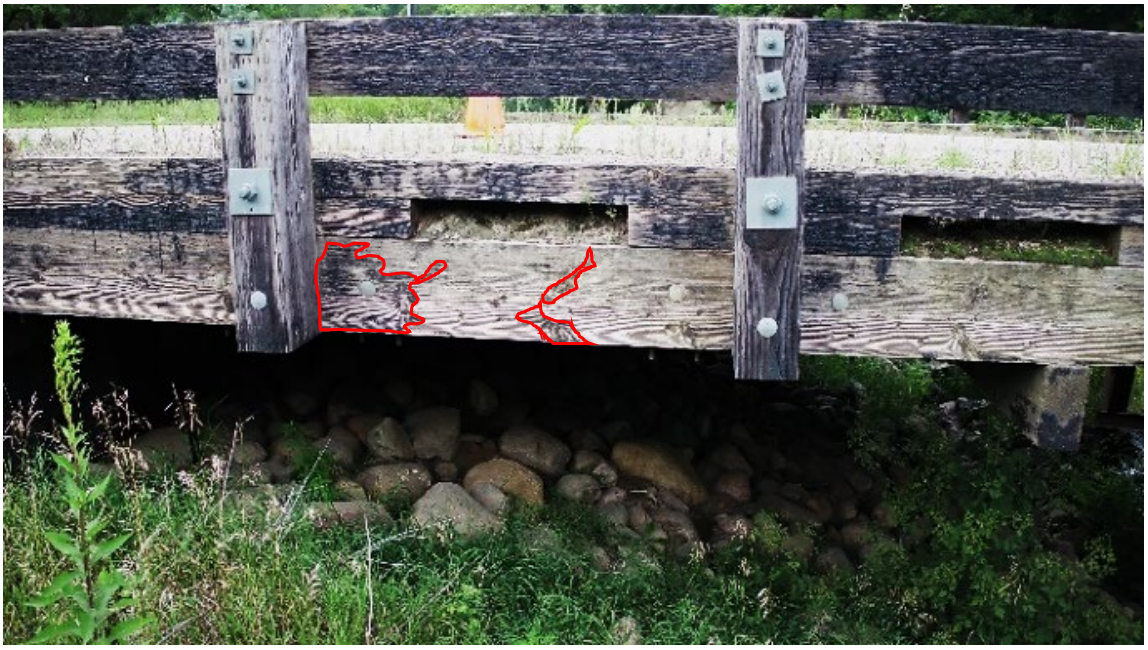


Figure 3. Image property adjustment application using inspection image (Figure 1b) adjusted with brightness -10%, contrast 30%, and sharpness 20%.

For this study, two image processing technologies, i.e., grayscale image enhancement and image property adjustment technologies, were applied in order to improve the visibility of the drone inspection images, which show representative defects due to weathering observed on the east side of the bridge. Although the visibility of the inspection images can be improved through the suggested image property adjustment technology, the improvement of the visibility of defect boundaries was limited. Compared to image property adjustment, the grayscale image enhancement technology was considered as an accurate and efficient methodology during the measurement of the defect having an area (i.e., weathering). Furthermore, additional areas of weathering on the side of the bridge (yellow boundaries in Figure 2c) were observed in the application image of grayscale enhancement technology, while this area was not identified through image property adjustment as depicted in Figure 3. Thus, for defect identification, the application of image property adjustment technology to inspection images can be recommended, whereas defect measurement will be more accurate and efficient through grayscale image enhancement technology.

Acknowledgment

Partial financial support for this research was provided by the United States Department of Agriculture (USDA) Forest Service–Forest Products Laboratory (FPL) through a cooperative research agreement (No. 18-JV-11111133-031). The assistance and cooperation of Lincoln County in Minnesota are gratefully acknowledged.

References

[1] American Society of Civil Engineers (ASCE) (2017) Infrastructure Report Card. American Society of Civil Engineers (ASCE), Washington, D.C., p. 110.
[2] American Society of Civil Engineers (ASCE) (2021) Report Card for Americas's Infrastructure. American Society of Civil Engineers (ASCE), Washington, D.C., p. 169.
[3] Atkinson, B. (2015) Snooper truck overturns on I-84 on-ramp, crushes bridge inspector in Connecticut. Equipment World.
[4] Canny, J. (1986) A Computational Approach to Edge Detection. IEEE Transactions on Pattern Analysis and Machine Intelligence PAMI-8(6), 679–98, Doi: 10.1109/TPAMI.1986.4767851.
[5] Chen, T.-W., Chen, Y.-L., Chien, S.-Y. (2008) Fast image segmentation based on K-Means clustering with histograms in HSV color space. 2008 IEEE 10th Workshop on Multimedia Signal Processing, pp. 322–5.
[6] Duque, L., Seo, J., Wacker, J.P. (2018) Timber Bridge Inspection Using UAV. Structures Congress 2018, Fort Worth, TX, pp. 186–96.



[7] Duque, L., Seo, J., Wacker, J.P. (2018) Synthesis of Unmanned Aerial Vehicle Applications for Infrastructures. Journal of Performance of Constructed Facilities 32(4), 04018046, Doi: 10.1061/(ASCE)CF.1943-5509.0001185.
[8] Duque, L., Seo, J., Wacker, J.P. (2018) Bridge Deterioration Quantification Protocol Using UAV. Journal of Bridge Engineering 23(10), 04018080, Doi: 10.1061/(ASCE)BE.1943-5592.0001289.
[9] Federal Highway Administration (FHWA) (1995) Recording and Coding Guide for the Structure Inventory and Appraisal of the Nation's Bridges. U.S. DOT FHWA, Washington, DC, p. 124.
[10] Federal Highway Administration (FHWA) (2012) Recording and Coding Guide for the Structure Inventory and Appraisal of the Nation's Bridges. U.S. DOT FHWA, Washington, DC, p. 124.
[11] Federal Highway Administration (FHWA) (2018) Recording and Coding Guide for the Structure Inventory and Appraisal of the Nation's Bridges. U.S. DOT FHWA, Washington, DC, p. 124.
[12] Grayson, W. (2015) Boom lift overturns, killing worker on Massachusetts jobsite. Equipment World.
[13] Jeong, E., Seo, J., Wacker, J.P. (2020) Literature Review and Technical Survey on Bridge Inspection Using Unmanned Aerial Vehicles. Journal of Performance of Constructed Facilities 34(6), 04020113, Doi: 10.1061/(ASCE)CF.1943-5509.0001519.
[14] Jeong, E., Seo, J., Wacker, J.P. (2020) New Bridge Inspection Approach with Joint UAV and DIC System. Structures Congress 2020, St. Louis, MO, pp. 349–59.
[15] Jeong, E., Seo, J., Wacker, J.P. (2020) Non-Contact Bridge Inspection and Damage Quantification Approach using UAS. US-Korea Conference (UKC) 2020 – Virtual Event, Korean-American Scientists and Engineers Association (KSEA).
[16] Jeong, E., Seo, J., Wacker, J.P. (2021) Grayscale Drone Inspection Image Enhancement Framework for Advanced Bridge Defect Measurement. Transportation Research Record 2675(8), 603–12, Doi: 10.1177/0361198121999605.
[17] Jeong, E., Seo, J., Wacker, J.P. (2022) UAV-aided bridge inspection protocol through machine learning with improved visibility images. Expert Systems with Applications 197, 116791, Doi: 10.1016/j.eswa.2022.116791.
[18] MATLAB (2020) MATLAB version 9.9.0. 1538559 (R2020b Update 3). The MathWorks Inc., Natick, Massachusetts.
[19] MATLAB & Simulink (2020) Enhance Grayscale Images. https://www.mathworks.com/help/images/contrast-enhancement-techniques.html. [accessed July 24, 2020].
[20] Robbins, C.H. (2017) Work & Safety analysis 2017. Industrial Rope Access Trade Association (IRATA) International, Ashford, UK, p. 81.
[21] Seo, J., Duque, L., Wacker, J.P. (2018) Field Application of UAS-Based Bridge Inspection. Transportation Research Record: Journal of the Transportation Research Board, 036119811878082, Doi: 10.1177/0361198118780825.
[22] Seo, J., Duque, L., Wacker, J.P. (2018) Drone-enabled bridge inspection methodology and application. Automation in Construction 94, 112–26, Doi: 10.1016/j.autcon.2018.06.006.
[23] Seo, J., Duque, L., Wacker, J.P. (2019) Glued-Laminated Timber Arch Bridge Inspection Using UAV. Computing in Civil Engineering 2019, pp. 336–42.
[24] Seo, J., Jeong, E., Wacker, J.P. (2020) Drone-Aided Bridge Inspection Coupled with Image Quality Improvement Processing Technique. NDE/NDT Structural Materials Technology for Highways and Bridges 2020, Online Only, OH.
[25] Seo, J., Jeong, E., Wacker, J.P. (2021) Visual Bridge Damage Measurement Using Drone-Captured Image Quality Optimization. In: Rizzo, P., Milazzo, A., (Eds.), European Workshop on Structural Health Monitoring, Springer International Publishing, Cham, pp. 503–13.
[26] Seo, J., Jeong, E., Wacker, J.P. (2021) Visible Damage Examination of Concrete Bridge Decking using UAS. ACI Virtual Concrete Convention, American Concrete Institue (ACI).
[27] Seo, J., Jeong, E., Wacker, J.P. (2021) Advanced Defect Identification and Quantification Using Grayscale UAS Inspection Images. US-Korea Conference (UKC) 2021, Korean-American Scientists and Engineers Association (KSEA), Los Angeles area, CA.
[28] Seo, J., Wacker, J.P., Duque, L. (2018) Evaluating the use of drones for timber bridge inspection. U.S. Department of Agriculture, Forest Service, Forest Products Laboratory, Madison, WI, p. 145.
[29] Seo, J., Wacker, J.P., Jeong, E. (2022) Evaluation of Unmanned Aircraft Systems as a Bridge Inspection Tool – Phase II. U.S. Department of Agriculture, Forest Service, Forest Products Laboratory, Madison, WI, In Press.

Conference Proceedings 4th ICTB (2022)
https://doi.org/10.24451/6j5j-qw13

ICTB 2021PLUS
4th International Conference on Timber Bridges
Biel/Bienne, Switzerland, 9 -12 May 2022



Evaluating the Efficacy of Ground-Penetrating Radar as an Inspection Tool for Timber Bridges

C. Adam Senalik[1], James P. Wacker, Xiping Wang

Abstract

Interest in using ground penetrating radar (GPR) as an inspection tool for wood and wooden structures has increased over the past two decades. GPR provides rapid scanning tool which can provide continuous subsurface information about the structure without the need for direct contact. It is accepted within the steel and concrete industries as a reliable inspection tool. By adapting the GPR for use on wood and wooden structures, the need for an inspector to learn an entirely unique technology is eliminated. Ideally, those familiar with GPR would only need minor instruction on how GPR can be used for wood inspection and hopefully increase the number of skilled inspectors faster than training with a completely unique technology. GPR inspection of wood has been shown to identify moisture, voids, and interior metal. The question remains as to whether GPR can detect internal decay in the absence of water, such as in the case of a covered bridge after a leaking roof has been repaired. This paper reports on a preliminary study, within a comprehensive multi-year effort to investigate GPR technologies, in which the dielectric orthotropy of wood is used to identify regions of interior decay.

1 Introduction

The use of ground penetrating radar (GPR) for inspection of wooden and wood-based structures has increased in the past two decades [1]. GPR has several desirable traits as an inspection tool: it is fast, non-contact, can locate subsurface defects, and is sensitive to the presence of moisture [2]-[8]. It also has several limitations. Radar wave propagation is affected by several factors including frequency of the radar waves, wood density, temperature, size of the specimen, size of the internal defect, and moisture content. Any one or a combination of these factors may be present during inspection [2], [7]-[9]. Despite complicating factors, the advantages of GPR inspection of wood are seen to outweigh the limitations. GPR is seen to have the potential to provide the same rapid, reliable, and non-destructive evaluations for wooden structures as it does for steel and concrete. Toward this end, the United States Department of Agriculture (USDA), Forest Service (FS), Forest Products Laboratory (FPL), in conjunction with the U.S. Federal Highway Administration (FHWA) initiated a multiphase study aimed at expanding the knowledge of GPR behaviour in wood with the goal of making it a more viable option as an inspection tool [10]-[11].

Early applications of GPR inspection of wood bridges occurred in 2002 in Queensland, Australia [4]-[5]. Researchers examined round wood girders during demolition and found excellent agreement between drilling surveys and defect locations as predicted by GPR. The author proposed an inspection regime which would begin with GPR for an initial assessment. In areas where the GPR results indicated the possibility of decay, other inspection tools like micro-resistance drilling or stress wave timing would be used for focused assessment. Another study examined the effect of a bituminous wear protection layer on the ability of GPR to assess the condition of nail laminated bridge decks [10]. The researcher found great potential to identify internal defects within a wooden structure, but widespread presence of the metal nails reflected GPR waves and masking nearby features within the bridge deck. As a result, the GPR signal was degraded which made feature identification within the deck more difficult.

1.1 Multiphase GPR Study

The overarching study, which the research in this paper is a part, has two phases; Phase 1, the tool selection phase, is complete, and Phase 2, the tool evaluation phase, is ongoing. In Phase 1, several non-destructive evaluation (NDE) tools were used to locate air-filled or wet sawdust-filled voids within laboratory constructed specimens. Inspectors with no knowledge of the internal voids were invited to demonstrate the capabilities of the NDE tools and to report their findings. GPR was selected for further study because it identified the highest number of defects and possessed the highest number of desired characteristics for an

[1] C. Adam Senalik, Research General Engineer, USDA, Forest Service, Forest Products Laboratory, United States of America, christopher.a.senalik@usda.gov



inspection tool [12]. In Phase 2, the sensitivity of GPR to moisture content (MC), temperature (T), and decay was explored. A laboratory study using dimensional lumber with varying MC and T were used to characterize how those variables affected GPR output. The method of specimen selection and fungal inoculation is documented in several publications and will only be briefly repeated here [10], [11], [13]. A total of 96 Douglas fir (*Pseudotsuga menziesii (Mirb)Franco*) specimens measuring 81.3 cm in length were inoculated with a brown rot fungus (*Fomitopsis pinicola (Sw.) P.Karst. (1881)*). The specimens had cross sectional dimensions typical of members used in wooden bridges. These field specimens were inoculated with a brown rot fungus and subsequently exposed to weather conditions in the southern United States that promotes rapid fungal growth. Scientists made regular visits and evaluated the wood specimens using a GPR device, collected MC measurements, and obtained stress wave time-of-flight (ToF) measurements. At 6-month intervals, a subset of 12 specimens were returned to the laboratory for further examination using X-ray computerized tomography (CT) and modified hardness testing at critical internal cross-sections [13].

1.2 Current GPR Research

The study is currently in the final portion of Phase 2 in which recorded wave characteristics from GPR are associated with internal decay. From previous studies mentioned above, it is known that GPR can identify moisture pockets and voids that are often associated with decay; however, the ability of GPR to identify decay itself, in the absence of moisture or voids, has not been established. Four fungal inoculated specimens (two glulam beams and two sawn timbers) were collected from the field exposure test site in the Harrison Experimental Forest, near Saucier, Mississippi, United States. This site is characterized as a high fungal decay hazard zone [14]. was chosen as the year-round temperature and humidity promote fungal growth. The middle 51-cm were covered with rigid corrugated plastic which prevented rainwater from contacting the middle portion of the beam. The desire was to have decay begin at the ends of the specimens and then spread to the middle portion through interior decay. The specimens in this study were exposed for over 3.5 years before being collected from the site and returned to FPL. When the specimens were returned, they were examined using X-ray CT. The CT revealed widespread interior moisture, which was corroborated using GPR. The specimens were placed in a humidity and temperature-controlled conditioning room which holds wood at an equilibrium moisture content (EMC) of 12% for three years. With sufficient time having passed for specimens to equilibrate, GPR was once again used to evaluate the specimens.

In this paper, the ability of ground penetrating radar to identify fungal decay in the absence of moisture or voids is examined. At the time of field data collection, there were no significant fungal voids, so the internal moisture was the primary characteristic visible in the GPR radargrams. As the antenna is moved along the surface of the specimen, the GPR sends transmits and receives a radar wave that travels through the depth of the specimen. The wave is transmitted every 2.5-mm of the antenna travel; the distance is measured by an encoder wheel attached to the antenna housing. The individual waves are then aggregated into a single image of through depth waves signals every 2.5-mm apart resulting in a two-dimensional picture known as a radargram. Effort has been made to associate internal features to characteristics within GPR radargrams [15], [16]. With knowledge of regions of internal decay from the CT scans, unique features of the GPR radargrams in the regions of decay can be used to identify indicators of decay in the absence of moisture [17]. This is useful when examining a structure during a dry season in which moisture content may be low, but decay is present. The objective of this paper is to investigate the potential of a new decay identification method using differences in perceived dielectric constant based upon GPR antenna orientation.

The dielectric constant (DC), also known as relative permittivity, is the ratio of the capacitance of a material to the capacitance of a vacuum. The DC governs the speed of an electromagnetic wave through the material; the square root of the DC equals the ratio of the speed of the wave in vacuum to the speed of the wave through the material. The DC, like many of its characteristics, varies based upon the angle of examination with respect to the grain. The DC parallel to the wood grain is greater than the DC perpendicular to the wood grain [9]. For Douglas-fir at 22.8°C and 12% MC, the DC values are around 2.3 parallel to the grain and 1.8 perpendicular to the grain [18]-[20]. As wood decays, the structure of the wood deteriorates. In a fully decayed piece of wood, there should be no differentiation between the DC parallel and perpendicular to the wood grain. In this paper, the relative change of the DC of the specimens is examined when the antenna is changed from parallel to the grain to perpendicular to the grain. It is hypothesized that in areas of extensive decay, the DC values parallel and perpendicular to the wood should be closer in value than in areas of sound wood.



2 Material and method

Four specimens were examined, each having different cross-sectional dimensions: A47, a six-layer glulam beam (13.0-cm × 22.7-cm); B47, a five-layer glulam beam (13.0-cm × 17.8-cm); C47, a solid sawn timber (8.9-cm × 14.0-cm); and D47, a solid sawn timber (8.9-cm × 18.4-cm). They were exposed to field conditions which promoted fungal growth. After a period 3 years and 10 months the four specimens examined in this study were returned to FPL. Upon return, the specimens were tested using GPR, stress wave ToF, and X-ray CT. The specimens were then placed in a humidity and temperature-controlled room at 22.8°C and 50% relative humidity (RH) for a period of 3 years to reach equilibrium at 12% MC. At 12% EMC, the specimens were once again examined using GPR. The GPR and antenna used in this study were a GSSI SIR® 4000 GPR data acquisition system (Nashua, NH) and a 2000 MHz dipole bowtie antenna (DBA) [21]. The GPR radargrams from the specimens were compared to information gained from GPR spans of undecayed control specimens.

The method explored here uses the relative change of DC parallel to the grain versus perpendicular to the grain as a metric for locating interior decay. GPR radargrams of Douglas-fir control specimens at 22.8°C and 12% MC were used to create a baseline threshold indicative of sound wood. The control specimen was a 5 lamina glulam beams with cross sections of 13.0-cm × 17.8-cm. The threshold was then applied to the decayed specimens. Areas of decay within the specimens were also identified using CT scans [22],[23]. The regions of relative change of the DC are then compared to the decay regions identified using the CT scans to determine if correlation exists.

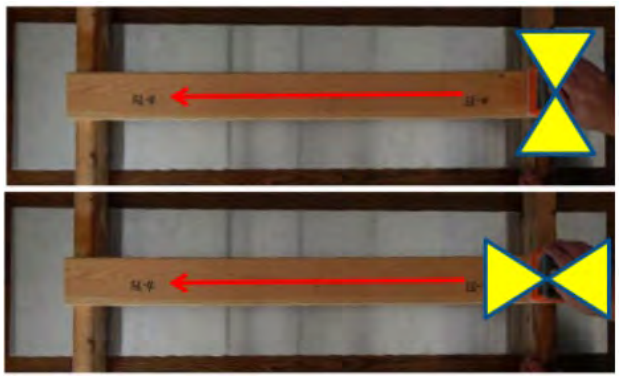


Figure 1: GPR scanning with dipole bowtie antenna, shown here in yellow, oriented perpendicular and parallel to wood grain. In the top (bottom) picture, the antenna is oriented perpendicular (parallel) to the wood grain and generates a field that is parallel (perpendicular) wood grain.

Figure 1 demonstrates the scanning process. The dipole bowtie antenna (DBA) was oriented either parallel to the wood grain or perpendicular to the wood grain. Please note, when the DBA was oriented perpendicular to the wood grain (DBA_{perp}), it generated a field that is parallel to the wood grain. Conversely, when the DBA was parallel (DBA_{para}) to the wood grain, it generated a field that was perpendicular to the wood grain. Therefore, when the DBA was oriented perpendicular (parallel) to the wood grain, it was used to examine the DC of wood parallel (perpendicular) to the wood grain. A thin aluminium sheet was placed under the beam to create a strong reflective boundary at the far side of the specimen. Figure 1 shows supports between the specimen and the aluminium sheet. The supports were not used when scanning the four specimens in this paper.

3 Results

Figure 2a shows the radargram generated using DBA_{perp} for specimen A47. Figure 2b shows the radargram generated using DBA_{para} on A47. In both Figure 2a and Figure 2b, there are notable distortions starting at 63-cm. A metal identification tag was placed on the top of each specimen; the metal tag causes the visible distortion. The dashed line represents the side of the specimen opposite of DBA. In both figures, the double arrow line shows the location of lowest DC of the scan which was used for normalization. For the normalization process, the all values along the dashed line were divided by the average DC value within ±25-mm of the highest DC value.

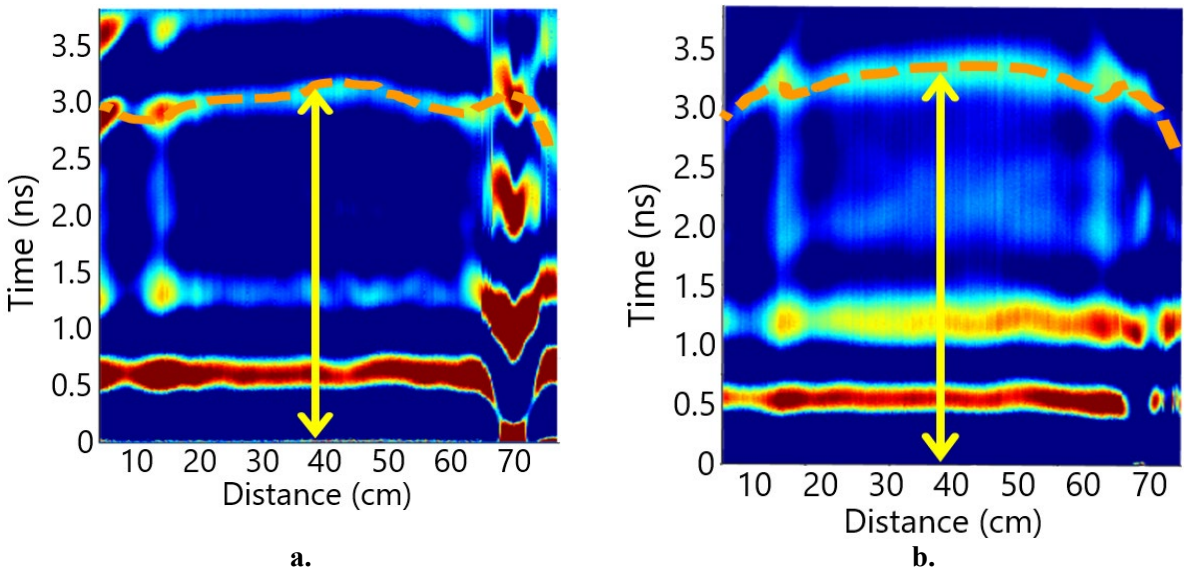


Figure 2: GPR radargram of Specimen A47 with dipole bowtie antenna (DBA). The doubled ended arrow represents the location of the beam used for normalization of the DC. a) DBA oriented perpendicular to wood grain. b) DBA oriented parallel to wood grain.

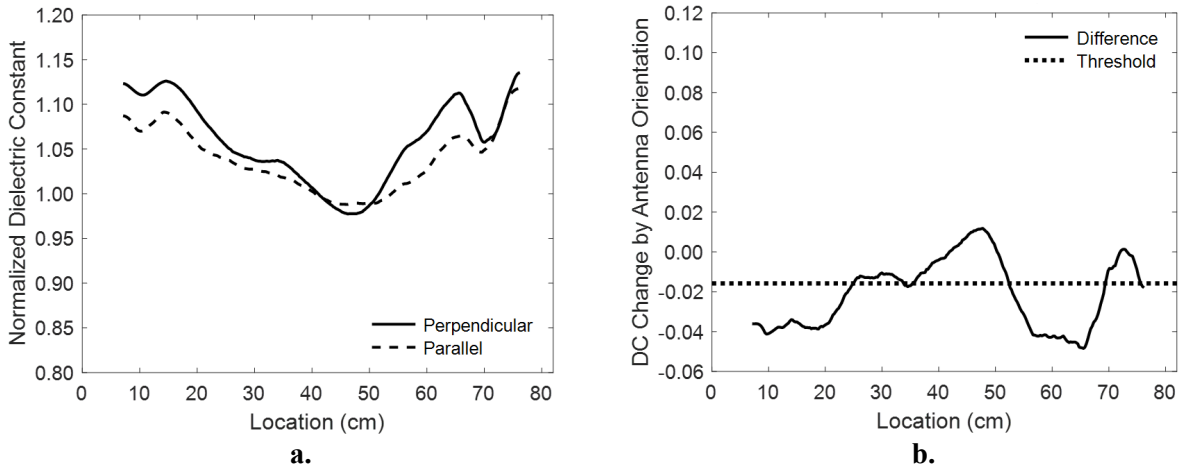


Figure 3: Locating decayed regions in specimen A47. a) Normalized DC along the length with the DBA oriented perpendicular and parallel to the grain. b) Difference in normalized DC for A47 with DBA oriented perpendicular and parallel to the wood grain. The control specimen decay line threshold (Figure 4b) is shown as a dotted line.

Figure 3a shows the normalized DC for the locations along A47. It is at this point the data from the control specimen is introduced. In Figure 4a, the normalized DC along the control specimen generated using DBA_{perp} and DBA_{para} is shown. The two curves tightly overlap. The difference between the values along the curve (perpendicular values minus parallel values) for the control specimen is shown in Figure 4b. The lowest observed value was -0.016 and was treated as the threshold for sound wood. The highest observed value was +0.013. This value was recorded for potential future work to establish an entire range of sound wood values. Figure 3b shows the difference in normalized DC along the curve for A47. The threshold line developed using the control specimen is also shown. Areas from 7-cm to 24-cm and from 53-cm to 68-cm were below the sound wood threshold. Above 68-cm the distortion caused by the metal identification tag obscures decay indicators within the cross section.

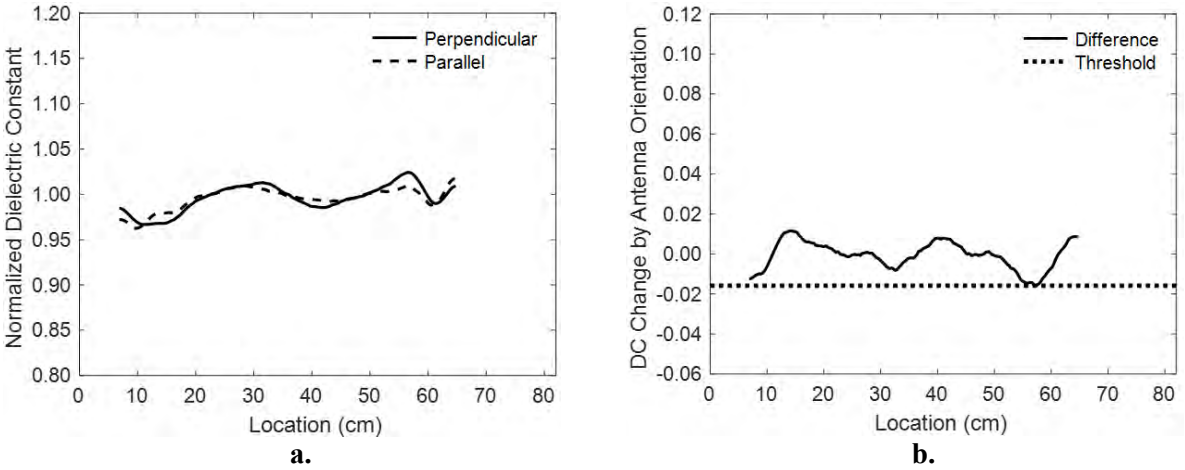


Figure 4: Control specimen threshold determination. a) Normalized DC along the length of the control specimen with the DBA perpendicular and parallel to the grain. b) Difference in normalized DC for control specimen with DBA oriented perpendicular and parallel to the wood grain. The threshold, -0.016, is shown as a dotted line.

Figure 5 shows the difference in normalized DC overlaid across the map in interior decay developed from the CT scan of A4. There was surface decay along the entire top face of A47. During scanning, the DBA was positioned along the top face. The DBA had decreased sensitivity to surface rot at the boundary between DBA housing and the top face of A47. However, the surface rot was easily identified during visual inspection.

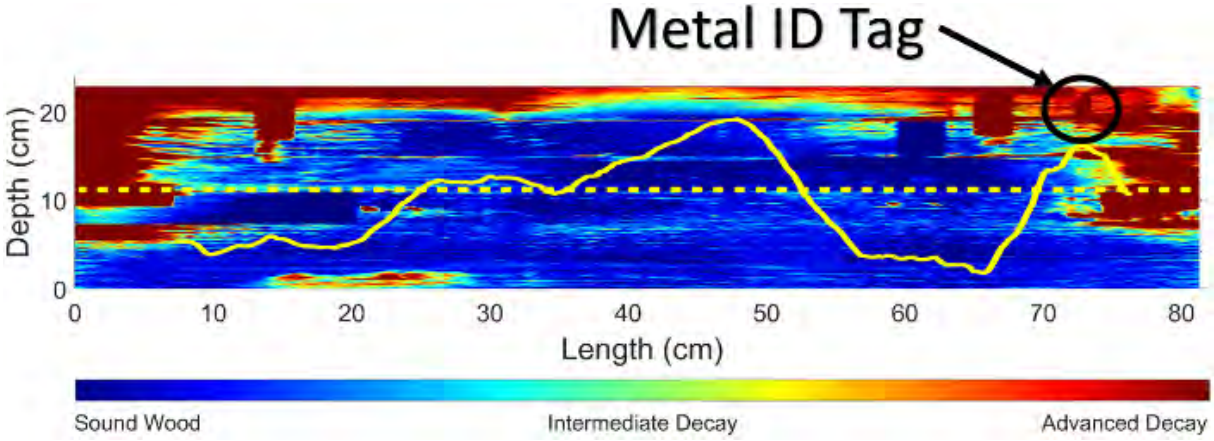


Figure 5: Difference in normalized DC for Specimen A47 with DBA oriented perpendicular and parallel to the wood grain overlaid on a map of decay regions for Specimen A47. Blue regions are sound wood and red regions are areas of advanced decay. The metal ID tag masks underlying decay

Figure 6 shows the normalized DC difference plots for all four specimens. Figure 6a shows A47 from Figure 3b. Figure 6b shows the normalized DC difference plot for specimen B47. The end opposite of the metal identification tag shows clear signs of decay. Like A47, the B47 metal identification tag masked decay beneath the tag. Throughout Phase 2, sawn timbers showed greater decay resistance than the glulam specimens. This resistance has been demonstrated by the decay resistance estimated from CT scans and ToF measurements of stress waves. The resistance was evident in the method examined here. Figure 6c shows the normalized DC difference plot for specimen C47. Two regions dipped below the threshold, at 15-cm and between 60-cm and 72-cm. The region at 15-cm corresponds to the fungal cavity where the specimen was inoculated with brown rot fungus. The region between 60-cm and 72-cm also surrounded a fungal cavity. Figure 6d shows the normalized DC difference plot for specimen D47. The method showed no decay within D47, which was supported by both the CT scan; however, the two fungal dips in the plot correspond to the location of the fungal cavities in D47.

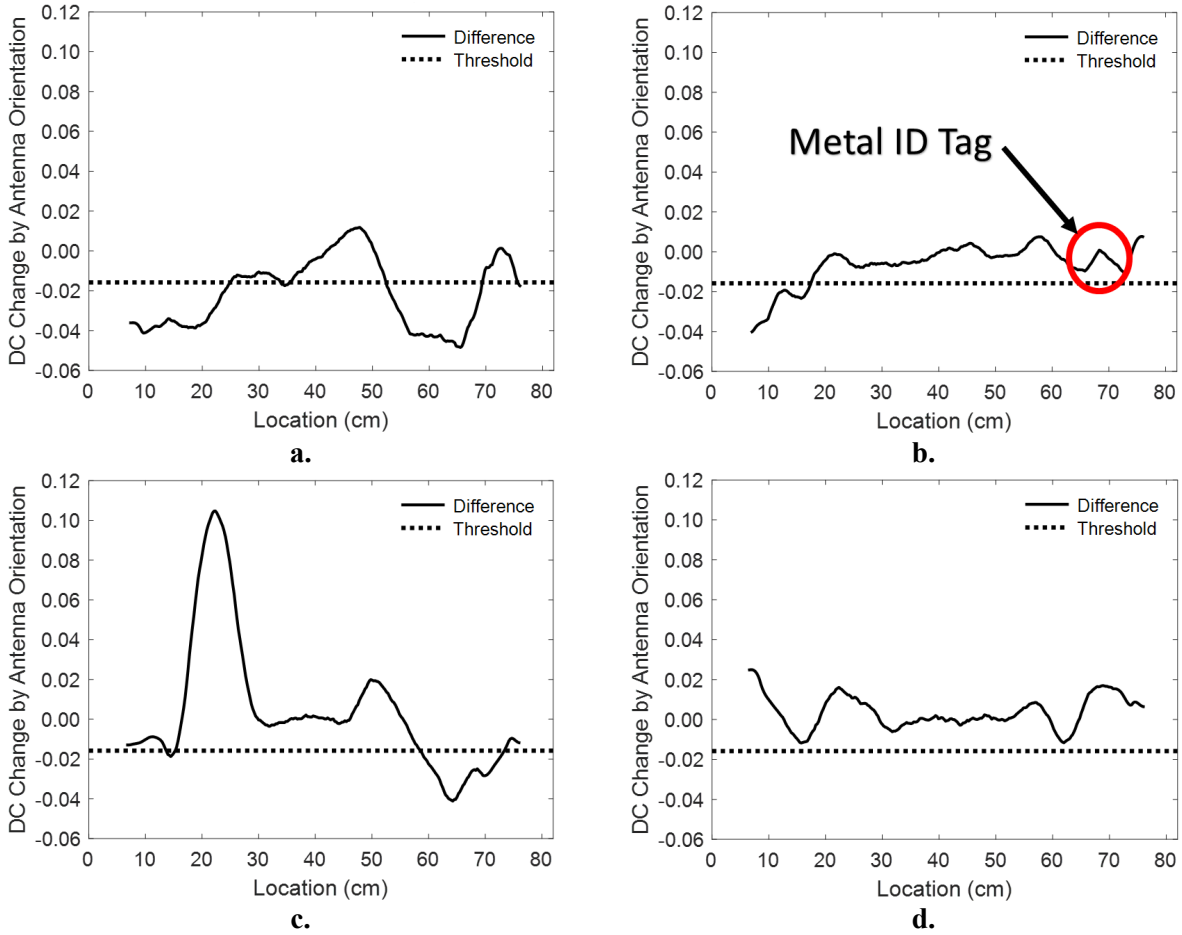


Figure 6: Difference in normalized DC for specimens with DBA oriented perpendicular and parallel to the wood grain. The threshold, -0.016, from Figure 4b is shown as a dotted line. a) A47 as shown in Figure 3b. b) B47. The metal ID tag masks underlying decay. c) C47. Sawn timber specimens have exhibited greater resistance to the brown rot. While the metal ID tag somewhat masks the underlying decay, it still shows the end decay. d) D47. Sawn timber specimens have exhibited greater resistance to the brown rot.

4 Conclusions

This study shows that internal decay may be detected by examining changes in the dielectric constant parallel and perpendicular to the wood grain as measured using a commercially available GPR unit and antenna. A difference in the normalized DC perpendicular to the wood grain minus the normalized DC parallel to the wood grain -0.016 was established as a threshold for sound wood using a control specimen. Good agreement was found between the regions below the threshold for glulam specimen A47 and B47. The sawn timber specimens C47 and D47 showed greater resistance to decay, but C47 exhibited the same differentiation in normalized DC in areas of decay A47 and B47. D47 showed no significant signs of decay in either the CT scan or normalized difference in DC values. The field scanning is rapid using GPR and the steps necessary to perform the procedure are easy to program into any number of computational software packages. The areas of advanced decay predicted by the DC orthotropy model matched the CT scan when only wood was in the region of scanning. The presence of the metal ID tags masked underlying decay. Further work on reducing the distortion caused by interior metal is necessary. The sample examined in this paper represent a small portion of the 96 specimens used in Phase 2. Early promise justifies expanding the number of examined specimens.

Acknowledgements

This study is part of the Research, Technology, and Education portion of the National Historic Covered Bridge Preservation (NHCBP) Program administered by the United States Department of Transportation, Federal Highway Administration. The NHCBP program includes preservation, rehabilitation, and



restoration of covered bridges that are listed or are eligible for listing on the National Register of Historic places; research for better means of restoring and protecting these bridges; development of educational aids; and technology transfer to disseminate information on covered bridges to preserve the Nation's cultural heritage.

References

[1] Rodrigues, Brunela Pollastrelli; Senalik, Christopher Adam; Wu, Xi; Wacker, James. 2021. Use of Ground Penetrating Radar in the Evaluation of Wood Structures: A Review. Forests. 12(4): 492. https://doi.org/10.3390/f12040492.

[2] Mai, T.C.; Razafindratsima, S.; Sbartaï, Z.M.; Demontoux, F.; Bos, F. Non-destructive evaluation of moisture content of wood material at GPR frequency. Constr. Build. Mater. 2015, 77, 213–217.

[3] Cassidy, N.J. Electrical and Magnetic Properties of Rocks, Soils and Fluids. In Ground Penetrating Radar Theory and Applications; Elsevier: Amsterdam, The Netherlands, 2009; pp. 41–72.

[4] Muller, W. Trial of ground penetrating radar to locate defects in timber bridge girders. In Proceedings of the Riding the Wave to Sustainability: IPWEAQ 2002 State Conference, Nossa Lakes, Queensland, Australia, 6–10 October 2002.

[5] Müller, W. Timber girder inspection using ground penetrating radar. Insight Non Destr. Test. Cond. Monit. 2003, 45, 809–812, doi:10.1784/insi.45.12.809.52990.

[6] Rodríguez Abad, I.; Martínez Sala, R.; García-García, F.; Capuz Lladró, R.; Diez Barra, R. A non-destructive method for the evaluation of density and moisture content. In Proceedings of the 12th International Conference on Ground Penetrating Radar, Birmingham, UK, 16–19 June 2008.

[7] Hans, G.; Redman, D.; Leblon, B.; Nader, J.; La Rocque, A. Determination of log moisture content using early-time ground penetrating radar signal. Wood Mater. Sci. Eng. 2015, 10, 112–129.

[8] Hans, G.; Redman, D.; Leblon, B.; Nader, J.; La Rocque, A. Determination of log moisture content using ground penetrating radar (GPR). Part 1. Partial least squares (PLS) method. Holzforschung 2015, 69, 1117–1123.

[9] Torgovnikov, G.I. Dielectric Properties of Wood and Wood-Based Materials; Springer-Verlag Berlin Heidelberg 1993.

[10] Brashaw, B.K. Inspection of Timber Bridge Longitudinal Decks with Ground Penetrating Radar. Ph.D. Thesis, Mississippi State University, Starkville, MS, 39762 USA, December 2014.

[11] Senalik, C.A.; Wacker, J.P.; Wang, X.; Jalinoos, F. 2016. Assessing the Ability of Ground-Penetrating Radar to Detect Fungal Decay in Douglas-Fir Beams. In: 25th ASNT Research Symposium: Summaries and Abstracts. Paper presented at 25th Research Symposium, New Orleans (110-116). Columbus, OH: American Society for Non-destructive Testing, Inc. 7 p.

[12] Wacker, James P.; Senalik, C. Adam; Wang, Xiping; Jalinoos, Frank. 2016. Effectiveness of several NDE technologies in detecting moisture pockets and artificial defects in sawn timber and glulam. In: World Conference on Timer Engineering, WCTE 2016. 22-25 August 2016; Vienna, Austria. 7 pp.

[13] Senalik, C. Adam; Wacker, James P.; Wang, Xiping; Rodrigues, Brunella Pollastrelli; Jalinoos, Frank. 2017. Assessing ability of ground-penetrating radar to detect internal moisture and fungal decay in Douglas-fir beams. In: Wang, X.; Senalik, C.A.; Ross, R.J., eds. Proceedings, 20th international non-destructive testing and evaluation of wood symposium. General Technical Report. FPL-GTR-249. Madison, WI: U.S. Department of Agriculture, Forest Service, Forest Products Laboratory: 286-300.

[14] Scheffer, T.C. 1971. A climate index for estimating potential for decay in wood structures above ground. Forest Products Journal. 21(10): 25–31.

[15] Wu, XI; Senalik, Christopher Adam; Wacker, James; Wang, Xiping; Li, Guanghui. 2019. Using ground penetrating radar to classify features within structural timbers. In: Wang, X.; Sauter, U.H.; Ross, R.J., eds. 2019. Proceedings: 21st International Nondestructive Testing and Evaluation of Wood Symposium. General Technical Report FPL-GTR-272. Madison, WI: U.S. Department of Agriculture, Forest Service, Forest Products Laboratory. pp 502-510.

[16] Wu, Xi; Senalik, Christopher Adam; Wacker, James; Wang, Xiping; Li, Guanghui. 2020. Object detection of ground-penetrating radar signals using empirical mode decomposition and dynamic time warping. Forests. 11(2): 230.

[17] Wu, Xi; Senalik, Christopher Adam; Wacker, James P.; Wang, Xiping; Li, Guanghui. 2020. Ground-penetrating radar investigation of salvaged timber girders from bridges along Route 66 in California. Wood and Fiber Science. 52(1): 73-86. https://doi.org/10.22382/wfs-2020-007.

[18] Wittkopf, J.J.; MacDonald, M.D. 1949. Dielectric Properties of Douglas Fir at High Frequencies. Oregon State Engineering Experiment Station Bulletin 28, July 1949.

[19] Mai, T.C.; Sbartaï, Z.M.; Bos, F. Non-destructive evaluation of wood moisture content using GPR technique—Effect of fiber direction and wood type. In Proceedings of the International Symposium Non-Destructive Testing in Civil Engineering (NDT-CE), Berlin, Germany, 15–17 September 2015.

[20] Rodríguez-Abad, I.; Martínez-Sala, R.; García-García, F.; Capuz-Lladró, R. Non-destructive methodologies for the evaluation of moisture content in sawn timber structures: Ground-penetrating radar and ultrasound techniques. Near Surf. Geophys. 2010, 8, 475–482, doi:10.3997/1873-0604.2010048.



[21] Geophysical Survey Systems, Inc (2014) SIR 4000 manual. Geophysical Survey Systems, Inc., Nashua, NH. https://www.geophysical.com/wp-content/uploads/2017/10/GSSI-SIR4000-Manual.pdf .

[22] Senalik, Christopher Adam; Wacker, James; Wang, Xiping; Wu, Xi. 2019. Identifying incipient decay in Douglas-fir bridge components using x-ray computerized tomography. In: Wang, X.; Sauter, U.H.; Ross, R.J., eds. 2019. Proceedings: 21st International Nondestructive Testing and Evaluation of Wood Symposium. General Technical Report FPL-GTR-272. Madison, WI: U.S. Department of Agriculture, Forest Service, Forest Products Laboratory: 62-70.

[23] Bucur, V. 2003. Nondestructive characterization and imaging of wood. Berlin Heidelberg New York: Springer.

Conference Proceedings 4th ICTB (2022)
https://doi.org/10.24451/779w-2t59

ICTB 2021 PLUS
4th International Conference on Timber Bridges
Biel/Bienne, Switzerland, 9 -12 May 2022



History and development stages in timber bridge construction in Switzerland

Robert Widmann[1], Andreas Müller[2]

1 Introduction - Topography of Switzerland

Switzerland is a relatively small country in the heart of Europe (Figure 1). Its territory stretches 220 km from north to south and 348 km from east to west and covers an area of approximately 41,000 square kilometers. Switzerland is roughly divided into three geographic regions, the Jura mountains in the north-west, the Alps in the south and between these two mountains there is a relatively flat band that runs from north-east to south-west and forms the so-called Central Plateau. The Alps make up almost 60% of the total area and thus form the largest part of the total area. Due to its topography and the high rainfall of approx. 1430 mm/a [1], Switzerland has a widely dispersed network of streams and rivers with a total length of around 65,000 kilometers. There are also around 80 larger and more than 6,500 smaller lakes. No Swiss person lives further than 16 km from a lake and the distance to the next watercourse is likely to be even much shorter in most cases. The four largest Swiss rivers - Rhine, Aare, Rhone and Reuss - have their sources just a few kilometers apart in the Gotthard region. The Swiss rivers empty into the North Sea (Rhine), the western Mediterranean (Rhône), the eastern Mediterranean (Ticino via the Po) and the Black Sea (Inn via the Danube). For this reason, Switzerland is also known as Europe's Water Tower.

The mentioned geographical conditions had and still have a major influence on mobility in Switzerland. Mountains, rivers and lakes are massive obstacles to the unhindered transport of people and goods. Overcoming the mountains required the construction of passes and/or tunnels, while water had to be crossed by (mobile) ferries or – of course – mainly by (fixed) bridges.

The building materials available for early bridge construction also resulted from the topographical conditions in these days. Stones were available in endless numbers and sizes from boulders and debris in rivers and lakes, or they could be hewn directly from the rock. The building material wood was (and is) available almost endlessly, since the forest area in Switzerland (today) accounts for 32 percent of the total area. Below the tree line, wood was and is available locally as a building material practically throughout Switzerland and therefore does not have to be transported over long distances. Figure 2 shows the three dominating materials for the construction of historic Swiss bridges united in one picture.



Figure 1: Map of Switzerland highlighting the presence of mountainous areas, water (river valleys and lakes) as well as wood (forests, highlighted in green). Picture: geo.admin.ch



Figure 2: Timber, iron and stones (masonry). Kubelbridge (1776) with a span of 30 m in the first plane and Sitterviadukt (1910) with a length of 365 m and a maximum span of 120 m. With 99 m this is the highest railway bridge in Switzerland. Picture: R. Widmann

1 Robert Widmann, Civil Engineer, Empa – Structural Engineering Laboratory, CH, robert.widmann@empa.ch
2 Andreas Müller, Professor, BFH School of Architecture, Wood and Civil Engineering, CH, andreas.mueller@bfh.ch



2 Early days timber bridges

As Werner Stadelmann [3] explained, it is therefore not surprising that our ancestors preferred wood for their constructions for centuries. The rounded trunks of the early bridges were laid close to each other, and branches filled their gaps. This technique is still used today for temporary bridges, e.g. in the area of forest roads (Figure 3). Later the road was covered with gravel, earth and clay. However, the bridges required constant supervision by "bridge-keepers" and goalkeepers. Covered with earthen material, the bridges were soft and difficult to walk on in rainy weather, and therefor, from the 15th century, the decks were covered with sawn timber. For better bases, the craftsmen processed the round trunks into rectangular squared timber with an axe. Planks were laid over them, some of the covering laid at an angle or loosely, held down at the edges with battens.

Since the reliable span of a wooden beam was limited to six to ten meters, intermediate supports made of stone or wood had to be installed for wider rivers/spans. Probably the oldest yoke bridge in Europe is the famous Kapellbrücke in Lucerne with spans of approx. 7.65 m (Figure 4).

In the event of war, such structures could be quickly removed and later, after the danger had passed, being reinstalled. Floods and ice drifts repeatedly destroyed intermediate pillars and caused bridges to collapse. Parts of the bridge that were washed away endangered other bridges downstream. In this regard, Stadelmann [3] also quotes the Swiss novelist Jeremias Gotthelf with his story "Water Distress in the Emmental", how the flood of August 13, 1837 destroyed all wooden bridges over the Emme, with the exception of the Horben Bridge, the only one without an intermediate pillar. The connection between the two sides of the valley was limited to this single transition for years.



Figure 3: Modern interpretation of early log bridge by Prof Gehri. Untere Hürlisegg Bridge – Eggiwil BE – constructed in 2009. This comes close to the historic "Schlagen einer Brücke", which refers to "Schlagen eines Baumes", in English cutting a tree/trunk with an axe. The wood was locally cut and processed on-site in order to arrange it as a bridge (deck) for forest-traffic. Pictures: E. Gehri



Figure 4: Renowned Kapellbridge in Lucerne, central Switzerland with a total length of 205 m. This is the oldest existing bridge in Switzerland (1365). It almost completely burnt down in 1993 and was rebuilt in 1994. Pictures: R. Widmann and sgkgs



3 Larger span timber bridges

3.1 Strut- and post- framed trusses

In an effort to achieve larger spans, supporting structures were developed from the 15th century by joining beams to form triangles und thus trusses. There were/are three basic construction types:

- In German "Sprengwerk". These are trusses made from struts that are positioned below the deck. This results in all members (except the deck itself) being loaded axially in compression. Joining the single members is relatively easy, e.g. via direct contact. Regarding the position of the truss relative to the deck, such constructions could also be referred to as "deck trusses".
- In German: "Hängewerk". These are trusses made from posts and struts which are positioned above the deck. They resemble king- or queen-post structures used in roofing constructions. The deck is suspended ("hanging") and the vertically running posts are loaded in tension. The connections have to transfer tension and thus are more difficult to realize. Regarding the position of the truss relative to the deck, such constructions could also be referred to as "through trusses". An advantage of this construction is that there are no structural members below the deck and thus the flow section is not reduced.
- A combination of the two above mentioned trusses, could be referred to as "composite truss frame or "Swiss trussed bridge" (Figure *5*). Regarding the position of the truss relative to the deck, such constructions could also be referred to as "pony trusses". This kind of trusses, in particular when they were made as polygonal strutted frames, allowed for the biggest spans of timber bridges before arches were introduced and realized.

Stadelmann [3] and Blaser [4] mention that one of the first suspension bridges spanned the Martinstobel near St.Gallen in 1468 with a length of 30 meters. Two other examples with widths of up to approx. 20 meters are the Neubrügg built in 1535 over the Aare near Bern and the Saane overpass near Gümmenen built in 1555. For the bridge construction, the craftsmen used straight wood with as little knots as possible, such as fir, spruce and larch, and also oak for special purposes. Because of its density and resin content, larch wood was the most suitable.

The best material, careful design and execution have always influenced the service life. Covered wooden bridges reach an age of more than two hundred years. Even if they had to be renovated and strengthened several times in order to reach this age, this is a great achievement. Especially if you compare the envisaged lifetime of 80 to 100 years for modern steel and concrete bridges. In practically all areas of Switzerland, most timber bridges were given a roof and side panels to protect them from the weather. These roofs, often elaborately executed, also served to reinforce the supporting structure. These bridges are still referred to as "Hüslibrücken" ("little house-bridges") to this day.





Figure 5: Letzibrücke from 1853 crossing the river Necker in Canton Thurgau. This is an example for a composite truss frame. Since 1969 a pre-tensioned concrete bridge close to the timber bridge takes the road traffic. The picture on the right shows how historic timber bridges can be used in Switzerland nowadays. Like many others they can be, e.g. rented for events like weddings or birthdays. This possibility of use contributes to the fact that the local population often has a strong emotional bond with "their" wooden bridge and thus also takes care of the structure. Pictures: R. Widmann



In the 18th century, the manual construction of wooden bridges with its variety of load-bearing systems reached a peak that was hardly surpassed later. Successful master carpenters like Hans Ulrich Grubenmann (1709-1783) from Teufen in Canton Appenzell Innerrhoden, Eastern Switzerland, Josef Ritter (1745-1809) from Lucerne, central Switzerland and Blasius Baldischwiler (1752-1832) from Laufenberg, southern Germany and other talented professionals created important buildings, some of which were well known in large parts of Europe [3].

3.2 The impact of the Grubenmann Bridges

The internationally best-known bridge structures of this time came from the Grubenmann brothers, and here in particular from Hans Ulrich Grubenmann [5]. In addition to numerous large roof structures for churches, the Grubenmann brothers designed and built more than 10 large wooden bridges, some of which are listed in Table 1. Their bridges show how it was possible to build bridges with large spans of over 50 m using wood. The transition from dissolved multiple trusses and hanging structures to arch structures can already be seen here. The two best-known and most important Grubenmann bridges are those of Schaffhausen (completed 1758) and Wettingen (completed 1766). With spans of 63 m (longer of the two spans in Schaffhausen) and 61 m (Wettingen), they were definitely among the widest-span wooden bridges in the world in that era.

Table 1: Examples of bridges of the brothers Hans-Ulrich and Johannes Grubenmann. Unfortunately, only 3 of the Grubenmann bridges are still existing.

Bridge	Year	Span [m]	Destroyed
Ziegelbrücke	1743	38	1799
Schaffhausen	1755-1758	56 + 63	1799
Reichenau (2)	1757	ca. 35 (1) and ca. 70 (2)	1799
Wettingen	1764-1766	61	1799
Schindeleggi	1765	31	1946
Netstal	1766	ca. 30m-35m (?)	1799
Ennenda	1765	ca. 48m (?)	1799
Schwanden	1765	?	1799
Oberglatt	1767	28	
Hundwil	1778	29	
Kubel	1780	30	

However, there are indications in the literature that one of the two bridges of the same age, at the confluence of the Vorder- and Hinterrhein in Reichenau, clearly exceeded the above-mentioned bridges with their approx. 70 m span. Unfortunately, unlike the first two bridges mentioned, no technical documentation or models of the Reichenau Bridges (and especially the longer of the two) remain. Contemporary witnesses report in the literature that this bridge was superior to the Schaffhausen and Wettingen bridges, in addition to or despite the larger span, with its obviously lower susceptibility to vibration.

With regard to the span of the Schaffhausen Bridge, there is probably not a single relevant treatise in which the topic is not discussed whether it was a single-span 119 m long bridge or a two-span bridge with spans of 63 m and 56 m (Figure 6).It is undisputed that Grubenmann at least initially wanted and proposed to build a single-span bridge. He proved the suitability of his construction with a corresponding single-span model, which he loaded with his full body weight in front of the responsible Schaffhausen officials. It is also clear that the Schaffhausen councilors rejected this and forced Grubenmann to place his bridge on an existing central midspan pillar.

It is clearly visible that the executed bridge contains features for both, one-span and two-span structures, to a certain extent as a kind of hybrid. There are records that allegedly prove that it worked at least temporarily as a single span bridge, but also those that refer this to the realm of fables. However, the analysis of the floor plan clearly shows that a single-span bridge is difficult to imagine. The reason for this is the bend above the central support, which in this case would greatly encourage the pressure members to deviate to the side. When discussing the two bridges, it seems to be much more important to the authors that the change or further development and transformation from the dissolved polygonal strutted frame (Schaffhau-

sen) to the arch (Wettingen, Figure 7) is clearly visible. This transformation is also well described an documented in detail by Blaser [4] and Steurer [6]. Arched timber structures were probably already in use beforehand and other Swiss master timber builders also adopted this construction method at the same or subsequent time.

Other examples are the Emme bridges in Hasle Rüegsau (Figure 8) and Schüpbach (Figure 9), both from 1839. These arches have in common that the individual lamellae were clamped/bolted against each other and interlocking tooth-shaped recesses ensured the transmission of shear forces in the arch. In the period that followed, both types of construction existed side by side.

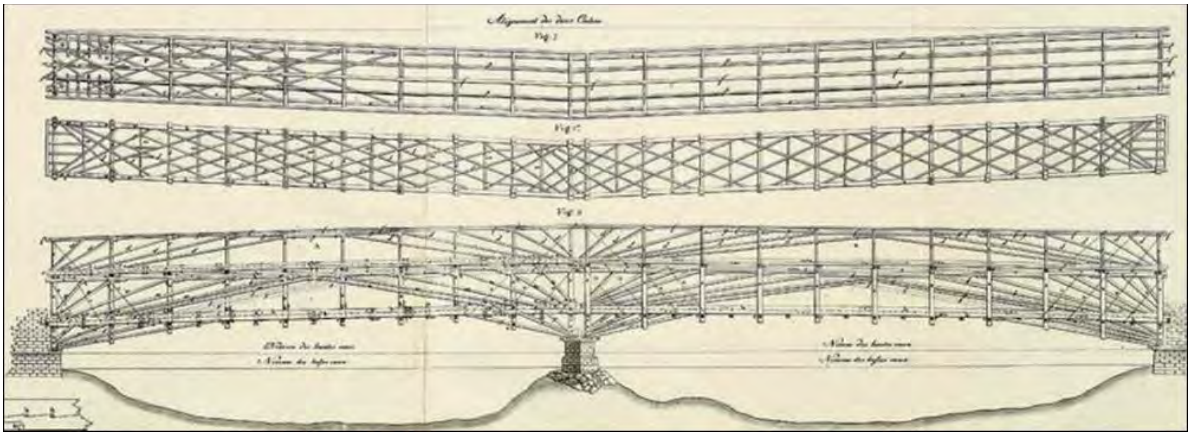


Figure 6: One of the two most important and renowned bridges of Hans Ulrich Grubenmann. is the Schaffhausen bridge crossing the river Rhine as shown here in a drawing from Christian von Mechel. The bridge was opened for traffic in 1758. The side view of the construction reveals that there are distributed arch-like polygonal struts that form a two-span structure as well as such that form only a one-span structure. From the plan view it can easily be recognized, that there is a bend at the middle support. Picture: B. Nebel

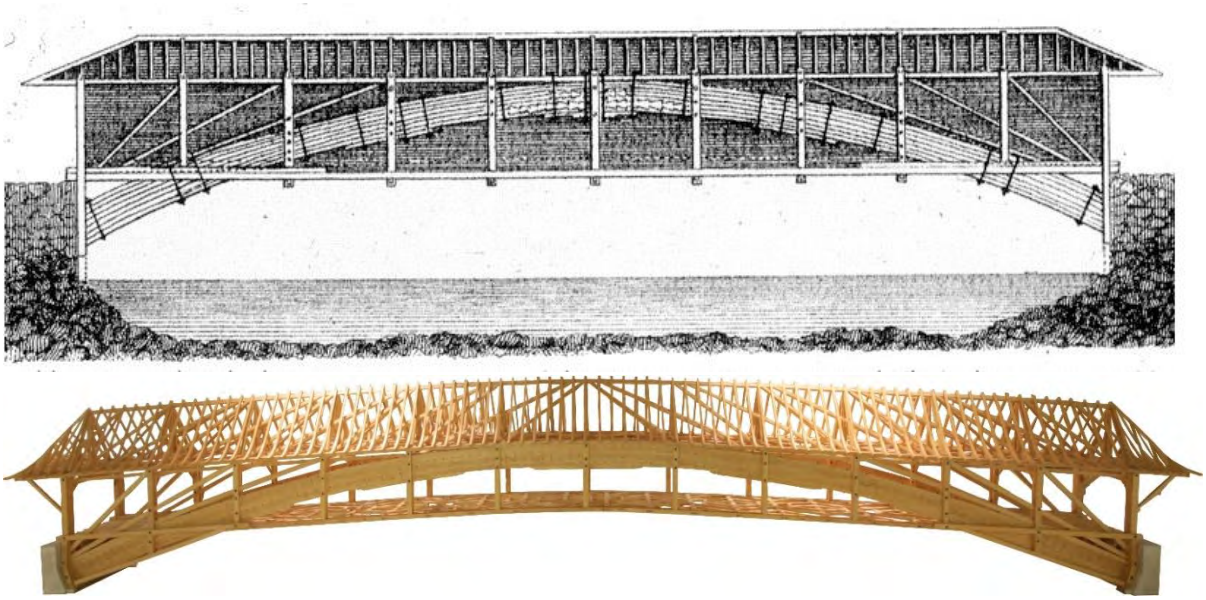


Figure 7: The other very important and renowned bridge of Hans Ulrich Grubenmann is the Wettingen bridge crossing the river Limmat with a span of 61 m. The bridge was opened for traffic in 1766. At this stage, the transition from combined polygonal struts and post constructions as used in Schaffhausen to an arched structure was performed. For the transfer of shear forces the single lamellae had to be spanned together. It is not clear, how it was realized. In the shown model (Zeughaus Teufen), as well in the original (?) model in Aarau, it has been realized by bolts whereas the drawing shows the use of braces. Pictures: B. Nebel, R. Widmann



Figure 8: Bridge at Hasle-Rüegsau BE crossing the river Emme. Built in 1839, it has a span of 58 m and thus is very similar to the Grubenmann Bridge in Wettingen, Picture: R. Widmann



Figure 9: Another Emme bridge (in Schüpbach) with an impressive 49 m span and similar construction as Hasle-Rüeggsau and Wettingen bridges. The picture shows nicely the technics used to create an arch with interlocking tooth-shaped recesses in the lamellae and/or hardwood dowels for the transfer of shear forces within the arch. Picture: E. Honegger (A. Steurer) [6]

3.3 US – Truss technology adopted for Swiss Timber bridges

They were supplemented by the lattice trusses developed in the USA at the beginning of the 19th century based on the designs of Ithiel Town ("lattice truss") and William Howe. Numerous bridges in Switzerland were built using this method, of which some impressive bridges still exist today, e.g. between Vaduz and Sevelen (Howe truss) over the Rhine and over the Necker (Town lattice truss) in the Canton of Sankt-Gallen.





Figure 10: Necker Bridge Anzenwil SG from 1863 with it's main structural elements being Town lattice trusses. The bridge spans 46 meters (with the addition of an intermediate support) and was under road traffic load until the year 2000, when a modern concrete-steel hybrid bridge was set next to it. The new bridge carries the main traffic load and leaves the slow traffic to the old timber bridge, Pictures: R. Widmann



Figure 11: Howe truss bridge crossing the river Rhine between Sevelen (CH) and Vaduz (LI). Built (opened) in 1871/1901 it was one of a series of more than 10 Howe truss bridges along the river Rhine, including one for railway. It is the only one that still exists. This bridge was under road-traffic load (6t) until in 1975 a new pre-stressed concrete bridge (from which the picture at the bottom was taken) was built next to it. www.swiss-timber-bridges.ch/ lists a total of 34 Howe truss bridges that exist(ed) in Switzerland. Pictures: Documentation: Die alte Rheinbrücke Vaduz–Sevelen

3.4 New (old) role for timber in bridge constructions

With the beginning of industrialization and the associated construction of railways and efficient roads, however, more and more bridges were built first of iron, then steel and concrete. Thus, the construction of (large) wooden bridges was strongly pushed back. In addition, numerous existing wooden bridges were destroyed and replaced by supposedly more efficient bridges made from modern building materials. After all, wood was still used in bridge construction for installations and scaffolding and formwork (Figure 12).



Figure 12: Renowned Salginatobelbrücke in Schiers, Graubünden, Eastern Switzerland by Robert Maillard (concrete structure) and Richard Coray (timber scaffolding) 1929-1930. These pictures highlight the transition of the role of timber in bridge constructions from being the dominant permanent solution in the past to serving as a temporary auxiliary construction. Pictures: L. Gianadda, R. Widmann

However, since the middle of the 1950s, a rethink has started. Numerous "Hüslibrücken" have been thoroughly renovated and placed under monument protection in order to preserve them for posterity. A few were left next to new concrete bridges as unused "siblings" (Figure 13).



Figure 13: Examples for timber bridges in Switzerland that lost their initial primary purpose as the main traffic bridge to their modern siblings. Left hand side shows the Lüthisburg bridge with length of 58m and its replacement can be seen in the background. Right hand side is the bridge from Figure 10 with its younger sibling just sitting next to it. Both timber bridges are well preserved and still serve for pedestrians and bycicles and in the Lüthisburg bridge can also be rented for event. Pictures: L. Gianadda, R. Widmann

4 Renaissance of timber road bridges in Switzerland

In the 1980s, timber road bridges experienced a renaissance in Switzerland. In 1985, the Dörfli Bridge was put into operation. The Bubenei Bridge followed in 1988. It is thanks to the canton of Berne that multi-lane road bridges in wood have once again been built in Switzerland, especially in the Emmental. There is probably no other region in Switzerland with such a high density of wooden bridges than the Emmental.

From the very beginning, attention was paid to excellent structural wood protection. Even then, only protected bridges were built. This was important to regain lost trust and has proven its worth to this day. The protection concept was initially based on a roof. The roadway deck was additionally protected with sealant and asphalt. Arches were predominantly used for the main structure. This supporting structure is excellently suited and efficient for bridges.



Figure 14: Dörfli-Bridge, Eggiwil, Canton Bern, built 1985, Span 30.6 m, Live load 28 Tons, Type Covered arch bridge, Design: H. Vogel and Prof. Gehri, ETH Zürich, Pictures: Archiv K. Schwaner.



Figure 15: Bubenei-Bridge, Canton Bern, built 1988, Length/Span: 50.0/43,4 m, Live load 28 Tons, Type Covered arch bridge, Design: H. Vogel, Bern, Moor Hauser & Partner AG, Bern, Pictures: Kolb



4.1 Adoption and further development of stress laminated timber deck plates in Switzerland

The QS plate certainly helped to achieve a breakthrough of the highly stressed road bridges in wood.

Around 1985, the system of transverse prestressing was adopted and further developed in Switzerland. The adaptation to the European requirements has led to the so-called "QS panels", which are frequently used in timber bridge construction and partly also in building construction reports Andreas Bernasconi in [10]. He explained that massive, slab-like roadway elements connected with nail plates were already used decades ago in Canada. Due to the vibrations caused by the traffic the nail connection has been detached. In order to improve the interaction of the elements as a slab-shaped load-bearing element, these roadway elements were pressed together in the transverse direction with the help of steel rods. This closed the open joints and the load-bearing effect was restored. From this rehabilitation measure the Stress Laminated Timber Deck Plates emerged. The QS panels were often formed by impregnated boards for simple forest bridges.

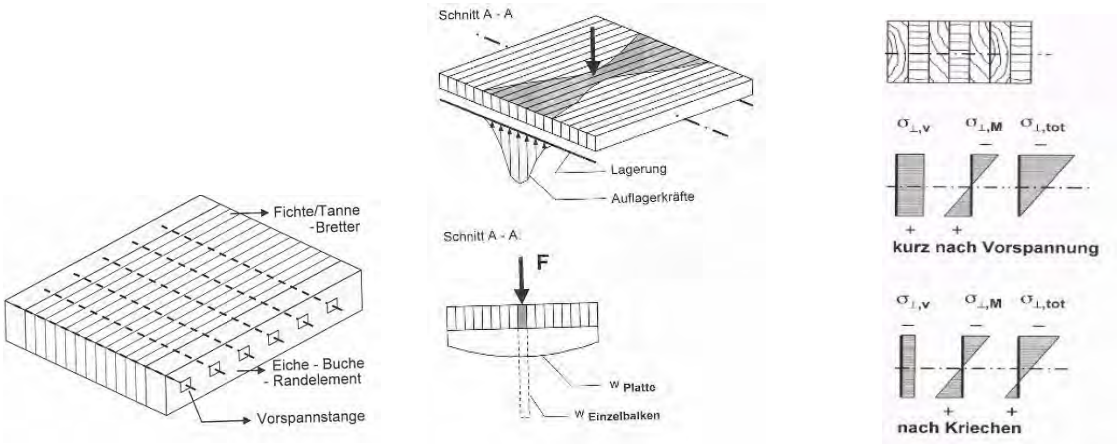


Figure 16: Stress Laminated Timber Deck Plates in: Schwaner K., Horsch B. (1999) Brücken aus Holz – Konstruieren, Berechnen, Ausführen, Tagungsband INFORMATIONSDIENST HOLZ [10], Pictures: Archiv K. Schwaner.



Figure 17: Forestry-Bridge-Typ with Stress Laminated Timber Deck Plates, Design: Prof. E. Gehri, Pictures: Archiv K. Schwaner.

4.2 Protection concept using lamella formwork

In addition to the road bridges, numerous footpath and cycle path bridges continue to be built in wood. An impressive example is the bridge over the Simme near Wimmis, Canton Bern. Julius Natterer used open lamella formwork instead of closed formwork. This type of cladding is widely accepted for the protection of wooden bridges. It is open and transparent and offers views for people of different sizes. Technically, it ensures excellent drying capacity for the protected components.



Figure 18: Cycle Path Bridge over Simme near Reutingen/Wimmis, Canton Bern, built 1989, Length 108 m, /Span 27/54/27 m, Type Covered truss bridge, Design: J. Natterer, Pictures: Kolb. Schwaner.

4.3 Protected bridges without roof

In the 1990s, the roof was dismissed for the first time. Confidence in the waterproofing systems has grown. The main reason, however, was to increase the economic efficiency. A covered bridge causes higher costs. As a result of the moisture input from the traffic, the deck must be carefully protected anyway. Between 2000 and 2010, 75% of the bridges have already been built without a roof [8].

High-performance materials also found their way into wooden bridge construction. In particular, components subjected to stress perpendicular to the grain were made with reinforcements of plywood and laminated veneer lumber (LVL).



Figure 19: Bridge San Nicla, Canton Graubünden, built 1993, Length/Span: 47,8/39 m, Live load 28 Tons, Type Arch Bridge, Design: A. Mayer, Sent, A. Deplazes, Chur, Prof. E. Gehri, Pictures: BFH



4.4 Timber-concrete composite bridges

In the same time period, timber-concrete composite bridges were built for the first time. The advantages were seen in the fact that the reinforced concrete carriageway slab perfectly protects the timber components underneath and at the same time ensures a significant part of the load-bearing capacity.

In particular, they ensure load distribution. The load distribution of the high individual loads of the load models does not cause a problem. The use of detail solutions from solid construction, which have been used and proven thousands of times, was seen as a major advantage. The most important of these are the connections of the scraper curbs, the roadway transitions and the anchoring of the crash barriers.

As is customary in Switzerland, different shear connections were developed and just used and tested on the current object.





Figure 20: Glenner-bridge, Graubünden, built 2002, Length 34,6 m, / Span 24,6 m, Live load 4x75 Tons, Design: Conzett, Bronzini, Gartmann AG, Chur, Pictures: Graubündenholz, Landquart/LIGNUM





Figure 21: Planchy, Bulle, built 2005, Span 25,9 m, 40 tons, Vial SA, Le Mouret, Pictures: BFH



Figure 22: Ronatobelbrücke in Furna, Graubünden, Timber-Concrete-Composite, built 1991; Span 12-12-13,75-12,25 m; 28 tons, Engineers Buchli + Joh. Fromm, Picture: Andrea Bernasconi HES-SO Yverdon/LIGNUM





Figure 23: Crestawaldbrücke in Sufers, Graubünden, Timber-Concrete-Composite, built 1996; Span 31 m; 28 tons, Engineers W. Zöllig, Arbon, M. Kratiger, Happerswil, Pictures: Archiv K. Schwaner

4.5 Competition for a new generation of timber bridges

In a competition for the renewal of four wooden bridges in the upper Emmental [12] a distinction was already made between timber bridges without roofs and timber bridges with roofs. The result of this competition was convincing. In the first stage (ideas competition) 45 designs were submitted. in the second stage 8 feasible bridge designs were developed. With this competition, the broad spectrum of timber bridge construction could be shown. This was important to convince even skeptical decision-makers of the quality of timber bridges.



Figure 24: Obermattbrücke, Canton Bern, built 2007, Through Bridge, vertically adjustable (70 cm) bridge when high water, span: 32 m live load 40 tons, Design: Paul Grunder AG, Täufen, *Pictures: BFH*

Heavy rainfalls often lead to the destruction of infrastructure structures/building. In this case rapid replacement is required. Every large-scale weather event was therefore also an opportunity for timber bridge construction. Innovative solutions for lifting, excavating and moving out of the danger zone were developed as important prevention measures. Due to their low dead weight, wooden bridges have an advantage here.

4.6 Timber bridge construction today

Today timber bridges are often made with block glued beams sometimes in combination with multilayer LVL or CLT deck plates as composite construction. Nevertheless, covered truss bridges are still being built today. These are very economical option for large spanned single-lane bridges. Some of these are designed for 66 tonnes.



Figure 25: Horenbrücke, Canton Aargau, built 2008, lenght: 30.87 m, span: 6,25 – 17,32 – 7,30 m, 40 tons, block glued girder bridge, Design: Makiol + Wiederkehr, Beinwil, Wilhelm+Wahlen, Aarau, Zimmermann Architekten, Aarau, Pictures: A. Müller BFH



Figure 26: Luthernbrücke, Canton Luzern built 2010, Lenght: 13,55 Span: 13.05 m, 40 tons, block glued girder bridge, Design: E. Winkler & Partner, Luzern, Makiol + Wiederkehr, Beinwil, Picture: Makiol + Wiederkehr



Figure 27: Kirchenbrücke Muotathal, Canton Schwyz built 2009, Lenght: 34,00 m Span: 33,40 m, 40 tons, arch bridge, Design: Pirmin Jung, Rain, BPP Ingenieure, Schwyz, E. Imhof, Luzern, Picture: BFH





Figure 28: Enningerbrücke, Malters, Canton Luzern, built 2010, Lenght: 46,0 m Span: 42,0 m, 28 tons, truss bridge, Design: Pirmin Jung, Rain, Emch + Berger WSB AG, Luzern, Pictures: Kolb, Pirmin Jung Ingenieure

4.7 Timber- ultra-high performance fibre composite (UHPC) composit structures

In the meantime, ultra-high performance fibre composite (UHPC) has found its way into timber bridge construction. The combination of wood and UHPC is promising. The material combination of timber with decks made of UHPC has already been used several times, especially in shear composite (wood-UHPC composite construction) in the new construction of wooden bridges (2018 Gletschersand bridge in Grindelwald, 2020 Fruttli bridge near Rigi Fruttli) [13].



Figure 29: Fruttlibrücke in Arth, Canton Schwyz built 2020, Span: 10,45 m, 40 Tons, Timber- UHPC composite structure, Design: Edgar Kälin, Einsiedeln, Neue Holzbau AG, Lungern, Prof. E. Brühwiler EPFL Lausanne [15], Pictures: E. Kälin



In contrast to the mastic asphalt structure, the UHPC layer serves to increase the load-bearing capacity of the roadway slab. With a roadway slab made of UHPC, 3 layers (waterproofing, protective layer, surface layer) can be replaced. According to [14] Brühwiler 2017), a UHPC layer thickness of 30 mm is "liquid-tight" up to an expansion of 1.2 ‰.

In expert circles, this type of construction in timber bridge building is considered to have good market chances, as the described advantages can significantly improve not only the increased performance but also the durability by protecting the underlying timber construction and thus also the economic efficiency of timber bridges.

References

[1] BAFU (2010) Hydrologischer Atlas der Schweiz, Tafel 6.6, Stand 2010. Bundesamt für Umwelt (Bafu): Bern
[2] BAFU (2021) Jahrbuch Wald und Holz 2021. Bundesamt für Umwelt (Bafu): Bern.
[3] Stadelmann W. (1990) Holzbrücken der Schweiz – ein Inventar, Verlag Bündner Monatsblatt, Chur, ISBN 3 905241 04 8.
[4] Blaser W (1982) Schweizer Holzbrücken, Birkhäuser Verlag, Basel, ISBN 3 7643 1334-X..
[5] Killer, J. (1942) Die Werke der Baumeister Grubenmann – Eine baugeschichtliche und bautechnische Forschungsarbeit., Dissertation ETH Zürich
[6] Steurer A., (2006) Developments in Timber Engineering The Swiss Contribution, Birkhäuser Verlag, Basel, ISBN 3 7643 1633
[7] Vaduz (2011) Dokumentation: Die alte Rheinbrücke Vaduz–Sevelen, Gemeinden Vaduz und Sevelen
[8] Bachofer R. und Conzett J. (2013), Brücken in Holz, Möglichkeiten und Grenzen, Forschungsprojekt AGB 2003/012 auf Antrag der Arbeitsgruppe Brückenforschung (AGB), Bundesamt für Strassen
[9] Kreuzinger H., Mohr B. (1995) Brücken – QS-Holzplattenbrücken, INFORMATIONSDIENST HOLZ, Entwicklungsgemeinschaft Holzbau in der DGFH et al.
[10] Andrea Bernasconi quervorgespannte Fahrbahnplatten in:
[11] Schwaner K., Horsch B. (1999) Brücken aus Holz – Konstruieren, Berechnen, Ausführen, Tagungsband INFORMATIONSDIENST HOLZ
[12] Stalder F. et al. (2000) Wettbewerb zur Erneuerung von vier Holzbrücken im oberen Emmental, Oberingenieurkreis IV, TBA Bern, Schweiz
[13] Kälin E., Roggenmoser P. (2022) Fruttli-and Rigiaa-Bridge, Timber-UHPC composite structure, 4. ICTB 2021, Biel
[14] Brühwiler (2017) Memorandum «UHFB als Abdichtung von Brückenfahrbahnplatten» vom 30. September 2017, Prof. Dr. E. Brühwiler, ENAC Faculté Environnement Naturel, Architectural et Construit, EPFL Lausanne
[15] Kälin E., Roggenmoser P. (2022) Fruttli-and Rigiaa-Bridge, Timber-UHPC composite structure, 4. ICTB 2021, Biel

Conference Proceedings 4th ICTB (2022)
https://doi.org/10.24451/0akb-5816

ICTB 2021 PLUS
4th International Conference on Timber Bridges
Biel/Bienne, Switzerland, 9 -12 May 2022



First Swiss wildlife bridge made with timber

Lukas Rüegsegger[1]

1 Introduction

With the building of roads, railways, infrastructure buildings, estates as well as industrial and commercial areas, wildlife connectivity is limited in heavily built-up Switzerland. The habitats of the animals are geographically demarcated with insurmountable barriers, which suppresses the animals' natural urge to move.

In Switzerland, 305 wildlife corridors of transregional importance are recorded. Of these, 14% are interrupted and can no longer be used by animals. More than half of the corridors (58%) are impaired and only 28% are classified as intact.

In 2001, the Federal Office for the Environment (FOEN) set the goal of rehabilitating 51 transregional wildlife corridors with wildlife-appropriate structures so that animal populations can mate again across different geographical areas.

In the Rynetel area, between Gränichen and Hunzenschwil, the wildlife corridor was restricted due to buildings and estate areas and completely desrupted by the A1 motorway. This is where the first wildlife overpass with timber construction was built.

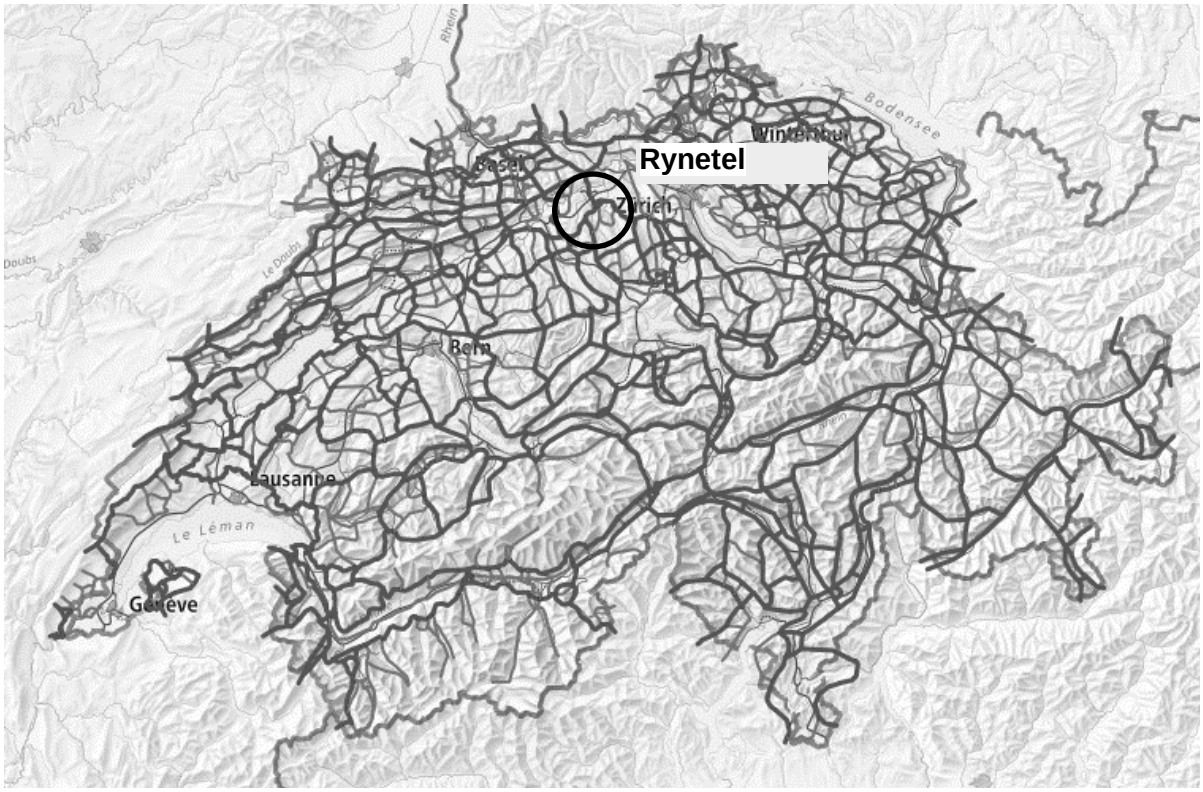


Figure 1 Wildlife corridors of supra-regional importance and location of the Rynetel wildlife crossing. Source: map.geo.admin.ch

[1] Lukas Rüegsegger, Timbatec Holzbauingenieure Schweiz AG, Switzerland,
Lukas.Ruegsegger@timbatec.ch

2 Wildlife Bridge Rynetel

The overpass structure should fit well into the topography and landscape. To equip the top of the bridge appropriately for wildlife, a useful width of 50 meters is predefined. In addition, an economical and low-maintenance construction with a durability of 100 years was required. A possible motorway expansion to 6 lanes was taken into account in the clearance gauge. As an important motorway link, the A1 cannot be completely closed. Therefore, the construction process had to be carried out while traffic was maintained.

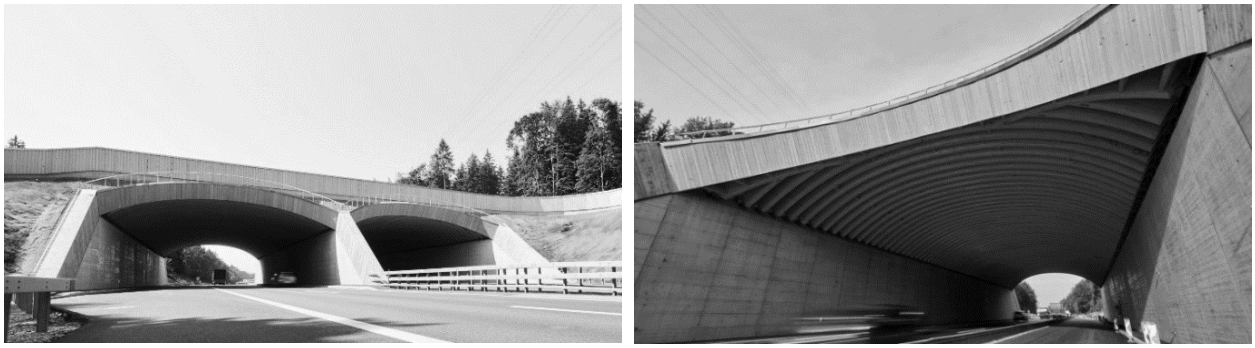


Figure 2 Photos of the completed bridge

2.1 Construction

In cross-section, the structure has a concrete wall with a thickness of 80 centimetres at the sides as well as in the middle. The approximately 17-metre span width on each side is traversed by arched trusses made of glulam GL28h. The trusses have profiles of 240 x 760 millimetres and are mounted on the concrete walls with a step span of 80 centimetres. A steel joint connects the wooden trusses to the solid construction.

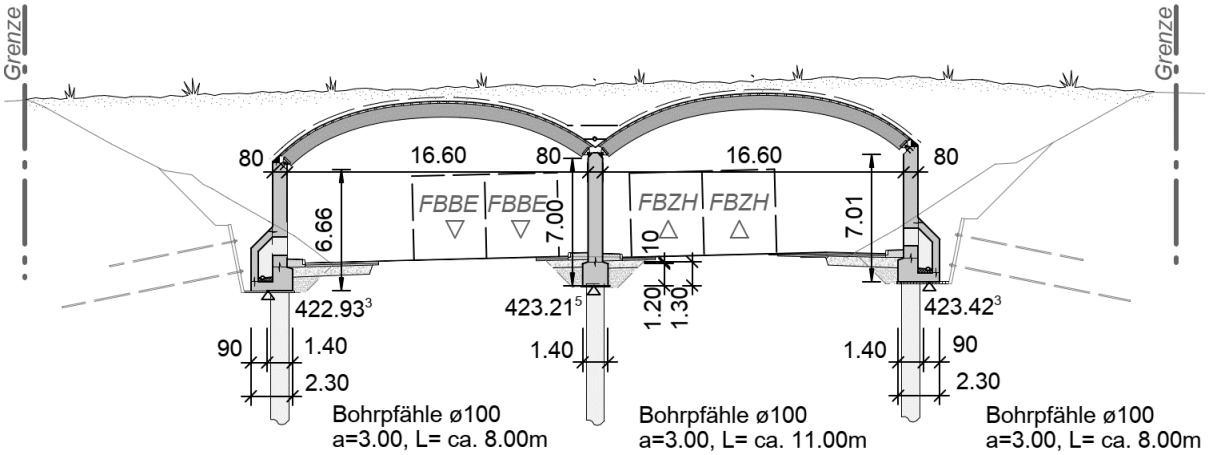


Figure 3 Cross section of the bridge

The secondary structure consists of unbent glulam beams with a profile of 100x400mm, which are fixed horizontally to the arched trusses. A laminated veneer lumber panel fixed to the secondary girders serves as the final substrate for the waterproofing. A coat of PUR bitumen serves as an adhesive base for the double and fully welded polymeric bitumen waterproofing. The root protection made of a TPO plastic cover is consistently welded and thus protects the substrate from root penetration. For mechanical protection, the waterproofing is additionally covered with a rubber mat. A drainage layer of seepage gravel is covered with a filter fleece and conducts the seepage water from the apex to the side walls, where it seeps away, or to the centre of the double arch where the water is collected by means of a seepage pipe and fed to the road drainage system via a downpipe. The final layer consists of soil with various substrates, which is planted.

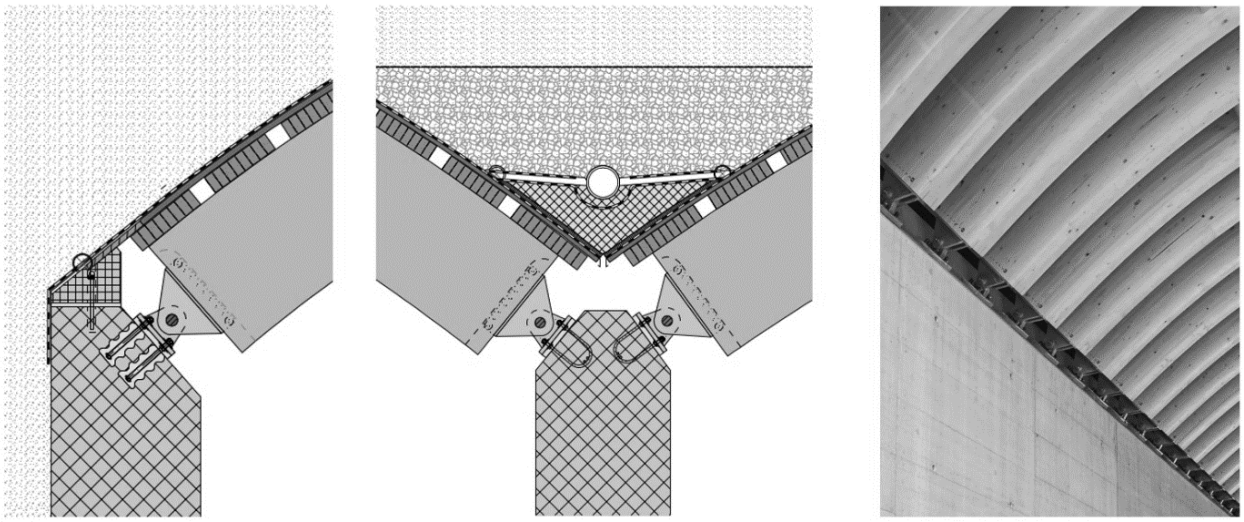


Figure 4 Construction of the support areas of the side wall (left) and the centre wall (right). Middle: Section through steel joint

In the apex area, the construction is covered with 70 centimetres of soil and seepage gravel, and in the outer walls over 4 metres high.

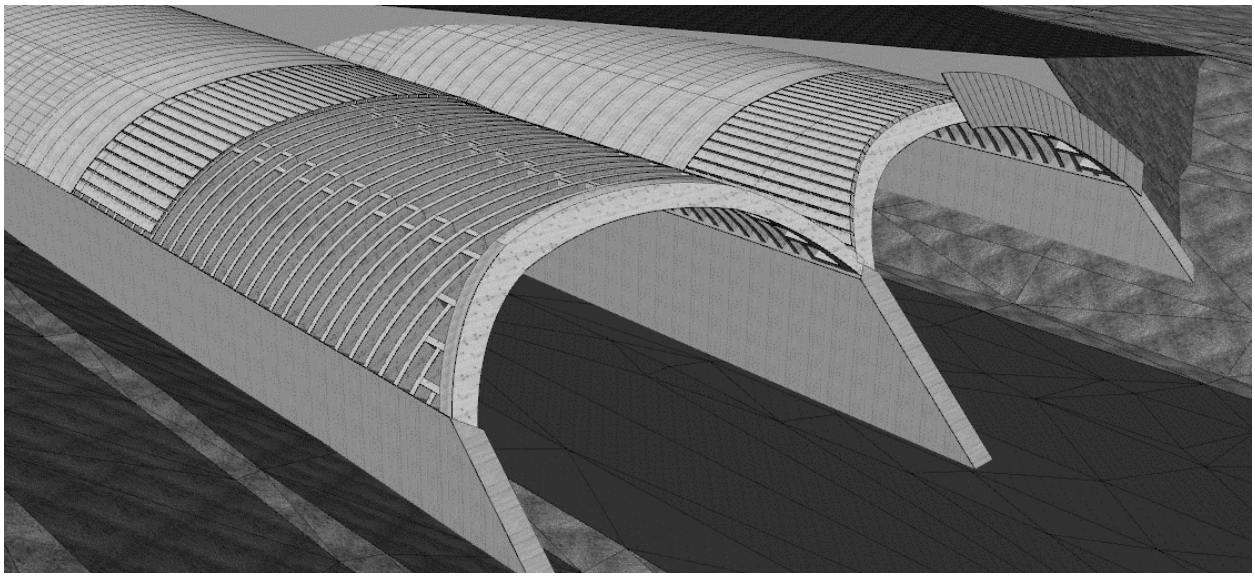


Figure 5 Visualisation of the design of the construction components

To generate the smallest possible earth loads on the structure and thus also to optimise the earth movements of the backfill or cover to a minimum, the supporting structure was arranged higher than would have been necessary due to the clearance profile for road use. This created an almost even area for the wildlife to pass. The two portals are inclined so that the various cover heights can be closed off with an embankment.

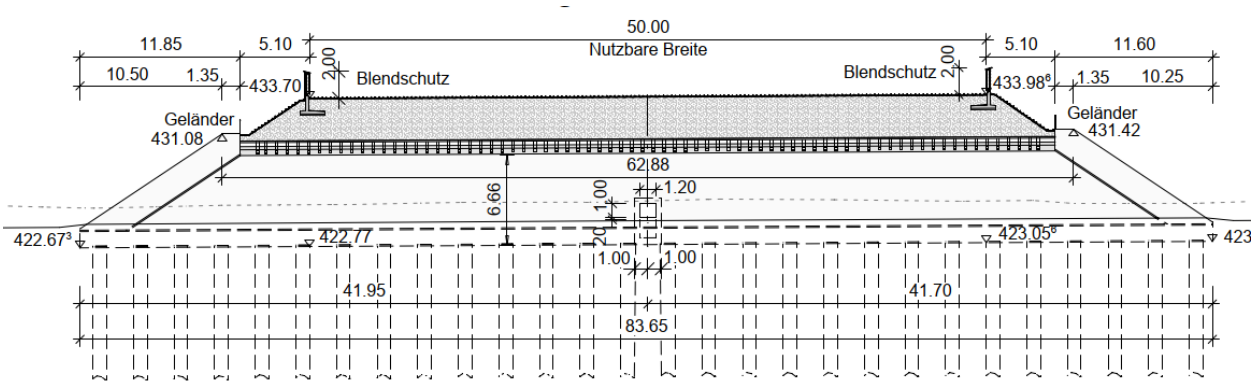


Figure 6 Longitudinal section of the bridge with inclined portals and the anti-glare elements as demarcation.

A two-meter-high glare shield delimits the bridge. On the side of the bridge, the glare shield is connected to the wildlife fence so that no animals cannot step onto the motorway. The glare shield is an important element that protects against headlights so that the animals can cross the bridge as undisturbed as possible.

2.2 Assembly

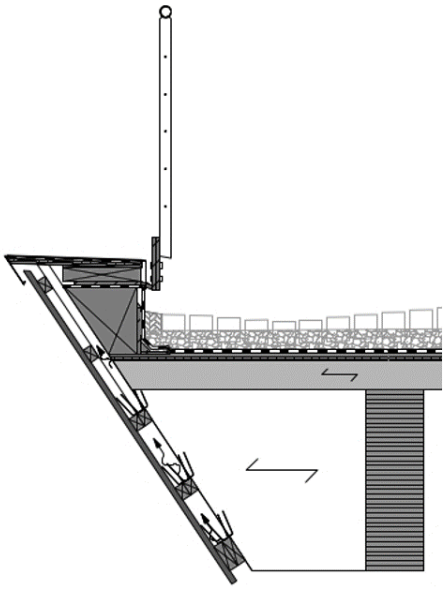




Figure 7 Section through portal and glare shield at the apex of the arch

The bridge structure had to be erected while the motorway was in operation. Therefore, the timber construction was completely assembled during the night. For this purpose, traffic could be diverted to the opposite carriageway so that the work could be carried out directly from the carriageway.

Due to the complex work on the portals, they were pre-assembled as modules on a nearby company site and transported to the construction site and assembled by special transport. The intervening trusses were erected individually, the secondary supporting structure and the veneer plywood were then assembled. As the last night work process, the portal cladding and the portal railing were mounted so that the sealing work could be carried out during the day.



Figure 8 Assembly of the individual trusses between the portal modules.

2.3 Project participants

Building owner:
Federal Roads Office FEDRO
Zofingen branch

Builder support:
Helbling Consulting + Construction Planning AG

Planning:
Engineering consortium IG WUEF:
- Bänziger Partner AG (lead)
- Timbatec Timber Construction Engineers AG

Landscape architecture:
SKK Landscape Architects AG

Execution:
ARGE FERA:
- Solid construction: Aarvia Bau AG
- Timber construction: Häring AG

Conference Proceedings 4th ICTB (2022)
https://doi.org/10.24451/t6nk-7h98

ICTB 2021 PLUS
4th International Conference on Timber Bridges
Biel/Bienne, Switzerland, 9 -12 May 2022



Climate and moisture monitoring in the timber wildlife bridge "Rynetel"

Sébastien Bonifacio[1], Marcus Schiere[2], Andreas Müller[3]

1 Introduction

With the first Swiss timber wildlife bridge 'Rynetel' over the A1 highway in Suhr (CH), timber is also introduced for the construction of wildlife crossings in Switzerland [1]. Approximately 70,000 vehicles pass through the structure daily. The construction was required to be durable and robust to allow a service life of 100 years, comparable to that of concrete structure [2]. The design was based on the first positive experience and knowledge gained from the four wildlife bridges built in Germany since 2005 [3][4]. For the wildlife bridges in Germany, wood species with a higher natural durability such as larch or Douglas fir were used. These are not available in sufficient quantities (regionally) in Switzerland for a structure of this type and size.

At the moment there is not enough knowledge about the prevailing climate conditions in a wildlife crossing over a highway to predict wood moisture and thus evaluate the use of native available spruce and fir ensuring the desired lifespan.

The project «Climatic conditions at timber overpasses for wild animals» aims to record and scientifically evaluate the general climate conditions thanks to a systematically monitoring of the structure. Special emphasis was also placed on the impact of traffic movements on the climate inside the structure. The timber construction is expected to be exposed to large volumes of water from spray carried inwards by traffic during rainfall. On the other hand, the traffic could also have a positive impact on air change (flow) in the structure and, hence, improve the drying capacity of the structure.

The impact of the cross-sectional shape and design of the tunnel-like bridge structure on the moisture levels and drying speed of the wood will also be analyzed in the future. This paper explains the properties of the implemented monitoring system to obtain all the data needed to perform the data analysis and achieve the project objectives mentioned above.

2 Measurement equipment

2.1 Wood moisture

Moisture content of the timber can generally be monitored either by performing local (spot) or global (surface) methods (Figure 1). To monitor a single spot, the electrical resistance measurement method, the sorption method and passive RFID are used. The electrical resistance measurement method is technically very simple and robust. The sorption method provides high accuracy and requires the installation of humidity and temperature sensors at the critical spot. [5]. One type of RFID tag measures the humidity in the immediate environment of the tag according to the principle of capacitive measurement. The use of RFID tags is low cost, and wireless [6].

[1] Sébastien Bonifacio, Bern Universitiy of Applied Sciences, Institute for Timber Construction, Structures and Architecture IHTA, currently: Projectingeneer, Timbatec Timber Construction Engineers Switzerland Ltd., Switzerland, sebastien.bonifacio@timbatec.ch
[2] Currently: Product Manager, Hupkes Wijma B.V., The Netherlands, mjs@hupkeswijma.com
[3] Bern University of Applied Sciences, Institute for Timber Construction, Structures and Architecture IHTA

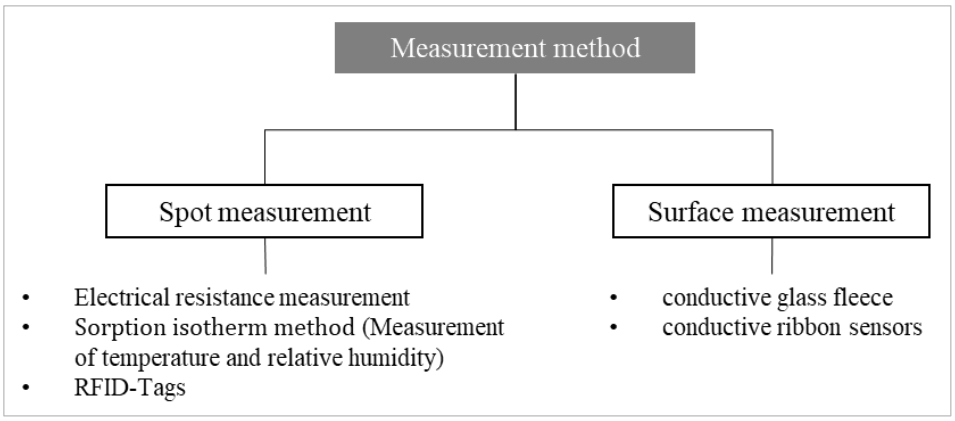


Figure 1 Overview of measurement methods used in monitoring systems in timber structures

With the surface measurement method, the moisture content of wood is measured over a large area. Surfaces can be reliably monitored with conductive glass fleece or with ribbon sensors. Both solutions are based on electric potential measurements. When the moisture changes or when water is present, the electrical potential changes. This way it is possible to monitor moisture over a wide area [6].

The project's purposes can only be achieved with accurate and reliable data. The above listed surface measurement systems are suitable for a surveillance system of the waterproofing system but do not provide sufficient accuracy for the scientific evaluations. The presence of salt and other chemical elements as well as measurements at temperatures below zero affect negatively the accuracy of the measurements with the electrical resistance system. For these reasons it was chosen to use the sorption method for wood moisture measurement. The RFID system did not allow for continuous measurements and are typically used for occasional measurements and could not be used to measure changes in conditions with a frequency of 3 hours.

Wood moisture is monitored with sensors that measure temperature and humidity inside a cavity (Figure 2 and Figure 3). Using a sorption curve, wood moisture is calculated [5].

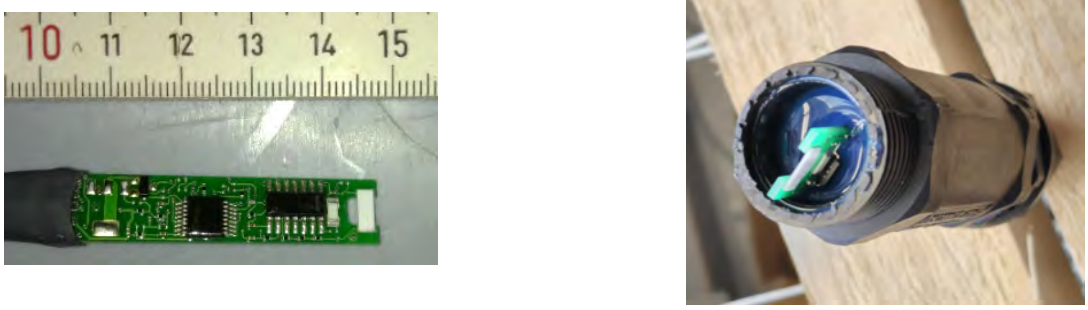


Figure 2 Air humidity and temperature sensor for measuring wood moisture by sorption method



Figure 3 Preparation of holes in wood (left) and drawing for moisture measurement at 40 mm and 100 mm depth (right).

2.2 Outdoor climate sensor

The measurement of humidity and temperature is made with the same temperature and humidity sensor as the one with which the wood climate is determined. This is placed in a plastic box, which is connected to the outside air through a hole. The box is protected from radiation of heat/cold towards the underlying roadway by a steel plate.

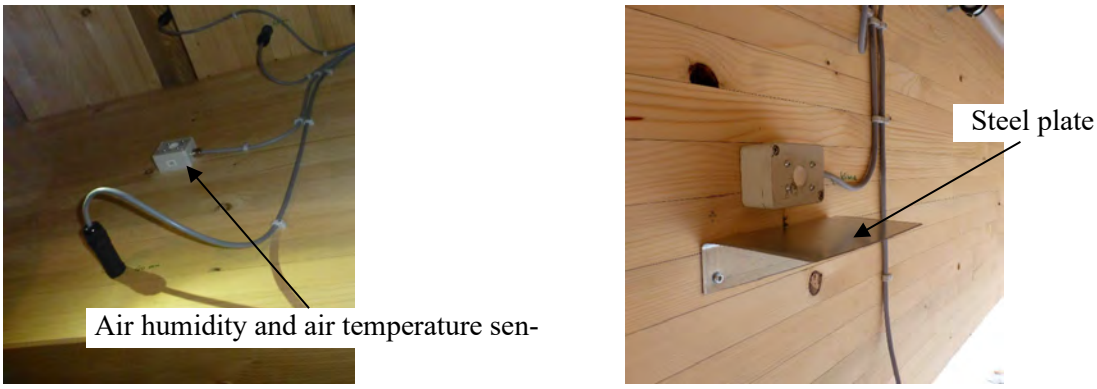


Figure 4 Air humidity and air temperature sensor (left) and steel plate as radiation protection (right).

2.3 Spray cloud and air exchange measurement

The measurement of spray cloud is carried out with rain sensors. If water lands on the surface of the beams, this is detected as spray cloud by the rain sensors. The air exchange due to the traffic in the structure is measured with a cup anemometer. Both systems were not calibrated and are used for qualitative comparisons of changes in the conditions within the wildlife bridge such as more are circulation, less air circulation.

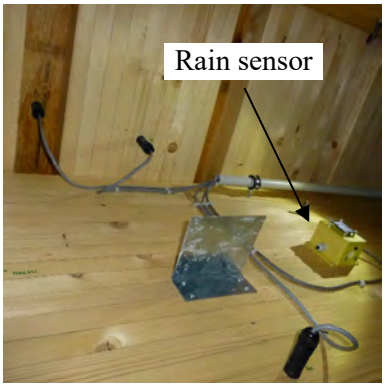


Figure 5 Rain sensor to detect spray cloud



Figure 6 Cup anemometer to detect movement of the air due to the traffic

3 Measuring points

The wildlife bridge (Figure 7) encloses the A1 highway with a double arch structure over a length of 50 meters. Wet roads and the combination of fast light traffic (left lane) and slow heavy traffic (right lane) can introduce water spray of varying heights and quantities into the structure. Due to the soil covering of the structure, larger temperature differences between the air in the structure and the adjacent, cooler timber structure are to be expected. This can lead to condensation on the timber members, the amount of which is estimated by measurements and calculation models.

Sensors were positioned in both the arch beams, the secondary structure, and the deck panels. Different points of the structure are monitored in order to detect differences between the area near the portals and the central area and differences between the two directions of travel (Figure 7). In addition to wood moisture, other parameters are measured such as climate, wood surface temperature, rain (spray cloud) and air velocity inside the wildlife bridge.



In total, the following sensors have been installed: 26x wood moisture measurement with temperature and humidity sensors, 4x outdoor climate sensors, 2x rain sensors and 1x air velocity sensor. To collect the necessary data 33 sensors were installed throughout the structure.

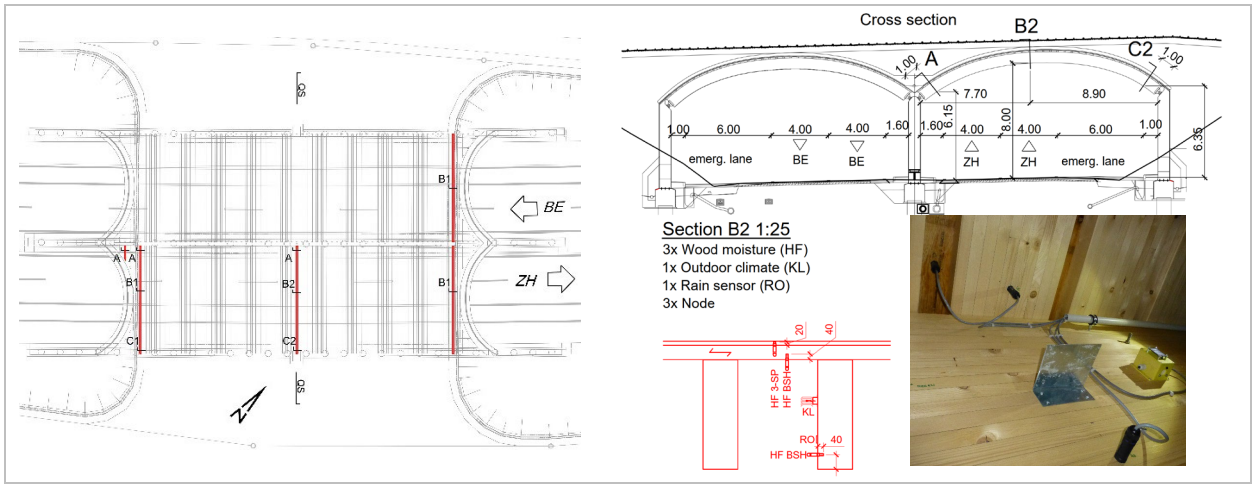


Figure 7 Wildlife bridge plan with monitoring sections indicated (left) and section with detail and photo sensor equipment point B2 (right)

4 Monitoring system

The sensors installed in the wood structure are connected to nodes for data transmission. The nodes are connected to a gateway that is linked to a web interface (swissMon©) from terra vermessungen Ltd (Figure 8). The monitoring system measures since October 2020 and provides the data in real time.

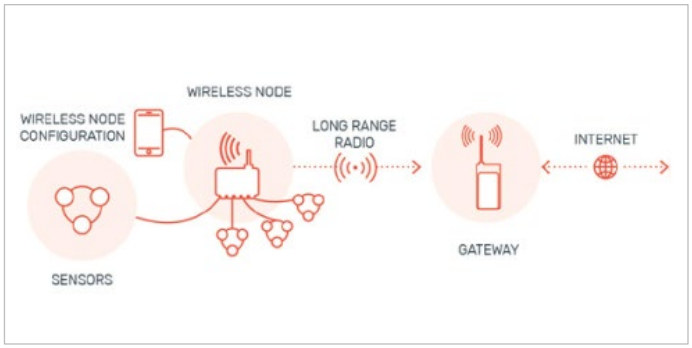


Figure 8 System design and data flow (swissMon©)

The data measured by the measuring system mounted on the wildlife bridge are supplemented with data from weather stations from the Swiss Federal Office MeteoSwiss and vehicle counting points from the Swiss Federal Roads Office FEDRO. These data together with the data measured by the monitoring system form the basis for the analyses that will be carried out in the duration of the project.

5 Wood moisture and conclusion

Measured values show that wood moisture in the various elements in timber varies with the seasons. Some elements show greater fluctuations while others have a more or less constant moisture content. The following picture shows the wood moisture (monthly average) at three different points: (1) slow lane, entrance area (2) slow lane, central area (3) emergency lane, central area. In correspondence of these three points the wood humidity of the glumal 760/240 beam is shown. In the central zone, slow lane, the humidity of the LVL is also shown.

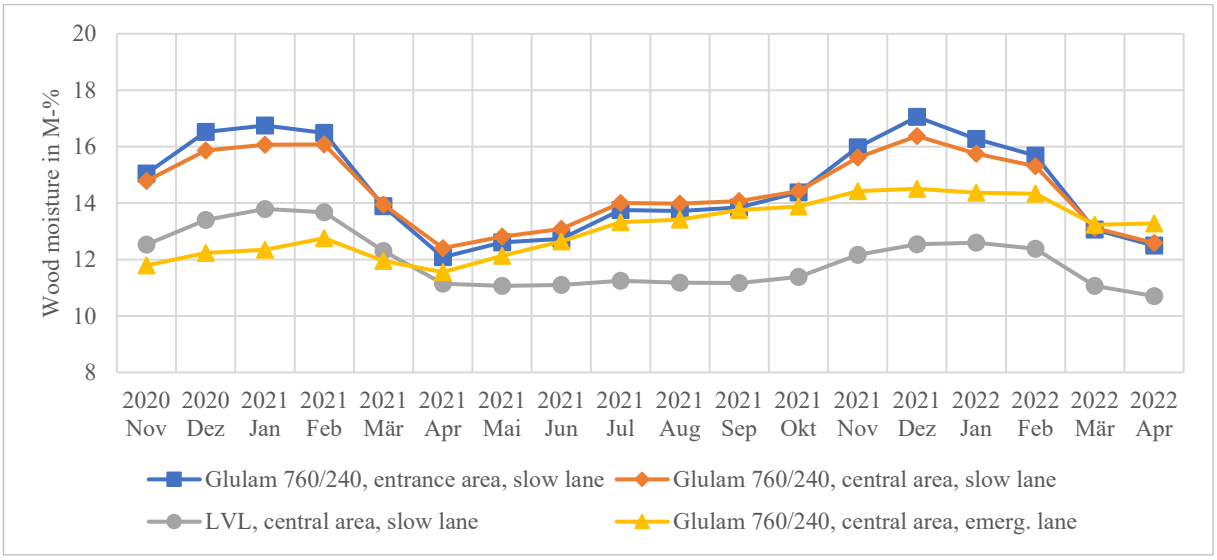


Figure 9 wood moisture (monthly average) from opening to traffic in November 2020 through April 2022

Since the opening of the wildlife bridge in November 2020 until today, in over one year period, there are no noticeable trends that indicate an increase in moisture and furthermore the maximum values are 17 M-%. The parts with higher moisture content are located above the slow lane. The moisture content of the LVL in contact with the soil has a lower moisture content than the glulam 760/240 beam. Above the emergency lane there is less moisture fluctuation than in the area above the slow lane, probably due to less spray cloud. The measurements carried out in the last 1.5 years confirm the correct choice of the type of structure and the use of wood for wildlife bridges.

The data collected from the monitoring system will be analyzed with special attention to the influence of traffic: (1) Due to water spray carried along by traffic during rainfall outside the wildlife bridge, the timber structure is exposed to larger amounts of water than a regular protected structure. (2) On the other hand, traffic could have a positive effect on the air exchange (flow) in the structure and on the drying capacity of the structure. These influences on the wood moisture content and wood moisture fluctuations will be quantified by two years of monitoring and simulations. Subsequently, the use of native spruce and fir as a load-bearing material in wildlife bridges will be further investigated. Simulations and further data analysis will allow prediction of wood moisture for other types of structures as well. All results will be published in the final report of the research project.

Acknowledgement

The research is performed in the scope of grant “2020.08 Klimabedingungen bei Wildtier-überführungen in Holzbauweise” by Federal Office for the Environment FOEN, Wald- und Holzforschungsförderung Schweiz (WHFF-CH). The project partners Timbatec Holzbauingenieure Schweiz AG, Häring AG, Roth Burgdorf AG, terra vermessungen AG and Lignum accompanied the project.

References

[1] Ingenieurgemeinschaft 2B (2918) UEF Wildüberführung Rynetal (AG 6) Suhr, Detailprojekt 2018.
[2] Müller A., Bonifacio S. (2019) Fachliche Stellungnahme zu der geplanten Wildtierüberführung über die A2 in Tenniken/Dietgen und deren Gebrauchstauglichkeit über 100 Jahre vom 27.9.2019, Institut für Holzbau, Tragwerke und Architektur, Berner Fachhochschule AHB.
[3] Bauer M. (2016) Erfahrungsbericht über die Grünbrücke bei Luckenwalde, 4. Internationale Holzbrückentage IHB 2016.
[4] ProTimb (2019) Wartungshandbuch - Prüfplan, Erfurt Deutschland.
[5] Bonifacio S. (2020) Untersuchung der Grundlagen zur Messung des Raumklimas in einen Holzgebäude, Berner Fachhochschule Architektur, Holz und Bau, Schweiz
[6] Berner Fachhochschule, IMP Bautest AG, Aeschlimann AG, Asphaltbeläge auf Holzbrücken - Untersuchung der schubfesten Fahrbahnaufbau-ten für Holzbrücken, Forschungsprojekt ‘Abdichtungssysteme und Bitumenhaltige Schichten auf Brücken mit Fahrbahnplatten aus Holz’

Conference Proceedings 4th ICTB (2022)
https://doi.org/10.24451/5qga-vs74

ICTB 2021 PLUS
4th International Conference on Timber Bridges
Biel/Bienne, Switzerland, 9 -12 May 2022



Preliminary moisture-relevant monitoring results of a timber wild-life bridge 'Rhynetel'

Karim Ghazi Wakili[1], Jan Maurer, Andreas Mueller

1 Introduction

Wild-life bridges are of central importance for animal friendly habitats in densely populated regions where motorways and railways necessary for the connectivity between urban centres and the countryside cut the whole landscape into disconnected pieces. Central Europe and especially Switzerland represents such an environment in need of corridors and connections to help the animals overcome these obstacles.

The first wooden wild-life bridge in Germany has been built already in 2004 and first investigation results reported by M. Bauer [1]. In 2016 there were already 37 with tendency to much more. The first such wooden wild-life bridge in Switzerland has been built in 2019 by Timbatec [2]. This is the one we are investigating the influence of climatic and traffic conditions on the moisture behaviour on its different wooden elements for the first time with an elaborate monitoring procedure.

The following represents an initial evaluation of a selection of sensors used in this project over the period from around October 2020 to July 2021. Measurements from a total of three sources were available. The sensors for determining the wood moisture and wood temperature (90 measured values) from the company "terra", weather data from a weather station near the wildlife crossing (22 measured values) from Meteo-Swiss and traffic data (9 different vehicle classes) from the Swiss Federal Road Office FEDRO.

2 Material and method

A complete overview of the monitoring system installed in this construction is presented by Bonifacio et al. [3] at this conference and the measurement procedures explained elaborately.

For reasons of clarity, a representative selection of sensors was made from the large number of measuring probes mentioned above, with the main emphasis on «wood moisture», «climate» and «traffic». This was done in order to obtain an initial basis for investigating any correlations between these three parameters. In the course of the project, the remaining data will also be used to check and confirm these correlations.

Figure 1 shows an overview of the locations where temperature and humidity sensors are located on the inside of the wildlife crossing. A detail of the sensor positioning is shown in Figure 2.

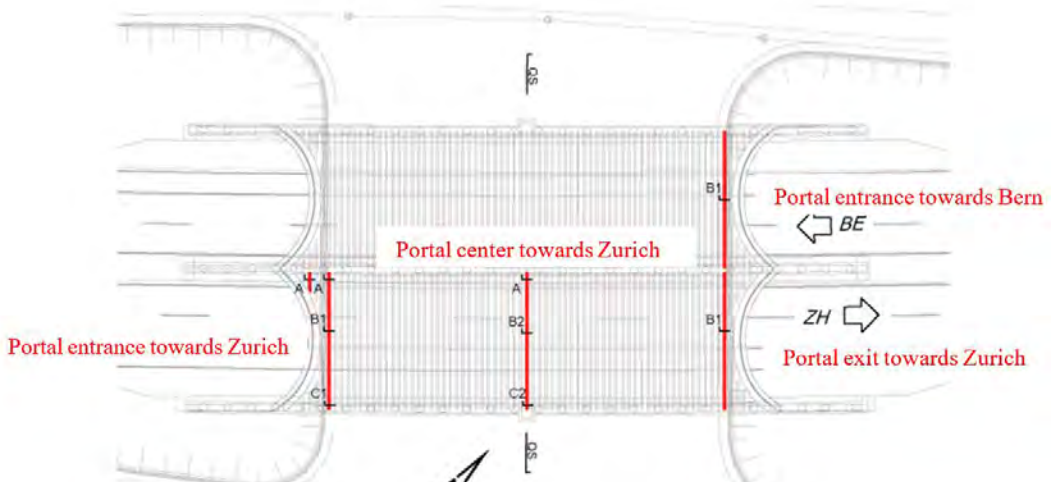


Figure 1. Drawing representing the top view of the timber wild-life bridge and the positions of the installed sensors

[1] Karim Ghazi Wakili, Senior Scientist, Institute for Timber Construction, Structures and Architecture, Bern University of Applied Sciences, Switzerland, karim.ghaziwakili@bfh.ch



Figure 2. Detail showing the position of the moisture sensors in the wooden elements (glue laminated timber).

3 Results

3.1 Temperature and moisture in the wooden elements

Figure 3 shows the measured surface values for the moisture content on the wooden elements [3] parallel to the lanes and covering the curved glue laminate timber elements (HF, red, blue, and yellow lines) in mass percent on the left y-axis. The amount of rain in mm/h (green line) is also shown on this axis. The right y-axis shows a dual value of 0 or 1 meaning no rain and rain. The time on the x-axis stretches over the period between October 9th, 2020, and July 7th, 2021. The dotted pink line corresponds to a preliminary hygrothermal simulation of the moisture content. This will be discussed in a future investigation comparing measured and simulated values.

The moisture contents fluctuate mainly between 10 and 15 mass percent of moisture which is not critical, and their mean value shows an increase from the starting point until March 2021 and decreases slightly afterwards. This is most probably the initial condition of a quasi-steady-state behaviour. There seems no immediate correspondence with the Amount of rainfall. This is not unusual as the moisture movement by diffusion is a slow transient process. No moisture accumulations have been detected for this period.

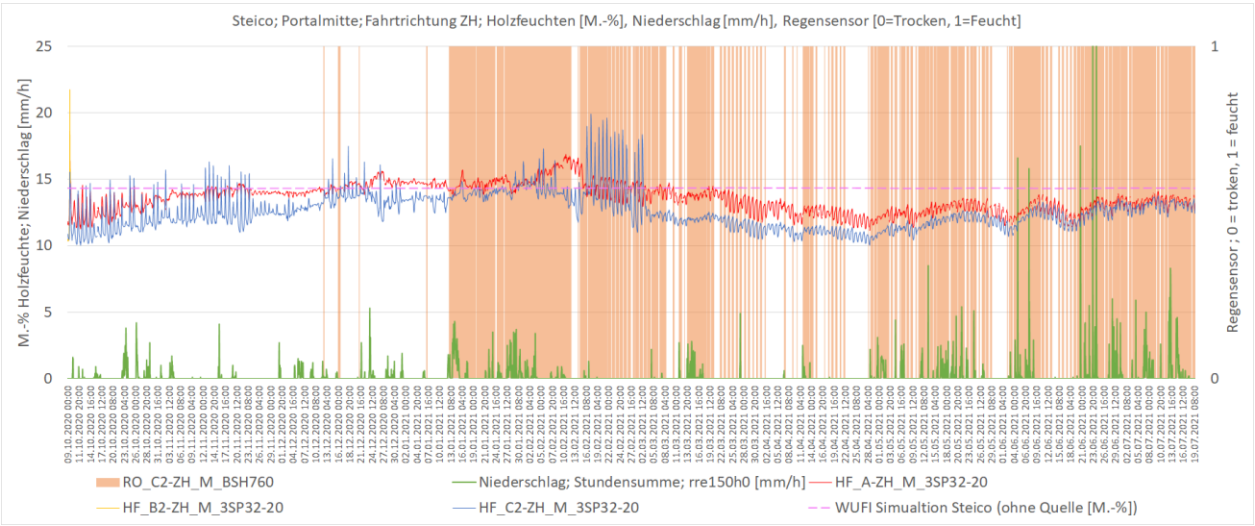


Figure 3. Measured moisture content in wooden elements at the center on the Zurich Lane, amount of rain and rain sensor (right y-axis).



An example of the spot moisture measurements [3] in two different depths in a curved laminated timber element is shown in Figure 4 together with the amount of rain (green line). The lines in yellow and blue (both 40 mm depth) show slightly higher variations in the measured period (the same as in Figure 3) compared to the grey line corresponding to a depth of 100 mm. The moisture contents are sub-critical and do not show an immediate correlation with the amount of rain as well.

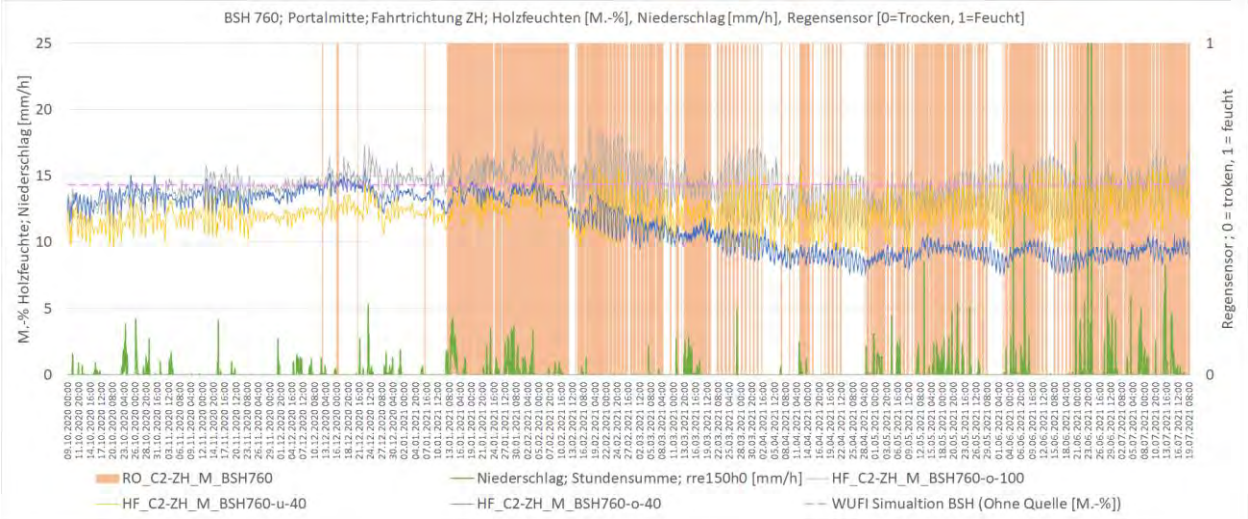


Figure 4. Measured wood moisture in two depths of 40 and 100 mm in a glue laminated timber element at the point C2 portal centre on the Zurich Lane, the measured precipitation, and the rain sensor (right y-axis).

3.2 Relative humidity of the air

The next two figures (Figs. 5 and 6) compare the measured air temperature and humidity (both yellow lines) in the space beneath the wild-life bridge (four measuring points) and the values obtained from the nearby meteorological station. During the colder season (Nov. 2020 to Feb. 2021), a slightly cooler temperature and correspondingly higher relative humidity is measured at some points in the space beneath the wildlife bridge. The use of these different climate data in a hygrothermal simulation will provide information about the effect of these differences on the wood moisture content (measured and simulated).

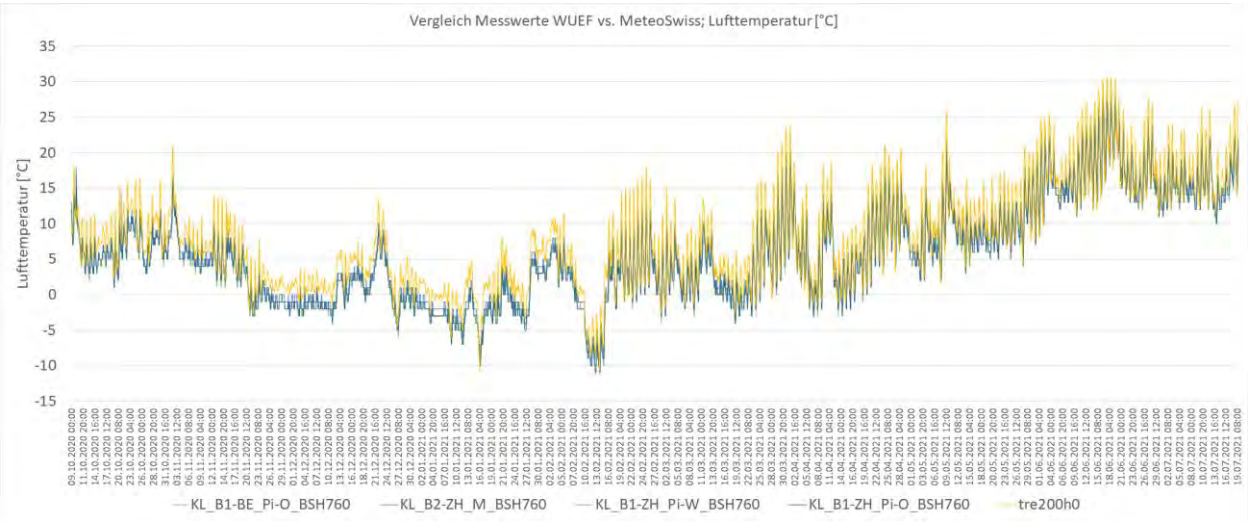


Figure 5. Measured air temperature in the space beneath the wildlife bridge and the nearby Meteo-Schweiz weather station (2m above ground).

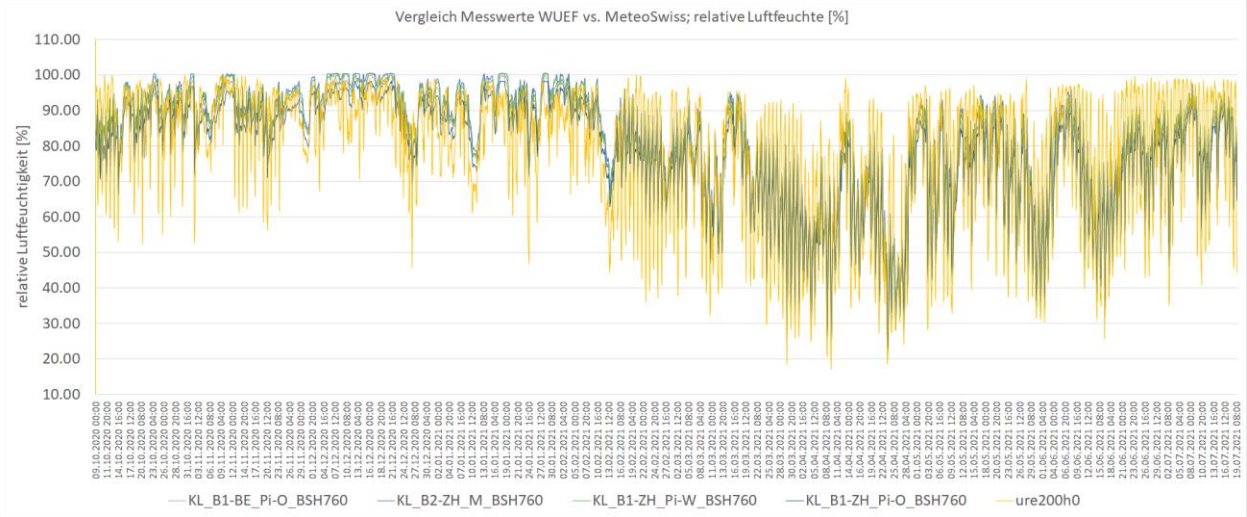


Figure 6. Measured air humidity (rel.) in the space beneath the wildlife bridge and the nearby Meteo-Schweiz weather station (2m above ground).

The relative humidity in the space beneath the wildlife bridge shows much smaller diurnal fluctuations which can be expected as the Meteo-Data are measured in an open field in contrast to the relatively closed space beneath the wildlife bridge. This explanation holds also for the lower temperature during the summer period (Apr. to Jul. 2021) The whole time period on the x-axis the same as in the previous figures.

3.3 Traffic data

According to the FEDRO guideline for traffic counters, the data for all vehicle classes was available individually. From these, however, the LW-like vehicles (types 1, 8, 9 and 10 see Table 1) were combined and summarized for the direction of travel in Figure 7. The reason is that these vehicles, due to their size, can spray the rainwater much more and much higher water, enable the formation of haze and can thus influence the moisture content in the wooden structure.

For the sake of clarity, the sum over a whole year of the counted vehicles (Figure 7) is divided into 6 periods of 4 hours each. This means that the first part in Figure 5 (top left) shows the total for the first 4 hours of the day (0, 1, 2 and 3) and the subsequent parts each show the total for the 2nd, 3rd, 4th, 5th and last 4 hours of the day correspondingly.

Table 1: Vehicle types according to 'Swiss 10' of FEDRO

Type	Vehicle
1	Bus
8	Truck
9	Truck with Trailer
10	Articulated Lorry

As mentioned above the diffusion of water is a slow process and a quasi-steady state would only be reached after 1-2 years depending on the climatic boundary conditions. An evaluation of moisture content in the wooden elements needs monitoring data for a corresponding period. This will also serve for robust hygro-thermal simulations to enable an extrapolation to longer time periods including and forecasting the impact of climate change.

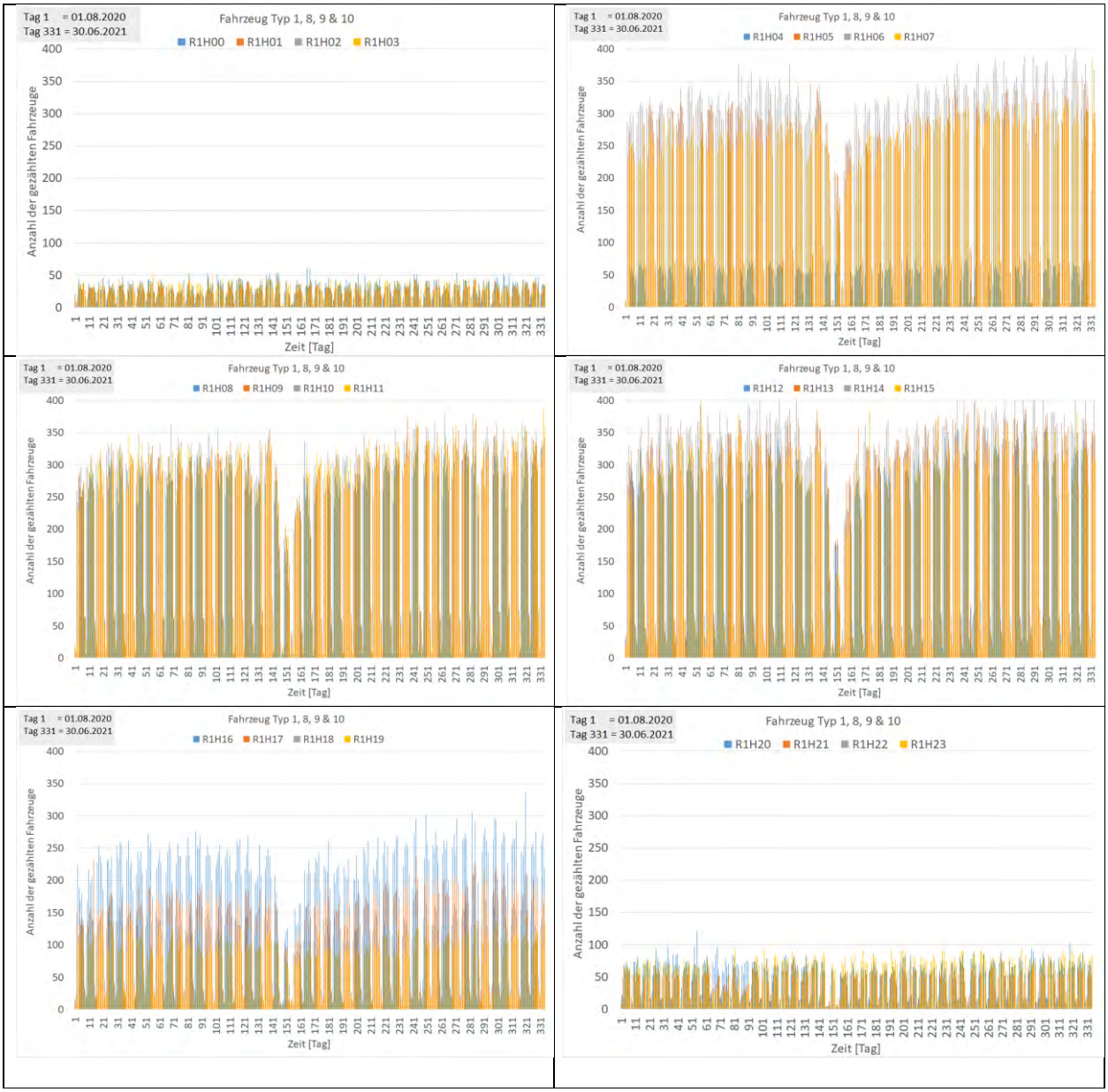


Figure 7. Number of counted large vehicles (types 1, 8, 9 and 10) in the direction of Zurich (R1) from July 2020 to June 2021. For the sake of clarity, summarized in 6 parts of 4 hours each.

4 Acknowledgement

The project has been financed by the grant “2020.08 Klimabedingungen bei Wildtier-überführungen in Holzbauweise” by the Swiss Federal Office for the Environment FOEN, Wald- und Holzforschungsförderung Schweiz (WHFF-CH). The support of the project partners “Timbatec”, “Häring AG/Roth Burgdorf”, “terra vermessungen “ and Lignum Switzerland is greatly appreciated.

5 References

[1] Bauer M. (2016) Erfahrungsbericht über die Grünbrücke bei Luckenwalde. In: 4. Internationale Holzbrückentage IHB 2016 , 8-9 June 2016, MPA Stuttgart. https://www.forum-holzbau.com/pdf/14_HBS_2016_Bauer.pdf

[2] Timbatec (2020) First Swiss wildlife bridge made of wood https://www.timbatec.com/en/aktuelles/meldungen/8087175055-Rynetel.php

[3] Bonifacio S., Schiere M., Mueller A. (2022) Climate and moisture monitoring system in the timber wildlife crossing ‘Rynetel’, ICBT 2021 PLUS, 9-12 May 2022, Biel, Switzerland.

Conference Proceedings 4th ICTB (2022)
https://doi.org/10.24451/w9sn-2964

ICTB 2021 PLUS
4th International Conference on Timber Bridges
Biel/Bienne, Switzerland, 9 -12 May 2022



Structural yield of a pedestrian bridge made of CLT-concrete, connected by screws and by notches

Gonzalo Moltini[1], Gonzalo Cabrera[2], Vanesa Baño[3]

Abstract

The structural design of a simply supported pedestrian bridge made of Cross-Laminated-Timber-Concrete-Composites (CLTCC) was studied for two different connections between CLT and concrete: i) 45º crossed-pairs of screws of 9 mm of diameter; and ii) longitudinal notches in the CLT (40 mm depth and 100 mm width). The composites were manufactured from CLT of Radiata pine from Spain, visually graded as C24, and concrete H25/B/25/I. Experimental push-out tests were made on 30 specimens of CLT-concrete according to EN 26891, 15 for each type of connection, to obtain the maximum load and the force-displacement curve, which were used to estimate the shear strength (f_v) and the slip modulus (K_{ser}) of the connection. In both cases, shear strength and slip modulus, the notched connections (1) resulted in higher values than those of the screws connections. The values of shear strength were 11.6 kN (CoV=36%) and 29.8 kN (CoV=34%) for the screws and notched connections, respectively. The values of slip modulus were 20,3 kN/mm (CoV=18%) and 68.4 kN/mm (CoV=21%) for screws and notches, respectively. Experimental screws connection showed a value of slip modulus higher than that obtained from the theoretical equation given by the Eurocode-5 (K_{ser} = 13.5 kN/mm). The experimental values were used to estimate the stress, strength and stiffness of the CLT-concrete slabs used as pedestrian bridges and residential buildings for both connection solutions. The notched connections showed a better performance than screwed connections in the bridge structural design, with a span over thickness ratio 4-5% higher for the same number of CLT layers.

1 Introduction

In the last decades, timber construction is experiencing a global worth, due in part to the need of reducing carbon emissions in a political model of transition into bioeconomy [1]. The growing use of cross laminated timber (CLT) in construction has been reported by several authors [2][3][4][5], mainly used as slabs and walls in buildings. The need to obtain a better structural behaviour, mainly associated to serviceability, of CLT panels used as floors in buildings on one hand, and the need to improve the sustainability criteria in the current concrete building sector on the other hand, had led to an increase in the use of CLT-concrete composites (CLTCC) in construction.

The first patent for Timber-Concrete-Composites (TCC) can be found in 1922; however, during the XX century reinforced concrete and steel structures were dominant in construction. TCCs have experienced a great growth in the last 20 years [6], initially focused on rehabilitation of buildings, in a system where timber beams (solid timber or glued laminated timber beams) are connected to a compression layer of concrete.

Nowadays, the current version of the Eurocode 5, EN 1995-1-1 [7], does not include the regulations for the design of CLT panels or TCC, which will be included in the new version [8], currently in discussion in the WG1 and WG2 of CEN/TC 250/SC 5; however, it does not include the case of CLT and Concrete Composites (CLTCC). Several authors have reported results of studies of TCC combining concrete slabs with timber beams [9] [10], but finding examples for CLTCC is not as common [11].

This work proposes to study the influence of two different connection types (notched and screwed connections) in the design of a pedestrian bridge designed as a CLT-concrete composite slab, from the experimental values of the slip modulus and the shear strength of the CLT-concrete connections.

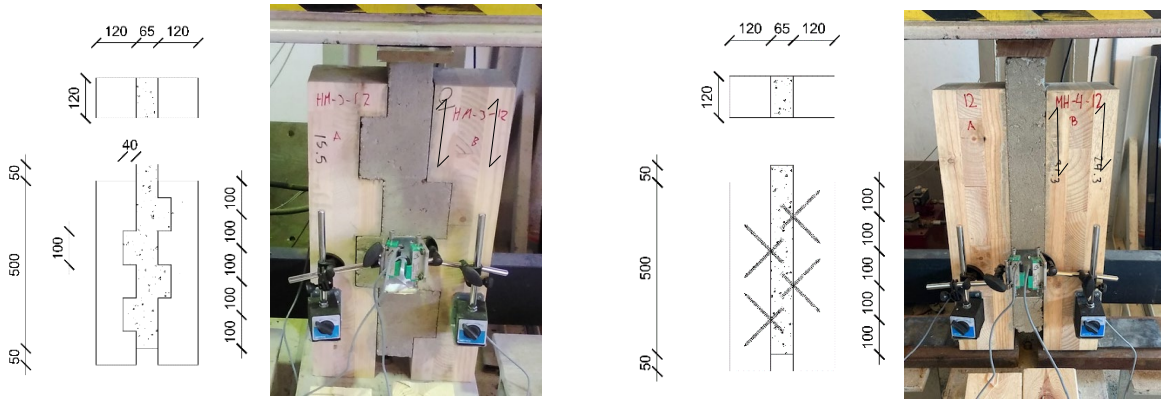
[1] PhD student, Civil Eng, Cesefor. Mail gonzalo.moltini@cesefor.com
[2] MEng. student, Civil Eng, Cesefor. Mail gonzalo.cabrera@cesefor.com
[3] Dr. Forest Eng., Head of the timber structures research group, Cesefor, Spain, vanesa.bano@cesefor.com



2 Material and method

2.1 CLT-Concrete Composite types

Thirty specimens of CLT-Concrete composites of Radiata pine (*Pinus radiata* D. Don) were manufactured in the facilities of the Cesefor Foundation (Spain), using timber of strength class C24 for the longitudinal layers and C16 for the transversal layers, and mass concrete H25/B/25/I. Two configurations for the connection between CLT and concrete were considered, a) notched and b) screwed (Fig. 1), fifteen from type a) and fifteen from type b). The notched connection had a depth of 40 mm (equal to the thickness of the first lamella), and the thickness of the specimens was 120 mm, the separation between notches was 200 mm. No fastener was used, assuming that the results provide conservative properties. For the screwed connection, crossed pairs at 45º timber-concrete screws CTC9160 from Rothoblaas were used, separated 200 mm along the longitudinal direction.

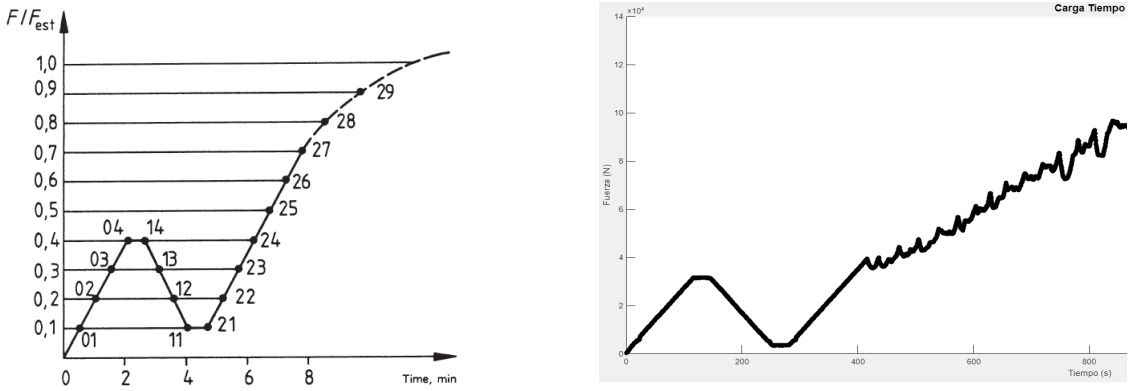


a) Notched connection b) Screwed connection

Figure 1: Experimental shear test specimens

2.2 Experimental testing

Fifteen double shear tests were carried out according to UNE EN 26891:1991 [12] for each connection type. The load was applied as shown in Fig. 2. The mean value of the relative displacement between CLT and Concrete measured with 4 extensometers located by pairs in both front and back faces as shown in Fig. 1 was used to calculate individual values of slip modulus (K_{ser}) in the initial elastic period (Between points 01 and 04 of Fig 2.a). Average value of K_{ser} was calculated.



a) Loading procedure according to EN 26891 b) Experimental loading procedure

Figure 2: Loading procedure

It was considered that each connection takes up a fourth part of the load applied. Individual strength values (F_i) were calculated according to Eq. 1 and the characteristic values were derived according to EN 14358:2016 [13] assuming a log-normal distribution of strength values.

$$F_i = \frac{F_{max}}{4} \qquad \text{Eq. 1}$$



2.3 Structural design methodology for a pedestrian bridge

2.3.1 Geometry

A simply supported 2 m wide CLTCC pedestrian bridge with both connection types over a span l was designed (Fig 3.). The total height of CLT is nh_l, being n the number of layers and h_l the CLT layer thickness (40 mm). Each layer was placed orthogonally to the next, being the upper and lower layers disposed in the longitudinal direction. The separation of the connectors was considered constant (200 mm) and the depth was considered equal to the layer thickness, in order to maintain the same conditions of the experimental shear tests. The thickness of the concrete compression layer (h_c) was defined with the aim that the neutral axis of the total CLTCC section is in the interface of the first and second layer of the CLT panel.

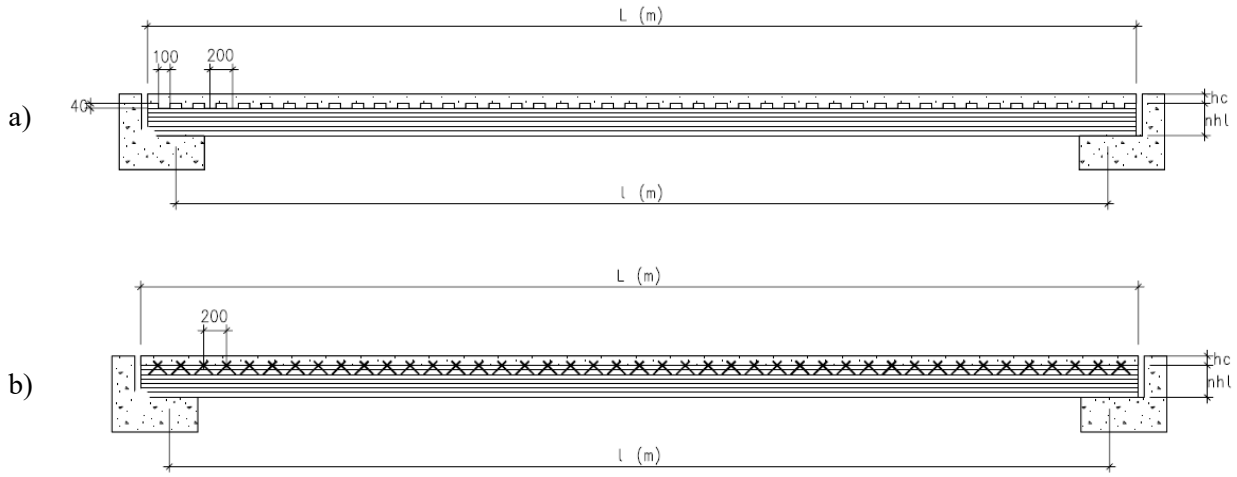


Figure 3: Pedestrian bridge geometry: a) notched connections and b) screwed connections

2.3.2 Design hypothesis

The timber physical and mechanical properties of strength classes C24 and C16 were taken from EN 338:2016 [14] and the rolling shear properties from the pro:Holz Cross-Laminated Timber Structural Design Manual [15]. Mechanical properties of concrete were calculated as given by EN 1992:2004(16) for concrete of $f_{ck} = 25\ N/mm^2$.

The basis for the structural design was taken from Eurocode 0 (17) for ultimate limit state (ULS) and deformation in serviceability limit state (SLS), considering a uniform imposed load of 5 kN/m^2 taken from Eurocode 1 [18]. The vibration serviceability limit state was not considered. The stiffness of the composite section was calculated using the Gamma method defined in the Annex B of Eurocode 5 for both ULS and SLS. Apart from these, several hypotheses were made:

i) Transverse layer contribution was neglected in the stiffness.
ii) Shear deformation was considered for the transverse layers of CLT and not in the longitudinal layers.
iii) Values of slip modulus were obtained from the experimental campaign. Since the tests were made in specimens of 120 mm wide, the results were multiplied by 8.33 to obtain the K_{ser} applied to an unitarian bridge width (1 m)($K_{ser,bridge} = K_{ser,exp}1000/120$)
iv) For notched connection the slip modulus in ULS was considered equal to that of SLS, $K_{ser,ULS} = K_{ser,SLS}$
v) For screwed connection the slip modulus in ULS was considered as two thirds of that of SLS $K_{ser,ULS} = 2/3\ K_{ser,SLS}$
vi) Concrete creep deformation was not considered in the calculation.
vii) Service class 2 was considered.
viii) Imposed loads were considered as short term.
ix) For the design of the CLTCC, the most restrictive value of rolling shear of the CLT panel was taken into account to calculate the stiffness (upper layer of CLT)



x) Hardening in the concrete is not considered

To calculate the effective stiffness (EI_{ef}) of the composite section, the Gamma method was used. A slip between 1) CLT and concrete; and 2) the longitudinal layers of the CLT (result of the rolling shear deformation of the transverse layer) were considered. The slip modulus between longitudinal layers of CLT was calculated using Eq. 2.

$$K_{ser,CLT} = \frac{G_{R,mean}B}{h_l} \quad \text{Eq. 2}$$

Being $G_{R,mean}$ the rolling shear modulus, B the width of the panel and h_l the layer's thickness.

$$EI_{ef} = E_c I_c + \gamma_c E_c A_c a_c^2 + \sum_{i=1}^{N} (E_i I_i + \gamma_i E_i A_i a_i^2) \quad \text{Eq. 3}$$

$$\gamma_C = \left(1 + \frac{\pi^2 E_c A_c s}{K_{ser} l^2}\right)^{-1} \quad \text{Eq. 4}$$

$$\gamma_i = \left(1 + \frac{\pi^2 E_i A_i}{K_{ser,CLT} l^2}\right)^{-1} \quad \text{Eq. 5}$$

where, E_C is the elastic modulus of concrete, A_c is the area of the cross section of concrete, s is the separation between connections, K_{ser} is the slip modulus of the connection (in either SLS or ULS), l is the span, I_C the individual moment of inertia of concrete, a_c the distance between the barycentre of the whole CLTCC section and the barycentre of the concrete layer section, N is the amount of longitudinal layers of CLT, E_i is the elastic modulus of the longitudinal layers, I_i is the individual moment of inertia of each layer, A_i is the area of the cross section of each CLT layer, a_i is the distance between the barycentre of the whole CLTCC section and the barycentre of the CLT longitudinal layer section.

2.3.3 Limit States

Two ultimate limit states were considered 1) $1.35PL$ 2) $1.35PL + 1.5IL$, being PL the permanent loads and IL the imposed loads. The following verifications were made: shear in the connection ($\max(V_{con}/F_{V,d}) \leq 1$); rolling shear in the CLT transverse layer ($\max(f_{v,rs}/f_{v,rs,d}) \leq 1$); Concrete compression ($\max(f_c/f_{c,d})$); and CLT tension in the bottom layer ($\max(f_m/f_{m,d}) \leq 1$). Given the geometry of the section, the compression in the CLT top layer always verified with the values of compression parallel to grain.

Two different load states were considered for the instantaneous and creep effect of the permanent and imposed loads. The creep effects for the imposed loads were null. Three verifications were made: integrity of the constructive elements (Eq. 6), user comfort (Eq. 7) and construction appearance (Eq. 8).

$$(\delta_{i,IL} + \delta_{d,PL}) / \frac{l}{400} \leq 1 \quad \text{Eq. 6}$$

$$(\delta_{i,IL}) / \frac{l}{350} \leq 1 \quad \text{Eq. 7}$$

$$(\delta_{i,IL} + \delta_{i,PL} + \delta_{d,PL}) / \frac{l}{300} \leq 1 \quad \text{Eq. 8}$$

Where, $\delta_{i,IL}$ is the instantaneous effect of the imposed loads, $\delta_{i,PL}$ is the instantaneous effect of the permanent load, $\delta_{d,PL}$ is the creep effect of the permanent load (considering $K_{def} = 1$) and l is the span.



3 Results

3.1 Experimental results of the connections

Experimental results of the shear strength ($F_{V,k}$) and the slip modulus ($K_{ser,i}$) of the CLT-concrete connections, described in point 2.1 and 2.2, are presented in Table 1. The eccentricity produced by the asymmetry in the connections of the test specimens was neglected, assuming that the results should be on the safety side for the structural design.

Table 1: Experimental results

Property	Notched connections	Screwed connections
$F_{V,mean}\ (kN)$	29.8	11.6
$CoV\ (\%)$	34	36
$F_{V,k}\ (kN)$	9.3	4.9
$K_{ser,i}\ (kN/mm)$	68.4	20.3
$CoV\ (\%)$	21	18

It was observed that the notched connections showed higher values of strength (90% higher) and slip modulus (237% higher) than the screwed connections. Given that the draft for the new Eurocode 5 (8) provides an equation to estimate the slip modulus of a concrete to timber connection, experimental result for screwed connections was compared with the theoretical value (Eq. 9). The experimental slip modulus was 50% higher than that proposed by the design code.

$$K_{ser,E5} = \frac{2\rho_m^{1.5} d}{23} = 13.5 \frac{kN}{mm} \qquad \text{Eq. 9}$$

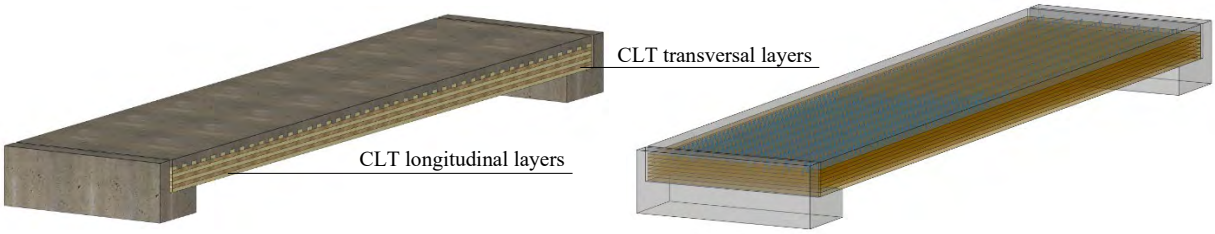
3.2 Design results

3.2.1 Geometry

The simply supported pedestrian bridge with both connection types was designed for different CLTCC thickness (Fig. 4). The geometry of the CLTCC depending on the number of layers of the CLT panels is shown in Table 2, where increasing the number of CLT layers implies an increase in the concrete layer thickness. The lightest colour of the CLT in Fig. 4a indicates the longitudinal layers and the darkness colour the transversal layers. The screwed bridge of the Fig. 4b is made with transparent materials with the aim to see the location of the screws and the disposition of the layers is equal to that in Fig. 4a.

Table 2: Cross-section geometry of the bridge

	CLT layers		
	5	7	9
Thickness CLT (mm)	200	280	360
Thickness concrete, h_c (mm)	46	81	116
Thickness CLTCC (mm)	246	361	476



a) Notched connection b) Screwed connection

Figure 4: CLTCC pedestrian bridge: a) notched connections and b) screwed connections



3.2.2 Structural design

The structural design of the CLTCC bridge was studied varying the span in steps of 100 mm for 5-, 7- and 9- layers of CLT and for the two connection types, to obtain the maximum span complying with the requirements described in point 2.3.3. The verifications are shown in Table 3.

Table 3: Structural verifications for the CLTCC bridge

	Notched connections			Screwed connections		
CLT layers	5	7	9	5	7	9
$EI_{ef,SLS}$ (kNm^2)	9593	25880	53768	8100	21669	45121
$EI_{ef,ULS}$ (kNm^2)	9593	25880	53768	7599	20248	42098
max $(V_{con}/F_{V,d})$	0.81	0.99	0.99	0.78	0.96	0.99
max $(f_{v,rs}/f_{v,rs,d})$	0.03	0.03	0.03	0.03	0.04	0.04
max $(f_c/f_{c,d})$	0.75	0.77	0.68	0.86	0.88	0.80
max $(f_m/f_{m,d})$	0.61	0.67	0.61	0.70	0.77	0.72
Eq. 6	0.97	0.98	0.78	1.00	0.98	0.83
Eq. 7	0.62	0.58	0.45	0.64	0.58	0.48
Eq. 8	0.92	0.97	0.79	0.95	0.97	0.83
Maximum span (m)	6.4	8.7	10.2	6.1	8.2	9.8
Span/thickness (STR)	26.0	24.1	21.4	24.8	22.7	20.6

As expected, notched connections showed a better structural yield than screwed connections. The span over thickness ratio (STR) was defined to compare the obtained results. For the same number of CLT layers, the STR of notched connections showed values between 4-5% better than those of screwed connections.

In both type of connections, the limits are imposed by the SLS for 5 layers CLT, shifting to ULS for 9 layers CLT, showing an equilibrium in the limits for 7 layers CLT. The increase from 5- to 9- layers produced a similar span increase in both cases (3.8 m and 3.7 m respectively). However, the 5 layers CLT showed the better structural yield measured as STR. The STR values are 21.5% and 20.4% higher for 5 layers CLT than that of 9 layers CLT for notched and screwed connections, respectively.

The structural yield of these CLTCC used as slabs in residential buildings (imposed load 2 kN/m^2) increased between 14% and 21% with respect to the use in pedestrian bridges (Table 4). It should be noticed that the use of CLTCC slabs for residential buildings is always limited by SLS.

Table 4: Structural verifications for the CLTCC bridge

	Notched connections			Screwed connections		
CLT layers	5	7	9	5	7	9
Maximum residential slab span (m)	7.4	9.7	12.3	7.0	9.3	11.7
$STR_{residential}$	30.1	26.9	25.8	28.5	25.8	24.6
$STR_{residential}/STR$	1.16	1.12	1.21	1.15	1.14	1.19

4 Conclusions

- Experimental results for shear strength and slip modulus were obtained for notched and screwed connections between CLT and concrete. The notched connection with a depth equal to the layer thickness, resulted in a 90% higher shear strength and 237% higher slip modulus than screwed connections.
- The experimental value of slip modulus for screwed connections was 50% higher than that proposed by the draft of the new Eurocode 5 for timber-concrete-composites.
- A simply supported CLT-concrete-composite pedestrian bridge was designed considering two different connection types experimentally studied.



- The notched connections showed a better performance than screwed connections in the bridge structural design, with a span over thickness ratio 4-5% higher for the same number of CLT layers.
- The structural design was limited by the serviceability limit state for 5 layers CLT, and by ultimate limit state for 9 layers CLT.
- This slab bridge typology made from CLT-concrete-composite shows a better structural yield for lower thicknesses. When increasing the bridge span, the material volume decreases its efficiency, thus, it is advisable to change the bridge typology, such as beams and concrete slab.
- Future works will include different notches depth and vibration studies in the CLT-concrete-composite, as well as different bridge typology performances.

Acknowledgments

This research project has been sponsored by the Projects: i) SOE4/P1/E1115 «Eguralt: Application and dissemination of innovative solutions for the promotion of mid-rise timber construction in the SUDOE area», co-financed by FEDER funds within the framework of the Interreg SUDOE program; and ii) 04/18/PA/0010 MEDGON: Design and development of a mixed wood-concrete industrialized construction system for high-rise buildings, funded by *Instituto para la Competitividad Empresarial de Castilla y León* in the call 2018 *PROYECTOS DE I+D.*

References

[1] Bouhala L, Fiorelli D, Makradi A, Belouettar S, Sotayo A, Bradley DF, et al. (2020) Advanced numerical investigation on adhesive free timber structures. Composite Structures [Internet]; 246:112389. Available from: https://doi.org/10.1016/j.compstruct.2020.112389

[2] Dangel U. (2016) Turning point in timber construction. Basel: Birkhäuser; 192 p.

[3] Gagnon S. (2012) CLT In Construction. Wood Design Focus; 22 (2):31–8.

[4] Pei S, Rammer D, Popovski M, Williamson T, Line P, Lindt JW van de Kuilen. (2016) An Overview of CLT Research and Implementation in North America. In: WCTE 2016 - World Conference on Timber Engineering

[5] Basterra A, López G, Vallelado P, García I, Baño V, Moltini G, Cabrera G. (2022) Aplicación y difusión de la innovación para la promoción de la construcción en altura con madera en el espacio Sudoe: identificación y análisis (Application and dissemination of innovative solutions for the promotion of mid-rise timber construction in the SUDOE area: Identification and analysis). ISBN:9788412487282. 2022. 518 pp.

[6] Yeoh D, Fragiacomo M, de Franceschi M, Heng Boon K. (2011) State of the Art on Timber-Concrete Composite Structures: Literature Review. Journal of Structural Engineering; 137(10):1085–95.

[7] CEN. EN 1995-1-1. (2006) Eurocode 5: Design of timber structures. Part 1-1: General. Common rules and rules for buildings

[8] CEN. prEN 1995-1-1 (2021). Consolidate draft of Eurocode 5. Design of timber structures.

[9] Dias AMPG, Jorge LFC. (2011) The effect of ductile connectors on the behaviour of timber-concrete composite beams. Engineering Structures; 33(11):3033–42.

[10] Fragiacomo M, Amadio C, MacOrini L. (2007) Short- and long-term performance of the "tecnaria" stud connector for timber-concrete composite beams. Materials and Structures/Materiaux et Constructions; 40(10):1013–26.

[11] Thilén J. (2017) Testing of CLT-Concrete Composite decks. Report TVBK – 5259. ISSN 0349-4969. ISRN: LUTVDG/TVBK-17/5259 (62)

[12] CEN. EN 26891. (1992) Timber structures. Joints made with mechanical fasteners. General principles for the determination of strength and deformation characteristics.

[13] CEN. EN 14358. (2016) Timber structures. Calculation and verification of characteristic values.

[14] CEN. EN 338. (2016) Structural timber. Strength classes.



[15] Wallner-Novak M, Koppelhuber J, Pock K. (2014) Cross-Laminated Timber Structural Design-Basic design and engineering principles according to Eurocode.

[16] CEN. EN 1992-1-1 (2004) Eurocode 2. Design of concrete structures - Part 1-1: General rules and rules for buildings

[17] CEN. EN 1990. Eurocode 0. (2002) Basis of structural design.

[18] CEN. EN 1991-1-1. (2002) Eurocode 1: Actions on structures. Part 1-1: General actions-Densities, self-weight, imposed loads for buildings.

Conference Proceedings 4th ICTB (2022)
https://doi.org/10.24451/w5qb-fy46

ICTB 2021 PLUS
4th International Conference on Timber Bridges
Biel/Bienne, Switzerland, 9 -12 May 2022



Notched Connections for Timber-Concrete Composite Bridges – Investigations on the Fatigue Behaviour

Simon Mönch[1], Ulrike Kuhlmann[2]

1 Introduction

Based on the combination of timber and concrete, timber-concrete composite bridges (TCC bridges) enable economical bridge constructions. Both materials are used according to their advantageous properties. In the case of typical single-span TCC bridges subjected to bending, the timber cross-section is placed in the tension area and the concrete cross-section in the compression area. In order to allow for high single and distributed loads, connectors between timber and concrete with high strength and stiffness are required.

A notched connection is characterized by very high strength and stiffness as well as an easy manufacturing and therefore is optimal suitable as connection between timber and concrete for TCC road bridges with heavy loads. Thus, notches as TCC shear connectors enable the construction of efficient TCC bridges with large spans. For road bridges, however, the verification of sufficient fatigue strength under frequently recurring traffic loads is required.

In the case of covered wooden bridges, which were built more and more often in Europe from the 13th century and onwards, a roof served as protection against the weather. Figure 1 (left) shows an example of a covered pedestrian bridge over the river Saane near Gümmenen (CH) [1]. Even today there are still many very well preserved covered wooden bridges. For innovative TCC bridges, the concrete deck, which extends sideways over the timber cross-section, acts as structural timber protection (see Figure 1 (right)). Kerbs, roadway expansion joints and railings can be designed by using common constructional details for concrete bridges. The use of timber as a regenerative building material significantly reduces the total weight of the bridge compared to conventional concrete constructions. A high degree of prefabrication of the timber elements also allows for a significant reduction in construction time.



Figure 1: Timber bridge with roof near Gümmenen (CH), built in the 15th century [1] (left) and TCC bridge across the river Agger in Lohmar with 28 m midspan, built in 2014 [2] (right).

Due to their high values of strength and stiffness, notches form ideal connectors between timber and concrete for TCC bridges. Figure 2 shows a notched connection with the relevant geometrical parameters: h_n = notch depth, l_n = notch length, l_v = timber length in front of the notch, h_t = timber thickness, h_c = concrete thickness, α = notch inclination of the edge and screws for preventing uplift.

In this contribution, first an overview of the current state of research is given. Subsequently, experiments on the fatigue behaviour of notched connections on push-out tests are presented, which were conducted among others at the University of Stuttgart in recent years. In the next step, experiments on TCC beams as test specimens measuring 4 m in length are presented, which were performed in 2021. Finally, S-N-curves for the fatigue verification derived from the TCC push-out and beam tests are discussed.

[1] Simon Mönch, Scientific Researcher, University of Stuttgart, Institute of Structural Design, Germany, simon.moench@ke.uni-stuttgart.de
[2] Ulrike Kuhlmann, Head of Institute, University of Stuttgart, Institute of Structural Design, Germany, sekretariat@ke.uni-stuttgart.de

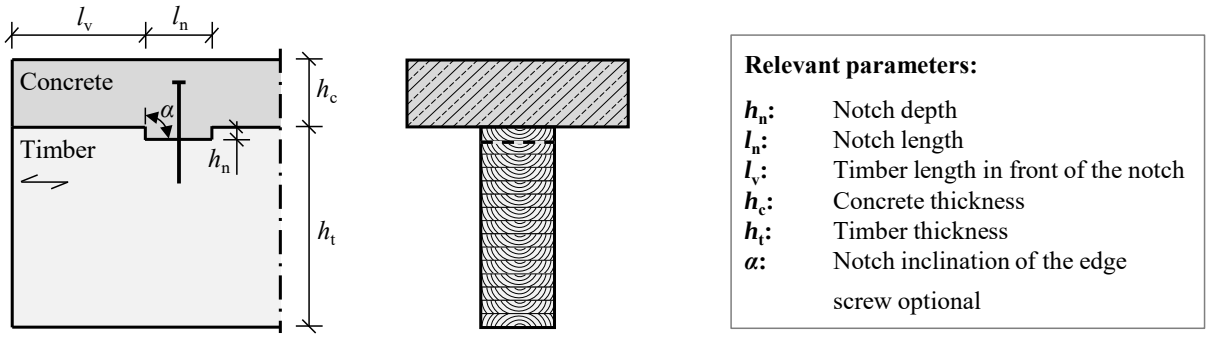


Figure 2: Drawing of a notched connection with geometrical parameters: side view (left) and cross section (right).

2 State of the art

CEN/TS 19103 [3], a European Technical Specification (TS) for the design of timber-concrete composite structures was published in November 2021. This Technical Specification was adopted by the European Committee for Standardization (CEN) in July 2021, and it will be applied as a future standard for provisional application. The aim is to subsequently transfer the CEN/TS into a part of Eurocode 5. Rules in the CEN/TS are partially based on results of extensive static TCC push-out and beam tests with notched connections, carried out by the Institute of Structural Design at the University of Stuttgart in recent years, (see [4] to [8]).

As a result, TCC elements can safely be designed as economical, wide-span slabs for multi-storey and industrial buildings and are already used more often. For TCC bridges (especially subjected to road traffic) this currently applies only to a limited extent. Therefore, a verification of sufficient fatigue strength under frequently recurring traffic loads is required. Currently, design rules for the fatigue verification of TCC bridges and of appropriate connectors are not given in the standard.

In the current version of EN 1995-2, Annex A [9], a fatigue verification for pure timber structures is given. The timber strength is reduced by the coefficient k_{fat} as a function of the number of load cycles. This coefficient also includes the stress ratio R, which is the ratio of the numerically smallest to the numerically largest design stress ($\sigma_{d,min}$ / $\sigma_{d,max}$) due to relevant fatigue loading. At present, it has only been partially investigated to what extent the k_{fat} verification also applies to TCC structures and, in particular, to notches as shear connectors.

Initial tests on notches under cyclic loading were conducted by Kuhlmann & Aldi (2010) [10]. Simon (2008) [11] also conducted a small cyclic test series. However, due to low maximum loads, some run-outs occurred (no failure appeared after more than 2 million load cycles) [11]. The tests were stopped and the results consequently could not be used to derive S-N-curves. However, they showed tendencies to high fatigue strength in the range of low maximum loads.

3 Static and cyclic TCC push-out tests with notched connections

In order to significantly increase the amount of cyclic TCC tests with notched connections and to investigate further parameters, a research project [8] funded by the German Research Foundation (DFG) was realised. Extensive static and cyclic tests with notched connections on 36 push-out test specimens were conducted in a total of 13 test series, over a period of three years (2019-2021) [4], [6]. Based on the push-out tests, 9 TCC beam tests were performed in a total of 3 test series in 2021, results are discussed in section 4.

All test specimens were made of glued-laminated timber out of spruce of quality GL 28h according to EN 14080 [12] and concrete of quality C 30/37 according to EN 1992-1-1 [13]. For all specimens, the notch depth h_n was chosen to 4 cm, which is a common dimension in bridge construction (cf. multi-storey buildings: usually h_n = 2.0 cm). The timber length in front of the loaded edge of the notch l_v was always 40 cm (corresponding to 10 · h_n).

The influence of the notch depth h_n in relation to the timber length in front of the loaded edge of the notch l_v on the failure mode (ductile timber compression failure or brittle timber shear failure in front of the notch, with subsequent cracks in the concrete) has already been investigated in former static test series (see [7]).

In principle, a ductile failure is preferable, because deformations are recognized before fracture. However, to derive S-N-curves from cyclic tests, a clear safe sided failure criterion is needed. In order to achieve a clear brittle timber shear failure, the timber length in front of the loaded edge of the notch was chosen to $10 \cdot h_n$ for all TCC test series within the DFG research project [8].

The results obtained from the static tests, which served as input values for the cyclic test series, focused on the evaluation of values for strength and stiffness of the notched connection (see [4], [6]). Based on this, the number of load cycles before failure (timber shear failure in front of the loaded edge of the notch, see Figure 3 (left and middle)), was determined by means of cyclic push-out tests with single amplitude load spectrum for varied maximum loads F_{max}. Subsequently, S-N-curves for a stress ratio of $R = 0.1$ were derived together with results from [10] (see Figure 3 (right)).

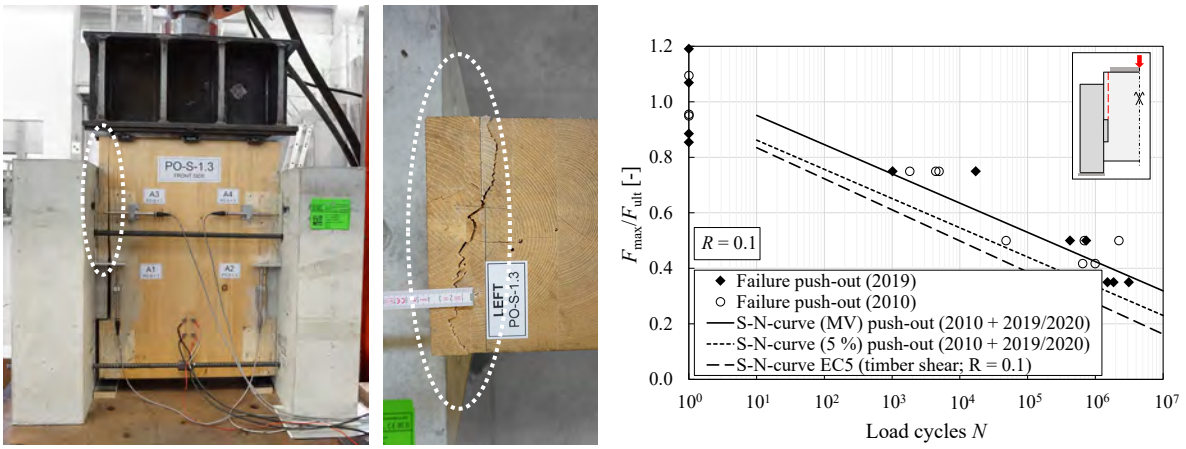


Figure 3: Push-out test specimen PO-S-1.3 after timber shear failure in front of the notch as front view (left), timber shear failure top view (middle) and S-N-curves for the stress ratio R = 0.1 derived from tests in 2019 and 2020 together with test results from Kuhlmann & Aldi (2010) [10] (right).

Figure 3 (right) shows the S-N-curve derived from the mean values (MV) of the tests for the relevant failure mode (timber shear failure) as well as the resulting statistically evaluated S-N-curve (5% fractile values). Both S-N-curves are located above the resulting S-N-curve for timber in shear according to EN 1995-2, A3 [9]. Therefore, the verification of the notches in shear according to the current rules seems to be on the safe side. Further information on the test evaluation and the statistical analysis can be found in [4], [6]. This confirms the already standardized fatigue verification given in [9] for timber in shear for a stress ratio of $R = 0.1$ also for the verification of the timber in front of the loaded edge of the notch in TCC systems.

Results obtained from cyclic push-out test series for a second stress ratio of $R = 0.4$, together with results obtained from TCC beam tests described in section 4, are shown as S-N-curves in Figure 8 (right). A stress ratio of $R = 0.4$ represents a typical stress ratio for TCC road bridges under traffic load in practice.

In addition, the verification that the fatigue rules are also applicable for real traffic by using the Palmgren-Miner Rule is still missing. Based on the cyclic test series with single amplitude load spectrum, mainly used to derive S-N-curves (series PO-C-2 and PO-C-5 in Figure 4 (right)), test series PO-C-6 was conducted with variable amplitude load spectrum (load protocol see Figure 4 (left)). A variable amplitude load protocol represents a more realistic scenario of recurring traffic loads on road bridges.

Figure 4 (right) shows that the linear interpolated mean value (corresponding to the linear damage accumulation hypothesis according to the Palmgren-Miner Rule [14]) is below the actual average of load cycles before failure in test series PO-C-6 and in this case on the safe side. However, this is only a single series of tests, which should not be considered as a complete validation of the Palmgren-Miner Rule for fatigue testing of timber, however, these test results give a positive indication. Further information on the evaluation of test series PO-C-6 can be found in [4], [6].

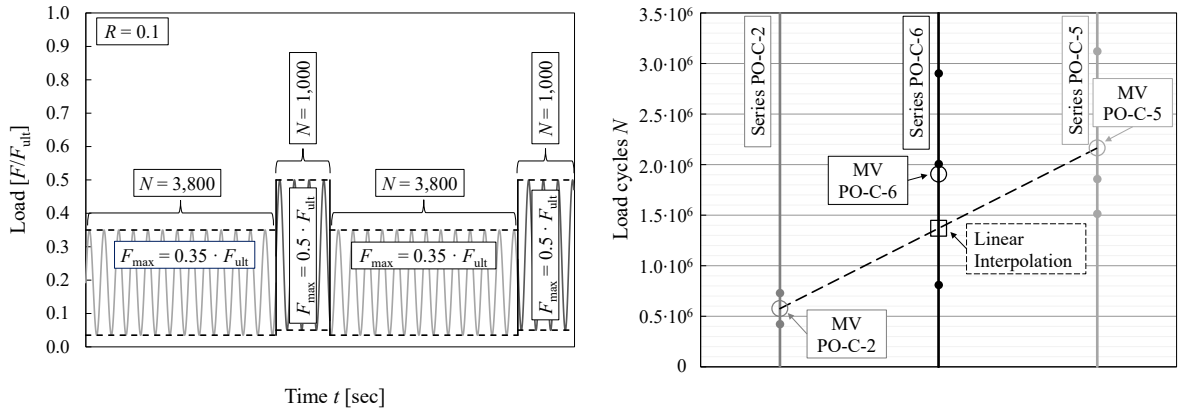


Figure 4: Load protocol of test series PO-C-6 with variable amplitude load spectrum (left) and comparison of the number of load cycles before failure of test series PO-C-6 with the results of test series PO-C-2 and PO-C-5 with comparable maximum load levels F_{max} conducted with single amplitude load spectrum (right).

4 TCC beam tests with stress ratio *R* = 0.4

4.1 Geometry, material and test programme

Based on the push-out test series, one static and two cyclic test series with a total of 9 tests on TCC beams (see Figure 5 and Figure 6) were conducted as 4 m long three-point bending tests at MPA, University of Stuttgart in 2021.

In comparison to push-out tests, the geometry of TCC beam test specimens is more similar to real TCC bridge constructions. Also, possible friction between timber and concrete can be simulated more realistically compared to push-out tests. As in practice, the timber elements in the area of the notches of both the push-out and the TCC beam test specimens were moisturized twice with water (30 min and 10 min before concreting the slab). However, there were no measurable differences in the influence of friction between the push-out and TCC beam tests. Initial adhesive friction break-off between timber and concrete was measurable, but similar for both test geometries and occurred at the beginning of the loading. Movable bearings were used for the TCC beam test setup to enable the TCC beam to move horizontally without restraint. As a single-span beam is purely governed by equilibrium, it can be assumed that the arrangement of only two notches (one on each side of the TCC beam) leads to evenly distributed forces to both notches. No strain gauges were used to measure the stress distribution on the beam, but for the range tested a linear elastic behaviour can be assumed.

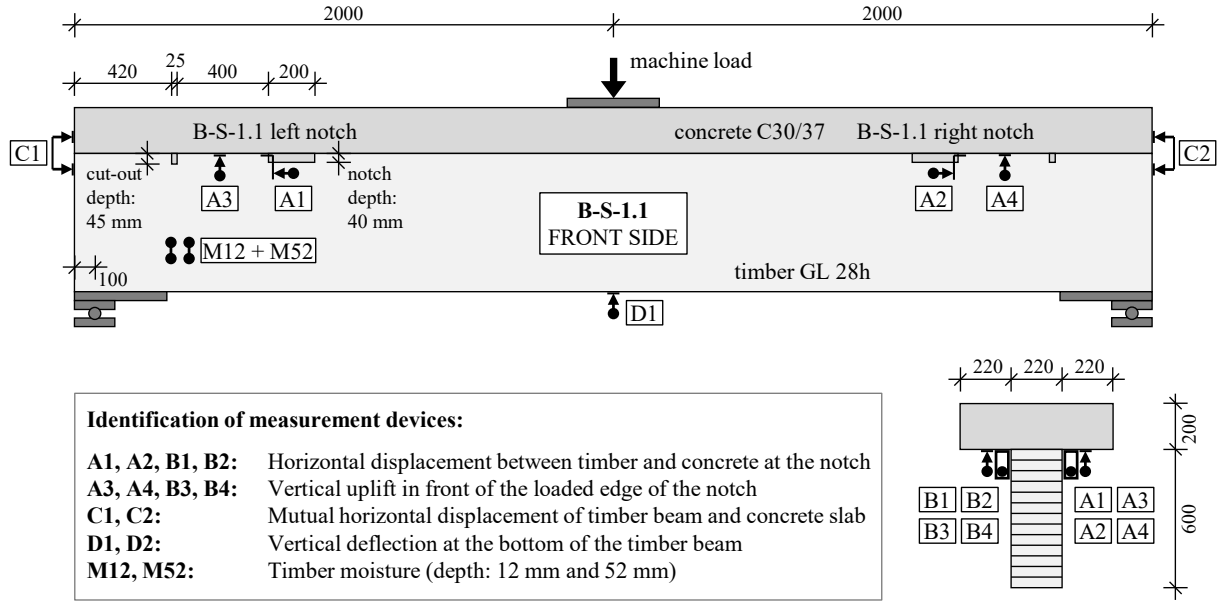


Figure 5: TCC beam test specimen with identification of measurement devices: front view (top) and cross section (bottom right), dimensions in mm [6].

The cyclic series were tested with a stress ratio of $R = 0.4$. These investigations aimed to confirm the results obtained from the push-out test series tested with the same stress ratio R and to derive even more accurate and meaningful S-N-curves based on the extended database.

The measurements of the notch, the timber length in front of the loaded edge of the notch and the material quality used are shown in Figure 5. They were similar to the push-out test specimens, already described in section 3. The TCC beams were manufactured in the same geometry as similar tests by Kuhlmann & Aldi (2010) [10], tested with a stress ratio of $R = 0.1$. The mean value of the carrying capacity F_{ult} determined from the static TCC beam tests of series B-S-1 was used as input value for determining the maximum loads F_{max} of the cyclic tests of series B-C-1 and B-C-2 (see Table 1).

Considering the maximum load F_{max} chosen in each case, the corresponding lower load F_{min} can be determined based on the stress ratio of $R = 0.4$. The resulting cyclic load protocol for the cyclic test series is shown in Figure 8 (left).

Table 1: Varied parameters of TCC beam test series conducted in 2021

Series No.	**Tests**	**Stress ratio** $\boldsymbol{R = \sigma_{min} / \sigma_{max}}$	**Frequency** $\boldsymbol{F}$ **[Hz]**	**Maximum load** $\boldsymbol{F_{max}}$ **[kN]**
B-S-1	3	-	Static loading	-
B-C-1	3	0.4	2.5	$0.75 \cdot F_{ult}$
B-C-2	3	0.4	2.5	$0.60 \cdot F_{ult}$

4.2 Results of TCC beam tests and derived S-N-curves

For all TCC beam tests, the failure occurred as brittle timber shear failure in front of the loaded edge of the notch (see Figure 6). However, the first cyclic test of series B-C-2 with a relatively small maximum load of $F_{max} = 0.60 \cdot F_{ult}$ showed a long crack in the timber in front of the loaded edge of the notch after more than 6 million load cycles, but no brittle failure occurred. Considering a frequency of $F = 2.5$ Hz, this corresponds to a test period of more than 27 days.

For that reason, the maximum load was first increased to $0.65 \cdot F_{ult}$ and finally to $0.70 \cdot F_{ult}$ (see Figure 8 (left)) until, after a total of 7.19 million load cycles, a brittle timber shear failure in front of the loaded edge of the notch occurred. Therefore, the second test within this series was started with a maximum load of $0.65 \cdot F_{ult}$, which, however, only initiated failure after increasing the load to $0.70 \cdot F_{ult}$.

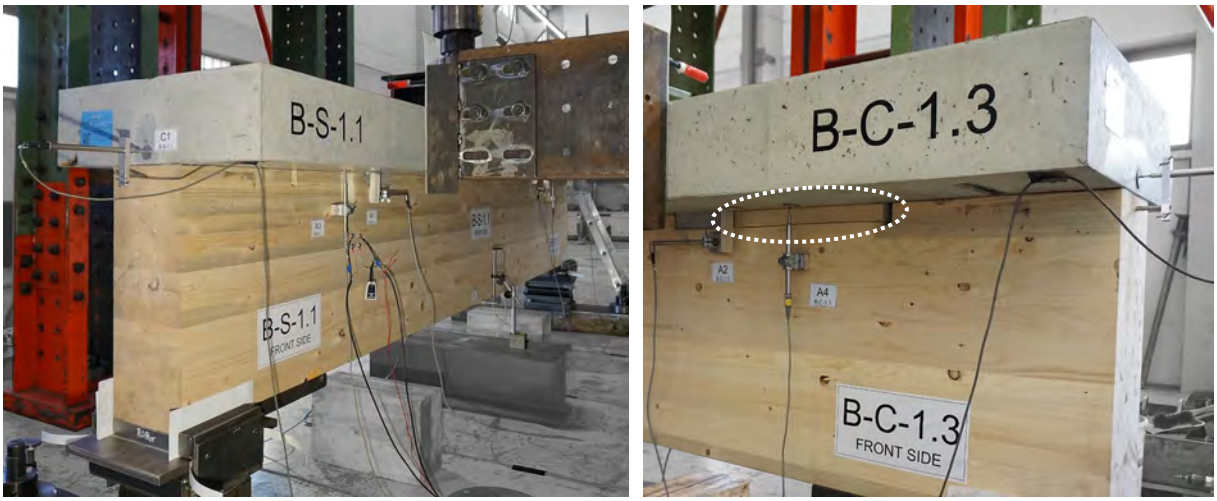


Figure 6: TCC beam specimen B-S-1.1 test setup at the MPA Stuttgart (left) and detail of the timber shear failure in front of the notch after cyclical loading of specimen B-C-1.3 (right).

Both run-outs could not be used for deriving the S-N-curves (but are shown in Figure 8 (left)). They confirm the tendency to high fatigue strength in the range of small maximum loads, as already observed by Simon [11]. Based on the results of the previous tests, the third test of series B-C-2 was finally started with a maximum load of $0.70 \cdot F_{ult}$. The failure occurred after 1.05 million load cycles. Thus, this test with single amplitude load spectrum could still be considered for the derivation of the S-N-curves with a stress ratio of $R = 0.4$.



All tests of series B-C-1 with a maximum load of $F_{max} = 0.75 \cdot F_{ult}$ failed at this load level (between $N = 71{,}880$ and $N = 516{,}980$ load cycles). Consequently, the results of series B-C-1 represent valuable input data for the S-N-curves derived in Figure 8 (right) based on all push-out and TCC beam tests with a stress ratio of $R = 0.4$. The measurement devices used for all TCC beam tests are marked at the respective locations in Figure 5. As an example, Figure 7 (right) shows the development in horizontal displacement at the notch for the corresponding side, where the brittle timber shear failure occurred.

All cyclic tests were first statically preloaded up to the mean load of the cyclic load protocol (shown in Figure 7 (left)). On average, the increase in displacement (between the start of cyclic loading and the brittle timber shear failure) was about 0.3 mm (see Figure 7 (right)).

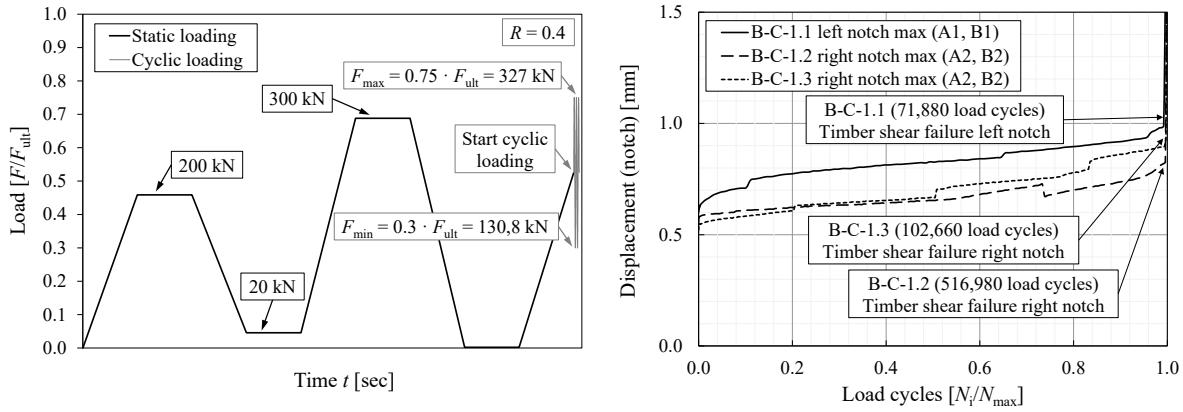


Figure 7: Static preloading together with the start of the cyclic loading for test series PO-C-1 (left) and horizontal displacement at the notch for all three tests of series B-C-1 (right).

Figure 8 (right) shows the S-N-curves derived from the mean values (MV) of the tests for the decisive failure mode (timber shear failure). In addition, the resulting statistically evaluated S-N-curves (5% fractile values) are shown as a combined evaluation of the TCC push-out and beam tests. This is shown in the same way for $R = 0.1$ in Figure 3 (right). For $R = 0.4$, the two S-N-curves are also above the resulting S-N-curve for timber in shear according to EN 1995-2, A.3 [9] and thus on the safe side.

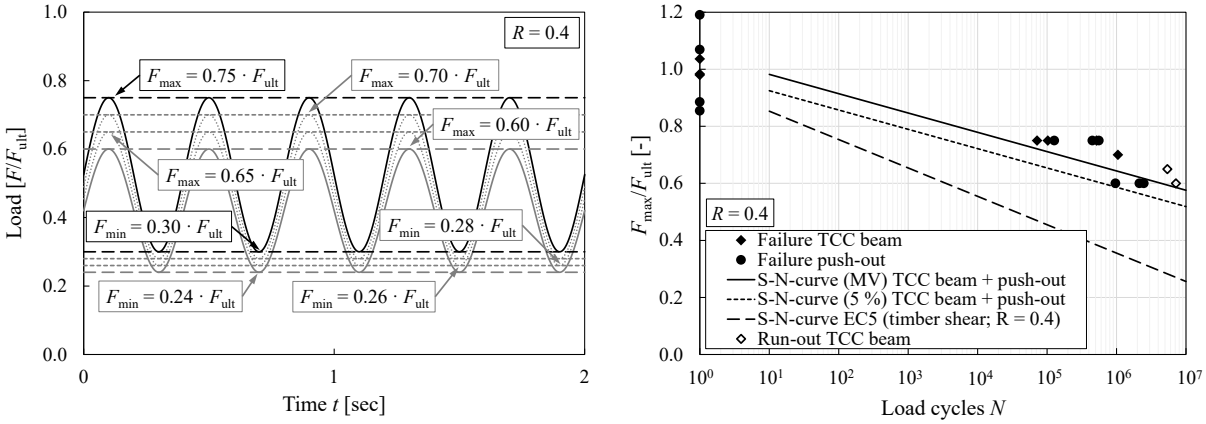


Figure 8: Load protocols of the cyclic loadings with a stress ratio of R = 0.4 (left) and S-N-curves for the stress ratio of R = 0.4 derived from TCC push-out and beam tests with marked run-outs (right).

A closer comparison shows that the distance between the S-N-curve derived from EN 1995-2, A.3 [11] and the S-N-curves derived from the tests with a stress ratio of $R = 0.4$ (Figure 8 (right)) is even larger than for the S-N-curves with $R = 0.1$ shown in Figure 3 (right). This indicates that the test results with a stress ratio of $R = 0.4$, which is more realistic in practice for TCC bridges, show an even higher fatigue strength compared to EN 1995-2, A.3 [9].



5 Summary and outlook

The discussed static and cyclic test series on TCC push-out and beam specimens with notched connections showed that the fatigue verification (decrease of strength by k_{fat}) for timber in shear, already implemented in EN 1995-2, A.3 [9], may also be applied with sufficient safety for the fatigue verification of notched connections in TCC bridges.

Within the future generation of the Eurocodes, the k_{fat} procedure will be maintained, but based now on a more elaborated background. Consequently, TCC-bridges with notched connections subjected to recurring traffic loads may be designed economically and safely. The spread of knowledge and a codification by the TS will allow for an increase in the use of sustainable timber constructions for bridges.

6 Acknowledgement

The investigations were funded by the German Research Foundation (DFG) – project number 397985109. This support is gratefully acknowledged.

We extend our appreciation to our DFG project partner, the Institute of Building Construction and Timber Structures at the Technical University of Braunschweig (Prof. Dr.-Ing. Mike Sieder and Peter Niebuhr, M.Sc.) for their very good cooperation.

Moreover, we thank SPAX International GmbH & Co. KG for providing screws for the specimens and MPA, University of Stuttgart for their great support in conducting the tests.

7 References

[1] Gerold, M. (2007) Holzbrücken am Weg (in German). Self-published, ISBN: 978-3-00-023624-2, Karlsruhe, Germany.

[2] Miebach F., Niewerth D., Wold F., Laraki J. (2018) Holz-Beton-Verbundbrücken – Erfahrungen und Perspektiven (in German). Qualitätsgemeinschaft Holzbrücken e.V.

[3] CEN/TS 19103 (2021) Eurocode 5: Design of Timber Structures – Structural design of timber-concrete composite structures – Common rules and rules for buildings. Technical Specification, CEN European Committee for Standardization, November 2021.

[4] Mönch S., Kuhlmann U. (2020) Fatigue Behaviour of Notched Connections for Timber-Concrete-Composite Bridges. In: International Network on Timber Engineering Research, INTER 2022, Online-conference, 17.-19. August 2020.

[5] Kudla K. (2017) Kerven als Verbindungsmittel für Holz-Beton-Verbundstraßenbrücken (in German). Institute of Structural Design, University of Stuttgart, No. 2017-02, PhD thesis.

[6] Mönch S. (2022) Performance of Notched Connections under Static and Cyclic Loading for Timber-Concrete Composite Systems. Institute of Structural Design, University of Stuttgart, PhD thesis, in preparation.

[7] Kuhlmann U., Mönch S. (2018) Design Parameters of Notched Connections for TCC Structures as Part of Eurocode 5. In: International Network on Timber Engineering Research, INTER 2018, Tallinn, Estonia, 13.-16. August 2018.

[8] Kuhlmann U., Sieder M., Mönch S., Niebuhr P. (2021) Ermüdungsverhalten von Kerven und selbstbohrenden Vollgewindeschrauben für die Anwendung als Verbindungsmittel bei Holz-Beton-Verbundträgern (Fatigue behaviour of notches and self-drilling screws for the application as connectors in TCC beams), (in German). University of Stuttgart, Institute of Structural Design and Technical University Braunschweig, Institute of Building Construction and Timber Structures, DFG-Research-Project, Project number: 397985109, 2018-2021.

[9] EN 1995-2 (2004) Eurocode 5: Design of timber structures – Part 2: Bridges. European Committee for Standardization (CEN), Brussels.

[10] Kuhlmann U., Aldi P. (2010) Fatigue strength of timber-concrete-composite bridges: Determination of a S-N-line for grooved connection and the "X-connector". In: World Conference on Timber Engineering, WCTE, Trento, Italy, 20-24. June 2010.

[11] Simon A. (2008) Analyse zum Trag- und Verformungsverhalten von Straßenbrücken in Holz-Beton-Verbundbauweise (in German). Bauhaus-Universität Weimar, PhD thesis.

[12] EN 14080 (2013) Timber structures – Glued laminated timber and glued solid timber – Requirements. European Committee for Standardization (CEN), Brussels.

[13] EN 1992-1-1 (2004) Eurocode 2: Design of concrete structures – Part 1-1: General rules and rules for buildings. European Committee for Standardization (CEN), Brussels with corrections and amendments + AC:2010.

[14] Miner A. (1945) Cumulative Damage in Fatigue. In: Journal of Applied Mechanics 12 (1945), pp. 159-164.

Conference Proceedings 4th ICTB (2022)
https://doi.org/10.24451/mgfx-n234

ICTB 2021 PLUS
4th International Conference on Timber Bridges
Biel/Bienne, Switzerland, 9 -12 May 2022



SHARP METAL FOR TIMBER CONNECTIONS

Stephan Schindlauer[1]

1 Introduction

Rothoblaas Sharp Metal is an innovative connection system suitable in all the application where the stiffness of the joints has a significant influence on the overall behaviour of the structure.

Sharp connector has a large number of fastening elements, distributed along the surface of the hooked plates. This guarantees excellent strength and stiffness, creating surface "apparent" adhesion with values comparable, for practical application, to a glued connection.

Since no chemical adhesion, as with the common gluing process, this application eliminates the variability and risks associated with the moisture variation and the treatment (sanding, cleaning, dust) of the surface in the practical field of application.

This aspect makes the application of these elements extremely interesting in case of restoration or structural reinforcement. Through the application of additional wooden elements, it is possible to create composite beams with significantly higher performance to make up for structural deficiencies or / and load increases.

The achievement of a high stiffness can be useful both for the reduction of the deformation and to improve the behaviour in terms of vibration (ie: floors).

Often the initial slippage due to the clearance between holes and dowels in steel plates can have a great influence on long span beams deflection even if the total design load bearing capacity is achieved. In this case, according to [2], the slippage "gap" should be added to the contribution stiffness of the fastener.

Another interesting field of application, currently under investigation, Is the use of hooked plate to reduce the splitting and other brittle failure on the loaded end of members connected by means of dowel type fasteners. This can ensure higher resistance spreading the loads on higher loading bearing area and creating higher confinement in joints of trussed subjected to higher loads (trusses diagonal in tension).

The development tests and experimental values indicated in this paper has been determined by laboratory tests at the Universität Innsbruck Institut für Konstruktion und Materialwissenschaften.

2 Sharp metal – overview

Sharp metal plates can transfer shear forces through a series of small pins organized in several (pair) rows.

Compared to the punched plates in which a limited number of large-sized teeth are made and bent from the sheet, the Sharp metal production process involves "lifting" of small size hooks by "scratching" the plate surface without a perforation, thus creating a very high number of small-sized teeth.

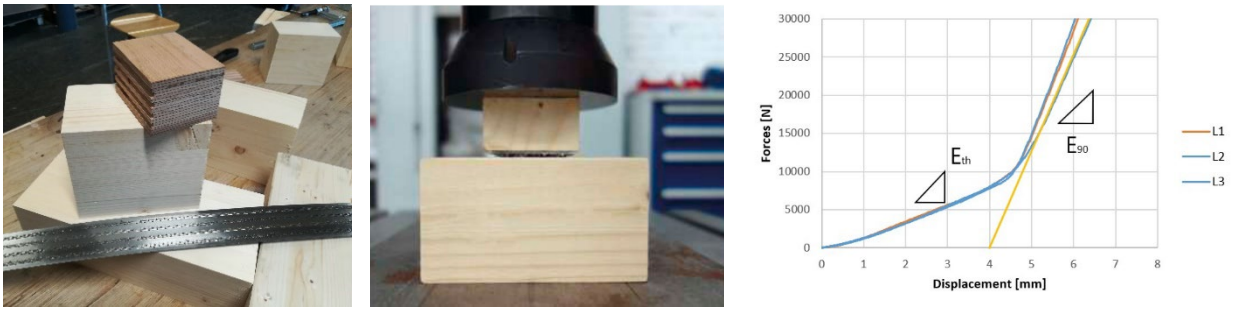
The plates are currently produced with two different "densities" of hooks on the surface, namely HL high density and LD low density. The plate has a thickness of 0.75mm and the teeth measure approximately 2mm on each side.

Plates with a larger number of teeth ensure higher stiffness and load bearing capacity. However, significative pressure forces should have to be applied to ensure these high values, while the system with lower density of hooks has less resistance and stiffness but requires lower pressure for penetration of the teeth.

The minimum pressure required to completely close the gap was determined experimentally with a universal testing machine. For HD plates this pressure is between 1.5 and 2 MPa, depending on timber density, while for LD it is approximately half.

The mean pressure was calculated from load displacement curves at the point where the path shows a variation in the slope (knee-shaped curves). The first part identifies the stiffness to the penetration of the teeth while the second the stiffness (EA/l) of the wood at 90 °.

[1] Stephan Schindlauer, field Engineer; Rothoblaas srl Italy; stephan.schindlauer@rothoblaas.com



(a) (b) (c)

Figure 1: Sharp metal LD 1200mmx50mm (a) – Tests to assess the force to close the gap (b) - Schematic shape of load displacement curve for compression tests.

In practical applications where presses or similar tools are not available, the clamping force can be applied using the axial capacity of large head screws - (washer head screws Rothoblaas TBS). In this case the performance is lower than the ideal condition since the penetration is potentially not complete, depending on the material density/wood species.

To facilitate the assembly phases, and reduce the penetration length required, applications with hammer insertion as in traditional single-sided punched plates have also been tested using hard wood tools with grooves that are inserted between the rows of teeth. The result in terms of effectiveness / time required seems to be positive.

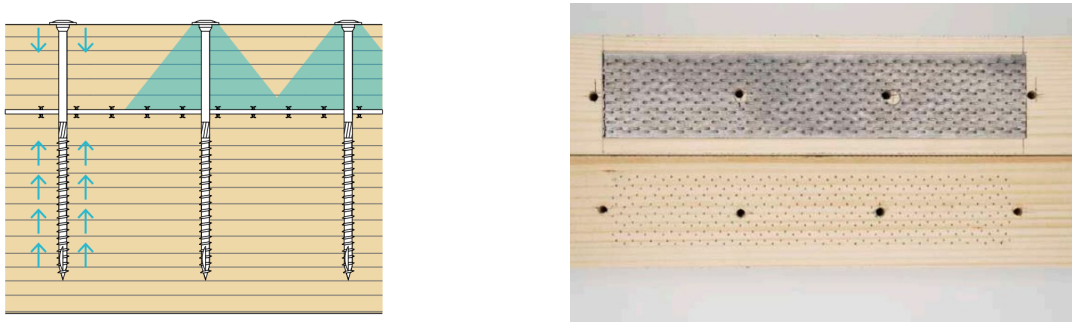
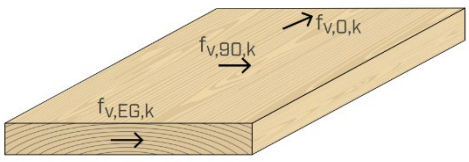


Figure 2: Installation of Sharp metal LD 1200mmx50mm with screws

The outcome of mechanical shear tests, in which screws were used to close the gap (condition of real application) shown good shear performance in all the different directions of the load; parallel (fv, 0), perpendicular (fv, 90) and along the wood fiber (fv, EG).

Table 1: Characteristic strength (without considering screws) The overall stiffness of the K_{ser} connection [N/mm] is determined by multiplying the k_{ser} coefficient by the plate surface.



Type	$F_{v,0,k}$ [MPa]	$F_{v,90,k}$ [MPa]	$F_{v,EG,k}$ [MPa]
LD	0.93	0.20	1.03
HD	1.15	0.51	1.03

Table 2: Characteristic strength (sharp metal + TBS 8x160 screws spacing 80mm)

Type	$F_{v,0,k}$ [MPa]	$F_{v,90,k}$ [MPa]	$F_{v,EG,k}$ [MPa]	$K_{ser,0}$ [N/mm]*[1/mm^2]	$K_{ser,90}$ [N/mm]*[1/mm^2]	$K_{ser,EG}$ [N/mm]*[1/mm^2]
LD	2.02	2.11	1.92	3.13	0.65	4.19
HD	2.24	2.42	1.92	6.47	0.90	5.00



Table 3: Characteristic parameters of the experimental tests (from UIBK test report-acc. to EN14358).

Screws	Sharp metal Type - length [mm]	F_{mean} [kN]	F_k [kN]	K_{ser} [N/mm]
3x TBS 8x160	-	15.8	13.2	2911
4x TBS 8x160	-	20.8	15.1	4346
4x TBS 8x160	LD 250	33.0	28.0	39133
4x TBS 8x160	HD 250	40.0	31.1	80876

Table 3 summarize the results of shear tests on joints with and without sharp metal. It worth notice the performance of the connections using sharp metal is significantly higher. To highlight the differences in terms of stiffness and strength, tests has been carried out using the same type, number of screws and timber grading.

For the sample with 4 screws an average experimental strength of 20.8kN and a stiffness of 4346N /mm was obtained. The same number of screws, same timber elements also using a strip of Sharp metal LD 50x250mm the strength was 32kN and the stiffness about 39133N/mm. Using an HD strip with the same dimensions the values increase to 39.9kN and 80876N /mm.

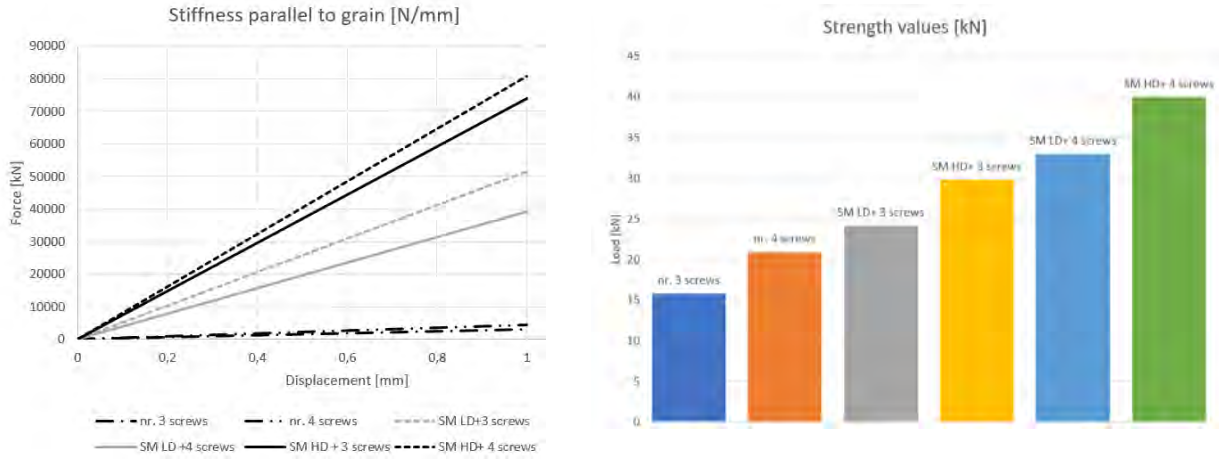


Figure 3: Outcome of tests- comparison of stiffness and strength.

With the aim of evaluate the effect of timber moisture variations several tests have been currently run at the University of Innsbruck. The first evidence shows a good behaviour of the connections in the case of an increase in humidity (swelling), while the effect of the decrease in water content creates distortions that lower the contact (shrinkage). To reduce this effect, screws should be positioned along the width during installation to reduce distortion (transversal deviation).

However, this problem affects all the rigid connection such as bonding or traditional joints. With sharp metal the main advantage is that only the shrinkage can affect the strength.

This aspect is important for timber bridge connections, given that humidity variations can often locally and for short periods reach high values even in protected structures (normally within service class 2). This problem could limit the application of adhesive for some particularly sensitive applications.

Regarding structural applications of sharp metal, one of the possible cases, where good results were obtained is the application on ribbed floors or hollow box build-up section.

For these type of structures, high stiffness is required to create an efficient load transfer between the component such as upper panels and ribs creating an efficient build up section. The modularity of strips with constant and reduced width (50mm) allows great versatility and timesaving.

In this case, especially when the application cannot be performed in shop, for instance due to transport limits, considerable costs and time are saved (curing, assembly, control). As already mentioned, in terms of results, during the tests, the fundamental parameter for evaluating the correct installation of Sharp metal is the closure of the gap. This is an easy and effective to control parameter.



Tests were carried out on ribbed floors which showed that the use of Sharp metal allows the achievement of excellent performance in terms of effective section.

Test were carried out on rib-floors composed of glue laminated timber beams (GL) with an integrative panel in cross laminated timber (CLT). All the tests were performed in the laboratory of the University of Innsbruck.

Different connection system has been tested to assess the different performances of screws, glue, and sharp metal. In this case, screws were used to ensure the embedment pressure of the hooks. The results shown in the table highlight that the solution with sharp metal has an intermediate behavior between glue and screws. Both in terms of strength and stiffness.

Table 4: Mean strength and stiffness values (F_{max}; K_{ser}) of rib panels assembled with screws, sharp metal and glued.

Test	Fmax [kN]	K_{ser} [N/mm]
Screwed (2 row 12d - TBSmax 8x240mm)	72.3	1473
	96.0	1617
	89.6	1439
Sharp metal (1 row 15d - TBSmax 8x240mm+HD 50/6000mm)	99.2	1935
Sharp metal (1 row 18d - TBSmax 8x240mm+LD 50/6000mm)	67.5	1489
Sharp metal (1 row 20d - TBSmax 8x240mm+LD 50/6000mm)	80.1	1169
	81.7	1341
Glued connection (2 row 20d)	128.3	2326
	145.5	2444

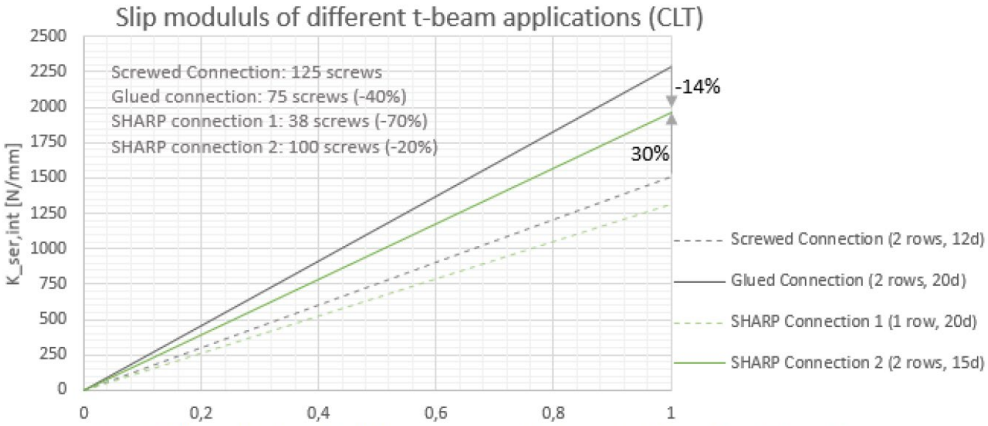


Figure 3: Slip modulus $k_{ser,int}$ for different t-beam applications with CLT-panels and Glulam-beams; Glued connection, screwed connection and SHARP-Metal connections

Figure 4: Stiffness of rib-panels (GL-CLT).

The advantage over structural bonding is a greater ductility of the connection (ultimate displacement) and less dependence on the assembly conditions. The use of this system can also be extended, as reported in the introduction, to the structural strengthening of elements of bridges or other structures that require a restoration due to localized degradation or a reinforcement for a variation of intended use. In this case, the intervention is easily removable.

Using sharp metal, as for structural bonding, surface preparation, such as flatness, presence of cracks, etc. has great influence on the results. Anyway, unlike gluing it is not necessary to use a primer or other similar treatment. This is because resistance is achieved by mechanical meshing and not by chemical adhesion.

Great importance for practical use is covered by the stiffness of the connected element since this value can affect the pressure value achievable with the screws. It has been observed that this parameter greatly influences the pressure needed to close the gap between the two elements.

In the case of panels with similar stiffness, the strips can be inserted on at least one element by hammering. This solution is easily achievable using "LD" type strips where the number of rows of teeth leave a flat non-



toothed parts that can be used to rest the protruding parts of the tool. According to this scheme, the tool can be made through a simple portion of hard wood with grooves corresponding to the teeth.

This application is more complex on the "HD" type but conceptually still feasible.



Figure 5: Use of sharp metal and alternative "traditional" methods using screws-tool to hammer the plates.

3 Conclusion

Sharp metal is an innovative connection technology, made with a surface hooked element, which can be used to transfer shear forces. The mechanical performance in terms of strength and stiffness are significantly higher than cylindrical dowel type connectors.

The type of connection allows its use in environment or part of the structure in which it is not possible/easy to guarantee the conditions in terms of humidity and temperature for correct bonding.

The maximum performance is obtained when the gap between the two parts to be connected is completely closed. This operation can be carried out using hydraulic or vacuum presses for mass production.

If screws are used, probably the maximum performance cannot be reached but anyway excellent performance for the main application can be achieved.

In case of moisture changing the main problems occur when the moisture content decrease (shrinkage). However, these problems are lower compared to the same geometry with a glued joint. Increasing the values of moisture this effect less problematic.

Future developments will concern the verification of extreme humidity conditions and applications to verify the operational application in reducing the distance from the edges of dowel type fasteners.

Acknowledgement

The authors would like to thank the scientific partners, University of Innsbruck. This paper and the research behind it would not have been possible without the exceptional support of Roland Maderebner. Special thanks also to Julian Meyer and all the staff of the laboratory for testing material.

References

[1] ETAG 015 - Three-dimensional nailing plates (EAD 130186-00-0603 - Three-dimensional nailing plates, 2018)
[2] UNI EN 1995-1-1:2014-06-01; Eurocode 5: Design of timber structures — Part 1-1: General — Common rules and rules for buildings
[3] Rothoblaas srl Datasheets product catalogue, Rothoblaas srl Via dell'Adige 2/1 39040, Cortaccia (Bz) Italy

Conference Proceedings 4th ICTB (2022)
https://doi.org/10.24451/7qwp-0972

ICTB 2021 PLUS
4th International Conference on Timber Bridges
Biel/Bienne, Switzerland, 9 -12 May 2022



The further Development of the Design of Timber Structures according to Eurocode 5 – Part 2: Bridges

Matthias Gerold [1]

1 Introduction

In 2004, the EU and several EFTA states introduced uniform design codes, the so-called EUROCODEs (EC). The goal of the European Committee for Standardization (Comité Européen de Normalisation, CEN) here was to replace the member states' differing or even missing design guidelines by a common set of technical rules that provide the same level of safety and thereby to further minimise barriers within Europe. In 2012, the European Commission issued a mandate for the development of a second generation of the Eurocodes to ensure their long-term applicability and reflect the constant technical developments and knowledge gains (see Figure 1).



Figure 1: European design codes – Eurocodes
Source: European Commission, 2021

For developing the second generation of the Eurocodes, the requirements and recommendations of the Eurocodes 0 and 1 had to be (mandatorily) taken into account. These codes, whose first generation was called "Code of the Code Writers," had originally been intended to serve as a guide for construction professionals.

For the series of standards "EN 1995 – Design of timber structures," experts regularly prepare drafts for specific topics in timber construction. To this purpose, six project teams (PT) had generally been convened since 2015. Today, their work is continued by ten working groups (WG), which had already before accompanied the thematic development of the EC5, in cooperation and coordination with the national standardisation bodies, see Figure 2. After extensive revision of the entire Eurocode 5 series, new versions will be available for all member states as of the year 2025/26.

In the following, Sect. 1 will provide an overview of the contents and differences of the new versions compared to the existing timber-construction standard. Sect. 2 will then compare the new versions with the existing EN 1995-2 (see /1/). Subsequently, Sect. 3 will detail the changes in the code for timber bridges.

In the following, Sect. 1 will provide an overview of the contents and differences of the new versions compared to the existing timber-construction standard. Sect. 2 will then compare the new versions with the existing EN 1995-2 (see /1/). Subsequently, Sect. 3 will detail the changes in the code for timber bridges.

Standardisation body CEN/TC 250/SC 5		Lead (chair): Stefan Winter (DE)		
Project team	Working group	Lead (convenor)	Code	Availability
PT 1	WG 1: Cross-laminated timber, laminated veneer lumber etc.	Tobias Wiegand (DE)	EN 1995-1-1	2025
PT 3		René Steiger (CH)		
PT 5	WG 3: Reinforcement, stability, oscillations etc.	Ulrich Hübner (AT)		
	WG 5: Connections and fasteners	Philipp Dietsch (DE)		
	WG 7: Breakthroughs and reinforcements	Julian Marcroft (UK)		
	WG 10: Basis of design			
PT 4	WG 4: Fire protection design	Andrea Frangi (CH)	EN 1995-1-2	2025
PT 6	WG 6: Timber bridges	Matthias Gerold (DE)	EN 1995-2	2026
PT 2	WG 2: Timber-concrete composites	Jörg Schänzlin (DE)	CEN TS 19103	2021

Figure 2: A part of the standardisation body CEN/TC 250/SC 5

[1] Matthias Gerold, Harrer Ingenieure GmbH, Karlsruhe / Ostfildern, Germany



2 Differences to the Existing Timber Design Code

The Eurocode 5 (EN 1995) remains divided into:

- Part 1-1: General – Common rules and rules for buildings
- Part 1-2: General rules – Structural fire design
- Part 2: Timber bridges

The old and the new code structure are compared in Table 1.

Since the introduction of the European design codes about 20 years ago, hardly any field has changed as much at product level as the field of timber construction. In accordance with the state of the art, the code is substantially expanded for materials and supplies such as cross-laminated timber, laminated veneer lumber, and hardwood products.

To meet past discussions and user feedback, the CEN has indicated the "ease of use," that is, the notion of practicability, as one of the core objectives for the second generation of the Eurocodes. In particular, this comprises:

- improved structure and clarity ("ease of use" – task 1)
- clearer linking and harmonisation/reduction of nationally determined parameters (NDP) (task 2)
- reduction of alternative equivalent application rules and procedures
- removal of little-used regulations
- explanation of the mechanical background of formulas

In timber bridge construction, PT6 should also treat the topic of fatigue (task 3).

In order to help planners eventually use several Eurocodes at once, particularly when working on hybrid constructions, the headings of the main chapters 1 to 11 (or 1 to 5, regarding fire) are identical across all 'material Eurocodes.' Chapters 2 and 3 were newly added to the existing structures.

In addition to the documents mentioned here, the Technical Specification (TS) CEN TS 19103 (as yet an informative document) was published for the design of timber-concrete composite structures. This document is intended to give users the opportunity for application tests, to prepare them for a possible EN 1995-1-3, and thus to provide the foundation for the rules-based design of timber-concrete composite structures.

Additionally, for the design and execution of glued-in threaded rods, a Technical Report (TR) about the state of the art of this special kind of connection is being prepared.

Furthermore, regulations relevant to the structural stability of timber constructions are being developed – possibly a new Part 3 of the series of standards.

For the design verifications of the following chapters, the revised Clause 7 "Serviceability limit states" of EN 1995-1-1 provides all the necessary boundary conditions. Clause 8 "Connections with metal fasteners" is divided into two thematic parts: The first part provides all proofs for a general design method, while the second part sets out design methods for construction elements with special requirements, e.g., notched beams or double-tapered beams (so far a part of the German National Annex / NA) as well as breakthroughs in beams (both reinforced and non-reinforced).



Table 1: Structural comparison of the codes EN 1995:2004 and 2027

	Cold-state design of timber constructions		Fire protection design of timber constructions		Timber bridges	
Chapter number / Chapter heading	EN 1995-1-1:2004	prEN 1995-1-1:2027	EN 1995-1-2:2004	prEN 1995-1-2:2027	EN 1995-2:2004	prEN 1995-2:2027
Scope	1	1	1	1	1	1
Normative references	1	2	1	2	1	2
Terms, definitions, and symbols	1	3	1	3	1	3
Basis of design	2	4	2	4	2	4
Materials	3	5	3	5	3	5
Durability	4	6			4	6
Structural analysis	5	7			5	7
Ultimate limit states	6	8			6	8, T/ΔT/Δmc/ΔL Annex E
Tabulated proofs			n.i.	6		
Simplified design methods			3,4,5	7		
More precise design methods			Annex B	8		
Design of timber constructions with natural fire curves			Annex A	Annex A		
Serviceability limit states	7	9			7	9, Annex C (only low seismic areas, bearings)
Fatigue	n.i.	10			Annex A	10
Joints and connections	8	11			8	11
Connections under fire exposure			6	8		
Composite construction elements and support structures	9	12				TCC Annex A
Roof, floor and wall diaphragm slabs	9	13				
Execution and monitoring	10	Separate document			9	Annex B – Inspection and Maintenance
Execution of details			7	10	-	Annex D (examples of structural timber preservation)
Foundation on timber piles	n.i.	14				
Oscillations caused by persons/pedestrians	7	9			Annex B	9 (incl. traffic)
Legend: n.i. = not included						



If multi-storey construction with timber is to be further advanced, the fatigue design should not remain limited to bridge constructions: increasing height means increasing dynamic actions not only in view of traffic loads but also, for example, in view of oscillations caused by industrial machines, bell vibrations, crane runways, and wind loads. For this reason, Clause 10 "Fatigue" was taken over from the bridge part (EN 1995-2) and adapted for the general design of building constructions with timber elements.

Part 2 of the series of standards complements the regulations for structural engineering which apply according to Part 1 and the new TS with those of bridge construction.

At the start of the development of prEN 1995-2 on the level of CEN/TC 250/SC 5, the project team SC5.T6 discussed and answered both the 78 comments from the 1st review of prEN 1995-2:2010-12 and the 149, 243, and 429 comments from the 1st, 2nd, and 3rd draft of prEN 1995-2:202x, respectively. The Final Document was published mid-December 2021 together with 8 Final Background Documents (BGD) in a zip file.

For the development of the English code texts, the use of verb forms was to be taken into account:

- "shall": requirement (strictly to be followed) ➔ previously: (P) principle
- "should": recommendation (highly recommended); alternative approach possible where technically justified
- "may": permission within the limits of the Eurocodes
- "can": possibility and capability ➔ only in NOTEs

The use of coloured images and flowcharts is allowed in standards (see https://boss.cen.eu). For figures there are guidelines as well.

It remains to be said that the EC5 regulations regarding the stability of buildings were revised, extended, and adapted according to the state of the art. Despite the tripled number of pages and the increased number of NDPs (essentially due to EC0 and EC1), the code writers have always kept a close eye on the question of practicability, for example, by providing simplified calculation procedures.

3 Sustainable Timber Bridge Construction

With a slight delay in time compared to the building construction codes 1-1 and 1-2, the code for timber bridges prEN 1995-2 was edited too. One of the main topics was the implementation of the specifications of EN 1990 and EN 1991-2, in particular the definition of requirements for reaching an operating life of 100 years. Since construction professionals speak the language of implementation planning, a new Informative Annex D with highly simplified figures exemplifies how timber bridges are to be protected basically. In order to meet this requirement, the Informative Annex B supplies additional requirements for the testing and maintenance of timber bridges. Both annexes can be rejected in whole or in parts (NDP) or else be supplemented nationally.

The previously known Annexes A (fatigue) and B (oscillations, damping) were integrated into the main part of prEN 1995. To increase the user-friendliness in both fields, the verification methods especially for bridges were simplified compared to prEN 1995-1-1 and EN 1990, respectively.

Like the building construction code, the code for timber bridges was extended to include requirements and regulations for the durability of structures, taking into account the issues of corrosion protection, deck plates, and timber-concrete composites. The creep factors for concrete in timber-concrete composite bridges are different from those in known building constructions, as the cross-sections are significantly larger. Accordingly, the new normative Annex A of prEN 1995-2 provides relevant conditional equations. prEN 1995-1-1 shall stipulate requirements for numeric analyses (keyword Finite Element Method, or FEM for short).

Eurocode 8, Part 2 ("Design of structures for earthquake resistance"), will from now on also take timber bridges into account. To this aim, the project team SC5.T6 and the working group WG6 developed an Informative Annex C, which was largely adopted by the EC8. The EC8 did not adopt supplementary regulations for the support of light timber bridges against vertical seismic forces and for timber bridges in areas with low seismic activity, with these regulations having therefore remained in prEN 1995-2. It is also relevant to point to the Informative Annex E, which contains suggestions to be considered in view of deformations and dimensional changes of timber constructions under changing environmental conditions such



as temperature or timber moisture, and notes on transversely prestressed timber deck plates (among other things for the "cupping" of the deck sides).

Most regulations on deck plates (timber decks) were added to the normative Annex of prEN 1995-1-1, as these regulations can also be applied to, e.g., nail-laminated timber constructions.

Project team SC5.T6 consisted of Roberto Crocetti (SW), Kristoffer Ekholm (SW), Matthias Gerold (DE) (lead), Frank Miebach (DE), and Andreas Müller (CH). It was supported by individual WG6 members such as Kjell Arne Malo (NO), Hauke Burkart (NO; secretariat), Rune Abrahamson (NO), Patrice Godonou (SW), Valentina Bruno Huré (FR), Antje Simon (DE), and Tobias Wiegand (DE), as well as by national experts from Germany (Durability: Helen Belschner; TCC: Jörg Schänzlin (SC5.T2), Jochen Marschall and Fabian Wolf; Vibrations: Patricia Hamm and Steffen zu Jeddeloh; Fatigue: Mike Sieder (SC5.T3), Peter Niebuhr, Ulrike Kuhlmann (EC3) and Simon Mönch).

With the technical work basically being done, there will now follow 'editorial' works (verb forms, NDPs, symbols, drawings), cross-checks with other Eurocodes, translations into the two other official languages of German and French, and the final coordination (enquiry) at the level of SC5 and CEN. The remaining steps of the standardisation process are shown in Figure 3.

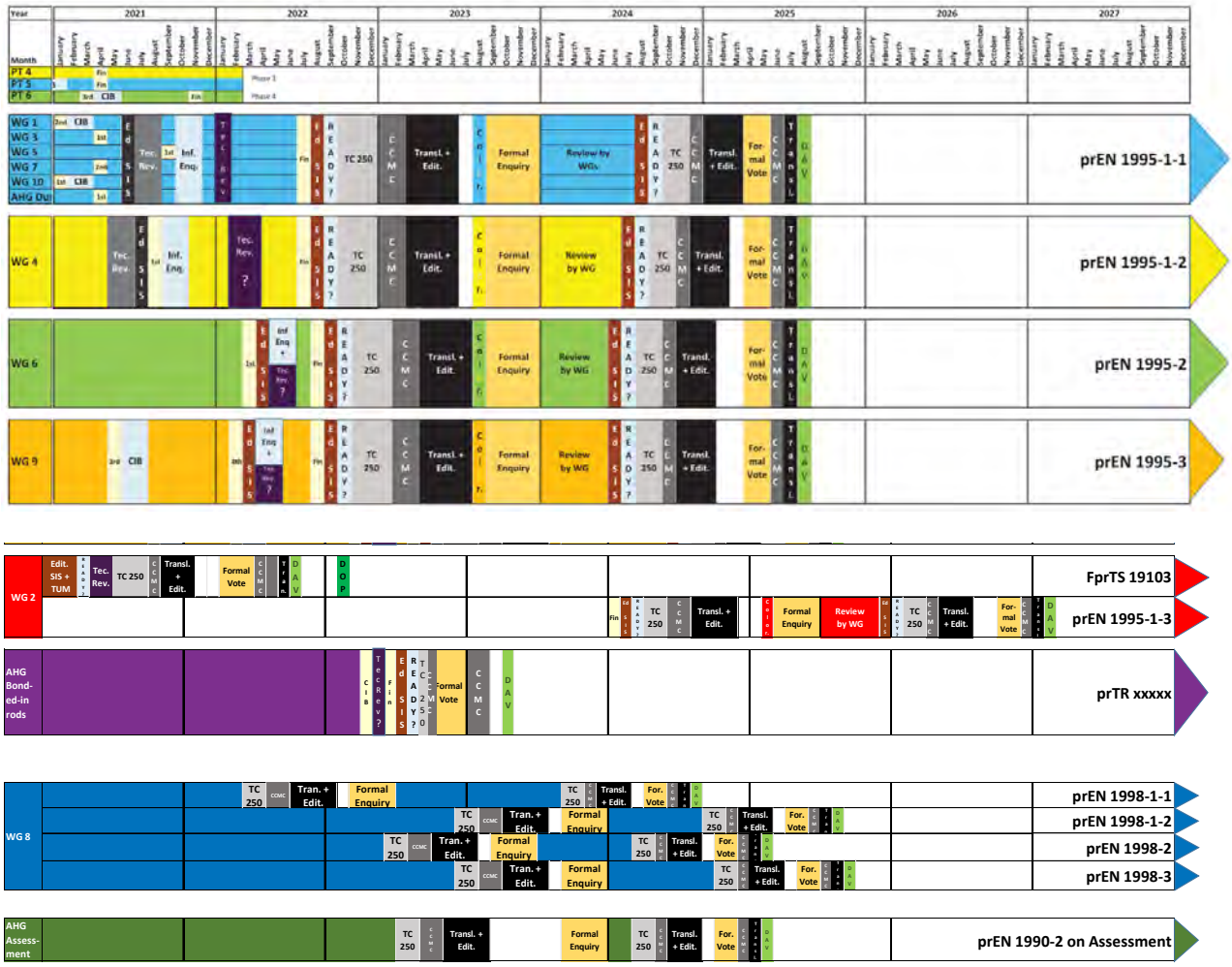


Figure 3: Planned timeline of the publication of the second generation of the EC5



4 Changes in prEN 1995-2 in Detail

4.1 Design Service Life T_{Life}

4.1.1 Specifications prEN 1990 A.2 Bridges

prEN 1990, ***3.1.2.26 Maintenance***

Set of activities performed during the service life of the structure so that it fulfils the requirements for reliability

Note 1 to entry: Activities to restore the structure after an accidental or seismic event are normally outside the scope of maintenance.

prEN 1990, ***A.2.4 Durability***

(1) All structural parts that rely on a design assumption of inspection or maintenance in order to satisfy their durability requirements over the design service life shall be designed to permit inspection and maintenance.

NOTE 1: See 4.6 for durability requirements.

NOTE 2: Inspection and maintenance are needed for structural members designed using the damage-tolerant method for fatigue. Material-related guidance on the damage-tolerant method is given in the relevant material Eurocodes.

NOTE 3: Maintenance activities can include the renewal of protective coatings, renewal of replaceable structural parts or elements other than structural, cleaning, treatment of detected fatigue cracks.

(2) If the inspection or maintenance of a structural part is not possible, it shall be designed to achieve adequate durability over the design service life without inspection or maintenance.

NOTE: See the other Eurocodes for measures to achieve adequate durability over the design service life without inspection or maintenance. Measures can include the provision of sacrificial material, protection of the part, use of materials with enhanced durability, control of the environment surrounding the part.

prEN 1990, ***4.8 Quality management***

(1) Appropriate quality-management measures should be implemented to provide a structure that corresponds to the design requirements and assumptions.

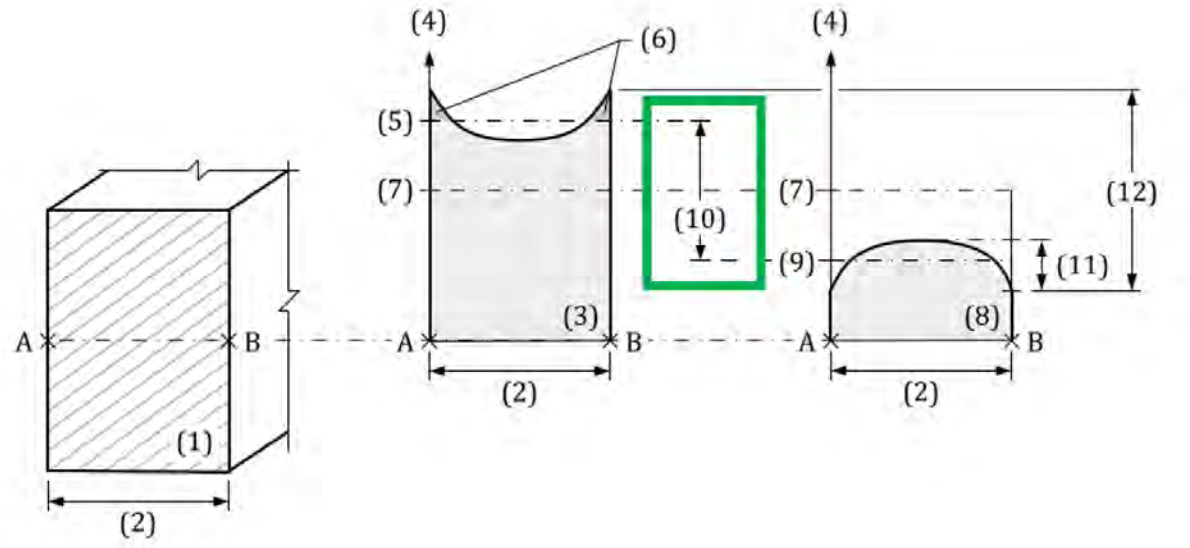
(2) The following quality-management measures should be implemented:

— organizational procedures in design, execution, use, and maintenance;

— controls at the stages of design, detailing, execution, use, and maintenance.

NOTE: See Annex B and the other Eurocodes for guidance on appropriate quality-management measures.

4.1.2 Basis prEN 1995-1-1 – Consolidated Version



Key

1 *Member cross-section*

2 *Width or depth of the cross-section*

3 *Moisture content profile, along the width or depth of the cross-section, under high relative humidity*

4 *Moisture content (vertical axis)*

5 *Upper limit of average moisture content, which is used to calculate the strength and stiffness of members and connections*

6 *Upper limit of moisture content may be exceeded for a few weeks per year*

7 *Yearly average moisture content, which is used to assign timber members to corrosivity categories for steel dowel-type fasteners*

8 *Moisture content profile, along the width or depth of the cross-section, under low relative humidity*

9 *Lower limit of average moisture content*

10 *Variation of the average moisture, which may be used to calculate dimensional changes of the section (in the case of unrestrained shrinkage)*

11 *Moisture difference, which may be used to estimate drying cracks in the zone of the member close to its surface*

12 *Moisture variation at the surface*

prEN 1995-1-1, *Figure 4.1 – Moisture content along the width or depth of a timber cross-section under high and low relative humidity*



4.1.3 Implementation prEN 1995-2: Design Service Life T_{Life}

For requirements see prEN 1990:2022, Annex A.2 Table A.2.2 Line 2 of the following Table 4.1 (NDP) was added for bridges used for sport and recreational purposes, after intense discussion with SC5.T6 with the Horizontal Group Bridges (HGB).

	Category of Timber Structures	*Design Service Life, T_{life} [years]*
1	*Protected timber bridges (including their foundations and steel tension components according EN 1993-1-11), other civil engineering structures supporting road or railway traffic* [a]	*100* [b]
2	*Timber bridges where the main structural members have a reduced protection* [a]	*50* [b]
3	*Replaceable structural parts* [d]	*25*
4	*Temporary structures* [c]	*≤ 10*

[a] *See EN 1990:202x, Table A.2.2 (NDP)*
Line 2 can be relevant, for example, for bridges in a low consequence class where the economic consequences of replacement after a shorter design service life are agreed to be acceptable by the relevant authority, or, where not specified, agreed for a specific project by the relevant parties.

[b] *See EN 1990:202x, Table A.2.2 (NDP)*

[d] *A value of 25 years may be given for the classification of replaceable structures or parts of structures as well. The protection of steel elements against corrosion should fulfil the design service life.*

Steel tension components according EN 1993-1-11 shall be designed with a design service life of 100 years (see 4.1.2.2) even if they should be replaceable.

Ancillary structures should be classified as replaceable parts of the main structure.

[c] *See EN 1990:202x, Table A.2.2 (NDP)*
Unprotected timber members should be classified as temporary structures.

prEN 1995-2, Table 4.1 (NDP) – Design Service Life T_{life}
– Categories for Timber Bridges

4.1.4 Relevant definitions prEN 1995-2

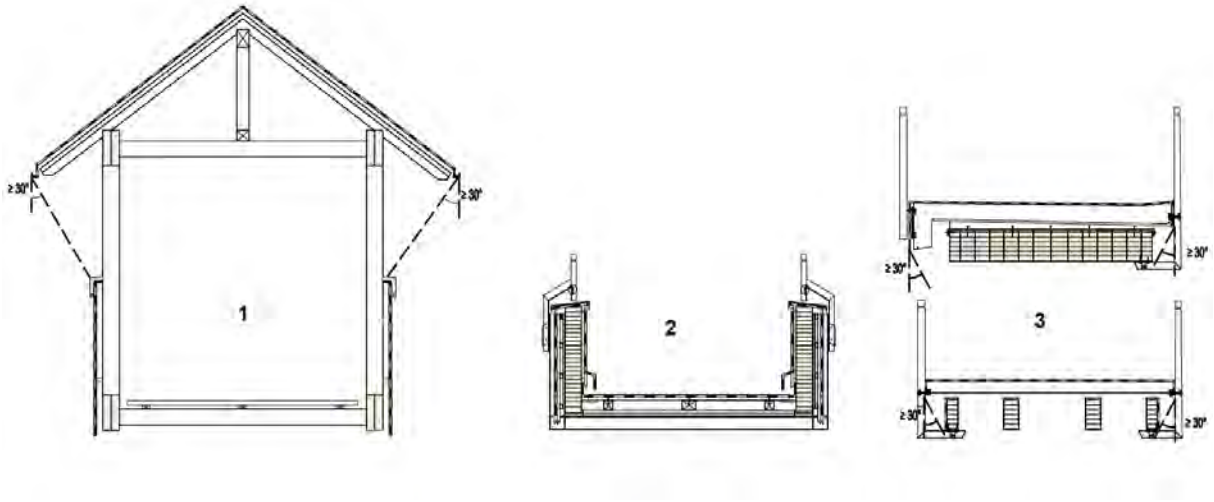
Protected Member

structural member not exposed to direct weathering such as rain, snow, or other sources of moisture ingress

Note 1 to entry: Protected members are provided with weather protection, e.g., in the form of claddings, sealed deck surface, or an adequate roof overhang in both longitudinal and transversal directions (see Figure 3.2), so that an accumulation of moisture is unlikely.

In the case of a protected bridge, all main bearing members of the superstructure are protected; for examples see Annex D.

Note 2 to entry: Protected members can typically be assigned to Service Class (SC) 2 and Use Class (UC) 3.1.



Key

membrane or weather-resistant layer

prEN 1995-1-1, Figure 3.2 – Examples of protected bridges:

1 Covered footbridge (bridge with a roof)
2 Trough bridge
3 Deck bridges

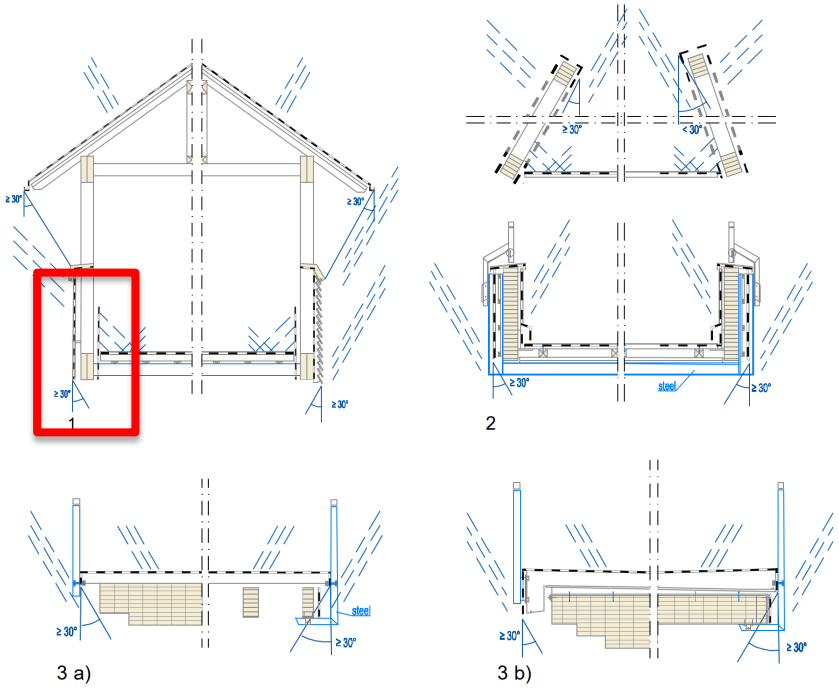


Unprotected Member

structural member that is not or only partially protected from weathering but is within the limits of Service Class (SC) 3

Note to entry: sufficiently allowing for an equilibrium moisture content mc of less than 24%; see paragraph 6.1 (5)

Figure 3.2 is shown in greater detail in Annex D as Figure D.1.



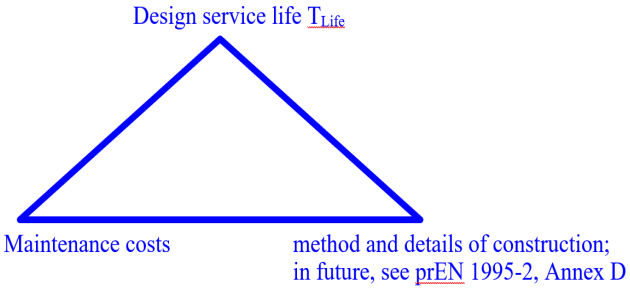
Key

membrane or weather-resistant layer

prEN 1995-1-1, Figure D.1 – Examples of protected timber bridges (extension of Figure 3.2):

1 Covered road bridge (with traffic inside)
2 Arch bridge (up) and trough bridge (down) with deck located at the base of the main bridge structure
3 Bridge with deck located above the main bridge structure, e.g.,
a) sealing system
b) timber-concrete-composite

Durability and thus sustainability ensure the economic viability of timber structures. Therefore, the following so-called "magic triangle" must be observed:



Basic structural timber preservation according to prEN 1995-1-1, prEN 1995-2, and national regulations (e.g., DIN 68800, DIN 1074, ZTV-ING)

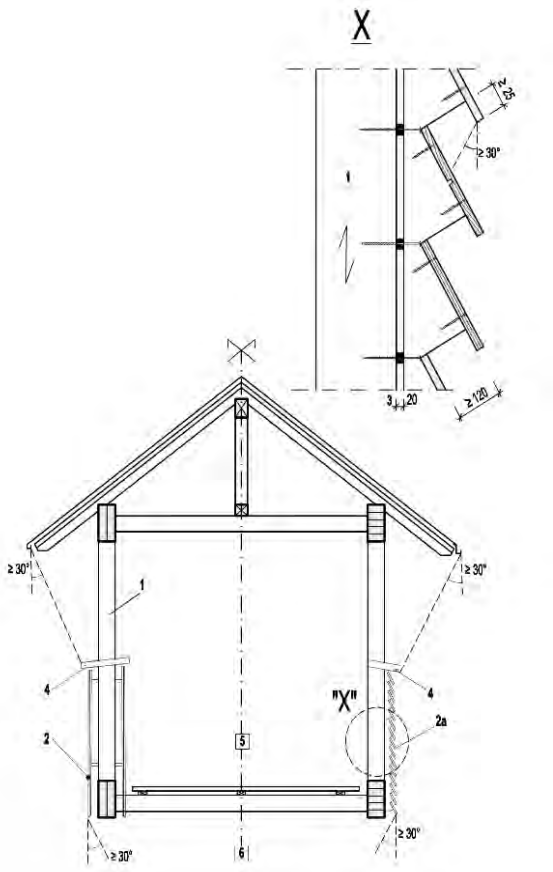
→ leads to a higher robustness



For this reason, the new EN 1995-2 shows users by means of concrete examples in Annex D how timber bridges can generally be protected: 5 possibilities for basic structural timber preservation, 3 examples for expansion joints, and 2 examples for connecting bridge caps to superstructures.

Furthermore, bridges of all materials are to be inspected at regular intervals. A monitoring can be helpful here. In the 11th drawing T-Mon, the example of an arch bridge is used to show at which points it makes sense to set up which monitoring systems – also with regard to the Use Class (UC) according to EN 355.

These examples in Annex D were also to be created in a language-neutral way. Therefore, each drawing in the prEN 1995-2 is on the next page followed by a key explaining the numbers and letters used in the drawing – as exemplified by the drawing T-Pos 1 below, with the drawing on the left and the key on the right.



Key to T-Pos 1

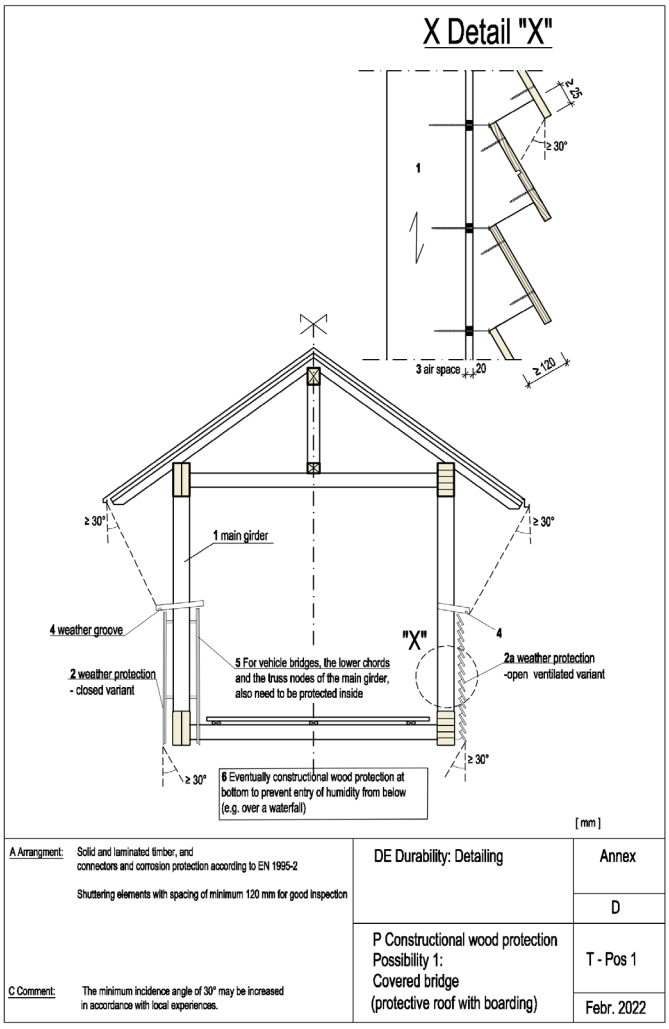
Annex

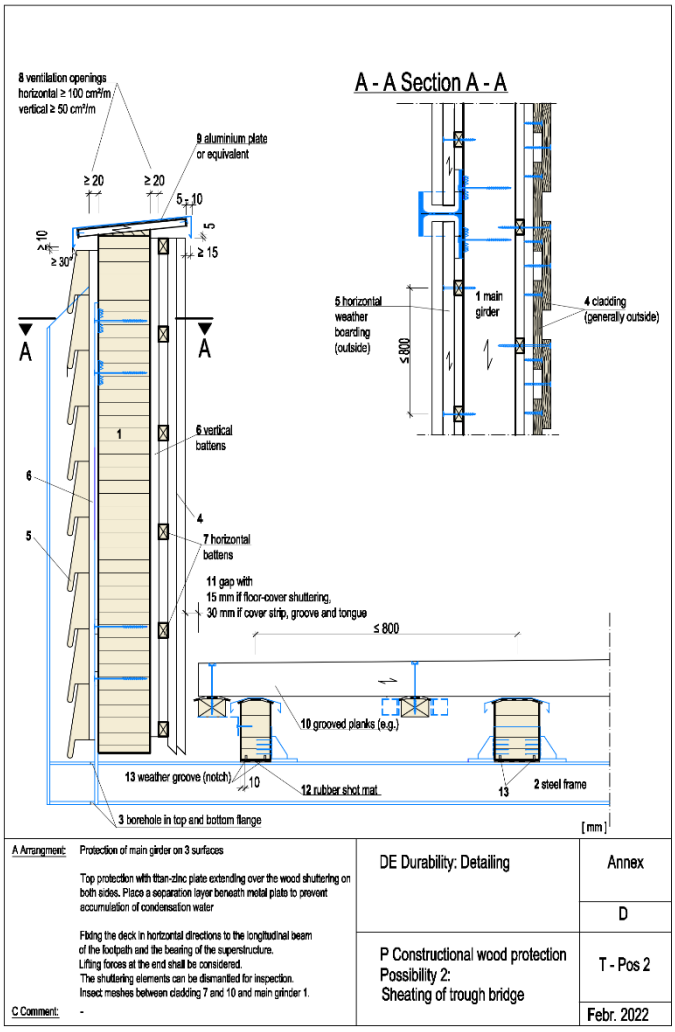
DE	Durability: Detailing	
P	Constructional wood protection Possibility 1: Covered bridge (protective roof with boarding)	
A	Arrangement:	Solid and laminated timber, and connectors and corrosion protection according to EN 1995-2 Shuttering elements with spacing of minimum 120 mm for good inspection
C	Comment	The minimum incidence angle of 30° may be increased in accordance with local experiences
X	Detail "X"	
1	main girder	
2	weather protection - closed variant	
2a	weather protection - open ventilated variant	
3	air space	
4	weather groove	
5	For vehicle bridges, the lower chords and the truss nodes of the main girder, also need to be protected inside	
6	Eventually constructional wood protection at bottom to prevent entry of humidity from below (e.g. over a waterfall)	

prEN 1995-1-1, Annex D – Durability, drawing T-Pos 1: Constructional wood protection
Possibility 1: Covered bridge (protective roof with boarding)

The lecture by Prof. Müller on the topics of durability / waterproofing systems / maintenance and inspection is followed by my second lecture, which provides additional information on the aforementioned 11 drawings (examples). To facilitate their understanding, the keys were here integrated into the drawings.

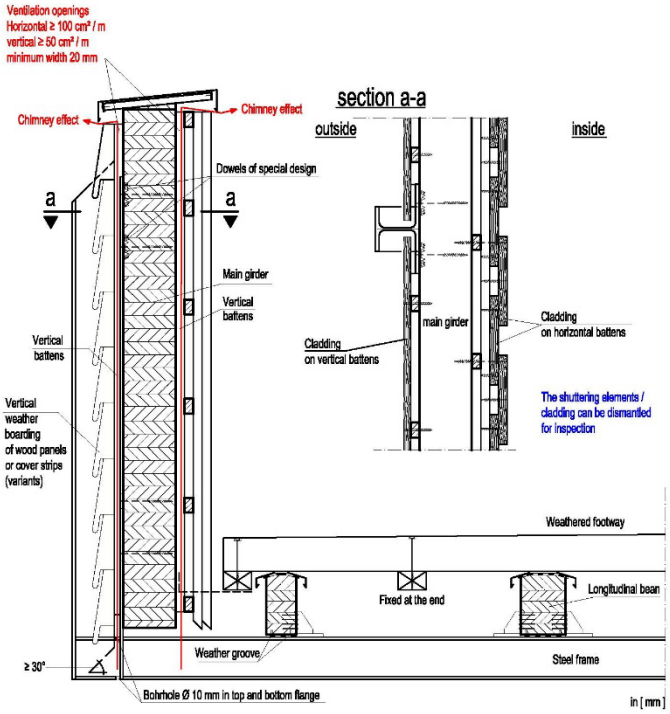


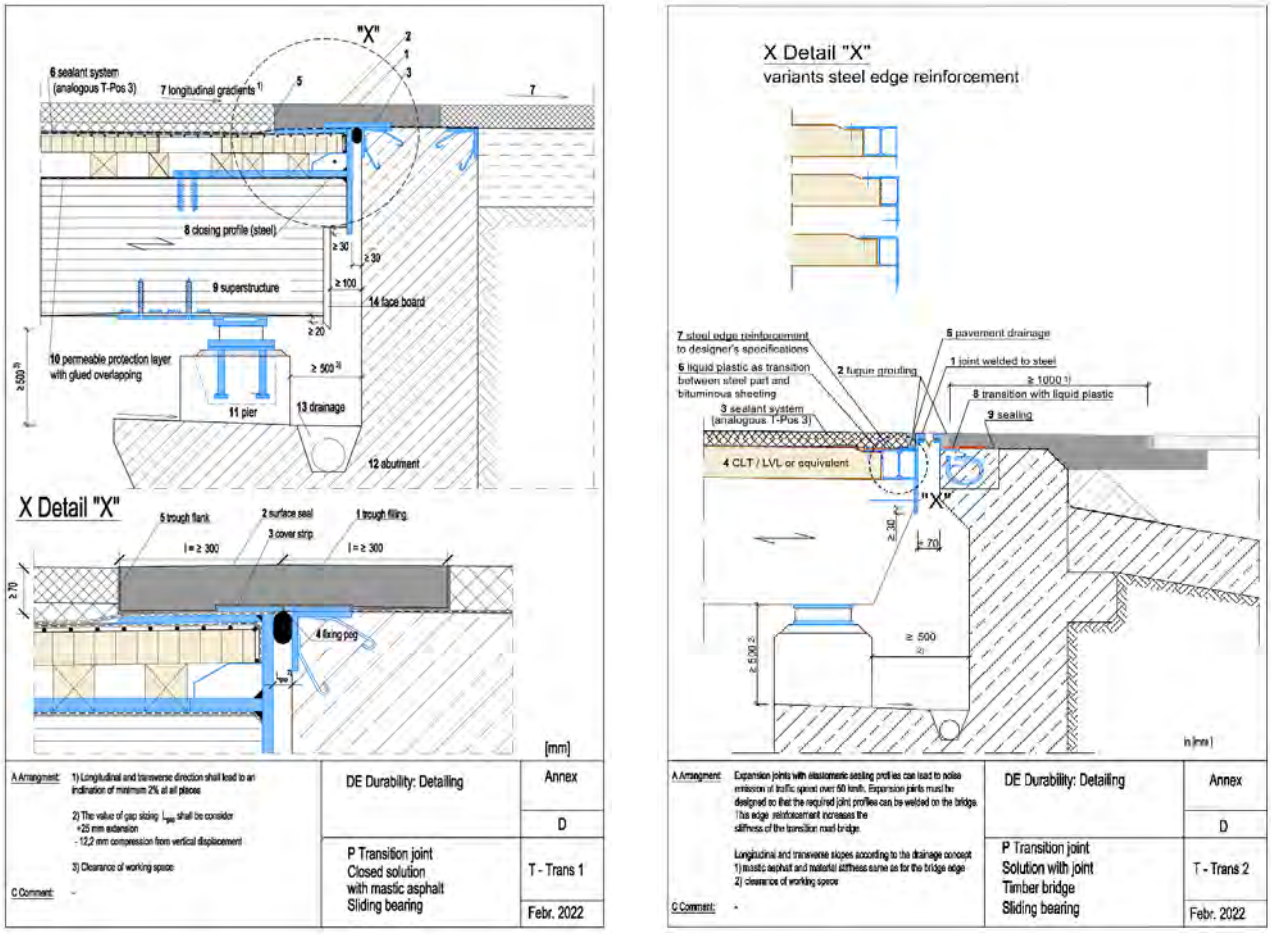


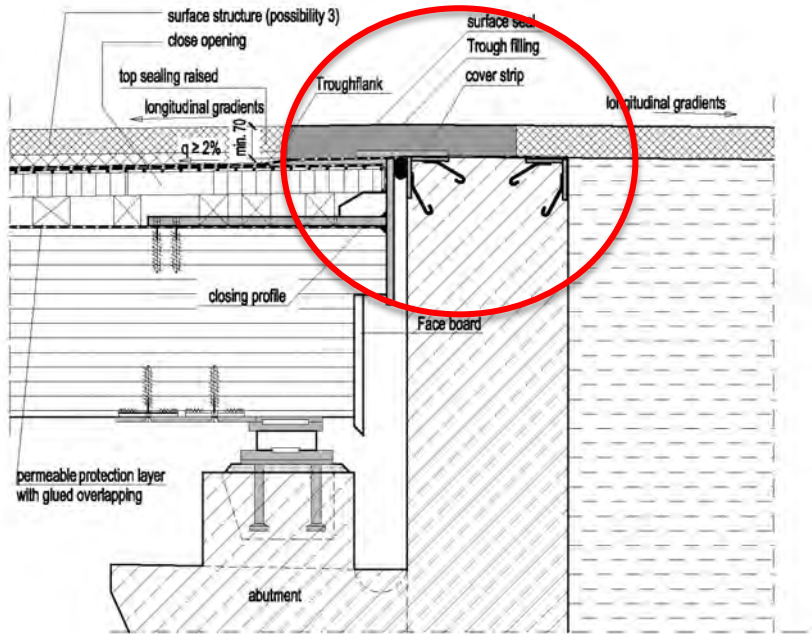


Possibility 2: Sheating of trough bridge

here: ventilation openings for chimney effect are shown







prEN 1995-1-1, Annex D – Durability, drawing T-Trans 1:
Transition road-bridge – here: closed transition joint is shown



The corrosion protection of steel fasteners in timber bridges is treated in Table 6.2 of prEN 1995-2; the protection of steel construction elements is dealt with in the series of standards Eurocode 3.

prEN 1995-2 – Table 6.2 – Timber exposure T_E-categories and atmospheric exposure C_E-categories with examples of minimum requirement for thicknesses for pure zinc coating, hot-dipped galvanized coating, and types of stainless steels for bridges (outdoor) with a design service life of 100 years [50 years]

Situation	**Timber exposure category** [a] **T_E**	**Service class SC**	**Atmospheric exposure category** [b] **C_E**	**Typical atmospheric exposure** [c] *(informative)*	**Examples of minimum**	
					zinc thickness	**stainless steel grade (type)** [d]
Protected outdoor with access of pollution	*T_E3*	*SC3*	*C_E2*	*L_{sea} > 10 km L_{street} > 100 m and/or low polluted area (< 5 µg/m³ of SO_2)*	*C_R2: 40 µm* [e] *(n.a.* [f] *if T_E4) [20 µm* [e] *(55 µm if T_E4)]*	*CRC II (e.g., 1.4301)*
	T_E3/T_E4	*SC3*	*C_E3*	*10 km > L_{sea} > 3 km 100 m > L_{street} > 10 m and/or medium polluted area (5 µg/m³ ≤ SO_2 ≤ 30 µm/m³)*	*C_R3: 110 µm [80 µm]*	*CRC III (e.g., 1.4401)*
	T_E3/T_E4	*SC3*	*C_E4*	*3 km > L_{sea} > 0,25 km L_{street} < 10 m and/or high polluted area (30 µg/m³ < SO_2 ≤ 90 µm/m³)*	*C_R4: n.a.* [f] * [110 µm]*	*CRC III (e.g., 1.4401)*
	T_E3/T_E4	*SC3*	*C_E5*	*L_{sea} < 0,25 km and/or very high polluted area (90 µg/m³ < SO_2)*	*C_R5: n.a.* [f] * [n.a.* [f] *]*	*CRC III (e.g., 1.4529)*
Permanent contact with ground or fresh-water [c]	*T_E5*	*SC4*	*n.a.* [f]		*C_R5: n.a.* [f] * [n.a.* [f] *]*	*CRC III to CRC V*

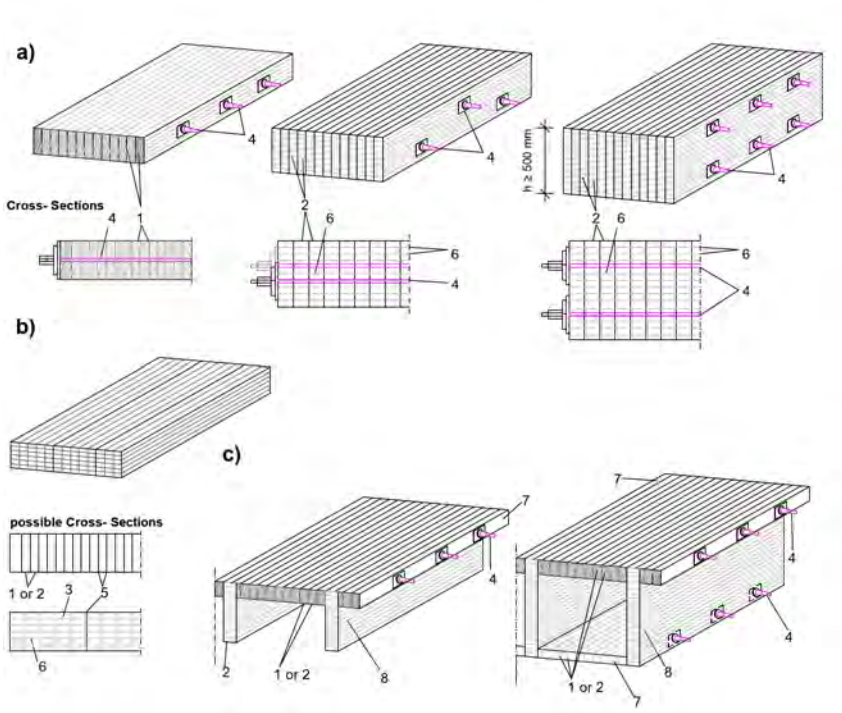
[a] *Timber exposure categories T_E3, T_E4, and T_E5 according EN 1995-1-1:202x, Table 6.1*
[b] *Atmospheric exposure categories C_E3, C_E4, and C_E5 according EN 1995-1-1:202x, Table 6.2 and 6.3*
[c] *The specified values for SO_2 are references values only and may vary.*
L_{sea} Indicates the distance from the sea. The actual exposure depends on the prevailing wind direction and the distance from the coast to saltwater seas e.g., Atlantic Ocean, North Sea, Baltic Sea, Mediterranean Sea, Black Sea, Irish Sea.
L_{street} Indicates the distance from roads with heavy traffic with de-icing salt
For T_E5/SC4 in case of seawater, each case should be evaluated individually.
[d] *Minimum corrosion resistance class for stainless steel grade shall be determined in accordance with EN 1993-1-4:2006/A1:2015*
[e] *CRC lll passivation may allow to reduce zinc thickness by 25%, and CRC Vl passivation by 50%*
[f] *not applicable*

4.2 Durability / Sealing / Maintenance / Inspection

Separate lecture by Prof. Dipl.-Ing. Andreas Müller

4.3 Timber Deck Plates

In Switzerland, you will probably all know the so-called QS construction method ("QS-Bauweise") developed by Prof. Gehri. Solid-wood beams are here arranged side by side in the direction of span and then clamped together by means of steel rods perpendicular to the grain direction (see Figure 8.1 a). As a result, the (punctual) wheel loads can be distributed over several beams (see Figure U.3). Nowadays, these deck plates (timber decks) are largely used in Scandinavian and Baltic states – and also made of laminated timber (GL) or cross-laminated timber (CLT), see Figure 8.1.



Key

a) Stress-laminated lumber or stress-laminated glulam (glued laminated timber) beams, prestressed, positioned edgewise

b) Glued laminated lumber or block glued glulam beams, positioned flatwise

c) Stress-laminated T-beams or stress-laminated box girder

1 Solid timber beam

2 Glulam beam

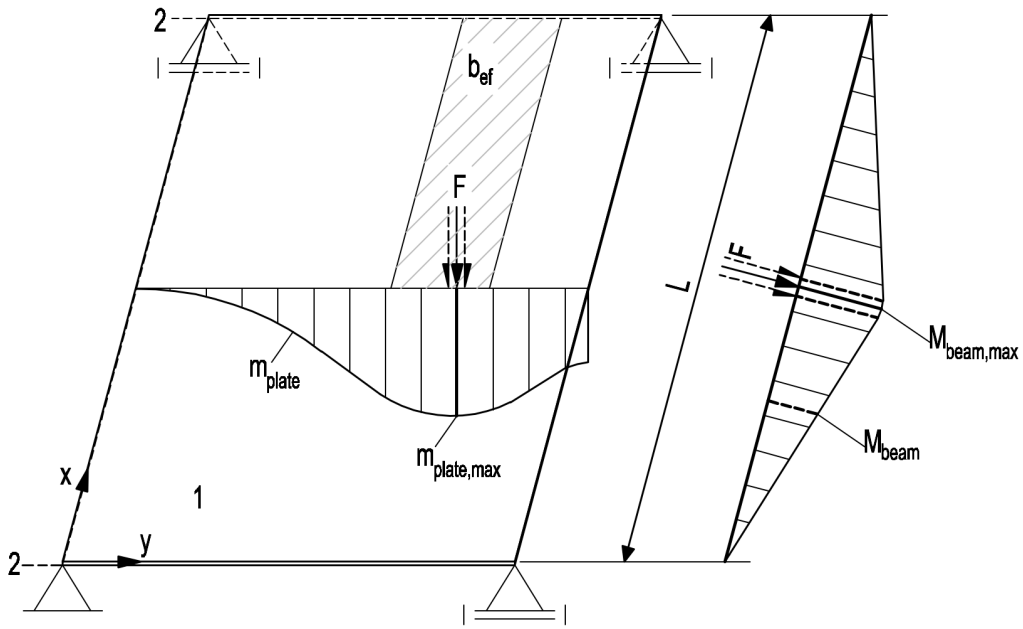
3 Block glued glulam beam

4 Prestressing bar or tendon

5 Glulam/GLVL beams as web

6 Planks, GLVL, or glulam beam as flange

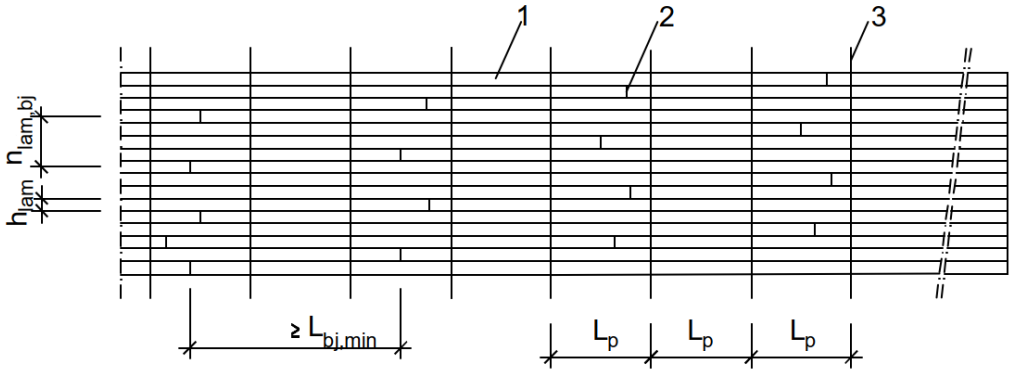
prEN 1995-2, Figure 8.1 Examples of timber decks for bridges made of lamellas (more examples than given in EN 1995-1-1, Annex U, Figure U.1)



Key

1	*Laminated timber deck*
2	*Support*
F	*Concentrated vertical load*
bef	*Effective width*
Mbeam	*Bending moment, calculated for a beam on two or more supports, in kNm*
Mbeam,max	*Maximum bending moment, calculated for a beam on two or more supports, in kNm*
mplate	*Bending moment, calculated by a numerical plate analysis, in kNm/m*
mplate,max	*Maximum bending moment, calculated by a numerical plate analysis, in kNm/m*

prEN 1995-1-1, Figure U.3 Example of bending moment distribution about y-axis in a plate for determining the effective width b_{ef}



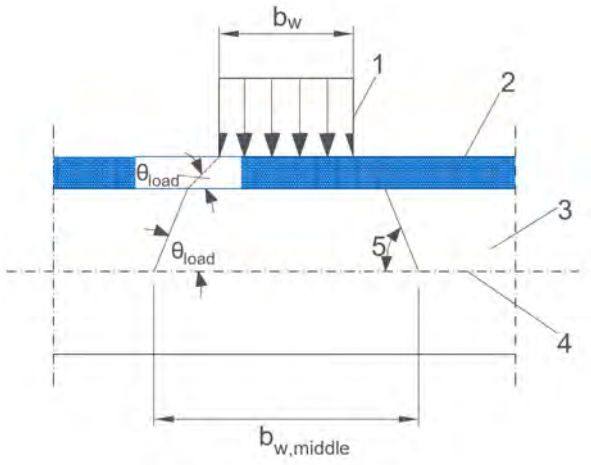
Key

1 Timber lamella
2 Butt-joint
3 Prestressing element

prEN 1995-1-1, Figure U.2 Butt joints in a prestressed-laminated timber deck with $n_{l,bj}$ = 4

In structural engineering, this system is used in so-called nail-laminated timber constructions. Both the automation of manufacturing processes and the desire for minimising timber waste are increasing, which raises the question of the influence of the butt joints (see Figure U.2) on the load-bearing capacity and the serviceability.

Figure U.4 illustrates the load distribution in in the longitudinal direction of the beam. If EN 1995-1-1 does not provide an angle of dispersion in horizontal direction for the laminated timber deck $\theta_{load,2}$, it should be taken as angle ß from EN 1991-2, 6.3.



Key

1	*Pressure*
2	*Pavement or planks*
3	*Laminated timber deck*
4	*Centroid (middle) plane*
b_w	*Width of the loaded area at the top of the pavement, in mm*
$b_{w,middle}$	*Width of the loaded area at the middle plane of the laminated timber deck, in mm*
$\theta_{load,1}$	*Angle of dispersion to the horizontal for the pavement or planks, in degrees;* $\theta_{load,1}$ *may be taken as* 45^o
$\theta_{load,2}$	*Angle of dispersion to the horizontal for the laminated timber deck, in degrees;* $\theta_{load,2}$ *may be taken as* 45^o *parallel and* 15^o *perpendicular to grain*
NOTE	*For CLT, the angle of dispersion is* 35^0 *in both directions, see 8.1.6.1(9).*

prEN 1995-1-1, Figure U.4 Dispersion of concentrated loads

In a query, most European states decided to take over the design methods, which the PT6 had adopted from prEN 1995-2:2010, into the normative Annex U of the main part of the new prEN 1995-1-1. The same applies to the compilation of numeric procedures for calculating the cut sizes of deck plates according to a plate theory. In a slightly generalised way, these basics were taken over into Annex V for prEN 1995-1-1.

For glulam decks, the bending stress perpendicular to grain caused by a concentrated load should be determined by a plate theory and limited to the tensile capacity perpendicular to the grain to Formula (8.7): $\sigma_{m,z,d} \leq f_{t,90,d}$, where $\sigma_{m,z,d}$ is the design bending strength of the glulam deck perpendicular to grain, and $f_{t,90,d}$ is the design tensile strength perpendicular to grain.

prEN 1995-1-1, Annex U, U.7, provides a simplified analysis for stress-laminated timber decks for system strength. When using the simplification, the minimum long-term residual compressive force $F_{p,min}$ due to prestressing between laminations shall be not less than 80 kN/m for bridges.

Stressing rods and bars of steel are given in Annex E (Dimensional Changes due to environmental effects), E4.3. The stress behind the anchorage plates should be verified by prEN 1995-1-1, 8.2.1.

Massive timber bridge decks may be regarded as continuously supported members. h may be taken as 280 mm (Figure 8.1 a). k_p may be set to Case B; see EN 1991-1-5, Table 8.1.

For circular anchorage plates, l_c may be set to $0{,}75 \cdot r$, where r is the radius of the circular plate.



In prEN 1995-2, 9.1, are given coefficients of friction μ between softwood timber laminations, and between softwood timber laminations and concrete, unless other values were verified. Taking into account irreversible deformations of prestressed timber decks, the values in Table 9.1 should be used only in outdoor structures.

	Perpendicular to grain	***Parallel to grain***
Lamination surface roughness	μ_{90}	μ_0
	[-]	*[-]*
Sawn timber to sawn timber	*0,40*	*0,30*
Planed timber to planed timber	*0,30*	*0,25*
Sawn timber to planed timber	*0,40*	*0,30*
Timber to concrete	*0,40*	*0,40*

prEN 1995-1-1, Table 9.1 Values of the coefficient of friction μ for softwood

The prestressing of timber decks is intended to prevent cupping of the deck sides due to moisture changes. Depending on the bridge span, a minimum force $F_{cupping}$ that constrains cupping at each transversal support may be taken into account as given in Formula (E.2) in Annex E.

Longitudinal fixated timber decks without an expansion joint may be designed by taking the forces from suppressed expansion on the abutment into consideration. E4.2 gives guidance on the minimum stress to be taken into account.



4.4 Timber-concrete Composites (TCC)

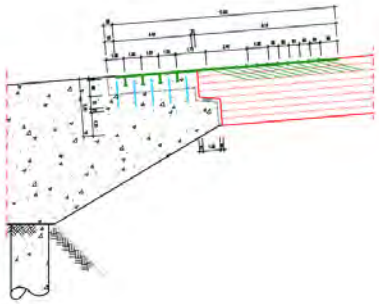
Timber-concrete-composites (TCC), prEN 1995-2, Annex A

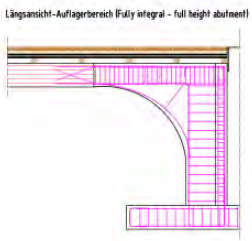
Separate lecture by Prof. Dr.-Ing. Jörg Schänzlin

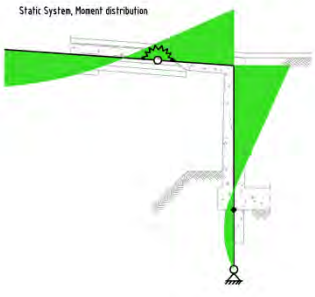
Integral bridges

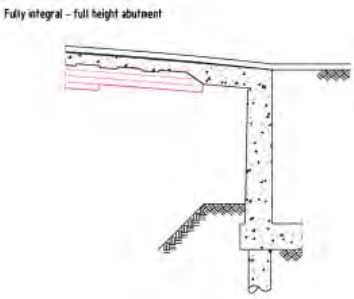


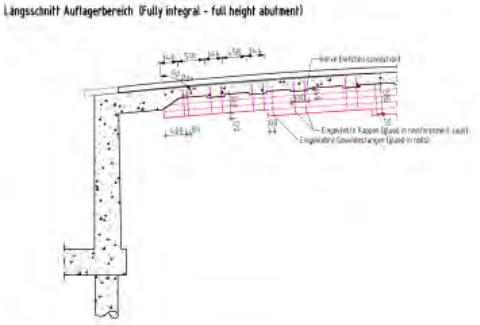


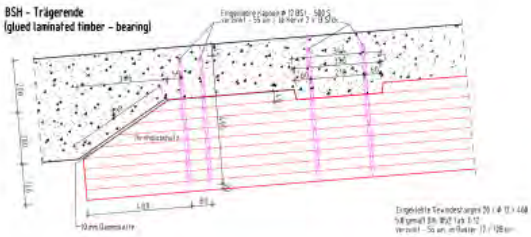


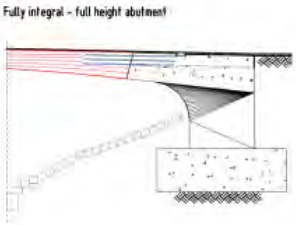


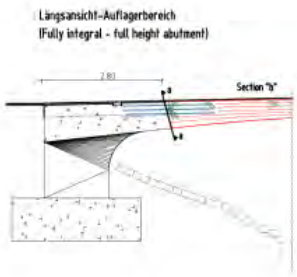


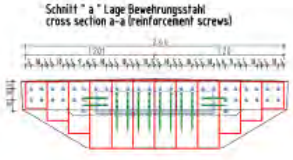


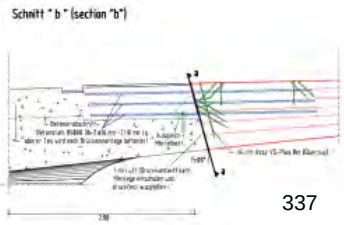














4.5 SLS: Deflections, Deformations

Deflections due to traffic-load and wind-force actions should be verified and limited in order to prevent unwanted dynamic impact due to traffic, infringe of required clearances, cracking of surfacing layer, and damage the drainage.

NOTE: Deflections of timber bridges are generally larger than those of bridges made of steel or concrete, due to the relatively low E-modulus of timber and the relatively low slip modulus typical of timber connections. The range of limiting values for beams, plates, or trusses with span L is given in Table 9.2. The recommended values are underlined. The application of these values can be chosen nationally and must then be specified in the National Annex. If the National Annex contains no information on the application, the values in Table 9.2 shall be used.

The maximum elastic deformation under variable load should be specified for comfort. The consideration of creep deformations may be omitted.

Table 9.2 (NDP) Limiting values for deflections of beams, plates, and trusses

Action (Frequent load value)	**Range of Limiting Values**	
	vertical	horizontal
Traffic loads on road bridges [1)]	<u>*L*/500</u> to *L*/650	-
Traffic loads on footways, cycle tracks and footbridges	<u>*L*/500</u> to *L*/900	-
Wind forces	-	<u>*L*/600</u> to *L*/1500
1) In the design, the vehicle may be positioned in the middle of a lane for laminated timber decks and positioned as close to the deck edge as possible for ancillary structural elements.		

In addition, the requirements for long-term deformations under permanent load including creep effects should be regarded.
The pre-camber should be at least equal to the long-time deformations caused by dead loads and quasi-permanent parts of life loads.
A pre-camber should be given to flat bridges due to water drainage issues and aesthetic reasons.

In 6.2 (1) NOTE, additional limits are given for sealing systems.

To prevent local damage to the sealant system of a bridge deck, the longitudinal tensile strain should not exceed the characteristic tensile strain capacity of the sealant membrane. If no information on the strain capacity is available, a value of 1,5‰ in the top surface of the deck may be used. The characteristic load combination should be used.

4.6 SLS: Oscillations, Damping

Vibrations, damping, simplified verification

Online lecture by Prof. Dr.-Ing. Patricia Hamm



4.7 Fatigue

The first proposal made by the project team SC5.T6 was to move the three subclauses A.1 (General), A.2 (Basic requirements and methods), and A.3 (Fatigue verification) of EN 1995-2:2010 Annex A (informative) into the main body (normative) of the new version of EN 1995-2:202x, Clause 10.
Having discussed several other verification models (see background paper), it was decided to "go back" to the old k_{fat}-model as it is in the current version of EN 1995-2:2010. Later, the plenary of TC 250 / SC 5 decided to move the major part of Clause 10 from prEN 1995-2 to prEN 1995-1, Clause 10. The reason is that the phenomenon of fatigue does not concern only timber bridges but any kind of timber structures, including towers for wind turbines, highway traffic sign posts, or bell towers. This means that in EN 1995-2, only those parts were kept that are relevant for timber bridges, in particular:

- some general parts concerning the fatigue assessment of timber structures
- parts of the document that deal with fatigue load models
- a simplified fatigue verification model especially for bridges

The k_{fat} values were determined for a "worst-case two-lane bridge" with a defined design service life. Adopting the k_{fat} values determined according to this model would correspond to the regular k_{fat} verification and would always be on the safe side (if the design service life and thus the maximum number of load cycles are not exceeded).

Since the k_{fat} values depend on R, a simplification is also required to offer a real advantage over the 'full' k_{fat} verification. Therefore, it is proposed to consider only whether the fatigue loading is alternating or not and to use the k_{fat} values for R = 0 or R = -1, respectively.

The k_{fat} values were evaluated according to current Annex A in EN 1995-2:2010 for $2*2*10^6$ trucks per year (worst case acc. to current EN 1991-2 Table 4.5, two lanes considered), 100 years design service life (according to Table 4.1 in the current draft), and ß = 3 (substantial consequences). This yields a design load cycle number of $1.2*10^9$.

	Compression	***Bending, tension and reversed axial***	***Connections with dowels***
$-1 \leq R < 0$ *(reversed loading)*	-	*0,13 [0,08]*	*0,04 [-]*
$0 \leq R$ *(non-reversed loading)*	*0,52 [0,49]*	*0,17 [0,13]*	*0,28 [0,24]*

prEN 1995-1-1, Table 10.1 Reduction factors k_{fat} for simplified verification for ß = 1 [ß = 3]

4.8 Earthquakes

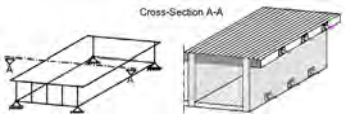
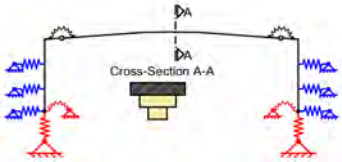
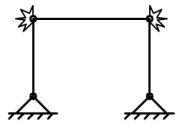
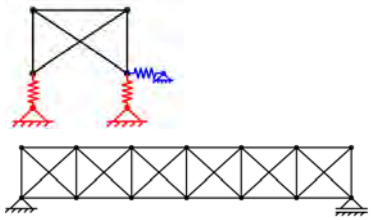
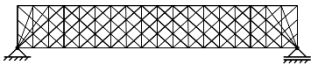
The Informative Annex C of prEN 1995-2 provdes supplementary information to EN 1998-2 Annex C on the design of

1. bearings and
2. timber bridges in low seismic areas.

NOTE: National choices regarding the application of this Informative Annex can be given in the National Annex. If the National Annex contains no information on the application of this Informative Annex, it can be used.

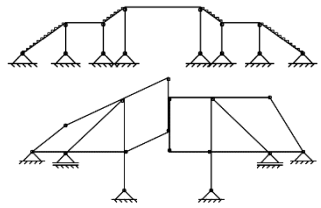
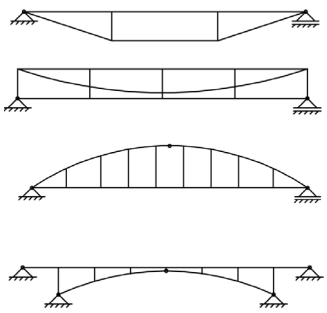
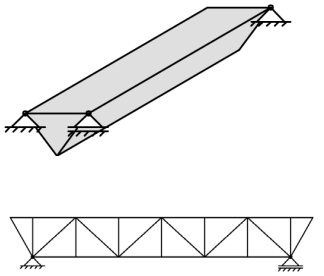
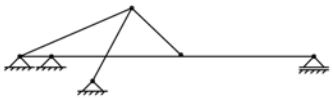
Annex C should be used for the design of timber bridges of the types indicated in prEN 1998-2, Table C.1, for horizontal earthquake action.



Examples of structural types of timber bridges	***Bridge type / used span L***	***Similar to building type in EN 1998-1-2 Table 13.1***	***Structural system; source of energy dissipation / ductility (if any)***	*NOTE: values to identify or to calculate*
	*c-b) Prestressed deck plates (materials see EN 1995-2 Figure 3.5; with solid or glulam or CL elements) L ≤ 25 m*	*c) Log structures*	*Single-span or continuous girder with friction between the beams or torsion-spring coupling*	*1st eigenfrequencies: horizontal + vertical + torsion (if hollow cross-section)*
 *see Figure C.1 as well*	*d-b) Integral abutment bridges L ≤ 45 m* *For embedding of the abutments and piles see paragraph C.2 (3)*	*d) Moment-resisting frame (MRF) structures (longitudinal direction of the bridge)*	*Frame with minimum two moment-transmitting joints with dowel-type fasteners / fastener plasticization*	*Torque hinges and/or embedding into ground* *For modelling soil, embedding of the abutments and Piles see paragraph C.2 (3)*
	*d–b) Portal frames of bridges (part of the bridge; e.g., entrance) L ≤ 10 m*	*d) Moment-resisting frame (MRF) structures (transverse direction of the bridge)*	*Frame with minimum two moment-transmitting joints with dowel-type fasteners / fastener plasticization*	*As for the main bridge*
	*e–b) Strutted (or truss) frame bridges with dowel-type connections L ≤ 50 m*	*e) Braced frame structure with dowel-type connections (longitudinal direction of the bridge)*	*Multi-span girder; joints between girder and piers with dowel-type fastener connections / fastener plasticization*	*1st eigenfrequencies: horizontal + vertical*
	*e–b) Timber pier made of a truss system (part of the bridge or the abutment) L ≤ 10 m* *Horizontal bracings of bridges (part of the bridge) L ≤ 90 m*	*e) Braced frame structure with dowel-type connections (transverse direction of the bridge)*	*Timber frame with dowel-type fastener connections / fastener plasticization*	*As for the main bridge* *For modelling soil, embedding of the abutments, and piles, see paragraph C.2 (3)*
	*g–b) Lattice-girder bridges (tunnel) protected by claddings fixed with nails or screws, face behaviour as box-type member L ≤ 90 m*	*g) Braced frame structures with carpentry connections and masonry infill*	*Single-span girder*	*1st eigenfrequencies: horizontal + vertical*

prEN 1998-2, Table C.1 (Part 1) Examples of structural types of timber bridges

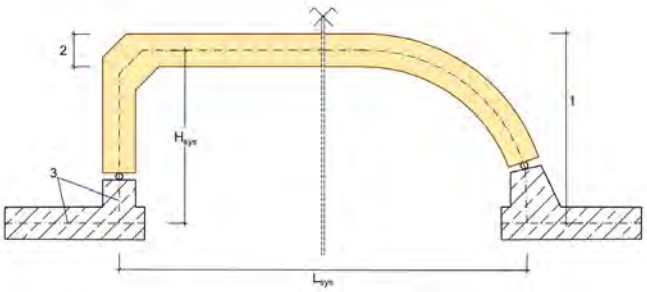


Examples of structural types of timber bridges	***Bridge type / used span L***	***Similar to building type in EN 1998-1-2 Table 13.1***	***Structural system; source of energy dissipation / ductility (if any)***	*NOTE: values to identify or to calculate*
	*h-b) Crossings;* *Draw bridges* *$L \leq 40$ m*	*h) Braced frame structures with carpentry connections*	*Strut and tie model; Modal mass*	*Eigenfrequencies* *horizontal + vertical + torsion*
	*i–b) Tied-arch bridges $L \leq 40$ m; suspension bridges $L \leq 50$ m; arch bridges with or without hangers $L \leq 90$ m; spandrel-braced bridges $L \leq 90$ m*	*i) Two-pin and three-pin arches, three-pin frames and dome structures*	*Single-span girder*	*1st eigenfrequencies: horizontal + vertical*
	*k–b) Hollow-box-girder bridges $L \leq 80$ m;* *Truss bridge $L \leq 150$ m*	*j) Large-span timber truss portal frame structures*	*Single-span girder*	*1st eigenfrequencies: horizontal + vertical + torsion*
	*k–b) Stressed ribbon bridges $L > 150$ m*	*j) Large-span timber truss portal frame structures*	*Continuous girder*	*1st eigenfrequencies: horizontal + vertical + torsion*
	*l–b) Cable-stayed bridges / Constructions with pylons* *$50 \text{ m} \leq L \leq 200$ m*	-	*Continuous girder*	*1st eigenfrequencies: horizontal + vertical + torsion (sometimes); effective modal mass*

prEN 1998-2, Table C.1 (Part 2) *Examples of structural types of timber bridges*

The drawings in EN 1998-2 Table C.1 depict the wooden or steel part of a structure.

In addition to bridge type d–b) “Integral abutment bridges,” see Figure C.1.



Key:
1 Height H for the design of the seismic earth pressure
2 Construtions Height h
3 System axis

(1)

Figure C.1 *Examples for the system length and height of frame constructions*

Type of ductile members of timber bridges	*Ductility class*			
	DC1	*DC2*		
	$q=q_s$	q_R	q_D	$q = q_S \cdot q_D \cdot q_R$
*c–b) Prestressed deck plates with solid or glulam or CL elements *)*	*1,5*			
- face sides of the beams not raised with glue; only friction		*1,1*	*1,2*	*2,0*
- others		*n.a.*	*n.a.*	*n.a.*
d–b) Moment-resisting frame structures, including portal frames, and integral abutment bridges	*1,5*	*1,1*	*1,3*	*2,2*
e–b) Strutted (or truss) frame bridges with dowel-type connections, timber piers, bracings of bridges	*1,5*	*1,0*	*1,3*	*2,0.*
f–b) Timber pier fixed on foundation	*1,5*	*1,1*	*1,2*	*2,0*
*g–b) Braced frame structures with carpentry joints *), protected by claddings fixed with nails or screws, face behaviour as with box-type member*	*1,5*	*1,1*	*1,2*	*2,0*
h–b) Crossings, draw bridges	*1,5*	*n.a.*	*n.a.*	*n.a.*
i–b) Tied-arch bridges, suspension bridges, two-pin and three-pin arches with or without hangers, spandrel-braced bridges	*1,5*	*n.a.*	*n.a.*	*n.a.*
k–b) Hollow-box-girder bridges, large-span timber truss portal frame structures	*1,5*	*n.a.*	*n.a.*	*n.a.*
l–b) Cable-stayed bridges	*1,5*	*n.a.*	*n.a.*	*n.a.*

**) The structural types c–b) and g–b) may be designed to DC 2 only for values of the seismic action index S_δ greater 4 m/s^2.*

n.a.: not applicable

prEN 1995-2, Table C.2 - Default values of q for timber bridges in areas of low seismic action



The values highlighted in yellow for bridge types c–b) and g–b) supplement EN 1998-2, Table C.2, and apply only in low seismic areas.

If Table C.2 contains different q-values for the longitudinal and for the transverse direction of the bridge, the q-value in the longitudinal direction should be used for modelling the system.

The supplementary information on the design of bearings is valid for bridges of all materials. Especially for light footbridges made of timber and steel, it has to be ensured that they do not slide down from the abutment due to a vertical impulse.

4.9 List of current NDPs in EN 1995-2

No.	Clause in EN 1995-2:2004	Corresponding clause in prEN 1995-2	Parameter e.g. characteristic values of self-weight	Recommended value e.g. nominal value	Category of NDP · Essential NDP · Other NDP	Status Retained Removed New	Comment Please provide: · justification for the retention of other NDPs; · confirmation as to whether consensus has been reached on NDPs to be removed; · justification for the introduction of new NDPs.
1		4.1.2.1 Table 4.1	Design service life	nominal value	Essential NDP	New	Design service life; see prEN1990-2 Annex A2
2	2.3.1.2 (1)	4.3.1.3 Table 4.2	Load-duration classes	nominal value	Essential NDP	Retained	Load-duration assignment
3	2.4.1	4.4.2 (1)	Characteristic material values	nominal value	Essential NDP	Retained	Partial factors for material properties; all factors should be mentioned in EN 1995-1-1
4	7.2.	9.3 Table 9.2	Limiting values for deflection	nominal value	Essential NDP	Retained	Limiting values for deflection
5	7.3.1 (2)	9.4.1.5 Table 9.4	Values of damping ratios	nominal value	Essential NDP	Retained	Damping ratios
7		B.1 (1)	Requirements for Insepection and Mainanance	Annex B (informative): Inspection and Maintenance of Timber Bridges	Essential NDP	New	To fulfill the requirements of a design service life of 100 years (see NDP No. 1) it is necessary especially for timber structures to have inspection and maintenance
8		Annex C	Additional information on Timber Bridges in zones with low seismicity action	Annex C (informative): Additional Information on Timber Bridges under Seismic Loads	Other NDP	New	EN 1998-2 does not reflect the input from the timber bridge specialists
9		Annex D	Because of readability / ease of use: Full page figures are given in Annex D instead of having these figures in the main text; the main text refers to the single figures	Annex D (informative): Examples for Detailing	Essential NDP	New	To fulfill the requirements of a design service life of 100 years (see NDP No. 1) it is necessary also to give detailed information how to protect timber bridges. The protection of timber bridges and the regular maintenance at least refer to safety – and not to execution. Other Examples can be added by national choice (NCI) to Annex D.
10		Annex E	Variations in temperature and moisture content; Dimensional Changes of elements	Annex E (informative): Dimensional Changes due to environmental effects	Other NDP	New	Temperature, moisture content, and therefor dimensional Changes of elements differ from country to country (see TS Annex A)
							30.11.2021

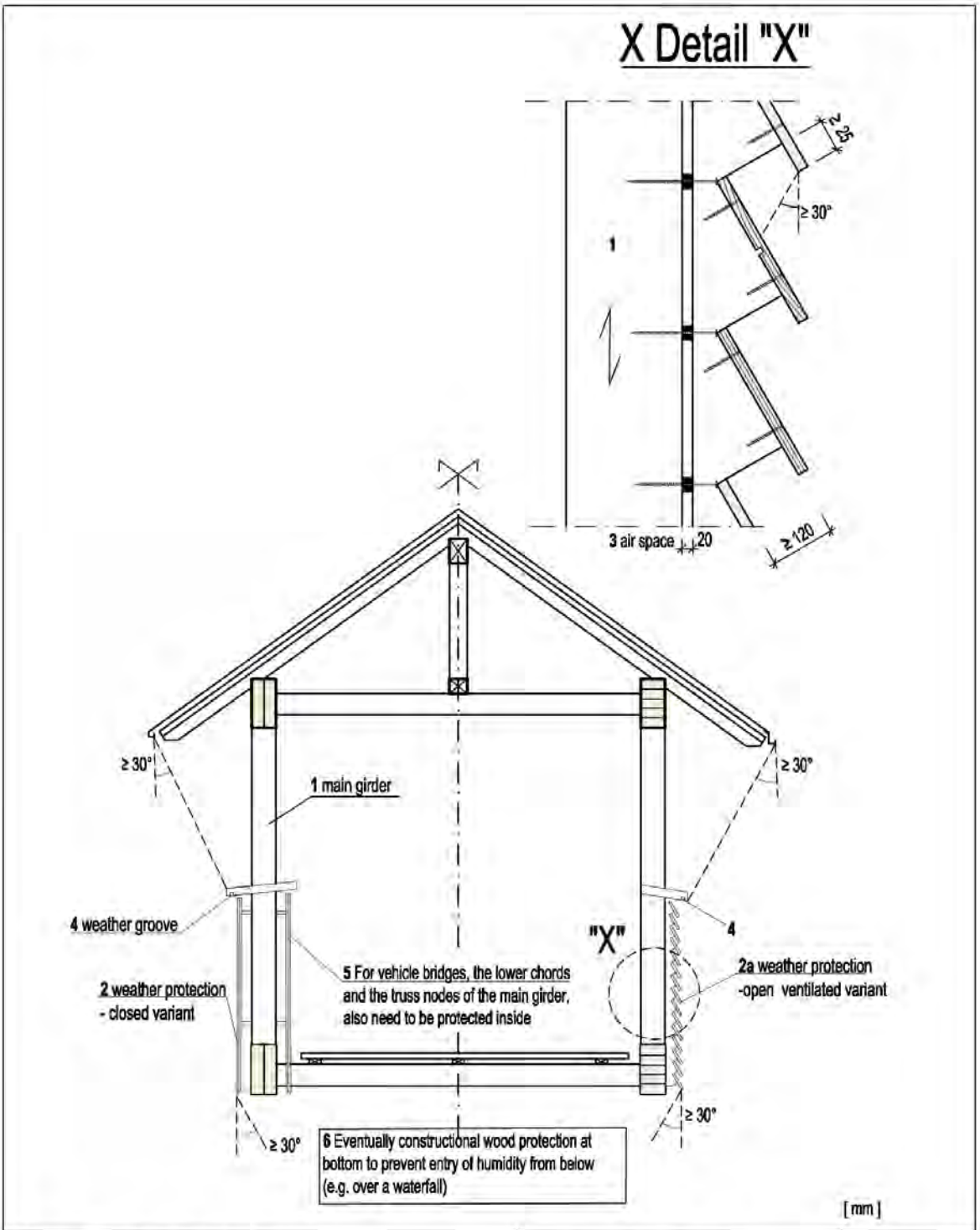


5 Perspective

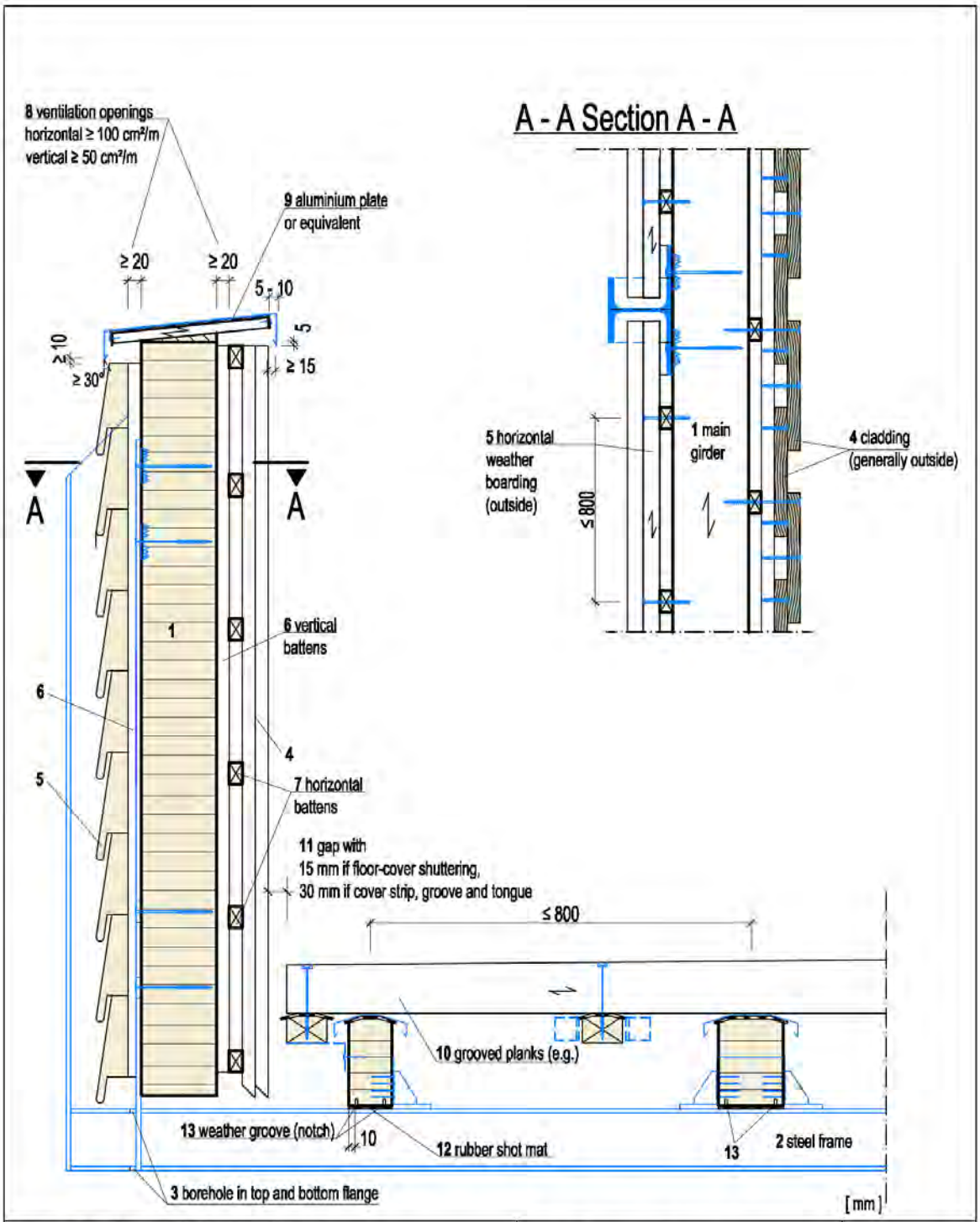
The completion of the work on the European timber construction standards scheduled for 2025 or 2026 still seems far-off, and the national application documents will probably only be available in 2027, but most of the essential changes are already known. The scope of the standard will inevitably grow, as new timber construction products need to be considered and known design approaches need to be extended and optimised. The update is guided by the central interest of increasing the user-friendliness – not only by profiting from digital availability and efficient search options but also by restructuring, homogenising, and simplifying the regulations. Nevertheless, as with the adjustment of the first generation of Eurocode 5, an additional process of learning, training, and education will be necessary, with this process starting already prior to the final publication. In conclusion, it may be stated: the second generation of Eurocode 5 is not a revolution but an evolution that consistently builds on the experiences and principles of the previous version.

6 Literature

[1] Schenk, M.; Werther, W.; Gerold, M. 2022 The Next Generation – Die Weiterentwicklung der Holzbaubemessun nach Eurocode 5.In: Quadriga, H.

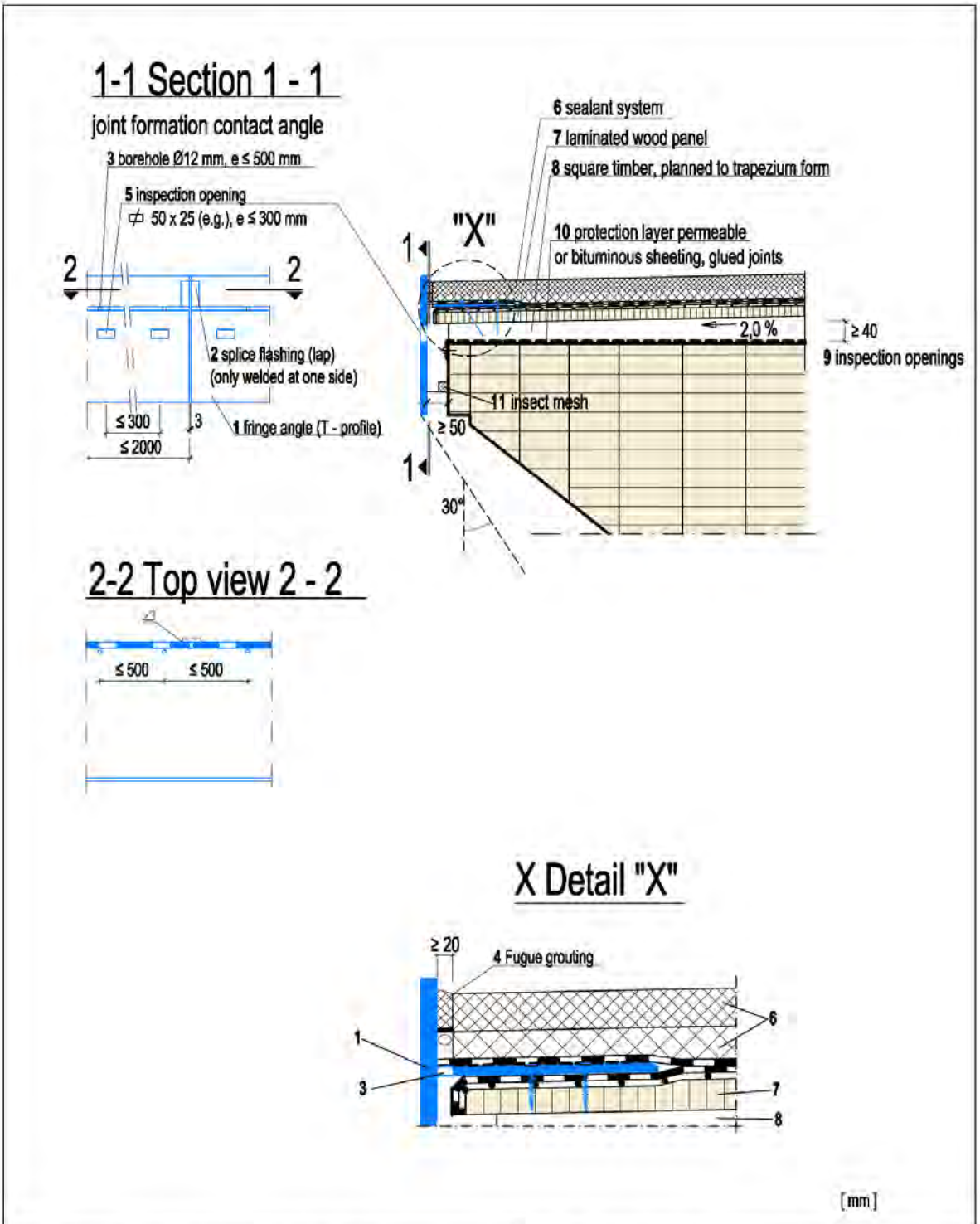


A Arrangment: Solid and laminated timber, and connectors and corrosion protection according to EN 1995-2 Shuttering elements with spacing of minimum 120 mm for good inspection	DE Durability: Detailing	Annex D
C Comment: The minimum incidence angle of 30° may be increased in accordance with local experiences.	P Constructional wood protection Possibility 1: Covered bridge (protective roof with boarding)	T - Pos 1 Febr. 2022

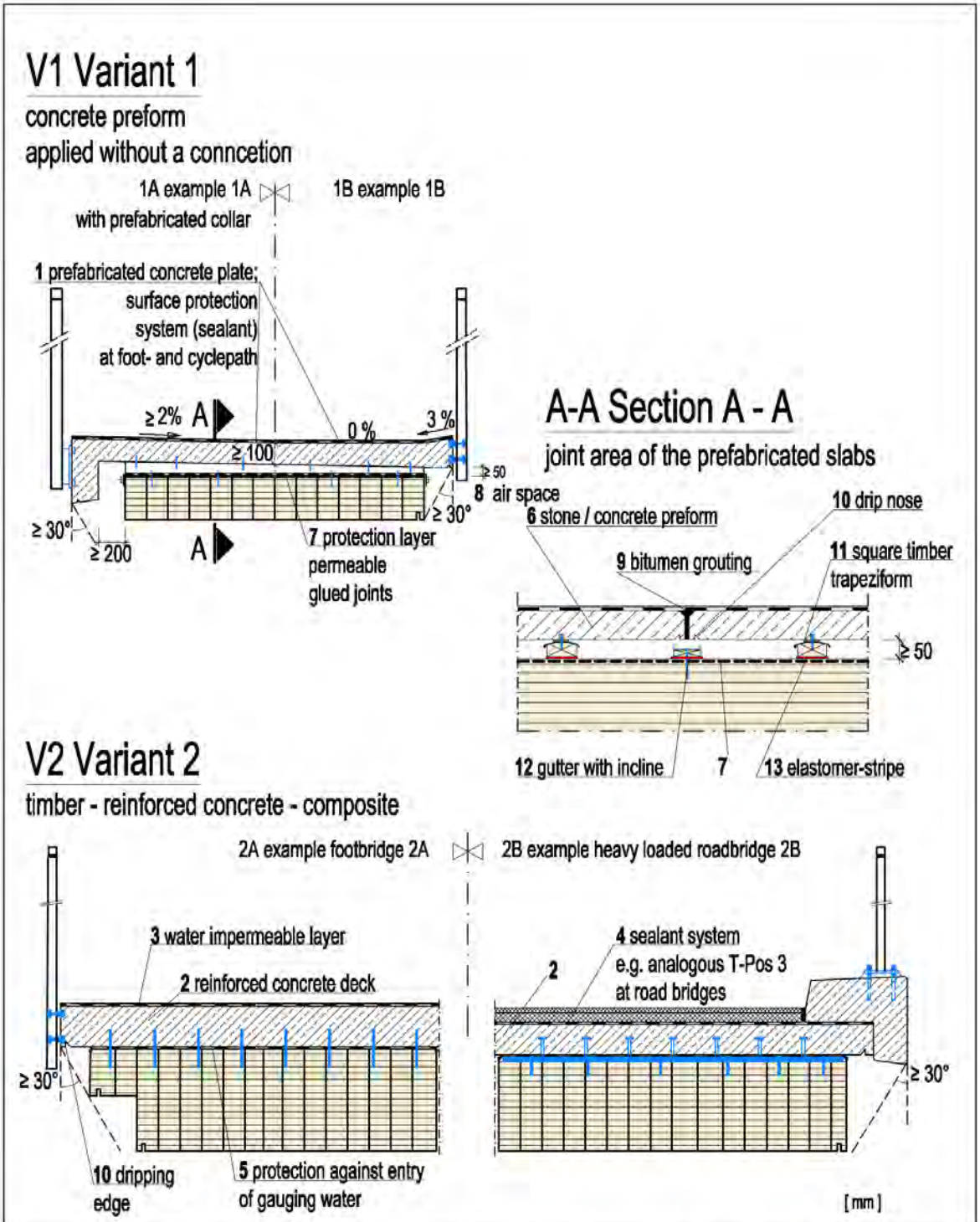


A Arrangment: Protection of main girder on 3 surfaces Top protection with titan-zinc plate extending over the wood shuttering on both sides. Place a separation layer beneath metal plate to prevent accumulation of condensation water Fixing the deck in horizontal directions to the longitudinal beam of the footpath and the bearing of the superstructure. Lifting forces at the end shall be considered. The shuttering elements can be dismantled for inspection. Insect meshes between cladding 7 and 10 and main grinder 1. C Comment: -	DE Durability: Detailing P Constructional wood protection Possibility 2: Sheating of trough bridge	Annex D T - Pos 2 Febr. 2022

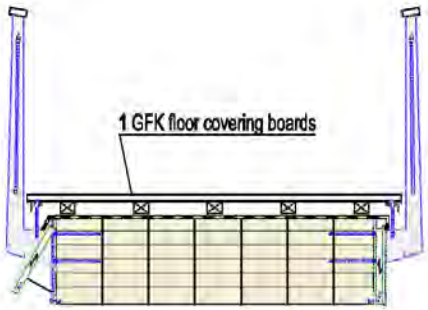



1-1 Section 1 - 1
joint formation contact angle
3 borehole Ø12 mm, e ≤ 500 mm
5 inspection opening
⊄ 50 x 25 (e.g.), e ≤ 300 mm
2
2
2 splice flashing (lap)
(only welded at one side)
≤ 300
≤ 2000
3
1 fringe angle (T - profile)
"X"
1
1
6 sealant system
7 laminated wood panel
8 square timber, planned to trapezium form
10 protection layer permeable
or bituminous sheeting, glued joints
2,0 %
≥ 40
9 inspection openings
11 insect mesh
≥ 50
30°
2-2 Top view 2 - 2
≤ 500
≤ 500
X Detail "X"
≥ 20
4 Fugue grouting
1
3
6
7
8
[mm]
A Arrangment:
Distance of bituminous road transitions normally every 50 m
The fringe angle has to be lapped in distances of 2 m maximum.
C Comemnt:
Avoid blistering on the bottom: e.g. by limiting the maximum thickness of the protection layer to 25 mm
Wearing boards should be provided on bridges with wooden pavements.
Disposition of bridge drains when necessary.
Construction of the deck layers and details according to national regulations
The installation of a monitoring system for surveillance and early warning of leakages in the sealing surface is recommended - especially if there are no horizontal ventilation and inspection openings.
The inspection openings with insekt mesh or equivalent may be omitted if there are other control mechanisms, e.g. monitoring systems.
DE Durability: Detailing
Annex
D
P Constructional wood protection
Possibility 3:
Closed road surface
Sealant systems
T - Pos 3
Febr. 2022



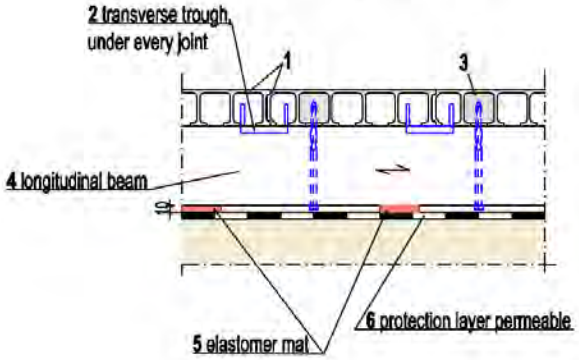

V1 Variant 1
concrete preform
applied without a conncetion
1A example 1A
with prefabricated collar
1B example 1B
1 prefabricated concrete plate;
surface protection
system (sealant)
at foot- and cyclepath
≥2%
A
0 %
3 %
≥100
≥50
8 air space
≥ 30°
≥ 30°
≥ 200
A
7 protection layer
permeable
glued joints
A-A Section A - A
joint area of the prefabricated slabs
6 stone / concrete preform
10 drip nose
9 bitumen grouting
11 square timber
trapeziform
≥ 50
12 gutter with incline
7
13 elastomer-stripe
V2 Variant 2
timber - reinforced concrete - composite
2A example footbridge 2A
2B example heavy loaded roadbridge 2B
3 water impermeable layer
2 reinforced concrete deck
4 sealant system
e.g. analogous T-Pos 3
at road bridges
2
≥ 30°
≥ 30°
10 dripping
edge
5 protection against entry
of gauging water
[mm]
A Arrangment: Variant 2 with gradients in longitudinal and sometimes in cross direction
guard rail, cap respectively impact protection, and pavement surface on road bridges, refer to national regulations. The shuttering elements can be dismantled for inspection
C Comment: A lateral concrete apron makes building control more difficult. Beneficial is a fixing of the concrete slabs over sideways attached angles
DE Durability: Detailing
Annex
D
P Constructional wood protection
Possibility 4:
Closed road surface:
Reinforced concrete-plates
T - Pos 4
Febr. 2022

ICTB 2021 PLUS
4th International Conference on Timber Bridges
Biel/Bienne, Switzerland, 9 -12 May 2022



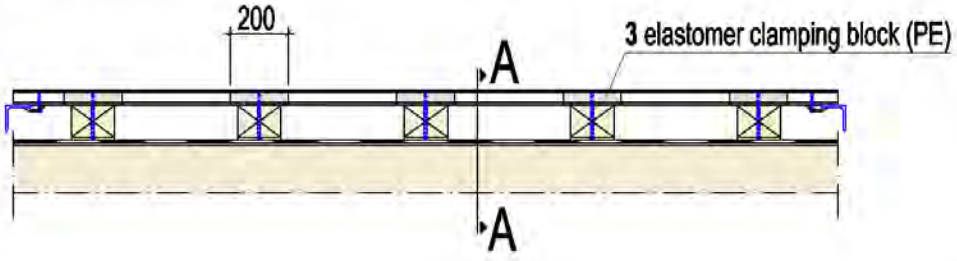
A-A Section A - A

b) in transverse direction
2 clampingblocks per plank



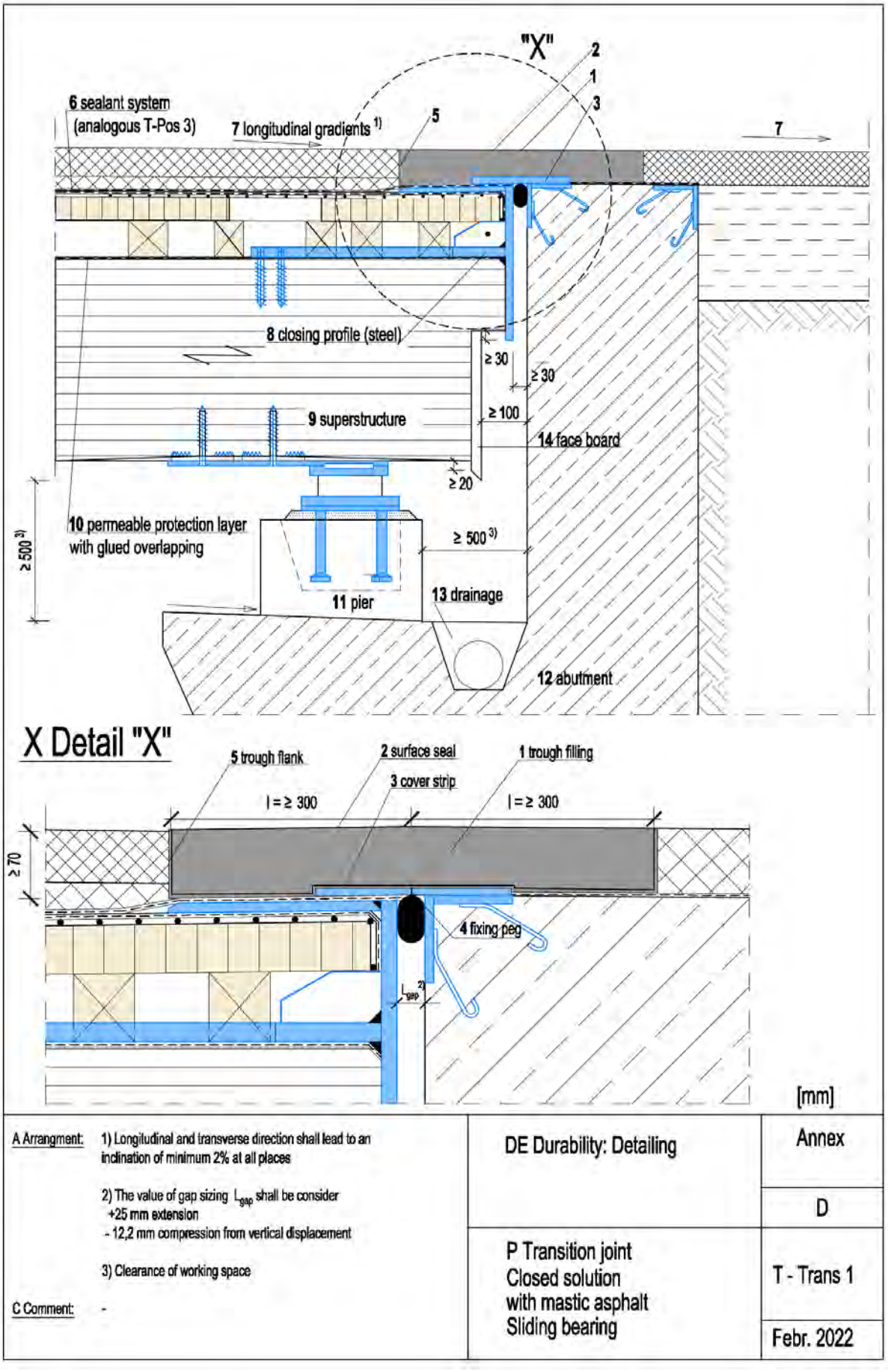
F Fixing of GFK floor covering boards

a) in longitudinal direction



[mm]

A Arrangment: If GFK-boards with a click system are used, no transverse trough under every joint (see Section A - A) is needed.	DE Durability: Detailing	Annex
		D
C Comment:	P Constructional wood protection Possibility 5: Closed road surface: GFK - board	T - Pos 5
		Febr. 2022



A Arrangment:

1) Longitudinal and transverse direction shall lead to an inclination of minimum 2% at all places

2) The value of gap sizing l_{gap} shall be consider
+25 mm extension
- 12,2 mm compression from vertical displacement

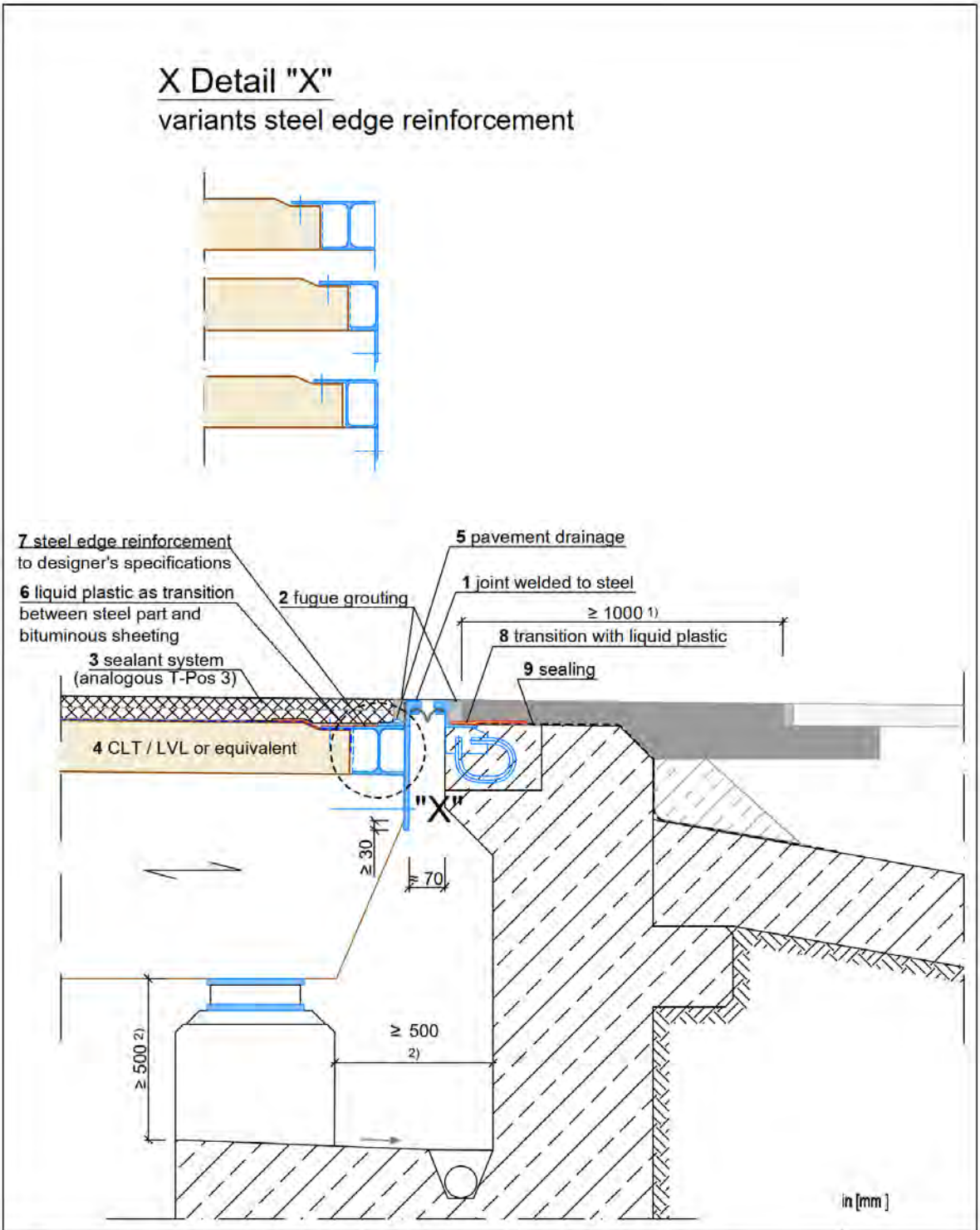
3) Clearance of working space

C Comment: -

DE Durability: Detailing	Annex
	D
P Transition joint Closed solution with mastic asphalt Sliding bearing	T - Trans 1
	Febr. 2022

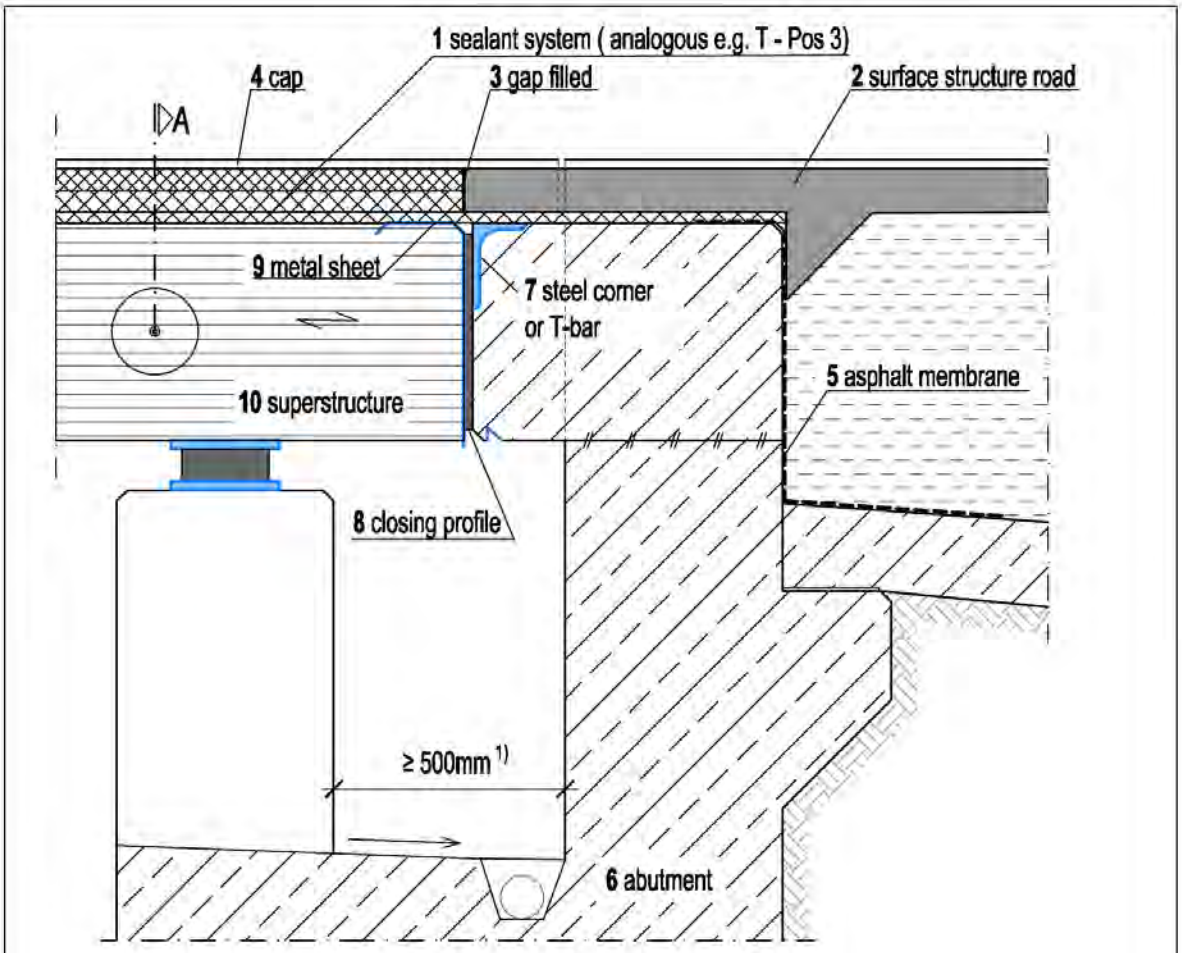
ICTB 2021 PLUS
4th International Conference on Timber Bridges
Biel/Bienne, Switzerland, 9 -12 May 2022

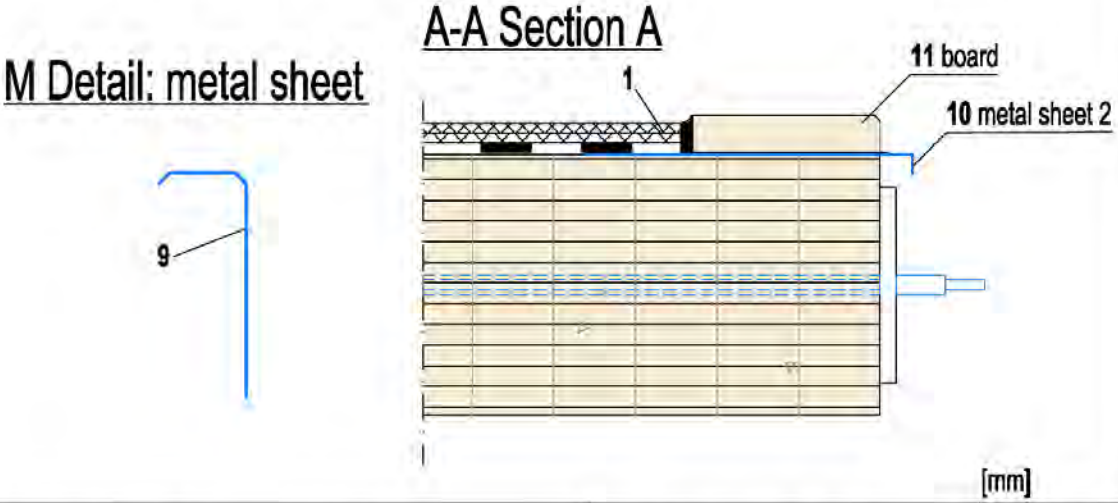




A Arrangment:	Expansion joints with elastomeric sealing profiles can lead to noise emission at traffic speed over 50 km/h. Expansion joints must be designed so that the required joint profiles can be welded on the bridge. This edge reinforcement increases the stiffness of the transition road-bridge. Longitudinal and transverse slopes according to the drainage concept 1) mastic asphalt and material stiffness same as for the bridge edge 2) clearance of working space	DE Durability: Detailing	Annex
			D
C Comment:	-	P Transition joint Solution with joint Timber bridge Sliding bearing	T - Trans 2
			Febr. 2022

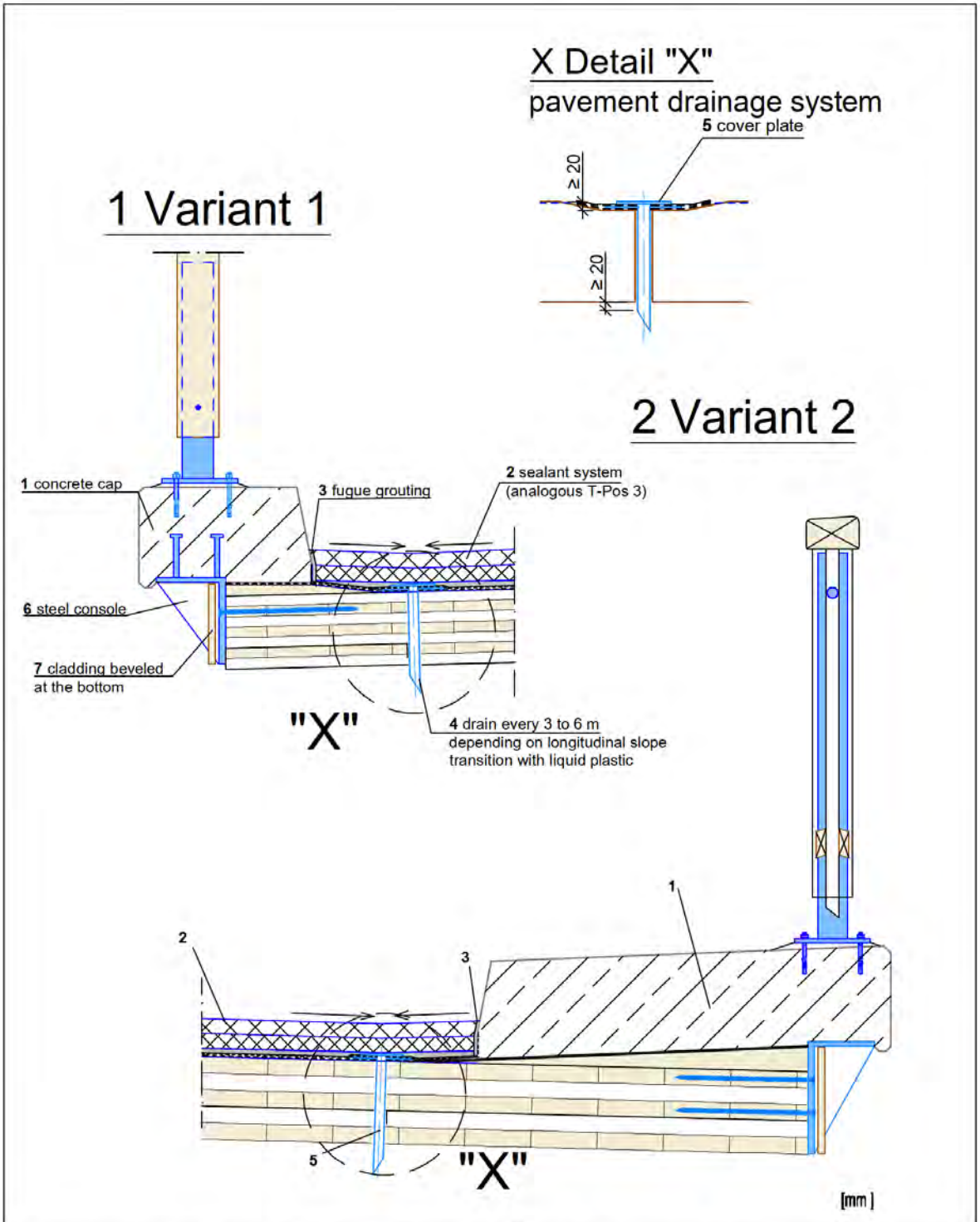




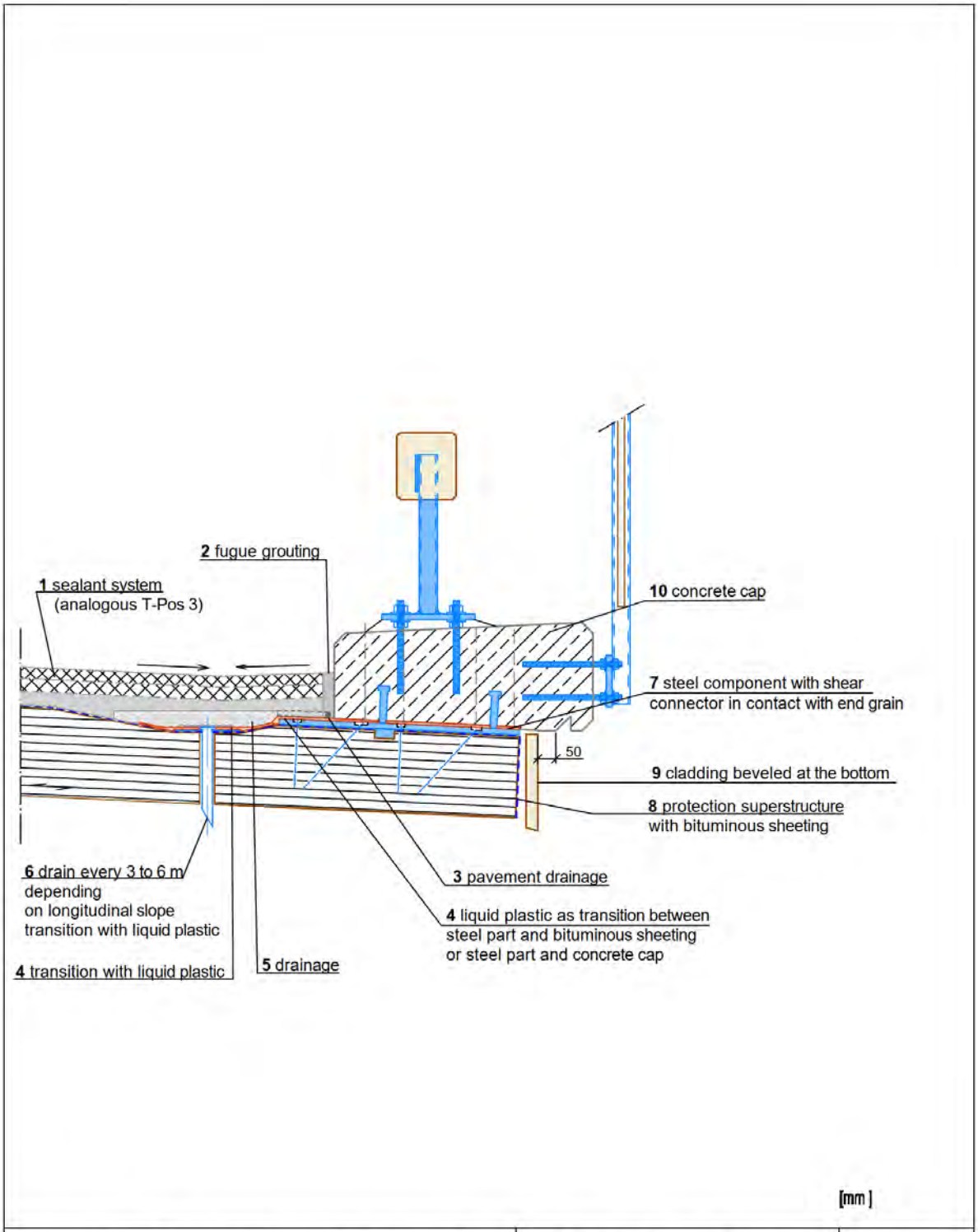


A Arrangment: Closing profile, if necessary, made out of rubber. Distance between bearing and abutment wide enough for inspection. 1) Clearence of working space	DE Durability: Detailing	Annex D
C Comment: Sealing with asphalt can crack between bridge and abutment by rotation	P Transition joint Solution with mastic asphalt Timber bridge Fixed bearing	T - Trans 3 Febr. 2022

ICTB 2021 PLUS
4th International Conference on Timber Bridges
Biel/Bienne, Switzerland, 9 -12 May 2022



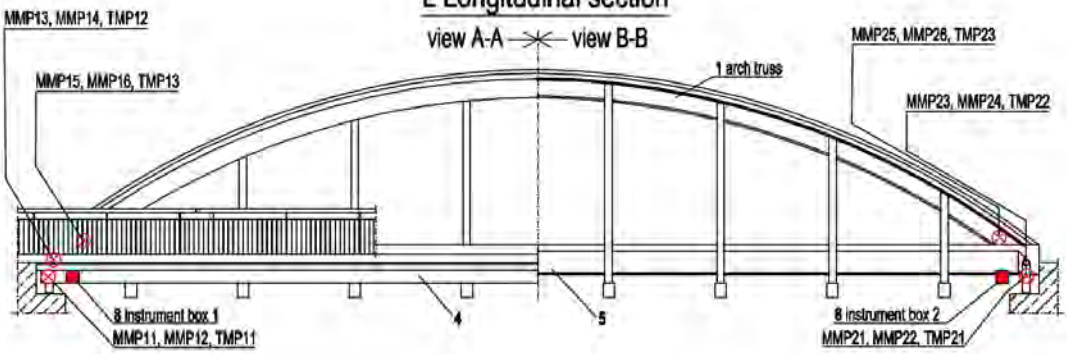
A Arrengment:	The cap should be connected to the bridge by means of shear connectors. The guard rail post are to be designed as a weak link in case of an impact (predetermined breakting spot). Longitudinal and transverse slopes according to the drainage conecpt.	DE Durability: Detailing	Annex
			D
C Comment:	-	P Edge sealant system on timber deck slab with concrete cap Solution 1	T - Cap 1
			Febr. 2022



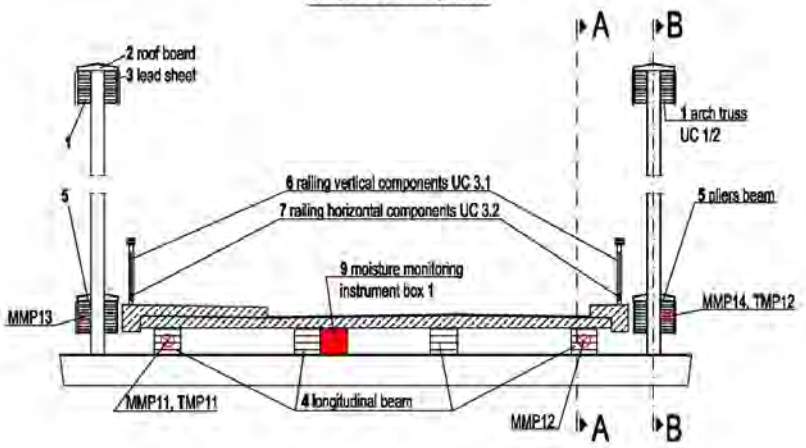
A Arrengment: The cap should be connected to the bridge by means of shear connectors. The guard rail post are to be designed as a weak link in case of an impact (predetermined breakting spot). Longitudinal and transverse slopes according to the drainage conecpt.	DE Durability: Detailing	Annex
		D
C Comment: -	P Edge sealant system on timber deck slab with concrete cap Solution 2	T - Cap 2
		Febr. 2022



L Longitudinal section



C Cross section



W Wood protection

Component	Use class (UC) [Service class (SC)]	Protective measure	Wood type	Durability class (DC)
	EN 335 [EN 1995-1-1]	EN 1995-2 sample drawings	EN 13556	EN 350 Table B. 1
Longitudinal beam	2 [2]	Weather protection through roadway slab and planking and transition 1, protection of the edges (grain-cut timber), protection against insect attack through technical drying, visibility and control of insect infestation	Spruce as glulam	4
Arch truss/ pliers beam	2 [2]	Weather protection by cladding and shuttering, protection against insects by technical drying and insect protection grid, visual inspection every 6 years by removal of claddings	Spruce as glulam	4
Railing	vertical: 3.1 [3] horizontal: 3.2 [3]	None, maintenance component	European larch	3

A Arrangment: Moisture Monitoring: Measurement depth 4 cm for MMP = Moisture measurement point TMP = Temperature measurement point	DE Durability: Monitoring	Annex D
C Comment: The monitoring system is showed by an arch road bridge (example). For other bridge types (see e.g. Figure D.1) the measurements should be planed similar.	P Moisture Monitoring Example arch truss Timber bridge Use classes	T - Mon Febr. 2022

Conference Proceedings 4th ICTB (2022)
https://doi.org/10.24451/ys1x-9w56

ICTB 2021 PLUS
4th International Conference on Timber Bridges
Biel/Bienne, Switzerland, 9 -12 May 2022



Vibration, Deflections

Patricia Hamm[1]

1 Introduction

The fact, that footbridges – independent of material – are likely to vibrate, is still actual. But there is a practical method to handle it. This method is presented here and is part of the draft of Eurocode 5-2 [1].

2 Designing the footbridge in ultimate limit state and deflections

2.1 Designing the footbridge in the ultimate limit state

Designing the footbridge in the ultimate limit state only leads to low frequencies. This is shown in [2] for steel bridges, but transferable to all materials.

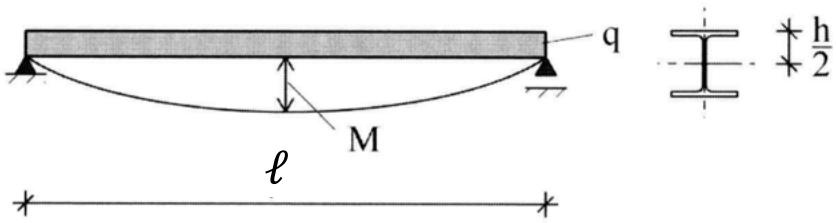


Figure 1: Bending moment of beam with constant load q, taken from [2]

The maximum bending moment of the girder is:

$$M_d = \gamma_{G/Q} \cdot \frac{q \cdot \ell^2}{8}$$

The maximum bending stress is:

$$\sigma_{m,d} = \frac{M_d}{W} = \frac{M_d \cdot h}{2 \cdot I}$$

In case of 100 % exploitation of the material, the maximum bending stress is equal to the strength.

$$\sigma_{m,d} = f_{m,d} = \frac{f_{m,k} \cdot k_{mod}}{\gamma_{m,timber}} or \frac{f_{y,k}}{\gamma_{m,steel}}$$

This leads to:

$$\frac{M_d \cdot h}{2 \cdot I} = \gamma_{G/Q} \cdot \frac{q \cdot \ell^2}{8} \frac{h}{2 \cdot I} = \frac{\gamma_{G/Q} \cdot q \cdot \ell^2 \cdot h}{16 \cdot I} = \frac{f_{m,k} \cdot k_{mod}}{\gamma_{m,timber}}$$

From this, the required area moment of intertia $I_{req,ULS}$ can be calculated, based on the ultimate limit state only. It is assumed that $\gamma_{G/Q} \approx 1{,}45$; $k_{mod} = 0{,}9$; $f_{m,k} = 24 \cdot 10^6 \frac{N}{m^2}$; see GL24h.

$$I_{req,ULS} = \frac{\gamma_{G/Q} \cdot \gamma_{m,timber} \cdot q \cdot \ell^2 \cdot h}{16 \cdot f_{m,k} \cdot k_{mod}} = \frac{1{,}45 \cdot 1{,}3 \cdot q \cdot \ell^2 \cdot h}{16 \cdot 24 \cdot 10^6 \cdot 0{,}9} = 5{,}45 \cdot 10^{-9} \cdot q \cdot \ell^2 \cdot h$$

[1] Patricia Hamm, Biberach University of Applied Sciences, Germany, hamm@hochschule-bc.de



2.2 Designing the footbridge to deflection criteria

Designing the footbridge to deflection criteria leads to the following:

The maximum deflection of a simple supported beam with constant load q is:

$$w = \frac{5}{384} \cdot \frac{q \cdot \ell^4}{EI}$$

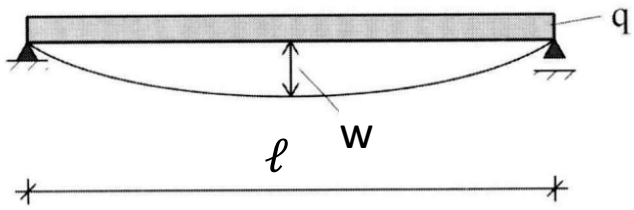


Figure 2: Deflection of beam with constant load q, taken from [2]

The limit of deflection is taken as $\frac{\ell}{x}$ and later as $\frac{\ell}{500}$.

This leads to the required area moment of inertia regarding the deflection criteria, with $E = 11500 \cdot 10^6 \frac{N}{m^2}$; see GL24h.

$$I_{req,Defl} = \frac{5}{384} \cdot \frac{q \cdot \ell^4 \cdot x}{E \cdot \ell} = \frac{5}{384} \cdot \frac{q \cdot \ell^3 \cdot 500}{11500 \cdot 10^6} = 5{,}66 \cdot 10^{-10} \cdot q \cdot \ell^3$$

2.3 Calculating the frequency

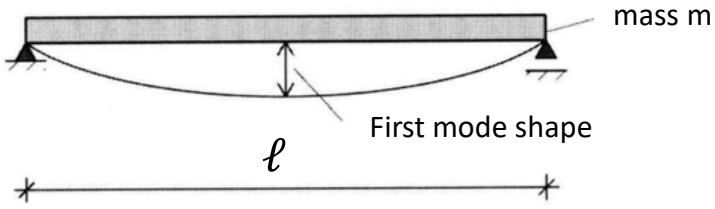


Figure 3: First mode shape of beam with constant mass m, taken from [2]

The frequency corresponding to the first mode shape of a simply supported beam can be calculated as:

$$f = \frac{\pi}{2 \cdot \ell^2} \cdot \sqrt{\frac{EI}{m}}$$

As the mass is taken to $m = \frac{q}{g}$, f is the frequency of the fully loaded bridge. $g = 9{,}81 \frac{m}{s^2}$ is the gravitational acceleration.

$$f^2 = \frac{\pi^2}{4 \cdot \ell^4} \cdot \frac{EI \cdot g}{q} = \frac{\pi^2}{4 \cdot \ell^4} \cdot \frac{11500 \cdot 10^6 \cdot I \cdot 9{,}81}{q} = \frac{278 \cdot 10^9 \cdot I}{\ell^4 \cdot q}$$

2.4 Combining the frequency and the required area moment of inertia

Replacing $I_{req,ULS}$ in this formula leads to the following frequencies:

$$f_{req,ULS} = \sqrt{\frac{278 \cdot 10^9 \cdot I}{\ell^4 \cdot q}} = \sqrt{\frac{278 \cdot 10^9 \cdot 5{,}45 \cdot 10^{-9} \cdot q \cdot \ell^2 \cdot h}{\ell^4 \cdot q}} = 38{,}9 \cdot \frac{\sqrt{h}}{\ell}$$

Assuming a beam with 1,5m height: $f_{ULS_1{,}5m} = 38{,}9 \cdot \frac{\sqrt{1{,}5}}{\ell} = 47{,}6 \cdot \frac{1}{\ell}$

Assuming a beam with 1,0m height: $f_{ULS_1{,}0m} = 38{,}9 \cdot \frac{\sqrt{1{,}0}}{\ell} = 38{,}9 \cdot \frac{1}{\ell}$

Assuming a beam with 0,5m height: $f_{ULS_0{,}5m} = 38{,}9 \cdot \frac{\sqrt{0{,}5}}{\ell} = 27{,}5 \cdot \frac{1}{\ell}$

Replacing $I_{req,Defl}$ in this formula leads to the following frequencies:

$$f_{Defl} = \sqrt{\frac{278 \cdot 10^9 \cdot I}{\ell^4 \cdot q}} = \sqrt{\frac{278 \cdot 10^9 \cdot 5{,}66 \cdot 10^{-10} \cdot q \cdot \ell^3}{\ell^4 \cdot q}} = 12{,}5 \cdot \frac{1}{\sqrt{\ell}}$$

The graph in figure 4 shows the interaction between designing for ultimate limit state or deflection and the resulting natural frequency for the fully loaded bridge.

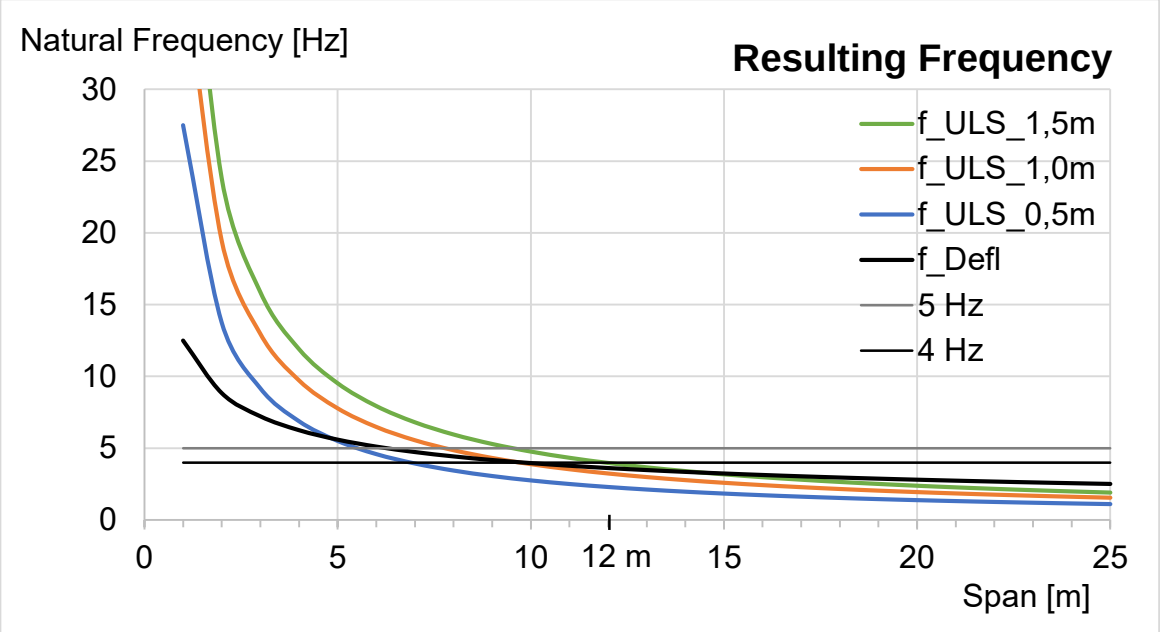


Figure 4: Resulting Frequency when designing the footbridge to ultimate limit state or deflection criteria

3 Method suggested in prEN 1995-2:202x (E). Eurocode 5 — Design of Timber Structures — Part 2: Bridges

3.1 Most of the footbridges are in resonance

Figure 4 shows, that most of the bridges with spans greater than (7m –) 12 m have natural frequencies lower than 5-Hz, or lower than 4 Hz, as the fully loaded bridge was based on the calculations above.

What does this mean? This means, that most of the bridges can be excited in resonance by the first or second harmonic part of the dynamic load to the underground while walking. Figure 5 shows, how to handle the low frequency footbridges in general: If the proof of vibration is not fulfilled, the installation of a tuned mass damper should be planned and regarded in the design of the bridge and in the costs. After the construction of the bridge, a vibration measurement can help to decide, whether the installation of the tuned mass damper is necessary or not.

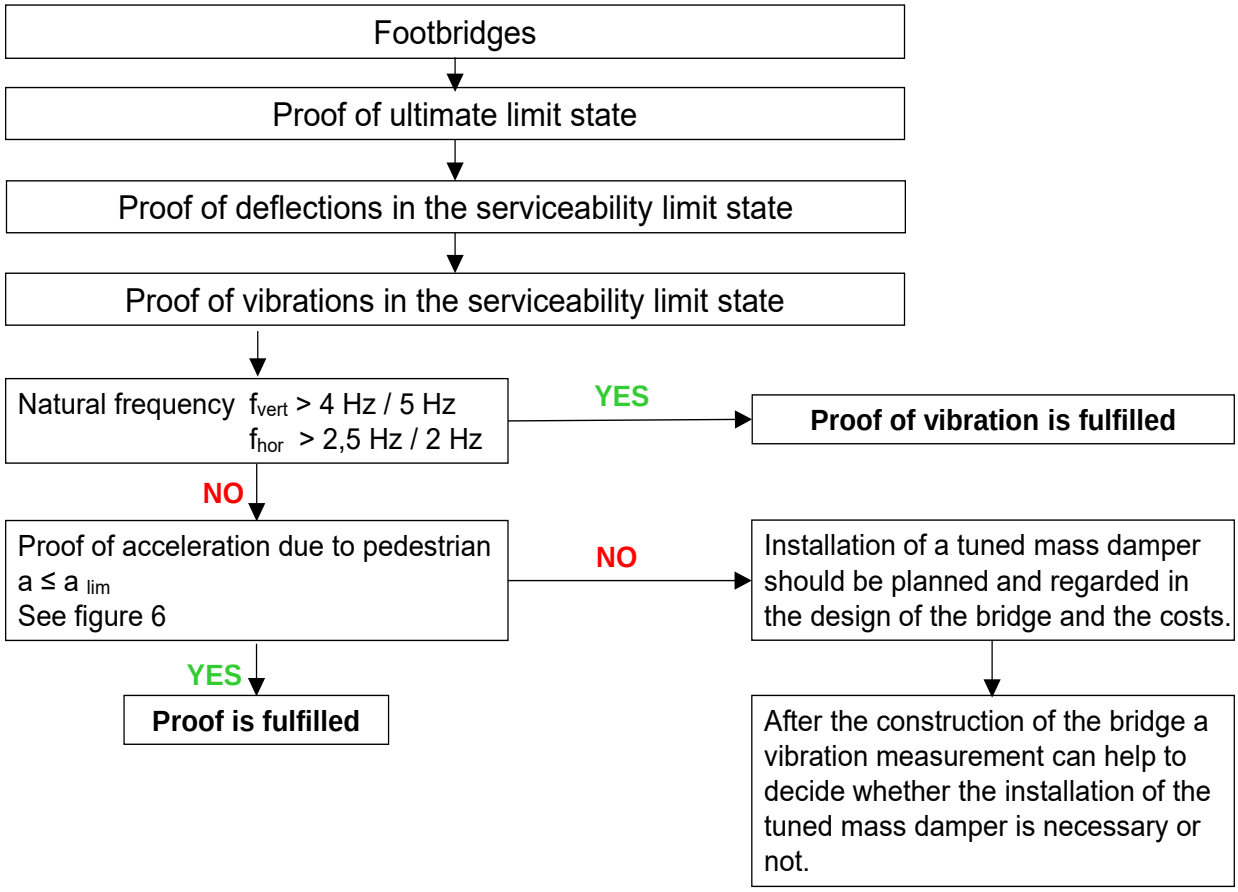


Figure 5: Flowchart how to handle low frequency footbridges in general, see [1], [3] and [4]

3.2 Calculation of the acceleration of the bridge in resonance

Eurocode 5-2 [1] gives formulas, how to calculate the resulting acceleration of the footbridge, when the bridges is excited in resonance. Table H.1 in Eurocode 0 [5] gives different limit values, which can be chosen for the limit acceleration depending on different comfort levels.

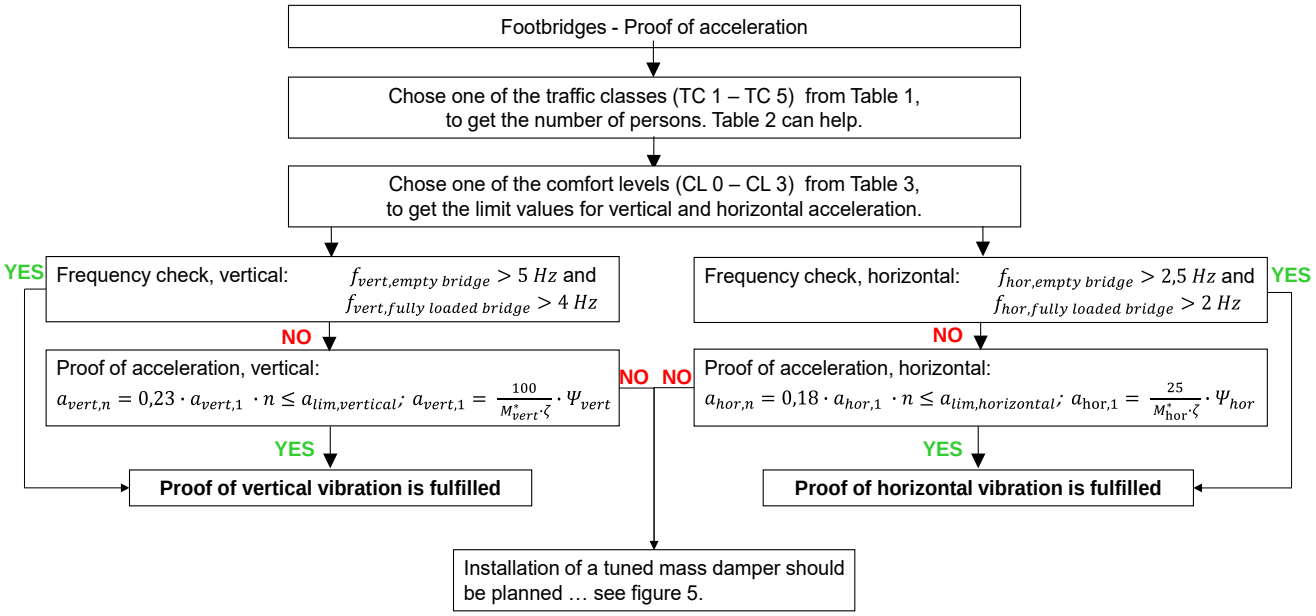


Figure 6: Flowchart of the simplified model to proof the acceleration of footbridges, see [1] and [6]

Table 1: Traffic Classes (move out from Table G.1, Eurocode 1 [6])

Traffic Class	Description	Explanation	Pedestrian Stream, given by density d [P/m²]
TC 1	Very weak traffic	Seldom used footbridge; bridge built to link sparsely populated areas	0.1
TC 2	Weak traffic	Footbridge for standard use; bridge that may occasionally be crossed by large groups of people but that will never be loaded throughout its bearing area	0.2
TC 3	Dense traffic	Urban footbridge linking up populated areas; bridge subjected to road traffic and that may occasionally be loaded throughout its bearing area	0.5
TC 4	Very dense traffic	Urban footbridge linking up high pedestrian density areas; bridge located for instance, nearby a rail or underground station	1.0
TC 5	Exceptionally dense traffic	Urban footbridge linking up exceptionally high pedestrian density areas; bridge located for instance, nearby an arena that may accommodate a large number of spectators	1.5



Normally no dynamic analyses are required for footbridges in traffic class TC1. For very light footbridges, e.g. girder-type bridges with pavement consisting of light material, it is advised to select at least TC2 to ensure a minimum amount of comfort. Very light footbridges may show high accelerations without any resonance.

The weight of a single person is 0.8 kN according to Annex A, Eurocode 0 [5].

The owner of the bridge should specify the appropriate traffic class, based on the level of pedestrian traffic that the bridge is expected to be subjected to. Table 2 can help.

Table 2: Recommended traffic classes for bridges according to their location

Location of the bridge	**Frequency of use**	**Recommended traffic class**
Outside of towns	sometimes	TC 1
	often	TC 2
Inside of towns	often	TC 2
In areas with huge events	often	TC 3
Close to stations	sometimes	TC 3
	often	TC 4
In areas with stadiums or parks	often	TC 4
On routes of fun runs	often	TC 5

Table 3: Comfort levels and corresponding allowed vertical and horizontal accelerations (move out from Table H.1, Eurocode 0 [5] and [7])

Comfort level	**Degree of comfort**	**Explanation**	**Vertical acceleration** $a_{lim,vertical}$ **[m/s²]**	**Horizontal acceleration** $a_{lim,horizontal}$ **[m/s²]**
CL 3	Maximum	Accelerations practically imperceptible to the users	≤ 0.5	≤ 0.1 ≈ 0.15
CL 2	Medium	Accelerations merely perceptible to the users	≤ 1.0	≤ 0.3
CL 1	Minimum	Accelerations perceived by the users, but not intolerable	≤ 2,5	≤ 0.8 ≈ 0.75
CL 0	No limit set	Accelerations strongly perceived by the users, intolerable by most	> 2,5	> 0.8 ≈ 0.75

M^*_{vert} and M^*_{hor} are the generalized masses of the bridge in kg for vertical or horizontal vibrations as a function of the mass per unit length of the bridge and the distance between the supports. The generalized mass M* may be different for vertical or horizontal accelerations.

The generalized mass of a single span girder or truss system with span ℓ is $M^* = \frac{1}{2} \cdot m \cdot \ell$

m is the mass per unit length of the bridge in kg/m including the permanent load plus the pedestrian load throughout the bridge bearing area, with a number of pedestrians per square meter – depending on the traffic class, see table 1.

ζ is the damping ratio to the relevant natural frequency, see table 4.

ψ_{vert} and ψ_{hor} are the reduction coefficients taking into account the probability that the footfall frequency (both jogging and walking) approaches the critical range of natural frequencies of the bridge, see Figures 7 and 8.



Table 4: Damping ratio according to Lehr

Static system of the bridge	Damping ratio ζ
cable-stayed bridges with very long cables vibrating themselves	0,5 %
cable-stayed bridges superstructures without mechanical joints timber-concrete-composite superstructures bridges with light-weight timber deck (e.g. roofed bridge with planked timber deck) with main girders with mechanical joints	1,0 %
superstructures with mechanical joints timber bridges with a heavy bridge deck (e.g stress laminated decks or block-glued decks) with a floating layer; e.g. a sealant system	1,5 %
bridge system consisting of a heavy deck supported by arches or trusses superstructures with a floating layer (e.g. a rear-ventilated road-surface)	2,0 %

In case of horizontal vibration of trough bridges (without torsion connection) with a lateral wind bracing (built with fasteners) the damping ratio values given above may be doubled.

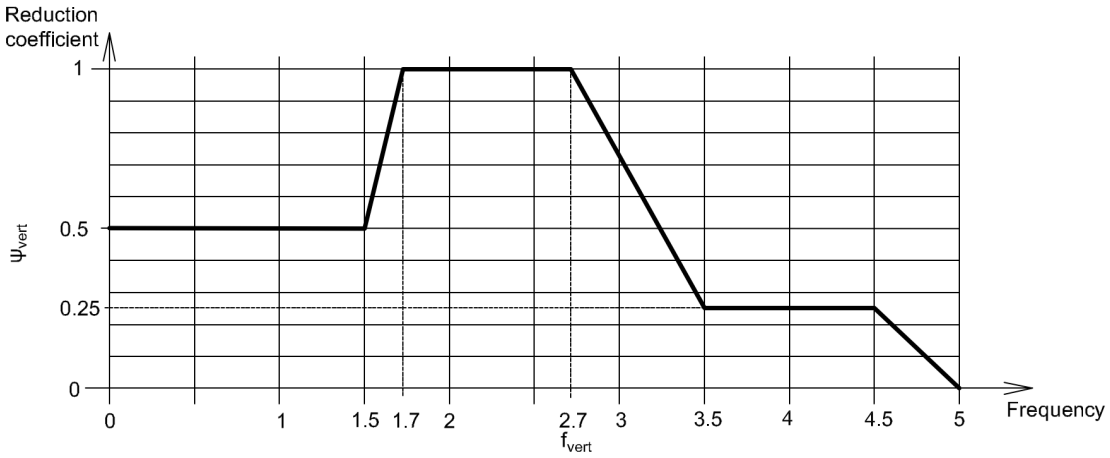


Figure 7: Relationship between the vertical natural frequency f_{vert} *and the reduction coefficient* ψ_{vert}*, taken from [1]*

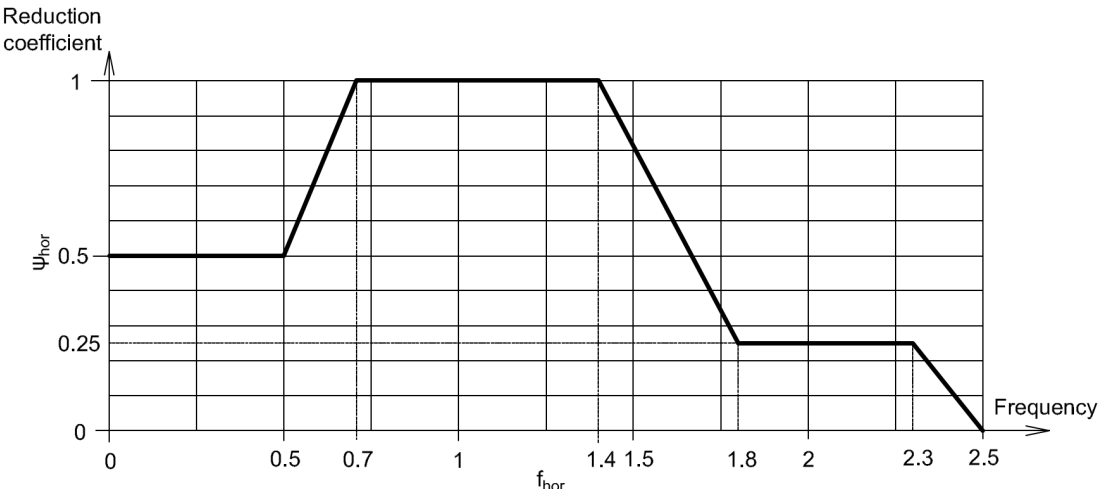


Figure 8: Relationship between the horizontal natural frequency f_{hor} *and the reduction coefficient* ψ_{hor} *taken from [1]*



4 Background

4.1 How are the higher harmonics considered?

The higher harmonics, namely the second harmonic are considered by the reduction coefficient. As the Fourier coefficient of the second harmonic (α_2 =0,1 – 0,2) is about one-half to one fourth of the first harmonic (α_1 =0,4), the reduction coefficient is $\Psi = 0{,}25$ in the range of two times step frequency ($2 \cdot f_S$ =2,5 – 5,0 Hz) – compared to $\Psi = 1$ in the range of step frequency (f_S =1,25 – 2,5 Hz), see Eurocode 1 [6], table G.2. Synchronisation with the second harmonic is rather unlikely, therefore $\Psi = 0{,}25$ is on the save side.

4.2 How are joggers considered?

The load function of runners (= joggers) has different Fourier coefficients compared to walkers. The main difference lies in the first harmonic, as the first Fourier coefficient for jogging ($\alpha_{1,jogging}$ =1,5) is about 4 times the Fourier coefficient of walking ($\alpha_{1,walking}$ =0,4). This leads to the following acceleration-relation due to 1 person: $a_{vert,1,jogging} = 4 \cdot a_{vert,1,walking}$

Eurocode 1 [6], table G.1 gives the number of persons, which should be regarded, see table 5:

Table 5: Number of persons in a pedestrian group (walking) and in a jogging group, taken from Eurocode 1 [6]

Pedestrian group n_w	Jogging group n_j	Relation n_w/n_j
1	0	-
2	0	-
4	1	4
8	2	4
16	4	4

One can see that the numbers of persons in a walking group is at least four times the number of persons in a jogging group. Therefore, the factor 4 for higher load while jogging cancels out the factor 4 for the bigger group while walking.

Figures 9 and 10 show the correlation. One can see that the black curves in figures 7 and 8 are the envelope curves of the mentioned cases “higher harmonics” and “joggers”.

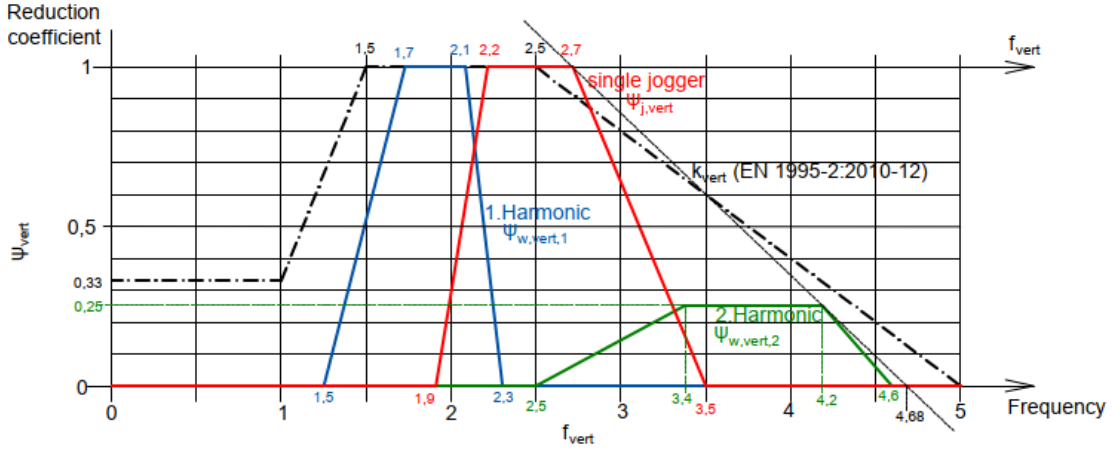


Figure 9: Relationship between the vertical natural frequency f_{vert} and the reduction coefficient $\psi_{w,vert}$ (walking) and $\psi_{j,vert}$ (jogging), taken from [11]

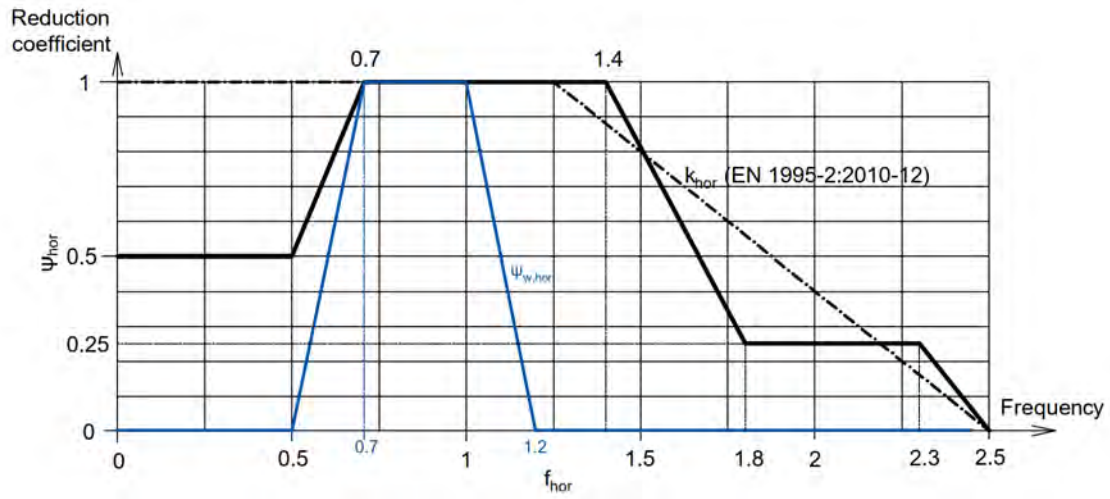


Figure 10: Relationship between the horizontal natural frequency f_{hor} and the reduction coefficient ψ_{hor} (both walking and jogging), taken from [11]

4.3 Why are pedestrian groups not regarded in the simplified model?

The simplified model builds on the load model pedestrian stream, given by a density d [P/m²], see table 1. The maximum number of persons in a pedestrian group is 16. This maximum number is rather equal to the minimum number for the pedestrian stream given in footnote 3, Annex G, Eurocode 1 [6]: "n ≥ 15 shall be assumed".

4.4 Why could there be a significant discrepancy between cold and warm weather?

When asphalt is used as paving, natural frequencies can vary depending on temperature. In cold weather, the asphalt becomes stiffer; this can lead to a higher frequency in cold weather. This can appear in both directions, for vertical and horizontal frequencies, see [10].

4.5 Is the simplified model applicable for all bridge types?

The simplified model may be adopted for any bridge type, provided that adequate generalized mass is adopted in the calculations.



4.6 How to do the advanced proof?

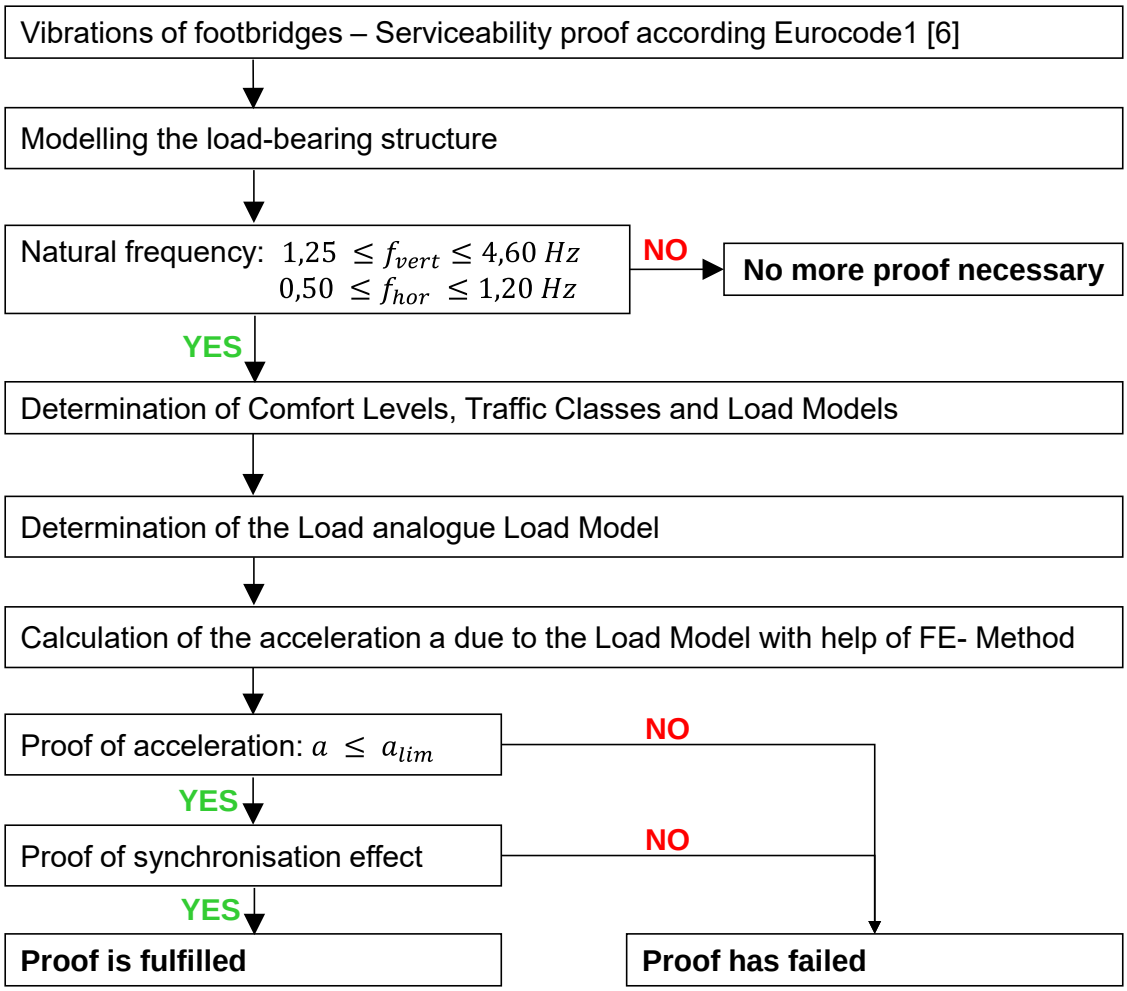


Figure 11: Flowchart for the advanced proof of vibration of footbridges according to Eurocode 1 [6], taken from [4]

4.7 Why are vibration analyses normally not required for foot and bicycle bridges with less than 12 m in span?

Figure 4 shows the correlation between the span of the bridge and the resulting natural frequency, depending on the design of the bridge. It shows that bridges with spans more than 12 m have quite likely frequencies less than 4 Hz (–-5-Hz). Bridges with spans less than 12m have natural frequencies greater than 4 Hz (– 5 Hz). Therefore, there is no risk of resonance between step frequency (or twice step frequency) and natural frequency. Nevertheless, it should be kept in mind that very light-weight structures can vibrate in a manner that it significantly reduces the comfort of the pedestrians using the bridge- even without resonance.



References

[1] Eurocode 5-2: prEN 1995-2:202x (E). Eurocode 5 — Design of Timber Structures — Part 2: Bridges.

[2] Kramer, H. (2007) Angewandte Baudynamik, Ernst & Sohn.

[3] Hamm, P. (2003) Ein Beitrag zum Schwingungs- und Dämpfungsverhalten von Fußgängerbrücken aus Holz. Dissertation. TU München, November 2003. Volltext unter: http://mediatum.ub.tum.de

[4] zu Jeddeloh, S. (2020) Untersuchungen zum Schwingungsverhalten von Holz-Beton-Verbundkonstruktionen (HBV). Masterarbeit, Universität Stuttgart, Institut für Konstruktion und Entwurf, Stahl-, Holz- und Verbundbau.

[5] Eurocode 0: prEN 1990:202x (E). Eurocode 0 — Basis of structural design.

[6] Eurocode 1-2: prEN 1991-2:202x (E). Eurcode 1 – Actions on structures - Part 2: Traffic loads on bridges.

[7] JRC-Scientific and Technical Report: Design of Lightweight Footbridges for Human Induced Vibration. 2009.

[8] Hamm, P.: Vibrations of wooden footbridges induced by pedestrians and a mechanical exciter. In: footbridge 2002, Proceedings of the International Conference on the Design and dynamic behaviour of footbridges. Paris, 20.-22. November 2002. Hrsg. AFGC and OTUA, 2002, S. 144-145 + CD.

[9] Hamm, P.: Serviceability limit states of wooden footbridges. Vibrations caused by pedestrians. In: International council for research and innovation in building and construction, Working Commission W18 - Timber Structures, CIB-W18, Meeting 2004, Edinburgh, Scotland, UK, 30.8.-3.9.2004. Hrsg.: Lehrstuhl für Ingenieurholzbau und Baukonstruktionen, Universität Karlsruhe.

[10] Crocetti R., Branco, J. and Barros, J: Timber Arch Bridges with V-shaped Hangers, Structural Engineering International 29(2):1-7, 2018

[11] Back ground document: EN 1995-2: BGD to «VIBRATIONS, DAMPING», not published yet.

Conference Proceedings 4th ICTB (2022)
https://doi.org/10.24451/ehwc-6323

ICTB 2021 PLUS
4th International Conference on Timber Bridges
Biel/Bienne, Switzerland, 9 -12 May 2022



Design of timber-concrete-composite structures

Jörg Schänzlin[1], Alfredo Dias[2]

1 Introduction

In recent years the advantages of timber-concrete-composite structures as increased stiffness and load capacity, have been a motivation for the wider use of these systems in buildings and bridges (see [1]). In order to support this higher demand, clear rules and a common understanding, how to design timber-concrete-composite structure is essential. For this reason the existing knowledge was collected and summarized (see [2]). Within the work of CEN/TC250/SC/PT5.2 this knowledge was transformed into the Technical Specification CEN/TS 19103 [3] focussing on buildings, which eventually will be the basis for a new part of [4] in the next generation of the Eurocodes.

In this paper the main contents of this Technical Specification and the main differences to the common design according to typical technical approvals are presented.

2 Range of application

Timber-concrete-composite structures show a large variability regarding the materials, the cross-sections, the connections that are used or even the design approaches that are followed. One reason is that the development of the structure but also of the design procedures takes place independently in the different countries. However not all this has been based on sufficient research studies and therefore an appropriate scientific background it is not available. For these reasons not all the conditions are covered and many limitations apply has described below:

- Timber: The Technical Specification [3] is linked to [4], consequently all wood based materials can be used which are allowed by [4]. However limitations apply in specific conditions such as for example in the field of application of the models provided to determine the mechanical properties of notch connections, where a minimum strength class of C24 and GL24 for solid timber and glued laminated timber respectively is required.
- Concrete: The concrete is limited to following strength classes
  - Normal concrete: ≥ C12/15; ≤ C60/80
  - Light weight aggregate concrete: ≥ LC12/15; ≤ LC60/80
- For the notched connections design models mentioned before, the lower limit of the concrete strength class is set to C20/25 since no sufficient information of lower concrete classes is available.
- Reinforcement: For the reinforcement reference to [5] is made, so all types of reinforcement defined in [5]can be used within TCC-structures designed according to the technical specification-
- Service class: The use of timber only be used in Service class 1 or 2 is motivated. However, the Technical Specification does not limit the application of TCC in Service class 3 except the Service class of the joint between timber and concrete. This joint has to be detailed in that way that the service conditions correspond to either Service class 1 or 2, the intention is to prevent water penetrating into the joint which is difficult to remove leading to a reduction of both the durability and performance.
- Dimensions: The thickness of the concrete slab should be between 50mm to 300mm, while the intermediate layers should not exceed the thickness of 50mm.

[1] Jörg Schänzlin, Biberach University of Applied Science, schaenzlin@hochschule-bc.de
[2] Alfredo Dias, University of Coimbra Coimbra, Portugal, alfgdias@dec.uc.pt



3 Short term behaviour

3.1 Loads/actions

During the life time of a composite timber-concrete structure two types of loads will act:

- "Common" external loads as dead load, live load, snow loads, wind loads, etc.
- Eigenstresses caused by inelastic strains such as different temperature elongation, shrinkage and swelling of the timber and shrinkage of the concrete

Once in many situations the temperature variations effects and the swelling/shrinkage of timber are not relevant. As simplification according to the Technical Specification [3] can be neglected, if the environmental conditions of the system are quasi constant. These quasi constant environmental conditions are defined by

- The initial moisture content is in the range of the final moisture content as already required in [4]
- The annual difference between the values of the maximum and minimum moisture content is lower or equal 6%
- The maximum difference of the air temperature is lower or equal 20°C.

This means that typical Service class 1 conditions as well as some conditions of service class 2 can be assigned to the quasi-constant conditions. In these situations shrinkage/swelling of timber and the effect of temperature variations may be neglected. Despite the shrinkage of concrete has to be considered in the ultimate as well as in the serviceability limit state.

When the three conditions listed above are not met the surrounding conditions are assigned to variable conditions. In these cases, the effects of the moisture variation and of the temperature variation have to be considered in the ULS as well as in the SLS. These additional inelastic strains are given by

- Temperature: The annual temperature variations as well as the variation between initial state and final state are defined in [6] and are already one common action in bridge design. In this case the temperature variations may be assumed constant over the cross section
- Shrinkage of concrete: The shrinkage of concrete may be obtained in Eurocode 2 [5].
- Shrinkage and swelling of timber: Comparable to the temperature two different moisture variations have to be considered
- Difference between the initial and the final moisture content
- Annual moisture variations: The procedure of the determination of the annuals moisture content of a sheltered system with direct access of the air is given in Annex A of the Technical Specification [3] as described below.

The determination of the annual moisture variations can be determined according to following procedure if more precise values are unknown:

- Identification of the climate zone according to the Köppen-Geiger-diagram (see Figure 1)
- Determination of the moisture content by interpolating the values given in [7] (see Tab 1)

Table 1: Variation of the moisture content in % averaged over the cross section Δmc = max mc - min mc (extract from [3,7])

	Minimum of the width, or twice the depth of the timber cross-section (mm)		
Bez.	38	125	>300
Temperate oceanic Stuttgart, Zurich, Paris, London CFB	15%	9%	3%
Temperate continental Southern region Warsaw, Berlin, Munich, Prague DFB.2	15.5%	9%	3.5%

- Determination of the inelastic strain by

$$\varepsilon = \alpha_{||} \cdot \Delta u \quad (1)$$

ε effective strain caused by moisture variation

Δu annual moisture variation determined according to Table 1

$\alpha_{||}$ Coefficient of swelling/shrinkage
= 0,01%/%Δu according to [8]

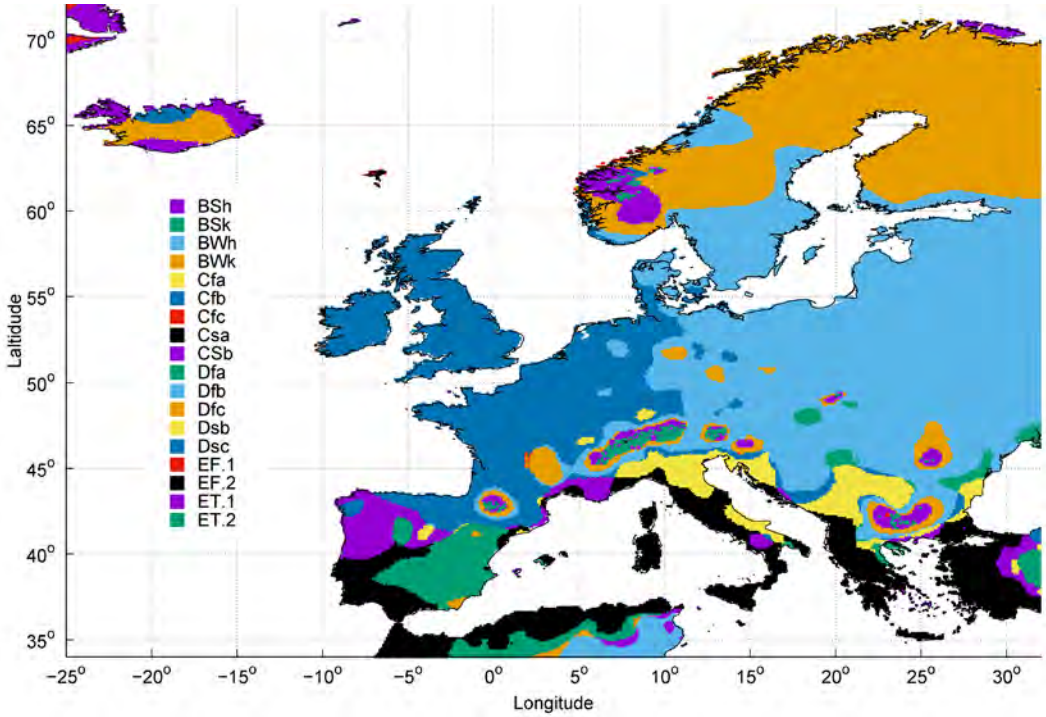


Figure 1: Köppen-Geiger-diagram (see [3,7])

In the current technical approvals, available for various connection devices the consideration of the variation of the moisture content is already required. The main difference between the Technical Specification and these technical approvals is in the way the moisture variation may be taken into account: by the global modification of the Modulus of Elasticity in technical approvals, whereas in the Technical Specification this effect is considered as an explicit load.

3.2 Modification factors

As for timber structures the influence of the moisture content and the time on the strength is taken into account with through modification factors of the strength k_{mod} given in Eurocode 5 [4].

Concerning the connection, the concept of the connection between two timber based products with different k_{mod}-values is applied on TCC-structures, assuming that the k_{mod}-value of the concrete is the modification of the strength of concrete given in Eurocode 2 α_{cc}.

$$k'_{mod} = \sqrt{k_{mod} \cdot \alpha_{CC}} \quad (2)$$



3.3 Determination of the forces

3.3.1 Methods

The performance of the connection, especially the stiffness, influences the distribution of the forces within the cross section. Therefore, the deformability of the connection has to be considered in the evaluation of the forces. Several analysis methods are available:

- Differential equation (see among others [9] and [10])
- γ-method according to [4], Annex B with the extension according to the Technical Specification, Annex B in order to consider the inelastic strains (see [7,11-14])
- Shear analogy method according to [15] (see among others [16] and [17])
- Modelling as strut&tie model (see among others [18])
- FE-modelling

The decision, which method is used, depends on the system and the target of the modelling of the system. Often FE is used within the scientific framework whereas the γ-method or the strut & tie model are often used to model the two layered timber-concrete-composite systems in simple systems. The technical Specification [3] does not introduce any limitation on this issue.

3.3.2 Behaviour of the material in the short term

For the evaluation of the internal forces the mean values of the Modulus of Elasticity of the timber cross section as well as the concrete cross section in compression may be assumed. Cracking of concrete has to be considered in the evaluation. This can be done by the introduction of a non-load bearing layer, representing the cracked area. The height of this layer is determined iteratively until no tensile stresses exceed the design strength in tension of the concrete (normally =0 N/mm²). The elastic behaviour in compression is also assumed when proofing the system.

The timber cross section is verified according to EN 1995-1-1 [4] by considering the interaction between the normal force and the bending moment in the timber cross section, as regular verification in timber members.

3.3.3 Compatibility

The verification of the TCC-cross section is done by the verification of the concrete cross section and the timber cross section separately. Additionally, the Technical Specification [3] requires the check of the compatibility of the cross section.

For the verification of the concrete cross section, it is assumed, that the reinforcement yields and the strain caused by the stresses reaches -3.5‰. Therefore, the strain at the reinforcement is greater or equal 2 ‰. This value is in the range of the maximum strain of the timber cross section, when reaching the strength of the timber (see Figure 2).

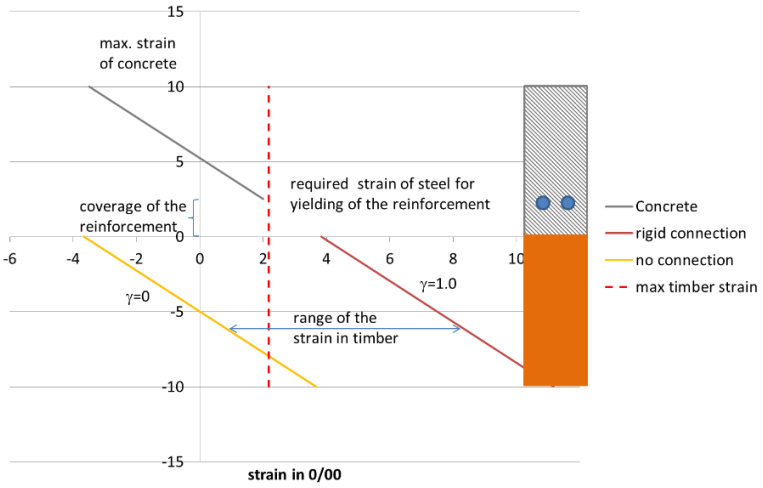


Figure 2: Strain distribution in the cross section



Since the timber cross section is installed underneath the concrete cross section in the tension zone, the strain in the timber cross section are larger than that in the reinforcement. Therefore, -- when considering the reinforcement as load bearing structure -- it has to be checked, which strain can be reached. In most of the cases, the reinforcement remains in an elastic strains due to this compatibility of the strains and the curvature of the concrete and the timber cross section.

3.3.4 Effective width

Often timber-concrete-composite structures are realised by connecting timber beams with a concrete slab. Due to the shear deformation of the concrete slab, the concrete slab cannot be activated fully over the complete width. In order to cover this influence an effective width is introduced. This effective width can be divided into the share caused by the normal force (= shell) and caused by bending. Since the reinforcement cannot be activated, only the share of the load distribution caused by normal force is considered. Comparing the different proposals available in existing standards, namely Eurocode 4 [2] and Eurocode 2 [5]. The proposal given in Eurocode 4 [2] shows a better correspondence to the shear lag, so the Technical Specification [3] proposes to use the effective width according to it.

4 Connection devices

4.1 General

The connection mechanical properties can be obtained from: laboratory tests, models given in the Technical Specification or from the connections technical approvals.

In order to avoid a separation of the concrete from the timber, a minimum uplift force of the concrete of 10% of the shear force in the connection should be transferred.

4.2 Dowel type fasteners installed 90° to the joint between timber and concrete

4.2.1 Load capacity

Since the theory according to [19] is derived by solving the equilibrium of forces at the joint, this theory can also applied to connections in timber-concrete-composite structures. The input values on the timber side are the one given in [4]. The embedment strength in the concrete is assumed to be strength under local compression. Therefore the embedment strength is proposed to be 3x of its compressive strength. With this embedment strength the load capacity of the connection can be determined according to the equations given in [4]

4.2.2 Stiffness

In the model it is assumed that the deformation in the concrete is negligible compared to the deformation in the timber cross-section. Therefore a same situation exists in TCC compared to steel to timber-connection. For this reason in a TCC connection with dowel type fasteners installed in 90° is the same as the stiffness in steel-to-timber connection as given in [4].



4.3 Notched connections

4.3.1 Range of application

Since the existing studies on the load and deformation behaviour of notched connection do not cover the whole possible range of parameters, the application of the equations in Technical Specification [3] are limited to following parameters (see Figure 3):

- Concrete strength greater or equal C20/25 with a maximum diameter of the aggregate size of 16mm
- Timber strength class greater or equal C24 and GL24 resp. or LVL according to EN 14374
- Geometry of the notch
  - Depth of the notch $h_N \geq 20mm$ for normal loads (e.g. in buildings) and $h_N \geq 30mm$ for normal loads (e.g. bridges, warehouses)
  - Length of the timber in front of the notch $l_v \geq 12.5 \cdot t_v$ for robustness reasons, however only $l_v \leq 8\ t_v$, may be considered in the design as load bearing length
  - Length of the notch in the timber $l_N \geq 150mm$ and min. $12.5 \cdot t_v$
  - Diameter of the screw $Ø \geq 6mm$ in order to prevent uplift between timber and concrete
  - Inclination of the load transferring contact area

$$80° \leq \alpha \leq \min \begin{cases} 115° \\ 90° + \Theta \end{cases} \tag{3}$$

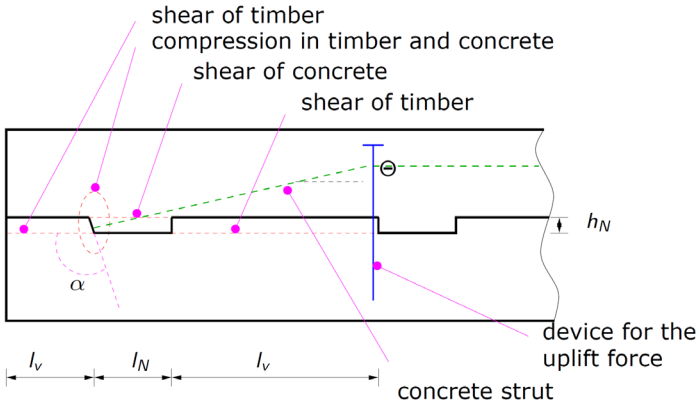


Figure 3: Notched connection

4.3.2 Stiffness

The stiffness of the notched connection is mainly determined by experimental and numerical models, since the load distribution in the anisothropic timber can hardly be described analytically (see [20] and [21]). The model proposed is based on the experimental data available for this connection type.

$$K_{ser} = \begin{cases} 1000 \frac{kN}{mm \cdot m_{width}} & \text{für } t = 20mm \\ 1500 \frac{kN}{mm \cdot m_{width}} & \text{für } t \geq 30mm \end{cases} \tag{4}$$

The notched connection behaves more or less linear elastic until the failure. Therefore the stiffness in the ULS is the same as in the SLS and does not need to be reduced by a factor of 2/3 as for the other typical connectors.



4.3.3 Load capacity

The load capacity can be determined by evaluating the single failure modes (see [20], [22] and Figure 3). These failure modes can be determined by following equations:

$$F_{R,k} = \begin{cases} f_{v,c,d} \cdot b_N \cdot l_N & \text{shear of concrete} \\ f_{c,d} \cdot b_N \cdot h_N & \text{crushing of concrete} \\ f_{v,h,d} \cdot k_{cr} \cdot b_N \cdot \min(l_V; l_S) & \text{shear of timber} \\ f_{c,0,d} \cdot b_N \cdot h_N & \text{crushing of timber} \end{cases} \quad (5)$$

$F_{R,d}$ Design value of the load capacity

$f_{v,c,d}$ „shear strength" of the concrete

$= \frac{\nu \cdot f_{c,d}}{cot\Theta + tan\Theta}$

ν Reduction factor taking into account the effects of crack on the shear transfer

$= 0{,}6 \cdot \left(1 - \frac{f_{ck}}{250\ [N/mm^2]}\right)$

k_{cr} Crack-Factor according to [4]

b_N Width of the notch

l_N Length of the concrete notch

$f_{c,d}$ Design value of the compressive strength of the concrete

$f_{c,0,d}$ Design value of the compressive strength of the timber member parallel to the grain

h_N Depth of the notch

$f_{v,d}$ Design value of the shear strength of the timber

l_V Length of the timber in front of the notch

l_S Length of the timber between the concrete notches

Θ Inclination of the compressive strut

In addition to these failure modes, an uplifting force should be considered in the evaluation. It depends on the assumed inclination Θ of the concrete strut.

$$F_{\perp,d} = \max \begin{cases} F_{\perp,d} & \text{according to Eq. (5)} \\ F_{R,d} \cdot tan\Theta \end{cases} \quad (6)$$

In the Technical Specification [3] this inclination is defined as the inclination of the compressive strut between the contact area of timber and concrete and the anchorage of the device transferring this uplift force. The lower boundary of the inclination is limited by the following equations

$$\Theta \geq \max \begin{pmatrix} \arctan\left(\frac{h_N}{2 \cdot (l_N + l_S)}\right) & intaraction\ between\ the\ notches \\ arctan\left(\frac{h_N}{l_N}\right) & required\ width\ of\ the\ concrete\ strut \end{pmatrix} \quad (7)$$

The first boundary ensures that the interaction between the notches can be neglected, since the elements transferring the uplift force are installed in between the notches. The second boundary ensures that the thickness of the concrete strut is not influenced by the non-load transferring edge of the notch. So the position of the device transferring the uplift force can be chosen "freely" within these boundaries. With increasing distance of this device from the edge of the notch, the forces in the device can be reduced.



However, the load capacity of the notch is also reduced. So it is up to the designer to develop the appropriate solution to balance between the decreasing load capacity of the concrete and the decreasing uplift force with increasing distance.

5 Long term behaviour

5.1 Critical point in time or "stiffness attracts forces"

In structures, where the long term behaviour influences the load and deformation behaviour often the points in time $t = 0$ and $t = \infty$ (~ t=50 years) are verified. The point in time t=0 is identified as that point in time where the design load (or relevant parts of this load) is applied on the structure.

If the courses of the development of the creep strains of timber and concrete are related to their final values and then compared to each other, it can be shown that the concrete creeps stronger within the first 3 to 7 years compared to the timber. This results to a time dependent change in the ratio between the stiffness of the concrete cross section and the stiffness of the timber cross section. Since stiffness attracts forces, the stresses mainly caused by bending increase in the timber cross section, whereas the stresses in the concrete are reduced. After that period concrete hardly creeps, so the timber cross section can transfer some stresses back to the concrete cross section when creeping. Therefore not only the points in time *t=0* and $t = \infty$ but also the period of *t=3 to 7 years* have to be considered in the design process. This additional point in time leads to an extra effort in the design process. On the other hand often the SLS, namely the limitation of the long term deflection, governs the cross section dimension. Within the development of the Technical Specification [3] studies were performed discussing the increase of the stresses at *t=3-7 years* related to the stresses at $t = 0$ and $t = \infty$. As result this additional point in time does not need to be verified, if the stresses in the timber cross section, obtained for the quasi-permanent combination are increased 25% in the verification. In this way the designer can decide whether this additional point in time has to be verified or may be neglected.

5.2 Creep of timber and concrete

Generally spoken the long term behaviour is often classified in the case "pure creep deformation" and "pure relaxation". In the case of "pure creep strain" the stresses are constant over time, where as in the cases with relaxation the total strain is constant over time. However, composite structures are somewhere in between. The long term behaviour cannot be classified as pure creep phenomenon since the creep deformation of the single components lead to stress redistributions within the composite cross section, resulting in non-constant stresses over the time. On the other hand, all components are deformable so the strain is not constant over time, which is necessary to classify the long term behaviour as a relaxation phenomenon.

This time dependent behaviour is not unique in timber-concrete-composite structures. [22] derived the solution o for the effective creep coefficients for concrete structures when an additional layer of concrete is place on top of an existing concrete deck. [23] (see [24]) extended this procedure for timber-concrete-composite structures especially with regard to the deformability of the connection assuming a smeared stiffness along the joint between timber and concrete. In [12] the different temporal development of the creep strain was implemented into the existing procedure. So the effective creep coefficient can be analytically determined, taking into account all relevant parameters as cross section dimension, material properties and different temporal development of the creep strains. However, these equations are not feasible for the daily design process. In the Technical Specification [3] the approach indicated in steel-concrete-composite structures is adopted, so the material creep coefficients from the material standards [4] and [5] are modified by a factor ψ (see Table 2)



Table 2: ψ -factors for the evaluation of the effective creep coefficient for slab systems (bt=bc; 1/5 < Ac,eff/At<1) and beam systems (b_t << b_c; 1 < $A_{c,eff}/A_t$ < 5) in dependence on the composite coefficient γ_1 according to [4] Annex B

Concrete φ = 3,5; k_{def} = 0,6		Concrete φ = 2,5; k_{def} = 0,6		Timber in all cases	
$\psi_c(t = 3 - 7a)$	$= 2{,}5 - \gamma_1^{1,1}$	$\psi_c(t = 3 - 7a)$	$= 1{,}9 - 0{,}6\,\gamma_1^{1,1}$	$\psi_t(t = 3 - 7a)$	= 0,5
$\psi_c(t = \infty)$	$= 2{,}6 - 0{,}8\,\gamma_1^{2}$	$\psi_c(t = \infty)$	$= 2{,}0 - 0{,}5\,\gamma_1^{1,9}$	$\psi_t(t = \infty)$	= 1,0
Concrete φ = 3,5; k_{def} = 0,8		Concrete φ = 2,5; k_{def} = 0,8		Connection in all cases	
$\psi_c(t = 3 - 7a)$	$= 2{,}2 - 0{,}8\,\gamma_1^{1,2}$	$\psi_c(t = 3 - 7a)$	$= 1{,}7 - 0{,}5\,\gamma_1^{1,1}$	$\psi_{conn}(t = 3 - 7a)$	= 0,65
$\psi_c(t = \infty)$	$= 2{,}3 - 0{,}5\,\gamma_1^{2,6}$	$\psi_c(t = \infty)$	$= 1{,}8 - 0{,}3\,\gamma_1^{2,5}$	$\psi_{conn}(t = \infty)$	= 1,0

For the point in time t=0 all *ψ-values are equal 0*

γ_1 according to [4] Annex B

In order to evaluate the effects of the creep deformation the Modulus of Elasticity and the stiffness of the connection are modified by

$$E_t(t) = \frac{E_0}{1+\psi_t \cdot k_{def}};\ E_c(t) = \frac{E_0(t_{load})}{1+\psi_c \cdot \varphi};\ K = \frac{K_0}{1+\psi_{conn} \cdot k\prime_{def}} \tag{8}$$

The effective creep coefficient of the connection can be determined by

$$k'_{def} = 2 \cdot k_{def} \tag{9}$$

The increase of the creep coefficient of the connection by the factor 2 is caused by the local high stresses in the range of the anchorage of the connection device.

Since creep and shrinkage interact and the effects of shrinkage are partly reduced by the creep deformation (~ relaxation), the shrinkage value of concrete at *t=3 to 7 years* may be reduced to 60% of its end shrinkage value and for the point in time $t = \infty$ it may be reduced to 90% of its end value.

In propped constructions, the shrinkage begins after the end of the post-treatment of the concrete, even if the system is still propped. The reason behind is the fact that the shrinkage leads to eigenstresses which cannot be reduced by creeping during the short period of propping. Therefore, the building process does not have an effect on the magnitude of the shrinkage value applied in the structural analysis.

6 Application for bridges

The focus of the Technical Specification [3] is the application of timber-concrete-structures in buildings. To enable the application in bridges, EN 1995-2 [25] will give some additional rules. The major differences to the rules given in the Technical Specification [3] are:

- Range of application
  - In order to avoid an increase of moisture in the joint between timber and concrete, the concrete has to be protected by a water impermeable layer, e.g. surface protection or bituminous sealing, since the concrete is usually not water-impermeable enough without any protection due to water-vapor penetrating through the deck
  - The concrete cross section height should be between 100mm and 400mm.
  - In difference to buildings, adhesive bonded timber-concrete-composite bridges are allowed.
- Design
  - The application of the γ-method is explicitly excluded, since the some boundaries of this method, as e.g. uniform distributed loads are not fulfilled in bridge design.
  - For dowel-type fastener, the application of the rope effect is not allowed.
- Effective creep coefficients: In order to consider the effect of the composite action on the effective creep coefficient, ψ -factors are given in the Technical Specification [3]. However, the range of application of these values is focussed on the application in buildings, which does not often fit the range of application in bridges. For that reason, the Annex A of [25] provides rules, how to determine the creep coefficients for geometries outside the boundaries defined in [3].



- Fatigue: The fatigue section will be shifted from the EN 1995-2 to the main part EN 1995-1-1. Additionally the determination of the fatigue resistance will be transferred from the level of forces to the stress level. Therefore, the application in timber-concrete-concrete should be possible, since the stresses are evaluated.

7 Design process

The design process according to [3] for the ULS and SLS is summarized in Fig 4 and Fig 5, resp.. The mayor differences in the design compared to the design according to common technical approvals are highlighted in red.

Compared to the design of pure timber elements, the mayor difference is, that the loads are separated into permanent and short term loads, whereas only the permanent loads lead to creep deformations. The short term loads act to short, so no relevant creep deformations are expected. The internal stresses are evaluated separately with different effective stiffness, representing the effect of creep of the material. Finally, the internal forces are superimposed and the proof of the system is done with these superimposed internal forces and stresses resp.

Since the internal stresses are influenced by the relation of the stiffness and not by the absolute value of the stiffness, the point in time of 3 to 7 years has to be considered in the ULS. However the deformation increases constantly, this point in time t=3-7y does not have to be considered in the SLS. For the evaluation of the effects of vibration, no creep deformation has to be considered, since the effective stiffness with the reduced MoE is not a real stiffness but represents the effect of creep.

8 Summary and Outlook

The load and deformation behaviour of timber-concrete-composite structures has been widely studied. As one output of these studies technical approvals of connections have been developed. These technical approvals often also cover the design procedure.

Nevertheless, it is planned to introduce clauses about the design of timber-concrete-composite structures within the next generation of the Eurocodes. In preparation for this a Technical Specification [3] has been developed and will be continuously improved, which could be the basis of a new part of [4].

This Technical Specification [3] differs from the typical technical approvals in following issues:

- Loads: In the Technical Specification the loads and actions caused by different elongation of the composite members due to shrinkage, swelling or temperature changes are determined explicitly and are not covered in a global modification factor. So the design can be adjusted to the existing surrounding and boundary conditions. The required partial safety factors of these loads and modifications factors assigned to these loads are given in the Technical Specification
- Design method: One of the most popular design method is the so called γ-method given in [4] Annex B. Unfortunately this method cannot consider inelastic strains, so the Technical Specification Annex B provides an extension in order to cover the effect of different temperature elongation, shrinkage and swelling within this method, by transferring these inelastic strains in a fictitious load.
- Connections: In the Technical Specification, design equations and provisions for dowel type fasteners and glued in rods installed perpendicular to the joint and notches are given. Additionally, the required parameters for the application of the Technical Specification are defined, namely load capacity, stiffness in the ULS and SLS. So technical approvals of other systems can be "docked" to the provisions given in this Technical Specification.
- Long term behaviour: Concerning the long term behaviour it might be necessary to verify an additional point in time, if some limits are exceeded. The effect of stress redistributions on the effective creep coefficients will be covered by the modification of the material creep coefficient.

The Technical Specification is published in February 2022. After a testing phase until January 2025 it is planned to convert the Technical Specification into a new part 1-3 of [4] dealing with the design of timber-concrete-composite structures.

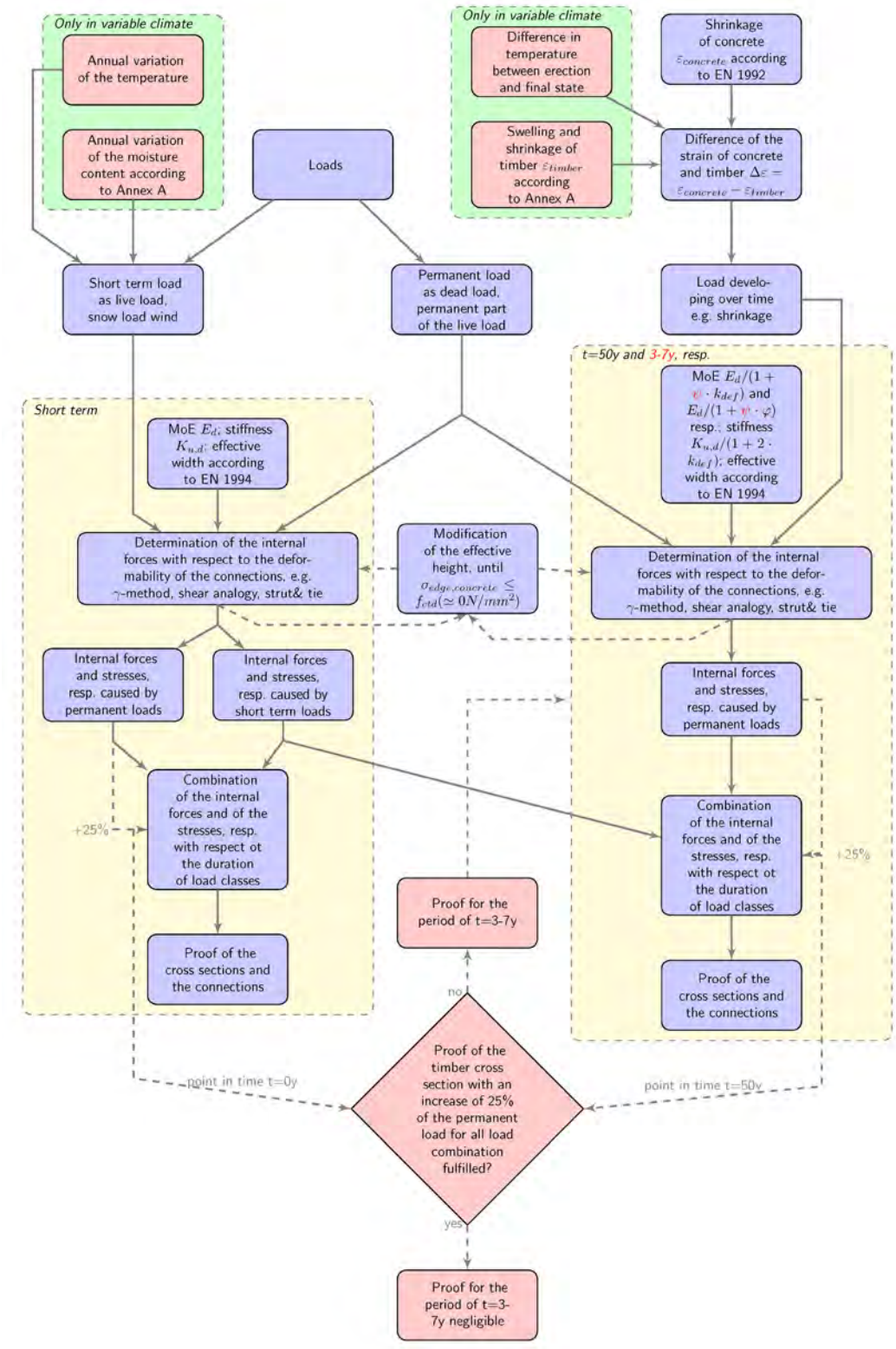


Figure 4: Design process in the ULS

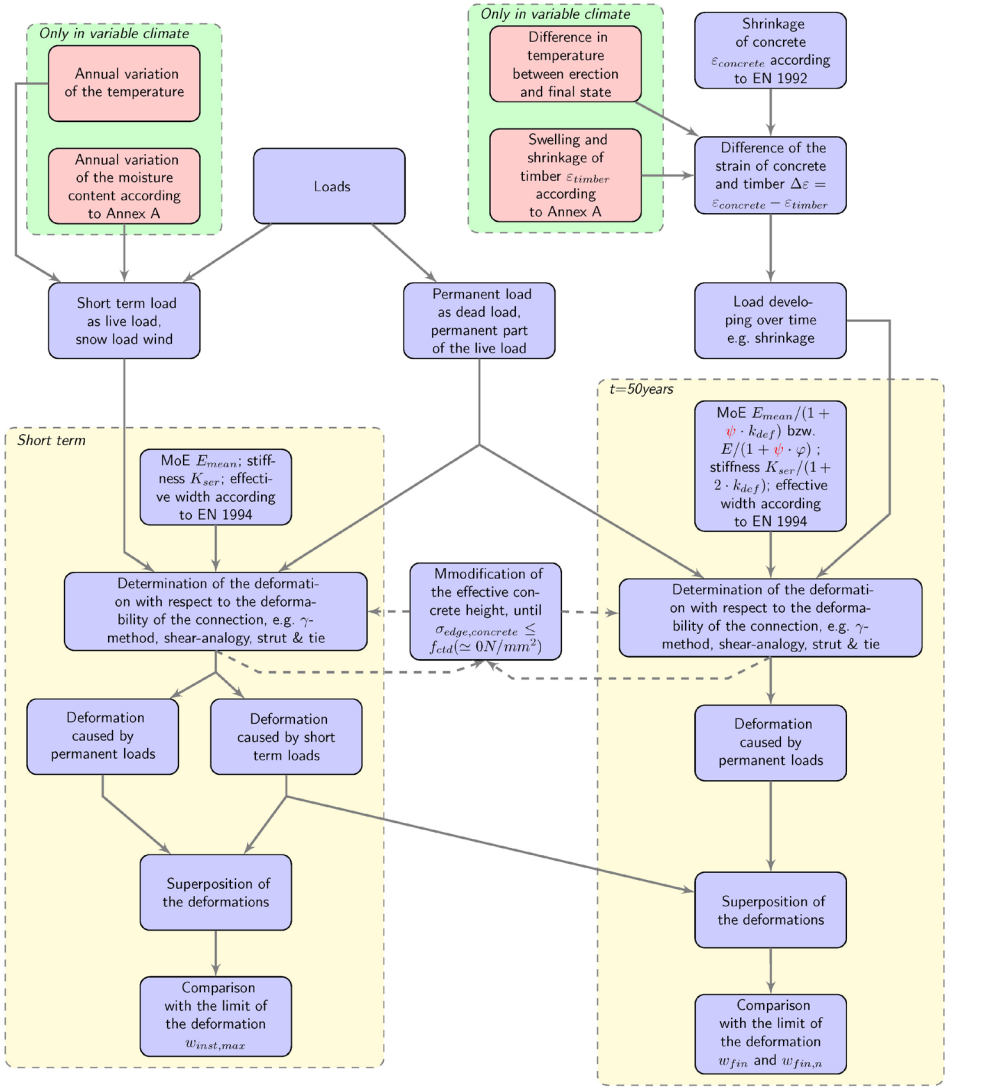


Figure 5: Design process in the SLS

9 References

[1] Jung, P.: Holz-Beton-Verbunddecken in der Praxis und ihre Wirtschaftlichkeit. In: Holz-Beton-Verbunddecken in Theorie und Praxis, Hrsg.: Bau und Wissen, CH-Wildegg, 2012

[2] DIN EN 1994-1-1: Eurocode 4: Bemessung und Konstruktion von Verbundtragwerken aus Stahl und Beton - Teil 1-1: Allgemeine Bemessungsregeln und Anwendungsregeln für den Hochbau; Deutsche Fassung EN 1994-1-1:2004 + AC:2009. DIN-Deutsches Institut für Normung e.V., 2010

[3] CEN/TS 19103: Eurocode 5: Design of Timber Structures. Structural design of timber-concrete composite structures. Common rules and rules for buildings; CEN European Committee for Standardization

[4] DIN EN 1995-1-1: Eurocode 5: Bemessung und Konstruktion von Holzbauten - Teil 1-1: Allgemeines- Allgemeine Regeln und Regeln für den Hochbau. DIN-Deutsches Institut für Normung e.V., 2010

[5] DIN EN 1992-1-1: Eurocode 2: Bemessung und Konstruktion von Stahlbeton- und Spannbetontragwerken - Teil 1-1: Allgemeine Bemessungsregeln und Regeln für den Hochbau; Deutsche Fassung EN 1992-1-1:2004 + AC:2010. DIN-Deutsches Institut für Normung e.V., 2010



[6] DIN EN 1991-1-5: Eurocode 1: Einwirkungen auf Tragwerke - Teil 1-5: Allgemeine Einwirkungen, Temperatureinwirkungen. DIN-Deutsches Institut für Normung e.V., 2010
[7] Dias, A.; Fragiacomo, M.; Harris, R.; Kuklic, P.; Rajicic, V.; Schänzlin, J.: Technical Specification – Final Draft - Eurocode 5: Design of Timber Structures - Part 1-3: Structural design of timber concrete composite structures / Project Team CEN/TC 250-SC5.T2. 2018.
[8] DIN EN 1995-1-1 / NA: Nationaler Anhang - Eurocode 5: Bemessung und Konstruktion von Holzbauten - Teil 1-1: Allgemeines- Allgemeine Regeln und Regeln für den Hochbau. DIN-Deutsches Institut für Normung e.V., 2013
[9] Fries, J.: Beitrag zum Tragverhalten von Flachdecken mit Hutprofilen, Institut für Konstruktion und Entwurf, Universität Stuttgart (Mitteilung 2001-1), Dissertation, Dezember 2001
[10] Dabaon, M.; Tschemmernegg, F.; Hassen, K.; Lateef, T. A.: Zur Tragfähigkeit von Verbundträgern bei teilweiser Verdübelung. In: Stahlbau 62 (1993), S. 3–9
[11] Schänzlin, J.; Fragiacomo, M.: Extension of EC5-Annex B formulas for the design of timber-concrete composite structures. In: CIB-40-10-1, 2007 (International council for research and innovation in building and construction– working commission W 18 – timber structures)
[12] Schänzlin, J.: Zum Langzeitverhalten von Brettstapel-Beton-Verbunddecken, Institut für Konstruktion und Entwurf, Universität Stuttgart, Dissertation, 2003
[13] Dias, A.; Fragiacomo, M.; Harris, R.; Kuklic, P.; Rajicic, V. ; Schänzlin, J.: Hintergrundbericht zur Technical Specification – Final Draft - Eurocode 5: Design of Timber Structures - Part 1-3: Structural design of timber concrete composite structures / Project Team CEN/TC 250-SC5.T2. 2018. – Forschungsbericht
[14] Dias, A. (Hrsg.); Schänzlin, J. (Hrsg.); Dietsch, P. (Hrsg.): Design of timber-concrete composite structures: A state-of-the-art report by COST Action FP1402 / WG 4. Shaker Verlag Aachen, 2018 https://www.costfp1402.tum.de/home/
[15] Kreuzinger, H.: Flächentragwerke: Platten, Scheiben und Schalen; Berechnungsmethoden und Beispiele. In: Brücken aus Holz (1999), S. 43–60
[16] Scholz, A.: Eigenspannungszustände an Verbundquerschnitten infolge von Dehnungsunterschieden Anwendung eines neueren Rechenverfahrens auf einem bewährten Lösungsansatz. In: Bautechnik 81 (2004), März, Nr. 3, S. 180–188
[17] Scholz, A.: Ein Beitrag zur Berechnung von Flächentragwerken aus Holz, TU München, Diss., 2003
[18] Grosse, M.; Hartnack, R.; Lehmann, S.; Rautenstrauch, K.: Modellierung von diskontinuierlich verbundenen Holz-Beton-Verbundkonstruktionen. In: Bautechnik 80 (2003), S. 534 – 541 und 693 – 701
[19] Johansen, K. W.: Theory of timber connections. In: International Association of Bridge and Structural Engineering 9 (1949), S. 249-262
[20] Michelfelder, B.: Trag- und Verformungsverhalten von Kerven bei Brettstapel-Beton-Verbunddecken, Universität Stuttgart, Institut für Konstruktion und Entwurf, Dissertation, 2006. http://nbn-resolving.de/urn:nbn:de:bsz:93-opus-28911
[21] Kudla, K.: Kerven als Verbindungsmittel für Holz-Beton-Verbundstraßenbrücken, Institut für Konstruktion und Entwurf, Diss., 2017
[22] Kupfer, H.; Kirmair, H.: Verformungsmoduln zur Berechnung statisch unbestimmter Systeme aus zwei Komponenten mit unterschiedlichen Kriechzahlen. In: Bauingenieur 62 (1987), S. 371–377
[23] Kreuzinger, H.: Verbundkonstruktionen Holz / Beton. 1994
[24] Blass, H.-J.; Ehlbeck, J. ; Linden, M. v. d. ; Schlager, M.: Trag- und Verformungsverhalten von Holz-Beton-Verbundkonstruktionen. 1995 (T2710)
[25] prEN 1995-2:202x: Eurocode 5 — Design of Timber Structures — Part 2: Bridges; CEN/TC 250/SC 5/WG 6 N374

Sponsoring Advertisements

Bern University
of Applied Sciences



Research and Development in Partnership with Industry

▸ Engineering and Information Technology

Empa
Materials Science and Technology

Empa -
Swiss Federal Laboratories for Materials Science and Technology

1 Empa – The Place where Innovation Starts

- Empa is the interdisciplinary research institute for materials science and technology of the ETH Domain and conducts cutting-edge research for the benefit of industry and the well-being of society.
- Within national and international networks we develop science-based solutions for pressing challenges of society and industry in the areas of energy, mobility, building technologies, personal health and the environment as well as advanced materials and surfaces.
- Together with our partners we turn research results into innovations, thus boosting the innovative capacity and the international competitiveness of the Swiss economy.
- Furthermore, Empa works out the scientific basis for the sustainable development of our society and for political decisions. We actively engage in public debate about novel technologies and their wider societal implications – all this to one end: to shape our future economically successful and environmentally sustainable at the same time.

2 Research Areas

To deliver solutions to today's increasingly complex challenges Empa has concentrated its efforts in five Research Focus Areas (RFAs):

- Energy for a secure, clean and efficient energy supply and innovative building and mobility concepts
- Natural Resources & Pollutants for a sustainable and efficient use of our natural resources and a sound environment
- Health & Performance to safeguard and maintain personal health and wellbeing, especially of the elderly
- Sustainable Built Environment to develop solutions for the sustainable design, construction, renewal, and preservation of the built environment
- Nanostructured Materials as a cross-sectional RFA providing solutions for all of the above mentioned challenges and research areas

Empa's RFAs are geared towards developing inter- and transdisciplinary solutions, which can be realized within due time and thus have an impact on society and at the same time strengthen the competitiveness of Empa's partners.

3 Figures and Facts

Empa is based at three locations within Switzerland: Duebendorf, Sankt Gallen and Thun. At the end of 2021, 1012 people were working at Empa. Scientific staff, including PhD and postdoctoral students, comprises 574 individuals. Of these, 101 are Senior Scientists. Technical and administrative staff comprised 395 persons. The proportion of women, at 28 percent, reflects the gender distribution among graduates from Swiss universities and ETH in the scientific disciplines represented at Empa. The proportion of foreign citizens is 45 percent of the total staff.

In 2021 Empa researchers and engineers published over 850 scientific papers and patented 13 developments. By the end of the year, over 110 projects funded by the Swiss National Science Foundation (SNSF), nearly 100 projects supported by Innosuisse, and roughly 70 EU projects were underway at Empa. In 2021 Empa also attracted almost 74 million Swiss francs in third-party funding for projects. The 32 spin-offs together with other start-ups in Empa's two business incubators employ a total of around 1100 employees.

Timber and Technology

Timbatec – Ihr Spezialist für Infrastrukturbauten aus Holz



www.timbatec.com

Timbatec
Timber and Technology

Always a **STRONG CONNECTION**

CLT INSIDE CORNER

One of our new products is the CLT internal corner system. Strong wall junction connections are created when it is used in combination. The internal corner system is also an unbeatable solution for timber / timber joints.



Sample application for the CLT internal corner system with KonstruX

KONSTRUX FULLY THREADED SCREW

KonstruX fully threaded screws maximise a joint's load-bearing capacity with high thread extraction resistance in both components. If partially threaded screws are used, the joint's load-bearing capacity is limited by the considerably lower characteristic yield strength in the attached part.



KonstruX, countersunk head galvanised

LIFTING ANCHOR & BALL SUPPORTING BOLT

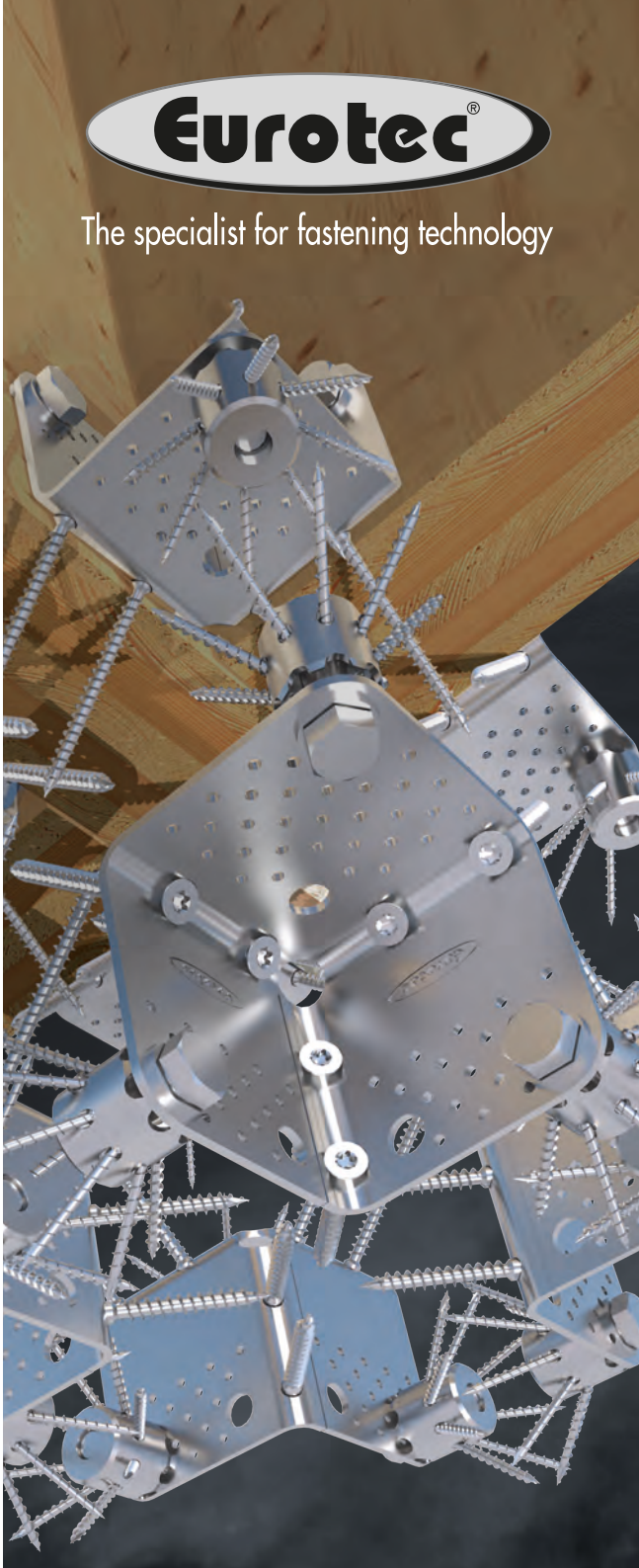
The clever HebeFix was designed for use with a ball support bolt. Pre-fabricated wall elements can be easily lifted and transported with the lifting anchor. Use with screws allows the lifting anchor to be used several times.



Sample application for the HebeFix in combination with the ball support bolt

Eurotec®

The specialist for fastening technology



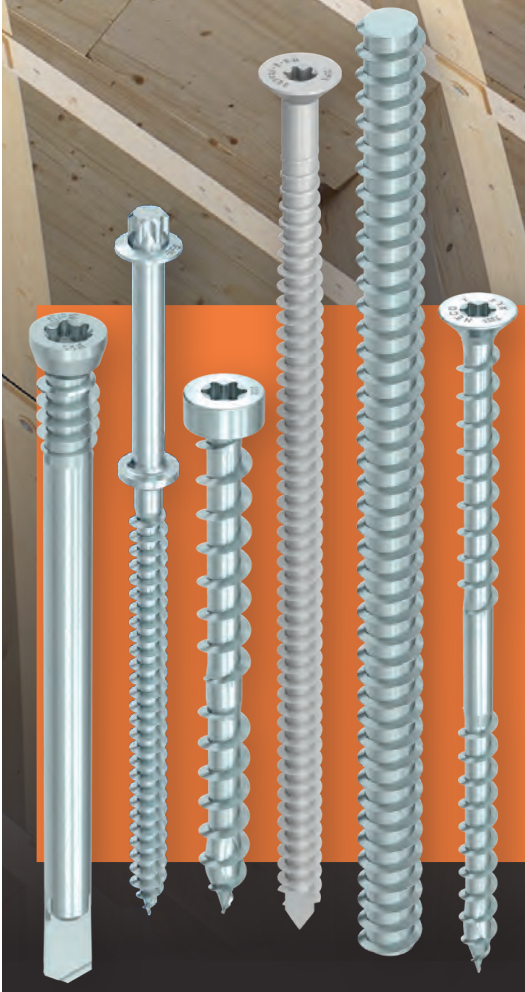
Find out more about our timber engineering solutions!

E.u.r.o.Tec GmbH • Unter dem Hofe 5 • D-58099 Hagen
Tel. +49 2331 62 45-0 • Fax +49 2331 62 45-200 • E-Mail info@eurotec.team

HECO SCHRAUBEN



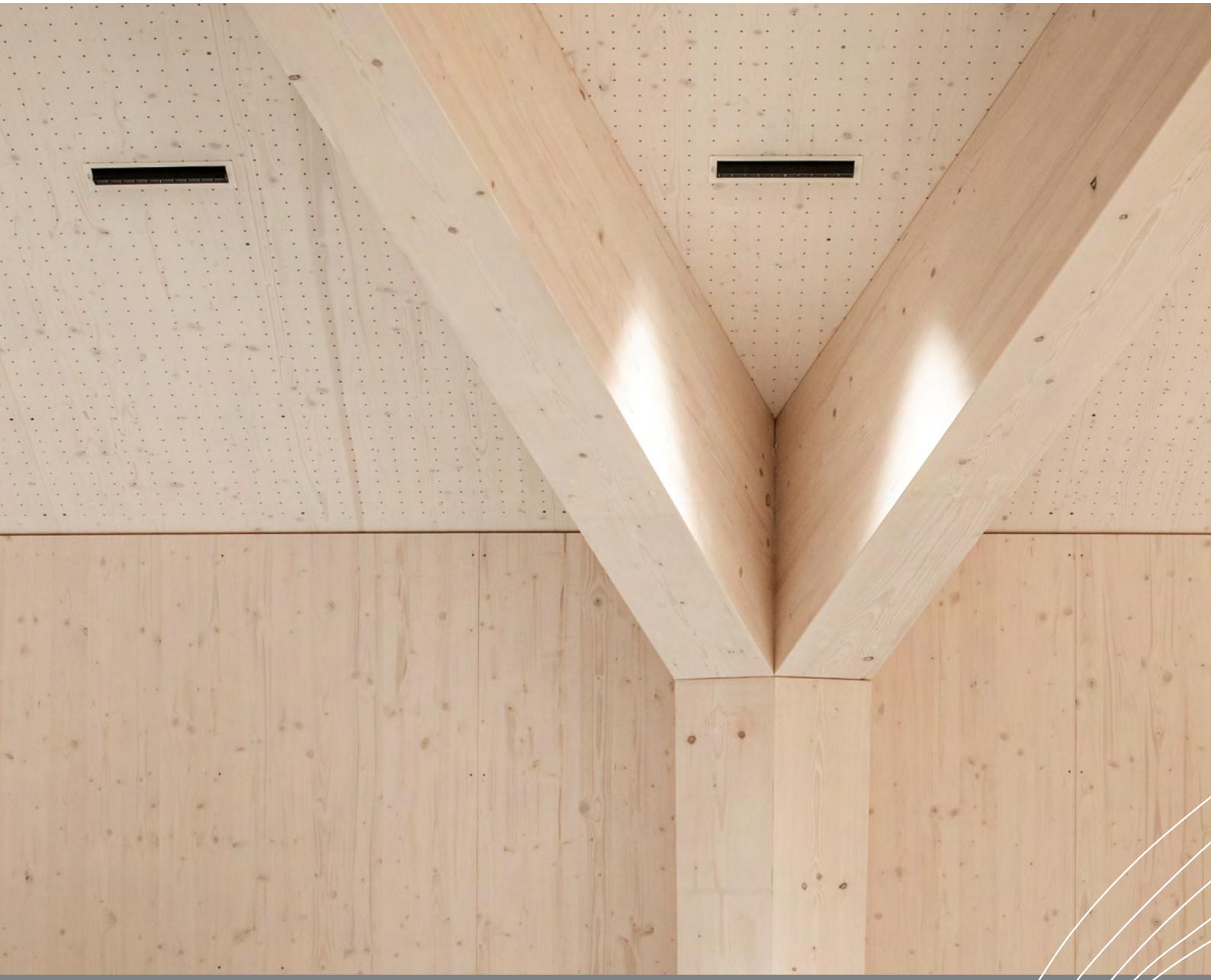
Swatch HCI © by Blumer-Lehmann AG



HECO Befestiger: Entwickelt für den konstruktiven Holzbau.

Erhältlich bei ihrem Fachhändler oder unter www.allchemet.ch

HÜSSER
HOLZLEIMBAU AG



State-of-the-art technology for timber construction.

huesserholzeimbau.com

IMMER AG

A competent and solution-oriented partner for wood processors across all language barriers

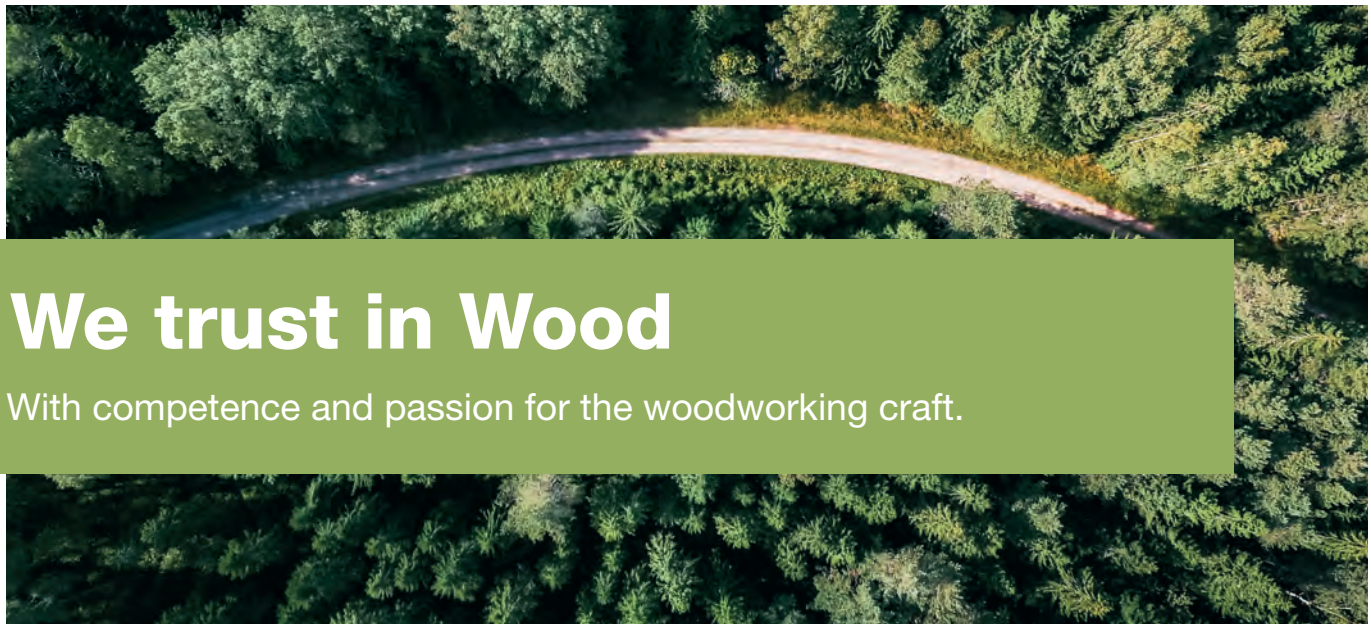
IMMER AG is a trading company with a long tradition. Founded in 1835, the company operates throughout Switzerland and now has around 180 employees. It is represented at several locations in Switzerland with its headquarters in Uetendorf, a branch in Rothenburg and a sales office in Farvagny. Thanks to a wide-ranging brand and product portfolio and a large number of general imports, wood processors benefit from a wide selection of products and strong brands. Whether in the online store, in the sales premises, by telephone or sales representatives visit – at IMMER AG, help is provided in a pragmatic and solution-oriented manner. Trained specialists are available to provide competent advice across all product ranges – from fittings to machines, tools, fastening- and locking technology. The modern logistics with its own delivery service, the in-house repair and service center and the inspection of PPE articles, round off the attractive package.





IMMER AG
Uetendorf | Rothenburg | Farvagny

www.immerag.ch



We trust in Wood

With competence and passion for the woodworking craft.

athmer FESTOOL Lamello metabo PROFESSIONAL POWER TOOL SOLUTIONS fein

PREBENA makita mafell PB SWISS TOOLS rothoblaas

GSA Technology AG · Obseestrasse 11 · CH-6078 Lungern
+41 41 679 70 99 · www.gsa-technology.ch · info@gsa-techonology.ch

GSA Technology – A powerful connection!

Bonded-in profiled rods are among the most efficient fasteners in modern timber construction. Whether glued in parallel or perpendicular to the grain direction, high forces can be applied in small areas of the wooden components. Since the late 1990s, neue Holzbau AG (n'H) has been researching and developing in this field in collaboration with Professor Emeritus Ernst Gehri of the ETH Zurich. Under the brand name "GSA Technology", a range of solutions has since been developed which are being successfully applied in various timber structures all over the world.
GSA stands for the German term „Gewindestangen-Anker" which means threaded rod anchor. In this connecting and reinforcing method, wood, GSA resin and steel form a composite system, requiring the adjustment of the three components' properties. To achieve optimal connections, certain rules must be followed and requirements complied with. To prevent the brittle failure modes of the wood or the adhesive, the joint must be designed such that the (ductile) steel rods fail first in the ultimate limit state. GSA rods enable high-performance connections of components in softwood and hardwood.

GSA Technology has advantages for all stakeholders:

- Building owners can have individual projects built on a cost-efficient basis thanks to standardised elements.
- Architects can plan slender and aesthetically pleasing structures with GSA technology, with visual appearances unimpaired by visible connectors.
- Contractors can focus on efficient erection. Thanks to modern CAD/CNC technology, ingenious and assembly-friendly plug-in connections are created with the highest possible precision.
- Engineers are convinced by the system's easy and thorough design concept. The GSA Technology guarantees the three essential criteria of stiffness, load-carrying capacity and ductility.
- With the connectors protected by the wood cover, the GSA components provide optimum fire behaviour.
- GSA Technology is continuously being developed in our own test laboratory. This enables design models to be verified. The applications in various products are constantly being expanded.
- We are convinced that GSA Technology has a strong future. Together with our licensing partners, we are scaling up GSA Technology and pushing timber construction forward.

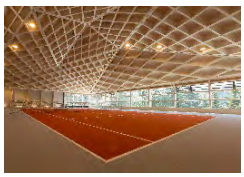
Realised projects

1) Cable car to Mount Weissenstein, Solothurn
2) Fabrication shop Schindler Scheibling AG, Uster
3) Production facility Strüby Holzbau AG, Root
4) Indoor tennis centre Bürgenstock, Obbürgen
5) Production facility Pilatus Aircraft Ltd, Stans


Weissenstein


Schindler Scheibling


Strüby


Bürgenstock


Pilatus Aircraft

www.gsa-technology.ch

SWISS MADE

smartex®
MONITORING-SYSTEMS

intelligently prevent moisture damages...



for all kinds of massive and wooden constructions

DETECT LEAKS AND MOISTURE IN REAL TIME

smartex® monitoring systems monitor your building in real time for leaks and wetness, even where you can't look. Around the clock, day by day. This means that damages are detected at an early stage, before long-term damages can occur.

AUTOMATICALLY LOCATE DAMAGES

If damages occur, smartex® not only sends an alarm, but also information where the damage occurred. Thus, many damages remain a small bagatelle, because you do not have to search for long to find them.

CARRY OUT TARGETED REPAIRS

Particularly with moisture damages, the earlier you repair, the less consequential damages occur. With smartex® you can repair quickly, which saves trouble and costs. And what doesn't break doesn't need to be repaired. That' s sustainable, too.

PROGEO MONITORING
SYSTEME UND SERVICES
GMBH & CO. KG

HAUPTSTRASSE 2
DE-14979 GROSSBEEREN
PHONE: +49-33701-22-0

PROGEO.COM

SOLUTIONS THAT SUIT EVERY NEED



- FASTENING
- AIRTIGHTNESS AND WATERPROOFING
- SOUNDPROOFING
- FALL PROTECTION
- TOOLS AND MACHINES

Rothoblaas is the multinational Italian company that has made innovative technology its mission, making its way to the forefront for timber buildings and construction safety in just a few years. Thanks to its comprehensive product range and the technically-prepared and widespread sales network, the company promotes the transfer of its know-how to the customers and aims to be a prominent and reliable partner for developing and innovating products and building methods. All of this contributes to a new culture of sustainable construction, focused on increasing comfortable living and reducing CO_2 emissions.

For further information:
www.rothoblaas.com

rothoblaas
Solutions for Building Technology



“ONE-SHOT-SYSTEM” – PARKHAUSSANIERUNG IN REKORDZEIT

Sikalastic®-8800 – SANIEREN – VERSIEGELN – NUTZEN – IN WENIGEN STUNDEN

Der hochreaktive Polyurea-Flüssigkunststoff reduziert Schliessungszeiten von Parkhäusern während der Sanierung auf ein Minimum. Das innovative Parkdecksystem nutzt die Polyurea-Technologie als Abdichtungs- und Verschleissschicht. Eine Aushärtung innert Sekunden ermöglicht das Aufbringen der Nutzschicht unmittelbar nach Applikation der Abdichtungsschicht. Die Zuschlagstoffe werden während der Beschichtung direkt in den Flüssigkunststoff eingeblasen. Dank einer schnell härtenden Versiegelung können die Flächen innert weniger Stunden nach Aufbringen der letzten Schicht wieder genutzt werden. **www.sika.ch**

BUILDING TRUST

Timber and Technology

Timbatec – Ihr Spezialist für Holzbrücken



www.timbatec.com

Timbatec
Timber and Technology


Queensferry Crossing Bridge,
Scotland - 2017
The World's longest three-tower cable-stayed bridge.
WE MAKE IT POSSIBLE.
www.vsl.com
VSL
A member of
Bouygues Construction

Bern University of Applied Sciences
Architecture, Wood and Civil Engineering
Solothurnstrasse 102
CH-2504 Biel

ictb21@bfh.ch
www.bfh.ch/ictb

Funding Partners

Schweizerische Eidgenossenschaft
Confédération suisse
Confederazione Svizzera
Confederaziun svizra

Swiss Confederation

Federal Office for the Environment FOEN
Action Plan Wood

Swiss National Science Foundation

Sponsor PLUS

Eurotec
IMMER AG
Ihr Partner für das Handwerk
HÜSSER HOLZLEIMBAU AG
n'H neue Holzbau AG
PROGEO the monitoring people
rothoblaas Solutions for Building Technology
Timbatec Timber and Technology
Holzbauingenieure·Thun·Bern·Zürich·Wien
Ihr Partner für anspruchsvolle Holzbauten
TS3 Timber Structures 3.0
VSL A member of Bouygues Constructio

Sponsors

Sika
ceseFor
Interreg Sudoe
EGURALT

